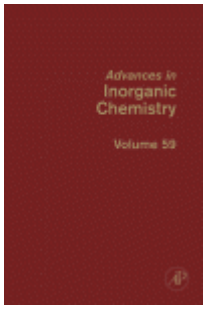

Advances in Inorganic Chemistry, volume 59

Template Effects and Molecular Organization
Elsevier, 2006

Edited by: Rudi van Eldik and Kristin Bowman-James
ISBN: 978-0-12-023659-6

PREFACE

At the 228th ACS Meeting in Philadelphia, Pennsylvania, August 22–26, 2004, a marathon symposium was held in the Inorganic Division that ran four days from Sunday morning through Wednesday afternoon. The title of the symposium, *From the Template Effect to Spontaneous Intermolecular Organization, A Celebration of Daryle Busch's First 50 years of Leadership, Teaching, Research, and Service*, only hints at the many contributions that Daryle H. Busch has made over the last five decades and more. The symposium was largely organized by two of Busch's former graduate students, Rebecca Roesner, currently at Illinois Wesleyan University, and Elena V. Rybak-Akimova, now at Tufts University, along with Kristin Bowman-James, a former postdoctoral associate, currently at the University of Kansas. A total of 49 of Daryle's former students, postdoctoral associates, colleagues, and friends, including internationally recognized leaders in their fields of research, presented talks at the symposium.

Since 1988, Daryle has held the Roy A. Roberts distinguished professor of chemistry position. He is currently also the deputy director of the Center for Environmentally Beneficial Catalysis at the University of Kansas. Prior to his current position, Daryle was a faculty member at The Ohio State University, where he held the rank of presidential professor.

Daryle's career has indeed been stellar. Seminal work early in his career resulted in the founding of macrocyclic chemistry and the molecular template effect. He was also a pioneer in ligand reaction chemistry and the burgeoning field of bioinorganic chemistry in the 1950s and 1960s. In the 1970s, he was the first to describe the phenomenon now so important in supramolecular chemistry known as preorganization. Throughout the years Daryle's research has evolved from the early foundations of basic transition metal coordination, macrocyclic and bioinorganic chemistry that he provided to the community has evolved to a focus on homogeneous catalysis and green chemistry in addition to his first love for bioinorganic and macrocyclic

chemistry. Daryle has also worked closely with industry throughout his career and holds twelve patents joint with five major industrial companies and two universities. Perhaps one of his greatest contributions to science has been in education, where he has been a tremendous role model for more than 200 PhDs and postdoctoral researchers.

The scope of the science presented in the four day symposium was breathtaking, ranging from the first talks on bioinorganic aspects of oxygen chemistry to anion coordination chemistry, self assembly, molecular devices and capsules, chemistry in supercritical fluids, biological imaging, cluster chemistry, and even touched on industrial academic liaisons. Many of the talks involved macrocyclic chemistry, and served to illustrate the tremendous synthetic advances that the field has made from the first simple monocyclic macrocycles to complex molecular knots and Borromean rings, capsules, catenanes and knotaxanes, a whole universe of elegantly interwoven molecules. Daryle gave a memorable talk providing historical perspective on the consequences of the kinetic and equilibrium template principles, which ultimately have led to this synthetic artwork, "From templates and molecular organization to catalysis," and illustrated the role that these principles played in the evolution of his own research program.

The Symposium was truly a tribute to the elegant science of the founding father of macrocyclic chemistry. As was evident by the participants in the symposium, Daryle's former students and postdoctoral associates as well as colleagues and friends alike all have the utmost regard and respect for Daryle both as a scientist and a human being.

As a consequence, we invited several speakers at the Symposium to contribute to a thematic issue of Advances in Inorganic Chemistry on Template Effects and Molecular Recognition. Kristin Bowman-James was invited to be co-editor for this volume since she has been associated with Daryle for many years. The authors were requested to write short reviews on their current research activity as presented at the symposium. This thematic issue contains eight contributions and covers a wide range of topics. In the first contribution, Lindoy and coworkers report on self-assembled metallo-supramolecular systems, incorporating β-diketonate motifs as structural elements. This is followed by a contribution by Suh and Moon on coordination polymer open frameworks constructed of macrocyclic complexes. Fabbrizzi and co-workers report on molecular devices based on metallo-cyclam subunits, which is followed by an impressive contribution from Roesner, Rybak-Akimova and co-worker on molecular recognition of neutral and charged guests using metallomacrocyclic hosts. The co-editor and co-workers report on supramolecular chemistry of environmentally relevant anions, which is followed by a contribution by Dye and coworkers on the role of cation complexants in the synthesis of alkalides and electrides. Riley and Schall cover the interesting topic of structure-activity studies and the design of synthetic superoxide dismutase (SOD) mimetics as therapeutics. Finally, the editor contributes with a

report on the electronic tuning of the lability of inert Co(III) and Pt(II) complexes.

We trust that every one will agree that the topics covered in this thematic issue are all very stimulating and report the most recent advances in inorganic chemistry accomplished in the area of template effects and molecular recognition.

Rudi van Eldik
University of Erlangen-Nürnberg
Germany

Kristin Bowman-James
University of Kansas, Lawrence
USA
July 2006

SELF-ASSEMBLED METALLO-SUPRAMOLECULAR SYSTEMS INCORPORATING β-DIKETONE MOTIFS AS STRUCTURAL ELEMENTS

DAVID J. BRAY, JACK K. CLEGG, LEONARD F. LINDOY and DAVID SCHILTER

Centre for Heavy Metals Research, School of Chemistry, University of Sydney, NSW 2006, Australia

I. Introduction

Molecular self-assembly is a widespread phenomenon in both chemistry and biochemistry. Yet it was not until recent decades that the rise of supramolecular chemistry has resulted in the designed self-assembly of an extremely diverse array of synthetic supramolecular architectures (*1–4*). The incorporation of metals into the latter has, in many instances, enhanced both the form and function of the resulting assemblies. Typically, both the design of the organic components and the choice of the associated metal ion have been key elements in the strategy employed to achieve a given supramolecular structure (*5*). Overall, the metallo-supramolecular field continues to produce a range of novel materials – often of nanometer dimensions – many of which are endowed with unusual properties. The latter include novel redox-active, photoactive, conductive (including superconductive), catalytic and non-linear optical properties. The ability to act as synthetic zeolite-like materials is also characteristic of particular structural types.

It has long been documented that β-diketone ligands are versatile metal coordinating agents and have played a significant role in coordination chemistry for over a century (*6–13*). Indeed, the metal ion

ADVANCES IN INORGANIC CHEMISTRY
VOLUME 59 ISSN 0898-8838 / DOI: 10.1016/S0898-8838(06)59001-4

complexation chemistry of simple β-diketone ligands represents one of the most studied areas of coordination chemistry.

The β-diketone motif is attractive for incorporation into metallo-supramolecular structures. First, it has the potential to be readily derivatized using well-established procedures. Thus, the electronic and steric nature of this ligand type may be varied in a rational manner to probe structure/function relationships as well as to 'tune' features of interest. Second, β-diketones have been shown to readily form complexes with a wide range of metals from across the Periodic Table. This prior research provides a rich resource upon which the design of more elaborate metal–ligand systems might be based. Indeed, examples of elaborated β-diketone derivatives being employed for the formation of metal ion directed assemblies, with in many cases the metals serving as both structural and functional elements, have been reported; these include both di- and polynuclear discrete species as well as non-discrete polynuclear structures – the latter falling into the category of framework materials. Nevertheless, the incorporation of β-diketone motifs into larger metallo-supramolecular systems has received somewhat less attention than for other classical coordination entities such as, for example, di- and polypyridine ligand systems (*14*).

In the discussion now presented, aspects of the prior work concerned with the synthesis and properties of metal-containing molecular architectures incorporating β-diketonate motifs will be reviewed, along with an account of our own recent investigations in this expanding area. Emphasis in the discussion has been given to systems in which the use of *designed* metal-ion-directed assembly has been employed for constructing new supramolecular entities.

II. Simple β-Diketone Ligands and Their Complexes

In order to provide a relevant background for the discussions in following sections, it is appropriate that an outline of some aspects of 'simple' metal β-diketonate chemistry now be presented. The simplest β-diketone ligand is 2,4-pentanedione (acetylacetone, acacH). Mildly basic conditions induce deprotonation of this species and the resulting 2,4-pentanedionate anion readily complexes a range of metal ions, usually (but not exclusively) (*15,16*) yielding a six–membered chelate ring (Fig. 1); parallel behavior is observed for a wide range of other β–diketone derivatives.

β-Diketones such as acacH show a tendency to form neutral complexes – with the geometry adopted normally reflecting the preferred geometry of the metal ion involved. For example, copper(II) forms square planar complexes of the type M(β-diketonato)$_2$ **1** (*17–19*). On the other hand, with acacH, cobalt(II) and nickel(II) form oxygen-bridged tetrameric and trimeric octahedral complexes of types

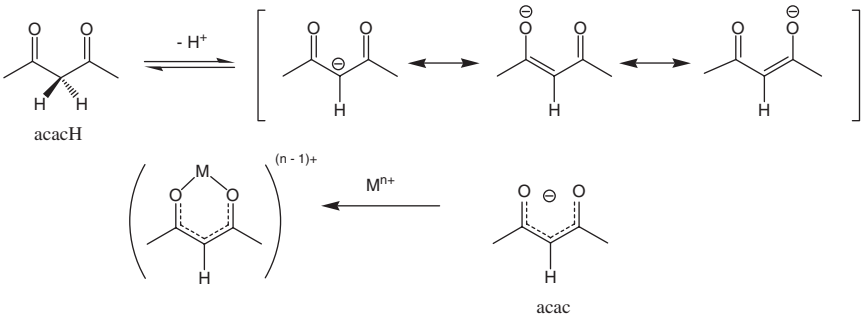

FIG. 1. Metal complexation by 2,4-pentanedione (acetylacetone, acacH).

$[Co_4(acac)_8]$ and $[Ni_3(acac)_6]$, respectively (*19,20*). However, in the case of cobalt(II), tetrahedral complexes can also result if a bulky β-diketonate ion is used. Chromium(III), manganese(III), iron(III) and cobalt(III) yield discrete octahedral complexes of the form [M(β-diketonato)$_3$] (*19,21–29*), as do several other trivalent metal ions including ruthenium, rhodium, aluminum, gallium and the lanthanides (although the lanthanide ions also form charged anionic species of the type $[M(acac)_4]^-$).

The ability to form higher coordinate species can be tuned through variation of the terminal R groups on the β-diketone (*30*). For example, it has been shown that the stepwise incorporation of electron-withdrawing trifluoromethyl groups serves to increase the affinity of the central metal ion for further ligation (*31*). Thus, the hexafluorinated analogue of 2,4-pentanedionate (1,1,1,5,5,5-hexafluoro-2,4-pentanedionate, hfac) has been documented to give the anionic copper(II) complex **2**, incorporating three such ligands (*32*).

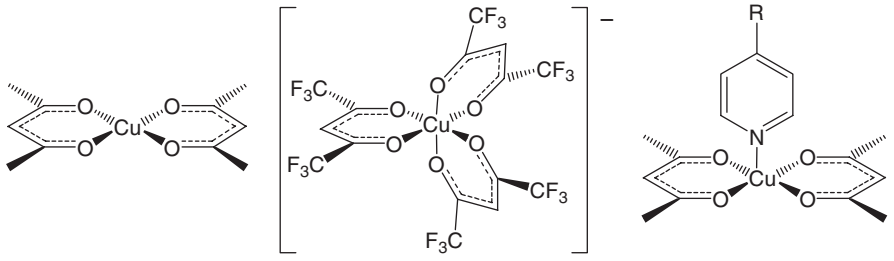

1 **2** **3a** R = CN
3b R = H
3c R = NH_2

A range of mixed-ligand complexes given by M(β-diketonato)$_2$L$_n$ (where, M = Co, Ni, Cu, Zn, n = 1 or 2, and L is a simple monodentate ligand such as an amine, alcohol, ether or water) are known (*19,33–39*). In some instances these species may be generated directly

from the corresponding coordinatively less-saturated precursor complex. Behavior such as this has been especially well documented for bis-β-diketonato complexes of copper(II) (*36,40*). When one axial site is occupied, as occurs in $VO(acac)_2$, the expected 1:1 adducts are formed; in this case products of type $[VO(acac)_2B]$ (where B is pyridine, 3- and 4-methylpyridine, 3,5-dimethylpyridine and 3- and 4-aminopyridine) have all been characterized (*41*).

The Lewis basicity of a potential axial ligand may also play an influential role with respect to adduct formation of the type mentioned above. For example, the five-coordinate copper(II) species **3a** is readily generated upon reaction of equimolar amounts of **1** and 4-cyanopyridine in dichloromethane, with the binding constant being $40\,M^{-1}$. The use of pyridine, a stronger base, gives adduct **3b**, with a binding constant that is approximately twice that of **3a**. Lastly, the analogous structure (**3c**) with 4-aminopyridine (a still stronger base) has a stability constant five times that of **3a** (*38*). It is also often possible to influence the formation of more than one adduct by altering the molar ratio of axial ligand to β-diketone complex. This is exemplified by the preparation of **4** and **5** from $[Cu(hfac)_2(H_2O)]$ in the presence of varying amounts of dabco (*42*). The formation of **4** also serves to illustrate that the use of ditopic base (such as dabco) can act to link two square planar precursor complexes. Further examples of such behavior are discussed below.

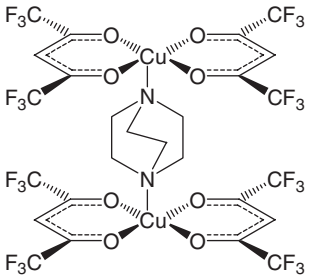

4

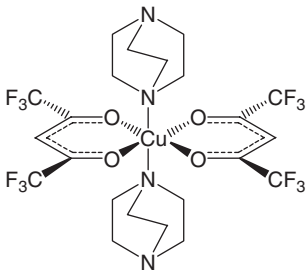

5

Soldatov *et al.* have carried out a series of investigations on complexes of type $M(dbm)_2$ (where dbm = dibenzoylmethanato) (*43*) and their heterocyclic amine base adducts (*44*). These studies were undertaken with the aim of investigating structure/function relationships underlying lattice inclusion behavior by the respective complexes as properties such as the nature of the axial ligands or the solvent involved were varied.

Four forms of the parent nickel(II) complex and two of the zinc(II) complex were characterized using powder and single-crystal X-ray diffraction analyses, differential scanning calorimetry, magnetic

susceptibility measurements and solid-state ^{13}C cross-polarization/magic angle spinning NMR (*43*). Thus, $Ni(dbm)_2$ forms three polymorphic forms (light-green, brown and green) and a fourth clathrate form with an included benzene as guest. With zinc, two polymorphic forms were isolated. The first is monomeric consisting of $[Zn(dbm)_2]$ entities, with each zinc center in a distorted tetrahedral environment of four oxygens from the two chelated dbm ligands. The second form is a dimer, $[Zn_2(dbm)_4]$, with each zinc coordinated to five oxygen atoms; in this, the Zn–Zn separation is 3.14 Å.

Mixed-ligand complexes of divalent nickel, zinc and cadmium with two bidentate dbm ligands equatorial and one or two monodentate heterocyclic amine ligands in axial sites have been reported (*45,46*). For example, the nickel(II) product, $[Ni(dbm)_2(2\text{-Mepy})_2]$ (2-Mepy = 2-methylpyridine), exists as the *trans* isomer in a number of structurally distinct forms and shows diverse solvent inclusion behavior. For zinc(II), only one 2-Mepy unit coordinates to give $[Zn(dbm)_2(2\text{-Mepy})]$ (and this does not exhibit inclusion behavior). With cadmium(II), two polymorphic forms of composition $[Cd(dbm)_2(2\text{-Mepy})_2]$ were isolated. The first is a metastable *trans* form, while the second (more stable) form contains the *cis* isomer. No solvent inclusion compounds were isolated in this case.

Parallel syntheses to those just mentioned have also been performed using the linear difunctional base 4,4′-bipyridine (bipy) (*47*). With this bis-monodentate derivative, linear one-dimensional structures were generated; these products are of type $[Ni(dbm)_2(bipy)]_n$ (*48*) and $[Zn(dbm)_2(bipy)]_n$ (*47,49*). Each structure may be considered to be a chain of alternating square planar $[M(dbm)_2]$ fragments connected by linear bipy units.

In a further more recent study, reaction of 1,2-bis(3-pyridyl)butadiyne with precursor complexes of type $M(hfac)_2 \cdot nH_2O$ (where M = Cu, Mn, or Zn) has been shown to produce three isostructural 'zig-zag' coordination polymers of stoichiometry $[M(hfac)_2(1,2\text{-bis}(3\text{-pyridyl})butadiyne)]_n$. These exhibit structures related to those just discussed above (*50*). Reaction of the corresponding 'bent' spacer, 1,2-bis(2-pyridyl)butadiyne, with $Mn(hfac)_2 \cdot 3H_2O$ also produced a related polymeric structure composed of one-dimensional chains.

In part, the above results extend an earlier study (*42*) in which an X-ray structure determination of the 1:1 adduct between dabco and $Cu(hfac)_2$ showed it to have a linear polymeric structure in which nitrogen donors from different dabco ligands occupy both axial sites of each copper center.

When one axial site is 'blocked', as occurs in $VO(hfac)_2$, the reaction with difunctional pyrazine (pyz) yields an axially linked dimer of type $[(VO(hfac)_2)_2(pyz)]$ (*51*); a similar linked-dimeric structure, $[(VO(hfac)_2)_2(dioxane)]$, is formed in the presence of dioxane (*52*).

The directed assembly of six M(II) complexes (M = Cu, Co and Ni) into infinite hydrogen-bonded chains has been achieved by combining

β-diketonato ligands with bifunctional ligands such as **6** containing a metal-coordinating pyridyl moiety as well as a self-complementary hydrogen-bonding moiety (*53*). In each case, the chelating β-diketonato ligand occupies the four equatorial coordination sites, with the bifunctional ligand coordinating in the axial positions. The supramolecular chemistry, which links individual coordination complexes into infinite one dimensional chains, is given by a combination of N–H···N and N–H···O hydrogen bonds.

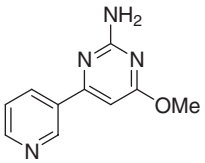

6

III. Supramolecular Systems Incorporating β-Diketone Motifs

A. β-Diketone Derivatives Substituted at Their 'Central' Carbon Atom

Numerous derivatives consisting of a single β-diketone group that contain a wide range of substituents on the 'central' carbon atom (the carbon between the keto groups) have been investigated for many years. When singly substituted, such derivatives maintain the potential to lose a proton and form a stable six-membered chelate ring on binding to a metal. Typical substituents include alkyl, aryl, halide, nitrile, azide, ether and thioether groups as well as other entities such as a 4-pyridyl ring. These groups may act as functional groups for further (organic) derivatization or serve to provide an additional donor site (or sites) for metal interaction. In particular, substitution at the γ-carbon in pentane-2,4-dione (acacH) has been employed to produce extended ligand systems for use in a number of studies, some of which fall into the supramolecular realm.

A number of reports of 3-(4-pyridyl)pentane-2,4-dione (pyacH) yielding metal-containing products have appeared (*54–60*).

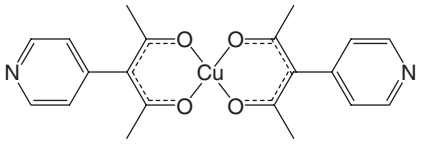

7

The choice of metal ion employed to prepare complexes of pyac can be used to direct the spatial arrangement of the terminal pyridyl groups in the 'β-diketonato' bound ligands. For example, on complexation with square planar copper(II), 'linear' $[Cu(pyac)_2]$ (**7**) is obtained (*56*). In contrast, generation of a *tris*-ligand complex of an octahedral metal ion, as occurs in $[Al(pyac)_3]$, yields a diverging arrangement of the three pyridyl groups (*54,55*). In this context, the aluminum complex has been demonstrated to act as a neutral guest for a large cyclic *tris*-porphyrin host to yield the impressive supramolecular host–guest assembly **8** (*54,55*).

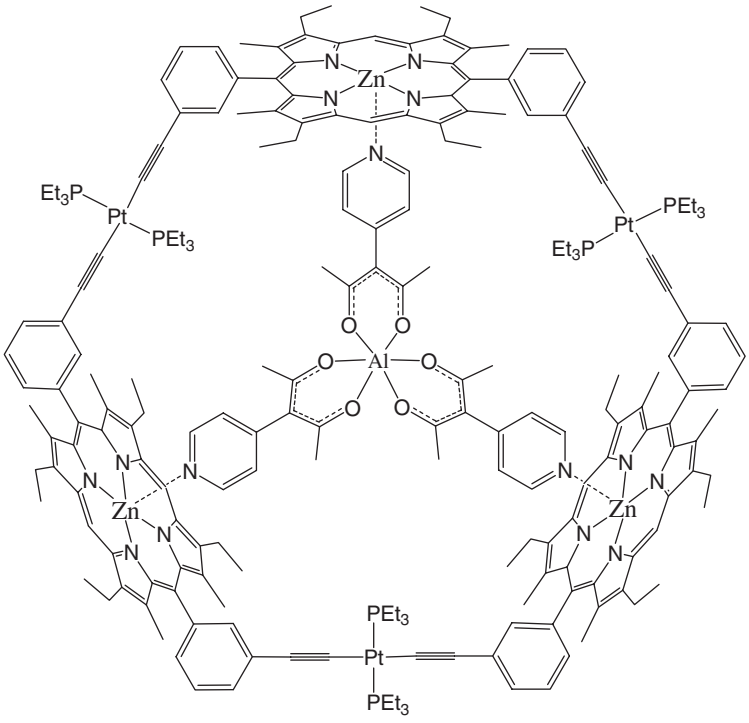

8

It is noted that in the solid state, the complexes $[M(pyac)_3]$ ($M = Al^{3+}$, Fe^{3+}) are not symmetric but have their pyridyl nitrogen lone pairs mutually oriented at angles of about 90° and 135° (*60*). The assembly of heterobimetallic arrays occurs when either the aluminum(III) or the iron(III) complexes react further with a second metal ion. Thus, these linker units form two dimensional heterobimetallic network structures incorporating square/octagonal coordination nets when reacted with cobalt(II) and cadmium(II) ions.

Although $Cu(pyac)_2$ incorporates both Lewis acid and Lewis base sites, only a very weak interaction occurs between the terminal pyridyl

lone pairs and adjacent copper centers in the solid state (*56*). Even so, this species crystallizes from anhydrous solvents in a square-grid topology; while in the presence of water, a doubly interpenetrating three-dimensional network forms instead. In each case, the copper(II) centers (*57*) exist in elongated octahedral N_2O_4 environments.

$Cu(pyac)_2$ also gives rise to mixed metal-organic frameworks upon reaction with cadmium(II) salts (*59*). Both the one-dimensional ladder formed with $CdCl_2$ and the two-dimensional grid afforded from $Cd(NO_3)_2$ are porous in nature, with the former incorporating two-dimensional channels and the latter one-dimensional channels. The copper sites in each of these structures are exposed to the pores and are coordinated by solvent molecules.

On reaction with beryllium(II), 3-(4-pyridyl)pentane-2,4-dionate once again forms a linear unit of type $Be(pyac)_2$; however, in this case, the β-diketonato groups are bound in a tetrahedral geometry around the beryllium(II) center (*58*). This arrangement has been exploited for the formation of heterobimetallic structures incorporating Co(II)/Be, Cu(II)/Be as well as mixed-valence (Cu(I)Cu(II)/Be) coordination systems. In the solid state, a discrete molecular arrangement is adopted in the case of $[Co\{BeL_2\}_2Cl_2]$ (L = pyac), a one-dimensional polymeric arrangement for $Cu_2X_3\{BeL_2\}_2$ (X = Cl, Br) and two-dimensional polymeric arrays in the case of $Co\{BeL_2\}(CH_3OH)_2SO_4$ and $Cu_2Br_2\{BeL_2\}_2$.

There have been a number of reports of systems incorporating ligands in which two β-diketonato fragments are linked through their 'central' carbon atoms. The simplest derivative of this type is tetraacetylethane, **9** ($taeH_2$), which in its doubly deprotonated form thus represents a further example of a linear ditopic linker unit (*61,62*). Owing to steric interaction between pairs of methyl groups, this molecule is twisted; the dihedral angle between the respective β-diketone fragments being quite large.

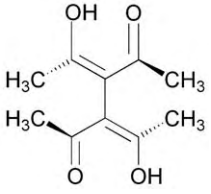

9

The structures of copper(II) and cobalt(II) complexes containing deprotonated tetraacetylethane (tae^{2-}) as a bridging ligand have been investigated (*63*). The reaction of copper(II) trifluoroacetate with $taeH_2$ and 2,2′-dipyridylamine (dpa) has been shown to yield the dinuclear complex, $Cu_2(dpa)_2(tae)(O_2CCF_3)_2$, which has an extended

hydrogen-bonded chain structure in the solid state. The uncoordinated axial positions on the copper ions have been exploited to provide extended geometries. Thus the reaction of 4,4′-dipyridyl (bipy) with this complex results in the formation of a polymeric compound of type $\{[Cu_2(dpa)_2(tae)(bipy)](O_2CCF_3)_2\}_n$, where the dinuclear unit is cross-linked via 4,4′-bipyridine spacer units. A similar reaction using cobalt(II) acetate yielded a helical dinuclear species of type $[Co_2(dpa)_4(tae)](O_2CCH_3)_2(H_2O)_2$. In this case, two $Co^{II}(dpa)_2$ units are linked via a tae bridge to give the helical arrangement, with the dpa units serving as 'terminating ligands'.

In an extension of the above study, under other conditions, it was demonstrated that the combination of cobalt(II) acetate, dpa and tetraacetylethane in CH_2Cl_2/CH_3OH results in the formation of a charge-neutral metallo-supramolecular square, incorporating four $[Co^{II}(dpa)]$ 'corners' and four tae 'sides' (*64*). The X-ray structure of the product is given in (Fig. 2). The combination of chelating β-diketonato ligands and octahedrally coordinated cobalt(II) ions results in each molecule being homochiral – indeed this is a rare example of a structurally characterized chiral molecular square. The Co–Co distance along each 'side' is 8.0 Å, with the enclosed cavity having dimensions of 4.2×4.2 Å. This and similar structures with larger cavity dimensions show promise for use as chiral reagents for molecular recognition and/or separation; for example, for use in chiral separation of larger drug molecules.

Dinuclear mixed complexes of ruthenium(III) incorporating tae have also been reported (*65*). These include $[\{Ru(acac)_2\}_2(tae)]$, $[\{Ru(phypa)_2\}_2(tae)]$ and $[(acac)_2Ru(tae)Ru(phpa)_2]$ (where phpa is the 2,2,6,6-tetramethyl-3,5-heptanedionate anion). The X-ray structure of $[\{Ru(acac)_2\}_2(tae)]$ shows a tae-linked structure of type **10** in which the bound acac groups of the tae-bridging unit are almost perpendicular to each other. A related dicationic, tae-linked species incorporating 2,2′-bipyridine (2,2′-bipy) of type $[\{Ru(2,2'\text{-bipy})_2\}_2(tae)]^{2+}$ was also characterized as part of this study.

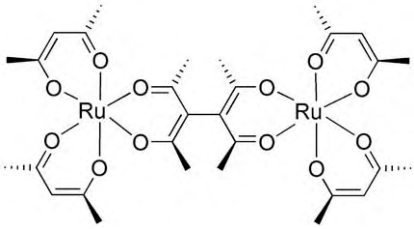

10

Alkyl-γ-linked ligands (*66,67*) and their corresponding copper(II) complexes of type **11** (*67*) have been investigated. It was postulated in this study that the solid complexes of the shorter-chain ($n = 6$, 8) branched ligands in their deprotonated form have the bis(β-diketonato)copper(II) entities linked to form polymeric species,

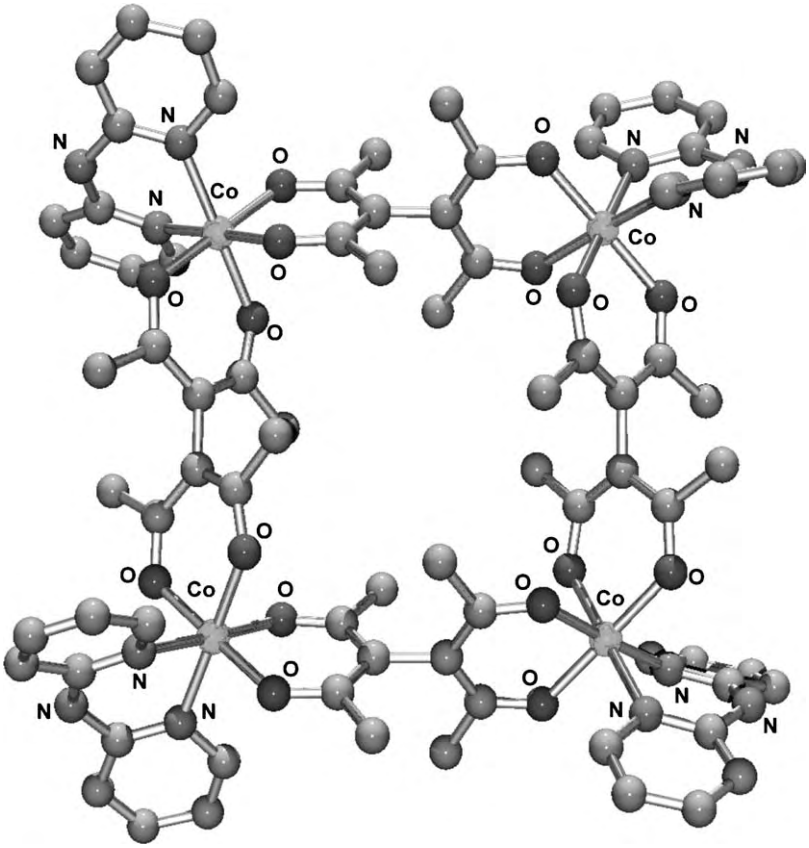

FIG. 2. The molecular square incorporating [Co^{II}(2,2′-dipyridylamine)] corners and tae sides (*64*).

whereas the longer-chain branched ligands either yield a monomeric species (for $n = 12$) or a monomer–polymer mixture (for $n = 10$).

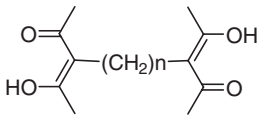

11

A report of the formation of triangular niobium(V) complexes of two related bis-β-diketonato ligands has appeared (*68*). The proposed structures, represented by **12**, contain three bis-β-diketonato ligands coordinated to three niobium centers, with the remaining two coordination sites on each center occupied by oxide and chloride ligands such that charge neutrality results. These trinuclear species were characterized by NMR, mass spectrometry and their electronic spectra.

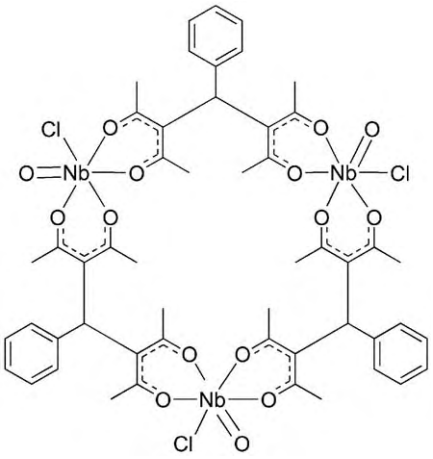

12

The interaction of linked diazo β-diketone ligand systems with selected lanthanide(III) ions (*69*) and ruthenium(II) (*70*) has been investigated. In the latter case the synthesis, spectroscopic, electrochemical (and antibacterial) studies of new dinuclear ruthenium(II) complexes, each containing an aryldiazo-linked bis(pentane-2,4-dionato) bridging ligand and 1,10-phenanthroline as co-ligands, were reported (*70*).

Thiobis(β-diketone) ligands, in which two β-diketone fragments are linked through their central carbon atom by a single sulfur atom or by a disulfide bridge, are known and in some cases their interaction with metal ions has been investigated (*71–75*). In a recent study it was demonstrated that such singly S-linked ligands readily give rise to a convenient synthesis of binuclear ruthenium(II) complexes of type $[RuCl(CO)(PPh_3)(B)_2L]$, where B is a monodentate ligand (such as PPh_3 or one of a range of amines) and L is the deprotonated thio-bis-β-diketone derivative; these products form on reaction of the corresponding precursor of type $[RuHCl(CO)(PPh_3)_2(B)]$ with the thio-bis-β-diketone ligand in benzene (*76*). The nature of the product complexes was assigned on the basis of their elemental analysis, IR, electronic, ^1H and ^{31}P NMR spectral data. In a subsequent study, further binuclear ruthenium(III) complexes of the above thio-bis-β-diketones were also obtained (*77*).

The disulfide-linked ligand **13** $(Hacac)_2S_2$ yields oxovanadium(IV) complexes that were postulated to be cyclic trinuclear species of type $[VO((acac_2)S_2)DMSO]_3$ and $[VO((acac_2)S_2)py]_3$ (where py = pyridine) on the basis of physical measurements (*78*).

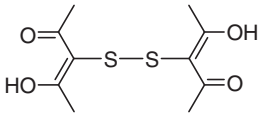

13

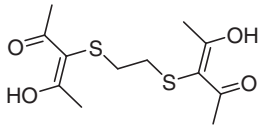

14

In a recent study, our group reported the formation of discrete cobalt(II) and nickel(II) complexes of type $[ML(H_2O)_2] \cdot H_2O$ (where LH_2 is the bis(2,4-pentanedione) derivative **14** incorporating a -SCH_2CH_2S- bridge between the γ-carbons of the β-diketone units). These products were obtained when the corresponding metal acetates were reacted with **14** in a methanol/acetone mixture (*79*). A molecular model confirmed that it is not possible for both β-diketone groups of **14** to coordinate to a single metal center and hence it was anticipated that on reaction with a suitable metal ion, either an extended metallo array or a discrete complex exhibiting an unusual coordination motif might result. Our study was undertaken to probe these possibilities.

The crystal structures of both the cobalt and nickel complexes mentioned above showed them to be isostructural. The structure of the cobalt(II) complex is given in Fig. 3. The bis-β-diketone **14** coordinates in its doubly deprotonated form via the two thioether sulfur atoms, but employs only two of its four oxygen atoms for metal binding. The metal center is pseudo-octahedral in each complex, with the sulfur donors arranged mutually *cis*, while the two bound β-diketone oxygen atoms

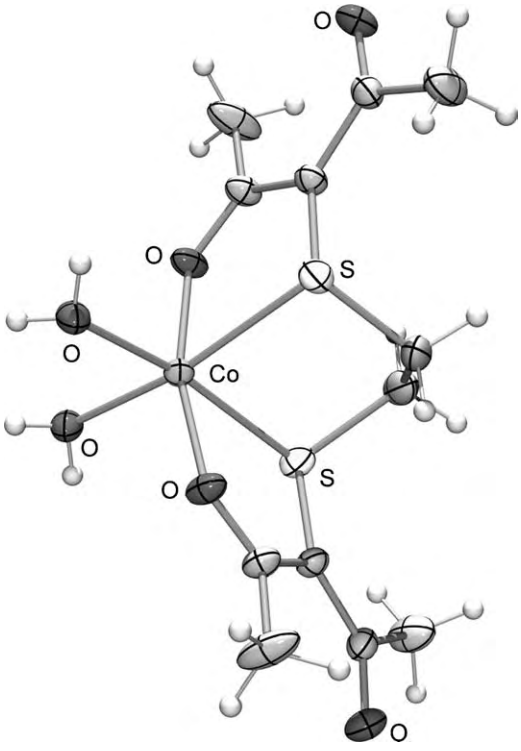

FIG. 3. The X-ray structure of the cobalt(II) complex of the bis(2,4-pentanedionato) derivative with a –SCH_2CH_2S-bridge between the γ-carbons of each β-diketone fragment (*79*).

are *trans*; the remaining two coordination sites are filled by water molecules. The latter complexes represent the first examples in which a γ-substituted thioether-containing β-diketone ligand coordinates via a sulfur and an oxygen donor in preference to the classical coordination mode involving both β-diketonate oxygens.

There is a report of an analog of **14** containing a disulfide bridge directly linking the two acetylacetone groups reacting with [Ru(acac)$_2$(MeCN)$_2$] to yield disulfide cleavage. The product is a mononuclear complex in which the acetonitrile groups are replaced by a cleaved ligand fragment acting as a bidentate ligand and coordinating via its thiolo sulfur donor and only one of the two available oxygen donors (*80*). A further complex in which a thiolo group attached to the 'central' carbon of a β-diketone unit combines with only one β-diketone oxygen to form a chelate ring has also been reported (*81*). In both of these latter systems, the thiolo moiety will act as a strong coordinating group toward the metal ions involved. This contrasts with the situation for **14** where the thioether groups are moderately weak donors toward both (high-spin) cobalt(II) and nickel(II).

Binuclear complexes of rhodium and iridium containing a bis(2,4-pentanedionato) ligand flexibly bridged through the respective γ-carbons by a 1,4-xylyl linker have also been synthesized (*82*). Thus, the reaction of [M(μ-Cl)(1,5-COD)]$_2$ (M = Rh, Ir; COD = cyclooctadiene) with 1,4-xylylbis(3-(2,4-pentanedione)), xylyl(acacH)$_2$ and two equivalents of KOH results in the formation of binuclear compounds of type [M(COD))$_2$(xylyl(acac)$_2$)]. The cyclooctadiene ligand in these complexes is readily displaced from the metal centers by either CO or PPh$_3$, leading to the formation of [(M(CO)$_2$)$_2$(xylyl(acac)$_2$)] and [(M(PPh$_3$)$_2$)(xylyl(acac)$_2$)], respectively.

A pioneering example of a bis-bidentate β-diketone derivative giving rise to a discrete molecular structure was reported by Maverick *et al*. in 1984 (*83*). The ligand system employed contained two β-diketone fragments separated by a *m*-xylene spacer; it acts as a bis(bidentate) ligand such that two molecules react with two copper(II) ions to form the non-solvated co-facial metallocyclic structure **15**. The separation between the two copper centers in this product is 4.908 Å. Such behavior results in a cavity that is too small to encapsulate anything larger than small solvent molecules. Addition of excess pyridine to the reaction solution used to prepare this species led to *exo* coordination of a molecule of this base to each of the copper(II) ions, resulting in each copper center becoming five coordinate (which differs from the situation in the related simpler species, [Cu(acac)$_2$(pyridine)$_2$], which contains six-coordinate copper(II)) (*38,84*).

Even acetonitrile appears too small to fit in the cavity of **15** (*85*). The X-ray structure of the solvated form of **15**, $Cu_2L_2(MeCN)_2 \cdot 1.5MeCN \cdot H_2O$ (LH_2 = 3,3′-[1,3-phenylene-bis(methylene)]bis(2,4-pentanedione) shows the presence of centrosymmetric Cu_2L_2 units (the Cu···Cu separation is 4.830 Å) with *exo* coordinated acetonitrile ligands.

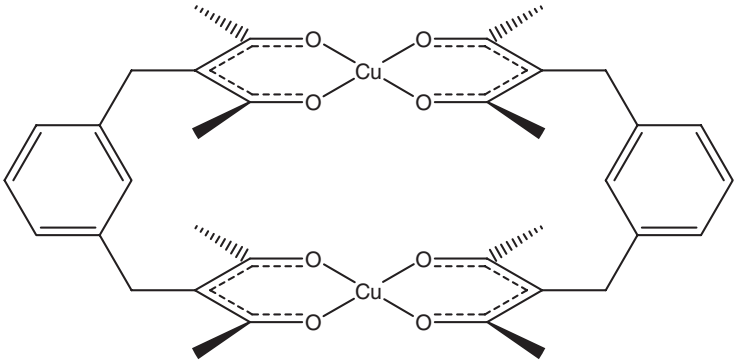

15

An extension of this work by the same group (*86*) involved a comparison of the complexation behavior of ligand **16** with the deprotonated forms of the five related derivatives **17**–**21**. Of the latter, only the less bulky ligand **17** (in its deprotonated form) gave a similar complex to that of **16** in satisfactory yield. This outcome was attributed to increased unfavorable steric interaction on coordination of **18**–**21** leading to the inhibition of the formation of square planar copper centers of the type observed in **15**.

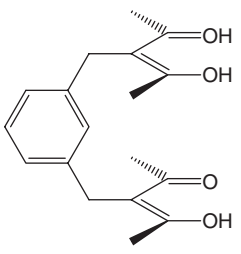

16

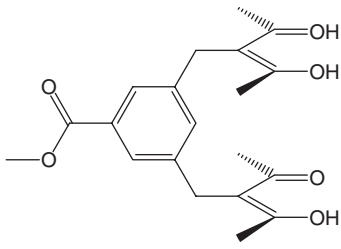

17

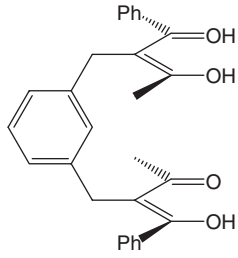

18

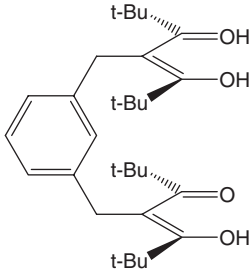

19

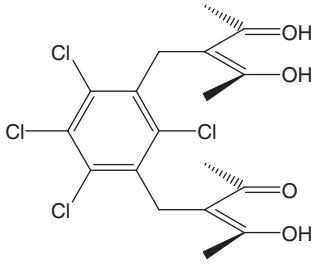

20

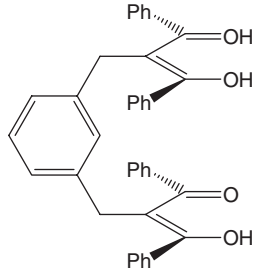

21

In a subsequent study, also by the same group, the related ligand in which the *m*-xylene spacer was replaced with a larger 2,7-napthylenediyl-bis(methylene) spacer was synthesized and its interaction with copper(II) investigated (*87*). The X-ray structure of the resulting copper(II) complex **22** confirmed the presence of a metallocyclic structure related to **15** but with a significantly larger cavity; the copper–copper distance now being 7.349 Å. A comparison of the 1:1 (base:complex) binding affinities of the nitrogen bases **23**–**26**, for which binding of the difunctional bases **24** and **26** is believed to occur within the cavity, indicated that both these bind the strongest to **22** – with the more basic difunctional base dabco (**26**) binding particularly strongly – presumably reflecting its strong attachment to *both* copper centers (Table I). In accord with this, the X-ray structure of the corresponding solid complex confirms that such an arrangement indeed also occurs in the solid state (Fig. 4). Subsequently, a further X-ray structure determination demonstrated that 2,5-dimethylpyrazine also binds in a similar fashion within the cavity of **22** (*88*). The number of *K* values for 1:2 Lewis base adduct formation by **22** was also extended in this latter report with binding constants for substituted pyridines being generally smaller than their corresponding unsubstituted derivatives.

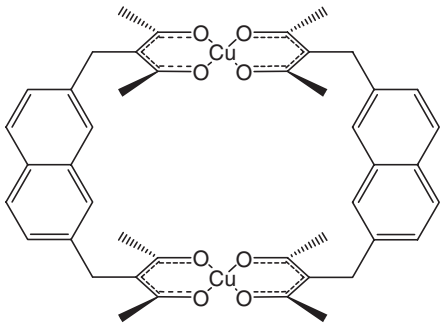

22

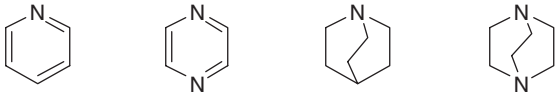

23 **24** **25** **26**

A more recent structural study has also confirmed the occurrence of internal (*endo*) coordination of 2-methylpyrazine to **22** (*85*). The synthesis of vanadium(II) and vanadium(III) complexes incorporating the deprotonated *m*-xylene-linked (parent) ligand acting as a bridging bisbidentate have also been synthesized (*89*). These products differ from the previously discussed dinuclear copper(II) complexes in that the vanadium(II) centers exhibit octahedral geometries. A vanadium(II)

TABLE I

BINDING CONSTANTS[a] FOR THE FORMATION OF 1:1 (M:L) COMPLEXES OF **22** WITH A SELECTION OF LEWIS BASES

Base	K/M^{-1}
Pyridine (**23**)	0.5 ± 0.2
Pyrazine (**24**)	5 ± 1
Quinuclidine (**25**)	7 ± 2
Dabco (**26**)	220 ± 20

[a]Determined spectrophotometrically in $CHCl_3$ at 20°C.

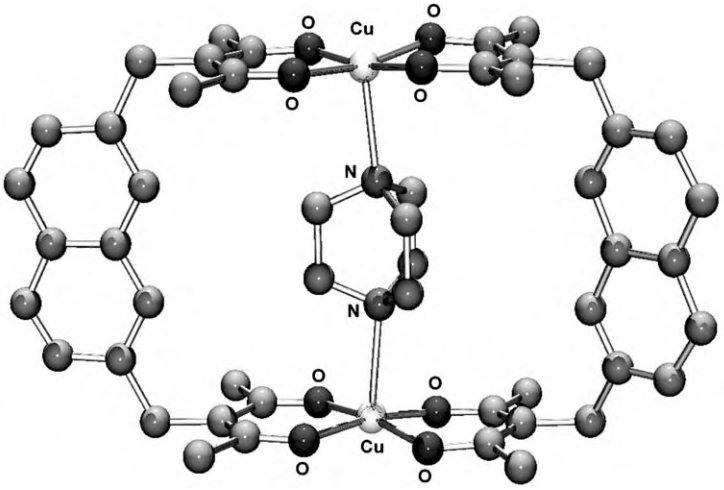

FIG. 4. The X-ray structure showing binding of dabco in the cavity of **22**.

product, whose X-ray structure is shown in (Fig. 5), incorporates two β-diketonate fragments bound to each vanadium complex in a *cis* manner, with the remaining two coordination positions in each coordination sphere being filled by a bidentate *N*,*N*,*N*′,*N*′-tetramethylethylenediamine ligand (*89*). Two vanadium(III) derivatives in which the fifth and sixth metal coordination positions are filled with a halide and a tetrahydrofuran ligand have also been characterized.

In a more recent development, Davidson et al. (*90*) reported the synthesis of an analogous copper(II) species incorporating a '*meta*' terphenyl spacer. As illustrated by **27**, the resulting larger cavity was able to encapsulate and bind a molecule of 4,4′-bipyridine; the X-ray structure of this product has been obtained (the Cu–Cu distance in the adduct is 11.8 Å). Interestingly, this large metallo-ring in the absence of its Lewis base shows no evidence of catenation. The hexagonal cavity delineated by the two terphenyl groups and the

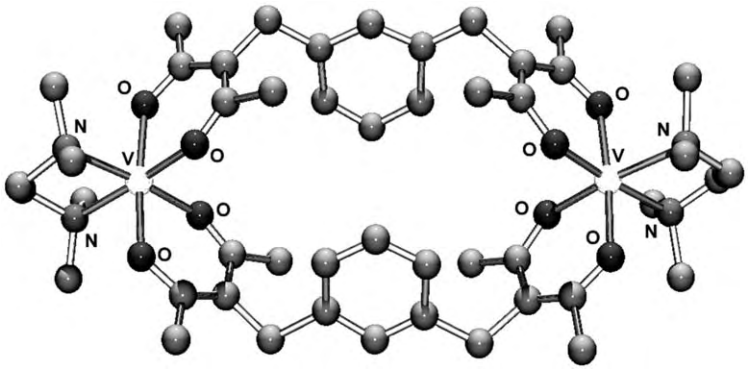

FIG. 5. The X-ray structure of the bridged vanadium(II) complex incorporating two m-xylene-linked, bis(2,4-pentanedionato) ligands and two bidentate *N*,*N*,*N*′,*N*′-tetramethylethylenediamine 'capping' ligands.

bis(diketonato)copper(II) moieties encompasses a volume of approximately 400 Å^3. Ten chloroform solvent molecules were found to occupy the cavity.

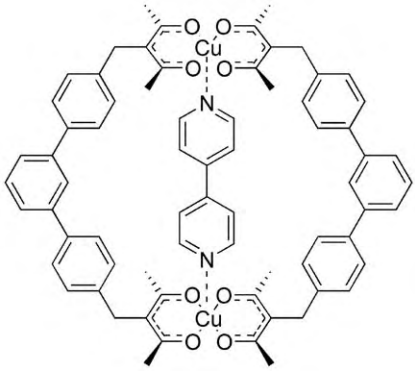

27

The use of two γ-substituted Cu(acac)$_2$ entities as linkers between the upper rims of two calix[4]arene molecules represents a novel method for obtaining biscalix[4]arenes (*91*). In one instance, the cavity generated between the two Cu(II)–chelate complexes has been found to be selective toward individual diamine substrates in an analogous manner to that discussed above for systems such as **15**, **22** and **27**.

B. 'END-LINKED' β-DIKETONE DERIVATIVES

It is well established that metal-ion binding by a macrocyclic host can give rise to both enhanced kinetic and thermodynamic

stabilities of the resulting metal complex over that obtained with the corresponding open-chain ligand derivative (*92*). The β-diketone motif has been incorporated into several macrocyclic systems. Macrocycles **28** and **29** were prepared from condensation of the appropriate precursors containing terminal acid chloride and acetylene groups in the presence of a Lewis acid catalyst (*93*). Ligand **28** was designed to act as a selective host for the uranyl (UO_2^{2+}) ion. It comprises three β-diketone fragments symmetrically spaced around a 24-membered ring. This macrocycle extracts uranyl ion from a dilute (10 ppm) aqueous phase into a benzene phase almost quantitatively. Related rings incorporating two, three, four and five malonates and various length alkyl spaces have also been synthesized and demonstrated to react with C_{60} regioselectively to form adducts (*94*).

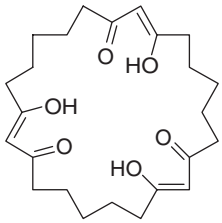

28

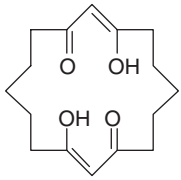

29

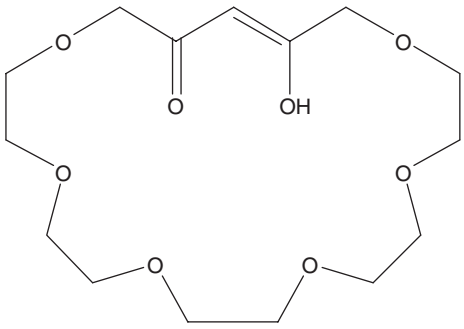

30

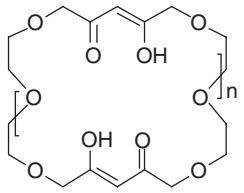

31, n = 1

32, n = 2

The incorporation of β-diketone motifs into crown ether systems has also been achieved. A number of both cyclic and related acyclic systems combining polyether linkages and β-diketone units were prepared by Cram *et al.* (*95,96*). Cyclic ligands **30–34** were prepared and their complexation toward a range of metal ions was compared with that for the open chain species **35–37**.

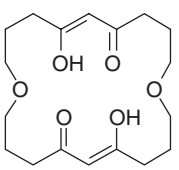

33

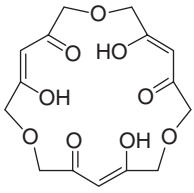

34

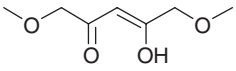

35

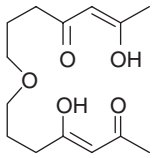

36

The stabilities of the cyclic systems were typically 2–5 orders of magnitude stronger than for the acyclic counterparts (*96*).

Cyclic systems have also been generated by using copper(II) or zinc(II) binding by two β-diketonato units to close each end of a connected polyether chain. Complexes **38–40** have been prepared in this manner and an investigation of the selectivity of the corresponding 'crown' polyether cavities toward alkali metals has been undertaken. A comparison of the copper(II) complexes **39** and **40** revealed that the larger cavity in **40** showed stronger binding for K^+ and Rb^+ than did **39**. In the absence of the divalent metal ion, these ligand systems showed minimal affinity for alkali metals. This study corresponded to one of the earliest reports of positive cooperativity occurring between the binding of two metal cations.

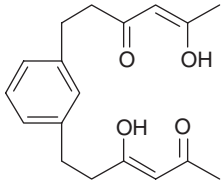

37

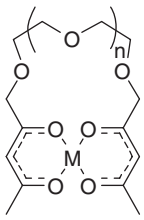

38 M = Zn, n = 2
39 M = Cu, n = 1
40 M = Cu, n = 2

Copper(II) complexes of alkyl-linked, bis-β-diketone derivatives related to the above have also been investigated (*67*). The series of ligands given by **41** with $n = 6$, 8, 10 or 12 (in their doubly deprotonated forms) each yield square planar copper derivatives with magnetically dilute [CuO_4] centers. In the solid state, these compounds were assigned linked-ligand polymeric structures of type $[CuL]_n$.

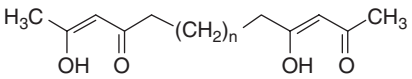

41

It is noted that in an extensive series of studies, Saalfrank and co-workers have employed a number of dialkyl malonate derivatives, closely related to β-diketone systems, for the synthesis of a variety of discrete tetrahedral ('adamantanoid') and trigonal prismatic (and related) coordination cages incorporating a variety of metal ion types (*97–104*). Many of these cages have been demonstrated to exhibit interesting guest inclusion behavior.

An example illustrating the encapsulation properties of these systems is given by the mixed valence Fe(II)/Fe(III) assembly illustrated in Fig. 6 (*100*). The superstructure is a regular tetrahedron with corners defined by one Fe(II) and three Fe(III) ions. The six edges of the tetrahedron are each formed by the bis(bidentate), doubly negatively charged ligands. Each of the four iron atoms is octahedrally coordinated by six oxygen atoms. This system has an ammonium ion trapped in the central cavity. In this case, the inclusion of the ammonium cation led to an overall neutral charge, which undoubtedly adds to the stability of the system. The complex has chiral 'corners' and exists as racemic isomers. Characterization of this product involved X-ray crystallography, Mössbauer, ESR and electrochemical studies.

The Saalfrank group has also investigated the template-mediated self-assembly of three-membered copper coronate **42** and sandwich

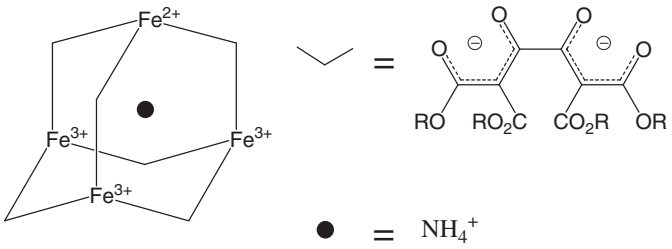

FIG. 6. A mixed valence Fe(II)/Fe(III) assembly with an encapsulated NH_4^+ ion.

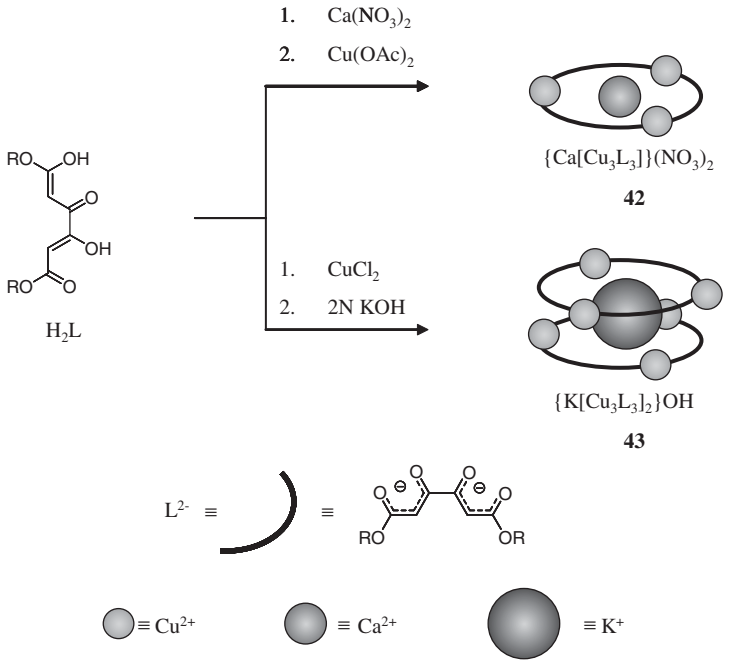

FIG. 7. Synthesis of template-mediated self-assembly of three-membered copper coronate **42** and sandwich complex **43**.

complex **43** starting from dialkyl ketipinates H_2L (Fig. 7) (*105–109*). A characteristic of these complexes is that encapsulated alkali or alkaline-earth metal ions are coordinated to the inner carbonyl oxygen donors.

The above studies were extended to the formation of 'hybrid metallocoronates' containing the glycolate-bridged, bis-1,3-diketonate ligand **44** as well as both copper(II) and alkali metals (*110,111*). These products are of type $\{M^I[Cu_2L_2]\}OAc \cdot 2MeOH$ (M = K, Rb, Cs; L = **44**). In the potassium complex each copper(II) center is square-pyramidal being bound to four diketonate oxygen donors and a methanol molecule. The potassium ion is eight-coordinate and is bound to four carbonyl and four ether oxygen atoms to yield a helical metallocrown-eight system. As part of these studies, a related (catecholate-bridged) bis-1,3-diketonate ligand ($CH_3COCH_2COCH_2O$-*o*-C_6H_4-OCH_2COCH_2-$COCH_3$; H_2L^1) was shown to react with nickel acetate and cesium ions to form a product of type $[\{Cs[Ni_2(L^1)_3]\}Cs \cdot 3MeOH]_n$. This [2]-metallocryptate species contains octahedral nickel(II); the latter is bound to diketonate oxygens and incorporates a 12-coordinate cesium ion in the void. The other (external) cesium atom is coordinated to two of the three methanol molecules as well as to two sets of three peripheral carbonyl oxygen donors to yield a one-dimensional, oxo-bridged metal string.

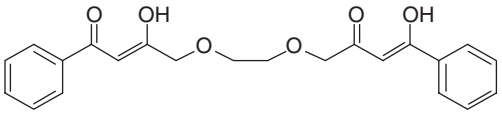

44

More recently, the one-pot synthesis of 'tetrahemispheraplexes' with ammonium, alkylammonium or alkali metal ions as *exo* guests using self-assembly or guest exchange processes has been described (*112*). The tetraammonium and tetraalkylammonium complexes $\{(NH_4)_4[Mg_4L_6]\}$ (where $L = (RO_2C)_2CHC(O)C(O)CH(CO_2R)$, R = Me or Et), $\{(MeNH_3)_4[Mg_4L_6]\}$, $\{(EtNH_3)_4[Mg_4L_6]\}$ and a mixed sodium/tris(ethylammonium) complex, $\{Na(EtNH_3)_3[Mg_4L_6]\}$, were all obtained in one-pot syntheses. Other species, such as the tetrakis(alkylammonium) derivative $\{(RNH_3)_4[Mg_4L_6]\}$ (R = Bu, hexyl, octyl) and the mixed diammonium-bis(*p*-methoxybenzylammonium) derivative, $\{(NH_4)_2(R'NH_3)_2[Mg_4L_6]\}$ ($R' = p\text{-}MeOC_6H_4CH_2$), were prepared by exchange of the ammonium ions in the above parent tetraammonium complex by alkylammonium ions. Similarly, exchange of the four ammonium ions by alkali metal cations yielded $\{M_4[Mg_4L_6]\}$ (M = K, Cs).

We have recently investigated the synthesis of a range of novel neutral nanometer-scale metallo-architectures that include discrete tetranuclear 'dimer of dimers', dinuclear helicates, supramolecular tetranuclear tetrahedral structures and related extended systems that fall in the category of framework materials (*113,114*). These diverse metallo-systems are based on 1,3- and 1,4-aryl-linked bis-β-diketonate ligands of types **45** and **46**.

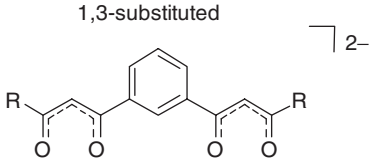

45

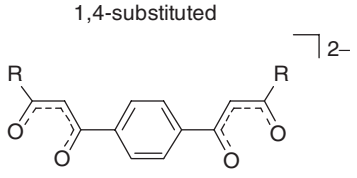

46

An attraction of these ligands is that their structures are readily varied and, for example, in our studies the terminal R groups were changed through Me, Et, Pr, *t*-Bu and Ph (*113,114*). As for simple β-diketone ligands, the structural versatility of the present systems thus result in both ligand types being able to be readily 'tuned' for particular synthetic and electronic outcomes.

The ^1H NMR spectra of the free ligands contain singlets at *c*. (δ)16.2, indicative of enolic protons, confirming that the (bis) enol tautomer

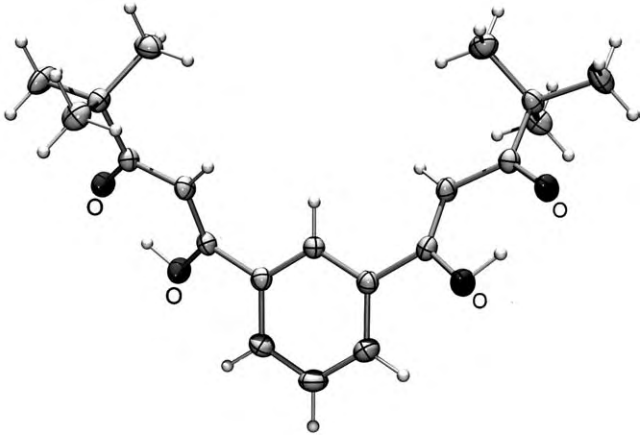

FIG. 8. X-ray structure of the protonated form of **45** (R = *t*-Bu).

is present in solution. An X-ray structure of the 1,3-aryl-substituted derivative incorporating *tert*-butyl terminal substituents confirms that the same tautomer persists in the solid and that the relative orientation of the bis-β-diketone fragments is such that the coordination vectors lie at ~120° to each other (Fig. 8).

Based on our studies so far (*113,114*) as well as on previous studies by others (*115–121*), it is clear that both the above ligand types are molecular components of uncommon promise for building metallo-supramolecular structures. Reflecting the available relative orientations of the β-diketonate groups in each ligand type, a range of both dinuclear (rectangular) and trinuclear (triangular) 'platform-like' products were isolated and characterized. Representative structures are given by **47** (*114*) (Fig. 9) and **48** (*113*) (Fig. 10). Thus an aim of the synthetic program, in the context of metallo-species such as **47** and **48**, was the possible exploitation of the coordinately unsaturated copper sites present in these planar dinuclear and trinuclear platform precursors. Such metal sites appeared ideal to serve as linking points for extending the platform structures from two to three dimensions through interaction with difunctional amine bases.

The ligand (**45**; R = Me, Et, Pr, *t*-Bu,) on reaction with copper(II) in the presence of base yielded dimeric complexes of stoichiometry $[Cu_2L_2](solvent)_n$ (where L is **45** and solvent is water or tetrahydrofuran) (*114*). It is noted that a complex of **45** with R = Me had been reported previously (*116*).

As mentioned above, the dinuclear complex with R = *t*-Bu crystallizes with each copper center bound to a tetrahydrofuran (thf) molecule such that the overall coordination geometry of each approaches square-pyramidal (Fig. 9). The planar, dinuclear copper complex with R = *t*-Bu has also been demonstrated to form 1:2 adducts with

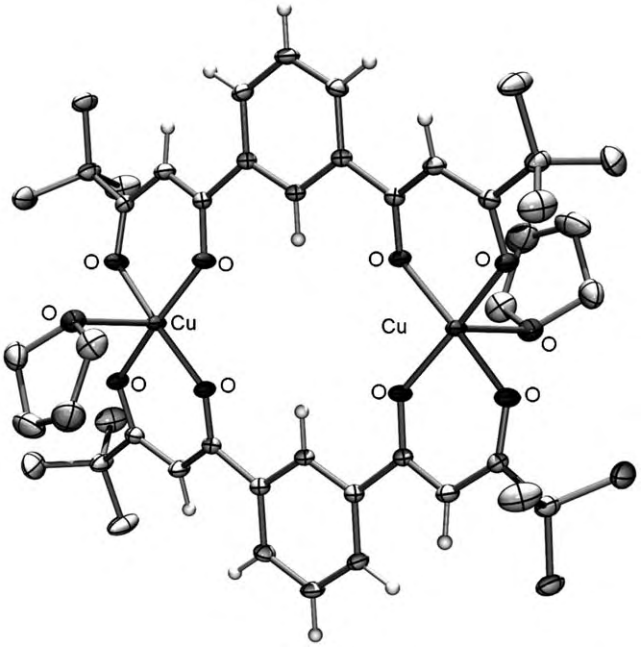

FIG. 9. X-ray structure of the dinuclear copper(II) complex **47** derived from **45** (R = *t*-Bu); a thf solvent molecule is weakly bound in an axial position to each copper center (*114*).

pyridine and 4-(dimethylamino)pyridine, with each adduct again incorporating five-coordinate metal centers. The structure of the bis-pyridine adduct is given in Fig. 11 (*114*).

The isolation of 2:2 complexes of a selection of the 1,3-aryl bridged ligands with cobalt(II), nickel(II) and zinc(II) in the prescence of pyridine have been carried out (*122*). In each of these species, two axial pyridine ligands are also bound to each metal center to yield octahedral coordination geometries.

Based on these studies, the prospect of linking copper centers in the dinuclear complex **47** (with R = *t*-Bu) using the difunctional heterocyclic bases, 4,4′-bipyridine, 4,4′-*trans*-azopyridine and pyrazine as co-ligands was probed (*114*). However, 4,4′-bipyridine was observed to coordinate through only one of its heterocyclic nitrogen atoms in the solid state to form a 1:2 ($[Cu_2L_2]$: 4,4′-bipyridine) adduct (Fig. 12). This is thus an analog of the structures obtained when the monofunctional monodentate nitrogen bases were employed. In contrast, the use of the related difunctional base, 4,4′-*trans*-azopyridine, was shown by X-ray diffraction to result in a structure in which 4,4′-*trans*-azopyridine ligands coordinate in a bridging fashion via both heterocyclic nitrogen atoms on alternate sides of each planar $[Cu_2L_2]$ unit to produce an infinite one-dimensional metallo-chain (Fig. 13).

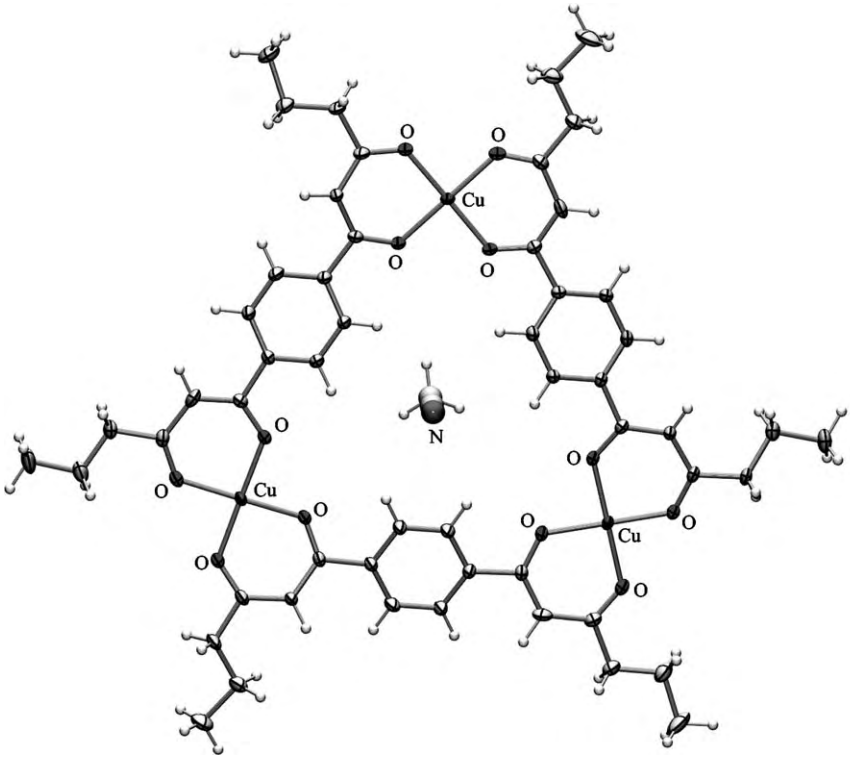

FIG. 10. X-ray structure of the trinuclear copper(II) complex **48** derived from **46** (R = Pr); an acetonitrile solvent molecule occupies the triangular void (*113*).

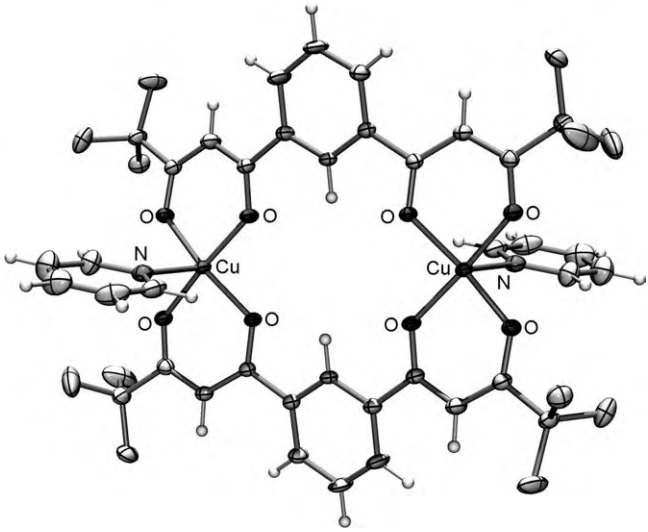

FIG. 11. X-ray structure of the di-pyridine adduct of **47** (*114*).

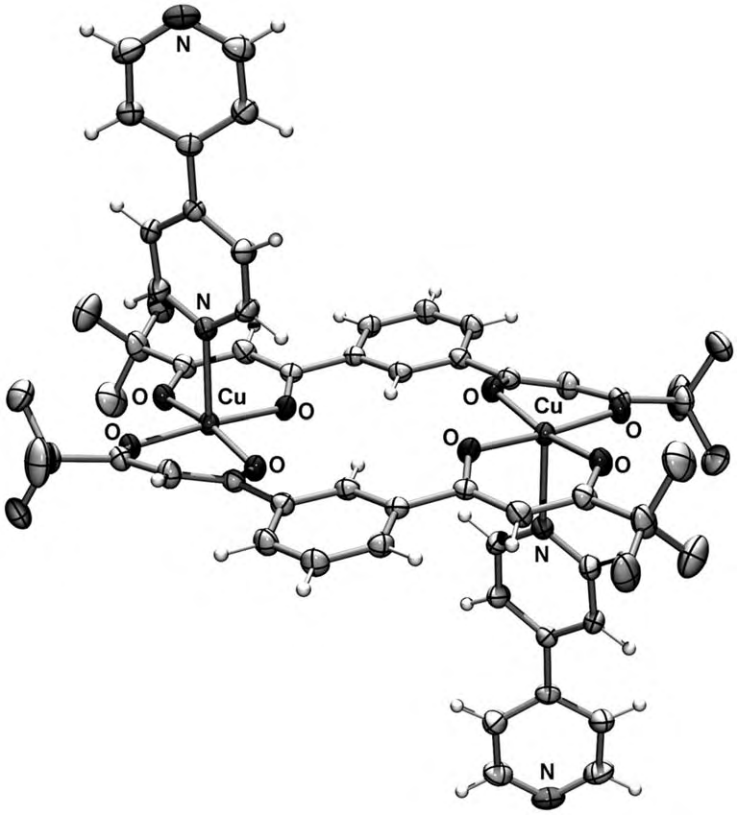

FIG. 12. X-ray structure of the discrete 1:2 adduct of **47** with 4,4′-bipyridine (*114*).

However, with the shorter difunctional base, pyrazine, a neutral, discrete assembly of type $[Cu_4L_4(pyrazine)_2]$ is formed. The X-ray structure (Fig. 14) of this product shows that two planar dinuclear complexes are linked by two pyrazine molecules in a sandwich arrangement such that the coordination environment of each copper ion is approximately square pyramidal; the overall tetranuclear structure thus adopts an arrangement corresponding to the 'dimer of dimers' mentioned previously.

The interaction of iron(III) with the 1,3-aryl bridged bis-β-diketones **45** with (R = Me and *t*-Bu) yielded neutral dinuclear species of type $[Fe_2L_3] \cdot n$(solvent) (*114*). These products gave UV–vis spectra that are similar to those of simple tris(β-diketonato)iron(III) complexes and the X-ray structure (Fig. 15) of $[Fe_2L_3] \cdot Et_2O$ (L is **45** (R = *t*-Bu)) showed that the two iron(III) centers are bridged by three ligands to produce a triple helical arrangement in which each iron(III) is surrounded by three β-diketonato fragments such that coordination saturation is

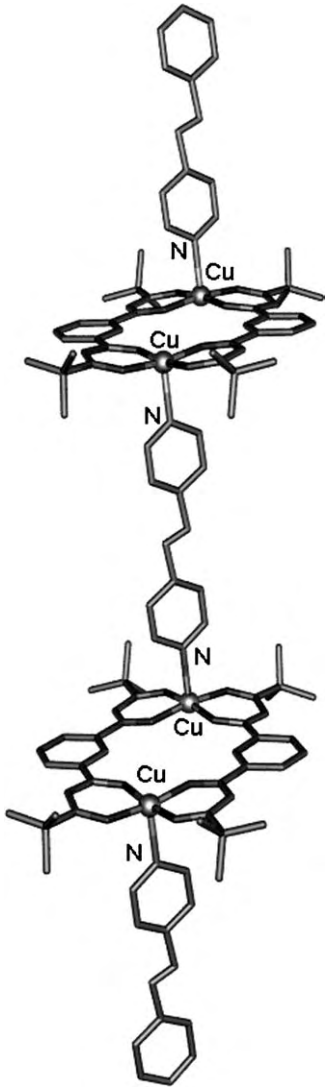

FIG. 13. X-ray structure of the stepped polymer formed from **47** and 4,4′-*trans*-azopyridine (*114*).

achieved. Each dinuclear complex has homochiral iron(III) centers (either Λ–Λ or Δ–Δ).

There are now several examples in which these and related difunctional ligands (incorporating similar 'parallel' donor moieties) produce dinuclear triple helicates upon coordination to a trivalent metal ion (*118,119,121*). For example, Christou *et al.* (*118*) have shown that **45** (R = Ph) reacts with trivalent titanium, vanadium, manganese and iron to yield dinuclear $[M_2L_3]$ complexes with helical structures. All

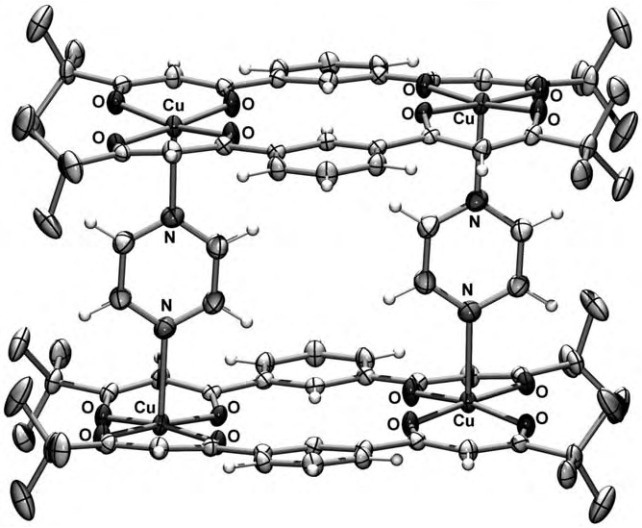

FIG. 14. X-ray structure of the 'dimer of dimers' formed from **47** and pyrazine (*114*).

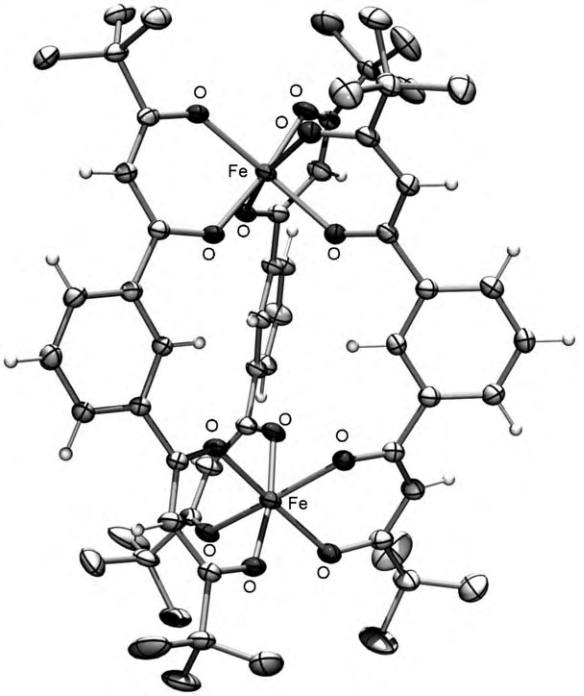

FIG. 15. X-ray structure of the dinuclear helical structure formed from **47** and iron(III) (*114*).

complexes in this series are isostructural, and cyclic voltammetry indicates that communication between metal centers is present in the titanium and vanadium species.

Similarly, in other studies (*121*) **45** (R = Ph) and its derivative with a 5-ethoxy substituent on the bridging aryl group have been used to prepare analogous dinuclear lanthanide derivatives for use as sensitizers in luminescence studies. Lanthanide(III) (or yttrium(III)) ions yield neutral triple-stranded complexes of type $[M_2L_3]$ where M = Eu, Nd, Sm, Y and Gd, and L is **45** (R = Ph) and $[M_2L'_2]$ where M = Eu or Nd and L′ is the ethoxy substituted ligand. An anionic quadruple-stranded derivative $[EuL'_4]^{2-}$ was also obtained in this study.

Parallel studies to those just discussed for the dinuclear platforms have also been carried out for the trinuclear platforms derived from 1,4-aryl substituted ligands of type **46** (*113*) mentioned previously. The interaction of the bis-β-diketones (with R = Me, Et, Pr, *t*-Bu and Ph) as well as a new naphthylene-linked species of this type with copper(II) yielded the corresponding triangular platforms of formula $[Cu_3(L)_3](\text{solvent})_n$. The X-ray structures of the complexes with R = Me and Pr confirmed their discrete triangular nature (see Fig. 10).

Interaction of selected copper(II) complexes of this type with both monofunctional and difunctional heterocyclic bases was found to lead to related 'adduct' behavior to that observed for the dinuclear platforms, except that the use of the difunctional bases in all cases yielded polymeric 'framework' products (*123*). Thus, in the latter case, the complex $[Cu_3L_3]$ (LH_2 = **46**; R = *t*-Bu) has been shown to generate polymeric structures of type $\{[Cu_3L_3(\mu_2\text{-bipy})(\text{thf})]\cdot 3.5\text{thf}\}_n$ and $\{[Cu_3L_3(\mu_2\text{–bipy})(\text{thf})]\cdot \text{thf}\cdot \text{bipy}\}_n$ on reaction with 4,4′-bipyridine, and $\{[Cu_3L_3(\mu_2\text{–pyz})]\cdot \text{thf}\}_n$ on reaction with pyrazine (pyz). The extended supramolecular architectures formed in each case have been confirmed by X-ray diffraction. These structures consist of alternating triangle/linker units to give rise to unusual one-dimensional polymeric chains in which two of the three copper sites in each triangular 'platform' are formally five-coordinate through interaction with a heterocyclic nitrogen donor. In contrast, when excess dabco was used as the linker unit, a symmetric prismatic structure of formula $\{Cu_3L_3(\text{dabco})_3\}_n$ was formed, incorporating only octahedral copper(II) ions. The different structures obtained can be rationalized (albeit tentatively) by consideration of linker size and basicity (*123*).

Ligand **46** (R = Ph) affords complexes with cobalt(II), nickel(II) and zinc(II) in the presence of pyridine (*120*). For the first two of these metal ions, the products are of type $[M_3(py)_6L_3]\cdot n\text{CHCl}_3$ and the structures of each were determined by X-ray diffraction. In each case discrete triangular structures form, with three bis(β-diketonato) ligands chelating three cobalt(II) or nickel(II) centers to form triangular (trinuclear) arrangements with two axially-coordinated pyridine ligands bound to each metal center. The complexes pack to form channels that accommodate chloroform, with both species showing potential for

zeolite-like behavior. In contrast to the above, the structure of $[Zn(py)_2L]_n \cdot n(py)$ is a one-dimensional coordination polymer in which the ligand adopts its *trans* conformation and chelates to two zinc(II) centers bridging them at 11.3 Å.

Related results to those observed above for cobalt and nickel were obtained with extended ligands of the above type incoporating 4,4′-biphenylene and 2,6-napthalylene spacer units (*122*). In the former case, a trianglar tri-cobalt(II) complex incorporating axial pyridine groups, with a central void of approximately twice the area of that observed for the related tri-copper(II) species (of type **48**) was obtained.

Interaction of ligands of type **46** with iron(III) (and in one instance gallium(III)) results in the spontaneous assembly of less-common, neutral molecular tetrahedra of formula $[Fe_4L_6](solvent)_n$ (L = all six ligand derivatives mentioned above) as well as a complex of type $[Ga_4L_6] \cdot 8.5thf \cdot 0.5H_2O$ (L = **46**, with R = Me); X-ray structure determinations of the iron(III) complexes (R = Et, Pr) (see Fig. 16) and the gallium(III) complex (R = Me) were undertaken. All structures have similar structures consisting of tetranuclear assemblies with pseudo-tetrahedral stereochemistries; in each case, the four trivalent metal ions are situated at the vertices of the tetrahedron with six ligands bridging the metal ions to define the edges. Each metal center is six-coordinate with approximate octahedral coordination geometry. All three structures encapsulate tetrahydrofuran in their central cavities. A magnetochemical investigation of $[Fe_4L_6] \cdot 6thf$ (L = **46**, R = Et) was also carried out (*113*). The susceptibility is Curie like and consistent with very weak coupling occurring between the iron(III) d^5 (high spin) centers.

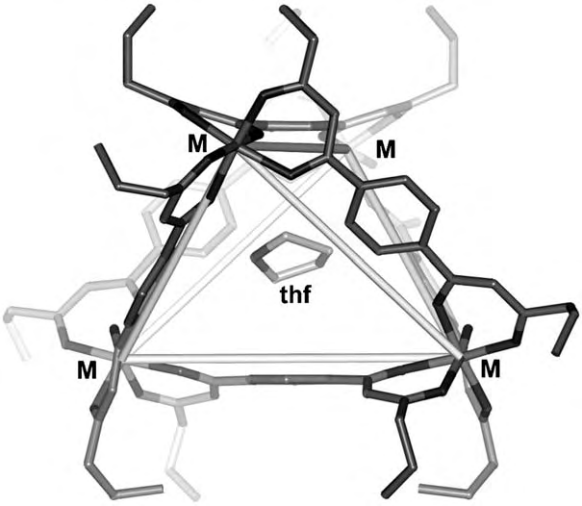

FIG. 16. X-ray structure of the tetrahedral complex of type $[M_4L_6]$ (L = **46**, R = Pr) showing an encapsulated thf molecule (*113*).

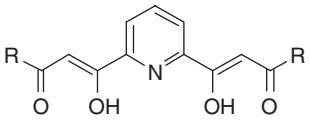

49

The reaction of 2,6-bis(2,4-pentanedione)pyridine (**49**, LH_2) in its doubly deprotonated form with divalent cadmium and manganese ions leads to octanuclear bis(triple-helical) metal(II) complexes of composition $[M_8O_2L_6]$ (*124*). NMR studies of the diamagnetic cadmium complex indicated the presence of six equivalent ligands. Full characterization of the manganese complex was achieved by X-ray crystallographic analysis. This showed that the product was a neutral, octanuclear, bis(triple-helical) chelate species. It contains a metallo core consisting of eight manganese(II) ions that form a two-fold capped, slightly twisted trigonal prism with a triply bound O^{2-} ion centered in each of the two inner faces. Each of the six doubly negatively charged pentadentate ligands binds to three manganese(II) centers. The two antipodal manganese ions are coordinated by three μ_1-and three μ_2-oxygen atoms from three ligands. The six remaining metal centers, describing a trigonal prism, are coordinated by one pyridyl nitrogen and two μ_2-oxygen atoms. Distorted octahedral coordination of these six manganese(II) ions is achieved by binding additional μ_3-O^{2-} ions. Consequently, in this complex, all the manganese(II) ions are octahedrally coordinated. As shown by X-ray analysis, the zinc complex is isostructural with the manganese species.

New trinuclear Cu(II)Ln(III)Cu(II) complexes (where Ln(III) is a wide selection of lanthanide ions) derived from **49** have been prepared by a one-pot reaction with $Cu(NO_3)_2.3H_2O$ and $Ln(NO_3)_3.nH_2O$ in methanol (*125*). X-ray structure determinations indicate that two deprotonated **49** ligands coordinate two copper(II) ions through their 1,3-diketonate entities to form a planar array with the Ln(III) ion bound to both pyridine moities to form the trinuclear CuLnCu core, bridged by the β-diketonate enolate oxygen atoms. The lanthanide ions adopted various coordination arrangements with bound nitrate ions such that normal (for these ions) high coordination numbers occur.

Reaction of **49** (R = Me, *t*-Bu) with potassium, strontium hydride, or lanthanum(III) chloride, followed by iron(III) chloride, has been reported to yield the corresponding di-iron, tris-ligand species in which the K^+, Sr^{2+} and La^{3+} ions occupy the central cavity of the respective complexes (*126,127*). In each complex, the iron(II) centers adopt their normal pseudo-octahedral coordination geometry. In the lanthanum-containing complex, the lanthanum(III) ion is eleven coordinate being bound by the six 'internal' oxygens from the β-diketonate groups, the three pyridyl nitrogens, a tetrahydrofuran group and

a water molecule. In contrast, a dinuclear iron, trispyridinium complex incorporating three protons in the cavity is generated from the reaction of the deprotonated form of **49** with (only) iron(III) chloride. The related potassium-containing species were formed from the triply-protonated complex on addition of potassium carbonate. From X-ray analyses, the strontium- and lanthanum-containing species and the pyridinium species form helical structures, whereas, in contrast, the potassium-containing species adopts a *meso*-arrangement.

Semiempirical PM3 computations have been carried out on the tris-ligand complex of **49** bound to two gallium(III) sites (*128*). Calculated structures agree well with the available X-ray structures of the corresponding iron(III) complexes. The calculations were also used to probe the relative energetics of metal/solvent occupancy of the central cavity in the above complex type.

The coordination properties of the phenol-containing derivative **50** (*129*) with Mn(II)/(III) have been described (*130*). Depending on the solvent employed, the reaction of this ligand with manganese(II) acetate yields either $[Mn_2L_2(py)_4]$ or $[Mn_3L_3]$ (where L is the doubly deprotonated form of **50**). The latter complex corresponds to an asymmetric triple-stranded helicate. Both complexes can be interconverted in solution by means of solvent control; the system thus resembles an interesting externally addressable switch. In the presence of manganese(III)/pyridine, partial degradation of **50** occurs through oxidative cleavage to yield **51** and the new complex $[Mn_2L'_2(py)_4]$ (where L′ is the triply deprotonated form of **51**) is generated. Variable-temperature magnetic susceptibility measurements were performed on each of the complexes. The fit for the first complex shows that the manganese(II) ions are not coupled ($g = 2.01$). The data for the second complex are in accord with the presence of an exchange coupled Mn(II)···Mn(II) pair next to a magnetically isolated manganese(II) center, while for the third complex the most satisfactory model corresponded to the manganese(III) ions being coupled antiferromagnetically (with $J = -1.48\,cm^{-1}$ and $g = 1.98$) together with weak ferromagnetic intermolecular exchange.

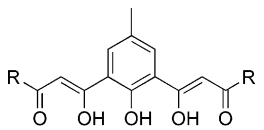

50

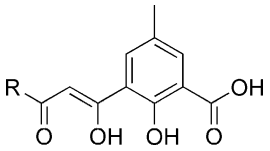

51

IV. Concluding Remarks

As is the case for other areas of contemporary metallo-supramolecular chemistry, the research discussed in this report clearly has implications for elucidating fundamental aspects of both supramolecular and host–guest inclusion behavior as well as giving promise of novel materials exhibiting unusual and potentially useful properties. In particular, it serves to emphasize the role that metal ions may play in the assembly of molecular architectures – an area of research pioneered by Daryle H. Busch more than 40 years ago.

References

1. Lehn, J.-M. *"Supermolecular Chemistry"*; VCH: Weinheim, **1996**.
2. Atwood, J. L.; Davies, J. E. D.; MacNicol, D. D.; Vögtle, F. (Eds.) *"Comprehensive Supramolecular Chemistry"*; vol. 11; Pergamon: Oxford, **1996**.
3. Rebek, J.; Conn, M. M. *Chem. Rev.* **1997**, *97*, 1647–1668.
4. Yeh, R. M.; Davis, A. V.; Raymond, K. N. Supramolecular Systems: Self-assembly. In: "*Comprehensive Coordination Chemistry II*"; vol. 7; Eds. McClevety, J. A.; Meyer, T. J. Elsevier: Oxford, **2004**, pp. 327–355.
5. MacGillivray, L. R.; Atwood, J. L. *Adv. Supramol. Chem.* **2000**, *6*, 157.
6. Werner, A. *Ber. Deut. Chem. Ges.* **1901**, *34*, 2594.
7. Swallow, A. G.; Truter, M. R. *Proc. Roy. Soc., A* **1960**, *254*, 205–207.
8. Dwyer, F. P.; Mellor, D. P. *"Chelating Agents and Metal Chelates"*; Academic Press: London, **1964**.
9. Bonati, F. *Organomet. Chem. Rev.* **1966**, *1*, 379–389.
10. Pike, R. M. *Coord. Chem. Rev.* **1967**, *2*, 163–172.
11. Gibson, D. *Coord. Chem. Rev.* **1969**, *4*, 225–240.
12. Casellato, U.; Vidali, M.; Vigato, P. A. *Inorg. Chim. Acta* **1976**, *18*, 77–112.
13. McCleverty, J. A.; Meyer, T. J. "*Comprehensive Coordination Chemistry II*"; vol. 1; Elsevier: Oxford, **2004**, p. 97.
14. Lindoy, L. F.; Atkinson, I. M. *"Self-assembly in Supramolecular Chemistry"*; Royal Society for Chemistry: Cambridge, **2000**.
15. Mehrotra, R. C. *Pure & Appl. Chem.* **1988**, *60*, 1349–1356.
16. Kawaguchi, S. *Coord. Chem. Rev.* **1986**, *70*, 51–84.
17. Shibata, S.; Sone, K. *Bull. Chem. Soc. Jpn.* **1956**, *29*, 852–856.
18. Fackler, J. P.; Cotton, F. A. *Inorg. Chem. 2*, **1963** 102–106 and references therein.
19. Cotton, F. A.; Wilkinson, G. W. *"Advanced Inorganic Chemistry"*; Wiley: New York, **1988**.
20. Bullen, G. J.; Mason, R.; Pauling, P. *Inorg. Chem.* **1965**, *4*, 456–462.
21. Padmanabhan, V. M. *Proc. Indian Acad. Sci.* **1958**, *47A*, 329–334.
22. Fay, R. C.; Girgis, A. Y.; Klabunde, U. *J. Am. Chem. Soc.* **1970**, *92*, 7056–7060.
23. Girgis, A. Y.; Fay, R. C. *J. Am. Chem. Soc.* **1970**, *92*, 7061–7071.
24. Kruger, G. J.; Reynhardt, E. C. *Acta Crystallogr. B* **1974**, *30*, 822–824.
25. Von Dreele, R. B.; Fay, R. C. *J. Am. Chem. Soc.* **1971**, *93*, 4937–4938.
26. Roof, R. B. *Acta Crystallogr.* **1956**, *9*, 781–787.
27. Iball, J.; Morgan, C. H. *Acta Crystallogr.* **1967**, *23*, 239–244.
28. Hon, P. K.; Pfluger, C. E. *J. Coord. Chem.* **1973**, *3*, 67–76.
29. Weatherburn, D. C.; Mandal, S.; Mukhopadhyay, S.; Bhaduri, S.; Lindoy, L. F. Manganese: Chapter 4. In: "*Comprehensive Coordination Chemistry II*"; vol. 5; Eds. McCleverty, J. A.; Meyer, T. J.; Elsevier: Amsterdam, **2004**, pp. 1–125.
30. Bailey, N. A.; Fenton, D. E.; Franklin, M. V.; Hall, M. *J. C. S. Dalton Trans.* **1980**, 984–990.

31. Funck, L. L.; Ortolano, T. R. *Inorg. Chem.* **1968**, *7*, 567–573.
32. Fenton, D. E.; Truter, M. R.; Vickery, B. L. *J. Chem. Soc., Chem. Commun*. **1971**, 93–94.
33. Bullen, G. J. *Acta Crystallogr.* **1959**, *12*, 703–708.
34. Fackler, J. P. *Inorg. Chem.* **1963**, *2*, 266–270.
35. Cotton, F. A.; Elder, R. C. *Inorg. Chem.* **1966**, *5*, 423–429.
36. Graddon, D. P. *Coord. Chem. Rev.* **1969**, *4*, 1–28.
37. Belford, R. L.; Chasteen, N. D.; Hitchman, M. A.; Hon, P.-K.; Pfluger, C. E.; Paul, I. C. *Inorg. Chem.* **1969**, *8*, 1312–1319.
38. Kwiatkowski, E.; Trojanowski, J. *J. Inorg. Nucl. Chem.* **1976**, *38*, 131–135.
39. Kwiatkowski, E.; Peplinski, Z.; Baranowski, J. *Trans. Met. Chem.* **1980**, *5*, 337–349.
40. Graddon, D. P.; Ong, W. K. *Aust. J. Chem.* **1974**, *27*, 741–747.
41. Martinez, J.; Martinez, A.; Doadrio, A. *Thermochim. Acta* **1985**, *87*, 281–287.
42. Belford, R. C. E.; Fenton, D. E.; Truter, M. R. *J. Chem. Soc., Dalton Trans.* **1972**, *20*, 2208–2213.
43. Soldatov, D. V.; Henegouwen, A. T.; Enright, G. D.; Ratcliffe, D. I.; Ripmeester, J. A. *Inorg. Chem.* **2001**, *40*, 1626–1636.
44. Soldatov, D. V.; Enright, G. D.; Ratcliffe, C. I.; Henegouwen, A. T.; Ripmeester, J. A. *Chem. Mater.* **2001**, *13*, 4322–4334.
45. Soldatov, D. V.; Enright, G. D.; Ripmeester, J. A. *Supramol. Chem.* **1999**, *11*, 35–47.
46. Soldatov, D. V.; Ripmeester, J. A. *Supramol. Chem.* **2001**, *12*, 357–368.
47. Soldatov, D. V.; Tinnemans, P.; Enright, G. D.; Ratcliffe, C. I.; Diamente, P. R.; Ripmeester, J. A. *Chem. Mater.* **2003**, *15*, 3826–3840.
48. Soldatov, D. V.; Ripmeester, J. A. *Mendeleev Commun. Electron. Version* 3, **2004**, 1–3.
49. Soldatov, D. V.; Moudrakovski, I. L.; Ratcliffe, C. I.; Dutrisac, R.; Ripmeester, J. A. *Chem. Mater.* **2003**, *15*, 4810–4818.
50. Zaman, Md. B.; Udachin, K. A.; Ripmeester, J. A. *Crystallogr. Eng. Commun.* **2002**, *4*, 613–617.
51. Haddad, M. S.; Hendrickson, D. N.; Cannady, J. P.; Drago, R. S.; Bieksza, D. S. *J. Am. Chem. Soc.* **1979**, *101*, 898–906.
52. Dichmann, K.; Hamer, G.; Nyburg, S. C.; Reynolds, W. F. *J. Chem. Soc., Chem. Commun*., **1970**, 1295–1296.
53. Aakeröy, C. B.; Schultheiss, N.; Desper, J. *Inorg. Chem.* **2005**, *44*, 4983–4991.
54. Mackay, L. G.; Anderson, H. L.; Sanders, J. K. M. *J. Chem. Soc., Chem. Commun*. **1992**, 43–44.
55. Mackay, L. G.; Anderson, H. L.; Sanders, J. K. M. *J. Chem. Soc., Perkin Trans.* **1995**, *1*, 2269–2273.
56. Turner, S. S.; Collison, D.; Mabbs, F. E.; Halliwell, M. *J. Chem. Soc., Dalton Trans*. **1997**, 1117–1118.
57. Chen, B.; Fronczek, F. R.; Maverick, A. W. *Chem. Commun*. **2003**, 2166–2167.
58. Vreshch, V. D.; Chernega, A. N.; Howard, J. A. K.; Sieler, J.; Domasevitch, K. V. *Dalton Trans*. **2003**, 1707–1711.
59. Chen, B.; Fronczek, F. R.; Maverick, A. W. *Inorg. Chem.* **2004**, *43*, 8209–8211.
60. Vreshch, V. D.; Lysenko, A. B.; Chernega, A. N.; Howard, J. A. K.; Krautscheid, H.; Sieler, J.; Domasevitch, K. V. *Dalton Trans*. **2004**, 2899–2903.
61. Fukuda, Y.; Mafune, K. *Chem. Lett*. **1988**, *17*, 697–700.
62. Lim, Y. Y.; Chen, W.; Tan, L. L.; You, X. Z.; Yao, T. M. *Polyhedron* **1994**, *13*, 2861–2866.
63. Zhang, Y.; Breeze, S. R.; Wang, S.; Greedan, J. E.; Raju, N. P.; Li, L. *Can. J. Chem.* **1999**, *77*, 1424–1435.
64. Zhang, Y.; Wang, S.; Enright, G. D.; Breeze, S. R. *J. Am. Chem. Soc.* **1998**, *120*, 9398–9399.

65. Koiwa, T.; Masuda, Y.; Shono, J.; Kawamoto, Y.; Hoshino, Y.; Hashimoto, T.; Natarajan, K.; Shimizu, K. *Inorg. Chem.* **2004**, *43*, 6215–6223.
66. Martin, D. F.; Fernelius, W. C.; Shamma, M. *J. Am. Chem. Soc.* **1959**, *81*, 130–133.
67. Bassetti, M.; De Cola, L.; Vallarino, L. M. *Inorg. Chim. Acta* **1985**, *105*, 141–145.
68. Sharma, R. K.; Shivahare, G. C. *Monatsh. Chem.* **1985**, *116*, 297–302.
69. Moustafa, M. M.; Amin, A. S.; Issa, R. M. *Monatsh. Chem.* **1997**, *128*, 423–430.
70. Mishra, L.; Yadaw, A. K.; Srivastava, S.; Patel, A. B. *New J. Chem.* **2000**, *24*, 505–510.
71. Oh, J. S.; Bailar, J. C. *J. Inorg. Nucl. Chem.* **1962**, *24*, 1225–1234.
72. Jones, R. D. G.; Power, L. F. *Aust. J. Chem.* **1971**, *24*, 735–742 and references therein.
73. Archer, R. D.; Tramontano, V. J.; Ochaya, V. O.; West, P. V.; Cumming, W. *Poly. Mater. Sci. Eng.* **1988**, *61*, 3176–3320.
74. Munro, H. S.; Finocciaro, P.; Mamo, A.; Recca, A. *Polymer Commun.* **1986**, *27*, 202–203.
75. Awawsarkar, P. A.; Gopinathan, S.; Gopiathan, C. *Synth. React. Inorg. Met-Org. Chem.* **1985**, *15*, 133–147.
76. Karvembu, R.; Natarajan, K. *Polyhedron* **2002**, *21*, 1721–1727.
77. Karvembu, R.; Jayabalakrishnan, C.; Natarajan, K. *Trans. Met. Chem.* **2002**, *27*, 574–579.
78. Grybos, R.; Paw, W. *Polyhedron* **1990**, *9*, 1397–1400.
79. Zheng, B.-S.; Zhang, X.-Y.; Zhu, H.-W.; Luo, S.-X.; Lindoy, L. F.; McMurtrie, J. C.; Turner, P.; Wei, G. *Dalton Trans.* **2005**, 1349–1351.
80. Hashimoto, T.; Endo, A.; Nagao, N.; Sato, G. P.; Natarajan, K.; Shimizu, K. *Inorg. Chem.* **1998**, *37*, 5211–5220.
81. Sharma, S.; Bohra, R.; Mehrotra, R. C. *Polyhedron* **1996**, *15*, 1525–1529.
82. Whitmore, B. C.; Eisenberg, R. *Inorg. Chem.* **1984**, *23*, 1697–1703.
83. Maverick, A. W.; Klavetter, F. E. *Inorg. Chem.* **1984**, *23*, 4129–4130.
84. Clack, D. W.; Farrimond, M. S. *J. Chem. Soc., Dalton Trans.* **1972**, 29–33.
85. Maverick, A. W.; Billodeaux, D. R.; Ivie, M. L.; Fronczek, F. R.; Maverick, E. F. *J. Incl. Phenom. Mac. Chem.* **2001**, *39*, 19–26.
86. Maverick, A. W.; Martone, D. P.; Bradbury, J. R.; Nelson, J. E. *Polyhedron* **1989**, *8*, 1549–1556.
87. Maverick, A. W.; Buckingham, S. C.; Yao, Q.; Bradbury, J. R.; Stanley, G. G. *J. Am. Chem. Soc.* **1986**, *108*, 7430–7431.
88. Maverick, A. W.; Ivie, M. L.; Waggenspack, J. H.; Fronczek, F. R. *Inorg. Chem.* **1990**, *29*, 2403–2409.
89. Bonitatebus, P. J.; Mandal, S. K.; Armstrong, W. H. *Chem. Commun.* **1998**, 939–940.
90. Davidson, G. J. E.; Baer, A. J.; Cote, A. P.; Taylor, N. J.; Hanan, G. S.; Tanaka, Y.; Watanabe, M. *Can. J. Chem.* **2002**, *80*, 496–498.
91. Fujimoto, K.; Shinkai, S. *Tetrahedron Lett.* **1994**, *35*, 2915–2918.
92. Lindoy, L. F. *"The Chemistry of Macrocyclic Ligand Complexes"*; Cambridge University Press: Cambridge, **1989**.
93. Tabushi, I.; Kobuke, Y.; Nishiya, T. *Tetrahedron Lett.* **1979**, *37*, 3315–3518.
94. Reuther, U.; Brandmüller, T.; Donaubauer, W.; Hampel, F.; Hirsch, A. *Chem. Eur. J.* **2002**, *8*, 2261–2273.
95. Albert, A. H.; Cram, D. J. *J. Chem. Soc., Chem. Commun.* **1976**, 958–959.
96. Albert, A. H.; Cram, D. J. *Am. Chem. Soc.* **1979**, *101*, 3545–3553.
97. Saalfrank, R. W.; Stark, A.; Peters, K.; von Schnering, H. G. *Angew. Chem. Int. Ed. Engl.* **1988**, *27*, 851–853.
98. Saalfrank, R. W.; Stark, A.; Bremer, M.; Hummel, H.-U. *Angew. Chem. Int. Ed. Engl.* **1990**, *29*, 311–314.

99. Saalfrank, R. W.; Horner, B.; Stalke, D.; Salbeck, J. *Angew. Chem. Int. Ed. Engl.* **1993**, *32*, 1179–1182.
100. Saalfrank, R. W.; Burak, R.; Breit, A.; Stalke, D.; Herbst-Irmer, R.; Daub, J.; Porsch, M.; Bill, E.; Muther, M.; Trautwein, A. X. *Angew. Chem. Int. Ed. Engl.* **1994**, *33*, 1621–1623.
101. Saalfrank, R. W.; Burak, R.; Reihs, S.; Low, N.; Hampel, F.; Stachel, H.-D.; Lentmaier, J.; Peters, K.; Peters, E.-M.; von Schnering, H. G. *Angew. Chem. Int. Ed. Engl.* **1995**, *34*, 993–995.
102. Johnson, D. W.; Xu, J.; Saalfrank, R. W.; Raymond, K. N. *Angew. Chem. Int. Ed.* **1999**, *38*, 2882–2885.
103. Saalfrank, R. W.; Glaser, H.; Demleitner, B.; Hampel, F.; Chowdhry, M. M.; Schunemann, V.; Trautwein, A. X.; Vaughan, G. B. M.; Yeh, R.; Davis, A. V.; Raymond, K. N. *Chem. Eur. J.* **2002**, *8*, 493–497.
104. Saalfrank, R. W.; Demleitner, B.; Glaser, H.; Maid, H.; Bathelt, D.; Hampel, F.; Bauer, W.; Teichert, M. *Chem. Eur. J.* **2002**, *8*, 2679–2683.
105. Saalfrank, R. W.; Löw, N.; Demleitner, B.; Stalke, D.; Teichert, M. *Chem. Eur. J.* **1998**, *4*, 1305–1311.
106. Saalfrank, R. W.; Löw, N.; Hampel, F.; Stachel, H.-D. *Angew. Chem.* **1996**, *108*, 2353–2354.
107. Saalfrank, R. W.; Löw, N.; Hampel, F.; Stachel, H.-D. *Angew. Chem. Int. Ed. Engl.* **1996**, *35*, 2209–2210.
108. Saalfrank, R. W.; Low, N.; Kareth, S.; Seitz, V.; Hampel, F.; Stalke, D.; Teichert, M. *Angew. Chem.* **1998**, *110*, 182–184.
109. Saalfrank, R. W.; Löw, N.; Kareth, S.; Seitz, V.; Hampel, F.; Stalke, D.; Teichert, M. *Angew. Chem. Int. Ed.* **1998**, *37*, 172–174.
110. Saalfrank, R. W.; Maid, H.; Mooren, N.; Hampel, F. *Angew. Chem. Int. Ed.* **2002**, *41*, 304–307.
111. Saalfrank, R. W.; Schmidt, C.; Maid, H.; Hampel, F.; Bauer, W.; Scheurer, A. *Angew. Chem. Int. Ed.* **2006**, *45*, 315–318.
112. Saalfrank, R. W.; Demleitner, B.; Glaser, H.; Maid, H.; Reihs, S.; Bauer, W.; Maluenga, M.; Hampel, F.; Teichert, M.; Krautscheid, H. *Eur. J. Inorg. Chem.* **2003**, 822–829.
113. Clegg, J. K.; Lindoy, L. F.; Moubaraki, B.; Murray, K. S.; McMurtrie, J. C. *Dalton Trans.* **2004**, 2417–2423.
114. Clegg, J. K.; Lindoy, L. F.; McMurtrie, J. C.; Schilter, D. *Dalton Trans.* **2005**, 857–864.
115. Fenton, D. E.; Regan, C. M.; Casellato, U.; Vigato, P. A.; Vidali, M. *Inorg. Chim. Acta* **1980**, *44*, L105–L106.
116. Fenton, D. E.; Regan, C. M.; Casellato, U.; Vigato, P. A.; Vivaldi, M. *Inorg. Chim. Acta* **1982**, *58*, 83–88.
117. Fenton, D. E.; Tate, J. R.; Casellato, U.; Tamburini, S.; Vigato, P. A.; Vivaldi, M. *Inorg. Chim. Acta* **1984**, *83*, 23–31.
118. Grillo, V. A.; Seddon, E. J.; Grant, C. M.; Aromi, G.; Bollinger, J. C.; Folting, K.; Christou, G. *Chem. Commun.* **1997**, 1561–1562.
119. Matsushita, M. M.; Yasuda, T.; Kawano, R.; Kawai, T.; Iyoda, T. *Chem. Lett.* **2000**, *29*, 812–813.
120. Soldatov, D. V.; Zanina, A. S.; Enright, G. D.; Ratcliffe, C. I.; Ripmeester, J. A. *Crystallogr. Growth and Design* **2003**, *3*, 1005–1013.
121. Basset, A. P.; Magennis, S. W.; Glover, P. B.; Lewis, D. J.; Spencer, N.; Parsons, S.; Williams, R. M.; De Cola, L.; Pikramenou, Z. *J. Am. Chem. Soc.* **2004**, *126*, 9413–9424.
122. Clegg, J. K.; Hayter, M. J.; Lindoy, L. F.; Schilter, D. unpublished results.
123. Clegg, J. K.; Lindoy, L. F.; McMurtrie, J. C.; Schilter, D. *Dalton Trans.* **2006**, 3114–3121.
124. Saalfrank, R. W.; Löw, N.; Trummer, S.; Sheldrick, G. M.; Teichert, M.; Stalke, D. *Eur. J. Inorg. Chem.* **1998**, 559–563.

125. Shiga, T.; Ohba, M.; Okawa, H. *Inorg. Chem*. **2004**, *43*, 4435–4446.
126. Saalfrank, R. W.; Seitz, V.; Caulder, D. L.; Raymond, K. N.; Teichert, M.; Stalke, D. *Eur. J. Inorg. Chem*. **1998**, 1313–1317.
127. Saalfrank, R. W.; Seitz, V.; Heinemann, F. W.; Göbel, C.; Herbst-Irmer, R. *J. Chem. Soc., Dalton Trans*. **2001**, 599–603.
128. Puchta, R.; Seitz, V.; van Eikema Hommes, N. J. R.; Saalfrank, R. W. *J. Mol. Modeling* **2000**, *6*, 126–132.
129. Aromi, G.; Gamez, P.; Berzal, P. C.; Driessen, W. L.; Reedijk, J. *Synth. Commun*. **2003**, *33*, 11–18.
130. Aromi, G.; Gamez, P.; Roubeau, O.; Berzal, P. C.; Kooijman, H.; Spek, A. L.; Driessen, W. L.; Reedijk, J. *Inorg. Chem*. **2002**, *41*, 3673–3683.

COORDINATION POLYMER OPEN FRAMEWORKS CONSTRUCTED OF MACROCYCLIC COMPLEXES

MYUNGHYUN PAIK SUH and HOI RI MOON

Department of Chemistry, Seoul National University, Seoul 151-747, Republic of Korea

I. Introduction

Crystal structure affects the chemical and the physical properties of a compound, such as stability, solubility, color, and optical properties. Therefore, if the crystal structure is designed and predicted, the desired physical and chemical properties can be generated in the compound, which is referred to as “crystal engineering”. By employing

ADVANCES IN INORGANIC CHEMISTRY
VOLUME 59 ISSN 0898-8838 / DOI: 10.1016/S0898-8838(06)59002-6

crystal engineering, advanced materials including porous coordination polymers can be prepared.

Coordination polymers with various structures have been self-assembled from a wide variety of metal ions and organic building blocks. Self-assembled coordination polymers with well-defined channels or pores have attracted significant interests because they are considered as zeolite analogues and have great potential in the applications to adsorption and separation processes (*1–10*), ion exchange (*11,12*), catalysis (*13,14*), and sensor technology (*15,16*). Zeolites have uniform pore sizes and shapes and are thermally stable, and thus they are widely employed as adsorbents and catalysts. However, the pore size and shape of zeolites cannot be easily modified. On the other hand, the pore size and shape of coordination polymers can be easily controlled by selecting the metal and organic building blocks. In addition, various chemical environments can also be generated on the surface of the voids or channels, which are advantageous in selective guest binding, recognition, storage of molecules, and catalysis.

Despite the extensive studies, however, the applications of coordination polymer open frameworks are limited as compared to zeolites. This is because of the following reasons. (1) The self-assembly of a simple metal ion and connecting ligand often provides self-interpenetrating or catenated structures in which the channels or pores are blocked. (2) Even if an open structure is constructed, the pores are filled with guest molecules. On removal of the guest molecules, the entire framework structure collapses. (3) Coordination polymers are, in general, thermally unstable as compared with inorganic zeolites and are destroyed at high temperatures ($>200^{\circ}$C) or even at low temperatures under vacuum condition. (4) They are often soluble in solvents and dissociate into their building blocks (*7–9,17–21*).

Therefore, in the design of coordination polymer open frameworks as functional materials, we should consider the manner in which permanent porosity, insolubility, and thermal stability can be generated.

In the self-assembly of porous coordination polymers, free metal ions are commonly used as the metal building blocks, and macrocyclic complexes have seldom been employed (*6–10,17–22*). This is because the synthesis of macrocyclic complexes is known to be difficult. However, simple one-pot template synthetic methods for Ni(II) and Cu(II) hexaaza macrocyclic complexes have been developed and are well documented (*23*). Various Ni(II) or Cu(II) hexaaza macrocyclic complexes thus synthesized contain various pendants such as methyl, hydroxyethyl, cyanoethyl, and pyridyl groups at the bridgehead positions (*23–25*).

The utilization of macrocyclic complexes offers several advantages over free metal ions in the assembly of multidimensional coordination polymer networks. Free metal ions contain many binding sites for the ligand, and thus the extending direction of the network cannot be easily controlled. However, the macrocyclic complexes in square-planar

geometries contain only two empty coordination sites at the *trans* positions, thereby acting as linear linkers for the ligands. Therefore, the utilization of macrocyclic complexes enables the control of the extending direction of networks, which simplifies the design and prediction of the network structures. Furthermore, macrocyclic complexes simplify the coordination mode of the ligand because of the bulkiness of the macrocycle. For example, a free metal ion binds 1,4-benzenedicarboxylate with the coordination modes of a–c. However, macrocyclic complexes in a square-planar geometry bind the ligands only in the c mode due to the steric hindrance between the macrocyclic ligands in the a mode. In the b mode, the macrocyclic complexes exhibit a folded structure that might experience significant strain. Furthermore, various functional groups can be attached to the macrocyclic frameworks to induce intermolecular interactions. Macrocyclic complexes are expected to prevent the interpenetration of the network, which can be considered as a major impediment in the construction of open structures.

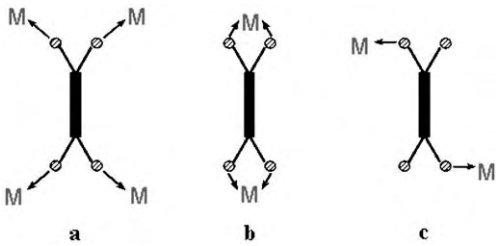

We built various coordination polymer open frameworks by utilizing macrocyclic complexes and organic ligands (*6–10,17–22*). The assembly and properties will be reviewed in this article. The macrocyclic complexes employed in the assembly of coordination polymer open frameworks are described as follows.

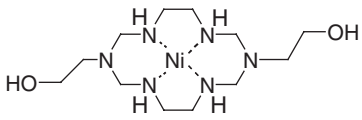

$[Ni(L_1)]^{2+}$

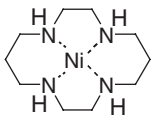

$[Ni(L_2)]^{2+}$

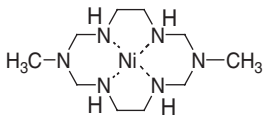

$[Ni(L_3)]^{2+}$

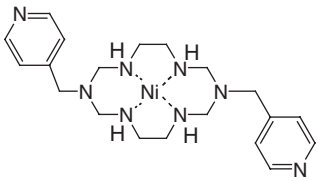

$[Ni(L_4)]^{2+}$

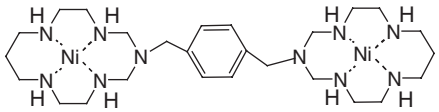

$[Ni_2(L_5)]^{4+}$

The organic building blocks (ligands) and their abbreviations are as follows.

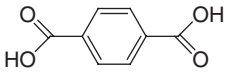

H_2BDC

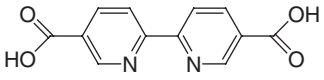

H_2BPyDC

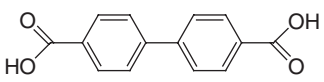

H_2BPDC

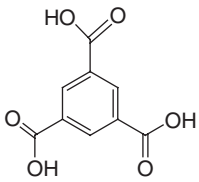

H_3BTC

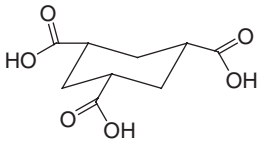

H_3CTC

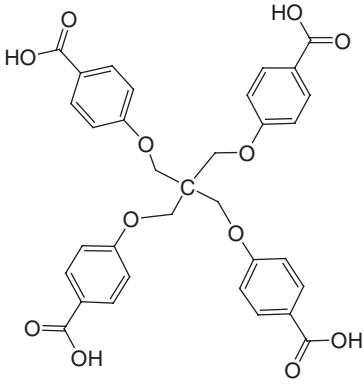

H_4TCM

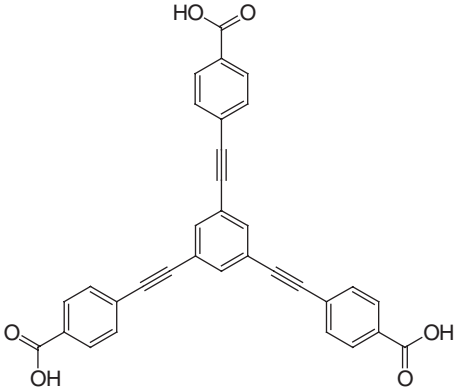

H_3TCPEB

The abbreviations of the organic building blocks and solvents are provided in Chart 1.

The coordination polymers of open structures thus prepared are able to exhibit porosity, gas storage capabilities, and selective guest binding properties for various guest molecules. Many of them show single-crystal-to-single-crystal transformations on the removal and reintroduction of guest molecules, which involve changes in the framework structures by the dynamic motions of the molecular components. In addition, the coordination polymers incorporating Ni(II) macrocyclic species can be employed in the preparation of small-sized silver nanoparticles by using their redox property.

CHART 1.

H_2BDC	1,4-benzenedicarboxylic acid
H_2BPyDC	2,2′-bipyridyl-5,5′-dicarboxylic acid
H_2BPDC	4,4′-biphenyldicarboxylic acid
H_3BTC	1,3,5-benzenetricarboxylic acid
H_3CTC	*cis*,*cis*-1,3,5-cyclohexanetricarboxylic acid
H_4TCM	tetrakis[4-(carboxyphenyl)oxamethyl]methane
H_3TCPEB	1,3,5-tris[2-(4-carboxylphenyl)-1-ethynyl]benzene
DMF	*N*,*N*′-dimethylformamide
DMSO	dimethylsulfoxide
MeOH	methyl alcohol
EtOH	ethyl alcohol
iso-PrOH	isopropyl alcohol
BzOH	benzyl alcohol
BuOH	butyl alcohol
PhOH	phenol
MeCN	acetonitrile
Pyr	pyridine
HAP	4-hydroxyacetophenone
THB	1,3,5-trihydroxybenzene

In this review, we will describe assembly, functions, and single-crystal-to-single-crystal transformations of coordination polymer open frameworks incorporating Ni(II) or Cu(II) macrocyclic complexes.

II. Design Strategies for the Construction of Porous Coordination Polymers

1D, 2D, and 3D strategies have been applied in the construction of coordination polymer open frameworks (Scheme 1). In the 1D strategy, 1D chains are assembled from metal and organic building blocks, which are packed in particular modes to generate the channels. In the 2D strategy, 2D layers with pores are constructed and are stacked by the interlayer interactions to align the pores and generate the channels. A pillared bilayer network, where 2D layers with pores are connected with covalent bonds, is also assembled. In the 3D strategy, 3D diamondoid networks are constructed by connecting the tetrahedral organic building blocks with linear metal linkers.

Although this review deals with polymeric crystalline coordination polymer open frameworks constructed of macrocyclic complexes, the structural design principles are quite similar to those for supramolecular materials, for which host–guest chemistry has been reported (*26,27*).

A. 1D STRATEGIES

When Ni(II) macrocyclic complexes with a square-planar geometry are connected by linear bidentate ligands, 1D chains are formed. The

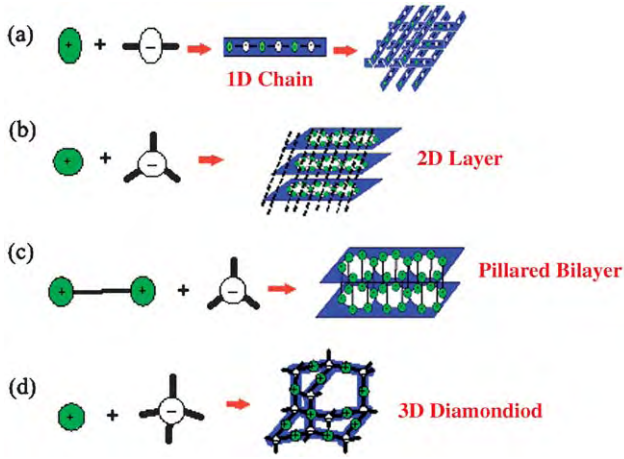

SCHEME 1. Various strategies for self-assembly of coordination polymer open frameworks.

1D chains are packed in various modes, as described in Scheme 2. In most cases, linear rods pack in a parallel manner, which cannot yield a porous structure. However, when the molecular building blocks constructing the linear rods have an appropriate shape and length, the rods would pack such that pores or channels are generated. Various rod packing modes have been mathematically analyzed in the literature (*28*).

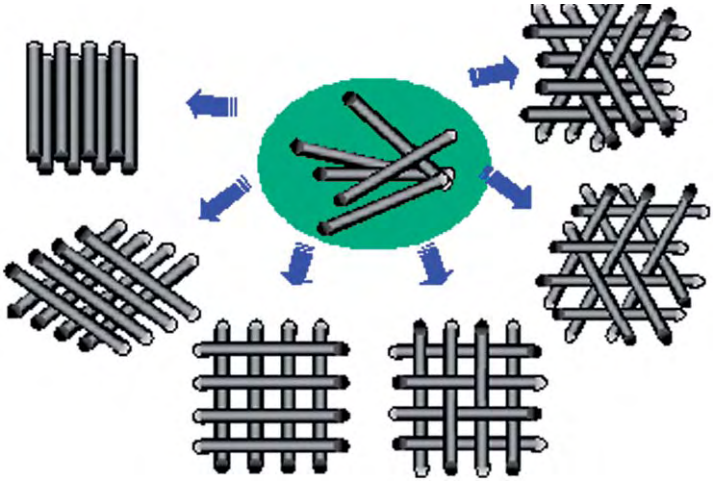

SCHEME 2. Rod packing modes.

A.1. Self-assembly of Ni(II) hexaaza macrocyclic complex $[Ni(L_1)]^{2+}$ ($L_1 = C_{12}H_{30}N_6O_2$) with 1,4-benzenedicarboxylate (BDC^{2-}) (20)

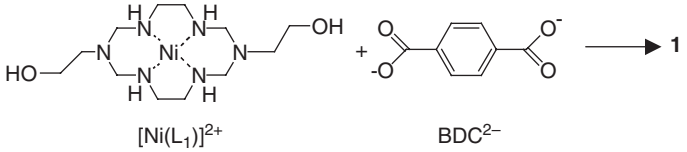

When a Ni(II) macrocyclic complex with hydroxyl pendants $[Ni(L_1)]^{2+}$ is mixed with Na_2BDC in $MeCN/H_2O$, each Ni(II) ion in the macrocyclic complex is coordinated with two carboxylate oxygen atoms of BDC^{2-} at the *trans* position, and each BDC^{2-} binds two metal ions in an *exo*-bidentate mode, which results in linear coordination polymer chain $\{[Ni(L_1)(BDC)]\}_n \cdot 4nH_2O$ (**1**) (Fig. 1). In the solid state, two different series of 1D chains extend in different directions. Within the same series of the 1D chains, the closest distance between the chains is 9.0 Å. The two different series of chains pack alternately in a manner similar to plywood, generating 1D channels. They are interconnected by the hydrogen-bonding interactions between the pendant hydroxyl groups of the macrocycles belonging to a polymer chain and the secondary amines of the macrocycles belonging to the other polymer chain. The lattice water molecules occupy the open space. The TGA data indicates that all the guest water molecules can be removed at 56–130°C, and the remaining framework is thermally stable up to 200°C. The void volume per unit cell estimated by PLATON (*29*) is 14.8%. The XRPD patterns indicate that the structure changes on desolvation. However, when the desolvated solid is suspended in water only for 1 min, the structure of the original crystal is restored.

A.2. Self-assembly of $[Ni(L_2)]^{2+}$ (L_2 = cyclam = 1,4,8,11-tetraazacyclotetradecane) with 2,2′-bipyridyl-5,5′-dicarboxylate ($BPyDC^{2-}$) (6)

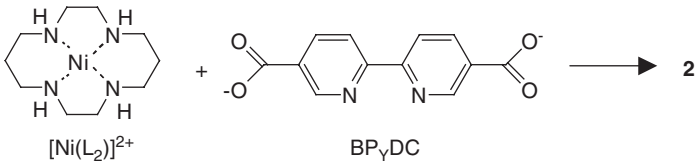

Although various linear coordination polymers have been constructed (*20,21*), (*30–32*), the ones exhibiting permanent porosity, gas adsorption (*33*), or selective guest binding ability are limited. A 1D coordination polymer $\{[Ni(L_2)(BPyDC)] \cdot 5H_2O\}_n$ (**2**) has been assembled from the Ni(II) macrocyclic complex $[Ni(L_2)](ClO_4)_2$ and $BPyDC^{2-}$. Within a chain, Ni···Ni separation is 15.56 Å, which is ~4 Å greater than that of $[Ni(L_1)(BDC)]_n \cdot 4nH_2O$ (**1**) (11.5 Å). The $BPyDC^{2-}$ ligand is planar and is located in a direction almost perpendicular to the coordination plane

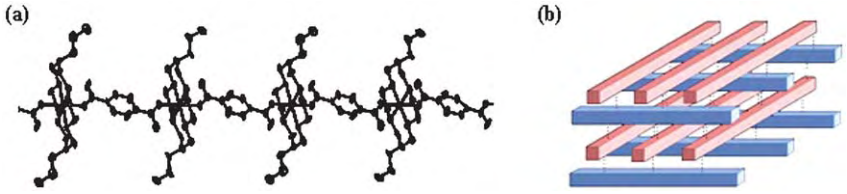

FIG. 1. (a) 1D linear coordination polymer chain constructed of $[Ni(L_1)]^{2+}$ and BDC^{2-}. (b) Schematic diagram showing how 1D linear chains pack to form channels. Dashed lines indicate hydrogen-bonding interactions between 1D chains.

of the macrocycle (dihedral angle = 85.1(1)°), which results in grooves between the macrocycles in the 1D chain. In the crystal structure, three series of 1D coordination polymer chains extend in three different directions (Fig. 2), and they are packed in the form of a double network of threefold braids (*28*). In other words, two threefold braids of slanting rods are packed with an inversion of the braids when translated in the perpendicular direction. In the threefold braids, three rods are entangled by fitting the macrocycles of the chain into the grooves of other chains. Furthermore, the second threefold braids pack over the first braids such that the macrocycles are located on the grooves of the first ones to fit in a key-and-lock style, which results in a remarkably robust framework. The 1D chains are linked to each other by C–H-π interactions between carbon atoms of the macrocycles and the pyridyl rings of $BPyDC^{2-}$. The packing of 1D coordination polymer chains generates 1D channels that have honeycomb-like openings with a diameter of 10.0 Å

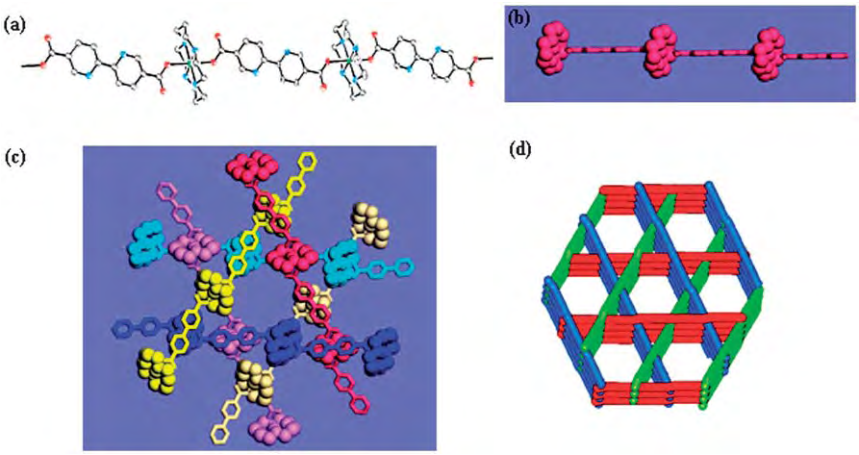

FIG. 2. X-ray structure of **2**. (a) An ORTEP view of the linear coordination polymer chain. (b) a CPK view of (a). (c) Double network of threefold braids where macrocycles fit into the grooves created by $BPyDC^{2-}$ ligands. (d) A view showing the stacking of the linear chains to generate 1D channels.

(effective size: 5.8 Å). The channels are filled with the guest water molecules. The free volume of the materials estimated using the N_2 gas sorption data is 37%.

The solid material is insoluble in water and common organic solvents. It is stable up to 300°C. Solid **2** is extremely robust such that its open structure is retained during several cycles of the dehydration and rehydration processes. In addition, it exhibits a permanent porosity, H_2 gas storage ability, and selective guest binding property, which will be discussed in Sections III and IV.B.

3. Self-assembly of $[Ni(L_3)]^{2+}$ (L_3 = 3,10-dimethyl-1,3,5,8,10,12-hexaazacyclotetradecane) and 4,4′-biphenyldicarboxylate ($BPDC^{2-}$) (34)

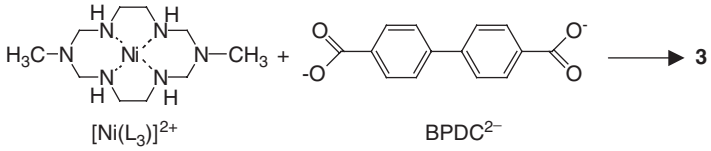

The self-assembly of $[Ni(L_3)](ClO_4)_2$ and Na_2BPDC in a H_2O/pyridine mixture results in $\{[Ni(L_3)]_3(BPDC)_3\} \cdot 2pyr \cdot 6H_2O$ (**3**; BPDC = 4,4′-biphenyldicarboxylate), which has a similar structure as **2**. In the crystal state of **3**, the linear coordination polymer chains pack as a double network of threefold braids (*28*), which generates 1D channels with honeycomb-shaped windows (diameter = 9.7 Å and effective pore size = 7.3 Å).

In general, when any of the building blocks or the solvent system is changed in the self-assembly, it would result in a framework of different structure (*18,35*). However, in this case, even if the metal and organic building blocks as well as the solvent system are changed, a structure similar to that of **2** is created. Furthermore, in the structure of **3**, the flat $BPDC^{2-}$ ligands form grooves between the macrocycles in a linear coordination polymer chain, and the macrocycles of the other chain fit into the grooves of the former in the key-and-lock style, thereby resulting in a robust framework (Fig. 3). Solid **3** is insoluble in water or organic solvents. A thermogravimetric analysis indicates that all the guest molecules can be removed at 138°C and the apohost is stable up to 250°C. The X-ray powder diffraction (XRPD) pattern of the desolvated solid is same as that of the as-prepared solid, indicating that the open structure created by the packing of 1D linear coordination polymer chains is intact even after the removal of the guest molecules. Solid **3** shows a permanent porosity and the H_2 gas adsorption capability, which will be discussed in Section III.

B. 2D Strategies

2D networks having honeycomb-like cavities can be created when triangular building blocks are placed at every corner of a hexagon and

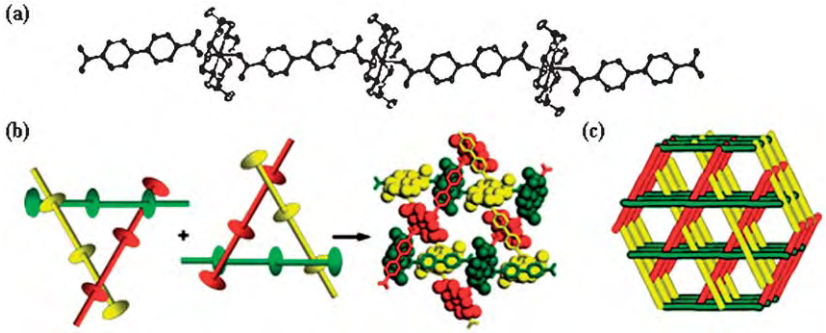

FIG. 3. X-ray structure of **3**. (a) An ORTEP view of the linear coordination polymer of **3**. (b) Double network of threefold braids where macrocycles fit into the grooves created by $BPDC^{2-}$. (c) A view showing the stacking of the linear chains to generate 1D channels.

linked by the linear linkers. In other words, if a tricarboxylate ligand is employed as the triangular building block and a macrocyclic complex with a square-planar geometry is used as the linear linker, a 2D coordination polymer with honeycomb cavities is created (Scheme 3). Then, each honeycomb cavity consists of six macrocyclic complexes and six carboxylate ligands. Every M(II) macrocyclic complex is shared by two cavities and every carboxylate ligand is shared by three cavities, and thus the stoichiometry of the 2D network becomes M^{II}:L = 3:2. If Ni(II) or Cu(II) macrocyclic complexes are self-assembled using tricarboxylate ligands, an electronically neutral 2D network will be formed.

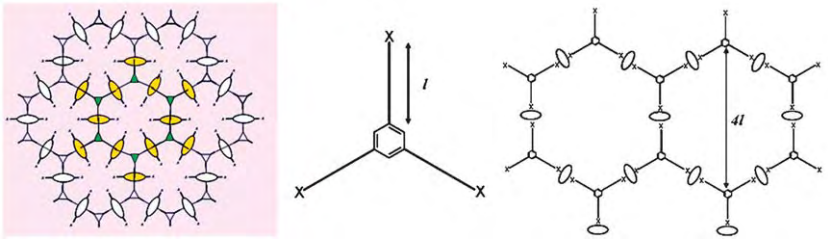

SCHEME 3. Control of cavity size of 2D network by triconnecting ligand.

If the 2D layers were stacked by the interlayer interactions such as hydrogen-bonding or π–π stacking interactions, the pores of the 2D layers would be aligned to create the channels. In order to induce the layers to stack via interlayer interactions, functional pendants such as hydroxyl or pyridyl groups can be attached to the macrocyclic ligands. The pore size of the 2D network depends on the size of the tricarboxylate ligands. Mathematically, the diagonal length of the honeycomb cavity will be four times that of the length of an arm of the tricarboxylate. That is, if a tricarboxylate ligand with an arm length of

l Å is used as an organic building block, the resulting structure would contain hexagonal cavities with a diameter of $4l$ Å.

The 2D structures are affected by the type of macrocycle, metal ion, the size of the tricarboxylate ligand, and the solvent system, as discussed in this section.

B.1. Noninterpenetrating 2D networks

(a) Self-assembly of Ni(II) macrocyclic complex with hydroxyl pendants $[Ni(L_1)]^{2+}$ with 1,3,5-benzenetricarboxylate (BTC^{3-}) (*18*). The self-assembly of a square-planar Ni(II) macrocyclic complex containing hydroxyl pendant chains $[Ni(L_1)]^{2+}$ and BTC^{3-} salt in H_2O/DMF results in a 2D coordination polymer $\{[Ni(L_1)]_3[BTC]_2 \cdot 18H_2O\}_n$ (**4**) with brick-wall cavities (Fig. 4a). When either a similar self-assembly is performed in the presence of pyridine or **4** is re-assembled in water in the presence of an excess amount of pyridine, a 2D coordination polymer with honeycomb cavities $\{[Ni(L_1)]_3[BTC]_2 \cdot 14H_2O \cdot 2pyr\}_n$ (**5**) is formed (Fig. 4b).

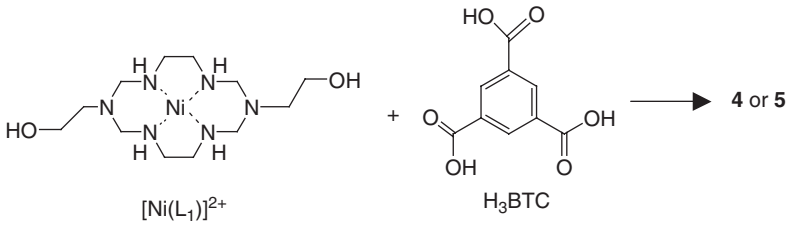

In the crystal structures of **4** and **5**, each Ni(II) macrocyclic complex binds two BTC^{3-} in the *trans* position and each BTC^{3-} is coordinated with three Ni(II) macrocyclic units to construct a 2D layer. The formation of different cavity shapes in **4** and **5** is attributed to the different coordination modes of the BTC^{3-} anion. The BTC^{3-} coordinates metal ions via C_1 symmetry in **4**, while it coordinates metal ions via C_3 rotational symmetry in **5**. The layers are interconnected by the

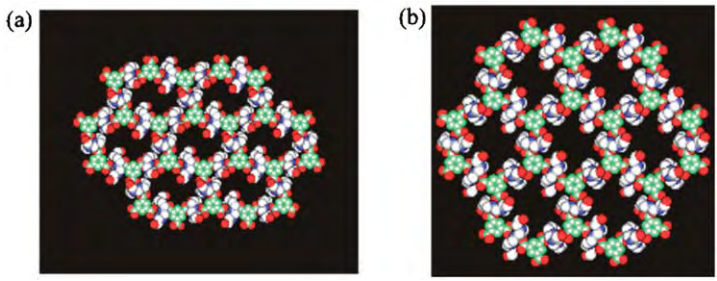

FIG. 4. CPK representations of the 2D layers for (a) $[Ni(L_1)]_3[BTC]_2 \cdot 18H_2O$ (**4**) and (b) $[Ni(L_1)]_3[BTC]_2 \cdot 14H_2O \cdot 2pyr$ (**5**).

hydrogen-bonding interactions between the hydroxyl pendants of the macrocycle in a particular layer and the secondary amines of the macrocycle located in the neighboring layers, which results in 3D structures generating 1D channels. The symmetrical binding mode of BTC^{3-} in **5** is induced by the π–π interactions of the included pyridine molecules with the benzene rings of BTC^{3-} anions in the host layers. The effective cavity sizes of **4** and **5** with the consideration of van der Waals surfaces are $\sim 6.7 \times 13$ and $11.4 \times 11.4\,\text{Å}^2$, respectively.

Solids **4** and **5** are stable up to 190°C and 200°C, respectively. The XRPD patterns for the desolvated solids indicate the structural changes that occur on the removal of guest molecules when compared with those of the as-prepared samples. The distance between the layers might change due to the removal of the guest molecules.

In **4** and **5**, the macrocyclic complex acts as a bifunctional building block that involves coordination of ligands as well as interlayer hydrogen-bonding interactions in order to result in a 3D structure from the 2D network. In particular, the results indicate that even a partial change in the guest molecules affects the topology of the host structure in the self-assembly of metal and organic building blocks.

(b) Self-assembly of $[Ni(L_2)]^{2+}$ and BTC^{3-} (*9*). A 3D network $\{[Ni(L_2)(H_2O)_2]_3[BTC]_2\}_n \cdot 24nH_2O$ (**6**) is assembled from $[Ni(L_2)]^{2+}$ and BTC^{3-}. The $[Ni(L_2)]^{2+}$ complex binds water molecules at the axial sites (*23*), which form hydrogen bonds with the carboxylate oxygen atoms of BTC^{3-}.

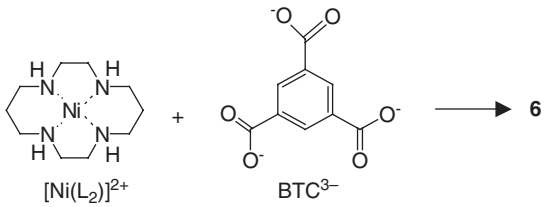

In **6**, each Ni(II) macrocyclic complex coordinated with water molecules forms hydrogen bonds with two BTC^{3-} units in the up and down directions with respect to the macrocyclic plane, and each BTC^{3-} interacts with three Ni(II) units. Thus, the positively charged macrocyclic complex layers and negatively charged organic layers are alternately packed closely (3.70 Å), leaving no open spaces on the *side* directions (Fig. 5). The network forms 1D channels with honeycomb apertures in a direction perpendicular to the 2D layers. The effective window size of the honeycomb channels is 10.3 Å (in diameter), as measured from the distance between the van der Waals surfaces of the opposing macrocyclic walls.

The TGA data for **6** indicates a loss in weight at 54, 85, and 135°C, which correspond to the loss of twelve simple guest molecules, twelve hydrogen-bonded water guest molecules, and two coordinated water

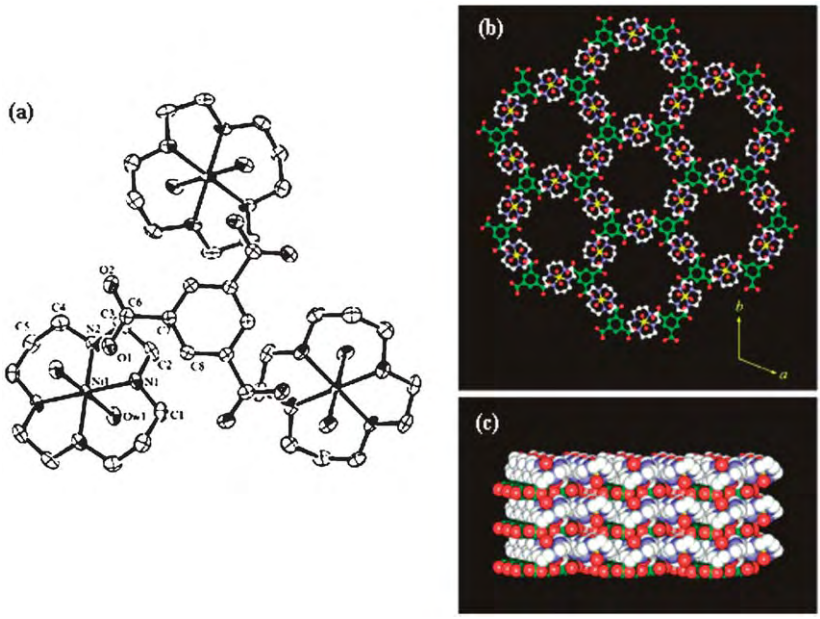

FIG. 5. X-ray structure of **6**. (a) An ORTEP drawing of the asymmetric unit. (b) View of the *ab* plane. Water molecules included in the channels are omitted for clarity. (c) CPK representation of the *ac* and *bc* planes.

molecules, respectively, per formula unit. The compound is stable up to 210°C. When the solvent guest molecules are removed, the X-ray diffraction (XRD) pattern of the dried solid exhibits a deformed framework structure. However, when the dried solid is suspended in water for 5 min, the same XRD pattern as that of the original crystal (**6**) is regenerated. The dried solid of **6** is used to differentiate glucose and maltose, as discussed in Section IV.B.

(c) Self-assembly of $[Ni(L_3)]^{2+}$ and BTC^{3-} (10). When the macrocycle of the metal building block was changed from L_2 to L_3 in the self-assembly with BTC^{3-}, $[Ni(L_3)]_3[BTC]_2 \cdot 18H_2O$ (**7**), whose network structure is different from **6**, was formed (Fig. 6).

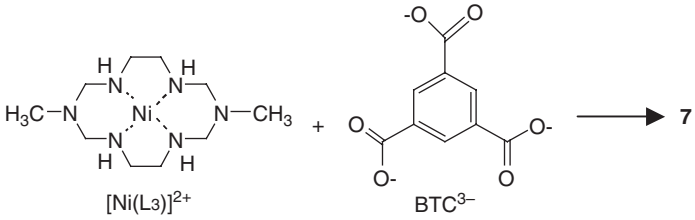

The azacyclam complex $[Ni(L_3)]^{2+}$ exhibits a considerably smaller equilibrium constant (K) when compared with $[Ni(L_2)]^{2+}$ for water

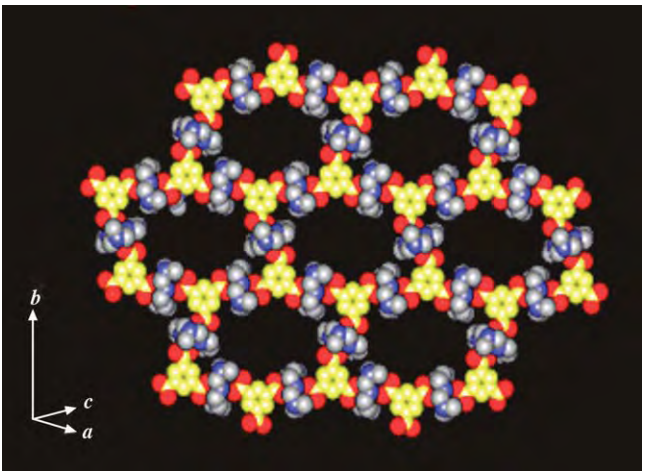

FIG. 6. A CPK representation showing the top view of a 2D layer of $[Ni(L_3)]_3[BTC]_2 \cdot 18H_2O$ (**7**).

binding (*23*), and the self-assembly between $[Ni(L_3)]^{2+}$ and BTC^{3-} in DMF/H_2O leads to the direct coordination of carboxylate groups of BTC^{3-} to the Ni(II) ion, which results in a 2D network with brick-wall cavities. The solid is insoluble in any solvent except H_2O. The accessible void of the channel is $12.5 \times 6.8\,\text{Å}^2$ after taking into consideration of the van der Waals surfaces. The apohost of **7** is thermally stable up to 240°C. A few lines in the XRPD pattern of **7** are slightly broadened when crystal **7** is heated at 100°C for 1 h, but their positions remain unaltered. When water vapor is diffused into the dried solid of **7**, the same XRPD pattern as that of the original crystal is regenerated.

(d) Self-assembly of Ni(II) hexaaza macrocyclic complex having pyridyl pendants ($[Ni(L_4)]^{2+}$) with cis,cis-1,3,5-cyclohexanetricarboxylate (CTC^{3-}) (*8*). The self-assembly of $[Ni(L_4)]^{2+}$ with H_3CTC in pyridine and TEA results in the 3D open frameworks $[Ni(L_4)][H_2CTC]_2 \cdot 4H_2O$ (**8**) and $[Ni(L_4)]_3[CTC]_2 \cdot 16H_2O$ (**9**), respectively, depending on the degree of deprotonation of H_3CTC.

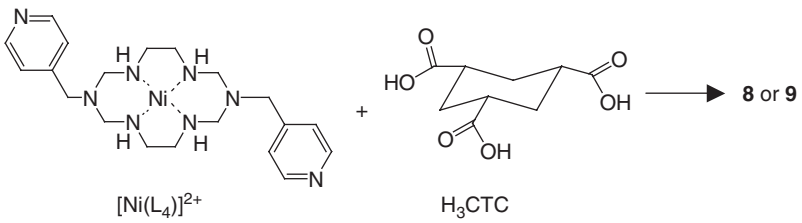

Solid **8** consists of a belt-like 1D chain with rectangular synthons (Fig. 7). The 1D chains are linked together by means of lattice water molecules by the hydrogen-bonding interactions, thereby generating

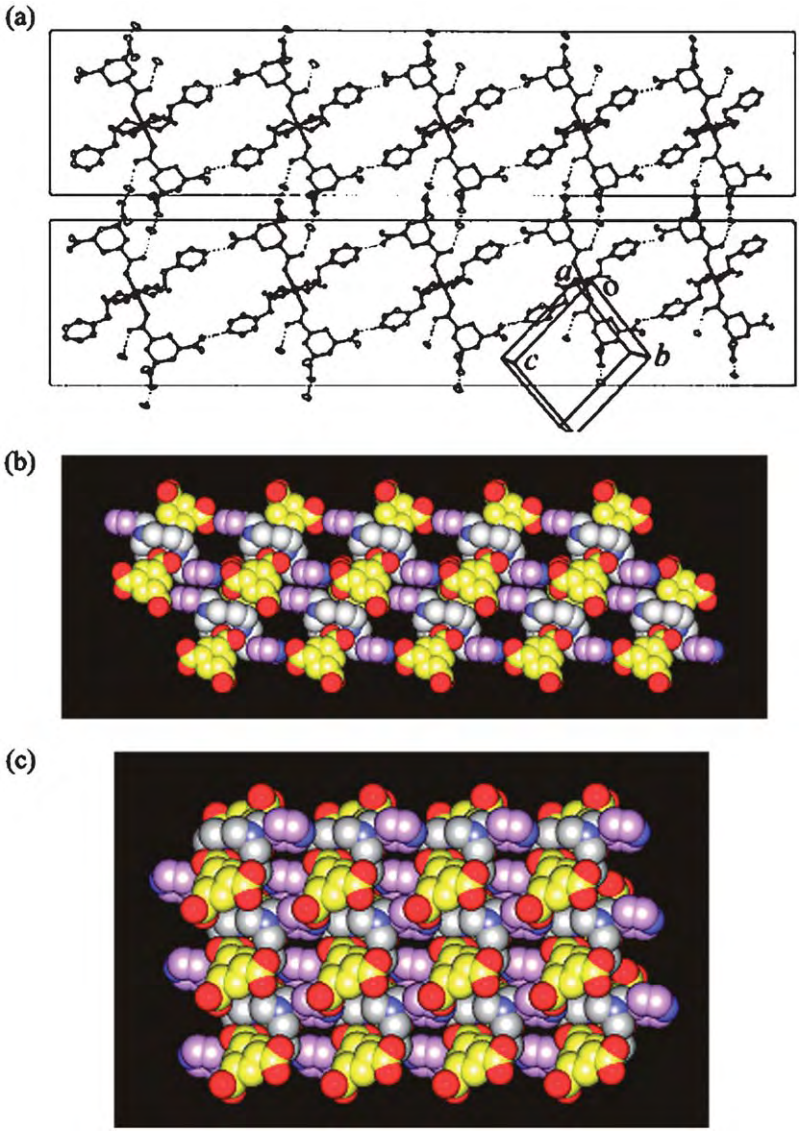

FIG. 7. (a) One-dimensional chains of **8**, which are linked by hydrogen-bonding interactions. Hydrogen bonds are indicated by dashed lines. (b) A CPK representation showing offset π–π stacking interactions between the two 1D chains of **8**. The effective void size of **8** is about $3.8 \times 9.8\,\text{Å}^2$. (c) A CPK representation of the 3D structure of **8**.

2D networks, which are further connected to one another by the offset π–π stacking interactions between the pendant pyridine rings to result in a 3D structure generating the channels. Solid **9** consists of puckered honeycomb-like sheets in which the pendant pyridine rings are involved in the hydrogen-bonding and edge-to-face π–π interactions

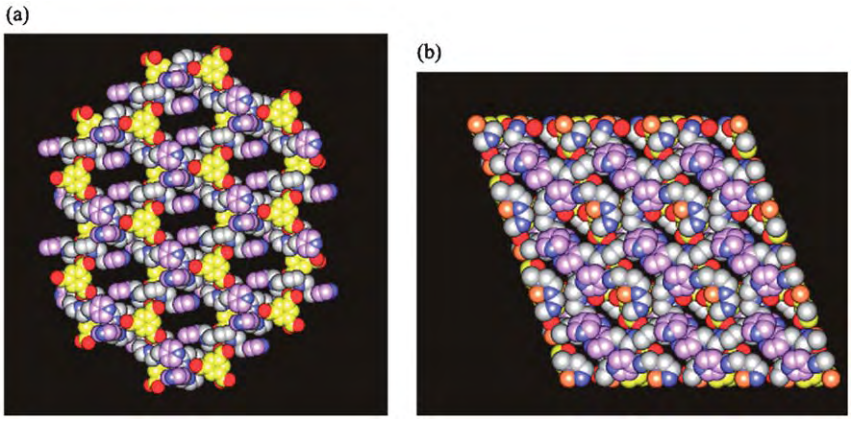

FIG. 8. (a) A CPK representation of a single layer of **9**. The effective size of a void is about $4.0 \times 8.5\,\text{Å}^2$. (b) A CPK view of the packed structure of **9** showing the channels.

(Fig. 8). Between the layers, the pendant pyridine rings belonging to the neighboring layers participate in the offset π–π stacking interactions, which result in a 3D network structure. Solids **8** and **9** are insoluble in all solvents. The XRPD patterns indicate that the frameworks of **8** and **9** are deformed when the guest water molecules are removed, but they are restored upon the rebinding of water.

(e) Self-assembly of $[Cu(L_3)]^{2+}$ with BTC^{3-} (7). The construction of a water column or an organic network is possible by the assembly of coordination polymer network. A coordination polymer $[Cu(L_3)]_3[BTC]_2 \cdot 18H_2O$ (**10**) was constructed by the self-assembly of Cu(II) complex of hexaaza macrocycle L_3 ($L_3 = C_{10}H_{26}N_6$) with BTC^{3-} in $DMSO/H_2O$.

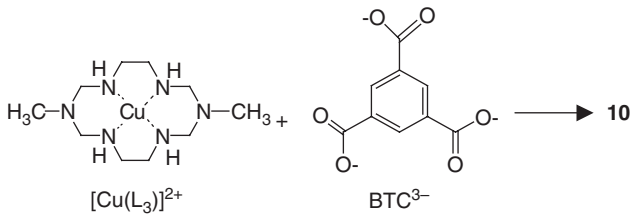

The X-ray crystal structure of **10** indicates that 2D coordination polymer layers with honeycomb cavities (effective size: 8.1 Å) are formed, and these layers are packed to generate 1D channels in a direction perpendicular to the 2D layers. In the channels of **10**, hexagonal water columns are formed, which cannot exist in the bulk water state. By the treatment of **10** with an aqueous solution of phenol, a hybrid solid $[Cu(L_3)]_3[BTC]_2 \cdot 9PhOH \cdot 6H_2O$ (**11**) was assembled (Fig. 9). In **11**, highly ordered 2D noncovalent phenol layers are formed

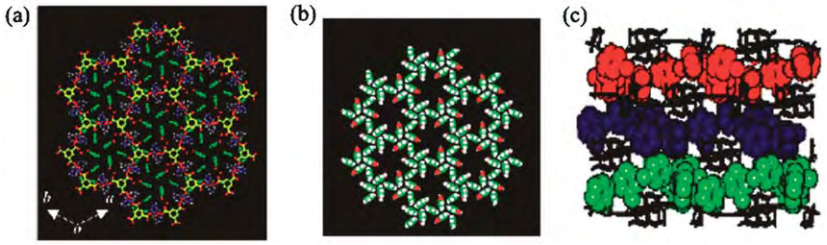

FIG. 9. X-ray structure of $[Cu(L_3)]_3[BTC]_2 \cdot 9PhOH \cdot 6H_2O$ (**11**). (a) Top view. (b) Noncovalent phenol layer. (c) Side view showing alternately packed host frameworks and phenol layers.

by the edge-to-face π–π interactions between the phenol molecules, and they are alternately packed with the coordination polymer host layers in the crystal lattice.

B.2. Interpenetrating 2D networks

(a). Self-assembly of $[Ni(L_2)]^{2+}$ and 1,3,5-tris[2-(4-carboxylphenyl)-1-ethynyl]benzene ($TCPEB^{3-}$) (36). In most cases, macrocyclic complexes provide non-interpenetrating coordination polymer networks. However, the self-assembly of macrocyclic complexes with a considerably larger tricarboxylate ligand, results in an interpenetrating or interwoven structure. The self-assembly of $[Ni(L_2)]^{2+}$ complex with $TCPEB^{3-}$ in a mixture of DMF/H_2O/pyridine (1.5/2/3, v/v) results in the 2D (6,3) network $[Ni(L_2)]_3[TCPEB]_2 \cdot 6pyr \cdot 4H_2O$ (**12**).

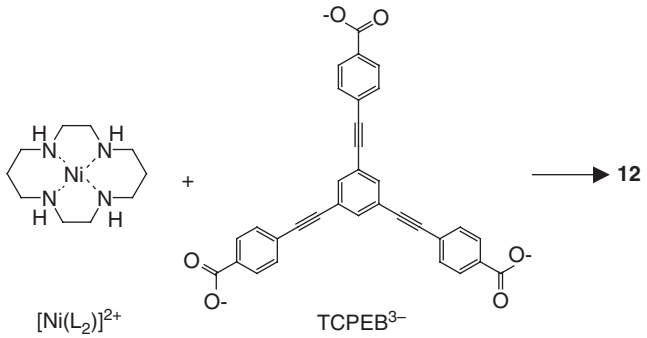

12 is expected to have honeycomb cavities with diameters of ~49–53 Å, which are significantly greater than those in the 2D networks constructed from BTC^{3-}. However, the cavities are extremely large and the 2D layers are triply interwoven, thereby generating smaller triangular voids of dimensions 23.6 Å × 23.5 Å × 23.7 Å with an effective cavity size ~18.4 Å × 14.7 Å × 9.5 Å. In this structure, two layers are not interpenetrated, but the third layer interweaves them resulting in 3-borromean layers (Fig. 10).

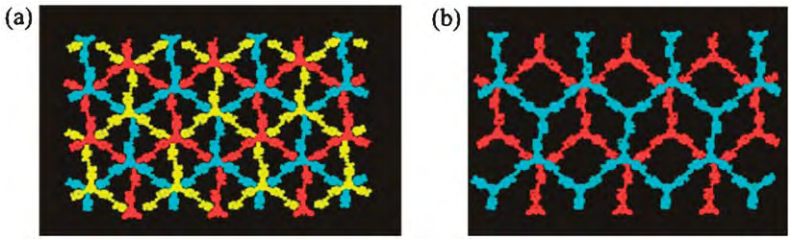

FIG. 10. X-ray structure of $[Ni(L_2)]_3[TCPEB]_2 \cdot 6pyr \cdot 4H_2O$ (**12**). (a) Triply interwoven structure of **12**. (b) Any two layers of triply interwoven structure in **12** are not interpenetrated.

Solid **12** contains 35% free volume of the crystal volume, as estimated by PLATON (*29*), and exhibits thermal stability up to 300°C. Although the free H_3TCPEB ligand itself emits fluorescent light, the emission is quenched in **12** due to the paramagnetic Ni(II) ions that are coordinated to the carboxylate groups of $TCPEB^{3-}$.

B.3. Self-assembly of pillared bilayer network (17)

A pillared bilayer network $[Ni_2(L_5)]_3[BTC]_4 \cdot 6pyr \cdot 36H_2O$ (BOF-1, **13**; $L_5 = C_{26}H_{52}N_{10}$) was assembled from Ni(II) bismacrocyclic complex $[Ni_2(L_5)]^{4+}$ and BTC^{3-} (Scheme 4). Since each Ni(II) ion of the macrocyclic complex is involved in the formation of the 2D network, two 2D layers are formed. The xylyl groups of the bismacrocyclic complexes act as the pillars linking the two 2D layers. The X-ray structure

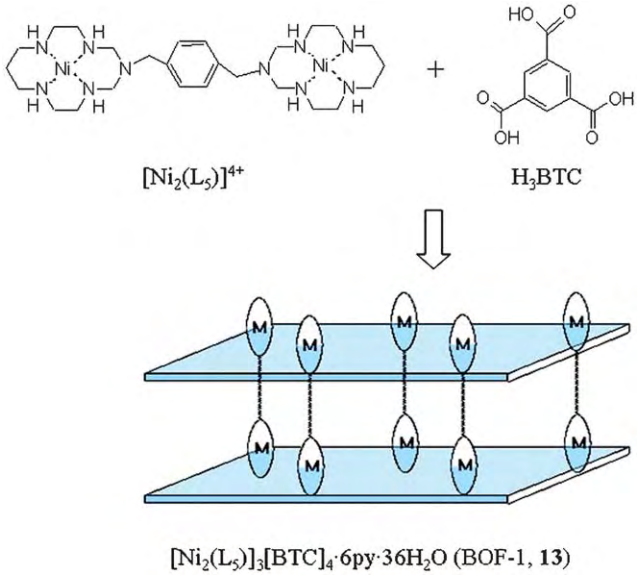

SCHEME 4. Construction of pillared bilayer network.

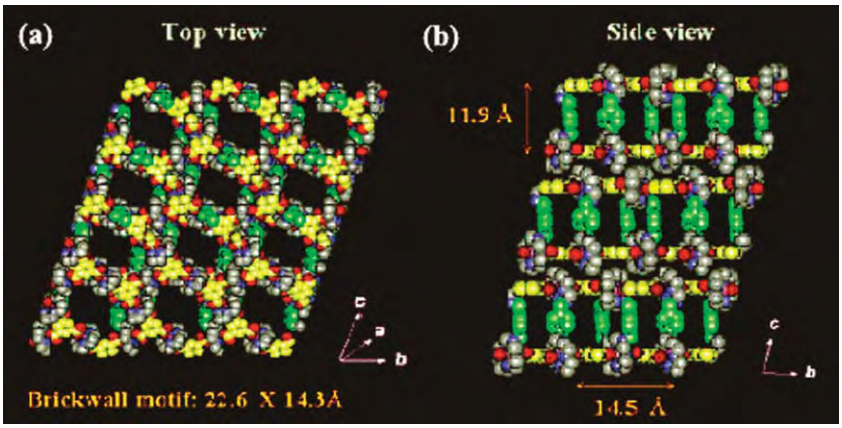

FIG. 11. X-ray structure of BOF-1 (**13**). (a) Top view showing 2D layers of brick-wall motif. (b) Side view showing pillared bilayer structure [thickness of bilayer, 11.91(1) Å].

of **13** (Fig. 11) shows that the 2D layers have brick-wall cavities with a size of 23 Å × 14 Å, and they are linked by xylyl pillars. Solid **13** contains 3D channels. The interlayer distance is ~11.9 Å and the side window is 14.5 Å. The void volume of **13** is 61%, which is considerably greater than that of zeolites.

When the single crystal of **13** is dried in air and then heated at 75°C for 1.5 h, $[Ni_2(L_5)]_3[BTC]_4 \cdot 30H_2O$ (**13-1**) and $[Ni_2(L_5)]_3[BTC]_4 \cdot 4H_2O$ (**13-2**) are formed with the retention of the single crystallinity. The X-ray structures of **13-1** and **13-2** reveal a sponge-like dynamic behavior of the bilayer framework that reduces the interlayer distance in response to the amount of guest molecules, as described in Section V.B. When **13** is immersed in pyridine and benzene, the guest molecules were exchanged with the retention of the single-crystal nature, resulting in $[Ni_2(L_5)]_3[BTC]_4 \cdot 20pyr \cdot 6H_2O$ (**13-3**) and $[Ni_2(L_5)]_3[BTC]_4 \cdot 14benzene \cdot 19H_2O$ (**13-4**), respectively. Solid **13-2** shows a function to differentiate various alcohols, as described in Section IV.B. Furthermore, crystal **13** reacts with I_2 via a single-crystal-to-single-crystal transformation to produce $[Ni_2(L_5)]_3[BTC]_4(I_3)_4 \cdot nI_2 \cdot 17H_2O$ (**13-5**) that consists of a positively charged framework incorporating Ni(III) and Ni(II) ions and the channels including I_3^- and I_2, as described in Section VI.A.

C. 3D STRATEGIES

C.1. Self-assembly of $[Ni(L_2)]^{2+}$ with tetrakis[4-(carboxyphenyl)oxamethyl]-methane (TCM^{4-}) (37)

If tetrahedral building blocks are linked by the linear linkers, a diamondoid network with adamantanoid cages would be formed. The

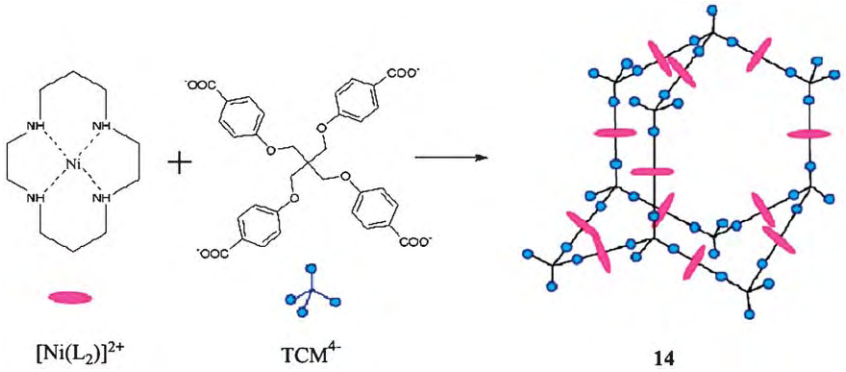

SCHEME 5. Construction of 3D diamondoid network.

self-assembly of $[Ni(L_2)](ClO_4)_2$ and Na_4TCM in DMF/H_2O (1:1, v/v) results in the diamondoid network $[Ni(L_2)]_2[TCM] \cdot 2DMF \cdot 10H_2O$ (**14**) (Scheme 5). In **14**, each Ni(II) ion is coordinated with two different TCM^{4-} ligands at the axial sites to exhibit a distorted octahedral coordination geometry, and each TCM^{4-} ligand binds four $[Ni(L_2)]^{2+}$ complexes in a tetrahedral manner, which gives rise to a diamondoid network comprising large adamantanoid cages with dimensions of 49.2 Å × 50.8 Å × 44.3 Å (the longest intracage distances). Such a large cavity induces an unusual 8-fold interpenetration of the networks in the [4+4] mode (Fig. 12). In other words, four networks form a set and the other four networks form the other set, and they are interpenetrated. Occasionally, interpenetration becomes an impediment to

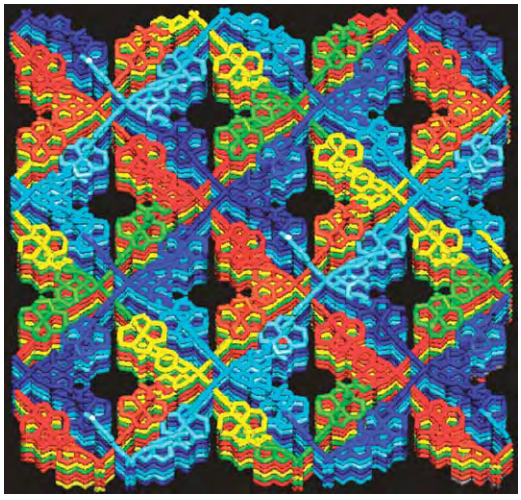

FIG. 12. X-ray structure of **14**. The 8-fold interpenetrating diamondoid networks in the [4+4] mode, which generate 1D channels (effective window size, 4.7 × 6.7 $Å^2$).

achievement of large-sized channels or cavities, although it sometimes results in a permanent porosity in the structure (*38,39*). Despite the high-fold interpenetration, compound **14** generates 1D channels with an effective window size of 6.7 Å × 4.7 Å. The network exhibits a flexible behavior: it becomes nonporous on the removal of the guest molecules that occupy the channels, as verified by the N_2 gas sorption measurement. However, the open structure is restored when the desolvated solid is immersed in a mixture of H_2O/DMF (1:1, v/v) for 5 min, as evidenced by the XRPD patterns.

III. Porosity

A. Types of Gas Sorption Isotherms

When the solid adsorbs a significant amount of gases, it is regarded as a porous material. When the solid adsorbs gas, its porosity is defined as the ratio of volume of open spaces to the total volume of the solid, and this value is estimated from the gas sorption data. Table I shows the classification of pore types according to the pore size.

The BET (Brunauer–Emmett–Teller) or Langmuir surface areas, pore volume, and pore size can be estimated from the gas sorption data. A porous material is considered as an adsorbent and the gas as an adsorbate. Adsorption occurs due to the forces between the adsorbent and the adsorbate. Based on the interacting forces, there are two types of sorptions: physisorption and chemisorption. In physisorption, van der Waals forces cause the condensation of vapor to liquid, while chemisorption involves a covalent bond formation between the adsorbent and the adsorbate.

According to the pore size and the adsorption force, the gas sorption isotherms can be classified into six types (Fig. 13) (*40,41*). Type I isotherm curves are exhibited by microporous solids, zeolites, molecular sieves, and activated carbon. This curve is characterized by a high knee at the initial step leading to saturation, where the plateau indicates the adsorbed amount. A Type I isotherm curve implies that the adsorbate forms a monolayer in the pore. Type II isotherm is exhibited by the unrestricted monolayer–multilayer adsorption on nonporous or macroporous adsorbents. Type III and V isotherm curves are characterized by convexity towards the P/P_o axis, beginning at the origin,

TABLE I

Classification of Pores (*40,41*)

	Width
Micropores	Less than ~20 Å (2 nm)
Mesopores	Between ~20 and ~500 Å (2 and 50 nm)
Macropores	More than ~500 Å (50 nm)

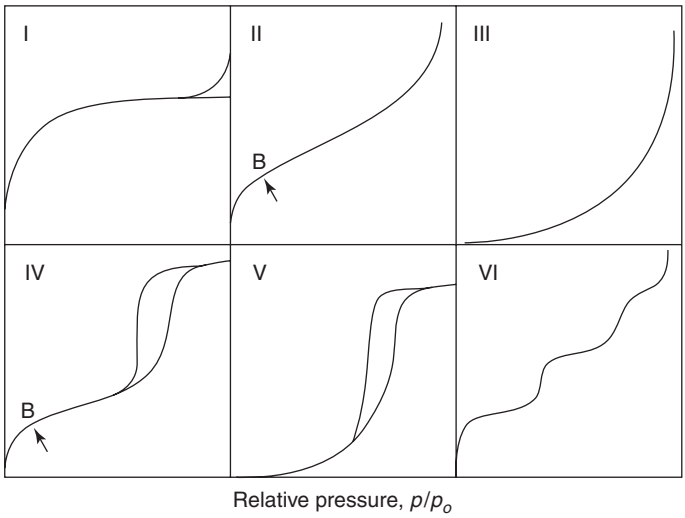

FIG. 13. Various types of gas sorption isotherms (*40,41*).

which implies a weak adsorbent–adsorbate interaction. Type III isotherms are seldom encountered. A well-known example is the adsorption of water vapor on nonporous carbon. Type IV and Type V isotherms are the characteristics of mesoporous adsorbents. The initial differences in P/P_o are due to the difference in the strength of the adsorbent–adsorbate and the adsorbate–adsorbate interactions. Type VI isotherms are associated with capillary condensation in the mesopores, indicated by the steep slope observed at a higher value of P/P_o. The initial part of the Type VI isotherm follows the same path as that of Type II.

The adsorption mechanism of a gas adsorbate on a solid is expressed by the Langmuir equation or the BET model. The former is with regard to the monolayer adsorption of the adsorbate and the latter is with regard to multilayer adsorption (*10,40,41*). The surface area, pore volume, and pore distribution of microporous materials are estimated using the Langmuir equation, Dubinin–Radushkevich isotherm equation, and Horvath–Kawazoe pore size distribution equation, respectively. The Dubinin–Radushkevich equation provides a reliable assessment of the total micropore volume when all the pores are narrow, thereby resulting in a primary micropore filling. The Horvath–Kawazoe method estimates the pore size distribution of a microporous solid from the low relative pressure region of the adsorption isotherm.

Table II shows the various adsorbates with their measuring temperatures and molecular areas (A_M). For evaluation of both the surface area and the pore size distribution of a solid from a single isotherm, N_2 gas is the most suitable adsorbate. For the determination of only the surface area, Ar provides an alternative, although Ar cannot be used for the assessment of pore size distribution at temperatures around

TABLE II

VALUES OF MOLECULAR AREA A_M (*40*)

Adsorbate	A_M in Å^2 (T/K)
N_2	16.2 (78)
Kr	15.2,[a] 20.8[b] (78)
	29.7,[a] 43.4[b] (195)
Butane	32.1,[a] 46.9[b] (273)
	24.7,[a] 37.5[b] (195)
Freon-21	26.4,[a] 40.1[b] (273)
Ar	13.8 (from liquid, 87.29)
	16.6 (nonporous solid, 78)
Xe	18.2–25 (77 K–90 K)
	17.0 (on metal)
Water	20(298)
Benzene	43
O_2	14.3 (77.3 K), 15.4 (90 K)
CO_2	14.1∼22.0 (195 K)
	20.6 (carbon black)
	19.1 (porous alumina)

[a]Values obtained from the equation of $A_M = 1.091(M/\rho_L L)^{2/3}$ (ρ_L = density in the liquid phase).
[b]Values revised experimentally by comparison of the surface area of various materials.

77 K. If the specific surface area is very low ($< 5\,m^2\,g^{-1}$), Kr also offers considerably high precision in the actual measurement of adsorption.

B. N_2 GAS SORPTION OF VARIOUS COORDINATION POLYMER SOLIDS

The gas sorption should be measured on the dried solid of the open framework. However, the open framework often collapses and exhibits non-porosity when the guest molecules included in the pores are removed.

Solids **2** and **3** that are constructed by the packing of the linear coordination polymer chains exhibit a permanent porosity. They adsorb N_2 gas and exhibit reversible Type I isotherms (Fig. 14). The Langmuir surface area and pore volume are $817\,m^2\,g^{-1}$ and $0.37\,cm^3\,cm^{-3}$, respectively, for **2**, and $691\,m^2\,g^{-1}$ and $0.45\,cm^3\,cm^{-3}$, respectively, for **3**. These are compared favorably with those of zeolites (pore volume: 0.18–0.47 $cm^3\,cm^{-3}$) (*42*). The data are compared with those of the other porous metal-organic frameworks that were prepared from the solvothermal reactions of free metal ions and organic building blocks (Table III).

Solids **4–13**, which are formed of 2D layers, do not exhibit porosity even though they contain channels or pores. This is probably because the stacking of the layers is deformed upon desolvation. Solid **14** with an eight-fold interpenetrating 3D diamondoid network also becomes nonporous upon desolvation.

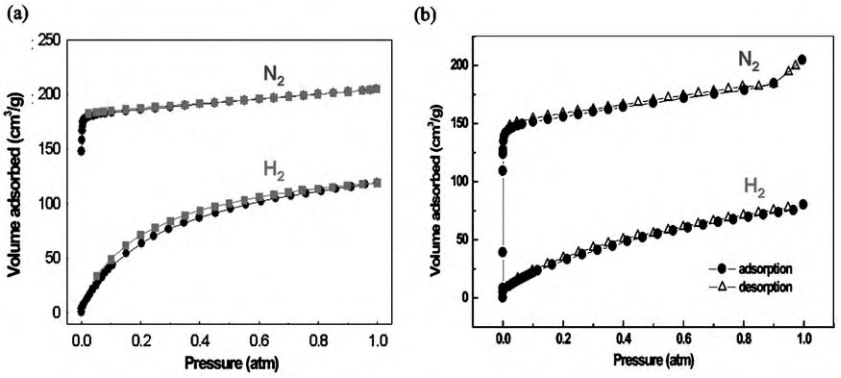

FIG. 14. N_2 and H_2 gas sorption isotherms for (a) **2** and (b) **3**.

TABLE III

POROSITY OF VARIOUS COORDINATION POLYMERS[a]

Compound	Cavity size (Å), (void volume, %)	Surface area ($m^2 g^{-1}$), (pore volume)	Thermal Stability (°C)	Ref.
$[Ni(L_2)(BP_YDC)]$ (**2**)	5.8 –	817 (0.37 cm3 cm−3)	300	*6*
$[\{Ni(L_3)_3(BPDC)_3]$ (**3**)	7.3 –	691 (0.45 cm3 cm−3)	250	*20*
$[Zn_4O(NTB)_2]$	5.0 (39.7)	1121 (0.51 cm3 cm−3)	430	*46*
$[Cu_3(BTB)_2(H_2O)_3]$	9.88–11.85, 16.4 (67)	1502 (0.53 cm3 g−1)	250	*38*
$[Zn_4O(BTC)_3]$	5.1, 15.1 (55–61)	2900 (0.61–0.54 cm3 g−1)	300	*43*
$[Zn_4O(BTB)_2]$	10.8 (81)	4500 (0.69 cm3 cm−3)	350	*41*
$[Cu_3(BTC)_2(H_2O)_3]_n$	9 (41)	918 (0.333 cm3 g−1)	240	*44*
$[Cu_2(ATC)]$	6.5 (50)	560 (0.20 cm3 g−1)	260	*45*

[a]NTB = 4,4′,4″-nitrilotrisbenzoic acid, BTB = 4,4′,4″-benzene-1,3,5-triyl-tribenzoic acid, ATC = 1,3,5,7-adamantane tetracarboxylic acid.

C. H_2 GAS SORPTION OF VARIOUS COORDINATION POLYMER SOLIDS

Compounds that adsorb 6.0 wt% of H_2 gas at room temperature can be practically employed as H_2 gas storage materials with respect to U. S. Department of Energy guidelines. Porous materials **2** and **3** that are constructed of 1D coordination polymer chains incorporating Ni(II) macrocyclic complexes adsorb H_2 gas. Solid **2** adsorbs H_2 gas up to 1.1 wt% at 77 K and 1 atm. Solid **3** adsorbs H_2 gas up to 0.72 wt% of H_2 gas at 77 K and 1 atm. They are expected to adsorb less amount of H_2 gas even under high pressures at room temperature. In addition, it stores much less amount of H_2 gas as compared with that (1.9 wt%) of $[Zn_4(O)(NTB)_2]$, which has been prepared in our laboratory by the

TABLE IV

H_2 Gas Sorption Data of Various Coordination Polymers[a]

Compound[b]	H_2 sorprtion capacity (wt%)	Number of H_2 molecule/formula unit	Ref.
$[Ni(L_2)(BPyDC)]$ (**2**)	1.1	3.2	*6*
$[Ni(L_3)_3(BPDC)_3]$ (**3**)	0.72	5.7	*34*
$[Zn_4(O)(NTB)_2]$	1.9	9.7	*46*
$[Zn_4(O)(BDC)_3]$	1.3	5.0	*47*
$[Zn_4(O)(NDC)_3]$	1.5	6.9	*47*
$[Zn_4(O)(HPDC)_3]$	1.6	9.3	*47*
$[Zn_4(O)(TMBDC)_3]$	0.89	4.2	*47*
$[Zn_4(O)(BTB)_2]$	1.25	7.1	*47*
$Ni_2(bipy)_2(NO_3)_4\cdots C_2H_5OH$	0.66	2.7	*48*
$Ni_2(bipy)_2(NO_3)_4\cdots CH_3OH$	0.99	4.1	*48*

[a]At 77 K and 1 atm of H_2.

[b]bipy = 4,4′-bipyridyl, NTB = 4,4′,4″-nitrilotrisbenzoic acid, NDC = naphthalene-2,6-dicarboxylate, HPDC = 4,5,9,10-tetrahydropyrene-2,7-dicarboxylate, TMBDC = tetramethyl- benzene-1,4-dicarboxylate, BTB = benzene-1,3,5-tribenzoate.

solvothermal reaction of Zn^{2+} ion and 4,4′,4″-nitrilotrisbenzoic acid (H_3NTB) in DEF (*46*). The H_2 adsoprtion data of **2** and **3** are compared with those of some other porous metal-organic frameworks that have been prepared from the solvothermal reactions of free metal ions and organic building blocks in Table IV.

IV. Guest Binding Properties

Porous coordination polymers capable of the selective sorption of guest molecules would be useful as molecular filters or for molecular separation. Some porous coordination polymers exhibit the selective binding of guest molecules such as D-glucose, metal complexes, alcohols, and aromatic compounds (*6–10,43,49*).

A. Estimation of Formation Constants (K_f) of the Host Solid with Guest Molecules

In open framework solids, the voids or channels are filled with guest molecules (in most cases with solvent molecules) when the coordination polymers are prepared by the self-assembly in the solvent. This is because the solids tend to form condensed materials. If the open space is maintained even after the guest molecules are removed, the host solid can bind other guest molecules depending on the size and chemical environment of the voids. The guest molecules could be gases, solvent molecules, organic compounds, and even transition metal complexes. They are recognized by the cavities due to the intermolecular interactions such as hydrogen bonds and/or π–π stacking interactions. The

molecular-scale cavities of the hosts can potentially serve as storage compartments (*50*), miniaturized reaction chambers (*51*), and catalytic environments (*52*) in a manner that is similar to the ones used for (*53*) more well-established zeolites (*42*).

For the host–guest complex (BS · G) formed between a binding site (BS) of the insoluble host and a guest molecule (G), the formation constant K_f can be defined as k_{ad}/k_{de} [Eq. (1)] by using the analogy with the Langmuir isotherm for gas adsorption on solid surfaces (*6–10,45,54*).

The plots of the concentration of G bound to BS ([BS · G]) against [G] should be prepared. Then, K_f and $[BS]_o$ values can be estimated by the analysis of the data according to Eq. (2). In this experiment, the total concentration of the guest ($[G]_o$) should be varied such that the θ values (degree of saturation) are maintained in the range from 20 to 80%.

$$BS + G \underset{k_{de}}{\overset{k_{ad}}{\rightleftharpoons}} BS \cdot G$$

$$K_f = \frac{k_{ad}}{k_{de}} = \frac{[BS \cdot G]}{[BS][G]} \tag{1}$$

If θ is defined as the fractional coverage,

$$\theta = \frac{[BS \cdot G]}{[BS]_o} = \frac{[G]}{([G] + 1/K_f)}$$

$$\text{Then, } [BS \cdot G]/\omega = \frac{([BS]_o/\omega)[G]}{([G] + 1/K_f)} \tag{2}$$

where ω is the amount of host solid per unit volume of the solution ($g\,L^{-1}$) and $[BS]_o/\omega$ is the binding capacity for the guest per gram of the host.

An accurately measured amount of the dried host solid is immersed in an appropriate solvent containing guest organic molecules at a fixed temperature until equilibrium is attained. The solvent selected should not interact with the host solid. The time required to attain equilibrium for the host–guest complex formation is estimated by monitoring the change in the guest concentration using spectrophotometry or the gas chromatography (GC) method. The concentration changes in the guest molecules are analyzed using any of the methods mentioned above and then fitted into Eq. (2).

B. Selective Guest Binding Properties of Various Framework Solids

The dried solid of **2** is used to differentiate various organic guest molecules such as EtOH, PhOH, pyridine, and benzene in an isooctane medium (Fig. 15). It binds EtOH and PhOH with high affinity by forming hydrogen bonds with the carbonyl group exposed on the channel surface of the host, and it less satisfactorily binds aromatic guests (Table V).

The dried solid of **6** is used to differentiate D-glucose and maltose due to the size fit of glucose into the channels (Fig. 16) (*9*). In methanol containing 5% water at 30°C, host **6** binds D-glucose with $K_f = (1.38+0.01) \times 10^4$ and by 0.405–0.004 mol% with respect to the number of glucose relative to the binding sites for the formula unit of

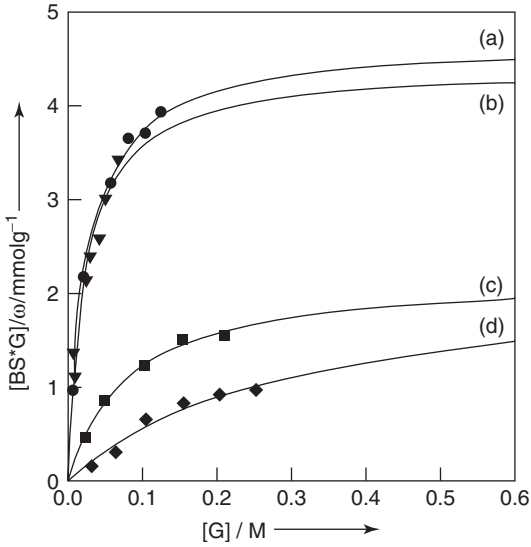

Fig. 15. Binding of host solid **2** with organic guests: (a) EtOH (●), (b) PhOH (▼), (c) pyridine (■), and (d) benzene (◆) in isooctane medium.

TABLE V

Guest Binding Data for Dried Solid of **2** (*6*)

Guest	K_f, M^{-1}	$[BS]_0/\omega$ (mmol g^{-1})	Guest inclusion capacity (mol)/ unit formula of host solid
EtOH	41.1 ± 3.4	4.65 ± 0.11	2.33
PhOH	42.6 ± 10.7	4.41 ± 0.44	2.21
Pyridine	12.9 ± 1.8	2.18 ± 0.12	1.09
Benzene	3.37 ± 1.73	2.31 ± 0.71	1.11

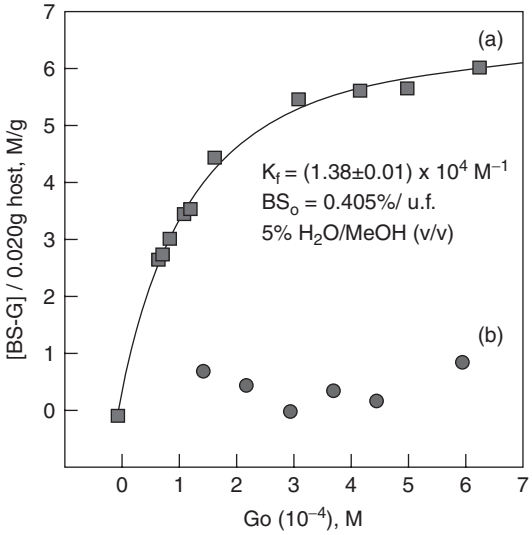

FIG. 16. Selective binding of **6** with (a) D-glucose (■) vs. (b) maltose (●) in water medium.

the host. The small number of binding sites occupied by glucose suggests that the inclusion of a glucose molecule effectively blocks successive inclusions of glucose deeper into the channels. In contrast to glucose, the complexation of maltose to the dried host solid of **6** was negligible since maltose is too big to occupy the channel.

Host solid **6** also binds various organic molecules and metal complexes as guests (Table VI) (*10*).

Besides the size effect, host–guest interactions are important in the selective inclusion process. Host solid $[Ni(L_3)]_3[BTC]_2 \cdot 18H_2O$ (**7**) binds PhOH selectively over PhCl and PhBr (Fig. 17 and Table VI) (*10*). The hydrogen-bonding interaction between the host solid and guest molecules plays an important role in the selectivity.

The host solid of $[Cu(L_3)]_3[BTC]_2 \cdot 18H_2O$ (**10**), which is prepared using a similar method as that used for $[Ni(L_3)]_3[BTC]_2 \cdot 18H_2O$ (**7**), binds the guests in the following order: EtOH > MeOH > PhOH (Fig. 18 and Table VII) (*7*). However, the total volume (1533 $Å^3$) of the PhOH inclusions that is estimated by the guest binding curve is considerably greater than the void volume (566 $Å^3$) of the host, indicating that phenol guests must be intercalated between the host layers instead of being included in the channels. The self-assembly in the presence of PhOH offers a 2D open framework with highly ordered 2D noncovalent PhOH networks (**11**), which are alternately packed with the host layers, as shown in Fig. 9.

Host solids **8** and **9** bind $[Cu(NH_3)_4](ClO_4)_2$ in MeCN with the binding constants (K_f) of 210 and 710, respectively, while they do not bind $[Cu(en)_2](ClO_4)_2$ (en = ethylenediamine) (*8*). The dried solids of **8** and

TABLE VI

INCLUSION OF DRIED SOLIDS OF **6** AND **7** WITH VARIOUS ORGANIC AND INORGANIC GUEST MOLECULES (*9,10*)

Host	Guest	Log K_f (M^{-1})	$[BS]_o/\omega$ (mmol g^{-1})	Guest inclusion capacity (mol)/ unit formula of host solid
6	MeOH[a]	1.82 ± 0.11	4.62 ± 0.35	6.00 ± 0.458
	PhOH[a]	–	–	7.6[c]
	THB[a]	2.41 ± 0.21	1.38 ± 0.12	1.79 ± 0.16
	HAP [a]	1.14 ± 0.12	2.91 ± 0.36	3.78 ± 0.46
	$[Cu(NH_3)_4](ClO_4)_2$[b]	2.81 ± 0.03	1.90 ± 0.00	3.30 ± 0.00
	$[Cu(en)_2](ClO_4)_2$[b]	0.98 ± 0.14	3.70 ± 0.90	6.41 ± 0.85
	$[Cu(Ht)_2](ClO_4)_2$[b]	1.57 ± 0.37	0.90 ± 0.50	1.56 ± 0.87
	$[Cu(3,2,3\text{-}N_4)](ClO_4)_2$[b]	0.78 ± 0.65	1.30 ± 1.50	2.25 ± 2.60
7	PhOH[a]	1.58 ± 0.20	4.09 ± 0.61	5.24 ± 0.78[a]

[a]Dried host solids were used in the binding experiment: $[Ni(L_2)(H_2O)_2]_3[BTC]_2$ for **6** and $[Ni(L_3)]_3[BTC]_2$ for **7**.

[b]Host solid as prepared, $[Ni(L_2)(H_2O)_2]_3[BTC]_2 \cdot 24H_2O$ (**6**), was used. en = ethylenediamine, Ht = Histamine 3,2,3–N_4 = *N*,*N*′-bis(3–aminopropye)ethylenediamene.

[c]Estimated from the observed maximum $[BS \cdot G]/\omega$ value.

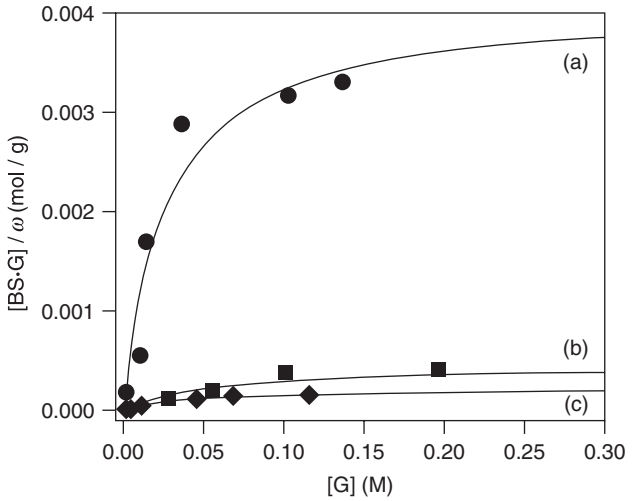

FIG. 17. Binding of host solid **7** with (a) PhOH (●), (b) PhBr (■), and (c) PhCl (◆) in *n*-hexane medium.

9 do not interact with benzene and toluene. However, they can be used to differentiate MeOH, EtOH, and PhOH in toluene, which have K_f values of 42, 14, and 12, respectively, for **8**, and K_f values of 13, 8.2, and 8.9, respectively, for **9**. In terms of the binding sites for guest molecules, the capacity of solid **9** is greater than that of solid **8** (*8*).

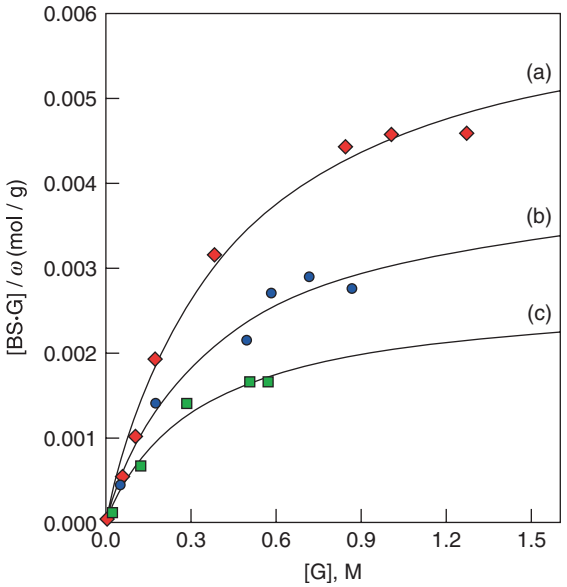

FIG. 18. Binding of host solid **10** with organic guests: (a) PhOH, (b) MeOH, and (c) EtOH in toluene medium.

TABLE VII

BINDING OF HOST SOLID **10** WITH VARIOUS GUEST MOLECULES (*7*)

Guest	K_f (M^{-1})	$[BS]_0/\omega$, (mmol g^{-1})	Guest inclusion capacity (mol)/ unit formula of host solid
PhOH	2.29 ± 0.36	6.48 ± 0.40	10.5
MeOH	2.59 ± 0.90	4.19 ± 0.58	6.78
EtOH	3.02 ± 1.15	2.70 ± 0.46	4.38

The dried solid of **13** is used to differentiate MeOH, EtOH, isopropyl alcohol, and benzyl alcohol in toluene (Fig. 19 and Table VIII). It binds benzyl alcohol the best because of the existence of a phenyl ring in benzyl alcohol, which can interact with the xylyl pillars of the host by π–π interactions (*17,54*).

The desolvated solid of **14** differentiates EtOH, pyridine, and *n*-BuOH, exhibiting different binding capacities (Fig. 20 and Table IX). It does not bind *t*-BuOH. The K_f value for *n*-BuOH is greater than EtOH, implying that hydrophobic interactions between the host and guests are important because the interior of the channel surface is covered with hydrocarbons of the macrocycles (*37*).

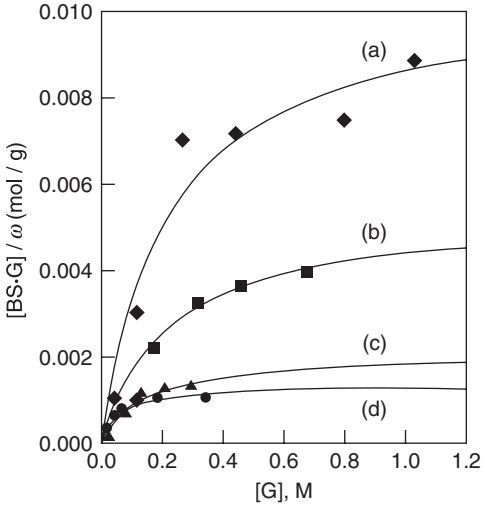

FIG. 19. Binding of dried solid **13** (BOF-1) (powder form) with guest organic molecules: (a) MeOH, (b) EtOH, (c) *iso*-PrOH, and (d) BzOH in toluene medium.

TABLE VIII

GUEST BINDING DATA FOR DRIED BOF-1 (**13**) (*17,54*)

	K_f (M^{-1})	$[BS]_o/\omega$ ($mmol\,g^{-1}$)	Guest inclusion capacity (mol)/ unit formula of host solid
MeOH	4.61 ± 1.82	10.5 ± 1.34	29.1
EtOH	4.55 ± 1.31	5.35 ± 0.50	14.8
iso-PrOH	6.49 ± 3.88	2.11 ± 0.58	5.84
BzoH	18.8 ± 8.54	1.31 ± 0.19	3.62

V. Single-Crystal-to-Single-Crystal Transformations and Sensing Properties

Some coordination polymers exhibit crystal-to-crystal transformations without a change in their framework structure upon guest removal (*2,33,44,45,55–62*), whereas some exhibit a change in their structures upon guest removal or guest exchange with the retention of their single-crystallinity (*43,46,63–68*), which is very important for the development of certain devices and sensors. X-ray crystal structures indicate that they show the dynamics of molecular components such as sponge-like shrinkage/swelling (*17,54,66*), sliding (*63,64*), swinging (*68*), and rotational motion (*46*).

TABLE IX

GUEST BINDING DATA FOR DESOLVATED HOST **14** (*37*)

	K_f (M^{-1})	$[BS]_o/\omega$ (mmol g^{-1})	Guest Inclusion Capacity (mol)/ Unit Formula of Host Solid
EtOH	0.84 ± 0.36	12.7 ± 3.4	14.4
Pyridine	0.93 ± 0.36	6.87 ± 1.84	7.81
n-BuOH	4.36 ± 1.22	0.75 ± 0.07	0.85

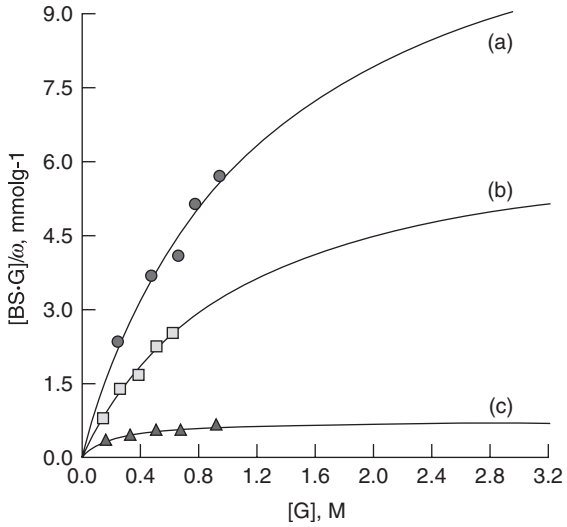

FIG. 20. Binding of desolvated solid **14** (powder form) with various guest molecules in the isooctane medium: (a) EtOH (●), (b) pyridine (■), and (c) *n*-BuOH (▲).

A. COLOR CHANGE WITH RETENTION OF NETWORK STRUCTURE ON DESOLVATION AND RESOLVATION (*6*)

In general, the crystallinity and framework structure of a coordination polymer open framework are destroyed when the guest inclusions are removed from the pores or channels. When solid **2** is dehydrated by heating the crystal at 150°C under 10^{-5} torr for 2–40 h the color changes from yellow to pink. On exposure to moisture, it rapidly becomes yellow again (within 5 min for the crystal and immediately for the powder). During the several cycles of dehydration and rehydration processes, the single-crystal nature can be retained (Fig. 21). The X-ray structures of the dehydrated and rehydrated crystals indicate that the porous framework structure is maintained and that only the bond distances and angles involving the Ni(II) center and the

FIG. 21. Photographs of (a) original crystal **2** in the mother liquor, (b) after evacuation of **2** at 150°C and 10^{-5} torr for 2 h (**2′**), and (c) after exposure of **2′** to water vapor for 5 min (**2″**).

carboxylate ligand are changed slightly. Since this compound is extremely sensitive to moisture, it can be employed as a moisture sensor.

B. Sponge-like Behavior with Retention of Single-Crystallinity upon Guest Removal and Rebinding (*17,54*)

The novel sponge-like behavior of the crystal responding to the amount of guest molecules was revealed for the first time using complete single-crystal structural characterization.

When the crystal of **13** (BOF-1) is allowed to stand in air for 2 h, most of the pyridine guests and some of the water guests are removed, resulting in $[Ni_2(L_5)]_3[BTC]_4 \cdot 30H_2O$ (**13-1**), with the retention of single-crystallinity. The X-ray structure of **13-1** shows that the interlayer distance reduces from 11.9 to 11.3 Å (Table X). When the single crystal of **13** is dried at 75°C for 1.5 h in a furnace, $[Ni_2(L_5)]_3[BTC]_4 \cdot 4H_2O$ (**13-2**) is formed with the retention of single-crystallinity. Crystallographic parameters including the cell volume change significantly during this transformation, as shown in Table X. The X-ray structure of **13-2** shows that the xylyl pillars are significantly tilted resulting in a reduction in the interlayer distance to 6.8 Å, although the 2D layers are completely intact. The results of **13-1** and **13-2** indicate a novel

TABLE X

CRYSTALLOGRAPHIC PARAMETERS OF BOF-1[a] (*17,54*)

Compound	**13**	**13-1**	**13-2**	**13-3**	**13-4**
Space group	$P\bar{1}$	$P\bar{1}$	$P1$	$P\bar{1}$	$P\bar{1}$
a (Å)	*16.505*	*16.420*	*12.382*	*16.467*	*16.460*
b (Å)	19.945	19.817	16.375	20.134	19.849
c (Å)	20.664	20.439	19.952	20.720	20.419
α (deg)	73.00	70.32	74.51	72.53	70.50
β (deg)	68.24	68.55	89.26	67.94	71.08
γ (deg)	76.07	76.19	84.18	75.04	76.30
V (Å^3)	5974.3	5777.9	3877.9	5990.4	5887.0
Thickness of bilayer (Å)	11.91(1)	11.27(2)	6.82(2)	11.71(2)	11.75(2)

[a] R_1 (unweighted, based on F^2) values are 0.0899 for **13**, 0.1839 for **13-1**, 0.1491 for **13-2**, 0.1279 for **13-3**, and 0.1299 for **13-4**.

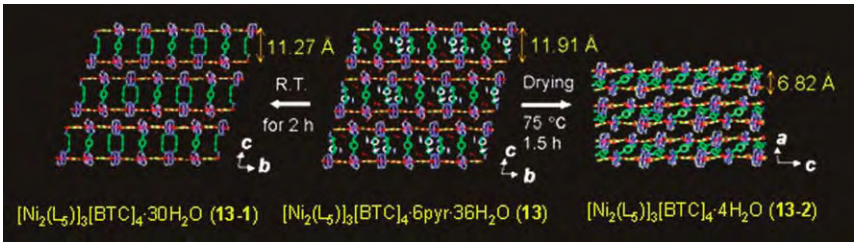

FIG. 22. X-ray structures of **13**, **13-1** and **13-2**, exhibiting sponge-like behavior of the single crystal in response to amount of guest.

sponge-like dynamic behavior of the crystal that shrinks and swells depending on the number of guest molecules (Fig. 22).

C. Retention of Single Crystallinity on Guest Exchange (*17,54*)

BOF-1 (**13**) also undergoes the guest-exchange process in pyridine and benzene, where solid **13** is completely insoluble, in the single-crystal-to-single-crystal manner. In pyridine and benzene media, parts of the guest molecules are exchanged with the corresponding solvent molecules, which results in $[Ni_2(L_5)]_3[BTC]_4 \cdot 20pyr \cdot 6H_2O$ (**13-3**) and $[Ni_2(L_5)]_3[BTC]_4 \cdot 14benzene \cdot 19H_2O$ (**13-4**), respectively. In **13-3**, pyridine molecules are included in the channels of the framework via face-to-edge π–π interactions with the phenyl rings of BTC^{3-} of the 2D layers and the aromatic ring planes of the pillars. They are also intercalated between the bilayer units via hydrogen-bonding interactions with the host. In **13-4**, benzene molecules are included only in the channels by the π–π interactions with the host. The size of the brick-wall motif in the 2D layer and the thickness of the bilayer in the guest-exchanged structures are unaltered as compared to those of as-synthesized BOF-1 (**13**) (Fig. 23). Retaining the single-crystal nature is attributed to the fact that the framework contains 3D channels, which imparts no stress onto the crystal during the guest-exchange processes.

VI. Redox Properties

The coordination polymer solid incorporating the Ni(II) macrocyclic complex can be oxidized because Ni(II) species reacts with the oxidizing agent to become Ni(III) species that can be stabilized by a macrocyclic ligand and additional anionic axial ligands, even though Ni(III) is in an unusually high oxidation state (*23*).

Coordination polymer open frameworks that are able to alter their framework charge as a result of the redox reaction are extremely limited (*69*). However, if a neutral open framework is oxidized, it should include free counter anions in the channels or pores. Then, the oxidized framework can be applied as an anion exchange material (*11,12*).

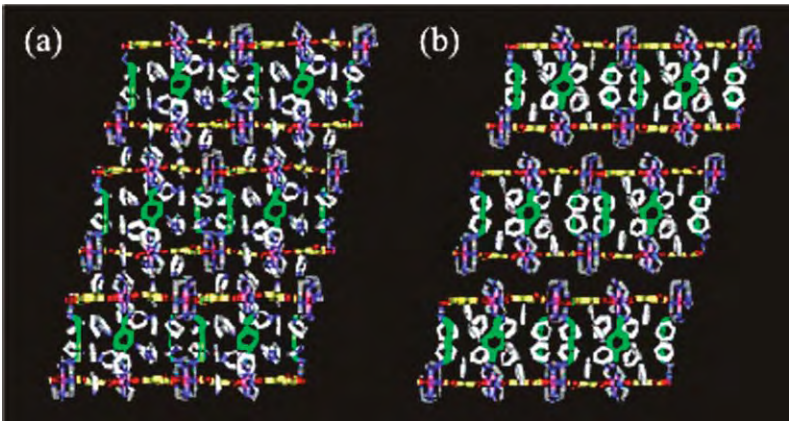

FIG. 23. X-ray structures (side views) of (a) **13-3** and (b) **13-4**. Organic guest inclusions are indicated as off-white, and water guest molecules are omitted for clarity.

In particular, retaining the single crystallinity (*17,58,63–65,69–71*) even *after the chemical reactions* is important for the development of certain devices.

Some coordination polymers that incorporate Ni(II) macrocyclic complexes react with I_2 and Ag(I) to produce I_3^- anion and Ag(0) nanoparticles (*34,54*), respectively, which are included in the oxidized frameworks containing Ni(III) species (*34,54*).

A. REDOX REACTION WITH IODINE: OXIDATION OF FRAMEWORK WITH RETENTION OF SINGLE CRYSTALLINITY (*54*)

When a crystal of BOF-1 (**13**) is immersed in a DMSO/H_2O solution of I_2, the color of the crystal changes from pink to dark brown, with retention of the single crystallinity, and forms $[Ni_2(L_5)]_3[BTC]_4 \cdot (I_3)_4 \cdot nI_2 \cdot 17H_2O$ (**13-5**) (Fig. 24). The cell parameters are not significantly altered in comparison with those of BOF-1 (**13**) (Table XI), even though the density of **13-5** (1.359 g cm^{-3}) remarkably increases (~28%) in comparison to that of BOF-1 (**13**) (1.061 g cm^{-3}).

In the X-ray crystal structure of **13-5** (Fig. 25), two-third of the Ni(II) ions are oxidized to Ni(III), and I_2 molecules are reduced to I_3^- anions that are included in the channels. The two nickel ions belonging to the same bismacrocyclic complex are in the same oxidation state. The Ni–N and Ni–O bond distances involving Ni(III) are shorter than those involving Ni(II) ions. The average Ni(III)–N and Ni(III)–O bond distances are 1.966(6) and 2.103(6) Å, respectively, and those for Ni(II)–N and Ni(II)–O are 2.000(8) and 2.130(8) Å, respectively. As for the included counter I_3^- anions, the I–I distances range from 2.653(17) to 2.923(2) Å with I–I–I angles of 164–180°. The I_2 inclusion has an I–I distance of 2.70(2) Å. Even though many I_3^- ions are introduced into the

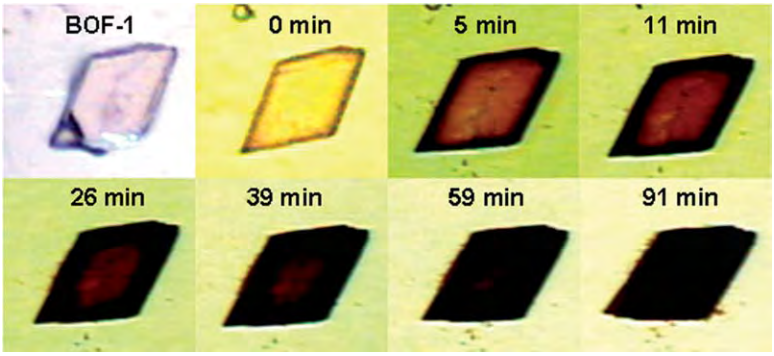

FIG. 24. X-ray structure of **13-5**, showing oxidized framework with I_3^- and I_2 included in the channels. (a) Top view. (b) Side view.

TABLE XI

CRYSTALLOGRAPHIC PARAMETERS FOR **13** AND **13-5**[a] (*54*)

Compound	***13***	**13-5**
Space group	$P\bar{1}$	$P\bar{1}$
a (Å)	16.505	16.434
b (Å)	19.945	19.914
c (Å)	20.664	20.338
α (deg)	73.00	71.26
β (deg)	68.24	70.07
γ (deg)	76.07	74.83
V (Å^3)	5974.3	5837.8
Thickness of bilayer(Å)	11.91(1)	12.20(1)

[a] R_1 (unweighted, based on F^2) values are 0.0899 for **13** and 0.1547 for **13-5**.

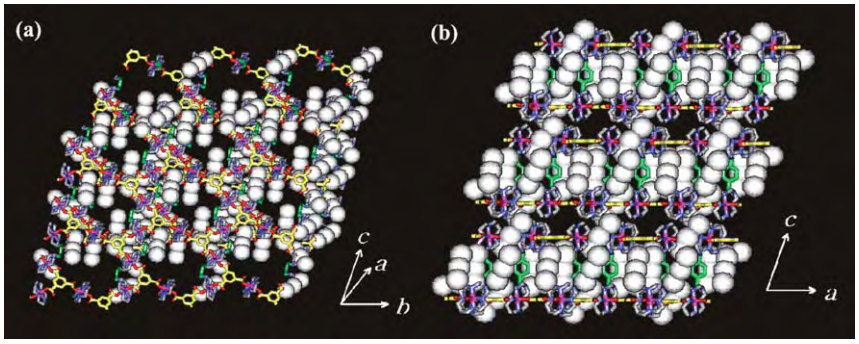

FIG. 25. Photographs showing single-crystal-to-single-crystal transformation of **13** on oxidation with the DMSO/H_2O (1:1, v/v) solution of I_2.

channels of **13-5**, the thickness of the bilayer [12.20(1) Å] is slightly changed as compared with that of BOF-1 (**13**) [11.91(1) Å]. The presence of Ni(III) ions in the framework is demonstrated by the EPR spectra showing anisotropic signals at $g_{||} = 2.024$ and $g_{\perp} = 2.182$ as well as the variable temperature magnetic susceptibility data of $\mu_{\text{eff}} = 5.26\ \mu_{\text{B}}$ at 301 K, corresponding to the spin diluted system having four low-spin Ni(III) and two Ni(II) ions per formula unit. Even though the redox reaction involves the oxidation of the framework, introduction of I_3^- anions in the channels, and an increase in the crystal density by approximately 30%, single-crystallinity is maintained due to the existence of the 3D channels in the framework (Fig. 25).

B. Redox Reaction with Ag(I) Solution: Preparation of Silver Nanoparticles (*34*)

Silver nanoparticles were prepared for the first time by using a redox-active coordination polymer network (*34*). The fabrication of silver nanoparticles with a size less than 5 nm has been known to be difficult because of its strong tendency to aggregate as compared to gold or platinum nanoparticles. However, mono-dispersed silver nanoparticles with a size of 3 nm are prepared by using solid **3**.

When the insoluble dried solid of **3** is immersed in an $AgNO_3$ solution for 10 min, 3 nm-sized Ag nanoparticles are formed (Fig. 26). Even after 18 h, the size of the nanoparticles does not change. The formation of silver nanoparticles is attributed to the auto-redox reaction between Ag(I) and Ni(II) ions incorporated in the host. The EPR spectrum for the solid shows anisotropic signals indicating Ni(III) species ($g_{\perp} = 2.183$ and $g_{||} = 2.024$) as well as an Ag(0) peak ($g = 2.005$). X-ray photoelectron spectra ($3d_{5/2}$ and $3d_{3/2}$ peaks for Ag, 368.0 and 374.1 eV; $2p_{3/2}$ and $2p_{1/2}$ peaks for Ni^{III}, 855.4 and 872.8 eV) also show that Ag and Ni atoms coexist in the solid (*72–74*). The XRPD patterns show that after immersion for 10 min, the host framework structure is retained, although the structure is destroyed

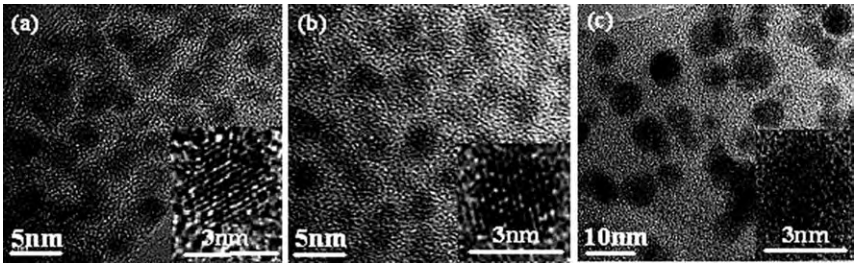

Fig. 26. HRTEM images for the solid isolated after immersion of the desolvated solid of **3** in the MeOH solution of $AgNO_3$ (8.0×10^{-2} M) at room temperature (a) for 10 min, (b) for 18 h, and (c) after removal of the host framework by heating the solid of (b) in dioctyl ether in the presence of oleic acid.

after immersion in the $AgNO_3$ solution for 18 h. The host-free Ag nanoparticles are also isolated by heating the solid in dioctyl ether in the presence of oleic acid, which exhibits silver lattice peaks at $2\theta = 38^\circ$ and 44°. It has been suggested that the silver atoms are collected in the channels, diffused into the surface of the host, and aggregated to the nanoparticles.

VII. Summary

Coordination polymer open frameworks having voids and channels of various aperture sizes and shapes can be assembled by using metal azamacrocyclic complexes and organic carboxylates as molecular building blocks. In the assembly, the azamacrocyclic complexes in square-planar geometries act as linear linkers for the carboxylate ligands that have linear, triangular, and tetrahedral shapes to provide primary 1D, 2D, and 3D networks. The primary networks pack three-dimensionally in the solid state to generate open structures with pores and channels. Some of the coordination polymer open frameworks show porosity and hydrogen storage capabilities (up to 1.0 wt% at 77 K and 1 atm). The hydrogen storage data are better than those for zeolites but not as good as those of the metal-organic frameworks prepared from free metal ions. The coordination polymer open frameworks generate various degrees of hydrophobic or hydrophilic environments on the surface of the voids, which are advantageous for the selective binding of organic guest molecules. In addition, some coordination polymers containing flexible molecular components show sponge like shrinkage on removal of the guest molecules that involves dynamic motions of molecular components. In particular, the coordination polymer frameworks incorporating Ni(II) macrocyclic species are redox-active in the solid state and react with the solutions of oxidizing agents such as I_2 and Ag^+ to produce oxidized frameworks incorporating Ni(III) species and the reduced substrate such as I_3^- anions and the small-sized silver nanoparticles. A variety of azamacrocyclic complexes that contain various functional groups attached to the macrocycles can be prepared by the simple template condensation reactions. By employing them as the metal building blocks, various types of networks are expected to be prepared, which would show high specificity for particular guests, novel crystal dynamics, and the formation of nanoparticles from various metal ions.

Acknowledgments

This work was supported by the Korea Research Foundation Grant funded by the Korean Government (MOEHRD, Basic Research Promotion Fund) (KRF-2005-084-C00020).

References

1. Chae, H. K.; Siberio-Perez, D. Y.; Kim, J. H.; Go, Y. B.; Eddaoudi, M.; Matzger, A. J.; O'Keeffe, M.; Yaghi, O. M. *Nature* **2004**, *427*, 523–527.
2. Eddaoudi, M.; Moler, D. B.; Li, H.; Chen, B.; Reineke, T. M.; O'Keeffe, M.; Yaghi, O. M. *Acc. Chem. Res.* **2001**, *34*, 319–330.
3. Eddaoudi, M.; Li, H.; Yaghi, O. M. *J. Am. Chem. Soc.* **2000**, *122*, 1391–1397.
4. Kitaura, R.; Fujimoto, K.; Noro, S.; Kondo, M.; Kitagawa, S. *Angew. Chem. Int. Ed.* **2002**, *41*, 133–135.
5. Uemura, K.; Kitagawa, S.; Kondo, M.; Fukui, K.; Kitaura, R.; Chang, H.-C.; Mizutani, T. *Chem. Eur. J.* **2002**, *8*, 3586–3600.
6. Lee, E. Y.; Suh, M. P. *Angew. Chem. Int. Ed.* **2004**, *43*, 2798–2801.
7. Ko, J. W.; Min, K. S.; Suh, M. P. *Inorg. Chem.* **2002**, *41*, 2151–2157.
8. Min, K. S.; Suh, M. P. *Chem. Eur. J.* **2001**, *7*, 303–313.
9. Choi, H. J.; Lee, T. S.; Suh, M. P. *Angew. Chem. Int. Ed.* **1999**, *38*, 1405–1408.
10. Choi, H. J.; Lee, T. S.; Suh, M. P. *J. Inclusion Phenom. Macrocyclic Chem.* **2001**, *41*, 155–162.
11. Min, K. S.; Suh, M. P. *J. Am. Chem. Soc.* **2000**, *122*, 6834–6840.
12. Yaghi, O. M.; Li, H. *J. Am. Chem. Soc.* **1996**, *118*, 295–296.
13. Pan, L.; Liu, H.; Lei, X.; Huang, X.; Olson, D. H.; Turro, N. J.; Li, J. *Angew. Chem. Int. Ed.* **2003**, *42*, 542–546.
14. Sawaki, T.; Aoyama, Y. *J. Am. Chem. Soc.* **1999**, *121*, 4793–4798.
15. Albrecht, M.; Lutz, M.; Spek, A. L.; van Koten, G. *Nature* **2000**, *406*, 970–974.
16. Real, J. A.; Andrés, E.; Muñoz, M. C.; Julve, M.; Granier, T.; Bousseksou, A.; Varret, F. *Science* **1995**, *268*, 265–267.
17. Suh, M. P.; Ko, J. W.; Choi, H. J. *J. Am. Chem. Soc.* **2002**, *124*, 10976–10977.
18. Choi, H. J.; Suh, M. P. *J. Am. Chem. Soc.* **1998**, *120*, 10622–10628.
19. Suh, M. P.; Choi, H. J.; So, S. M.; Kim, B. M. *Inorg. Chem.* **2003**, *42*, 676–678.
20. Choi, H. J.; Suh, M. P. *Inorg. Chem.* **1999**, *38*, 6309–6312.
21. Min, K. S., Suh, M. P. *Eur. J. Inorg. Chem.* 2001, 449–455.
22. Ferlay, S.; Mallah, T.; Vaissermann, J.; Bartolome, F.; Veillet, P.; Verdaguer, M. *Chem. Commun.* **1996**, *21*, 2481–2482.
23. Suh, M. P. *Adv. Inorg. Chem.* **1997**, *44*, 93–146.
24. Suh, M. P.; Shim, B. Y.; Yoon, T. S. *Inorg. Chem.* **1994**, *33*, 5509–5514.
25. Suh, M. P.; Kang, S.–G. *Inorg. Chem.* **1988**, *27*, 2544–2546.
26. Moulton, B.; Zaworotko, M. J. *Chem. Rev.* **2001**, *101*, 1629–1658.
27. Hosseini, M. W. *Acc. Chem. Res.* **2005**, *38*, 313–323.
28. Lidin, S.; Jacob, M.; Anderson, S. *J. Solid State Chem.* **1995**, *114*, 36–41.
29. Spek, A. L. *"PLATON99, A Multipurpose Crystallographic Tool"*; Utrecht University: Utrecht, The Netherlands, **1999**.
30. Li, Y. H., Su, C. Y., Goforth, A. M., Shimizu, K. D., Gray, K. D., Smith, M. D., zur Loye, H. C. *Chem. Commun.* 2003, 1630–1631.
31. Belcher, W. J., Longstaff, C. A., Neckening, M. R., Steed, J. W. *Chem. Commun.* 2002, 1602–1603.
32. Abourahma, H.; Moulton, B.; Kravtsov, V.; Zaworotko, M. J. *J. Am. Chem. Soc.* **2002**, *124*, 9990–9991.
33. Takamizawa, S.; Nakata, E.; Yokoyama, H.; Mochizuki, K.; Mori, W. *Angew. Chem. Int. Ed.* **2003**, *42*, 4331–4334.
34. Moon, H. R.; Kim, J. H.; Suh, M. P. *Angew. Chem. Int. Ed.* **2005**, *44*, 1261–2165.
35. Prior, T. J.; Rosseinsky, M. J. *CrystEngComm.* **2000**, *2*, 128–133.
36. Choi, H. J.; Suh, M. P. *Inorg. Chem.* **2003**, *42*, 1151–1157.
37. Kim, H.; Suh, M. P. *Inorg. Chem.* **2005**, *44*, 810–812.
38. Chen, B.; Eddaoudi, M.; Hyde, S. T.; O'Keeffe, M.; Yaghi, O. M. *Science* **2001**, *291*, 1021–1023.

39. Reineke, T. M.; Eddaoudi, M.; Moler, D.; O'Keeffe, M.; Yaghi, O. M. *J. Am. Chem. Soc.* **2000**, *122*, 4843–4844.
40. Sing, K. S. W.; Gregg, S. J. *"Adsorption, Surface Area and Porosity"*; 2nd edn.Academic Press: London, **1982**; (Chaps 1–5).
41. IUPAC manual of Symbols and Terminology, Appendix 2, Pt. 1, Colloidand Surface Chemistry. *Pure Appl. Chem*. **1972**, *31*, 578.
42. Breck, D. W. *"Zeolite Molecular Sieves"*; Wiley: New York, **1974**; Chap. 8.
43. Li, H.; Eddaoudi, M.; O'Keeffe, M.; Yaghi, O. M. *Nature* **1999**, *402*, 276–279.
44. Chui, S. S.–Y.; Lo, S. M.–F.; Charmant, J. P. H.; Orpen, A. G.; Williams, I. D. *Science* **1999**, *283*, 1148–1150.
45. Chen, B.; Eddaoudi, M.; Reineke, T. M.; Kampf, J. W.; O'Keeffe, M.; Yaghi, O. M. *J. Am. Chem. Soc.* **2000**, *122*, 11559–11560.
46. Lee, E. Y.; Jang, S. Y.; Suh, M. P. *J. Am. Chem. Soc.* **2005**, *127*, 6374–6381.
47. Rowsell, J. L. C.; Millward, A. R.; Park, K. S.; Yaghi, O. M. *J. Am. Chem. Soc.* **2004**, *126*, 5666–5667.
48. Zhao, X.; Xiao, B.; Fletcher, A. J.; Thomas, K. M.; Bradshaw, D.; Rosseinsky, M. J. *Science* **2004**, *306*, 1012–1015.
49. Suresh, E.; Boopalan, K.; Jasra, R. V.; Bhadbhade, M. M. *Inorg. Chem*. **2001**, *40*, 4078–4080.
50. Toda, F., Hyoda, S., Okada, K., Hirotsu, K. *J. Chem. Soc., Chem. Commun*. 1995, 1531–1532.
51. Kiang, Y.–H.; Gardner, G. B.; Lee, S.; Xu, Z.; Lobkovsky, E. B. *J. Am. Chem. Soc.* **1999**, *121*, 8204–8215.
52. Aoyama, Y.; Endo, K.; Yamaguchi, Y.; Sawaki, T.; Kobayashi, K.; Kanehisa, N.; Hashimoto, H.; Kai, Y.; Masuda, H. *J. Am. Chem. Soc.* **1996**, *118*, 5562–5571.
53. Hailian, L.; Laine, A.; O'Keefe, M.; Yaghi, O. M. *Science* **1999**, *283*, 1145–1147.
54. Choi, H. J.; Suh, M. P. *J. Am. Chem. Soc.* **2004**, *126*, 15844–15851.
55. Biradha, K.; Hongo, Y.; Fujita, M. *Angew. Chem. Int. Ed*. **2000**, *39*, 3843–3845.
56. Ohmori, O.; Kawano, M.; Fujita, M. *J. Am. Chem. Soc.* **2004**, *126*, 16292–16293.
57. Abrahams, B. F.; Jackson, P. A.; Robson, R. *Angew. Chem. Int. Ed*. **1998**, *37*, 2656–2659.
58. Rather, B., Zaworotko, M. J. *Chem. Commun*. 2003, 830–831.
59. Takamizawa, S.; Nakata, E.; Saito, T. *Angew. Chem., Int. Ed*. **2004**, *43*, 1368–1371.
60. Abrahams, B. F.; Moylan, M.; Orchard, S. D.; Robson, R. *Angew. Chem. Int. Ed*. **2003**, *42*, 1848–1851.
61. Kitagawa, S.; Kitaura, R.; Noro, S. *Angew. Chem. Int. Ed*. **2004**, *43*, 2334–2375.
62. Toh, N. L.; Nagarathinam, M.; Vittal, J. J. *Angew. Chem. Int. Ed*. **2005**, *44*, 2237–2241.
63. Biradha, K.; Fujita, M. *Angew. Chem. Int. Ed*. **2002**, *41*, 3392–3395.
64. Biradha, K.; Hongo, Y.; Fujita, M. *Angew. Chem. Int. Ed*. **2002**, *41*, 3395–3398.
65. Kepert, C. J., Rosseinsky, M. J. *Chem. Commun*. 1999, 375–376.
66. Takaoka, K.; Kawano, M.; Tominaga, M.; Fujita, M. *Angew. Chem. Int. Ed*. **2005**, *44*, 2151–2154.
67. Wu, C.-D.; Lin, W. *Angew. Chem. Int. Ed*. **2005**, *44*, 1958–1961.
68. Dybtsev, D. N.; Chun, H.; Kim, K. *Angew. Chem. Int. Ed*. **2004**, *43*, 5033–5036.
69. Oh, M.; Carpenter, G. B.; Sweigart, D. A. *Angew. Chem. Int. Ed*. **2001**, *40*, 3191–3194.
70. Atwood, J. L.; Barbour, L. J.; Jerga, A.; Schottel, B. L. *Science* **2002**, *298*, 1000–1002.
71. Maspochi, D.; Ruiz-Molina, D.; Wurst, K.; Domingo, N.; Cavallini, M.; Biscarini, F.; Tejada, J.; Rovira, C.; Veciana, J. *Nat. Mater.* **2003**, *2*, 190–195.
72. Wagner, C. D. In: "*Handbook of X-ray Photoelectron Spectroscopy, A Reference Book of Standard Data for Use in X-ray Photoelectron*

Spectroscopy"; Ed. Muilenberg, G. E. ; Eden Prairie, Minnesota. Perkin-Elmer Corp. **1979**.
73. Yue, Z. R.; Jiang, W.; Wang, L.; Toghiani, H.; Gardner, S. D.; Pittman, C. U. Jr. *Carbon* **1999**, *37*, 1607–1618.
74. Davidson, A.; Tempere, J. F.; Che, M. *J. Phys. Chem.* **1996**, *100*, 4919–4929.

MOLECULAR DEVICES BASED ON METALLOCYCLAM SUBUNITS

LUIGI FABBRIZZI[a], FRANCESCO FOTI[a], MAURIZIO LICCHELLI[a], ANTONIO POGGI[a], ANGELO TAGLIETTI[a] and MIGUEL VÁZQUEZ[b]

[a]Dipartimento di Chimica Generale, Università di Pavia, via Taramelli 12, 27100 Pavia, Italy
[b]Departamento de Química Inorgánica, Universidad de Santiago de Compostela, Santiago de Compostela, Spain

I. Some Peculiar Properties of Metal Complexes of Cyclam

Cyclam (1,4,8,11-tetra-aza-cyclotetradecane, **3**) is the prototype of synthetic aza-macrocycles. It tends to encircle transition metal ions to give complexes of *trans*-octahedral geometry, which display some peculiar properties: (i) high thermodynamic stability (the *thermodynamic macrocyclic effect*) (*1*); (ii) extreme inertness to demetallation (the so-called *kinetic macrocyclic effect*) (*2*); (iii) rich redox activity of the metal centre and stabilisation of unusually high oxidation states: Ni^{III} (*3*), Cu^{III} (*4*), Ag^{II} and Ag^{III} (*5*) and, as a transient, Hg^{III} (*6*). Such properties are indisputably related to the cyclic nature of the ligand, but they also depend upon the size of the macrocyclic ring. This can be clearly discerned considering the complete series of cyclic tetramines, whose atomicity ranges from 12 to 16 and whose formulae are sketched in Chart 1.

A. Kinetic Stability

Nickel(II) and copper(II) complexes with ammonia and open-chain tetramines are typically labile and in an acidic solution decompose in a

ADVANCES IN INORGANIC CHEMISTRY
VOLUME 59 ISSN 0898-8838 / DOI: 10.1016/S0898-8838(06)59003-8

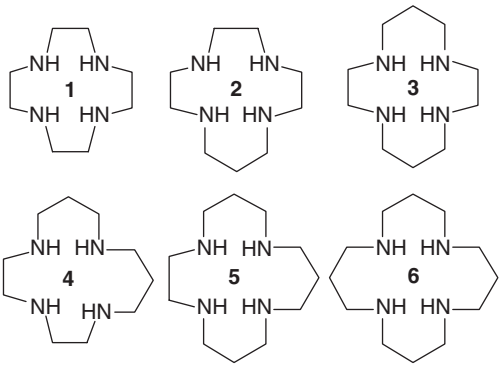

CHART 1. Cyclic tetramines, whose atomicity ranges from 12 to 16 and which, on metal complexation, form five- and/or six-membered chelate rings.

TABLE I

DEMETALLATION OF $[Ni^{II}([13–16]aneN_4)^{2+}$ IN 0.3 M $HClO_4$. LIFETIMES, τ, AT 25°C

[13]aneN$_4$ (**2**)	1.4 h
[14]aneN$_4$ (**3**)	–[a,b]
[15]aneN$_4$ (**5**)	4.3 h
[16]aneN$_4$ (**6**)	5.3 s

[a]No detectable demetallation after several months (*7*).
[b]In 1 M $HClO_4$ a lifetime of 30 years has been estimated (*8*).

twinkling of an eye, with the formation of polyammonium ion and metal aquaion. On the other hand, corresponding complexes with macrocyclic tetramines are substitutionally inert and last in acidic solution for a period ranging from seconds to years, depending upon the ligand's ring size. Such an aspect was investigated by Busch, who considered the demetallation of the nickel(II) complexes with 13- to 16-membered tetramine macrocycles in an aqueous solution 0.3 M in $HClO_4$ (*7*). Pertinent lifetimes, τ, at 25°C, are reported in Table I.

It was observed that, whereas other nickel(II) macrocyclic complexes decomposed in acidic solution over a period ranging from seconds to hours (see τ values in Table I), the $[Ni^{II}(cyclam)]^{2+}$ complex persisted intact for several months, indicating a lifetime of at least some years. Later, Billo was able to estimate for $[Ni^{II}(cyclam)]^{2+}$ in 1 M $HClO_4$ a lifetime of 30 years (*8*). (Indeed, being 14-membered makes a difference!)

B. THERMODYNAMIC STABILITY

The especially high thermodynamic stability of tetra-amine macrocycle complexes with respect to corresponding complexes with open-chain counterparts results from both favourable enthalpy and entropy contributions. The entropy advantage derives from the fact that the macrocycle

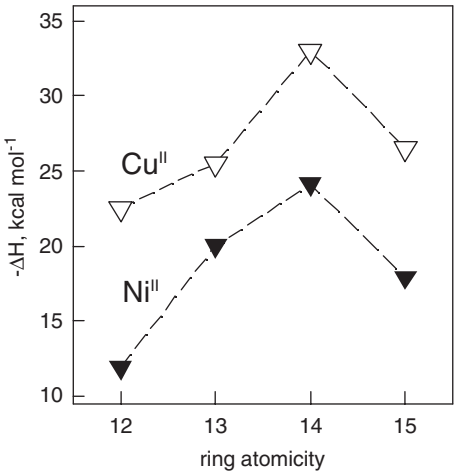

FIG. 1. Enthalpy changes, ΔH°, for the complexation equilibria, $M^{2+}+L \rightleftarrows [ML]^{2+}$ in aqueous solution, at 25°C. Open triangles: copper(II) complexes (*10*); filled triangles: high-spin nickel(II) complexes (*9*).

is pre-oriented for coordination and does not lose any conformational entropy on metal binding, as non-cyclic tetramines do, and is assumed to be independent upon ring size. On the other hand, the enthalpy term is highly dependent upon the atomicity of the macrocycle.

In Fig. 1, the calorimetrically determined enthalpy changes for the equilibria of complex formation with macrocycles **1**–**3**, **5** in aqueous solution, at 25°C, are plotted vs. ligand's atomicity, for Ni^{II} (high-spin) (*9*), and Cu^{II} metal ions (*10*). For both metals, the most exothermic complexation process is observed for the 14-membered macrocycle cyclam, whereas both expansion and contraction of the ring cause a drastic and progressive decrease of the heat effect. Notice that a second 14-membered macrocycle exists, **4**, isocyclam, which, on complexation, gives a 5,5,6,6 sequence of chelate rings (whereas cyclam provides the symmetric pattern 5,6,5,6). Complexation of isocyclam is by far less exothermic than for cyclam, for both high-spin Ni^{II} and Cu^{II}. The enthalpy change principally reflects the intensity of the metal–amine interaction: cyclam has the right size to encircle Ni^{II} and Cu^{II} and can place its donor atoms in the required coordinative positions (the corners of a square), without suffering any serious conformational rearrangement (*11*).

C. REDOX BEHAVIOUR

Also the redox behaviour of tetra-aza-macrocyclic complexes is extremely affected by ligand's ring size. As an example, Fig. 2 displays the half-wave potential values for the Ni^{III}/Ni^{II} couple within macrocycles **1**–**6**, in an MeCN solution made 0.1 M in Bu_4NClO_4 (*12*). It is shown that the easiest attainment of the Ni^{III} state, expressed by the

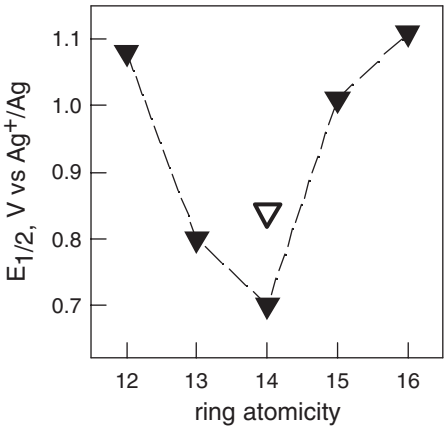

FIG. 2. Half-wave potential values for the Ni^{III}/Ni^{II} couple, $E_{1/2}(Ni^{III}/Ni^{II})$ within macrocycles **1–6**, in an MeCN solution made 0.1 M in Bu_4NClO_4. At atomicity 14, the filled triangle refers to the cyclam (**3**) complex, the open triangle to isocyclam (**4**).

less positive value of $E_{1/2}(Ni^{III}/Ni^{II})$, takes place within the symmetric 14-membered macrocycle, cyclam, and that both expansion and contraction of the ring make the Ni^{II}-to-Ni^{III} oxidation more and more difficult. Half-wave potentials are strictly related to the intensity of the metal–ligand interaction: in particular, strong in–plane interactions raise the energy of the Ni^{II} orbital from which the electron is abstracted on oxidation. The Ni^{II}-to-Ni^{III} oxidation process is comparatively disfavoured with isocyclam, due to the less propitious position and orientation of the amine nitrogen donor atoms (*13*). The $[Ni^{III}(cyclam)]^{3+}$ complex is extremely stable also in water (provided the solution is acidic): the $E_{1/2}(Ni^{III}/Ni^{II})$ value for the cyclam complex in 1 M HCl is 0.71 V vs. NHE. Consider that $E_{1/2}$ for the $[Fe^{III}(H_2O)_6]^{3+}/[Fe^{II}(H_2O)_6]^{2+}$ couple is 0.77 V vs. NHE. The Fe^{II} aquaion is currently used as a mild reducing agent (for instance, as $(NH_4)_2SO_4$ $[Fe^{II}(H_2O)_6)]SO_4$, in the standardisation of a solution of permanganate); $[Ni^{II}(cyclam)]^{2+}$ is a (slightly) stronger reducing agent, but its use in redox titrimetry is not (yet) so widespread.

All the mentioned properties make cyclam and its metal complexes convenient and versatile subunits for building multicomponent systems displaying a variety of functions: some of them will be discussed in the next sections.

II. The Template Synthesis of Cyclam and Azacyclams

The synthesis of cyclic molecules is intrinsically disfavoured by the entropy term and its achievement typically involves a multistep pathway and is characterised by relatively low yields. Busch demonstrated

that in some favourable cases a transition metal centre can be used as a template in the synthesis of cyclic molecules displaying ligating tendencies, which makes the process much easier and substantially improves the yield (*14*). This is the case for 14-membered tetra-aza macrocycles, including cyclam. The nickel(II) template synthesis of cyclam is illustrated in the Scheme 1 below (*15*).

The Ni^{II} ion preorganises the open-chain tetramine $3 \cdot 2 \cdot 3$-tet, by placing its donor nitrogen atoms at the corners of a square. The two primary amine groups are in the correct position to undergo Schiff base condensation with glyoxal, thus allowing cyclisation to occur. Then, the two $C = N$ double bonds are hydrogenated, e.g. with $Na[BH_4]$, to produce the $[Ni^{II}(cyclam)]^{2+}$ complex. The metal centre can be removed from the cyclam ring by boiling in presence of excess cyanide. Axial binding of a CN^- ion is the first step of the demetallation process, which eventually leads to the the formation of $[Ni^{II}(CN)_4]^{2-}$ (*16*). The free macrocycle can be isolated as a solid and made to react with other metal ions, if desired. Or it can be functionalised to give a multicomponent system, for instance by appending a chosen subunit to one of the amine groups of cyclam. This typically requires the multistep procedure of (i) selective protection of the amine groups, (ii) substitution at the unprotected nitrogen atom, (iii) deprotection. Indeed, it could be more comfortable to profit from a template reaction giving in a one-pot process the metal complex of the functionalised macrocycle. Such a reaction already exists and its mechanism is illustrated in Scheme 2.

The reaction involves the pre-orientation of the linear tetramine $2 \cdot 3 \cdot 2$-tet by a metal centre capable of imposing a square coordination (Ni^{II}, Cu^{II}). Each one of the two primary groups of the coordinated tetramine undergoes Schiff base condensation with formaldehyde. Then, an AH_2 molecule, displaying the properties of a diprotic

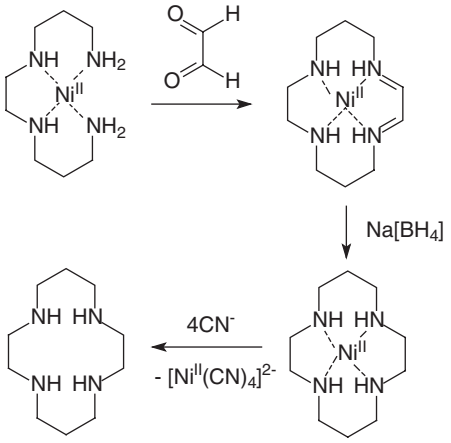

SCHEME 1. Nickel(II) template synthesis of cyclam (15).

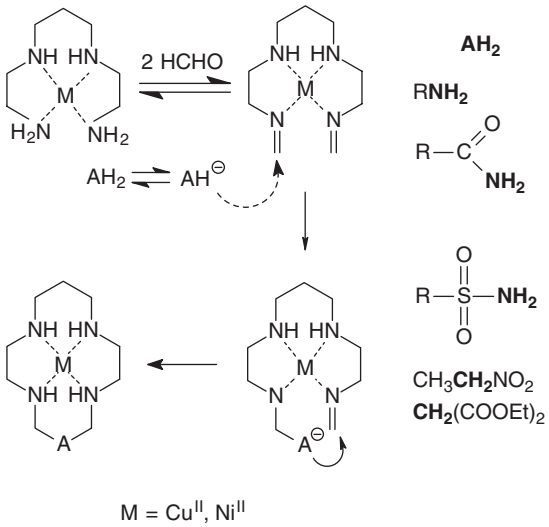

SCHEME 2. Metal template synthesis of azacyclam. AH_2 is a diprotic acid at nitrogen (primary amine, primary carboxyamide, primary sulphonamide) or at carbon (nitroethane, diethylmalonate).

Brønsted acid, transfers its first proton to an auxiliary base, e.g. excess triethylamine, and the AH^- fragment which forms gives a nucleophilic attack at one of the C = N double bonds. Subsequently, the covalently bound –AH fragment further deprotonates: the $-A^-$ fragment that forms attacks the other proximate C = N imine bond, accomplishing the cyclisation. Thus, the $\mathbf{AH_2}$ molecule behaves as a *padlock*, which firmly locks the tetramine around the metal centre. Padlocks include the carbon acids nitroethane, $CH_3\mathbf{CH_2}NO_2$, (*17*) and diethylmalonate, $\mathbf{CH_2}(COOEt)_2$, (*18*). Primary amines, $R\mathbf{NH_2}$, which can be formally considered diprotic acids, also give successful cyclisation processes (*19*). However, the most versatile cyclisation was observed when using as padlocks primary amides, both carboxyamides, $RCO\mathbf{NH_2}$ (*20*) and sulphonamides, $RSO_2\mathbf{NH_2}$ (*21*). The ring that forms (azacyclam) is isostructural with that of cyclam (the amide nitrogen atom merely plays an architectural role and is not involved in coordination) and metal azacyclam complexes (of Ni^{II} and Cu^{II}) display the same peculiar properties observed with cyclam complexes: in particular, inertness to the demetallation and enhanced redox activity. Very interestingly, by using this template procedure, almost any functional group can be appended to the 14-membered tetramine framework. In fact, given a desired fragment R, it is almost always possible to obtain its amide derivative, in particular sulphonamide, RSO_2NH_2, which can be used as a locking fragment in the preparation of the corresponding Ni^{II} or Cu^{II} azacyclam complex.

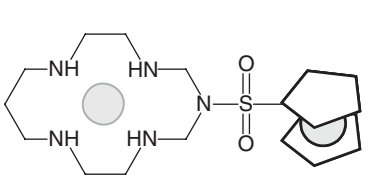

7

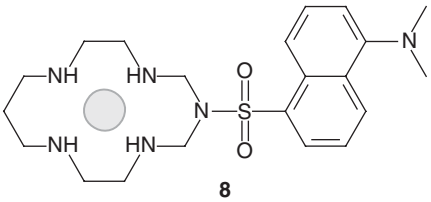

8

For instance, on reaction of $[Ni^{II}(2.3.2\text{-tet})]^{2+}$ with 1-ferrocene sulphonamide, the conjugate system **7** was obtained, in which two distinct and non-equivalent redox active subunits (through the Ni^{II}/Ni^{III} and Fc/Fc^{+} couples) are covalently linked (*22*). On reaction of $[Ni^{II}(2.3.2\text{-tet})]^{2+}$ with dansylamide, the two component system **8** was obtained (*23*). **8** is the prototype of a rich family of metal-based redox switches of fluorescence (*24*). In particular, the $[Ni^{II}(\mathbf{8})]^{2+}$ complex is fluorescent due to the emission of the dansyl (Dans) subunit. However, if the Ni^{II} centre is oxidised to Ni^{III}, either chemically (with $S_2O_8^{2-}$, in MeOH) or electrochemically (at a platinum anode, in MeCN), fluorescence is fully quenched due to the occurrence of an electron transfer (eT) from the excited fluorogenic subunit, Dans*, to the Ni^{III} ion, a process characterised by a distinctly negative ΔG° value. On chemical (with NO_2^- in MeOH) or electrochemical (in MeCN) reduction of Ni^{III} to Ni^{II}, fluorescence is fully restored. In particular, the occurrence of an eT process from Ni^{II} to Dans* is thermodynamically disfavoured. Thus, the nickel-azacyclam subunit behaves as a switch of dansyl fluorescence, which can be quenched-revived at will on oxidation–reduction of the metal centre. Other fluorogenic fragments can be connected to the nickel-azacyclam subunit through reaction of $[Ni^{II}(2.3.2\text{-tet})]^{2+}$ with the appropriate sulphonamide derivatives (e.g. 1-naphthalene sulphonamide) to generate efficient redox switches of fluorescence.

III. Scorpionands and Scorpionate Complexes

An ethylamine side-chain can be covalently linked to a nitrogen atom of cyclam to give a quinquidentate ligand, which combines the rigid nature of macrocycles to the flexibility of open-chain polyamines: *N*–aminoethyl-cyclam (**9**) (*25*).

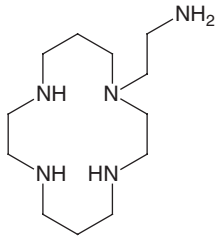

9

As an example, the nickel(II) complex of **9** in a strongly acidic solution exists as a square-planar low-spin complex, of yellow colour. In particular, the primary amine group of the pendant arm is protonated and stays far away from the metal centre. On the other hand, the closed and rigid arrangement strongly disfavours the occasional detachment of the four amine nitrogen atoms of the cyclam ring, thus preventing their protonation. On addition of standard base, the solution takes a pale blue-violet colour, due to the formation of the high-spin complex. Such a spin conversion is associated with the deprotonation of the ammonium group of the pendant arm: the primary amine group coordinates the metal, to give a complex of different geometry: probably octahedral (with a water molecule occupying the sixth position of the octahedron, see Scheme 3).

The process is quickly reversible and the pendant arm can be made to oscillate between two defined positions (on the metal and far away from it), through consecutive additions of acid and base, the intramolecular movement being signalled by the blue-to-yellow colour change. The pK_a associated to the process is quite low (2.9), much lower than the pK_a of ethylammonium: 10.8. This indicates that coordination to the metal centre enhances the acidity of the $-CH_2CH_2NH_3^+$ fragment by ca. 8 orders of magnitude. This huge energy gain (RT $\ln(\Delta pK_a) = 14.7\,\text{kcal mol}^{-1}$) must include the favourable enthalpy contribution associated to the formation of a fifth metal–amine coordinative bond. However, such a term cannot exceed $5.5\,\text{kcal mol}^{-1}$ (quantity estimated by dividing the enthalpy change associated to the reaction of Ni^{II} with the open-chain tetramine 2.3.2-tet by 4) (*26*). It is suggested that a significant entropy term contributes to make pK_a low, which is related to the high probability of the ethylammonium pendant arm to collide with the metal centre, compared to an individual ethylammonium, which moves in the whole solution. Thus, a chelate effect exists that favours intramolecular binding and deprotonation of the ammonium side chain.

Noticeably, metal binding in a scorpionate arrangement can also enhance the acidity of carbon acids, in an indirect mode. A recent example refers to the deprotonation of a 2-nitrobenzyl fragment. Tendency of 2 nitrobenzene to undergo tautomerisation to the corresponding nitronic

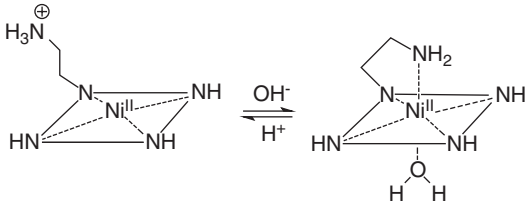

SCHEME 3. pH controlled coordination of the pendant arm in a scorpionate complex.

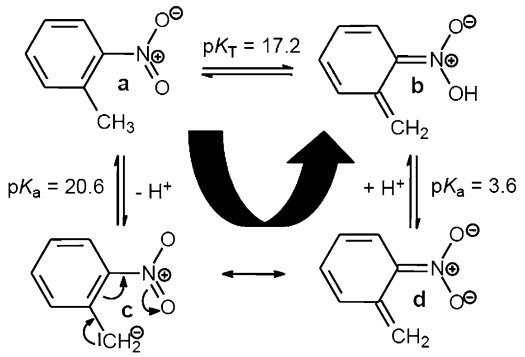

SCHEME 4. The tautomeric equilibrium of 2-nitrotoluene.

acid is rather low, which is expressed by $pK_T = 17.2 \pm 0.2$ (*27*). The constant of the tautomerisation equilibrium has been calculated through the thermodynamic cycle illustrated in Scheme 3.

The thermodynamic cycle shows that the scarce tendency of 2-nitrotoluene (**a**) to convert into the aci-nitro tautomer (**b**) depends upon the very low Brønsted acidity of the $-CH_3$ group ($pK_a = 20.6$). The low acidity is most likely related to the circumstance that deprotonation leads to the formation of the nitronate ion (formula **d** in Scheme 4), in which aromaticity has been lost. In order to profit from the scorpionate effect, molecule **10** was considered, in which a 2-nitrobenzyl pendant arm is covalently linked to the nitrogen atom of a cyclam ring (*28*). In particular, the 2-substituted positional isomer is expected to favour the coordination of the nitro-nitronate group to transition metal centre, encircled by the cyclam ring.

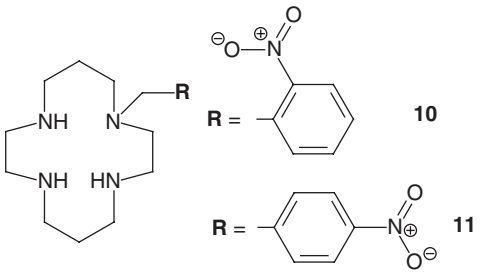

The Ni^{II} complex of **10**, indicated in the following as $[Ni^{II}(LH)]^{2+}$, displays in aqueous solution an intense absorption band centred at 330 nm, due to the 2-nitrobenzyl chromophore, with a shoulder at 450 nm, which is ascribed to the d-d transition of the low-spin square-planar Ni^{II} centre. Such a coordinative arrangement has been confirmed by the crystal structure of the $[Ni^{II}(LH)](ClO_4)_2$ complex salt,

which shows that the nitro group is not involved in coordination and stays far away from the metal centre, at quite a long distance: 4.83 Å, from Ni^{II} to the closest oxygen atom of the -NO_2 fragment. On increasing the pH of the solution, through addition of standard NaOH, no modification of the spectrum was observed, until pH 10, when the shoulder at 450 nm began to decrease and a new, less intense, band developed at 550 nm (see Fig. 3).

Such a spectral behaviour indicates the occurrence of the low-spin to high-spin conversion, associated to a change of coordination geometry from square-planar to octahedral. It is therefore suggested that in basic solution the -CH_2- group linking the cyclam ring to the 2-nitrobenzene fragment undergoes deprotonation. –CH_2– deprotonation is associated with the following events (which do not necessarily take place according to a temporal sequence): (i) the 2-nitrobenzyl pendant arm moves towards the metallocyclam subunit; (ii) an electronic rearrangement takes place, to give the anion of the nitronic acid; (iii) a coordinative bond forms between one oxygen atom of the $–NO_2^-$ (nitronate) group and the Ni^{II} centre: then, a water molecule goes to occupy the remaining site of the coordination octahedron, while the metal electrons rearrange to the high-spin configuration. The overall process is pictorially illustrated in Scheme 5.

On non-linear least-squares fitting of the sigmoidal plot of absorbance at 450 nm vs. pH (see Fig. 3, inset) a pK_A value of 10.71 ± 0.01 was

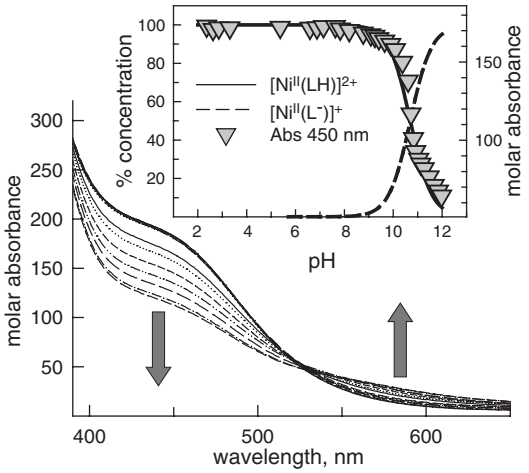

FIG. 3. Visible spectra recorded over the course of the titration of an aqueous solution of $[Ni^{II}(\mathbf{10})](CF_3SO_3)_2$ with standard base: the decrease of the band at 450 nm indicates the disappearance of the planar low-spin complex, to which the formation of the octahedral high-spin species corresponds (band at ca. 580 nm). Inset: change of the absorbance at 450 nm with pH: the sigmoidal profile discloses a $pK_a = 10.71 \pm 0.01$, associated to the deprotonation of the –CH_2– group of the nitrobenzyl pendant arm.

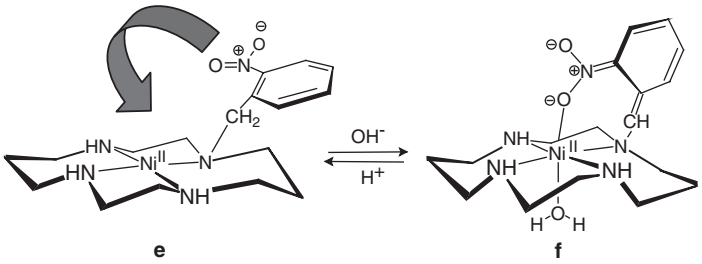

SCHEME 5. The metal-controlled deprotonation of the pendant 2-nitrobenzyl group in an Ni^{II} scorpionate complex.

calculated for the acid dissociation equilibrium: $[Ni^{II}(LH)]^{2+} \leftrightarrows [Ni^{II}(L^{-})]^{+} + H^{+}$. Solid and dashed lines in the inset indicate the % concentration of the two species present at the equilibrium, **e** and **f**, respectively, over the investigated pH range. It has to be noted that on addition of standard acid, the band at 450 nm is fully restored, demonstrating the reversibility of the process. Quite interestingly, no spectral changes are observed on titration of a solution of the yellow diamagnetic Ni^{II} complex of the positional isomer **11**, containing a 4-nitrobenzyl pendant arm, whose coordination to Ni^{II} is sterically prevented.

The pK_a values of the $[Ni^{II}(LH)]^{2+}$ complex (10.7) must be compared with the corresponding value for 2-nitrotoluene (20.6), which emphasises the role metal ions can play in enhancing acidity of carbon acids. This is a consequence of the scorpionate arrangement, which provides favourable enthalpy (establishment of Ni^{II}–NO_2^- and Ni^{II}–OH_2 bonds) and entropy contributions (the facilitated coordination of the pendant arm). The use of the Ni^{II} ion provides, as a further advantage, the occurrence of the low-to-high spin conversion, which allows visual and spectrophotometric monitoring of the process.

IV. Sensors and Dosimeters Based on the Cyclam Motif

The well-recognised propensity of cyclam to include transition metals has encouraged synthetic chemists to design molecular sensors based on its coordinating framework. However, the primary requirement of a sensor is the quick and full reversibility of interaction with the analyte: this is not the case with cyclam, whose metal complexes exhibit extreme inertness (the previously discussed kinetic macrocyclic effect). Indeed, sensors based on a 14-membered tetra-aza arrangement have been developed, but they are based on dioxocyclam (**11**), a macrocycle displaying the same framework of cyclam, but containing two adjacent amide nitrogen atoms. Dioxocyclam is obtained in good yield (*29*), through the reaction of diethylmalonate with the open-chain tetramine 2.3.2-tet (see Scheme 6).

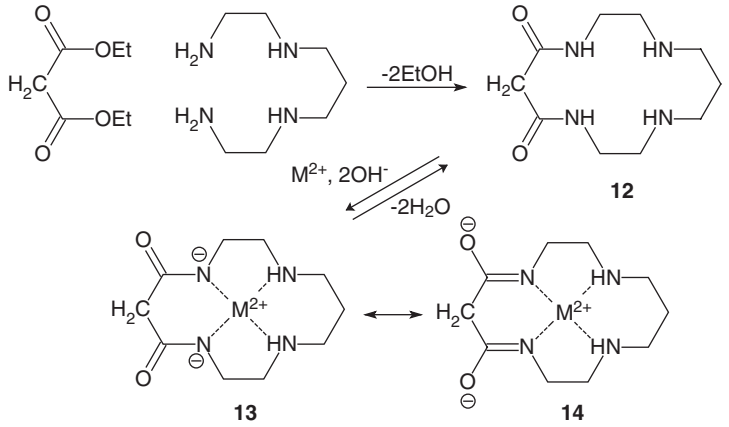

SCHEME 6. The synthesis of dioxocyclam and the pH-controlled formation of dioxocyclamato(2−) complexes.

Dioxocyclam, in presence of 2 equiv. of base, is able to include a divalent cation, M^{2+}, with the simultaneous extrusion of two protons from the two amido groups (*30*). In the electrically neutral [M^{II}(dioxocyclamato(2–)] complex that forms, the negative charge is delocalised over the two NCO fragments of the macrocyle, a situation which can be illustrated through a classical resonance representation, as shown in Scheme 6 (**13** ↔ **14**). On titration with standard base, a pale blue aqueous solution containing equimolar amounts of dioxocyclam and $Cu^{II}(ClO_4)_2$, plus excess acid, turns pink violet at a pH around 5, due to the formation of the [Cu^{II}(dioxocyclamato(2–)] complex. On back addition of standard acid, the pink violet colour disappears, owing to an instantaneous demetallation process. Fast demetallation may seem in contrast with the cyclic nature of the coordinated ligand and to its mechanical resistance to expose nitrogen atoms to the incoming protons. However, the dioxocylamato(2–) complex offers an easy way to demetallation, not accessible to tetramine analogues: in particular, two H^+ ions protonate the negatively charged oxygen atoms of the macrocycle (resonance formula 14 in Scheme 6), according to a process too fast to be detected in the timescale of stopped-flow experiments (*31*). On formation of the neutral ligand (enol form), the negative charge is withdrawn from the two amide nitrogen atoms, which completely lose their coordinating tendencies: the Cu^{II} ion is no longer firmly bound by the tetra-aza donor set, the two amine groups can now be protonated and fast demetallation takes place. On these premises, a fluorescent chemosensor of Cu^{II} has been designed, by linking an antracenyl subunit to the dioxocyclam framework (**15**) (*32*).

In an MeCN/H_2O solution (4:1 v/v), the functionalised macrocycle displays the typical anthracene fluorescence over the 2–12 pH interval (see Fig. 4, diamonds). However, when the solution contains equimolar amounts of **15** and $Cu^{II}(ClO_4)_2$, on increasing pH, e.g. on addition of

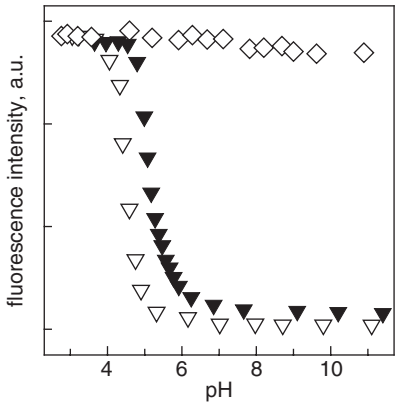

FIG. 4. Fluorimetric titration profiles obtained on addition of standard NaOH to an MeCN/H_2O solution (4:1 v/v) containing: (i) **15** plus excess acid (diamonds); (ii) equimolar amounts of **15** and Cu^{II} plus excess acid (open triangles); (iii) equimolar amounts of **16** and Cu^{II} plus excess acid (filled triangles). The separation of the two sigmoidal profiles reflects the greater thermodynamic stability of the macrocyclic complex.

standard base to an acidified solution, fluorescence is quenched at pH 4.5 ± 1 according to a well-defined sigmoidal profile (open triangles in Fig. 4). Quenching reflects Cu^{II} inclusion into the dioxocyclamato(2–) cyclic moiety, and is due to the occurrence of an electron transfer (eT) process from the metal to the excited fluorophore. The eT process is made possible by the capability of the dioxocyclamato(2–) coordinative arrangement to favour the access to the Cu^{III} state. A similar behaviour is displayed by the open-chain counterpart **16**. An analogous sigmoidal profile is observed, but displaced towards the basic region by one pH unit (Fig. 4, filled triangles). This reflects the higher thermodynamic stability of the complex of dioxocyclam compared to the complex of the non-cyclic ligand (the thermodynamic macrocyclic effect).

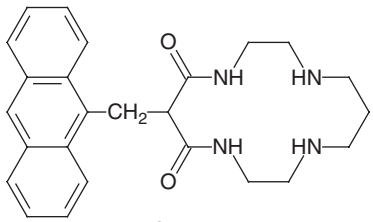

15

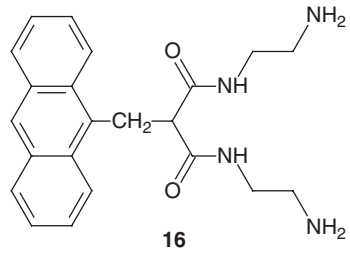

16

Cyclam, because of the inertness of its complexes, cannot be used as a sensor, but can be used as a dosimeter, i.e. an irreversible device, which progressively accumulates the dose, each time summing up the signal,

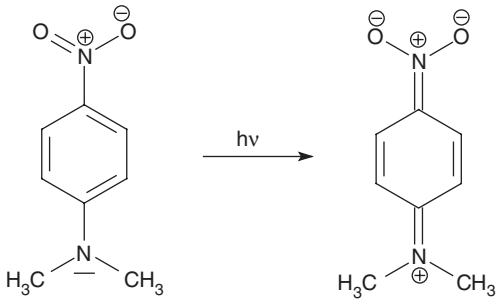

17

SCHEME 7. The charge transfer optical transition in dimethyl-(4-nitrophenyl)-amine.

and, after extended use, should be discarded. In particular, we were interested in designing a colorimetric dosimeter for transition metals, based on the cyclam framework. In this sense, we made use of a push-pull chromophore. Typically, push-pull chromophores consist of a molecular system in which a donor group (D) and an acceptor group (A) are connected by an electron permeable fragment. Colour results from a charge transfer transition from D to A. For instance, in the classical chromophore dimethyl-(4-nitro-phenyl)-amine (**17**), the transition responsible for the bright yellow colour involves a charge transfer process from the tertiary amine group to the nitro group, as illustrated in Scheme 7.

In principle, a coordinative interaction of the dimethylamine group of **17** with a d block metal ion should alter the energy of the charge transfer transition and modify the colour, thus giving rise to a convenient procedure of visual detection of transition metals in solution. However, addition of even a large excess of transition metal ions to an aqueous solution of **17** neither induced a colour change nor modified the absorption spectrum: this has to be ascribed to the fact that the aniline nitrogen atom of **17** exhibits very poor donating properties and cannot be engaged in a metal–ligand interaction.

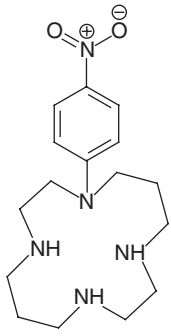

18

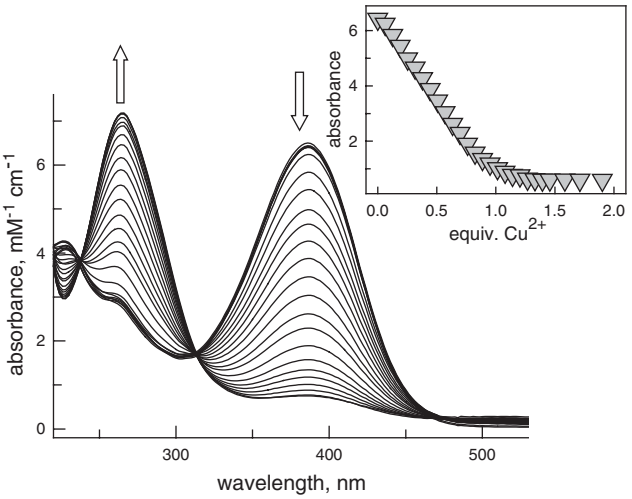

FIG. 5. Titration of an aqueous solution 5×10^{-5} M in **18**, buffered at pH = 4.75, with a standard solution of Cu^{II}. On metal addition, the band at 386 nm, due to **18**, decreases, while a new band develops at 266 nm, pertinent to the $[Cu^{II}(\mathbf{18})]^{2+}$ macrocyclic complex. On titration, the yellow solution discolours. Inset: absorbance at 386 nm vs. equivalents of Cu^{II}.

Thus, we considered the opportunity of incorporating the dimethyl-(4-nitro-phenyl)-amine moiety into the framework of cyclam, with the aim of bringing the envisaged metal at interaction distance with the aniline nitrogen atom. In this connection, the functionalised cyclam macrocycle **18** was synthesised, in which the nitrogen atom of the 4-nitro-phenyl-amine fragment is part of a 14-membered ring (*33*).

Inclusion of transition metal ions was investigated by titrating an aqueous solution of **18**, adjusted to pH = 4.75 (CH_3COO^-/CH_3COOH buffer), with an aqueous standard solution of the metal salt and looking at colour changes and modifications of the absorption spectrum. In particular, addition of Cu^{II} made the yellow solution discolour, inducing a decrease of the band at 386 nm and the development of a new band at 266 nm (see Fig. 5). In particular, the family of spectra recorded over the titration experiment showed the presence of two well defined isosbestic points. Very significantly, the absorbance at 386 nm ceased decreasing after the addition of 1 equiv. of Cu^{II} (see inset to Fig. 5), thus indicating the formation of a Cu^{II}/**18** complex of 1:1 stoichiometry.

Such a 1:1 adduct was isolated in a crystalline form and its molecular structure was determined. It was observed that the Cu^{II} ion is fully encircled by the tetra-aza subunit of **18** according to a square geometry. More interestingly, the distance of the Cu^{II}-N(aniline) bond, 2.07 Å, is only slightly larger than those of the three Cu^{II}-N(amine) bonds (average

value: 2.00 ± 0.01 Å), indicating the existence of a regular metal–ligand interaction. Quite interestingly, the macrocycle adopts a configuration of type *trans-I* (with the substituents on the nitrogen atoms, hydrogens and 4-nitro-phenyl, all above the N_4 plane; nitrogen configuration *R,S,R,S*; with the Cu^{II} centre on the same side, at 0.03 Å above the N_4 plane). On the basis of structural features, colour and spectral changes observed in titration experiments could be fully accounted for. In fact, the coordinative interaction of the Cu^{II} ion with the lone pair of the aniline nitrogen atom modifies the electronic and spectral properties of the 4-nitro-phenylamine chromophore. In particular, the metal–aniline group interaction raises the energy of the charge transfer to the nitro group, inducing a hypsochromic shift of the pertinent absorption band from 386 to 266 nm.

Analogous titration experiments were carried out with a variety of metal ions, which included Mn^{II}, Fe^{II}, Fe^{III}, Co^{II}, Ni^{II}, Zn^{II} Pb^{II}: in all cases, neither a colour change nor a modification of the spectral features of **18** were observed, indicating that the metal does not interact with the aniline group of the chromophore and, presumably, with the tetra-aza macrocycle. Lack of interaction may be due to both thermodynamic and kinetic effects. In particular, the presence of the aniline nitrogen atom in the donor set is expected to reduce the donating tendencies of the macrocycle, which forms a stable complex only with the metal leading the Irving-Williams series, Cu^{II}. Moreover, it should be considered that the macrocyclic subunit of **18** (L) at pH = 4–5 is present in solution with two amine group protonated (LH_2^{2+}). This feature may prevent the approach of the cation to the doubly protonated ligand and formation of the complex, due to electrostatic repulsive effects. Inference of a kinetic factor is demonstrated by the fact that Ni^{II} reacts with **18** in boiling MeOH, to give, only after prolonged reflux of the solution, a yellow diamagnetic salt of formula $[Ni^{II}(\mathbf{18})](ClO_4)_2$, displaying a square-planar coodination geometry. Lack of interference by the above mentioned metals can be demonstrated by titrating with a standard Cu^{II} solution an aqueous solution containing **18** plus 10 equiv. of the interfering metal: in all cases, the family of spectra and the titration profile shown in Fig. 4 were not altered. Thus, **18** is capable to detect Cu^{II} through the well perceptible disappearance of its yellow colour and, if desired, through a distinct change of the spectrum. It has to be noted that the inclusion of the Cu^{II} ion within the macrocycle is not reversible. For instance, Cu^{II} is not removed from the poly-aza ring of **18**, even after the addition of a large excess of strong acid, due to the kinetic macrocyclic effect. Thus, **18** has to be considered as a sensitive and efficient *dosimeter* of Cu^{II}.

V. An Anion Sensor for Citrate

There exists a general interest in the design of molecular systems (receptors) capable to selectively interact with anions and possibly to

signal to the outside the occurrence of the recognition process (*34*). Typically, the receptor offers a suitable cavity in which some positively charged groups have been strategically positioned. First examples in the field referred to macropolycyclic systems containing either ammonium (*35*) or tetraalkylammonium groups (*36*). Selectivity derived from size and shape matching of anion and receptor's cavity. The nature of the anion–receptor interaction is electrostatic, thus not particularly strong. It may happen that interaction energy is not high enough to compensate the dehydration terms, a circumstance that confines anion recognition studies to non-aqueous solvents. In addition, in the case of polyammonium receptors, in order to keep amine groups protonated, one must operate under acidic conditions, in any case at a pH lower than 7, a situation that prevents studies in a biological context. On the other hand, positive charges within the receptor's cavity can be provided by metal ions. Thus, the anion–receptor interaction falls in the field of coordination chemistry, profiting from some convenient features: (i) the energy of metal–ligand interaction is relatively high, in any case overcoming the dehydration terms, so that recognition studies can be performed in pure water (and at pH = 7); (ii) the metal–ligand interaction, when using d block centres, is typically directional, which may offer further elements of selectivity. During the last decade, we have reported a number of receptors containing coordinatively unsaturated metal ions (mainly Cu^{II}), which are capable of selective interactions with anions and ionisable analytes, including amino acids, in water (*37*). For instance, in a recent example, we have described the selective inclusion of dicarboxylates into a dicopper(II) bis-tren cryptate: the dimetallic receptor was able to recognise the length of both aromatic and aliphatic dicarboxylates (*38*), a feature which allowed specific recognition and sensing of glutamate in presence of a variety of anionic neurotransmitters (*39*).

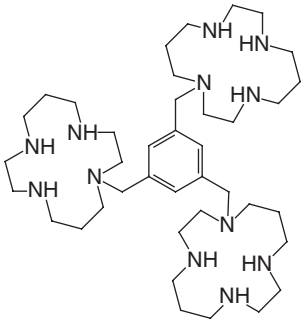

19

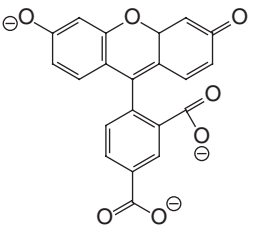

20

In the perspective of extending the metal–ligand approach to the recognition of tricarboxylates, we have recently considered the design

of a receptor containing three unsaturated Cu^{II} centres (*40*). In particular, we considered system **19**, in which three cyclam subunits have been implanted on a 1,3,5-mesityl platform and we prepared the corresponding tri-copper(II) complex, $[Cu^{II}_3(\mathbf{19})]^{6+}$. Copper(II) complexes with cyclam derivatives tend to coordinate one X^- anion, giving a stable five-coordinate species of square pyramidal geometry, in which X^- occupies the apical position (*41*). A very important feature deriving from the use of cyclam subunits is that the Cu^{II} ion (like Ni^{II}) cannot be removed from the macrocyclic ring by any competing ligand (*42*). Such a circumstance ensures the stability of the $[Cu^{II}_3(\mathbf{19})]^{6+}$ receptor even in presence of a large excess of the envisaged anion. The 1,3,5-trimethyl benzene scaffold was chosen because, when appropriately functionalised, it can favour the formation of a bowl suitable for the inclusion of anions.

The interaction of $[Cu^{II}_3(\mathbf{19})]^{6+}$ with carboxylates was investigated by taking profit from the indicator displacement paradigm (*43*). According to this approach, the receptor binds not too strongly and fully quenches the emission of an anionic fluorescent indicator. Then, in a titration experiment, the envisaged anion displaces from receptor's cavity the indicator, which can release its natural fluorescence, thus signalling, through an OFF/ON mechanism, the occurrence of the recognition process. 5-Carboxy-fluorescein (**20**) was chosen as an indicator, as it possesses two carboxylate groups and a phenolate oxygen atom, capable of interacting with the Cu^{II} centres of the receptor. 5-carboxy-fluorescein is highly fluorescent in its anionic form, the dominating species at pH = 7. Complete quenching

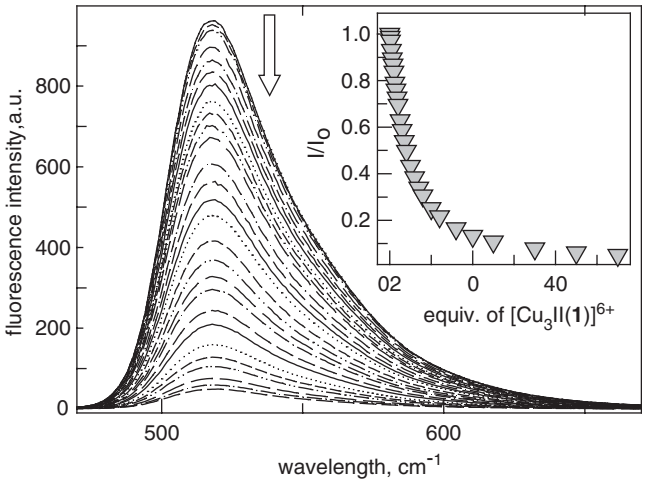

FIG. 6. Emission spectra taken on titration of an aqueous solution of 5-carboxy-fluorescein (2.5×10^{-7} M), buffered at pH 7 with HEPES 0.01 M, with an aqueous solution of $[Cu^{II}_3(\mathbf{19})]^{6+}$ ($\lambda_{exc} = 450$ nm).

of the 5-carboxy-fluorescein emission was observed when titrating a degassed solution of the indicator **20** with a standard solution of $[Cu_3^{II}(\mathbf{19})]^{6+}$ (as shown by the family of spectra displayed in Fig. 6).

Curve fitting of the titration profile (fluorescent intensity vs. concentration of $[Cu_3^{II}(\mathbf{19})]^{6+}$, shown in the inset of Fig. 6) indicated the formation of a 1:1 receptor–indicator complex, whose association constant log K_{in} was 5.78 ± 0.01. Quenching is ascribed to the occurrence of an intramolecular electron or energy transfer process involving the photoexcited fluorescein subunit and the paramagnetic Cu^{II} centres within the complex. Then an aqueous solution containing $[Cu_3^{II}(\mathbf{19})]^{6+}$ (2×10^{-5} M) and **20** (5×10^{-7} M) and buffered to pH 7 was titrated with an aqueous solution of 1,3,5-benzene-tricarboxylate, **21**. It was observed that progressive addition of 1,3,5-benzene-tricarboxylate induced a complete recovery of the 5-carboxy-fluorescein emission.

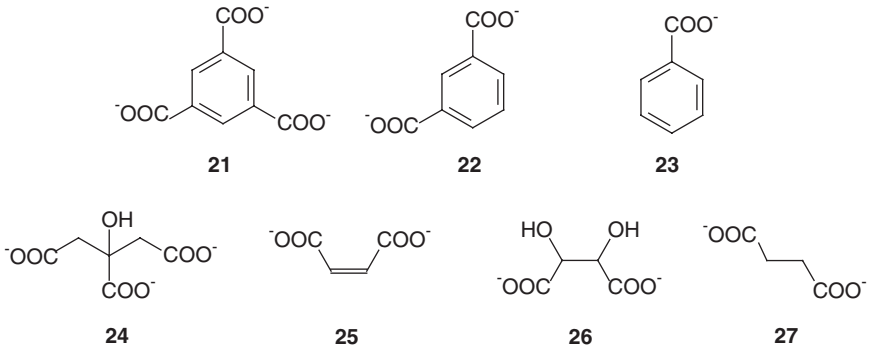

The corresponding titration profile (fluorescent intensity vs. anion equiv.) is shown in Fig. 7 (circles) and clearly indicates that the $[C_6H_3(COO)_3]^{3-}$ anion fully displaces the indicator from the host cavity.

On non-linear least-squares treatment of titration data a log $K_{ass} = 5.81 \pm 0.01$ was calculated for the 1:1 complex between $[Cu_3^{II}(\mathbf{19})]^{6+}$ and $[C_6H_3(COO)_3]^{3-}$. The high value of the association constant probably has to be ascribed to the geometrical complementariety of the $[Cu_3^{II}(\mathbf{1})]^{6+}$ receptor and of the $[C_6H_3(COO)_3]^{3-}$ anion, both possessing a C_{3v} symmetry. In particular, the negatively charged oxygen atom of each carboxylate group establishes a coordinative interaction with the copper(II) centre of each metallocyclam subunit. In this connection, it should be noted that the bidentate anion 1,3-benzene dicarboxylate (isophthalate, **22**, triangles in Fig. 7) and the monodentate benzoate (**23**, diamonds) gave much shallower titration profiles, to which much smaller values of log K_{ass} correspond (< 3). This further demonstrates the natural affinity of the tripodal $[Cu_3^{II}(\mathbf{19})]^{6+}$ receptor for triply negatively charged anions of triangular shape.

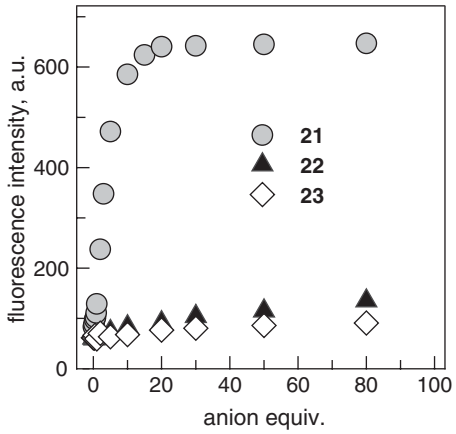

FIG. 7. Profiles obtained over the course of the titration with a given anion of an aqueous solution 2×10^{-5} M in $[Cu_3^{II}(\mathbf{19})]^{6+}$ and 5×10^{-7} M in **20**, and buffered to pH 7 with HEPES (0.01 M). The 1,3,5-benzene-tricarboxylate anion, **21** (circles) displaces from receptor's cavity the fluorescein indicator **20**, which can release its full fluorescent emission.

Not surprisingly, receptor $[Cu_3^{II}(\mathbf{19})]^{6+}$ forms a very stable 1:1 complex with the triply negatively charged anion citrate (**24**, log $K_{ass} = 5.59 \pm 0.01$, the titration profile is shown in Fig. 8), whose three carboxylate groups can coordinate the three Cu^{II} centres. Similar titration experiments were carried out on a variety of dicarboxylates, none of which could compete with citrate, as shown by the shallower titration profiles reported in Fig. 8. This is probably due to the fact that dicarboxylates can interact with only two of the three available copper(II) centres. However, affinity towards $[Cu_3^{II}(\mathbf{19})]^{6+}$ varies significantly with the nature of the dicarboxylate anion. In particular, maleate (**25**) forms a relatively stable complex with $[Cu_3^{II}(\mathbf{19})]^{6+}$ (log $K_{ass} = 4.5 \pm 0.1$), more stable than tartrate (**26**, log $K_{ass} = 4.1 \pm 0.1$) and succinate (**27**, log $K_{ass} = 3.8 \pm 0.1$). In the three envisaged anions **25**–**27** the two COO^- groups are separated by the same number of carbon atoms, with a similar bite length for encompassing the metallocyclam subunits of two arms: the observed affinity sequence (**25** > **26** > **27**) reflects the increase of the flexibility of anion framework and the consequent increasing loss of conformational entropy, which takes place on complex formation. Very poor affinity towards $[Cu_3^{II}(\mathbf{19})]^{6+}$ is displayed by the spherical chloride and by the trigonal nitrate, for which K_{ass} values $< 10^3$ could be estimated. Indeed, NO_3^- possesses a C_{3v} symmetry, but it detains only one negative charge and behaves as a poorly coordinating ligand for 3d metal ions, also when acting as monodentate. Moreover, the small size of NO_3^- does not allow a favourable fitting within the rather large cavity provided by $[Cu_3^{II}(\mathbf{1})]^{6+}$. In particular, such a cavity is tailor-made for the much

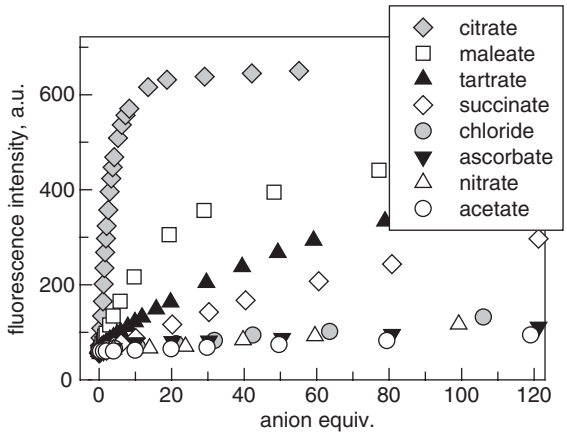

FIG. 8. Profiles obtained over the course of the titration with a given anion of an aqueous solution 2×10^{-5} M in $[Cu_3^{II}(\mathbf{19})]^{6+}$ and 5×10^{-7} M in **20**, and buffered to pH 7 with HEPES (0.01 M).

larger 1,3,5-benzene-tricarboxylate ion. To make a fair comparison with receptors operating through electrostatic interactions, it has to be mentioned that the 1,3,5-ethyl benzene scaffold had been previously functionalised with three arms contaning guanidinium groups (*44*), to generate a tricationic receptor, which formed a stable complex with the citrate anion in water ($\log K_{ass} = 3.8$). Affinity towards citrate has been more recently increased (*45*), through the use of side chains containing the guanidium-carbonyl pyrrole functionality ($\log K_{ass} = 4.9$ at pH = 6.3). We have shown that the metal containing receptor $[Cu_3^{II}(\mathbf{19})]^{6+}$, in an aqueous solution buffered at neutral pH, forms with citrate a 1:1 complex with $\log K_{ass} = 5.6$, thus becoming the most efficient artificial receptor for the binding of citrate in water reported thus far.

The moral of the story is that the use of receptors containing metallocyclam subunits should be encouraged in anion recognition studies, for two main reasons: (i) the metal centre is coordinatively unsaturated and leaves room for the binding of one anion donor atom, without any particular steric constraint, and (ii) it is kinetically inert and cannot be demetalated even in presence of a huge excess of analyte or of any other competing ligand.

VI. A Molecular Fluorescent Thermometer Operating Through the Ni^{II}/Ni^{III} Redox Change

Sensing, in a chemical context, refers to the detection of a molecular species, whose presence and amount is signalled through the drastic change of a property, e.g. fluorescence. However, even a physical

quantity, e.g. temperature, can be sensed at the molecular level, using a quite similar approach. In the simplest way, a molecular fragment sensitive to temperature is connected to a fluorogenic subunit. In particular, the temperature sensitive unit must exist in two different states of comparable stability A and B. Then, A and B must be in equilibrium and the equilibrium should be affected by temperature, being distinctly exo- or endo-thermic. As a second requirement, A and B should exhibit a different perturbing effect on the proximate fluorophore: state A quenches fluorescence and state B does not (or *vice versa*). In these circumstances, one could modulate the intensity of the fluorescent emission by changing the relative concentration of A and B by a temperature variation. As a consequence, the temperature of the solution can be measured from the fluorescence intensity, I_F, on the basis of an I_F vs. temperature calibration curve.

A convenient temperature sensitive subunit is provided by the coordination chemistry of polyamine macrocycles: the $[Ni^{II}(cyclam)]^{2+}$ complex. In fact, $[Ni^{II}(cyclam)]^{2+}$ in a polar solvent S – water (*46*), MeCN and DMSO (*47*) – exists in two forms of comparable stability, which differ for their electronic properties and stereochemistry: (i) an octahedrally elongated form, $[Ni^{II}(cyclam)S_2]^{2+}$, in which the four nitrogen atoms of cyclam span the equatorial plane, and two solvent molecules S occupy the axial sites: the complex has two unpaired electrons (high-spin form) and exhibits a blue-violet colour; (ii) a square species, $[Ni^{II}(cyclam)]^{2+}$, in which the macrocycle is coplanarly coordinated to the metal: the two highest energy electrons are now paired (low-spin form) and the colour is yellow, due to a relatively intense d–d band centred at 450 nm, molar absorbance $\varepsilon = 65\,M^{-1}\,cm^{-1}$, in aqueous 0.1 M $NaClO_4$, at 25°C. The two forms undergo a fast and reversible interconversion equilibrium, which is strongly temperature dependent:

$$\underset{\text{blue, high-spin}}{[Ni^{II}(cyclam)S_2]^{2+}} \rightleftarrows \underset{\text{yellow, low-spin}}{[Ni^{II}(cyclam)]^{2+}} + 2S$$

In particular, a temperature increase favours the formation of the yellow, low-spin species; a temperature decrease favours the formation of the blue, high-spin form. The high-to-low-spin conversion is distinctly endothermic (in aqueous solution, $\Delta H^\circ = 5.4\,kcal\,mol^{-1}$), and this reflects the loss of the two axial Ni^{II}-S bond, when moving from the octahedral to the square stereochemistry. At 25°C, in aqueous solution, there exists 25% of the low-spin species, and 75% of the high-spin species: however, the solution appears yellow, owing to the higher absorbance of the low-spin complex (*46*). Distribution varies with the solvent's nature and is also affected by structural modification on cyclam backbone (e.g. presence of alkyl substituents on nitrogen and carbon atoms).

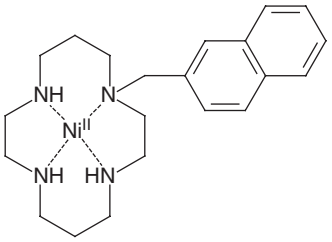

28

On these premises, the $[Ni^{II}(cyclam)]^{2+}$ fragment was linked through a $-CH_2-$ group to the classic naphthalene fluorophore, to give the two-component assembly **28** (*48*). It has now to be verified whether the two metal spin states have a different perturbing effect on the nearby photoexcited naphthalene fragment. This can be assessed by studying the emission behaviour of complex salts of formula $Ni^{II}(\mathbf{28})X_2$. In an $Ni^{II}(\mathbf{28})X_2$ salt, in the solid state, the Ni^{II} centre experiences an octahedrally elongated coordination geometry, in which the two X^- anions occupy the two apical positions. The spin-state of the metal centre is determined by the coordinating tendencies of X^-: (i) strongly coordinating anions (e.g. Cl^-) stabilise the high-spin state (Ni^{II} 'feels' an *octahedral* stereochemistry); (ii) weakly coordinating anions stabilise the low-spin state (Ni^{II} 'feels' a *square* stereochemistry). The complex salts $Ni^{II}(\mathbf{7})X_2$, when dissolved in $CHCl_3$, in view of solvent's non-coordinating tendencies, keep intact their donor set and maintain their spin state. Thus, measuring the emission spectra of $CHCl_3$ solutions of different $Ni^{II}(\mathbf{7})X_2$ salts allows one to evaluate the effect of the Ni^{II} spin state on the emission properties of the nearby naphthalene fragment. Quite interestingly, this effect is substantially different for high- and low-spin complexes.

Table II reports the quantum yields Φ of a series of $Ni^{II}(\mathbf{28})X_2$ complex salts of different spin multiplicity. High-spin complexes ($X^- = Cl^-$, NO_3^-, NCS^-) show a quantum yield 3–4 times lower than low-spin complexes ($X^- = ClO_4^-$, $CF_3SO_3^-$). It should be noticed that the quantum yield is in any case distinctly lower than observed with plain naphthalene, thus indicating that the metal centre has a more or less pronounced quenching effect on the nearby excited fluorophore. It has been observed that the quenching mechanism has an energy transfer nature (in fact, the fluorescence intensity is not restored when the solution is frozen to 77 K). In particular, it has been hypothesised that the energy transfer takes place through a double electron exchange (Dexter mechanism). Quantum yield values in $CHCl_3$ solution show that such a process is remarkably more efficient for the high-spin metal centre than for the spin paired complex, whose electronic structure is definitively more compact.

On these bases, one should expect that the spin-state effect on fluorescence should be observed also in a polar and coordinating medium,

TABLE II

QUANTUM YIELDS VALUES (Φ) DETERMINED FOR DIFFERENT SALTS OF $[Ni^{II}(\mathbf{28})]^{2+}$ COMPLEX IN A $CHCl_3$ SOLUTION. Φ OF PLAIN NAPHTHALENE, IN AN EtOH SOLUTION, IS 0.21

Anion	Cl^-	NO_3^-	NCS^-	ClO_4^-	$CF_3SO_3^-$
Φ	0.007	0.009	0.005	0.019	0.020

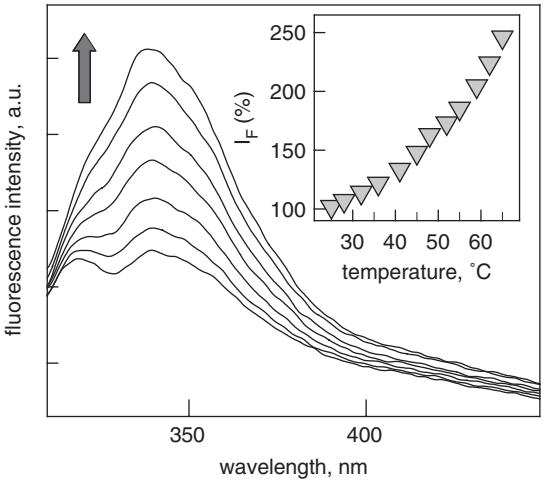

FIG. 9. Emission spectra of an MeCN solution 10^{-5} M in the $Ni^{II}(\mathbf{28})(ClO_4)_2$ complex salt recorded over the 27–65°C range ($\lambda_{exc} = 290$ nm). On increasing temperature, fluorescence increases, owing to the conversion of the high-spin into the low-spin state of the Ni^{II} centre. The inset shows the variation of the fluorescence intensity at 335 nm, I_F, with temperature and represents the calibration curve of the molecular fluorescent thermometer $Ni^{II}(\mathbf{28})(ClO_4)_2$.

where the axial position are not longer occupied by the X^- anions, but by solvent molecules and where the high- and low-spin species coexist, according to a temperature-dependent equilibrium. Indeed, the emission intensity of a solution of an $Ni^{II}(\mathbf{28})(ClO_4)_2$ complex in an MeCN solution was observed to vary with temperature and, in particular, it increases with increasing temperature. Fig. 9 displays the family of emission spectra recorded over the 27–65°C range.

The spin conversion equilibrium taking place in the MeCN solution is illustrated by the following equation:

$$[Ni^{II}(\mathbf{28})(MeCN)_2]^{2+} \rightleftharpoons [Ni^{II}(\mathbf{28})]^{2+} + 2MeCN$$

At lower temperatures the $[Ni^{II}(\mathbf{28})(MeCN)_2]^{2+}$ complex, high-spin, dominates, which has the more pronounced quenching effect on the nearby naphthalene fluorophore. Owing to the endothermic nature of

the high-to-low-spin conversion, on raising temperature the concentration of the low-spin form, $[Ni^{II}(cyclam)]^{2+}$, increases, causing a concurrent enhancement of the fluorescent emission. The inset of Fig. 9 shows the variation of the maximum of the emission intensity with temperature. Such a diagram represents a sort of calibration curve of the $[Ni^{II}(\mathbf{28})]^{2+}$ system, which behaves as a thermometric probe. The response of the thermometer is fully reversible and extremely fast, as the fluorescent emission change is related to the release-uptake of solvent molecules from the axial positions of the metal and to the consequent electron rearrangement, a process taking place well below the millisecond timescale.

Systems of this type could be gainfully used for measuring the temperature of biological fluids, including intracellular ones. In particular, fluorescence microscopy measurements would allow one to determine temperature changes inside a cell domain, in which the fluorescent probe had been injected, with both spatial and temporal resolution. The advantage of systems like $[Ni^{II}(\mathbf{28})]^{2+}$ is that, due to the high sensitivity of the fluorescent signal, they can be used at very low, non-invasive concentration levels. In particular, temperature changes of a solution of $[Ni^{II}(\mathbf{28})]^{2+}$ can be distinctly perceived at a 10^{-7} M concentration. However, the rather lipophilic system $[Ni^{II}(\mathbf{28})]^{2+}$ itself cannot be used as a thermometric probe for biological fluids due to its very poor solubility in water. The obstacle can be circumnavigated by appending to the cyclam framework a more hydrophilic fluorogenic fragment than naphthalene.

VII. Conclusion

We have tried to demonstrate that metal complexes of cyclam derivatives, including scorpionands, can perform some elementary functions at the molecular level (signalling, sensing, controlling of molecular motions). These, and other, functions result from the combination of the unique properties displayed by cyclam and related synthetic macrocycles. Daryle Busch invented this topic, devising the template synthesis of macrocyclic complexes and characterising their distinctive behaviour, related to the cyclic and constrained nature of the ligand. His papers have inspired hundreds of researchers all over the world and remain fundamental for the development of macrocyclic and supramolecular chemistry. Long live Professor Busch and cyclam!

References

1. Cabbiness, D. K.; Margerum, D. W. *J. Am. Chem. Soc.* **1969**, *91*, 6540–6541.
2. Cabbiness, D. K.; Margerum, D. W. *J. Am. Chem. Soc.* **1970**, *92*, 2151–2153.
3. Lovecchio, F. V.; Gore, E. S.; Busch, D. H. *J. Am. Chem. Soc.* **1974**, *96*, 3109–3118.
4. Olson, D. C.; Vasilevskis, J. *Inorg. Chem.* **1971**, *10*, 463–470.

5. Barefield, E. K.; Mocella, M. T. *Inorg. Chem*. 1973, 12, 2829–2832.
6. Deming, R. L.; Allred, A. L.; Dahl, A. R.; Herlinger, A. W.; Kestner, M. O. *J. Am. Chem. Soc* **1976**, *98*, 4132–4137.
7. Busch, D. H. *Acc. Chem. Res.* **1978**, *11*, 392–400.
8. Billo, E. J. *Inorg. Chem*. **1984**, *23*, 236.
9. Fabbrizzi, L.; Micheloni, M.; Paoletti, P. *Inorg. Chem*. **1980**, *19*, 535–538.
10. Fabbrizzi, L.; Micheloni, M.; Paoletti, P. *J. Chem. Soc*., *Dalton Trans*. **1979**, 1581–1584.
11. Anichini, A.; Fabbrizzi, L.; Paoletti, P.; Clay, R. C. *J. Chem. Soc., Chem. Commun*. 1977, 244–245.
12. Bencini, A.; Fabbrizzi, L.; Poggi, A. *Inorg. Chem*. **1981**, *20*, 2544–2549.
13. Sabatini, L.; Fabbrizzi, L. *Inorg. Chem*. **1979**, *18*, 438–444.
14. Thompson, M. C.; Busch, D. H. *J. Am. Chem. Soc.* **1964**, *86*, 3651–3656.
15. Barefield, E. K. *Inorg. Chem*. **1972**, *11*, 2273–2274. Barefield, E. K.; Wagner, F.; Herlinger, A. W.; Dahl, A. R. *Inorg. Synth*. **1976**, *16*, 220.
16. Hinz, F. P.; Margerum, D. W. *Inorg. Chem*. **1974**, *13*, 2941–2949.
17. Comba, P.; Curtis, N. F.; Lawrance, G. A.; Sargeson, A. M.; Skelton, B. W.; White, A. H. *Inorg. Chem*. **1986**, *25*, 4260–4267.
18. Fabbrizzi, L.; Licchelli, M.; Poggi, A.; Vassalli, O.; Ungaretti, L.; Sardone, N. *Inorg. Chim. Acta* **1996**, *246*, 379.
19. Fabbrizzi, L.; Manotti Lanfredi, A. M.; Pallavicini, P.; Perotti, A.; Taglietti, A.; Ugozzoli, F. *J. Chem. Sac., Dalton Trans*. **1991**, 3263.
20. De Blas, A.; De Santis, G.; Fabbrizzi, L.; Licchelli, M.; Manotti Lanfredi, A. M.; Morosini, P.; Pallavicini, P.; Ugozzoli, F. *J. Chem. Soc., Dalton Trans.* **1993**, 1411–1416.
21. Abbà, F.; De Santis, G.; Fabbrizzi, L.; Licchelli, M.; Manotti Lanfredi, A. M.; Pallavicini, P.; Poggi, A.; Ugozzoli, F. *Inorg. Chem*. **1994**, *33*, 1366–1375.
22. De Blas, A.; De Santis, G.; Fabbrizzi, L.; Licchelli, M.; Mangano, C.; Pallavicini, P. *Inorg. Chim. Acta* **1992**, *115*, 202.
23. De Santis, G.; Fabbrizzi, L.; Licchelli, M.; Sardone, N.; Velders, A. H. *Chem. Eur. J.* **1996**, *2*, 1243–1250.
24. Fabbrizzi, L.; Licchelli, M.; Pallavicini, P. *Acc. Chem. Res.* **1999**, *32*, 846–853.
25. Pallavicini, P.; Perotti, A.; Poggi, A.; Seghi, B.; Fabbrizzi, L. *J. Am. Chem. Soc.* **1987**, *109*, 5139.
26. Fabbrizzi, L.; Barbucci, R.; Paoletti, P. *J. Chem. Soc., Dalton Trans.* **1972**, 1529–1534.
27. Schwörer, M.; Wirz, J. *Helv. Chim. Acta* **2001**, *84*, 1441–1458.
28. Boiocchi; L. Fabbrizzi, M.; Foti, F.; Monzani, E.; Poggi, A. *Org. Lett.* **2005**, *7*, 3417–3420.
29. Fabbrizzi, L.; Poggi, A.; Seghi, B. *Inorg. Synth*. **1985**, *23*, 82.
30. Buttafava, A.; Fabbrizzi, L.; Perotti, A.; Poggi, A.; Seghi, B. *Inorg. Chem*. **1984**, *23*, 3917.
31. Siegfried, L.; Kaden, T. A. *J. Phys. Org. Chem*. **1992**, *5*, 549–555.
32. Fabbrizzi, L.; Licchelli, M.; Pallavicini, P.; Perotti, A.; Taglietti, A.; Sacchi, D. *Chem. Eur. J.* **1996**, *2*, 75–82.
33. Boiocchi, M.; Fabbrizzi, L.; Licchelli, M.; Sacchi, D.; Vázquez, M.; Zampa, C. *J. Chem. Soc. Chem. Commun*. **2003**, 1812–1813.
34. Bowman-James, K. *Acc. Chem. Res.* **2005**, *38*, 671–678.
35. Lehn, J. M.; Sonveaux, E.; Willard, A. K. *J. Am. Chem. Soc.* **1978**, *100*, 4914.
36. Schmidtchen, F. P. *Angew. Chem*. **1977**, *89*, 751.
37. Amendola, V.; Bastianello, E.; Fabbrizzi, L.; Mangano, C.; Pallavicini, P.; Perotti, A.; Manotti Lanfredi, A.; Ugozzoli, F. *Angew. Chem. Int. Ed. Engl*. **2000**, *39*, 2917. Fabbrizzi, L.; Leone, A.; Taglietti, A. *Angew. Chem. Int. Ed*. **2003**, *40*, 3066. Fabbrizzi, L.; Marcotte, N.; Stomeo, F.; Taglietti, A. *Angew. Chem. Int. Ed*. **2003**, *41*, 3811–3814. Hortala, M. A.; Fabbrizzi, L.; Marcotte, N.; Stomeo, F.; Taglietti, A. *J. Am. Chem. Soc.* **2003**, *125*, 20–21.

38. Boiocchi, M.; Bonizzoni, M.; Fabbrizzi, L.; Piovani, G.; Taglietti, A. *Angew. Chem., Int. Ed.* **2004**, *43*, 3847–3852.
39. Bonizzoni, M.; Fabbrizzi, L.; Piovani, G.; Taglietti, A. *Tetrahedron* **2004**, *60*, 11159–11162.
40. Fabbrizzi, L.; Foti, F.; Taglietti, A. *Org. Lett.* **2005**, *7*, 2603–2606.
41. Micheloni, M.; Paoletti, P.; Bürki, S.; Kaden, T. A. *Helv. Chim. Acta* **1982**, *65*, 587–594.
42. Boiocchi, M.; Bonizzoni, M.; Fabbrizzi, L.; Foti, F.; Licchelli, M.; Poggi, A.; Taglietti, A.; Zema, M. *Chem. Eur. J.* **2004**, *10*, 3209–3216.
43. Wiskur, S. L.; Ait-Haddou, H.; Lavigne, J. J.; Anslyn, E. V. *Acc. Chem. Res.* **2001**, *34*, 963–972.
44. Metzger, A.; Lynch, V. M.; Anslyn, E. V. *Angew. Chem., Int. Ed. Engl.* **1997**, *36*, 862–864. Metzger, A.; Anslyn, E. V. *Angew. Chem., Int. Ed.* **1998**, *37*, 649–652.
45. Schmuck, C.; Schwegmann, M. *J. Am. Chem. Soc.* **2005**, *127*, 3373–3379.
46. Sabatini, L.; Fabbrizzi, L. *Inorg. Chem.* **1979**, *18*, 438.
47. Boiocchi, M.; Fabbrizzi, L.; Foti, F.; Vázquez, M. *J. Chem. Soc., Dalton Trans.* **2004**, 2616–2620.
48. Engeser, M.; Fabbrizzi, L.; Licchelli, M.; Sacchi, D. *J. Chem. Soc. Chem. Commun*. **1999**, 1191.

MOLECULAR RECOGNITION OF NEUTRAL AND CHARGED GUESTS USING METALLOMACROCYCLIC HOSTS

IVAN V. KORENDOVYCH[a], REBECCA A. ROESNER[b] and ELENA V. RYBAK-AKIMOVA[a]

[a]Department of Chemistry, Tufts University, Medford, MA 02155, USA
[b]Department of Chemistry, Illinois Wesleyan University, Bloomington, IL 61702-2900, USA

I. Introduction

Macrocycles and metallomacrocycles are widely used as hosts for molecular recognition of various charge- and shape-complementary substrates (*1–6*). Each macrocyclic molecule incorporates several heteroatoms that can be involved in guest recognition. These large cyclic molecules adopt well-defined shapes, thus allowing for discrimination between guests. Additionally, macrocyclic ligands and their complexes can be easily modified, functionalized, or linked together, in order to create receptors suitable for high affinity binding of specific substrates.

ADVANCES IN INORGANIC CHEMISTRY
VOLUME 59 ISSN 0898-8838 / DOI: 10.1016/S0898-8838(06)59004-X

In the arsenal of intermolecular, non-covalent interactions responsible for substrate binding (electrostatic attraction, hydrogen bonding, hydrophobic interactions, aromatic π-stacking, etc.) coordinative bonding between a donor atom and a metal ion is among the strongest binding modes. The incorporation of metal ions into molecular receptors has resulted in the successful design of a variety of metallohosts (*3–8*). While the metal ion is itself a guest in these systems, it can, in turn, contribute to the recognition of secondary, non-metallic substrates. In addition to coordinative interactions between the donor atoms of guest molecules and vacant coordination sites on the metallohosts, such as those that operate when dioxygen binds to hemoglobin; metal cations can also participate in electrostatic interactions with negatively charged functional groups that may be present in guests. Through this second mode of interaction, transition metal complexes have been used in the design of high affinity anion receptors (*9–14*). Metal ions can also play a structural role in pre-organizing molecular receptors for substrate binding (*3,5*), and/or act as reporters in sensors due to their ability to signal a substrate binding event via changes in fluorescence, absorbance, or redox potential (*15–22*). Metallomacrocycles appear to be particularly attractive building blocks for the design of metallohosts, on account of their well-known thermodynamic stability and kinetic inertness (*23*). Thus, the metal ions incorporated into the macrocycles will remain in well-defined coordination sites during substrate recognition events, and no leakage of the metal is expected.

Although the presence of one or several metal ions in the macrocyclic hosts is clearly useful for designing high-affinity receptors, anion binding via multiple electrostatic interactions is also effective with protonated, metal-free macrocycles. Molecular recognition of anions with polyammonium- or polyalkylammonium macrocycles, pioneered by J.-M. Lehn and coworkers (*24,25*), is a very active area of research and has been extensively reviewed (*9,25–27*).

Molecular recognition, which implies preferential binding of certain substrates over others, is best accomplished in an enzyme mimetic fashion—by incorporating multiple binding sites in three-dimensional assemblies. Selective binding of complementary substrates is often reinforced by size and shape selectivity of guest inclusion within lacuna created by adding superstructure to macrocyclic platforms. A variety of molecular architectures have been employed in the preparation of efficient and selective hosts from macrocyclic receptors. Popular substrate binding modes include encapsulation of a guest within the hydrophobic cleft of a mononuclear macrocycle, guest coordination to the metal center supplemented by hydrogen bonding with the heteroatoms of the same macrocycle, guest interaction with receptor centers in the pendant arms attached to the macrocycle or metallomacrocycle, guest binding between two or more macrocycles, and coordination of the guest to two metal ions within one dinuclear

macrocyclic complex (*5*). Comprehensive coverage of this rapidly developing area of research is beyond the scope of the present paper. We will instead provide examples related to our own research on metallomacrocycles that recognize polyfunctional guests of various sizes. Many aspects of these studies were inspired by the seminal contributions of Professor Daryle Busch (*4*).

First, we would like to present molecular design principles that are applicable to selective recognition of small molecules such as O_2 and CO. Specifically, coordination of these small molecules to metal centers within the cleft-shaped cyclidene macrocycles will be considered. Next, strategies for expanding the hydrophobic cyclidene cavities to allow for incorporation of medium-sized organic molecules will be discussed. These systems were designed by Busch and coworkers in order to prepare fully synthetic models for the active sites of oxidative enzymes (e.g., cytochrome P450). Oxygen coordination to the metal accompanied by substrate encapsulation within the hydrophobic cavity may ultimately result in regio- and stereoselective, "enzyme-like" substrate oxidations (*28,29*). In the next section, we will discuss length- and shape-selective recognition of difunctional medium-sized organic cations (e.g., diammonium cations) and organic anions (e.g., dicarboxylates) that bind between two receptor sites appended to the edges of folded macrocyclic clefts. Finally, we will explore binding motifs that are promising for recognition of large hydrophobic species, including fullerenes and carbon nanotubes, and large inorganic polyanions, such as polyoxometalates. These polyhedral species can be sandwiched between two or more nearly planar macrocycles, encapsulated within cavities formed from one or more functionalized macrocycles, or bound by several pendant arms radiating from a single macrocyclic platform.

II. Mononuclear Clefts for Binding Neutral Molecules

The systems to be considered in this section are mononuclear macrocyclic complexes with non-planar conformations. While the metal center may provide a specific coordination site for binding a guest, the selective molecular recognition in these systems is based primarily on the shape complementarity between the host and the guest, and depends on multiple weak interactions (van der Waals forces, π-stacking, etc.) between the macrocyclic ligand (the "organic part" of the complex) and the guest. Multipoint substrate binding is the most effective way to accomplish selectivity. For this reason, axial coordination of mono- or bidentate guest ligands in the absence of secondary intermolecular forces, while important in its own right, will not be considered in this discussion.

Guest recognition using unmodified monocyclic hosts is often based on the inclusion of shape-complementary guests. The monocyclic

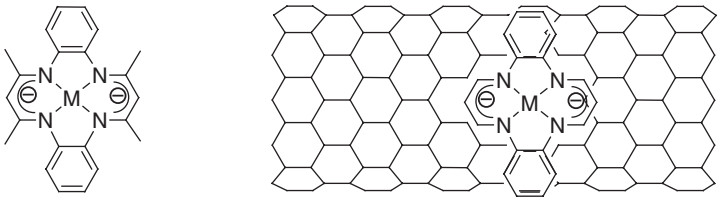

1

SCHEME 1. Macrocyclic complex 1 and its proposed binding to single-walled carbon nanotubes.

ligands fold to form clefts that serve to confine the guests (*30,31*). In the absence of direct bonding between the metal center and the (usually non-polar) organic guests, large contact areas between the host and guest can lead to sufficiently strong binding through van der Waals forces and/or π–π interactions. Large molecules and nano-objects, such as fullerenes (*30,32–36*) and single-walled carbon nanotubes (Scheme 1 (*37*)) are easily cradled in the clefts of folded aromatic macrocycles. Various aspects of using macrocycles for the recognition of large anions (polyoxometalates) will be considered in Section IV.

A. RECOGNITION OF SMALL MOLECULES

Weak non-covalent interactions are insufficient for small molecule (e.g., O_2, CO) recognition, such as that observed in synthetic oxygen carriers, because of the insufficient surface area for host–guest van der Waals contacts. In this case, stronger coordinative bonds between a small molecule, such as O_2, and the transition metal center (usually, iron(II) or cobalt(II)) account for binding strength, while the shape of the cleft or void is responsible for excluding larger substrates or preventing undesired host–host interactions. Fine-tuning of the binding pocket also allows for discrimination between two small molecules (e.g., the preferential binding of dioxygen over carbon monoxide).

Bi- and tricyclic host systems were designed in order to create a 3D void about the metal ion, thus allowing for steric discrimination between small (e.g., O_2) and large (e.g., 1-methylimidazole) guest ligands (*38*). The most thoroughly studied and robust of these totally synthetic, macrocyclic oxygen carriers are the superstructured cyclidenes of Busch and co-workers (*29,38,39*). These molecules were designed so that the O_2 binding site at the Co(II) or Fe(II) center is protected from autoxidation (μ-oxo dimer formation is prevented by the bridge). Although the rich chemistry of these complexes has been reviewed (*40*), we will briefly discuss the aspects important to molecular recognition here.

Cyclidene macrocycles (see Scheme 2 for representative structures) have been bridged across the cavity, creating sterically protected

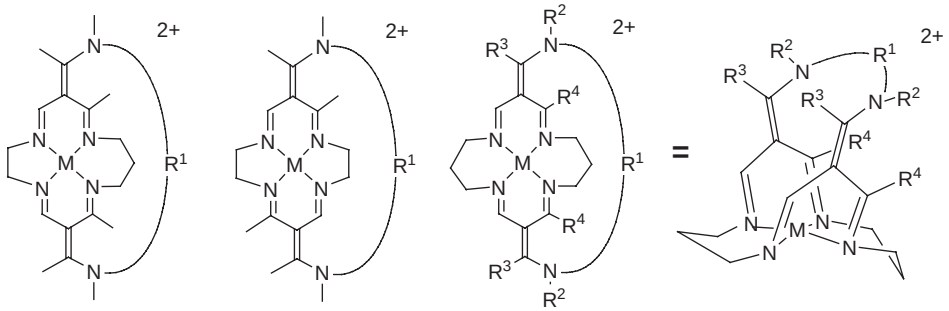

2: $R^1 = (CH_2)_6$ **3:** $R^1 = 2\ CH_3$ **4:** $R^1 = (CH_2)_{12}$

5: R^1= 2 Me, R^2=R^3=R^4=Me
6: R^1= $(CH_2)_3$, R^2=R^3=R^4=Me **12:** R^1= $(CH_2)_4$, R^2 =Ph, R^3=R^4=Me
7: R^1= $(CH_2)_4$, R^2=R^3=R^4=Me **13:** R^1= $(CH_2)_5$, R^2 =Ph, R^3=R^4=Me
8: R^1= $(CH_2)_5$, R^2=R^3=R^4=Me **14:** R^1= $(CH_2)_6$, R^2 =Ph, R^3=R^4=Me
9: R^1= $(CH_2)_6$, R^2=R^3=R^4=Me **15:** R^1= $(CH_2)_8$, R^2 =Ph, R^3=R^4=Me
10: R^1= $(CH_2)_8$, R^2=R^3=R^4=Me **16:** R^1= $(CH_2)_6$, R^2 =Me, R^3=R^4=H
11: R^1= $(CH_2)_{12}$, R^2=R^3=R^4=Me **17:** R^1= $(CH_2)_8$, R^2 =Me, R^3=R^4=H

SCHEME 2. Representative structures of cyclidene macrocyeles.

ligand binding pockets in the resulting lacunar complexes (*38*). The cavities in these compounds have been further expanded to form vaulted cyclidenes (compounds **18–24**, Section II.B) (*28,29,38,41*). The shapes of the cyclidene platforms depend on the size of the macrocyclic ring. The 16-membered macrocyclic platforms (**5–24**) fold because of the conformational requirements of adjacent chelate rings: the low energy chair or boat conformations of the 6-membered saturated rings force the adjacent unsaturated rings to tilt toward the MN_4 plane. In the most common geometry, both unsaturated "wings" are positioned on the same side of the MN_4 plane, forming a well-defined cleft. However, the unsaturated chelate rings can also tilt in opposite directions, giving the macrocycle a zig-zagged shape. This unusual conformation was reported for the *trans*-dimethyl cyclidenes (16-membered homologs of **3**) (*42*). The 14-membered cyclidenes, which commonly have *trans*-orientation of their methyl substituents (compounds **3** and **4,** Scheme 2), are essentially planar due to gauche conformations of the saturated 5-membered chelate rings (*43,44*). The 15-membered complexes, where conflicting requirements of the 5- and the 6-membered saturated chelate rings compete, can adopt either a planar or a saddle-shaped conformation (*38,44*).

Dioxygen affinity of the Co(II) and Fe(II) cyclidene complexes is governed by both electronic and steric factors. Coordination of a fifth donor ligand, such as pyridine or 1-methylimidazole, is required for efficient O_2 binding and is usually accomplished by adding the corresponding base to a solution of the macrocyclic complex. The sixth

coordination site of the metal should remain vacant or be occupied by a labile ligand, in order to allow for reversible binding of the O_2 ligand. The lacunar cyclidenes **6–17** are ideally suited for selectively binding small ligands (O_2, CO) inside the cavity while excluding larger monodentate basic ligands (pyridine, 1-methylimidazole). The iron(II) complexes of the C4- and C5-bridged cyclidenes (Fe(**12**), Fe(**13**)) exist in solution (in acetone–pyridine–water or acetonitrile–1-methylimidazole solvent systems) as high-spin, five-coordinate species, (*45–47*) while the iron(II) complex of the C6-bridged cyclidene Fe(**14**) displays a distinct spin equilibrium between a five-coordinate high-spin form and a six-coordinate low-spin form. This equilibrium is shifted toward formation of the low-spin, six-coordinate form at low temperature (–40°C). The C8-bridged Fe(**15**)$^+$ exists as a similar equilibrium mixture with a significant fraction of 6-coordinate complex present even at room temperature (*47*). Molecular modeling studies demonstrate that exclusion of axial base (1-methylimidazole) from the cavity is largely due to van der Waals repulsion between the guest and the bridge (the "roof" of the lacuna), while the interaction between the flat aromatic guest and the walls of the cleft is relatively less important (*48*). The behavior of d^7 Co(II) ions with respect to axial ligand binding is somewhat different from that of d^6 ions, such as cobalt(III) or iron(II): five-coordinate species dominate in solutions of both lacunar and unbridged Co(II) cyclidenes in the presence of excess pyridine or imidiazole derivatives, as evidenced by EPR spectroscopy (*38,40,49,50*) and electrochemical data (*50,51*). In the case of cobalt(II) cyclidenes (especially for the unbridged complexes), exclusion of the axial base from the sixth position is due to electronic factors (destabilization of the d_z^2 orbital in complexes with strong equatorial ligand fields) rather than the superstructure (*48*). In the absence of a sixth ligand, biomimetic principles suggest and molecular dynamics simulations corroborate (*52*) that the walls of the cleft and the bridge shield the cobalt(II) metal centers in Co(5) and Co(9) from the non-coordinating solvent (methanol) resulting in facilitated dioxygen binding (*53*).

The only crystal structure for a cobalt(II) cyclidene dioxygen adduct, that of [Co(**9**)(O_2)(MeIm)]$^{2+}$, shows that O_2 binds at an angle of 121°, as expected for coordinated superoxide, and that the hexamethylene bridge flips away from the guest. (Fig. 1) (*38*). This flipping, which has also been observed for Co(III)–NCS^- adducts (*40*), effectively eliminates the van der Waals repulsion between the flexible bridges and the included O_2. In this case, dioxygen affinity of the Co(II) complexes parallels the cavity width (Fig. 2), indicating that there are significant steric interactions between the walls of the cavity and the guest. The cavity width in cyclidenes, which is defined as the distance between the "edges" of the cleft, depends on the length of the bridge. Short bridges composed of tetra- or pentamethylene chains constrain the distances between the edges of the cleft and enforce narrow cavities.

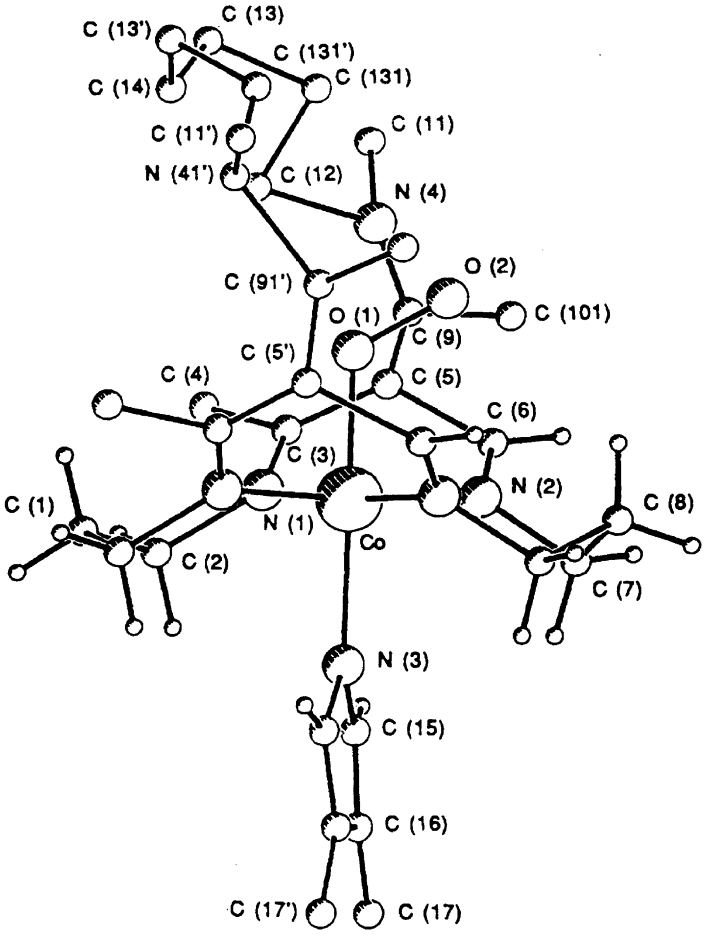

FIG. 1. X-ray crystal structure of the dioxygen adduct of the cobalt(II) cyclidene complex $[Co(\mathbf{9})(MeIm)(O_2)]^{2+}$. Reproduced with permission from Ref. (*38*). Copyright 1994, American Chemical Society.

The hexamethylene bridge has an optimal length for spanning the cavity of the 16-membered cyclidene, while longer bridges (C7 or C8) enforce wider separation between the "walls" of the cavity. Even longer bridges are flexible and can adopt various conformations, which allow the cleft to shrink back to its optimal width (~7 Å) (*40*).

The differences in oxygen affinities are primarily determined by the rates of O_2 binding rather than O_2 dissociation. Dioxygen binding is an entropically controlled, low barrier process (*53*). When the bridge–guest interaction is unavoidable, it severely diminishes the oxygen affinities. Examples include short, non-flexible C_3 and C_4 bridges in **6**, **7**, **12** (*38,40*); planar 14-membered cyclidenes **4** with low bridge heights (*43*); and unsubstituted cyclidenes **16**, **17**, where the

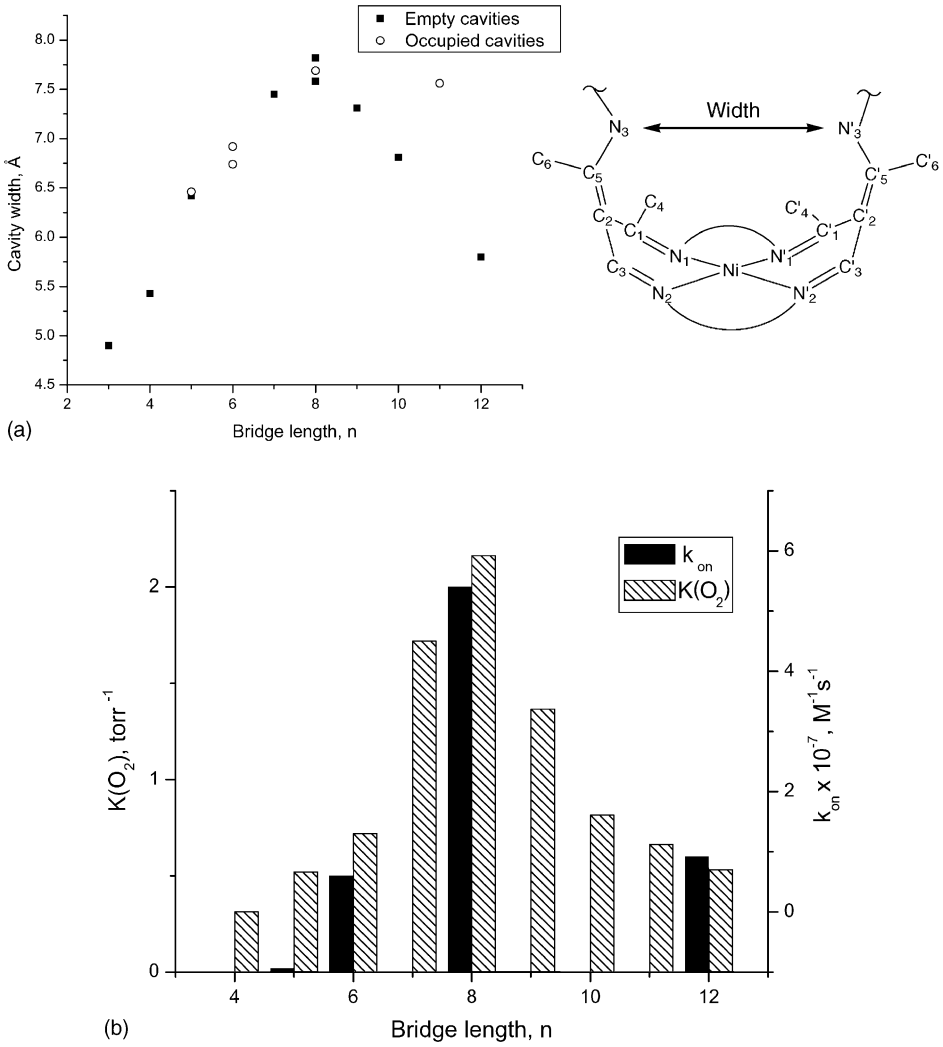

FIG. 2. Correlation between bridge length in polymethylene bridged cobalt(II) cyclidenes **7**–**11** and (a) cavity width of the complexes; (b) dioxygen affinities of cobalt(II) complexes measured in CH_3CN-1-methylimidazole (MeIm at 0 °C, and dioxygen binding rates of cobalt(II) complexes measured in acetone-MeIm at 70°C. Adapted from Refs. (*40*,*53*).

bridge adopts a zigzag straight-over-the cavity conformation (*54*). Various additional effects have been discussed in detail, using an impressive array of experimental data on cyclidene-O_2 binding constants (*40*).

The dioxygen affinities of iron(II) cyclidenes also depend on steric constraints for O_2 binding, resulting in van der Waals repulsions in dioxygen adducts. This effect is evident from comparisons between complexes having aliphatic bridges of different lengths (Table I).

TABLE I

KINETIC AND THERMODYNAMIC PARAMETERS FOR O_2 BINDING TO IRON(II) CYCLIDENE COMPLEXES MEASURED IN ACETONITRILE/1.5 M 1-MeIm USING STOPPED-FLOW SPECTROPHOTOMETRY (*55,56*)

R^1	R^2	R^3	$\Delta H^{\neq}_{on}$ (kJ mol^{-1})	$\Delta S^{\neq}_{on}$ (J K^{-1} mol^{-1})	$\Delta H^{\neq}_{off}$ (kJ mol^{-1})	$\Delta S^{\neq}_{off}$ (J K^{-1} mol^{-1})	ΔH° (kJ mol^{-1})	ΔS° (J K^{-1} mol^{-1})
$(CH_2)_4$	Me	Ph	12	−276	95	76	–84	–350
$(CH_2)_5$	Me	Ph	14	–229	50	−110	−37	−120
$(CH_2)_6$	Me	Ph	41	−75	ND	ND	ND	ND
$(CH_2)_8$	Me	Ph	54	−40	ND	ND	ND	ND
m-Xy	Me	Me	11.1	−252	ND	ND	ND	ND
m-Xy	Bz	Me	11.4	−253	ND	ND	ND	ND
m-Xy	Ph	Me	15.8	−228	ND	ND	ND	ND
m-Xy	Ph	Bz	9.1	−243	ND	ND	ND	ND

Note: Oxygen dissociation rates were determined from the non-zero intercepts of the plots of k_{obs} vs. $[O_2]$, using the equation $k_{obs} = k_{on}[O_2]+k_{off}$. Equilibrium constants were estimated as $K = k_{on}/k_{off}$. ND – not determined.

Oxygen binding to five-coordinate C4-, C5-, and *m*-xylene-bridged cobalt(II) or iron(II) cyclidenes is characterized by low activation enthalpies and large negative activation entropies, which are typical of associative processes. The six-coordinate C6- and C8-iron(II) cyclidenes release a solvent molecule in the course of oxygen binding. These ligand substitution reactions have substantially larger activation barriers, but less negative activation entropies (Table I) (*55,56*).

Electronic effects on the oxygenation rates are less pronounced, although in some cases still significant. The rates of oxygen binding increase by almost an order of magnitude with an increase in electron withdrawing properties of the R^2 and R^3 substituents in *m*-xylene-bridged ($R^1 = m$-Xy) iron (II) cyclidenes ($k_{on} = 186\,M^{-1}\,s^{-1}$ for $R^2 = R^3 =$ Me, and $1305\,M^{-1}\,s^{-1}$ for $R^2 =$ Ph, $R^3 =$ Bz at –20°C).

Iron(II) cyclidenes also bind carbon monoxide, which is forced by the bridge into a slightly bent configuration (the Fe–C–O angle = 170.6° in [Fe(**8**)(CO)(py)]) (*39*). As expected, this non-linear coordination mode results in relative destabilization of iron(II) cyclidene adducts with carbon monoxide (Table II) (*47,55,57*). Remarkably, the discrimination against CO is unusually high for the C5 bridged complex Fe(**13**): $K^{CO}/K^{O_2} = 0.03$ (*55*). There are only a few examples of iron(II) complexes that bind O_2 more strongly than CO. These include *Ascaris* Hemoglobin (*58*) and synthetic sterically hindered porphyrins (*59*). Molecular modeling suggests that selective recognition of O_2 by the complex Fe(**13**)$^{2+}$ is caused both by unfavorable van der Waals interactions between CO and the bridge (which is much less pronounced in the case of O_2 because of the greater bending of the latter ligand), and by favorable electrostatic interactions between the polar O_2 ligand and the walls of the cleft. The former effect destabilizes the CO adduct, while the latter one stabilizes the dioxygen complex (*47,55,57,60*).

B. Binding of Organic Molecules within Expanded Cavities

The regular bridged cyclidenes are well suited for small molecule recognition, because larger ligands cannot be accommodated inside their cavities. If encapsulation of molecules larger then O_2 or CO is desirable, the cyclidene cavity depth can be increased by appending piperazine or bipiperidine risers, and aromatic bridges can be introduced, in order to increase hydrophobic interactions with non-polar guests (*29,61*).

This design indeed proved to be successful in that the vaulted and supervaulted cyclidenes **18–24** (Scheme 3) were capable of binding alcohols and phenols in water (*41,62–64*). Diamagnetic low-spin nickel(II) vaulted cyclidenes displayed substantial ^{13}C NMR shifts upon interaction with *n*-propyl, *n*-butyl, *t*-butyl, and benzyl alcohols (the association constant, *K*, was estimated to be close to $7\,M^{-1}$ for each of these guests interacting with the 3,6-durene-bridged host, and varied from 3 to 8 for the various bridges, revealing no convincing trends).

TABLE II

KINETIC AND THERMODYNAMIC PARAMETERS FOR CARBON MONOXIDE AND DIOXYGEN BINDING TO IRON(II) CYCLIDENE COMPLEXES (R^2 = Ph, R^3 = Me) IN ACETONITRILE – 1.5 M 1-MeIm MIXTURE AT 25°C (*55,56*)

R^1	k_{on}^{CO} ($torr^{-1}\,s^{-1}$)	k_{off}^{CO} (s^{-1})	K^{CO} ($torr^{-1}$)	$k_{on}^{O_2}$ ($torr^{-1}\,s^{-1}$)	$k_{off}^{O_2}$ (s^{-1})	K^{O_2} (torr)	$M = K^{CO}/K^{O_2}$	$k_{on}^{O_2}/k_{on}^{CO}$
$(CH_2)_4$	2.2×10^{-4}	0.06	3.6×10^{-3}	4.0×10^{-4}	1.1	4×10^{-4}	12	1.8
$(CH_2)_5$	1.1×10^{-3}	0.022	5.0×10^{-2}	4.6×10^{-2}	0.03	1.6	0.03	42
$(CH_2)_6$	0.32	0.0026	1.2×10^{2}	14.9	7	2.1	60	46
$(CH_2)_8$	1.34	0.0041	3.3×10^{2}	21.3	53	0.4	800	16

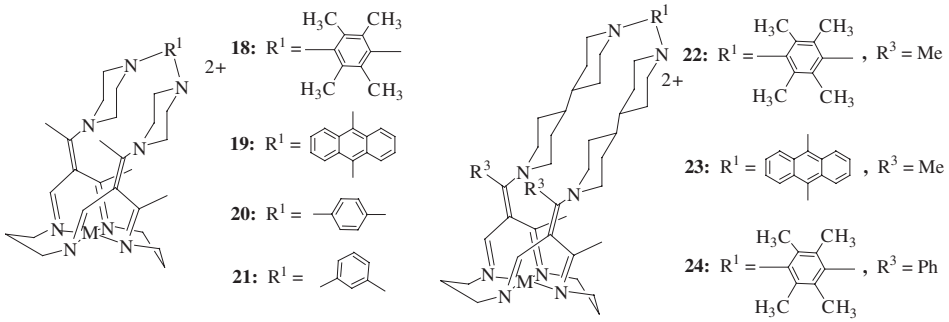

SCHEME 3. Structures of vaulted cyclidenes.

No shifts were observed when methanol was used as a guest, and only minor shifts were induced by ethanol (*62*). Phenol, 2,6-dimethylphenol, and 3,5-dimethylphenol interacted with Ni(**18**) with association constants of about $10\,M^{-1}$. Discrimination against alcohols with short hydrocarbon chains is indicative of predominantly hydrophobic interactions. The hydrophobic nature of these host–guest interactions was supported by a solvent effect study: no host–guest association was registered by NMR when an organic solvent (e.g., acetonitrile, acetone, or nitromethane) was used instead of water (*62*). NMR relaxation studies of paramagnetic copper(II) complexes confirmed this conclusion and provided detailed information on the orientation of the guests inside the host cavities (Fig. 3(c)) (*63,64*). Both alcohols and phenols are partly encapsulated inside the hydrophobic (remote from the metal ion) part of the cavity, with their hydrophilic OH groups being exposed to the solvent. The cavities of the vaulted cyclidenes with piperazine risers (**18**–**21**) are not sufficiently deep to completely accommodate phenols (Fig. 3(c)); but supervaulted cyclidenes (**22**–**24**) bearing bipiperidine risers are well suited to encapsulate phenols (Fig. 3(b)) (*41*). Interestingly, when vaulted cyclidenes were crystallized from polar solvents, acetonitrile (*62*) or benzonitrile (*41*), the nitrile guest occupied the cavity in a very different orientation, with its polar CN group directed toward the positively charged metal ion. The unbridged and C6-bridged cyclidenes were predicted, by molecular dynamics and free energy simulations, to have a similarly positioned weak binding site for 1-methylimidazole at the entrance into the cleft (*48*).

The experimental studies on hydrophobic host–guest interactions in vaulted cyclidenes culminated in the characterization by NMR relaxation studies of a unique ternary complex with both *n*-butanol and dioxygen shared the same cavity (Fig. 4) (*28*). Moreover, the vaulted cyclidene Co(**18**) catalyzed the oxidation of 2,6-dimethyl phenol with dioxygen, while cyclidenes with smaller cavities (capable of binding dioxygen, but not the substrate) did not act as catalysts (*49*). The authors proposed that the phenol was being oxidized by coordinated dioxygen while itself being a guest within the vaulted cyclidene cavity

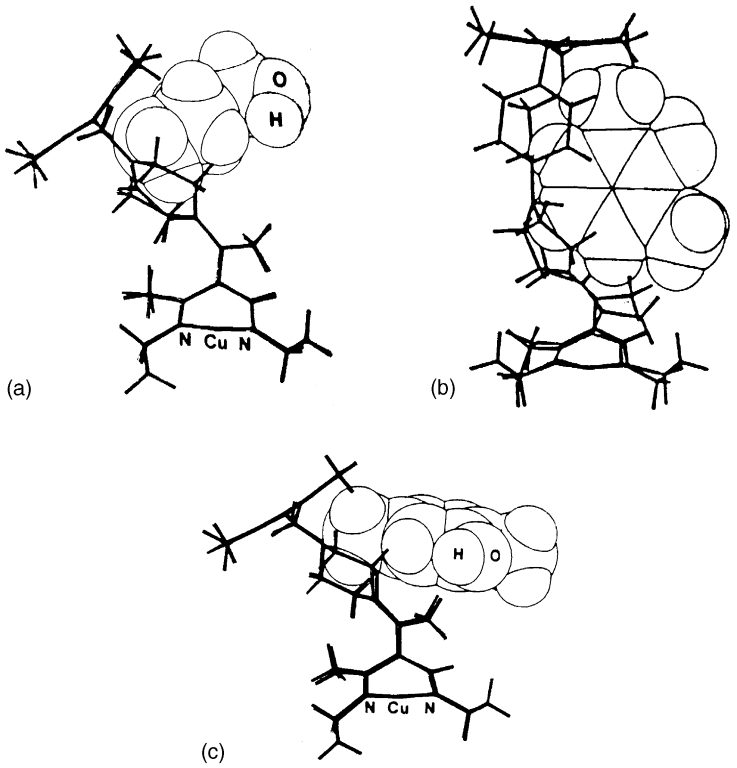

FIG. 3. Orientation of the guest in the inclusion complexes: (a) Cu(**18**)$^{2+}$ in *n*-butanol; (b) Cu(**22**)$^{2+}$-2,6-dimethylphenol, and (c) Cu(**18**)$^{2+}$-2,5-dimethylphenol, determined by NMR relaxation studies. Reproduced with permission from Refs. (*41,64*). Copyright 1986 and 1990 American Chemical Society.

(*49*). Thus even weak complexation of the substrate (phenol) inside the hydrophobic cavity may be critically important for catalytic reactions promoted by the metallomacrocyclic platform.

The hydrocarbon bridges in vaulted cyclidenes utilize weak hydrophobic interactions for guest binding, thus giving rise to low-affinity host–guest complexation. The bridges may also contain functional groups that account for stronger host–guest interaction. An interesting class of complexes that have the same topology as classical vaulted cyclidenes are face-to-face dimers of metallomacrocycles. In this case, a metal-containing macrocycle is incorporated into the expanded bridge. The first examples of face-to-face bicyclic cyclidenes were provided by Busch and coworkers (*65,66*). Recently, Korybut-Daszkiewicz and coworkers prepared homo- and heterodimetallic complexes with similar structures (*67–70*) that could be used as hosts for the recognition of small organic molecules, (*67*) and in the preparation of a switchable catenane (Scheme 4) (*68–70*). Neutral, face-to-face dinickel(II) complexes (Fig. 5, compounds **28** and **29**) were shown to be efficient hosts

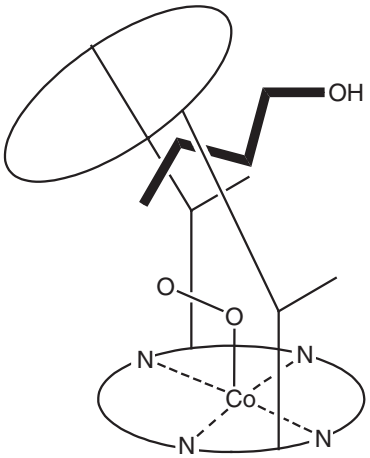

FIG. 4. The orientation of two guests, O_2 and *n*-butanol, inside the hydrophobic cavity of the host Co(**19**), determined by NMR relaxation studies. Adapted from Ref. (*28*).

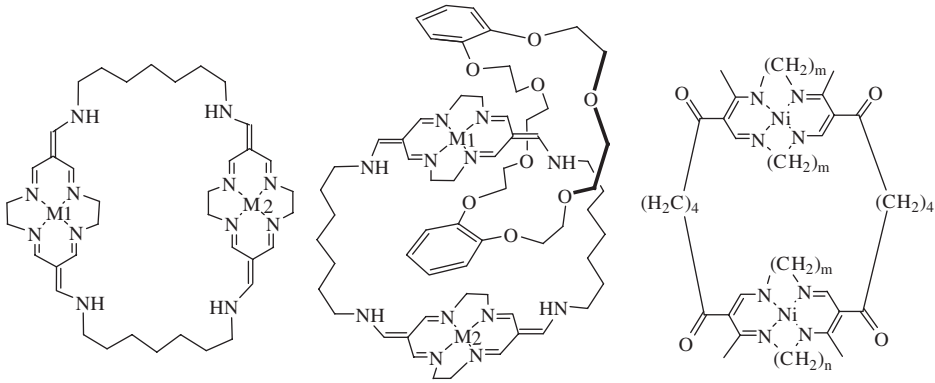

M_1=M_2=Cu^{2+} **25a**
M_1=M_2=Ni^{2+} **26a**
M_1=Cu^{2+} M_2=Ni^{2+} **27a**

M_1=M_2=Cu^{2+} **25b**
M_1=M_2=Ni^{2+} **26b**
M_1=Cu^{2+} M_2=Ni^{2+} **27b**

m=n=3 **28**
n=2 m=3 **29**

SCHEME 4. Structural formulas of the dicyclidene complexes and the corresponding catenanes as well as face-to-face nickel cyclidenes (*70*).

for aromatic guests: they bind toluene, TCNQ, or quinones, utilizing π–π interactions and forming charge-transfer complexes with redox active guests (such as TCNQ or quinones) (*67*). The assembly of catenanes **25b–27b** from monomeric cyclidene precursors, diamine linkers, and dibenzo-24-crown-8 also occurred due to π–π interactions between the benzene rings of the crown and the conjugated metallomacrocycle, as confirmed by X-ray crystallography of the catenanes (*68–70*). Since the benzocrown is the electron-rich partner of this

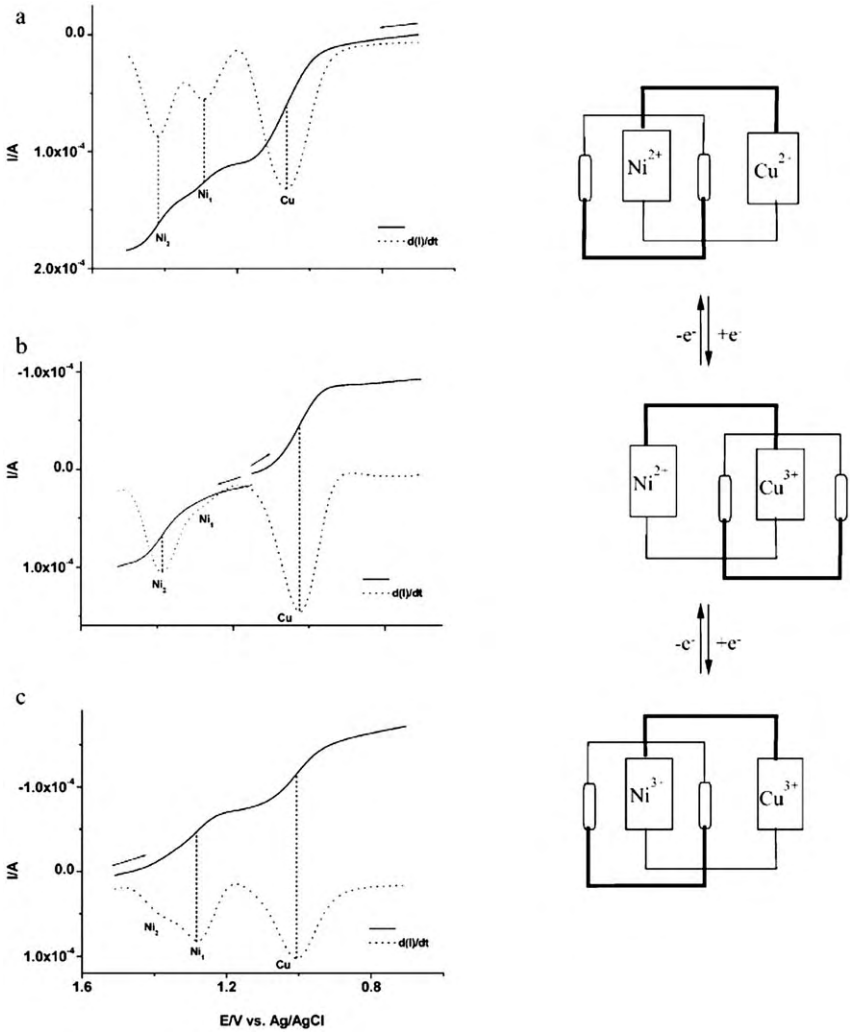

FIG. 5. RP voltammograms and their derivatives for 1 mM **27b** in 0.1 M TBAHFP in acetonitrile recorded on GCE, t_p50 ms, t_w2 s. *E*: (a) 0.70, (b) 1.15, (c) 1.50 V. Reproduced with permission from (*70*).

supramolecular assembly, it preferentially binds to the oxidized metal cyclidenes, which contain Ni^{III} or Cu^{III}, thus allowing for electrochemically induced motion of the crown ring between differentially oxidized cyclidene metallocomplexes (Fig. 5).

Introducing additional binding sites into metallomacrocycles with bridges allows for the design and preparation of selective receptors for important biological molecules. For example, combining two metal ions in the macrocycle with a pyrazole-based hydrogen-bonding site incorporated into the bridge was successfully applied to designing a metalloreceptor for dopamine. The dicopper complex of **30** binds this

neurotransmitter in water at physiological pH with affinity constants of approximately $10^4\,M^{-1}$ (the exact values depend on the extent to which dopamine and the pyrazole moiety in the bridge are protonated at a given pH); the proposed dopamine coordination mode is shown in Fig. 6 (*71*).

Another approach incorporates high affinity selective guest-binding receptors into the bridges that span the metallomacrocyclic cavities. Cyclodextrin (CD) receptor arms allow for strong binding of hydrophobic guests in water and thus open up exciting opportunities for molecular recognition accompanied by signaling from the metal centers. In the cyclodextrin appended lanthanide (Tb^{3+} or Eu^{3+}) complexes **31** and **32** (Scheme 5) a luminescence response can be triggered by aromatic

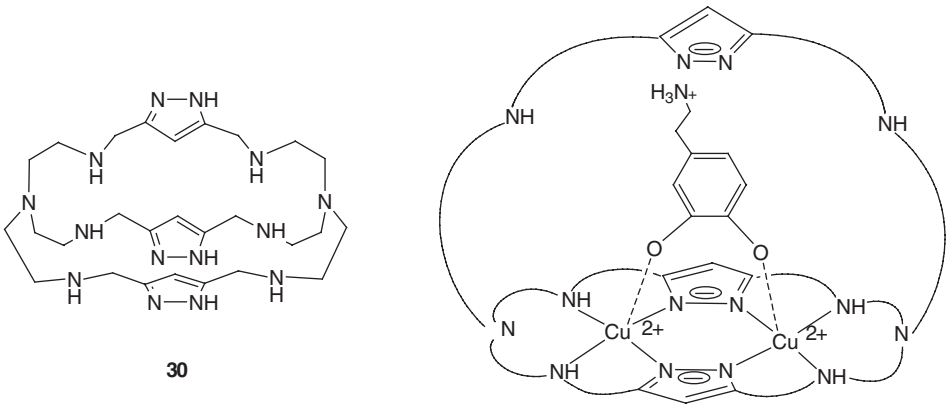

FIG. 6. Encapsulation of dopamine into the dinuclear copper (II) complex of the pyrazolate-containing cage **30**, according to Ref. (*71*).

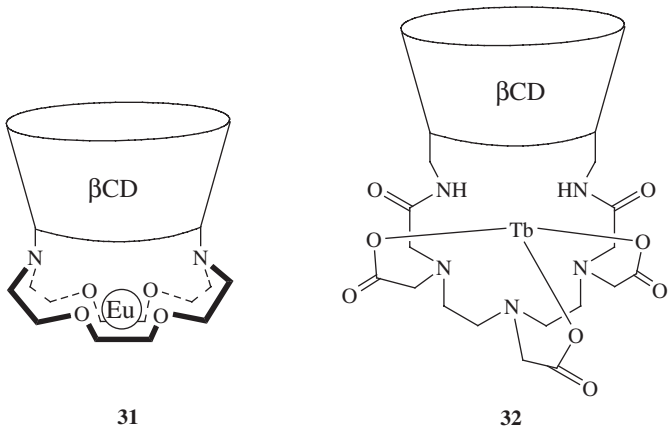

SCHEME 5. Schematic structures of cyclodextrin-appended lanthanide complexes **31** and **32**.

guest encapsulation into the CD cavity (*72–77*). This sensitization of luminescence is due to an energy transfer mechanism (absorption-energy transfer-emission, AETE) in which the light absorbed by the aromatic molecule is transferred to the lanthanide ion and excites it into a light emitting quintet state ($^5D_0$ for Eu^{3+} or $^5D_4$ for Tb^{3+}) (*74*).

The structure of the metallomacrocycle has an impact on both the affinity of guest binding to the appended cyclodextrin receptor and the efficiency of luminescent response. In **31**, the rigid two-point connection of the tripositive macrocycle to the CD cavity shields the hydrophobic binding site and leads to a dramatic decrease in guest binding affinities ($K < 10\,M^{-1}$ for the benzene-**31** complex, as compared to $K = 200\,M^{-1}$ for benzene-βCD); as a result, there is no increase in the luminescence of **31** in the presence of benzene (*74*). This electrostatic screening of a neutral, hydrophobic guest can be overcome by introducing negatively charged groups in the lanthanide-coordinating macrocycle. Indeed, the cradle geometry of a neutral **32** does not prevent the guest binding; moreover, a large (up to 25-fold) increase in the binding constants was detected ($K = 18{,}000\,M^{-1}$ for naphthalene and $4000\,M^{-1}$ for durene complexation with **32**, as compared to $K = 760\,M^{-1}$ for naphthalene-βCD) (*77*). In addition to this indirect influence of the metal complex on the guest binding affinities, direct interaction between the metal ion and a functional group on the substrate (e.g., pyridine, benzoic or picolinic acid) was reported to increase the luminescent response, likely due to stronger, multipoint binding (*76*). The luminescent response depends on the geometry of the supramolecular complex and is greatly improved in compounds with cradle geometry; a neutral complex **32** displayed even larger fluorescence enhancement upon guest binding (*73,74,76,77*).

Very rigid attachment of a substrate receptor (e.g., the cyclodextrin strap mentioned in the previous paragraph) to the metallomacrocyclic platform is not necessarily optimal, because this geometry creates significant kinetic barriers for host–guest complexation (it becomes difficult to bring the guest inside the host, especially in the presence of strong electrostatic screening by a +3 metal site, as was the case in **31**). A possible alternative design would "break" the bridge, incorporating two receptor arms that can be properly positioned for substrate binding by attaching them to the edges of the cleft. Examples of this approach will be considered in the following sections.

III. Metallomacrocyclic Clefts with Two Appended Receptor Sites for Ditopic Recognition

The concept of attaching two or more receptor sites to a scaffold is widely used in supramolecular chemistry in order to design selective

hosts (*1,9,27*). Although most commonly used scaffolds are organic molecules or fragments, metal-containing scaffolds are also gaining popularity (*3,5,6*). Combining reactive metal-containing platforms with guest-binding receptor groups is particularly attractive for biomimetic catalyst design, as was discussed above. For example, regioselective reagents and catalysts based on functionalized rigid metalloporphyrins were prepared and characterized by Breslow (*78–84*) and Woggon (*85–88*). Porphyrin scaffolds, however, are planar, and do not orient the attached receptor groups. It was therefore desirable to develop metal-containing clefts similar to organic "molecular tweezers" (*89–93*). Interestingly, macroscopic tweezers, which are commonly used for grasping and releasing small objects, are relatively flexible and can be opened and closed at will. In contrast, traditional polyaromatic "molecular tweezers" are very rigid and cannot change shape upon guest binding. Attaching receptor groups to somewhat more flexible clefts would allow for the preparation of "molecular tweezers" that are more similar to their mechanical counterparts. These hosts would encapsulate the guest by folding at their hinge and then, in response to an external signal, open up and release the guest.

Transition-metal complexes with cyclidene ligands, introduced in Section II.A, provide a promising framework for designing functional, tweezer-like, molecular receptors. Cyclidenes are desirable platforms for molecular tweezers because of their sometimes flexible, cleft-like conformations; their demonstrated catalytic activity; and the well-developed synthetic chemistry for their modification. The long-range effect of macrocyclic ring size on the overall molecular shape of cyclidenes is profound: the 14-membered complexes are planar, the 16-membered ones fold into a saddle-shaped conformation, and the 15-membered complexes can exist in either planar or cleft-like conformations (*40,44,94*). The high degree of conjugation in the unsaturated chelate rings accounts for the fact that the entire "wing" moves in response to the changing conformations of the saturated chelate rings of different sizes. As a result, the separation and relative orientation of substituents appended at the periphery of cyclidenes are highly sensitive to the size and geometry of the macrocycle.

Metal complexes with Jäger and analogous cyclidene macrocycles display catalytic properties (e.g., cobalt cyclidenes can catalyze phenol oxidation (*49*) whereas nickel complexes with Jäger macrocycles can catalyze the electroreduction of carbon dioxide to oxalate (*95*)). Chiral building blocks are easily incorporated into Jäger and cyclidene platforms (*96,97*) opening the possibilities for chiral recognition and enantioselective catalysis.

The great potential for using modified cyclidenes as building blocks in supramolecular chemistry was recognized by Busch, Korybut-Daszkiewicz, and others (*41,62–64,68,70*). Recently, selective molecular receptors have been prepared from cyclidenes functionalized with paired arms appended to opposite edges of the macrocyclic platforms

(*98–102*). Recognition of cationic and anionic guests with these ditopic molecular receptors ("molecular tweezers") is reviewed in the following sections.

A. Dication Recognition with Functionalized Cyclidenes

Protonated organic amines are often studied as guests, because amine functionality is commonly present in biomolecules, such as amino acids, proteins, and neurotransmitters. Crown ethers, which are known to form reasonably strong complexes with primary ammonium salts (*103*), can serve as receptor groups in multitopic hosts for ammonium cations. Molecules containing two crown ether fragments attached to a rigid scaffold or assembled about a metal center are known to bind diammonium salts and, in some cases, display substantial length selectivity (*104–117*). This structural motif is also known to be effective for cation binding to crown-decorated cyclidenes (Scheme 6).

In a recent series of experiments, either high-affinity (18C6) or low-affinity (15C5 or aza-15C5) binding groups were attached to the cyclidene platforms (14-membered or 15-membered), and the affinities and selectivities of the resulting ditopic receptors toward cationic guests were determined (*99,102,118*). For comparison, the binding of mono- and ditopic ammonium cations to crown ethers that are not attached to cyclidenes (*119–121*) will also be considered in this section.

Attaching crown–ether moieties to a planar 14-membered cyclidene platform yielded metalloreceptors (**33–36**) that could bind alkali or alkaline earth metal ions, (*99,118*) but demonstrated weak, essentially non-cooperative interaction with organic ammonium cations (*118*). Interestingly, despite the weak nature of these interactions, a shift in reduction potential was observed for both the copper(II)- and nickel(II)-containing receptors (**36a** and **36b**) when certain amino acids (β-alanine or lysine) were added to acetonitrile–water solutions of the receptor (*118*). These results are promising for designing selective receptors for biologically important species and it appears that the larger, cleft-shaped, 15- and 16-membered cyclidenes hold even more potential in this regard.

In contrast to planar 14-membered cyclidenes, the 15-membered cyclidene platforms can adopt both "open" (planar) and "closed" (saddle shaped) conformations (*40*). This non-rigidity is needed in order to eventually obtain switchable receptors. The saddle-shaped conformation of the 15-membered platform allows for the synthesis of shape-complementary host–guest assemblies. The question of whether these relatively flexible, functionalized [15]cyclidene clefts can act as ditopic receptors ("molecular tweezers") was addressed by Kryatova *et al*. (*102*). NMR titration data with molecular tweezers **37** and **38** in CH_3CN indicated complexation between the alkylammonim cations (Table III) and the crown ethers appended to the cyclidene platform. The resonances of the

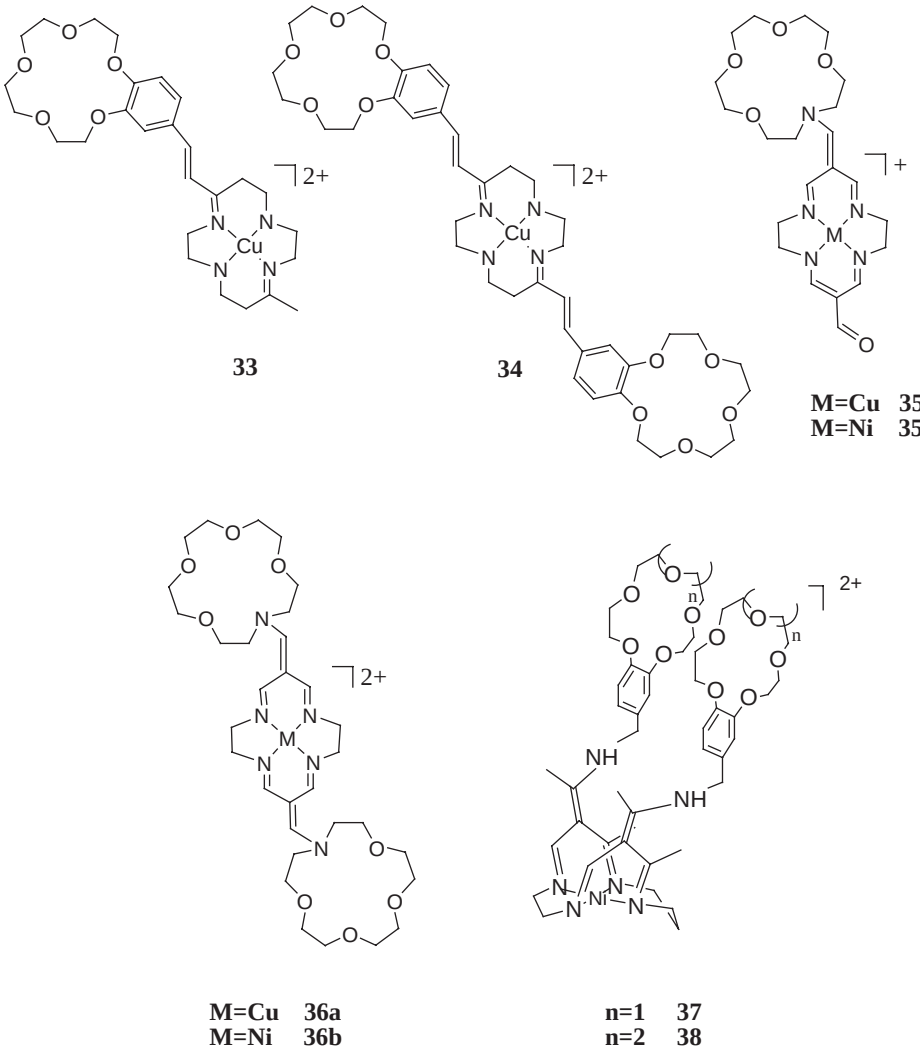

SCHEME 6. Structural formulas of crown-ether-appended cyclidenes.

crown ether moieties, and the resonances of the ammonium guests (especially α-CH_2 protons) shifted due to host–guest adduct formation. The ^{1}H NMR signals of the tetraaza macrocyclic platform also shifted upon difunctional guest binding to **37** or **38,** but no shifts of these platform resonances were observed upon monoammonium salt binding. These results suggested that both protonated mono- and diamines interact with the crown ether receptor sites, but their binding modes to crown-cyclidenes are different. Unlike monofunctional guests, the diammonium cations can be encapsulated between both receptor "arms", causing a conformational change in the cyclidene platform. Similar conformation-dependent NMR shifts of monoalkylated cyclidene complexes lacking

TABLE III

ASSOCIATION CONSTANTS (K_{assoc}, M^{-1}) FOR 1:1 HOST–GUEST COMPLEXES OF TWEEZERS **37** AND **38** AND BENZOCROWNS WITH DIAMMONIUM AND MONOAMMONIUM CATIONS AT 298 K, DETERMINED BY ^1H NMR TITRATION, DATA TAKEN FROM REF. (*102*)

Host	Guest	K_{assoc}	Log K_{assoc}	Solvent
B15C5	$NH_3(CH)_2C_6H_5^+$	5.5×10^2	2.74	CH_3CN
37	$(NH_3)_2(CH_2)_2C_6H_4^{2+}$	3×10^3	3.48	CH_3CN
	$(NH_3)_2(CH_2)_2^{2+}$	4×10^3	3.60	CH_3CN
	$(NH_3)_2(CH_2)_3^{2+}$	5×10^4	4.70	CH_3CN
	$(NH_3)_2(CH_2)_4^{2+}$	10^5	5.00	CH_3CN
	$(NH_3)_2(CH_2)_5^{2+}$	4×10^3	3.60	CH_3CN
	$(NH_3)_2(CH_2)_6^{2+}$	1.25×10^3	3.10	CH_3CN
B18C6	$NH_3(CH)_2C_6H_5^+$	5×10^4	4.70	CH_3CN
38	$(CH_3)_2(NH_2)_2(CH_2)_2^{2+}$	1.2×10^2	2.08	CH_3CN
	$(NH_3)_2(CH_2)_2^{2+}$	3×10^4	4.48	CH_3CN
	$(NH_3)_2(CH_2)_3^{2+}$	7×10^4	4.85	CH_3CN
	$(NH_3)_2(CH_2)_4^{2+}$	9×10^4	4.95	CH_3CN
		6×10^2	2.78	MeOH
	$(NH_3)_2(CH_2)_5^{2+}$	3×10^4	4.48	CH_3CN
	$(NH_3)_2(CH_2)_6^{2+}$	2×10^4	4.30	CH_3CN
		3×10^2	2.48	MeOH
	$(NH_3)_2(CH_2)_2C_6H_4^{2+}$	5×10^4	4.70	CH_3CN

receptor groups have been reported (*122,123*). Direct coordination of the diammonium guests to the nickel(II) centers in the cyclidene platform is unlikely, because no interaction between these guests and unfunctionalized cyclidenes was observed.

Addition of an excess of the parent monotopic receptor (benzo-15-crown-5 or benzo-18-crown-6) to the diammonium cations caused a smaller change in the chemical shifts of the aliphatic cation resonances than titration with equivalent amounts of ditopic tweezers **37** or **38**, respectively. These results are qualitatively consistent with the diammonium salts binding to both receptor sites of the tweezers.

Using Job's method, all of the tweezer-diammonium cation systems were found to form 1:1 complexes consistent with the difunctional guest inclusion depicted in Scheme 7. Control experiments showed a 2:1 complexation between simple parent crowns (B15C5 or B18C6) and diammonium cations, a 1:2 complexation between ditopic tweezers (**37** or **38**) and monoammonium cations, and a 1:1 complexation between monotopic crowns (B15C5 or B18C6) and monoammonium cations. These observations suggest that each RNH_3^+ group interacts with one crown ether ring. An alternative possibility exists for the 15-crown-5 derivatives, where two types of complexes with monoamonium salts in either 1:1 or 2:1 ratios are known, and their binding constants are comparable (*124*). In the 2:1 complexes, one ammonium group was sandwiched between two crown ether rings. Detailed studies described below (Section III.B) demonstrate that this "sandwiched" binding

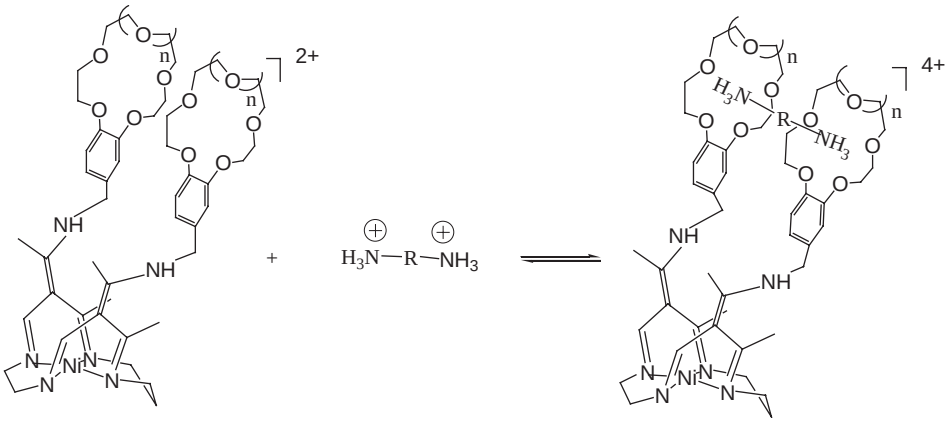

SCHEME 7. Proposed binding mode of diammonium salts to molecular tweezers **37** and **38**.

mode is not observed for alkylammonium complexation by benzo-15-crown-5 or B15C5-appended cyclidenes.

Variable-temperature NMR experiments indicate that the yields of crown-ammonium, host–guest complexes increase at lower temperatures as is expected for associative processes. The equilibrium was characterized quantitatively at room temperature by NMR titrations, and the association constants for 1:1 host–guest complexes of the diammonium salts (thiocyanate or perchlorate) with the ditopic molecular receptors **37** and **38** are summarized in Table III.

Despite the positive charge on the nickel(II)-containing platform, the ditopic cyclidene-based receptors **37** and **38** were found to have stronger binding affinities for organic diammonium salts than the corresponding simple benzo crowns have for the monoammonium salts. This can be attributed to preorganization of the receptor arms. A moderate chelate effect was registered for the B18C6 derivative **38** with 1,3-diaminopropane and 1,4-diaminobutane, while a substantial increase in alkyl diammonium binding affinities was registered in several cases for the B15C5 derivative **37** (Table III).

As expected, the B18C6-containing host **38** displays higher guest binding affinities than its B15C5-containing counterpart **37**. This behavior parallels the guest binding affinities of the monomeric crown ethers (*103,125,126*). The strong binding affinity of the B18C6 derivative **38** is also exemplified by its ability to complex secondary diamines (Table III). There was no evidence for piperidine binding to complex **37** under the same experimental conditions.

The recognition of α,ω-diamines as a function of length was investigated using a series of aliphatic difunctional guests with two primary ammonium groups separated by 2–6 carbons. Tweezer **37** bearing B15C5 arms showed substantial selectivity. The strongest complexation was observed for the cations of 1,3-diamino propane and

1,4-diaminobutane, while 1–2 orders of magnitude weaker binding was observed for shorter ($(CH_2)_2(NH_3^+)_2$) or longer ($(CH_2)_5(NH_3^+)_2$) and $(CH_2)_6(NH_3^+)_2$) diammonium salts (Table III). The optimal length of the diamine guests agrees well with the cavity width of saddle-shaped cyclidenes (~7 Å, Section II.A) (*40*). The results of molecular modeling studies on covalently bridged cyclidene systems (*48,52,127*) also demonstrate that a six-atom linker spans the cavity with the least steric strain.

The guest binding affinity of the B18C6-containing tweezer **38** reveals the same trend in optimal length of the diammonium substrates as was seen for the tweezer **37**, although the length selectivity is significantly less pronounced (Table III). One might suggest that the higher guest binding affinity of tweezer **38** masks its potential selectivity in encapsulating diammonium substrates of different length. Indeed, the equilibrium constants for supramolecular host–guest complexes with tweezer **38** showed strong binding for all primary diammonium cations studied (Table III). In order to test this hypothesis, NMR titrations of the diammonium salts with the strongest and weakest binding (C_4 and C_6 chains, respectively) were also carried out in methanol. As expected, binding constants were lower in the protic solvent than in acetonitrile, but the difference in the values of log K_{assoc} also remained small (Table III). It is therefore likely that the relatively small energy penalty upon reorganization of the host in order to bind a "non-optimal" guest is sensed by the low-affinity receptor **37**, but does not lead to discrimination against non-optimal guests by the high-affinity receptor **38**. The larger 18C6 rings afford greater conformational flexibility as the tweezer binds diammonium substrates of different lengths between its receptor arms.

B. Interaction of B15C5 and Other Crown Ethers with Ammonium Cations

In order to better understand the factors that govern the binding affinity and selectivity of diammonium salt complexation with metal-containing molecular tweezers, detailed characterization of the stoichiometry, thermodynamics of formation, and structural features of simpler crown ether complexes with ammonium cations was necessary for the rational design of functional and selective supramolecular receptors.

The stoichiometry and stability of the crown-ammonium adducts depend both on the size of the crown ether and on the nature of the ammonium cation (NH_4^+, RNH_3^+, etc). Of the common crown ethers, 18-crown-6 (18C6) and its derivatives have the highest affinity for ammonium cations (NH_4^+ and RNH_3^+) and invariably show a 1:1 binding stoichiometry both in solution (*103,125,128–130*) and in the solid state (*131–134*). A different stoichiometry (2:1) was found in all structurally characterized complexes of 15-crown-5 (15C5) and its derivatives with

NH_4^+ (*131,135–137*). These complexes have a sandwich structure with the NH_4^+ cation placed between two nearly parallel 15C5 residues. The same type of coordination is observed when B15C5 interacts with the hydronium ion to give the $[(H_3O)(B15C5)_2]^+$ complex (*138*). The smaller cavity size of the 15C5 family as compared to the 18C6 family is generally believed to be responsible for the different stoichiometries and structures of their host–guest complexes with NH_4^+ (*130,131,139*).

Until recently little information was available regarding the stoichiometries and structures of complexes formed between 15C5 (or its derivatives) and alkyl ammonium ions. The data that were available indicated that alkylammonium cations RNH_3^+, unlike NH_4^+, coordinate to only one 15C5 molecule (*120,129,140–142*). However, it remained unclear whether this stoichiometry is a general property of the interaction between 15C5 macrocycles and the protonated primary amino group, or whether it results from additional interactions present in all systems studied thus far. Two of the crystallographically characterized complexes are head-to-tail dimers of self-complimentary 15C5 derivatives with pendant ammonium arms: 2-ammoniomethyl[15-crown-5] (*140*) and 4′-ammoniomethyl[benzo-15-crown-5] (*120*), in which the 1:1 ammonium–crown binding motifs may have been enforced by a "chelate" effect and/or additional π-stacking of the benzene rings (see also Section III.C below). In another structural study, a 1:1 complex of substituted monoaza[15-crown-5] with $PhCH(CH_3)NH_3^+$ was reported, (*141*) but its interpretation is complicated by the presence of bulky substituents (on both components of the complex) and intermolecular cation-azacrown interactions in addition to those expected between the ammonium group and the lone pairs of the crown. In order to better understand host–guest complexation between 15-crown-5 derivatives and alkylammonium cations, simple 15-crown-5 systems have been investigated in some detail (*121*). Mixtures of B15C5 host and benzylammonium guest give rise to crystals of the 1:1 adduct regardless of the ratio of components in the starting solution. The composition of the solid product, $[PhCH_2NH_3(B15C5)](ClO_4)$ (complex **39**), was established by elemental analysis and single crystal X-ray diffraction (Fig. 7).

The complexation is driven by the formation of two hydrogen bonds between the protonated amino group of the ammonium fragment and two oxygen atoms of the crown residue. The oxygen atoms of the crown lie in an approximately planar arrangement with a mean deviation from the plane of 0.2858(17) Å. The macrocycle adopts a skew conformation, as it does when coordinated to inorganic ammonium, NH_4^+ (*131,136,137,143*). The N atom of the $PhCH_2NH_3^+$ group is displaced by 1.842(4) Å from the mean plane defined by the five oxygen atoms of the crown residue.

It is instructive to compare the structural features of complex **39** to those of other known adducts between 15C5 derivatives and

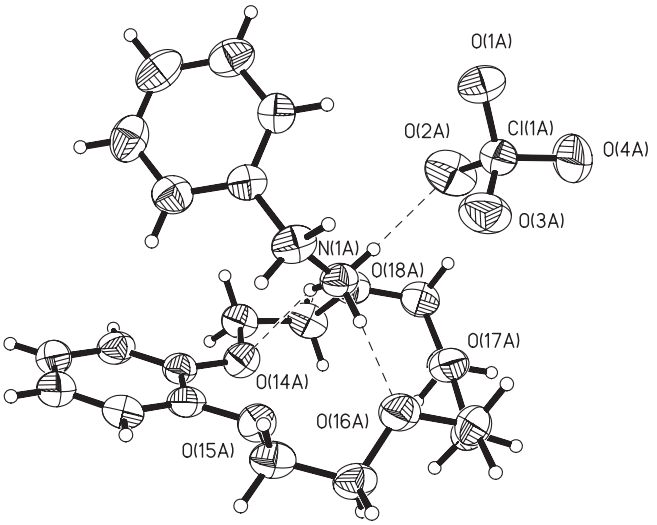

FIG. 7. Crystal structure of $[PhCH_2NH_3(B15C5)](ClO_4)$ (**39**) (*121*).

ammonium cations. In a family of well-known, structurally characterized 1:2 sandwich complexes of inorganic NH_4^+ with 15C5 and its derivatives, two hydrogens from the NH_4^+ cation form hydrogen bonds with one crown ether ring, and the remaining two hydrogens are H-bonded to a second macrocycle. In these cases the typical distances between the ammonium nitrogen and the O_5 plane of each crown molecule can be rather large and range from 1.82 to 2.34 Å (*131,135–137,143*).

On the other hand, organic primary ammonium cations with functionalized substituents were found to form two NH···O hydrogen bonds with a single crown ether host. The nitrogen atom in these complexes is displaced 1.89–1.95 Å from the mean O_5 plane (*120*). This short crown-ammonium separation was previously attributed, at least partially, to additional interactions in the host–guest adducts (e.g., the "chelate effect" of two simultaneous crown–ammonium interactions in self-complementary dimers (*120,140*) or an additional system of hydrogen bonding (*141*)). Another example of short crown–ammonium separation (1.93 Å) was observed between a secondary dialkylammonium ion, $Me_2NH_2^+$, and a B15C5 residue in the crystal structure of $[(H_3O)(B15C5)_2][Me_2NH_2]_2[PMo_{12}O_{40}] \cdot 2(B15C5)$ (*138*). In this case packing effects could not be ignored, as the 1:1 association complexes of $Me_2NH_2^+$ cations and crown ether molecules were packed in the voids of the crystal lattice formed by large polyoxometalate anions (see also Section IV).

The small RNH_3^+–15C5 separation found in **39,** where the complex is held together by just two hydrogen bonds (with no significant additional interactions present), strongly suggests that a distance of 1.8–1.9 Å between the ammonium nitrogen and the 15C5 ring is

typical in unconstrained 1:1 adducts. It can also be argued that alkylammonium cations typically form 1:1 adducts with 15C5 derivatives. Indeed, the RNH_3^+ group utilizes two of its hydrogen atoms for H bonding, with one crown ether, but the remaining hydrogen is not sufficient for effective H bonding with the second macrocyclic ring. Additionally, the alkyl substituent blocks access to the second crown molecule, thereby precluding the formation of sandwich complexes.

The stoichiometry of benzylammonium complexation with B15C5 in acetonitrile solution was determined to be 1:1 by Job's method (*121*). Mass spectroscopy of an acetonitrile solution of **39** also revealed that the 1:1 complex is the predominant species. No evidence for more complex structures was observed.

Association constants for the complexation of benzylammonium perchlorate by B15C5 in acetonitrile (at four different temperatures) have been determined by NMR titrations and are reported in Table IV. Association constants for several related systems are also included for comparison. As expected, the complexes between 18-crown-6 hosts and RNH_3^+ are stronger than the corresponding complexes between 15-crown-5 hosts and RNH_3^+; the former adducts are held together by three hydrogen bonds, while the smaller crown ethers in the latter adducts form only two hydrogen bonds with their ammonium guests (*103,125*). Based on the limited available data, it appears that the substituents appended to the host or guest molecules exert relatively little influence on complex stability in the ammonium—15-crown-5 systems (Table IV). For larger hosts (18-crown-6 derivatives), the binding affinity for amines followed the series $NH_4^+ > RNH_3^+ > R_2NH_2^+$ (*125*). While this general trend still holds for 15C5 derivatives, the difference between NH_4^+ and RNH_3^+ in protic solvents is smaller, and sometimes becomes negligible (*129,142*) (Table IV). The R group may be of greater importance in the 18C6 complexes because it interferes with hydrogen bonding to a greater extent (e.g., may decrease the number of hydrogen bonds from three in unsubstituted NH_4^+ complexes to two in RNH_3^+ complexes). Similarly, the benzo-substituted 18-crown-6 hosts (B18C6 and DB18C6) generally form weaker complexes than the parent unsubstituted 18C6 (*125*). This effect is also diminished for the smaller 15C5 ring, as 15C5 and B15C5 bind NH_4^+ comparably strongly in acetonitrile (*124,144*) (Table IV).

The enthalpic and entropic contributions to host–guest complexation for **39** were determined by Van't Hoff analysis (*121*). These thermodynamic parameters are very close to those obtained in CH_3CN for a 1:1 complex of B15C5 with NH_4SCN (*124*) (Table V), and agree reasonably well with previously reported values for reactions of 15C5 with alkylammonium ions in ethanolic solution (Table V) (*129,142,145*). Enthalpy–entropy compensation may be partially responsible for the similar binding constants between ammonium cations and 15C5 derivatives in different solvents; complexation in water, when occurs, is entropically driven (Tables IV and V).

TABLE IV

BINDING CONSTANTS FOR COMPLEXES OF AMMONIUM AND ALKYLAMMONIUM CATIONS WITH B15C5 AND 15C5

Guest	Host	T (K)	K_1 (M^{-1})	Log K_1	K_2 (M^{-1})	Log K_2	Solvent	Method	Reference
$C_6H_5CH_2NH_3^+$	B15C5	310	400 ± 10	2.60			CH_3CN	NMR, ^1H	(*121*)
	B15C5	298	550 ± 10	2.74			CH_3CN	NMR, ^1H	(*121*)
	B15C5	288	700 ± 10	2.85			CH_3CN	NMR, ^1H	(*121*)
	B15C5	280	950 ± 10	2.98			CH_3CN	NMR, ^1H	(*121*)
$CH_3NH_3^+$	15C5	313		2.61 ± 0.06			EtOH	Potentiostatic	(*142*)
	15C5	298		3.03 ± 0.11			EtOH	Potentiostatic	(*142*)
	15C5	283		3.20 ± 0.09			EtOH	Potentiostatic	(*142*)
	DB15C5	298		0.86 ± 0.14			H_2O	Spectrophotometric	(*129*)
	DB15C5	298		0.95 ± 0.05			H_2O	Spectrophotometric	(*129*)
$C_2H_5NH_3^+$	15C5	313		2.63 ± 0.10			EtOH	Potentiostatic	(*142*)
	15C5	298		2.76 ± 0.12			EtOH	Potentiostatic	(*142*)
	15C5	283		3.06 ± 0.07			EtOH	Potentiostatic	(*142*)
$C_6H_4(CH_2)_2(NH_3)_2^{2+}$	B15C5	298	1100 ± 100	3.04	400 ± 30	2.60	CH_3CN	NMR, ^1H	(*121*)
$(CH_2)_4(NH_3)_2^{2+}$	B15C5	298	1100 ± 100	3.04	300 ± 30	2.48	CH_3CN	NMR, ^1H	(*121*)
NH_4^+	B15C5	298		2.16 ± 0.15		1.97 ± 0.2	CH_3CN	Calorimetry	(*124*)
	15C5	298		2.0			CH_3CN	N/A	(*145*)
	15C5	298		3.17 ± 0.08			EtOH	Potentiostatic	(*142*)
	15C5	298		3.50		3.03	MeOH	Calorimetry	(*146*)
	DB15C5	298		0.85 ± 0.09			H_2O	Spectrophotometric	(*129*)

TABLE V

ENTHALPY AND ENTROPY VALUES FOR DIFFERENT COMPLEXES OF B15C5 AND 15C5 WITH AMMONIUM/ALKYLAMMONIUM IN DIFFERENT SOLVENTS

Alkylamonium/ ammonium	Crown ether	ΔH (kcal mol^{-1})	ΔS (cal mol^{-1} K^{-1})	Solvent	Reference
$C_6H_5(CH_2)NH_3^+$	B15C5	–4.9 ± 0.5	–3.8 ± 1	CH_3CN	(*121*)
NH_4^+	B15C5	–4.6 ± 0.4	–5.5 ± 1.4	CH_3CN	(*124*)
NH_4^+	15C5	–4.5 ± 0.5	1.2 ± 0.7	EtOH	(*142*)
$CH_3NH_3^+$	15C5	–5.6 ± 0.2	–5.0 ± 1	EtOH	(*142*)
$C_2H_5NH_3^+$	15C5	–5.6 ± 0.2	–5.7 ± 1	EtOH	(*142*)
NH_4^+	15C5	–2.0		MeOH	(*146*)
NH_4^+	B15C5	–0.74		MeOH	(*146*)
NH_4^+	15C5	–0.24 ± 0.04	+7.0	H_2O	(*145*)

In the studies described above (*121*), a 1:1 stoichiometry and fairly high thermodynamic stability for the benzylammonium–B15C5 complexes was established. The complexation in acetonitrile is enthalpically driven. The enthalpic effect is reasonably high, considering that only two hydrogen bonds were identified in the structure of the solid complex. Relatively high enthalpy of benzylammonium binding may be related to the close host–guest contact determined by X-ray crystallography.

Diammonium cations also form host–guest complexes with benzo-15-crown-5 (*121*). Complexes with an overall stoichiometry (B15C5):(diammonium salt) = 2:1 were isolated for $^{+}H_3NCH_2C_6H_4CH_2NH_3^{+}$ (complex **40**) and $^{+}H_3N(CH_2)_4NH_3^{+}$ (complex **41**), regardless of the ratio of components in solution. The formulas were determined by elemental analysis and confirmed by single crystal X-ray diffraction studies. Both compounds crystallized as centrosymmetric complexes with one crown ether ring per ammonium group (Fig. 8).

The composition and geometry of each crown ether-ammonium fragment is very similar to that determined for complex **39**. Substitution of the p-xylylenediammonium cation with the less bulky tetramethylenediammonium cation did not affect the geometry of the host–guest interactions in complex **41** compared to complex **40**.

Unlike the protonated monoamine, which clearly interacted with just one crown ether molecule, the protonated diamines $^{+}H_3NCH_2C_6H_4CH_2NH_3^{+}$ and $^{+}H_3N(CH_2)_4NH_3^{+}$ bind more than one crown ether residue in solution. The Job's plot shows the formation of two complexes with [host]/[guest] ratios of 1:1 and 1:2 in acetonitrile. Equilibrium constants for 1:1 and 1:2 complexation were determined from titration of the diammonium salts with B15C5 at 298 K, and

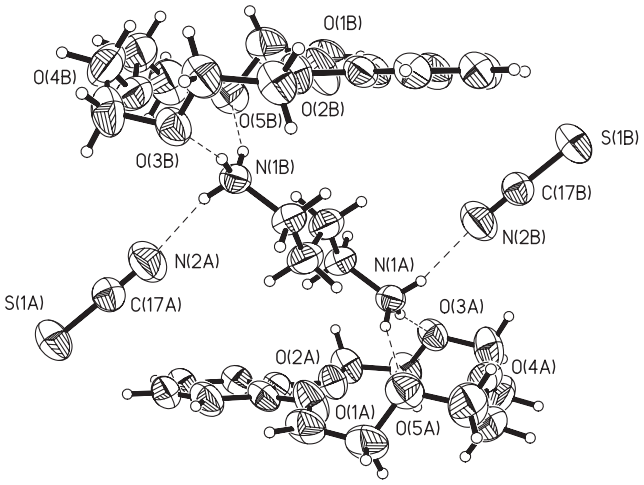

FIG. 8. Crystal structure of complex $[H_3N(CH_2)_4NH_3(B15C5)_2](SCN)_2$ (**41**) (*121*).

fitting the resulting binding curves to the following two-step association scheme:

$$\text{B15C5} + \text{H}_3\overset{+}{\text{N}}\text{–R–}\overset{+}{\text{N}}\text{H}_3 \underset{K_1}{\rightleftharpoons} [\text{B15C5}]\text{H}_3\overset{+}{\text{N}}\text{–R–}\overset{+}{\text{N}}\text{H}_3$$

$$\text{B15C5} + [\text{B15C5}]\text{H}_3\overset{+}{\text{N}}\text{–R–}\overset{+}{\text{N}}\text{H}_3 \underset{K_2}{\rightleftharpoons} [\text{B15C5}]\text{H}_3\overset{+}{\text{N}}\text{–R–}\overset{+}{\text{N}}\text{H}_3[\text{B15C5}]$$

The resulting values of K_1 and K_2 are reported in Table IV. The 1:2 complex predominated in solution when the B15C5 concentration exceeded 9.0×10^{-3} M for *p*-xylylenediammonium (0.01 M) and 5.0×10^{-3} M for tetramethylenediammonium (0.0012 M).

The studies described above demonstrate that each ammonium group of the alkyldiammonium ion binds one molecule of B15C5 with an affinity similar to that observed for the $PhCH_2NH_3^+$–B15C5 system. The overall stoichiometry of diammonium–crown interaction, determined from Job's plot, is 1:2. This is consistent with the exclusive formation of 1:1 complexes between the protonated monoamine ($PhCH_2NH_3^+$) and B15C5, and the lack of sandwich complex formation in that case. The stepwise equilibrium constants K_1 and K_2 also support a model where the two "ends" of the alkyldiammonium cations behave independently, with each "end" binding only one crown ether molecule. The ~2–3 fold decrease in K_2 as compared to K_1 can be attributed to a statistical effect (the decreased probability of RNH_3^+–crown "collision").

The length of the linker in ^+H_3N–R–NH_3^+ (tetramethylene vs. p-xylylene) did not influence the association constants for host–guest complexation with B15C5 (*121*). This result is consistent with the data previously reported for the complexation of different alkyldiammonium cations with 18-crown-6 (*125*).

Very different behavior was exhibited by the ditopic molecular tweezer **37** in its interaction with diammonium cations: (a) only 1:1 complexes were formed, suggesting an "end capped", or inclusion, binding mode; (b) binding affinity depended on the length of the linker (length selectivity for inclusion complexation) (*102*). Since B15C5 alone displays no selectivity with respect to diammonium cation binding, the selectivity of the ditopic host **37** toward $[(CH_2)_4(NH_3)_2]_2^{2+}$ is caused by preorganization of the two receptor fragments attached to the saddle-shaped macrocyclic scaffold. X-ray structural data show that the crown–crown centroid–centroid separation in **41** is about 2.5 Å shorter than the same parameter in **40** (8.29 Å vs. 10.74 Å), accounting for stronger binding of this shorter guest to the ditopic receptor **37**.

When two B15C5 residues were appended to a metallomacrocyclic platform, the length selectivity of the resulting host in the molecular recognition of alkyldiammonium cations was superior to the selectivity displayed by an analogous B18C6-containing ditopic receptor (Section

III.D). This effect can be related to the differences in ammonium–crown binding geometries for the crown ethers of different ring sizes. In ammonium complexes with B18C6, both "perched" and "nested" geometries are possible, where three symmetric hydrogen bonds are formed between the ammonium group and three alternate oxygen atoms of the crown in its preferred D_{3d} conformation. In the former case (perched), the ammonium nitrogen atom is positioned 0.8–0.9 Å above the mean plane of the oxygen atoms. In the latter case (nested), which is easily accessible when its stability is enhanced by other interactions (such as additional hydrogen bonds in a $H_3NRNH_3^{2+}$ complex), it moves almost to the center of the ring and is bound to the lower triangle of 18C6 oxygens (*131,134,147*). In contrast, only the perching complexes are stable for the B15C5 derivatives, with the ammonium group located ~2.0 Å above the mean plane of the oxygen atoms (*120,131*). With its B18C6 rings, and thus multiple ammonium binding modes, tweezer **38** is better able than tweezer **37** to accommodate guests of inappropriate length. Not surprisingly then, tweezer **37** shows greater length selectivity in binding guests than tweezer **38**.

C. Ditopic Crown/Ammonium Complexes in Self-Complementary Systems

In order to further examine the effects of ditopic binding on host–guest complexation between ammonium cations and crown ethers, systems that do not contain a metallomacrocycle were also investigated. Two new self-complementary molecules each composed of a crown-ether (benzo-18-crown-6 or benzo-15-crown-5) with a pendant, protonated primary amino-group (RNH_3^+) (compounds **42** and **43,** Scheme 8) have been recently reported (*119,120*). In addition to providing new insights into the nature of difunctional guest binding by cyclidene-based molecular tweezers, compounds **42** and **43** are interesting in their own right.

Self-complementary (plerotopic) molecules which can form dimers or oligomers due to weak non-covalent interactions have been used effectively as building blocks for supramolecular architertures (*148–155*). For example, Rebek and coworkers have developed molecular capsules based on self-complimentary bowl-shaped molecules rimmed with urea residues (*153*) and Stoddard and coworkers have designed different types of interlocked systems based on the host–guest interaction of molecules with protonated secondary amino or 4,4'-dipyridinium functionalities threaded through large ($\geq$ 24-membered) crown ether macrocycles (*149–151,156*).

Although structural data are of great value in studies of plerotopic dimers, very few of them have been characterized by X-ray crystallography (*154*). Comparison of the structural features of two recently reported plerotopic dimers $\mathbf{(42H^+)_2 \cdot 2(H_3BCNBH_2^-)}$ and $\mathbf{(43H^+)_2 \cdot 2PF_6^-}$ to features of the analogous monotopic

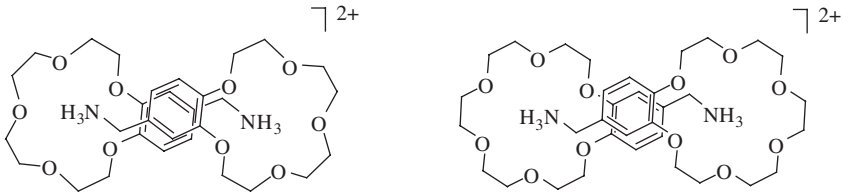

$(42H^+)_2$ $(43H^+)_2$

SCHEME 8. Plerotopic dimers $(42H^+)_2$ and $(43H^+)_2$.

crown-ammonium adducts (Section III.B), reveals the role of a two-point binding "chelate effect" and possible additional host–guest interactions (e.g., π-stacking). This information is helpful for predicting and understanding the structures and stabilities of other ditopic host–guest complexes, such as the inclusion complexes of diammonium salts in the clefts of crown-appended cyclidenes (**37** and **38**).

The dimeric supramolecules $(42H^+)_2$ and $(43H^+)_2$ self-assemble from the monomer (a crown ether with a pendant protonated amino arm) in the gas phase (as shown by electrospray mass-spectrometry), in the solid state (as follows from X-ray crystallography), and in solution (according to NMR). The dimers have unusually high thermodynamic and kinetic stability in solution and can be thought of as supramolecular cyclophanes, in which two aromatic rings are fixed in a π-stacked geometry by non-covalent interaction.

The X-ray crystallographic study of the solvate $\mathbf{43 \cdot HPF_6 \cdot 0.5MeOH}$ revealed the formation of a centrosymmetric (C_i) head-to-tail dimeric cation $(43H^+)_2$ in the solid state (Fig. 9). The ammonium group of each component of the cyclic dimer is coordinated by three oxygens of the complementary 18-crown-6 residue. The average N···O separation is 2.89 Å, which is typical for hydrogen bonds between RNH_3^+ and crown ethers (*131–134*). The oxygen atoms in the macrocyclic ring are in an approximately planar conformation with the mean deviation from the O_6 plane being 0.166 Å. The N atom of the ammonium group is displaced by 0.764 Å from the mean plane of the six macrocyclic oxygen atoms. This distance is among the shortest ammonium–crown ether separations reported in the literature for RNH_3^+–18C6 systems, which usually are in the range of 0.8–1.4 Å (*131–134*). Such a short distance might be explained by the "chelate effect" of two simultaneous crown–ammonim interactions and the π–π stacking between the aromatic rings of the monomers (interplanar separation 3.40 Å, centroid–centroid separation 3.87 Å). An example of a "push effect" was previously found for the $H_2NNH_3^+$ complex with 18C6, where a set of H bonds between the "upper rim" oxygens and the NH_2 group induced a nested configuration of the NH_3 group interacting with the "lower rim" oxygens and displaced by only 0.11 Å from the mean O_6 plane (*134*).

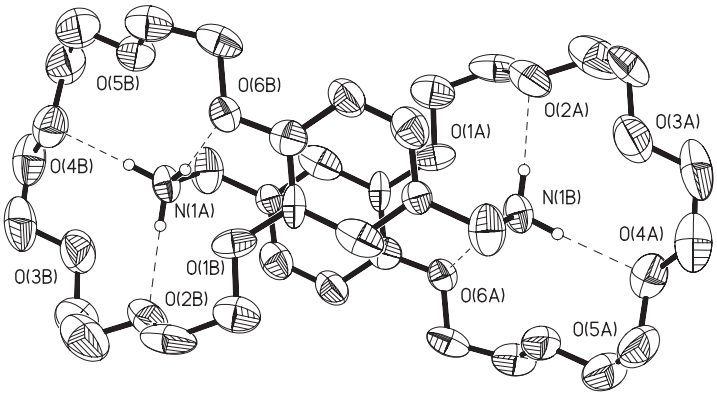

FIG. 9. Molecular structure of supramolecular cation $(43H^+)_2^{2+}$ (*119*)-Reproduced by permission of The Royal Society of Chemistry.

Another self-complementary dimer, $(B15C5CH_2NH_3^+)_2$, **$(42H^+)_2$** was also crystallographically characterized in the form of its salt with a unique $[H_3BCNBH_2CN]^-$ counterion. Here too the pendant crowns are organized as a centrosymmetric (C_i) head- to-tail cationic dimeric **$(42H^+)_2$**. The N···O bond lengths range from 2.864 [O4] to 3.144 Å [O2] with an average N···O separation of 3.00 Å. The oxygen atoms in the macrocyclic ring are approximately coplanar, with a mean deviation from the O_5 plane of 0.1977 Å. The N atom of the ammonium group is displaced by 1.889 Å from the mean plane of the five macrocyclic oxygen atoms. Although this distance is among the shortest ammonium–crown ether separations reported in the literature for the RNH_3^+–15C5 ring systems, which usually are in the range of 1.82–2.34 Å (*131,135,137,143,157,158*), it is fairly close to the ammonium out-of-plane displacement of the $PhCH_2NH_3^+$ adduct with B15C5 (1.842(4) Å, Section III.B) (*121*). The relatively small "chelate effect" arising from two simultaneous crown–ammonim interactions in **$(42H^+)_2$** is consistent with the B15C5 receptor having less orientational flexibility in ammonium binding than the larger B18C6 receptor (Section III.B).

Interestingly, the effect of π–π stacking between the aromatic rings of benzo-15-crown-5 moieties in the **$(42H^+)_2$** appears to be minimal compared to a pronounced effect in an analogous dimer based on a B18C6–NH_3^+ recognition motif (*119*). The interplanar separation of two parallel benzene rings (3.68 Å) in the B15C5 dimer is larger than that observed for the compound containing benzo-18-crown-6 (3.40 Å). Also, the two rings in the B15C5 system are shifted with respect to each other, resulting in a significantly larger centroid–centroid separation (4.53 Å) compared to 3.87 Å for the B18C6 dimeric analog (*119*). Metric parameters of a recently characterized $(15C5–CH_2NH_3)_2^{2+}$ dimer (*140*) are very similar to those reported here for **$(42H^+)_2$**. Since the former compound does not have aromatic rings, the geometry of both dimers is

defined primarily by the RNH_3^+–15C5 interactions and not by additional π–π stacking.

The single-crystal X-ray study of **(42H$^+$)** · $[H_3BCNBH_2^-]_2$ also revealed the formation of an unusual $[H_3BCNBH_2CN]^-$ anion. This anion has been known for some time but was never structurally characterized (*159–162*). The crystallographic data along with ^{11}B NMR and IR data confirmed the connectivity of the dicyanodiborohydride anion which had previously been assigned by other means (*159–162*).

The solution behavior of both the B15C5 and B18C6 dimers **(42H$^+$)$_2$** and **(43H$^+$)$_2$** were studied by variable temperature NMR. ^1H NMR spectra for dimethyl sulfoxide (DMSO) solutions at 295 K indicate an absence of aggregation. However, NMR spectra collected using acetonitrile solutions clearly show an associative process over a 238–343 K temperature range and 10^{-4}–10^{-2} M concentration range. NMR data also indicate significant π–π interaction between the catechol rings that may arise from the offset face-to-face stacking of the two aromatic units in the cyclic head-to-tail dimer **(43H$^+$)$_2$** (Fig. 9) (*119*).

The temperature-dependent ^1H NMR spectra of an acetonitrile solution of **42H**$[H_3BCNBH_2CN]$ indicate that the yield of the dimer increases with decreasing temperature as expected for an associative process, but even at 343 K the dimerization is substantial in acetonitrile. The dimerization is essentially quantitative for **(43H$^+$)$_2$**.

The dimers can be completely destroyed by the addition of KI to the acetonitrile solution due to the competitive complexation of K^+ by the crown ether. No π–π interactions between the catechol rings of the two B15C5 residues are observed by NMR in the K^+ complex of **42**.

Remarkably, the dimer formed from **43 · HPF$_6$** (*119*) is even somewhat more stable than the analogous "threaded" crown–ammonium self-associate observed by Stoddart and co-workers (*149,151*). The dimer **(43H$^+$)$_2$** is the predominant form in acetonitrile solution over a broad range of concentrations and temperatures (10^{-4}–10^{-2} M, 238–343 K), while the "threaded" dimer of Stoddart's alkylamino-substituted DB24C8 dissociates into the monomeric form upon heating a 10^{-2} M acetonitrile solution to 343 K or upon dilution to 10^{-4} M at room temperature (*151*). The relatively high stability of **(43H$^+$)$_2$** can be explained in terms of strong association between the primary ammonium group and B18C6 receptor of **43** ($K \sim 10^4\ M^{-1}$ in acetonitrile at 295 K) (*102,103,125,163*) compared to the weaker "threading" of a secondary ammonium cation through DB24C8 ($K \sim 10^2$–$10^3\ M^{-1}$ under similar conditions) (*103,125,163–165*).

The kinetic stability of the **(43H$^+$)$_2$** dimer is also unusual. Experiments with other B18C6 derivatives invariably showed rapid exchange of alkylammonium guests on the ^1H NMR timescale (CD_3CN, 295 K) (*102*). The slow exchange observed for **43 · HPF$_6$** solutions in acetonitrile at low temperatures, and intermediate exchange observed at room temperature, can be attributed to decreased decomplexation

rates arising from the "chelate effect" of two-point dimerization reinforced by π-stacking interactions. Slow exchange is typical for threaded complexes of ammonium cations with large crowns (*149–151*), but is unusual for perched complexes with medium-sized crown ethers (*103,125,163*). $(\mathbf{42H^+})_2$ undergoes fast exchange even at 240 K.

It can be concluded that ditopic ammonium–crown interactions improve both the thermodynamic and kinetic stability of the host–guest adducts. Attaching two crown ether receptor groups to the edges of metallomacrocyclic clefts shows significant promise for the preparation of shape- and length-selective receptors. The relative flexibility of the cyclidene complexes does not prevent length- and shape-selective recognition of polyfunctional guests, as described in detail in Section III.A (*102*). Moreover, the dipositive charge of the cyclidene platform in receptors **37** and **38** was not detrimental to the formation of stable adducts with diammonium guests of appropriate length.

D. Binding of Bifunctional Anionic Guests to Ditopic Cyclidene-Based Hosts

Early examples of dicarboxylate binding systems, reported by the research groups of J.-M. Lehn (*24,166,167*), E. Kimura (*168*), R. Breslow (*169*), and F.P. Schmidchen (*170–172*) in the early 1980s, clearly illustrate three approaches to preorganizing two carboxylate receptors: (a) incorporating polyammonium receptors into the macrocycles (*24,167,168,170*); (b) attaching two receptor groups to a linear spacer (*166,169,171*); and (c) placing the binding groups on the walls of a cleft (*172*). Recognition of dicarboxylate guests using macrocyclic cavities gave rise to topologically more advanced approaches employing 3D recognition by cryptands and cages (*173–181*). These highly preorganized hosts exhibit strong binding affinities and excellent length selectivity. This route is, however, quite synthetically challenging. In contrast, ditopic receptors connected by a linear spacer are relatively easy to synthesize, but allow for only limited preorganization of the host. While the flexibility of such tethered hosts does not necessarily compromise their affinity for dicarboxylate guests ("induced fit" binding) (*182,183*), and size selectivity can sometimes be achieved if rigid linkers are employed (*184,185*), the compositions and structures of these host–guest adducts are not easily predictable. One-to-one binding can give rise to either discrete host–guest pairs or oligomers with alternating dicarboxylate and direceptor monomers. A variety of crystalline oligomers have been isolated in the solid state and analyzed by X-ray diffraction (see (*186–188*) for some examples), suggesting that these systems are well-suited for crystal engineering, but not always appropriate for shape selective substrate recognition in solution. Rigid

cleft-like scaffolds, poetically advocated by Schmidtchen (*172*):

> Though encapsulation of ions
>
> In cages was first to rely on,
>
> The better perspective
>
> For being selective
>
> Have locular hosts for anions,

can be considered a reasonable, synthetically-accessible compromise between the first two approaches. Functionalized clefts successfully recognize dicarboxylate guests (*172,189–194*), and the search for new spacers continues to yield ditopic receptors with desirable properties (*109,195–205*).

Functional groups (e.g., polyamines, amidinium or guanidinium fragments, amidopyridines, etc.) that are capable of electrostatic and hydrogen bonding interactions with carboxylates (*206*) can be attached to a rigid molecular scaffold, yielding shape-selective receptors.

The advantages of incorporating metal ions into receptors for anion recognition (Section I) were demonstrated in numerous studies on specific hosts for dicarboxylates. For example, self-assembly of polyfunctional receptors has been accomplished via coordination of several receptor fragments to the metal ions (*108,207–210*); direct coordination to the metal centers was used for carboxylate binding (*179,181,211–214*); and binding affinities were increased due to favorable electrostatic interactions between positively charged metal centers in the hosts and the anionic guests (*202,215–217*). Metals also served as redox (*202,215,216*), fluorescent (*210*), or colorimetric (*207*) reporters of carboxylate binding events.

We applied our general design strategy, described in Section III.A, in order to prepare selective receptors for dicarboxylic acids (*98,100*). In the first example, two cyclic tetramine residues (cyclens), which are expected to strongly bind dicarboxylates due to a combination of electrostatic interactions and hydrogen bonding (*24,167,168,181,218–223*), were attached to a conformationally flexible 15-membered cyclidene, to yield the ditopic host **44** (Scheme 9) (*98*).

The metal-free tetraaza macrocycle cyclen has four secondary amino groups which can be protonated, with the first two protonation constants close to each other and typical of a strong base (*224*). Cyclen becomes a weaker base when it is appended to a nickel(II)cyclidene platform as the positive nickel center draws electron density away from the cyclen nitrogens through the conjugated cyclidene platform. As a result, NMR titration of complex **44** in d_6-DMSO with triflic acid showed that just one secondary amino group in each cyclen residue of **44** retained its strongly basic properties, while two other secondary amino groups in each cyclen behaved as weakly basic centers.

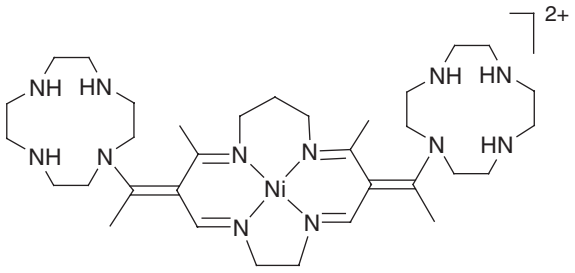

44

SCHEME 9. Structure of cyclen-appended cyclidene **44**.

TABLE VI

EQUILIBRIUM CONSTANTS OF DICARBOXYLIC ACID BINDING TO COMPLEX 44 (DMSO, 25 °C). EQUILIBRIA IN THE SYSTEM ARE DESCRIBED BY EQ. (1)–(6) *(98)*

Acid	K_{meas}	Log(K_{meas})	pK_{a1} *	pK_{a2} *	Log(K_{assoc})+Constant
Malonic	7000	3.85	1.38	5.68	10.901
Maleic	4000	3.60	1.92	6.22	11.74
Phthalic	3500	3.54	2.93	5.41	11.88
Fumaric	1100	3.04	3.03	4.38	10.45
Terephthalic	890	2.95	3.54	4.46	10.95
Isophthalic	680	2.83	3.7	4.6	11.13
Succinic	118	2.07	4.21	5.63	11.91
Glutaric	41	1.61	4.34	5.27	11.22
Sebacic	13	1.11	4.4	5.22	10.73

Complex **44** reacts with a number of dicarboxylic acids in organic solvents (DMSO or acetonitrile), as observed by ^{1}H NMR spectroscopy. The stoichiometry of these host–guest complexes has been established by the method of continuous variations (Job's method) as 1:1 for all dicarboxylic acids. Binding constants (Table VI) were determined by fitting the results of ^{1}H NMR titrations to a 1:1 host–guest binding model.

Relatively strong 1:1 complexation between complex **44** and several dicarboxylic acids, together with the weak binding observed for monocarboxylic acids, suggests that both cyclen receptor arms in **44** participate, cooperatively, in the encapsulation of dicarboxylate guests (Fig. 10).

This proposed binding mode implies that shape complementarity between the host (receptor **44**) and the guest (a dicarboxylic acid) is beneficial for high affinity binding. A comparison of the measured dicarboxylic acid binding constants (Table VI) does not immediately reveal this trend, because of the composite nature of K_{meas} values. In considering these systems, it is reasonable to assume that the

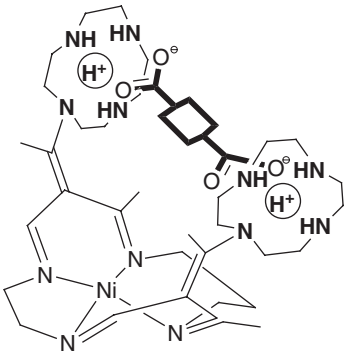

FIG. 10. Proposed binding mode of dicarboxylic acids to **44**.

following equilibria exist in the reaction solution:

$$R(CO_2H)_2 \rightleftharpoons {}^{-}O_2C - R - CO_2H + H^+ \qquad K_{a1} \tag{1}$$

$${}^{-}O_2C{-}R{-}CO_2 \rightleftharpoons {}^{-}O_2C{-}R{-}CO_2^- + H^+ \qquad K_{a2} \tag{2}$$

$$\text{Receptor} + 2H^+ \rightleftharpoons (\text{Receptor})H_2^{2+} \qquad K_{b(2)} \tag{3}$$

$$(\text{Receptor})H_2^{2+} + {}^{-}O_2C - R - CO_2^- \rightleftharpoons \text{Adduct} \qquad K_{assoc} \tag{4}$$

The measured binding constant K_{meas} can be expressed as the product of two sequential dissociation constants of an acid (K_{a1}, K_{a2}), the protonation constant of the complex **44** ($K_{b(2)}$), and an association constant for host–guest adduct formation (K_{assoc}).

$$K_{meas} = K_{a1}K_{a2}K_{b(2)}K_{assoc} \tag{5}$$

Although the measured binding constants depend on the strengths of the acids (Table VI), there is no linear correlation between the log K_{meas} and pK_a of the guests. A comparison between three relatively weak aliphatic dicarboxylic acids (succinic, glutaric, and sebacic) is particularly revealing: both pK_{a1} and pK_{a2} of these acids are nearly identical, while their binding constants with complex **44** differ by an order of magnitude. Clearly, factors other than guest acidity play a role in their binding to the host **44**. Another variable in Eq. (5) is the association constant K_{assoc} (a measure of association between the doubly protonated host **44** and the dianion of the guest). The remaining term, the protonation constant of complex **44** ($K_{b(2)}$), does not change

throughout the series. It is the K_{assoc} value that is expected to depend on the shape complementarity between the host and the guest.

$$\log K_{meas} + pK_{a1} + pK_{a2} = \text{Log } K_{assoc} + \text{Const} \qquad (6)$$

The calculated values of ($\log K_{assoc}$+Const) are summarized in Table VI and Fig. 11. Complex **44** shows substantial selectivity for succinic, phthalic, and maleic acids. In all three of these acids, two carboxylate groups are attached to neighboring carbon atoms and can be positioned *cis* to each other. The importance of having the appropriate distance between the two carboxylate groups is evident from a comparison of aliphatic diacids: the binding affinity, optimal for succinic acid, decreases for both shorter (malonic acid) and longer (glutaric and sebacic acids) homologs. While flexible aliphatic linkers allow for a variety of spatial arrangements of the two carboxylate groups, rigid unsaturated aliphatic or aromatic diacids fix the functional groups in a well-defined geometry. Since maleic acid (*cis*-isomer) is bound more strongly than fumaric acid (*trans*-isomer), it is clear that *cis*-orientation of the two carboxylates is beneficial for their interaction with the receptor **44**. Aromatic *ortho*-diacids are very similar to maleic acid with respect to orientation of the two carboxylate groups and it follows logically that *o*-phthalic acid is bound more strongly than the isomeric *m*- and *p*-derivatives (isophthalic and terephthalic acids). It thus appears that vicinal *cis*-1,2-dicarboxylates show the strongest interactions with the difunctional receptor **44.** Presumably, this guest geometry corresponds to an optimal binding conformation of the host **44**. This assumption is in agreement with structural data for the parent cyclidene complexes (*40*). The only crystallographically character-

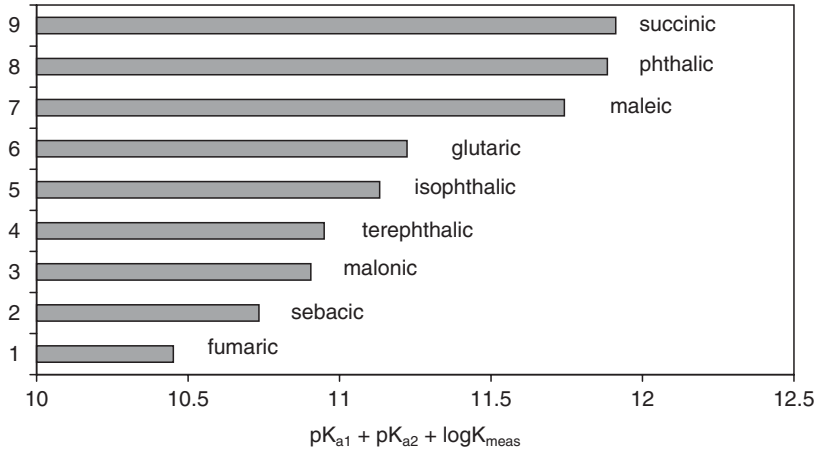

FIG. 11. Diagram of the relative values of association constants ($\log K_{assoc}$ +Const., see Eq. (6)) of the host–guest complexes formed between complex **44** and dicarboxylic acids (*98*).

ized saddle-shaped 15-membered cyclidene precursor has a cavity width of 7.23 Å, which is not substantially different from the cavity width in unbridged 16-membered cyclidenes (6.39–6.85 Å) (*44*). Extensive X-ray studies of covalently bridged 16-membered cyclidenes (Scheme 2) (*225*) and molecular modeling studies on these systems (*48,52,127*) demonstrated that the hexamethylene linker (R^1) has an optimal length to span the cyclidene cavity with the least steric strain. Notably, the dicarboxylate guests that bind most strongly to host **44** also have six atoms spanning the receptor cavity (two carboxylate oxygens, two carboxylate carbons, and two carbons in the linker) in a supramolecular fashion. In summary, analysis of the data in Fig. 11 shows that significant shape selectivity in dicarboxylate binding can be accomplished using the relatively flexible ditopic receptor **44** which acts as a pair of tweezers for shape-complementary substrates (*98*). Very similar length selectivity was also observed for diammonium recognition by crown-appended cyclidenes (Section III.A, Table III): again, the highest-affinity binding was reported for the guest containing six second-period atoms in a linear chain (two protonated nitrogens separated by four methylene units) (*102*).

The cyclen-appended cyclidene **44** binds carboxylic acids fairly strongly, but this host also decomposes in protic solvents, presumably via a base-promoted deacylation pathway (*226*). For systematic studies on dicarboxylate binding, another family of modified cyclidenes bearing aminopyridine receptor groups was synthesized (**45–52**, Scheme 10) (*100,101*).

These systems allowed us to explore the role of cyclidene molecular shape in the guest binding properties of receptors for dicarboxylates. A series of three nickel(II) cyclidenes (**45–47**), each bearing two ethylpyridine receptor sites, was prepared. These host molecules, which differ only with respect to size of the macrocyclic ring, were crystallographically characterized and the influence of their molecular shape on dicarboxylic acid binding affinity was examined (*100*).

The crystallographic data confirmed the expected geometries of the 14- and 16-membered macrocycles **45** and **47** as planar and saddle-shaped, respectively. The 15-membered complex **46** was found to crystallize in an "open", nearly planar, geometry that resembles the overall molecular shape of the 14-membered complex **45** (Figs. 12–14). Unlike the 14-membered complex **45**, in which the two unsaturated wings are almost coplanar with the NiN_4 fragment, the 15-membered **46** has its unsaturated wings tilted in opposite directions. It is thus likely that an alternative saddle-shaped conformation of **46** (with both unsaturated wings facing the same direction) is close in energy to the structure determined by X-ray diffraction (*40,44*). Furthermore, in covalently bridged 15-membered cyclidenes, the macrocyclic platform is invariably cleft-like and has a cavity size comparable to that of the corresponding 16-membered complexes (*40*). In contrast, the 14-membered platform could only be bridged using a long, C_{12} aliphatic chain that

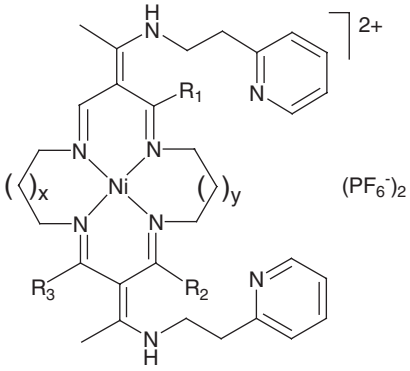

x=y = 0; $R_1 = R_3 = CH_3$; $R_2 = H$ **45**
x=0; y = 1; $R_1 = R_2 = CH_3$; $R_3 = H$ **46**
x=y = 1; $R_1 = R_2 = CH_3$; $R_3 = H$ **47**

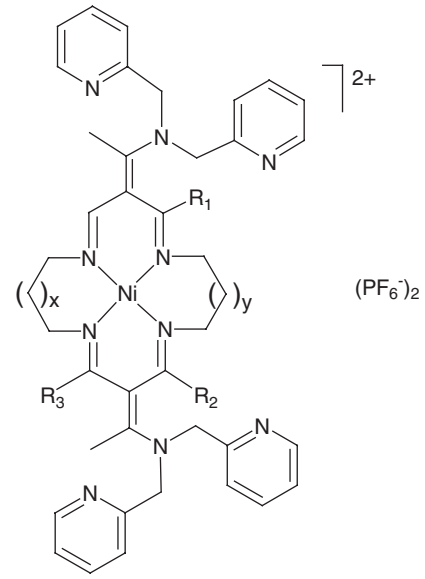

x=y = 0; $R_1 = R_3 = CH_3$; $R_2 = H$ **48**
x=0; y = 1; $R_1 = R_2 = CH_3$; $R_3 = H$ **49**
x=y = 1; $R_1 = R_2 = CH_3$; $R_3 = H$ **50**

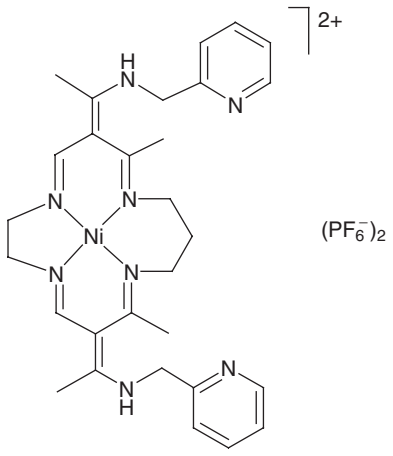

51

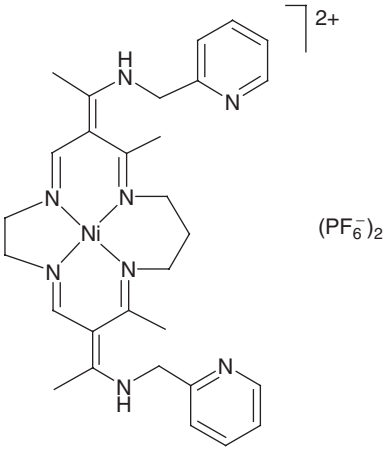

52

SCHEME 10. Structures of alkylpyridine-appended cyclidenes **45–52**.

can span the "open wings" of this nearly planar macrocycle (*43*). Molecular mechanics and molecular dynamics calculations also support the accessibility of a saddle-shaped geometry in 15-membered

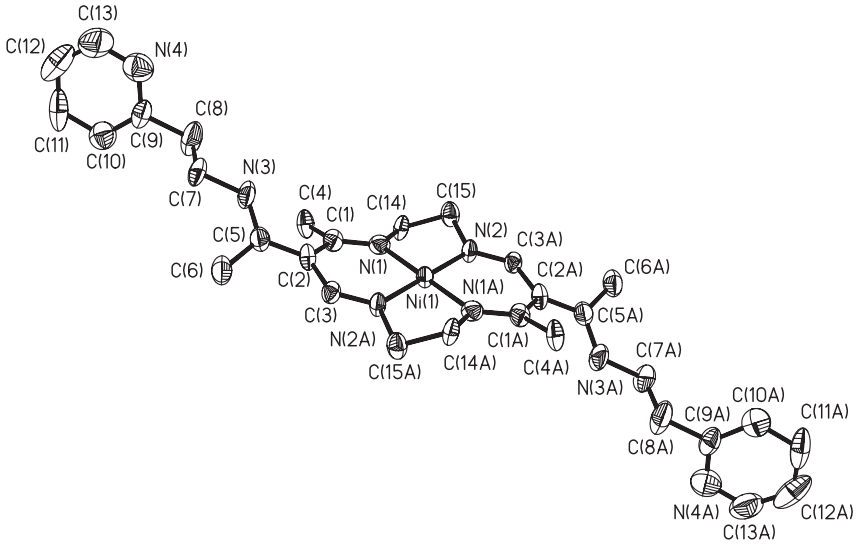

FIG. 12. ORTEP diagram of [Ni(2-pyEtNH[14]cyclidene)]$(PF_6)_2$ complex **45**. Hydrogen and counteranions are omitted for clarity. Thermal ellipsoids are shown at 50% probability. Reproduced with permission from Ref. (*100*). Copyright 2003, American Chemical Society.

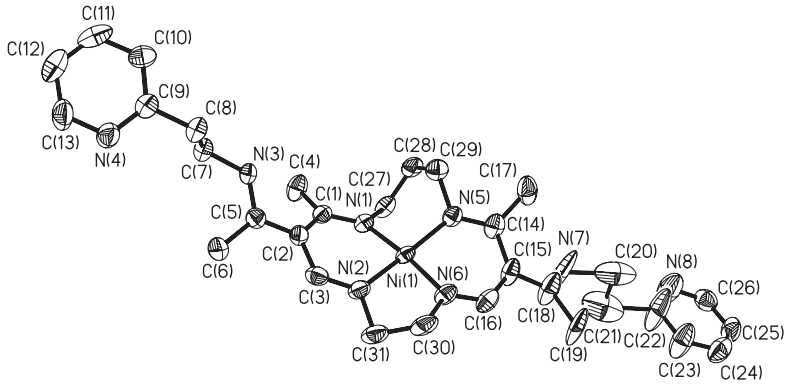

FIG. 13. ORTEP diagram of [Ni(2-pyEtNH[15]cyclidene)]$(PF_6)_2$ complex **46**. Hydrogen and counteranions are omitted for clarity. Thermal ellipsoids are shown at 50% probability. Reproduced with permission from Ref. (*100*). Copyright 2003, American Chemical Society.

cyclidenes and related molecules, and a predominantly planar conformation for the 14-membered complexes (*48,52,127*).

Both X-ray crystallography and NMR spectroscopy show that the ethylpyridine arms are the most flexible parts of complexes **45–47**. In the case of the 16-membered complex **47,** the asymmetric unit contained two non-equivalent complex cations, which differ in the

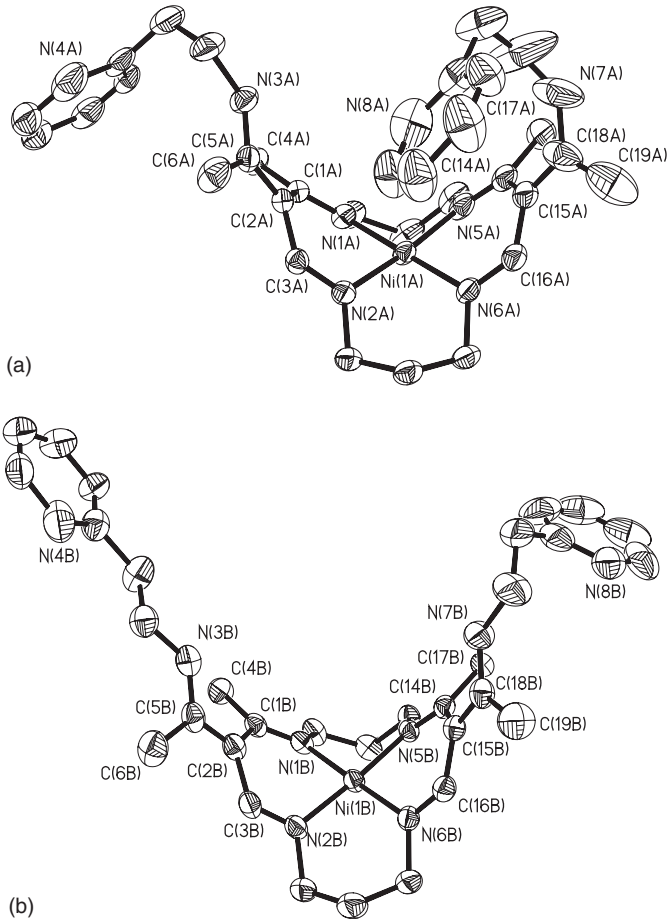

FIG. 14. ORTEP diagram of [Ni(2-pyEtNH[16]cyclidene)]$(PF_6)_2$ complex **47a** (top) and **47b** (bottom). Hydrogen and counteranions are omitted for clarity. Thermal ellipsoids are shown at 50% probability. Reproduced with permission from Ref. (*100*). Copyright 2003, American Chemical Society.

orientations of their ethylpyridine substituents. The flexibility of the aliphatic linkers that were used to attach the receptor groups to the cyclidene platforms allows the host geometry to adjust to the geometric requirements of the encapsulated guests.

All three complexes, **45–47**, were found to interact with carboxylic acids. The carboxylic acid binding can be attributed to partial protonation of the receptor arms and hydrogen bonding of the carboxylate anions with both the ethylpyridine fragment and an exocyclic NH group (see Fig. 15). No carboxylate coordination to the nickel(II) centers was observed. Hydrogen bonding between dicarboxylic acids and host macrocycles **45–47** is confirmed by NMR: the dicarboxylic acid-induced NMR shifts of the protons in the ethylpyridine fragments are

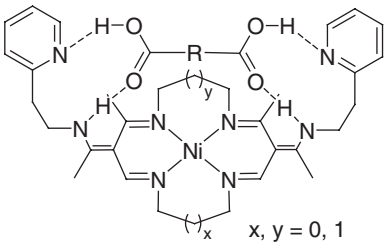

FIG. 15. Inclusion binding mode of dicarboxylic acids by **45–47**.

somewhat smaller than the shifts due to full protonation of the pyridine nitrogens in **45–47** with strong acid. Not surprisingly, the pyridine-appended host **46** does not bind dicarboxylic acids (e.g., maleic acid) as strongly as an analogous cyclidene host bearing polyamine macrocyclic receptor arms (host **44**) under the same experimental conditions (DMSO, 25°C) (*98*). The polyamine (cyclen) receptor is a much stronger base than the pyridine, and it has more possibilities for both hydrogen bonding and electrostatic interactions with carboxylate guests.

The relatively strong 1:1 complexation between complexes **45–47** and aromatic or unsaturated dicarboxylic acids, and the lack thereof in the case of monocarboxylic acids (Table VII) suggests that both ethylpyridine receptor arms participate, in a cooperative manner, in the encapsulation of dicarboxylate guests (Fig. 15).

Additional evidence in favor of the guest being encapsulated between the two receptor arms was obtained from Nuclear Overhauser Enhancement Spectroscopy (NOESY) studies of the maleic acid–**46** system. These spectra clearly show through-space correlations between the guest protons and protons from both the macrocyclic platform and the pyridine arms. The 3.0–3.5 Å distances between the maleic acid and the macrocycle, which were determined from the NOESY experiment, are consistent with an inclusion binding mode (*100*). In the case of the 16-membered complex **47**, difunctional guest binding inhibits flipping of the receptor arms between "outside-the-cavity" and "inside-the-cavity" orientations. An alternative 1:1 supramolecular motif, a linear oligomer with intermolecular binding of the dicarboxylate, was previously found in a number of solid-state structures (*186–188,227*), but is unlikely to dominate in dilute solutions. The stability of oligomeric adducts should depend on the overall concentration of host–guest solution, a behavior that was not observed in our systems.

The proposed intramolecular inclusion binding mode (Fig. 15) implies that shape complementarity between the host (receptors **45–47**) and the guest (a dicarboxylic acid) is beneficial for high affinity binding. Analysis of the binding constants (Table VII, Fig. 16) shows that the binding strength depends on the structures of both the host and

TABLE VII

EQUILIBRIUM CONSTANTS (K_A, M^{-1}) FOR CARBOXYLIC ACID BINDING TO MACROCYCLIC HOSTS 45–47 AT 298 K (*100*)

Guest	pK_a[a]	*[14]*NHET$_2$PY, **45**	*[15]*NHET$_2$PY, **46**	*[16]*NHET$_2$PY, **47**
Phthalic acid	2.95; 5.41	19 ± 2	121 ± 12	252 ± 3
3-Nitrophthalic	2.11; 4.48	20 ± 2[b]	45 ± 7	421 ± 15
5-Nitroisophthalic	3.93; 5.16[c]	64 ± 6	152 ± 7	51 ± 19
2-Nitroterephthalic	1.75; 3.60[d]		<10	<10
Maleic	1.92; 6.22	100 ± 14	159 ± 13[e]	213 ± 19
Benzoic	4.21		0[f]	
Fumaric	3.03; 4.38[d]		<10	
2-Nitrobenzoic	2.1		<10	<10
4-Nitrobenzoic	3.45		<10	<10
Nitrobenzene	–		0[f]	
Terephthalic	3.54; 4.34	(Insoluble)		
Isophthalic	3.5; 4.5 (H_2O)			
4.78; 5.98[c]	(Insoluble)			
Trifluoroacetic		2:1 at Saturation	2:1 at Saturation	

Note: Unless otherwise noted, the NMR titrations were performed in CD_3CN at 298 K. Unless otherwise noted, the data were taken from the *Dictionary of Organic Compounds*

[a]Ionization constants in water, for diacids, pK_{a1} and pK_{a2} are listed.

[b]$K_a = 27 \pm 3$ when repeated as reverse titration (i.e., host added to guest acid solution.).

[c]Data in a 1:1 methanol/water mixture. S.J. Gumbley, R. Stewart. *J. Chem. Soc. Perkin Trans. 2*, 1984, 529–531.

[d]W.E. Berger, *Helv. Chim. Acta 23*, 1940, 39–53.

[e]$K_a = 23 \pm 7\ M^{-1}$ in d-DMSO.

[f]No changes in spectrum were observed.

the guest. While acidity of the guest is clearly a factor that influences the binding strength, the orientation of the two carboxylate groups and the distance between them also play an important (and sometimes decisive) role in binding affinity. While 1,2- and 1,3-aromatic and *cis*-1,2-unsaturated diacids bind reasonably well (with affinity constants ranging from 20 to 400 in acetonitrile), the 1,4- aromatic and trans-1,2-unsaturated diacids show very small, if any, interaction with the macrocyclic hosts **45–47**. In some cases (e.g., with terephthalic acid or fumaric acid), the limited solubility of the diacid partially accounts for small NMR shifts and the lack of saturation on the binding curves. In some other cases, however, the diacids have sufficient solubility, and still demonstrate only weak binding to the macrocyclic hosts. A good example is 2-nitroterephthalic acid, which has sufficient solubility in acetonitrile and ionization constants comparable to or exceeding the values for other isomers of nitrophthalic acids (Table VII). The unfavorable orientation of the two carboxylate groups prevents a strong interaction between this acid and the macrocycles.

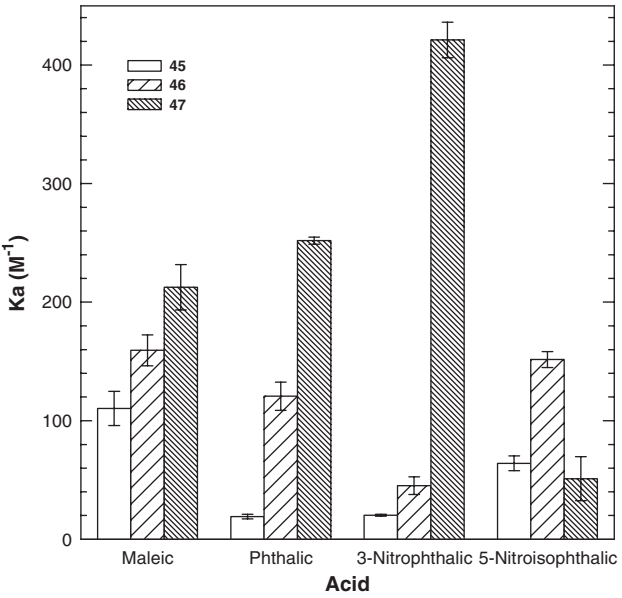

FIG. 16. Graphical comparison of binding constants for four dicarboxylic acids and compounds **45**, **46** and **47**. Reproduced with permission from Ref. (*100*). Copyright 2003, American Chemical Society.

The macrocyclic ring size (and, consequently, the shape of the host molecule) has a pronounced effect on the diacid binding affinity (Fig. 16). For all acids that bind relatively strongly, the planar 14-membered macrocycle **45** has the weakest binding affinity for diacid guests. In most cases, the saddle-shaped 16-membered macrocycle **47** is the best receptor. The 15-membered complex **46**, that can adopt either an almost planar, or a saddle-shaped conformation, usually displays an intermediate binding affinity. Interestingly, this trend holds for all 1,2-aromatic or *cis*-unsaturated diacids investigated in this work. However, the aromatic 1,3-diacid (5-nitroisophtalic acid) has a 3-fold higher binding affinity to **46** than it has to the saddle-shaped host **47**. Apparently, the average separation between the two pyridine receptor centers in **46** is greater than the distance between the pyridine receptors in **47**. This greater separation is unfavorable for the strong binding of 1,2-diacids, but becomes favorable for the corresponding 1,3-diacid. It can be concluded that the molecular shape of the cyclidene platform significantly influences the guest binding affinity of ditopic hosts, and in some cases even changes the selectivity of the hosts. This molecular shape effect is observed in systems that have flexible appended receptor arms, and this flexibility is beneficial for "induced-fit" guest binding. Indeed, the orientation of the pyridine arms in crystalline macrocycles **45–47** did not suggest substantial preorganization for dicarboxylate encapsulation. It can be assumed that the

host–guest interaction itself repositioned the ethylpyridine groups in order to accomplish a good fit between the host and the guest. In the case of the 14-membered platform that cannot fold, the conformational flexibility of the receptor arms was necessary to accommodate the bifunctional guests. For the 15-membered complex, it can be hypothesized that the platform adopted a saddle-shaped conformation in the host–guest complex that is favorable for guest encapsulation. This cleft-like confirmation of the platform already existed in the solid state of the 16-membered complex. The flexibility of the receptors allowed for only moderate selectivity in host–guest interactions between carboxylates and **45–47**. The effects of molecular shape and macrocycle-dependent size and shape selectivity may be even more pronounced in systems with rigid receptor groups directly attached to the cyclidene platforms. The exploration of such systems is being pursued.

Association constants for the 2-methylpyridine-appended host **51** and maleic, phthalic, and 3-nitrophthalic acids are less than $30\,M^{-1}$. Intramolecular hydrogen bonding between the pyridine and amine observed in the solid state for **51** inhibits the binding of carboxylic acids. However, the 3-pyridylmethylamine derivative **52** does react with dicarboxylic acids. Compound **52** binds smaller guests (i.e., maleic acid) more strongly than the larger phthalic and nitrophthalic acids (*101*) (Fig. 17).

Due to the presence of nickel(II) in the platform, binding of carboxyfluorescein to **47** resulted in fluorescence quenching. This effect could be used in competitive fluorescence assays for dicarboxylic acids: encapsulation of the guest will release carboxyfluorescein, and the assay will "light up" (*101*).

IV. Interactions between Polyoxoanions and Macrocyclic Cations

While the use of macrocycles and other polytopic receptors for the recognition of simple mineral anions (*9,26*) and carboxylates (*194*) has developed rapidly and prominently over the past 30 years, the molecular recognition of polyoxoanions has been less recognized as a cohesive area of investigation. A careful inspection of the literature reveals considerable interest in the non-covalent interactions between polyoxometalates and polytopic receptors, but this information is so scattered over time and disciplines that many groups have worked independently, in the context of specific goals and applications, with little sense of polyoxometalate host–guest recognition as a topic itself. Recent advances in (a) the design of discrete polyoxometalate-specific receptors (*228,229*), (b) the design of supramolecular, hybrid materials composed of polyoxoanions and organic or complex cations (*230–234*), and (c) the use of polyoxometalates to selectively precipitate prions (*235*) highlight the need for literature review of polyoxometalate/receptor interactions.

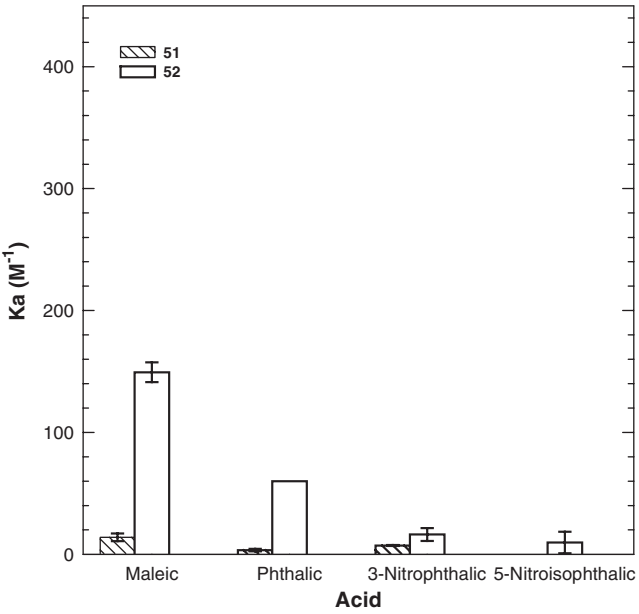

FIG. 17. Graphical comparison of binding constants for four dicarboxylic acids and compounds **51** and **52**.

In keeping with the theme of this chapter, the following sections will focus on polyoxometalate/receptor interactions from a molecular rather than materials perspective and special attention will be given to interactions between polyoxoanions and protonated or metallated macrocyles.

A. Interactions between Polyoxoanions and Crown Ethers

It is not surprising, given both the importance and commercial availability of crown ethers, that salts composed of $[M\text{-crown}]^+$ cations and polyoxoanions (POMs) have been widely investigated. The first of these salts to be structurally characterized was the monohydrate salt of potassium 18-crown-6 and the hexamolybdate ion, $(C_{12}H_{24}O_6)_2 \cdot K_2Mo_6O_{19} \cdot H_2O$ (*236*). As clearly seen in Fig. 18, the K^+-crown complexes are layered face to face, in approximate columns, with hexamolybdate ions or water molecules intercalated alternately between them. This columnar, sandwich structure can, perhaps, be attributed to the size complementarity between cation and anion. This material is also characterized by strong ion–dipole interactions between the potassium ions and the water molecules, as demonstrated by a 363 K thermogravimetric dehydration temperature. Strong interactions between crown-coordinated M^{n+} cations and co-crystallized water appear to be a structural theme in many M^+-crown POM salts (*237–241*). In some cases, aggregation of the crown cations with water appears to

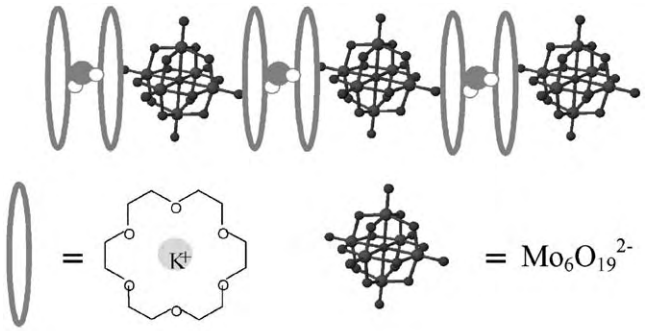

FIG. 18. Schematic illustration of the crystal structure of $(C_{12}H_{24}O_6)_2 \cdot K_2Mo_6O_{19} \cdot H_2O$ (*236*).

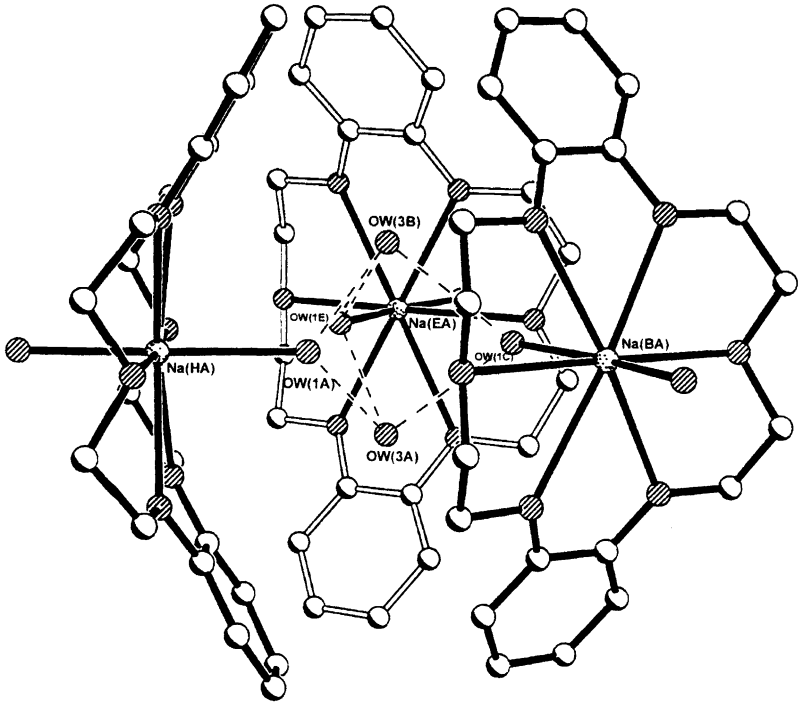

FIG. 19. Three $[Na(DB18C6)(H_2O)_2]^+$ ions and two additional water molecules form a hydrogen bonded supramolecular cage in the structure of $[\{Na(DB18C6)(H_2O)_2\}_3(H_2O)_2]XMo_{12}O_{40} \cdot 6DMF \cdot CH_3CN$ (X = P) Reproduced with permission from Ref. (*241*). Copyright 2003 American Chemical Society.

minimize crown-POM interactions as is the case with salts composed of Na^+-dibenzo-18-crown-6 cations and Keggin polyoxoanions, $[\{Na(DB18C6)(H_2O)_2\}_3(H_2O)_2]XMo_{12}O_{40} \cdot 6DMF \cdot CH_3CN$ (X = P or As) (*241*). As is apparent in Fig. 19, three $[Na(DB18C6)(H_2O)_2]^+$ ions and

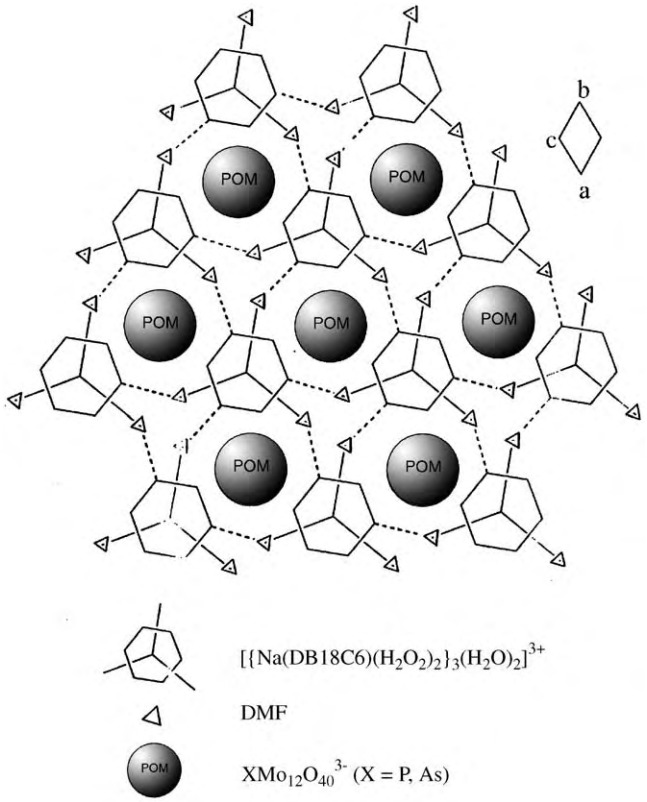

FIG. 20. Schematic representation of the crystal structure of [{Na(DB18-C6)$(H_2O)_2\}_3(H_2O)_2$]$XMo_{12}O_{40} \cdot 6DMF \cdot CH_3CN$ (X = P) from Ref. (*241*). Polyoxoanions are guests in a hydrogen-bonded network formed by [{Na(DB18C6)$(H_2O)_2\}_3(H_2O)_2]^{3+}$ units and DMF. Reproduced with permission from Ref. (*241*). Copyright 2003 American Chemical Society.

two additional water molecules form a hydrogen bonded supramolecular cage which effectively excludes the POMs from the concave surfaces of the macrocycles. At a higher organizational level, however, the POMs are clearly guests in the hydrogen-bonded network formed by [{Na(DB18C6)$(H_2O)_2\}_3(H_2O)_2]^{3+}$ units and DMF (Fig. 20). In another, more unusual example (*240*) the hexamolybdate ion, $[Mo_6O_{19}]^{2-}$, stabilizes a rare transition metal–crown ether complex, $[Cu^{II}(H_2O)_4$(dibenzo-24-crown-8] $[Mo_6O_{19}]$. In this case, the copper(II) sits in the geometric center of the crown cavity and is coordinated to two symmetrically opposed oxygen atoms of the dibenzo-24-crown-8 and four water molecules (Fig. 21). While one *trans*-oriented pair of ligated water molecules hydrogen bonds exclusively to four ethereal oxygen atoms of the crown ether, the other 2 ligated water molecules each form one hydrogen bond to the dibenzo-24-crown-8 and a second to a neighboring hexamolybdate ion. In this manner, the coordinated water

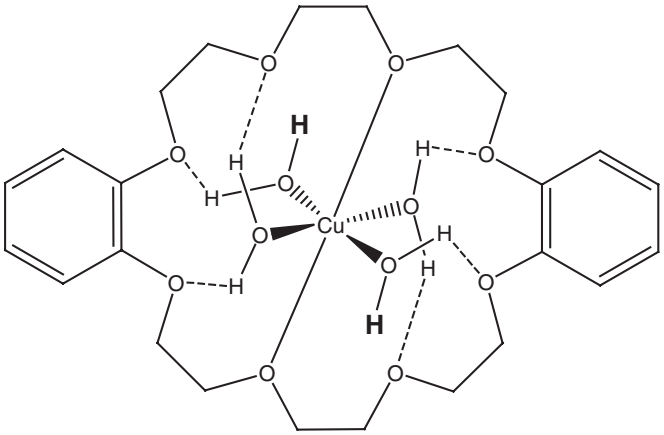

FIG. 21. Schematic representation of the copper coordination sphere and hydrogen bonding motifs in $[Cu^{II}(H_2O)_4$(dibenzo-24-crown-8] $[Mo_6O_{19}]$ (*240*). The hydrogen atoms emphasized with large, bold font hydrogen bond to bridging oxygen atoms of neighboring hexamolybdate ions. Reproduced with permission from Ref. (*240*). Copyright 2005 American Chemical Society.

molecules serve to link the crown complexes and polyoxoanions into 2D sandwich-like chains (Fig. 22).

While less common, strong, specific interactions between crown ether complexes and polyoxoanions are also possible. An illustrative example is a compound prepared from the Keggin anion, $[PMo_{12}O_{40}]^{3-}$, and sodium dibenzo-18-crown-6: $[\{Na(\text{dibenzo-18-crown-6})(MeCN)\}_3\{PMo_{12}O_{40}\}]$ (*242*). This material is prepared using a unique solid-state method. Dibenzo-18-crown-6, sodium chloride, and phosphomolybdic acid tetracosahydrate ($H_3 \cdot PMo_{12}O_{40} \cdot 24H_2O$) were ground for 30 min in an agate mortar, combined with a small volume of acetonitrile and then sonicated for five days. Orange crystals of the product formed in the suspended mixture and were manually separated from the other solids. While this method seems impracticable for isolating gram quantities of pure material, it is in another sense quite remarkable. It suggests the possibility of forming crystalline macrocycle/POM "complexes" even when the components do not share a common solvent. Keggin ions are composed of three Mo_3O_{12} triplets organized about a single PO_4^{3-} tetrahedron. In the product, $[\{Na(\text{dibenzo-18-crown-6})(MeCN)\}_3\{PMo_{12}O_{40}\}]$, the three terminal oxygen atoms of a single Mo_3O_{12} triplet are each coordinated to the sodium atom of a $[Na(\text{dibenzo-18-crown-6})(MeCN)]^+$ unit (Fig. 23). The authors attribute this arrangement both to coordinative bonding between the polyoxoanion and the sodium ions and to van der Waals attractions between the crown ether units.

Systems based on polyoxometalates and crown ethers have been used to selectively precipitate (*243–245*), extract (*246–251*), and detect (electrochemically) (*252–254*) a variety of metal ions. While

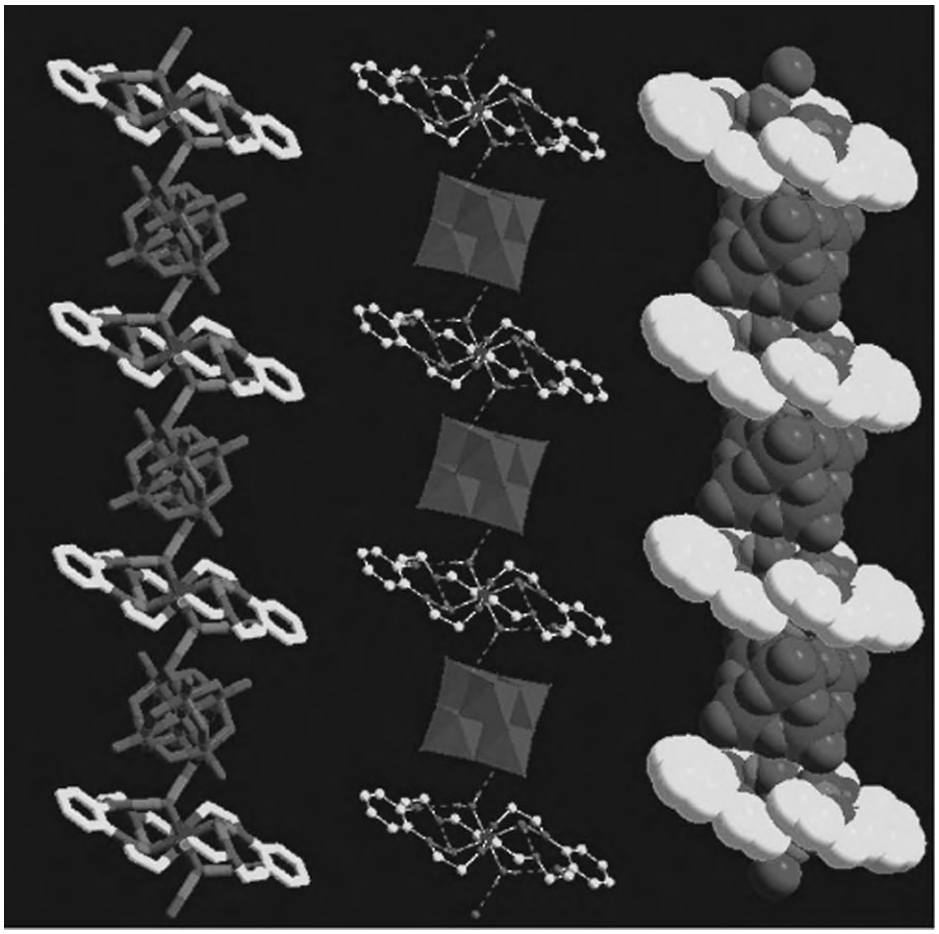

FIG. 22. Hydrogen bonded chains of crown ether coordination complexes and polyoxoanions in the solid state structure of $[Cu^{II}(H_2O)_4$(dibenzo-24-crown-8$][Mo_6O_{19}]$. Reproduced with permission from Ref. (*240*). Copyright 2005 American Chemical Society.

host–guest interactions have not been explicitly investigated in the majority of these systems, these studies have potential applications in nuclear waste and heavy metals remediation and thus provide motivation for further investigation of macrocycle-POM interactions. In a more recent study (*255*), a tripodal tris(benzo-18-crown[6]) receptor, 1,3,5-Tris-[*N*′-(4′-benzo-18-crown[6])-2-propynyl)-4,4′-trimethylenedipiperidino-N-(2-propyn-3-yl)]benzene, Fig. 24, was used to kinetically precipitate nanoscopic molybdate aggregates from aqueous solution (K^+ present) for TEM (transmission electron microscopy) analysis. In this case, the anionic particles were large and understood to have multiple tripodal crown molecules adhering to their surfaces.

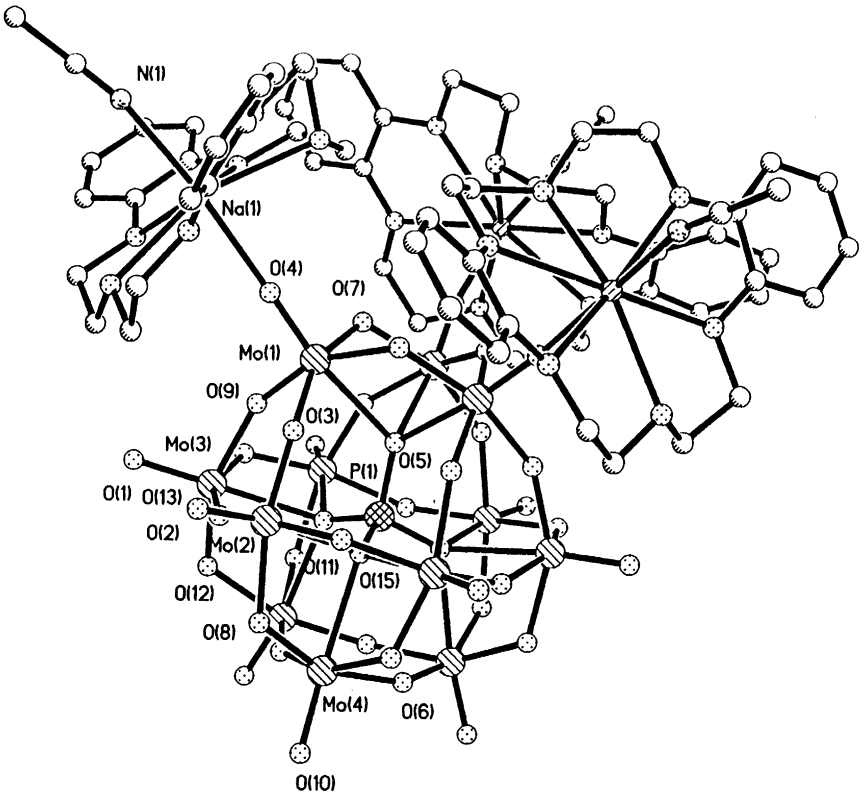

FIG. 23. Crystal structure of [{Na(dibenzo-18-crown-6)(MeCN)}$_3${P-$Mo_{12}O_{40}$}] (*242*). The three [Na(dibenzo-18-crown-6)(MeCN)]$^+$ units are bound to the terminal oxygen atoms of a single Mo_3O_{12} triplet. Reproduced with permission from Ref. (*242*). Copyright 2001 American Chemical Society.

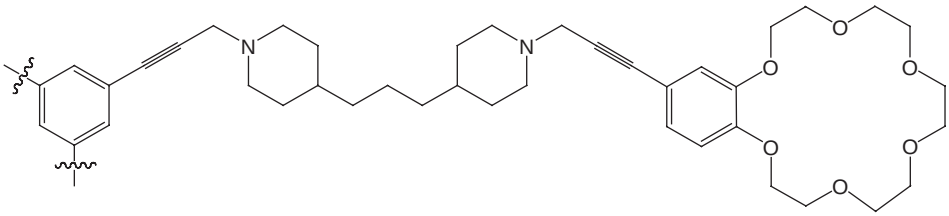

FIG. 24. Tripodal crown-ether receptor used to kinetically precipitate nanoscopic polymolybdate aggregates.

B. INTERACTIONS BETWEEN POLYOXOANIONS AND AZAMACROCYCLES

While crown ethers can clearly be crafted into complex POM receptors, there are inherent limitations to this approach. First, crown ethers typically bind monovalent cations, limiting the positive

charge to macrocycle ratio at one to one. Second, the ethereal oxygens have no possibility for protonation or further functionalization. Both of these limitations are removed when aza macrocycles are used in place of crown ethers, and the literature is replete with examples of multiply charged and/or N-substitued aza-macrocycles (*14,25,256–259*) as anion receptors. The relative absence of studies concerning polyoxometalates and non-conjugated aza-macrocyclic receptors (*260–262*), has prompted the recent preparation of salts composed of diprotonated or nickelated cyclam cations and the tungstosilicate anion: $[H_2Cyclam]_2$ $[\alpha\text{-}SiW_{12}O_{40}]$ and $[Ni(Cyclam)]_2$ $[\alpha\text{-}SiW_{12}O_{40}]$ (*263*). Efforts have also been directed toward the preparation of functionalized cyclam derivatives to be used in the preparation of aza-macrocyclic/POM materials (Fig. 25) (*264*).

To date, the most specific polyoxometalate receptors have been fashioned from highly conjugated, nitrogen containing receptors (*228,229,232*). The first of these was reported several years ago and involves recognition of two different Keggin polyoxoanions, $PW_{12}O_{40}^{3-}$ and $SiW_{12}O_{40}^{4-}$, by a cyclic porphyrin trimer (*228*), (Fig. 26). In this elegant example, the host cavity was calculated to have an interior diameter of approximately 13 Å, just slightly larger than the diameters of its anionic guests (e. g., 12.7 Å for $PW_{12}O_{40}^{3-}$). Host–guest interactions appear to be quite specific in this case, as the host–guest adducts have been observed by positive ion FAB mass spectrometry. By contrast, no adduct formation was observed in the mass spectrum of the same polyoxoanions with protonated porphyrin monomer (*228*) or

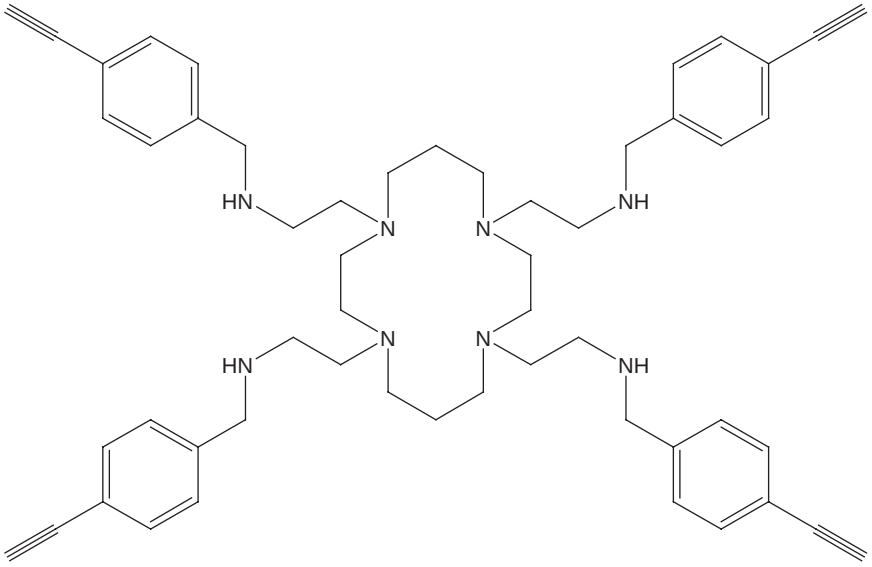

FIG. 25. Tetraalkynylsubstituted cyclam macrocycle as a potential POM receptor.

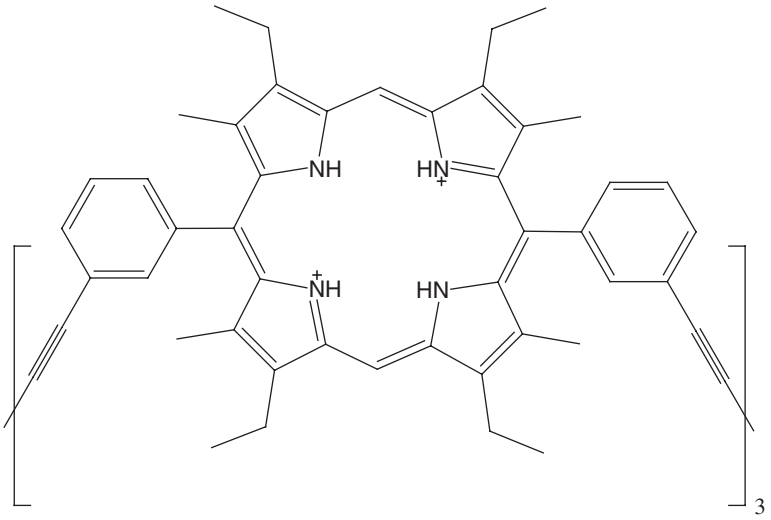

FIG. 26. Cyclic porphyrin trimer that binds the Keggin polyoxoanions, $PW_{12}O_{40}^{3-}$ and $SiW_{12}O_{40}^{4-}$. Adducts with both polyoxoanions were observed using positive ion FAB mass spectroscopy. No adducts were observed in the mass spectrum when $PW_{12}O_{40}^{3-}$ and $SiW_{12}O_{40}^{4-}$ were combined with the porphyrin monomer (*228*).

the FAB mass spectrum of $PW_{12}O_{40}^{3-}$ with $[(H_3O)$(dibenzo-18-crown-6)$]^+$ (*239*). More recently a polyoxoanion receptor with two guest sites has been prepared from $[Cu(MeCN)_4]_3PM_{12}O_{40}$ and 4,7-phenanthroline. The copper(I) ions and phenanthroline ligands self-assemble to form a hexanuclear host with two "bowls" ideally suited (size and charge complementarity) to accommodate $PM_{12}O_{40}^{3-}$ guests (Fig. 27). Moving beyond discrete macrocycles, into the realm of coordination polymer hosts and polyoxoanion guests, the examples rapidly become too complex and too numerous for discussion here. Fortunately, some of these materials have recently been reviewed (*232*).

V. Summary

Macrocycles and metallomacrocycles have been used in the design of high-affinity, selective receptors for a variety of substrates. Small molecule guest ligands can be bound to the metallomacrocyclic host through sigma-donor and pi-acceptor interactions. Furthermore, the macrocycle itself can adopt cleft-like conformations suitable for 3D encapsulation of substrates. Additional receptor groups can be readily appended to the macrocyclic complexes, in order to accomplish more complex multi-point guest recognition. The flexibility of the metallomacrocyclic receptors can be varied, so that either highly selective rigid hosts, or more versatile, flexible hosts can be obtained, as needed.

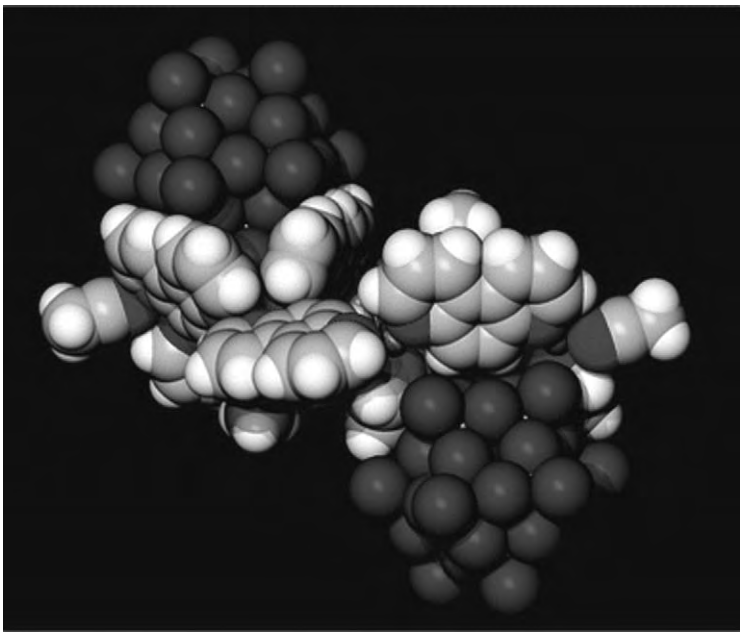

FIG. 27. Polyoxoanion receptor with two $PMo_{12}O_{40}^{3-}$ guests (*229*). Reproduced by permission of The Royal Society of Chemistry.

Relatively flexible macrocycles with appended receptor sites can display pronounced shape selectivity in the molecular recognition of cationic or anionic guests. Combining metal ion reactivity with the recognition properties of metallomacrocycles appears to be very promising for the development of new switchable receptors, as well as new, selective reagents and catalysts.

The field of molecular recognition using metallomacrocycles started out with small molecule binding within well-defined cavities. Later, the versatility of macrocyclic scaffolds provided numerous possibilities for cavity expansion. Advances in the design and preparation of polyfunctional macrocyclic platforms, which often contained deep cavities and/or several appended functional groups, resulted in an impressive array of supramolecular hosts for medium-sized guests. Examples included successful recognition of di- and polyamines, di- and polycarboxylates, and important biomolecules (such as neurotransmitters). Simultaneous binding of a small molecule (O_2) and medium-sized organic molecules within the same polymacrocyclic cavity was also accomplished, opening the way toward low-molecular-weight models of enzyme active sites. Due to the ability of the metal centers to act as spectrophotometric, fluorescent, or redox reporters of binding events, these selective molecular hosts can be applied in sensor design. Molecular recognition using functionalized metallomacrocyclic hosts has also been employed in the design of molecular

machines. Finally, macrocyclic compounds were recently shown to be effective in recognizing large guests, such as polyoxoanions, fullerenes, and carbon nanotubes. Hosts composed of several macrocyclic rings are often required for binding of these nanoscale objects. Alternatively, long tendrils extending from a monomacrocyclic scaffold may, through electrostatic, hydrogen bonding or π–π interactions, effectively "chelate" neutral or anionic guests. Just as the classic principles of coordination chemistry have recently been extended to the recognition of small anions (*26*), chemists are gradually developing a system and language for recognizing these even larger species.

Acknowledgments

We are grateful to our colleagues, past and present, who have contributed to our work on macrocyclic receptors. We would especially like to thank Professor Daryle Busch—both for his groundbreaking contributions to the field of molecular recognition and for fostering a spirit of inquiry and collegiality that has nurtured and sustained our careers. Research in the authors' laboratories is supported by the NSF (CHE0111202), a Tufts University Faculty Research Awards Committee grant (ERA), and an Illinois Wesleyan University Artistic and Scholarly Development grant (RR).

References

1. Hartley, J. H.; James, T. D.; Ward, C. J. *J. Chem. Soc. Perkin Trans.* **2000**, *1*, 3155–3184.
2. Perry, J. J. B.; Kilburn, J. D. *Contemp. Org. Synth.* **1997**, *4*, 61.
3. Canary, J. W.; Gibb, B. C. *Prog. Inorg. Chem.* **1997**, *45*, 1–82.
4. Busch, D. H. *Chem. Rev.* **1993**, *93*, 847–860.
5. Rybak-Akimova, E. V. *Rev. Inorg. Chem.* **2001**, *21*, 207–298.
6. Kersting, B. *Anorg. Allg. Chem.* **2004**, *630*, 765–780.
7. Fabbrizzi, L.; Poggi, A. (Eds.) "Transition Metals in Supramolecular Chemistry". Kluwer Academic Publishers: Dordrecht, **1994**.
8. Aoki, S.; Kimura, E. *Chem. Rev.* **2004**, *104*, 769–787.
9. Bianchi, A.; Bowman-James, K.; Garcia-Espana, E. (Eds.) "Supramolecular Chemistry of Anions". Wiley-VCH: New York, **1997**.
10. Gale, P. A. *Coord. Chem. Rev.* **2000**, *199*, 181–233.
11. Snowden, T. S.; Anslyn, E. V. *Curr. Opin. Chem. Biol.* **1999**, *3*, 740–746.
12. Beer, P. D. *Top. Curr. Chem.* **2005**, *255*, 125–162.
13. Beer, P. D.; Gale, P. A. *Angew. Chem. Int. Ed.* **2001**, *40*, 486–516.
14. Schmidtchen, F. P.; Berger, M. *Chem. Rev.* **1997**, *97*, 1609–1646.
15. Robertson, A.; Shinkai, S. *Coord. Chem. Rev.* **2000**, *205*, 157–199.
16. Fabbrizzi, L. *Coord. Chem. Rev.* **2000**, *205*, 85–108.
17. Rogers, C. W.; Wolf, M. O. *Coord. Chem. Rev.* **2002**, *233*, 341–350.
18. Beer, P. D.; Hayes, E. J. *Coord. Chem. Rev.* **2003**, *240*, 167–189.
19. Boiocchi, M.; Bonizzoni, M.; Fabbrizzi, L.; Piovani, G.; Taglietti, A. *Angew. Chem., Int. Ed.* **2004**, *43*, 3847–3852.
20. Fabbrizzi, L.; Licchelli, M.; Taglietti, A. *Dalton Trans.* **2003** 3471–3479.
21. Martinez-Manez, R.; Sancenon, F. *Chem. Rev.* **2003**, *103*, 4419–4476.

22. Amendola, V.; Fabbrizzi, L.; Mangano, C.; Pallavicini, P.; Poggi, A.; Taglietti, A. *Coord. Chem. Rev.* **2001** 219–221.
23. Lindoy, L. F. *"The Chemistry of Macrocyclic Ligand Complexes"*; Cambridge University Press: New York, **1989**.
24. Dietrich, B.; Hosseini, M. W.; Lehn, J.-M.; Sessions, R. B. *J. Am. Chem. Soc.* **1981**, *103*, 1282–1283.
25. Llinares, J. M.; Powell, D.; Bowman-James, K. *Coord. Chem. Rev.* **2003**, *240*, 57–75.
26. Bowman-James, K. *Acc. Chem. Res.* **2005**, *38*, 671–678.
27. Lehn, J.-M. *"Supramolecular Chemistry: Concepts and Perspectives"*; VCH: Weinheim, **1995**.
28. Meade, T. J.; Takeuchi, K. J.; Busch, D. H. *J. Am. Chem. Soc.* **1987**, *109*, 725–728.
29. Busch, D. H.; Stephenson, N. A. *J. Inclusion Phenom. Mol. Recog. Chem.* **1989**, *7*, 137–153.
30. Hardie, M. J.; Raston, C. L. *J. Chem. Soc., Chem. Comm.* **1999** 1153.
31. Hardie, M. J.; Nichols, P. J.; Raston, C. L. *Adv. Supramol. Chem.* **2002**, *8*, 1–41.
32. Dudic, M.; Lhotak, P.; Stibor, I.; Petrickova, H.; Lang, K. *New J. Chem.* **2004**, *28*, 85–90.
33. Perret, F.; Nishihara, M.; Takeuchi, T.; Futaki, S.; Lazar, A. N.; Coleman, A. W.; Sakai, N.; Matile, S. *J. Am. Chem. Soc.* **2005**, *127*, 1114–1115.
34. Haino, T.; Matsumoto, Y.; Fukazawa, Y. *J. Am. Chem. Soc.* **2005**, *127*, 8936–8937.
35. Wang, M.-X.; Zhang, X.-H.; Zheng, Q.-Y. *Angew. Chem. Int. Ed.* **2004**, *43*, 838–842.
36. Haino, T.; Yanase, M.; Fukazawa, Y. *Tetrahedron Lett.* **2005**, *46*, 1411–1414.
37. Basiuk (Golovataya-Dzhymbeeva), E. V.; Basiuk, V. A.; Rybak-Akimova, E. V.; Acosta-Najarro, D.; Puente-Lee, I.; Saniger, J. M. 203rd Meeting of The Electrochemical Society (April 27–May 2, 2003) vol. 13: Fullerenes and Nanotubes: The Building Blocks of Next Generation Nanodevices, Paris, **2003**; pp. 375–382.
38. Busch, D. H.; Jackson, P. J.; Kojima, M.; Chmielewski, P.; Matsumoto, N.; Stevens, J. C.; Wu, W.; Nosco, D.; Herron, N.; Ye, N.; Warburton, P. R.; Masarwa, M.; Stephenson, N. A.; Christoph, G.; Alcock, N. W. *Inorg. Chem.* **1994**, *33*, 910–923.
39. Busch, D. H.; Zimmer, L. L.; Grzybowski, J. J.; Olszanski, D. J.; Jackels, S. C.; Callahan, R. C.; Christoph, G. G. *Proc. Natl. Acad. Sci. USA* **1981**, *78*, 5919.
40. Busch, D. H.; Alcock, N. W. *Chem. Rev.* **1994**, *94*, 585–623.
41. Meade, T. J.; Alcock, N. W.; Busch, D. H. *Inorg. Chem.* **1990**, *29*, 3766–3776.
42. Cameron, J. H.; Nicol, D. P. Rosair, G. M. *Chem. Commun.* **1998** 1595–1596.
43. Chen, J.; Ye, N.; Alcock, N. W.; Busch, D. H. *Inorg. Chem.* **1993**, *32*, 904–910.
44. Alcock, N. W.; Lin, W. K.; Jircitano, A.; Mokren, J. D.; R Corfield, P. W.; Johnson, G.; Novotnak, G.; Cairns, C.; Busch, D. H. *Inorg. Chem.* **1987**, *26*, 440–452.
45. Herron, N.; Zimmer, L. L.; Grzybowski, J. J.; Olszanski, D. J.; Jackels, S. C.; Callahan, R. W.; Cameron, J. H.; Christoph, G. G.; Busch, D. H. *J. Am. Chem. Soc.* **1983**, *105*, 6585.
46.. Dickerson, L. D.; Sauer-Masarwa, A.; Herron, N.; Fendrick, C. M.; Busch, D. H. *J. Am. Chem. Soc.* **1993**, *115*, 3623–3626.
47. Buchalova, M.; Warburton, P. A.; van Eldik, R.; Busch, D. H. *J. Am. Chem. Soc.* **1997**, *119*, 5867–5876.
48. Rybak-Akimova, E. V.; Kuczera, K. *Inorg. Chem.* **2000**, *39*, 2462.
49. Deng, Y.; Busch, D. H. *Inorg. Chem.* **1995**, *34*, 6380–6386.
50. Deng, Y. Ph.D. thesis, Ohio State University, **1991**.
51. Chavan, M. Y.; Meade, T. J.; Busch, D. H.; Kuwana, T. *Inorg. Chem.* **1986**, *25*, 314.
52. Rybak-Akimova, E. V.; Kuczera, K.; Jas, G. S.; Deng, Y.; Busch, D. H. *Inorg. Chem.* **1999**, *38*, 3423.

53. Rybak-Akimova, E. V.; Marek, K.; Masarwa, M.; Busch, D. H. *Inorg. Chim. Acta* **1998**, *270*, 151–161.
54. Kolchinski, A. G.; Korybut-Daszkiewicz, B.; Rybak-Akimova, E. V.; Busch, D. H.; Alcock, N. W.; Clase, H. J. *J. Am. Chem. Soc.* **1997**, *119*, 4160–4171.
55. Buchalova, M. Ph.D. thesis, University of Kansas, **1997**.
56. Kryatov, S. V.; Rybak-Akimova, E. V.; Schindler, S. *Chem. Rev.* **2005**, *105*, 2175–2226.
57. Buchalova, M.; Busch, D. H.; van Eldik, R. *Inorg. Chem.* **1998** 1116–1120.
58. Gibson, Q. H.; Smith, M. H. *Proc. R. Soc.* **1965**, *163*, 206.
59. Collman, J. P.; Herrmann, P. C.; Fu, L.; Eberspacher, T. A.; Eubanks, M.; Boitrel, B.; Hayoz, P.; Zhang, X.; Brauman, J. I.; Day, V. W. *J. Am. Chem. Soc.* **1997**, *119*, 3481.
60. Rybak-Akimova, E. V.; Kuczera, K. *Unpublished results*.
61. Busch, D. H.; Stephenson, N. A. In: "*Inclusion Compounds*"; vol. 5; Eds. Atwood, J. L.; Davies, J. E. D.; MacNicol, D. D.; Oxford University Press: Oxford, **1991**.
62. Takeuchi, K. J.; Busch, D. H.; Alcock, N. W. *J. Am. Chem. Soc.* **1983**, *105*, 4261–4270.
63. Kwik, W.-L.; Herron, N.; Takeuchi, K. J.; Busch, D. H. *J. Chem. Soc., Chem. Comm.* **1983** 409–411.
64. Meade, T. J.; Kwik, W.-L.; Herron, N.; Alcock, N. W.; Busch, D. H. *J. Am. Chem. Soc.* **1986**, *108*, 1954–1962.
65. Hoshino, N.; Goldsby, K. A.; Busch, D. H. *Inorg. Chem.* **1986**, *25*, 3000–3006.
66. Hoshino, N.; Jircitano, A.; Busch, D. H. *Inorg. Chem.* **1988**, *27*, 2292–2300.
67. Bilewicz, R.; Wiekowska, A.; Korybut-Daszkiewicz, B.; Olszewska, A.; Feeder, N.; Wozniak, K. *J. Phys. Chem. B.* **2000**, *104*, 11430–11434.
68. Korybut-Daszkiewicz, B.; Wiekowska, A.; Bilewicz, R.; Domagala, S.; Wozniak, K. *J. Am. Chem. Soc.* **2001**, *123*, 9356–9366.
69. Wiekowska, A.; Bilewicz, R.; Domagala, S.; Wozniak, K.; Korybut-Daszkiewicz, B.; Tomkiewicz, A.; Mrozinski, J. *Inorg. Chem.* **2003**, *42*, 5513–5522.
70. Bilewicz, R.; Korybut-Daszkiewicz, B.; Rogowska, A.; Szydlowska, J.; Wiekowska, A.; Domagala, S.; Wozniak, K. *Electroanalysis* **2005**, *17*, 1463–1470.
71. Lamarque, L.; Miranda, C.; Navarro, P.; Escarti, F.; Garcia-Espana, E.; Latorre, J.; Ramirez, J. A. *Chem. Commun.* **2000** 1337–1338.
72. Skinner, P. J.; Beeby, A.; Dickins, R. S.; Parker, D.; Aime, S.; Botta, M. *J. Chem. Soc. Perkin Trans.* **2000**, *2*, 1329.
73. Rudzinski, C. M.; Hartmann, W. K.; Nocera, D. G. *J. Phys. Chem. A* **1998**, *102*, 7442.
74. Rudzinski, C. M.; Hartmann, W. K.; Nocera, D. G. *Coord. Chem. Rev.* **1998**, *171*, 115.
75. Pikramenou, Z.; Nocera, D. G. *Inorg. Chem.* **1992**, *31*, 532.
76.. Pikramenou, Z.; Yu, J.; Lessard, R. B.; Ponce, A.; Wong, P. A.; Nocera, D. G. *Coord. Chem. Rev.* **1994**, *132*, 181.
77. Mortellaro, M. A.; Nocera, D. G. *J. Am. Chem. Soc.* **1996**, *118*, 7414.
78. Breslow, R.; Yang, J.; Yan, J. M. *Tetrahedron* **2002**, *58*, 653–659.
79. Breslow, R.; Dong, S. D. *Chem. Rev.* **1998**, *98*, 1997–2011.
80. Breslow, R.; Gabriele, B.; Yang, J. *Tetrahedron Lett.* **1998**, *39*, 2887–2890.
81. Breslow, R. *Acc. Chem. Res.* **1995**, *28*, 146–153.
82. Belvedere, S.; Breslow, R. *Bioorg. Chem.* **2001**, *29*, 321–331.
83. Yang, J.; Breslow, R. *Tetrahedron Lett.* **2000**, *41*, 8063–8067.
84. Yang, J.; Weinberg, R.; Breslow, R. *Chem. Commun.* **2000** 531–532.
85. French, R. R.; Holzer, P.; Leuenberger, M. G.; Woggon, W.-D. *Angew. Chem., Int. Ed.* **2000**, *39*, 1267–1269.
86. French, R. R.; Holzer, P.; Leuenberger, M.; Nold, M. C.; Woggon, W.-D. *J. Inorg. Biochem.* **2002**, *88*, 295–304.
87. Woggon, W.-D.; Wagenknecht, H.-A.; Claude, C. *J. Inorg. Biochem.* **2001**, *83*, 289–300.

88. Woggon, W. D. *Acc. Chem. Res.* **2005**, *38*, 127–136.
89. Klarner, F.-G.; Kahlert, B. *Acc. Chem. Res.* **2003**, *36*, 919–932.
90. Fokkens, M.; Schrader, T.; Klarner, F.-G. *J. Am. Chem. Soc.* **2005**, *127*, 14415–14421.
91. Zimmerman, S. C.; VanZyl, C. M.; Hamilton, G. S. *J. Am. Chem. Soc.* **1989**, *111*, 1373.
92. Zimmerman, S. C. *Top. Curr. Chem.* **1993**, *165*, 71.
93. Colquhoun, H. M.; Zhu, Z. *Angew. Chem., Int. Ed.* **2004**, *43*, 5040–5045.
94. Alcock, N. W.; Padolik, P. A.; Pike, G. A.; Kojima, M.; Cairns, C. J.; Busch, D. H. *Inorg. Chem.* **1990**, *29*, 2599–2607.
95. Rudolph, M.; Dautz, S.; Jager, E. G. *J. Am. Chem. Soc.* **2000**, *122*, 10821–10830.
96. Du, G.; Ellern, A.; Woo, K. L. *Inorg. Chem.* **2003**, *42*, 873–877.
97. Cameron, J. H.; Clarke, C. A.; Harvey, H. B.; McCullough, K. J.; Rudolpf, P. A. *J. Chem. Soc., Dalton Trans.* **1996**, 1513–1518.
98. Kryatova, O. P.; Kolchinskii, A. G.; Rybak-Akimova, E. V. *J. Inclusion Phenom. Macrocycl. Chem.* **2002**, *42*, 251–260.
99. Taraszewska, J.; Zieba, K.; Korybut-Daszkiewicz, B. *Electrochim. Acta* **2004**, *49*, 2675–2681.
100. Disch, J. S.; Staples, R. J.; Concolino, T. E.; Haas, T. E.; Rybak-Akimova, E. V. *Inorg. Chem.* **2003**, *42*, 6749–6763.
101. Disch, J. S.; Rybak-Akimova, E. V. Manuscript in preparation.
102. Kryatova, O. P.; Kolchinski, A. G.; Rybak-Akimova, E. V. *Tetrahedron* **2003**, *59*, 231–239.
103. Izatt, R. M.; Pawlak, K.; Bradshaw, J. S.; Bruening, R. L. *Chem. Rev.* **1991**, *91*, 1721–2085.
104. Goodman, M. S.; Jubian, V.; Linton, B.; Hamilton, A. D. *J. Am. Chem. Soc.* **1995**, *117*, 11610–11611.
105. Tsubaki, K.; Tanaka, H.; Furuta, T.; Kinoshita, T.; Fuji, K. *Tetrahedron Lett* **2000**, *41*, 6089–6093.
106. Tsubaki, K.; Nuruzzaman, M.; Kusumoto, T.; Hayashi, N.; Wang, B.-G.; Fuji, K. *Org. Lett.* **2001**, *3*, 4071–4073.
107. Fuji, K.; Tsubaki, K.; Tanaka, K.; Hayashi, N.; Otsubo, T.; Kinoshita, T. *J. Am. Chem. Soc.* **1999**, *121*, 3807–3808.
108. Prevot-Halter, I.; Weiss, J. *New J. Chem.* **1998**, 869–874.
109. Jeong, K.; Park, J. W.; Cho, Y. L. *Tetrahedron Lett.* **1996**, *37*, 2795–2798.
110. Gunter, M. J.; Johnston, M. R. *Tetrahedron Lett.* **1992**, *33*, 1771–1774.
111. Fages, F.; Desvergne, J. P.; Kampke, K.; Bouas-Laurent, H.; Lehn, J. M.; Meyer, M.; Albrecht-Gary, A. M. *J. Am. Chem. Soc.* **1993**, *115*, 3658–3664.
112. Smeets, J. W. H.; Sijbesma, R. P.; Van Dalen, L.; Spek, A. L.; Smeets, W. J. J.; Nolte, R. J. M. *J. Org. Chem.* **1989**, *54*, 3710–3717.
113. Hamilton, A.; Lehn, J. M.; Sessler, J. L. *J. Am. Chem. Soc.* **1986**, *108*, 5158–5167.
114. Jones, N. F.; Kumar, A.; Sutherland, I. O. *J. Chem. Soc. Chem. Commun.* **1981**, 990–992.
115. Mageswaran, R.; Mageswaran, S.; Sutherland, I. O. *J. Chem. Soc. Chem. Commun.* **1979**, 722–724.
116. Johnson, M. R.; Sutherland, I. O.; Newton, R. F. *J. Chem. Soc. Chem. Commun.* **1979**, 306–308.
117. Johnson, M. R.; Sutherland, I. O.; Newton, R. F. *J. Chem. Soc. Chem. Commun.* **1979**, 309–311.
118. Korybut-Daszkiewicz, B.; Taraszewska, J.; Zieba, K.; Makal, A.; Wozniak, K. *Eur. J. Inorg. Chem.* **2004**, 3335–3344.
119. Kryatova, O. P.; Kryatov, S. V.; Staples, R. J.; Rybak-Akimova, E. V. *Chem. Commun.* **2002**, 3014–3015.
120. Kryatova, O. P.; Korendovych, I. V.; Rybak-Akimova, E. V. *Tetrahedron Lett.* **2003**, *44*, 4251–4255.

121. Kryatova, O. P.; Korendovych, I. V.; Rybak-Akimova, E. V. *Tetrahedron* **2004**, *60*, 4579–4588.
122. Cameron, J. H.; Clarke, C. A.; Rosair, G.; Scott, E. L. *Coord. Chem. Rev.* **1998**, *174*, 313–326.
123. Cameron, J. H.; Graham, S. *J. Chem. Soc., Dalton Trans.* **1989**, 1599–1608.
124. Strakhova, N. N.; Solov'ev, V. P.; Raevskii, O. A. *Koord. Khim.* **1989**, *15*, 483–485.
125. Izatt, R. M.; Bradshaw, J. S.; Nielsen, S. A.; Lamb, J. D.; Christensen, J. J. *Chem. Rev.* **1985**, *85*, 271–339.
126. Izatt, R. M.; Wang, T.; Hathaway, J. K.; Zhang, X. X.; Curtis, J. C.; Bradshaw, J. S.; Zhu, C. Y.; Huszthy, P. *J. Inclusion Phenom. Mol. Recog. Chem.* **1994**, *17*, 157–175.
127. Lin, W.-K.; Alcock, N. W.; Busch, D. H. *J. Am. Chem. Soc.* **1991**, *113*, 7603–7608.
128. Metzger, A.; Gloe, K.; Stephan, H.; Schmidtchen, F. P. *J. Org. Chem.* **1996**, *61*, 2051–2055.
129. Buschmann, H.-J.; Mutihac, L.; Jansen, K. *J. Inclusion Phenom. Macr. Chem.* **2001**, *39*, 1–11.
130. Gokel, G. W.; Goli, D. M.; Minganti, C.; Echegoyen, L. *J. Am. Chem. Soc.* **1983**, *105*, 6786–6788.
131. Doxsee, K. M.; Francis, P. E. J.; Weakley, T. J. R. *Tetrahedron* **2000**, *56*, 6683–6691.
132. Johnson, B. F. G.; Judkins, C. M. G.; Matters, J. M.; Shephard, D. S.; Parsons, S. *Chem. Commun.* **2000**, 1549–1550.
133. Cram, D. J.; Trueblood, K. N. *Top. Curr. Chem.* **1981**, *98*, 43.
134. Trueblood, K. N.; Knobler, C. B.; Lawrence, D. S.; Stevens, R. V. *J. Am. Chem. Soc.* **1982**, *104*, 1355–1362.
135. Owen, J. D. *J. Chem. Soc. Perkin Trans.* **1983**, *2*, 407–415.
136. Rogers, R. D.; Kurihara, L. K.; Benning, M. M. *Inorg. Chem.* **1987**, *26*, 4346–4352.
137. Ma, S.-L.; Lu, C.-X.; Fan, Y.-P. *Jiegou Huaxue* **1996**, *15*, 454.
138. You, W.; Zhu, Z.; Wang, E.; Xu, L.; Hu, C. *J. Chem. Crystallogr.* **2000**, *30*, 577–581.
139. Akutagawa, T.; Hashimoto, A.; Nishihara, S.; Hasegawa, T.; Nakamura, T. *J. Phys. Chem. B* **2003**, *107*, 66–74.
140. Coles, S. J.; Hursthouse, M. B.; Kilic, A.; Ciftci, G. Y. *Acta Crystallogr.* **2002**, *E58*, o83.
141. Ozbey, S.; Kaynak, F. B.; Togrul, M.; Demirel, N.; Hosgoren, H. *Z. Kristallogr.* **2003**, *218*, 381–384.
142. Pouretedal, H. R.; Shamsipur, M. *J. Chem. Eng. Data* **1998**, *43*, 742–744.
143. Rogers, R. D.; A-H., B. *Inorg. Chim. Acta* **1996**, *250*, 105.
144. Lednev, I. K.; Hester, R. E.; Moore, J. N. *J. Chem. Soc. Faraday Trans.* **1997**, *93*, 1551–1558.
145. Izatt, R. M.; Terry, R. E.; Nelson, D. P.; Chan, Y.; Eatough, D. J.; Bradshaw, J. S.; Hansen, L. D.; Christensen, J. J. *J. Am. Chem. Soc.* **1976**, *98*, 7626–7630.
146. Buschmann, H.-J.; Schollmeyer, E.; Mutihac, L. *Supramol. Sci.* **1998**, *5*, 139–142.
147. Timko, J. M.; Moore, S. S.; Walba, D. M.; Hiberty, P. C.; Cram, D. J. *J. Am. Chem. Soc.* **1977**, *99*, 4207–4219.
148. Amabilino, D. B.; Stoddart, J. F. *Chem. Rev.* **1995**, *95*, 2725.
149. Ashton, P. R.; Baxter, I.; Cantrill, S. J.; Fyfe, M. C. T.; Glink, P. T.; Stoddart, J. F.; White, A. J. P.; Williams, D. J. *Angew. Chem. Int. Ed.* **1998**, *37*, 1294–1297.
150. Ashton, P. R.; Parsons, I. W.; Raymo, F. M.; Stoddart, J. F.; White, A. J. P.; Williams, D. J.; Wolf, R. *Angew. Chem., Int. Ed.* **1998**, *37*, 1913–1916.
151. Cantrill, S. J.; Youn, G. J.; Stoddart, J. F.; Williams, D. J. *J. Org. Chem.* **2001**, *66*, 6857–6872.

152. Haino, T.; Fujii, T.; Fukazawa, Y. *Tetrahedron Lett.* **2005**, *46*, 257–260.
153. Hof, F.; Craig, S. L.; Nuckolls, C.; Rebek, J. *Angew. Chem. Int. Ed.* **2002**, *41*, 1488.
154. Lindner, H. J.; Yuan, D.-Q.; Fujita, K.; Kubo, K.; Lichtenthaler, F. W. *Chem. Comm.* **2003**, 1730–1731.
155. Higham, L. T.; Kreher, U. P.; Mulder, R. J.; Strauss, C. R.; Scott, J. L. *Chem. Comm.* **2004**, 2264–2265.
156. Sessler, J. L.; Andrievsky, A.; Gale, P. A.; Lynch, V. *Angew. Chem. Int. Ed.* **1996**, *35*, 2782.
157. Chen, D.-R.; Hu, Q.-P.; Meng, Y.-D.; Fan, Y.-P. *Jiegou Huaxue* **1994**, *13*, 235.
158. Akutagawa, T.; Hasegawa, T.; Nakamura, T.; Inabe, T. *J. Am. Chem. Soc.* **2002**, *124*, 8903–8911.
159. Kay, J. F.; Morris, J. H.; Reed, D. *J. Chem. Soc. Dalton Trans.* **1980**, 1917–1920.
160. Gyori, B.; Emri, J.; Feher, I. *Organomet. Chem.* **1983**, *255*, 17–28.
161. Jacobsen, G. B.; Morris, J. H. *J. Chem. Soc. Dalton Trans.* **1984**, 415–421.
162. Meina, D. G.; Morris, J. H. *J. Chem. Soc. Dalton Trans.* **1986**, 2645–2650.
163. Zhang, X. X.; Bradshaw, J. S.; Izatt, R. M. *Chem. Rev.* **1997**, *97*, 3313–3361.
164. Cantrill, S. J.; Fulton, D. A.; Heiss, A. M.; Pease, A. R.; Stoddart, J. F.; White, A. J. P.; Williams, D. J. *Chem. Eur. J.* **2000**, *6*, 2274.
165. Ashton, P. R.; Chrystal, E. J. T.; Glink, P. T.; Menzer, S.; Schiavo, C.; Spencer, N.; Stoddart, J. F.; Tasker, P. A.; White, A. J. P.; Williams, D. J. *Chem. Eur. J.* **1996**, *2*, 709–728.
166. Dietrich, B.; Fyles, D. L.; Fyles, T. M.; Lehn, J.-M. *Helv. Chim. Acta* **1979**, *62*, 2763–2787.
167. Hosseini, M. W.; Lehn, J.-M. *J. Am. Chem. Soc.* **1982**, *104*, 3525–3527.
168. Kimura, E.; Sakonaka, A.; Yatsunami, T.; Kodama, M. *J. Am. Chem. Soc.* **1981**, *103*, 3041–3045.
169. Breslow, R.; Rajagopalan, R.; Schwarz, J. *J. Am. Chem. Soc.* **1981**, *103*, 2905–2907.
170. Schmidtchen, F. P. *Chem. Ber.* **1981**, *114*, 597–607.
171. Schmidtchen, F. P. *J. Am. Chem. Soc.* **1986**, *108*, 8249–8255.
172. Schmidtchen, F. P.; Gleich, A.; Schummer, A. *Pure Appl. Chem.* **1989**, *61*, 1535–1546.
173. Dietrich, B.; Guilhem, J.; Lehn, J.-M.; Pascard, C.; Sonveaux, E. *Helv. Chim. Acta* **1984**, *67*, 91–104.
174. Hosseini, M. W.; Lehn, J.-M. *Helv. Chim. Acta* **1988**, *71*, 749–756.
175. Lehn, J.-M.; Meric, R.; Vigneron, J.-P.; Bkouche-Waksman, I.; Pascard, C. *J. Chem. Soc. Chem. Commun.* **1991**, 62–64.
176. Teulade-Fichou, M.-P.; Vigneron, J.-P.; Lehn, J.-M. *J. Chem. Soc. Perk. T.* **1996**, *2*, 2169–2175.
177. Hinzen, B.; Seiler, P.; Diederich, F. *Helv. Chim. Acta* **1996**, *79*, 942–960.
178. Shinkai, S.; Yoshioka, A.; Nakayama, H.; Manabe, O. *J. Chem. Soc. Perkin. Trans.* **1990**, *2*, 1905–1909.
179. Martell, A. E.; Motekaitis, R. J. *J. Am. Chem. Soc.* **1988**, *110*, 8059–8064.
180. Jullian, V.; Shepherd, E.; Gelbrich, T.; Hursthouse, M. B.; Kilburn, J. D. *Tetrahedron Lett.* **2000**, *41*, 3963–3966.
181. Bazzicalupi, C.; Bencini, A.; Bianchi, A.; Fusi, V.; Garcia-Espana, E.; Giorgi, C.; Llinares, J. M.; Ramirez, J. A.; Valtancoli, B. *Inorg. Chem.* **1999**, *38*, 620–621.
182. Eblinger, F.; Schneider, H.-J. *Angew. Chem. Int. Ed. Engl.* **1998**, *37*, 826–829.
183. Hossain, M. A.; Schneider, H.-J. *Chem. Eur. J.* **1999**, *5*, 1284–1290.
184. Garcia-Tellado, F.; Goswami, S.; CHung, S.-K.; Geib, S. J.; Hamilton, A. D. *J. Am. Chem. Soc.* **1990**, *112*, 7393–7394.
185. Fan, E.; Van Arman, S. A.; Kincaid, S.; Hamilton, A. D. *J. Am. Chem. Soc.* **1993**, *115*, 369–370.
186. Yang, J.; Fan, E.; Geib, S. J.; Hamilton, A. D. *J. Am. Chem. Soc.* **1993**, *115*, 5314–5315.

187. Garcia-Tellado, F.; Geib, S. J.; Goswami, S.; Hamilton, A. D. *J. Am. Chem. Soc.* **1991**, *113*, 9265–9269.
188. Kimura, E.; Ikeda, T.; Shionoya, M.; Shiro, M. *Angew. Chem., Int. Ed. Engl.* **1995**, *34*, 663–664.
189. Schiessl, P.; Schmidtchen, F. P. *Tetrahedron Lett.* **1993**, *34*, 2449–2452.
190. Rebek, J. Jr.; Nemeth, D.; Ballester, P.; Lin, F.-T. *J. Am. Chem. Soc.* **1987**, *109*, 3474–3475.
191. Hamann, B. C.; Branda, N. R. Jr. *J. Rebek Tetrahedron Lett.* **1993**, *34*, 6837–6840.
192. Alcazar Montero, V.; Tomlinson, L.; Houk, K. N.; Diederich, F. *Tetrahedron Lett.* **1991**, *32*, 5309–5312.
193. Tanaka, Y.; Kato, Y.; Aoyama, Y. *J. Am. Chem. Soc.* **1990**, *112*, 2807–2808.
194. Seel, A.; Galan, A.; de Mendoza, J. *Top. Curr. Chem.* **1995**, *175*, 101–132.
195. Sebo, L.; Diederich, F.; Gramlich, V. *Helv. Chim. Acta* **2000**, *83*, 93–113.
196. Sebo, L.; Schweiger, B.; Diedrich, F. *Helv. Chim. Acta* **2000**, *83*, 80–92.
197. Goswami, S.; Ghosh, K. *Tetrahedron Lett.* **1997**, *38*, 4503–4506.
198. Goswami, S.; Ghosh, K.; Halder, M. *Tetrahedron Lett.* **1999**, *40*, 1735–1738.
199. Goswami, S.; Ghosh, K.; Dasgupta, S. *J. Org. Chem.* **2000**, *65*, 1907–1914.
200. Benito, H. M.; Gomez-Garcia, M.; Jimenez Blanco, J. L.; Mellet, C. O.; Garcia Fernandez, J. M. *J. Org. Chem.* **2001**, *66*, 1366–1372.
201. Ahn, D.-R.; Kim, T. W.; Hong, J. I. *Tetrahedron Lett.* **1999**, *40*, 6045–6048.
202. Carr, J. D.; Coles, S. J.; Hursthouse, M. B.; Light, M. E.; Tucker, J. H. R.; Westwood, J. *Angew. Chem., Int. Ed. Engl.* **2000**, *39*, 3296–3299.
203. Kral, V.; Andrievsky, A.; Sessler, J. L. *J. Am. Chem. Soc.* **1995**, *117*, 2953–2954.
204. Lavigne, J. J.; Anslyn, E. V. *Angew. Chem. Int. Ed. Engl.* **1999**, *38*, 3666–3669.
205. Sessler, J. L.; Andrievsky, A.; Kral, V.; Lynch, V. *J. Am. Chem. Soc.* **1997**, *119*, 9385–9392.
206. Fitzmaurice, R. J.; Kyne, G. M.; Douheret, D.; Kilburn, J. D. *J. Chem. Soc. Perk. T.* **2002**, *1*, 841–864.
207. Goodman, M. S.; Hamilton, A. D.; Weiss, J. *J. Am. Chem. Soc.* **1995**, *117*, 8447–8455.
208. Goodman, M. S.; Jubian, V.; Hamilton, A. D. *Tetrahedron Lett.* **1995**, *36*, 2551–2554.
209. Prevot-Halter, I.; Smith, T.; Weiss, J. *J. Org. Chem.* **1997**, *62*, 2186–2192.
210. Watanabe, S.; Higashi, N.; Kobayashi, M.; Hamanaka, K.; Takata, Y.; Yoshida, K. *Tetrahedron Lett.* **2000**, *41*, 4583–4586.
211. Motekaitis, R. J.; Martell, A. E. *Inorg. Chem.* **1991**, *30*, 694–700.
212. Llobet, A.; Reibenspies, J.; Martell, A. E. *Inorg. Chem.* **1994**, *33*, 5946–5951.
213. Lu, Q.; Reibenspies, J. J.; Martell, A. E.; Motekaitis, R. J. *Inorg. Chem.* **1996**, *35*, 2630–2636.
214. Lacy, S. M.; Rudkevich, D. M.; Verboom, W.; Reinhoudt, D. N. *J. Chem. Soc. Perkin Trans.* **1995**, *2*, 135–139.
215. Beer, P. D.; Drew, M. G. B.; Hazlewood, C.; Hesek, D.; Hodacova, J.; Stokes, S. E. *J. Chem. Soc., Chem. Commun.* **1993**, 229–231.
216. Beer, P. D.; Hesek, D.; Kingston, J. E.; Smith, D. K.; Stokes, S. E.; Drew, M. G. B. *Organometallics* **1995**, *14*, 3288–3295.
217. Jeong, K.-S.; Lee, J. W.; Park, T.-Y.; Chang, S.-Y. *Chem. Commun.* **1999**, 2069–2070.
218. Hosseini, M. W.; Lehn, J.-M. *Helv. Chim. Acta* **1986**, *69*, 587–603.
219. Cudic, P.; Vigneron, J.-P.; Lehn, J.-M.; Cesario, M.; Prange, T. *Eur. J. Org. Chem.* **1999**, 2479–2484.
220. Kimura, E.; Kuramoto, Y.; Koike, T.; Fujioka, H.; Kodama, M. *J. Org. Chem.* **1990**, *55*, 42–46.
221. Bencini, A.; Bianchi, A.; Burguete, M. I.; Garcia-Espana, E.; Luis, S. V.; Ramirez, J. A. *J. Am. Chem. Soc.* **1992**, *114*, 1919–1920.

222. Bencini, A.; Bianchi, A.; Burguete, M. I.; Dapporto, P.; Domenech, A.; Garcia-Espana, E.; Luis, S. V.; Paoli, P.; Ramirez, J. A. *J. Chem. Soc. Perkin Trans.* **1994**, *2*, 569–577.
223. Alfonso, I.; Rebolledo, F.; Gotor, V. *Chem. Eur. J.* **2000**, *6*, 3331–3338.
224. Martell, A. E.; Smith, R. M. *"Critical stability constants"*; Plenum Press: New York, **1974**.
225. Alcock, N. W.; Lin, W. K.; Cairns, C.; Pike, G. A.; Busch, D. H. *J. Am. Chem. Soc.* **1989**, *111*, 6630–6643.
226. Nazarenko, A. Y.; Robinson, P. D.; Wilson, R. M.; Kolchinski, A. G.; Disch, J. S.; Rybak-Akimova, E. V. *J. Inclusion Phenom. Macrocyclic Chem.* **2002**, *42*, 83–87.
227. Min, K. S.; Suh, M. P. *Eur. J. Inorg. Chem.* **2001**, 449–455.
228. Anderson, H. L.; Sanders, J. K. M. *J. Chem. Soc., Chem. Commun.* **1992**, 946947.
229. Inman, C.; Knaust, J. M.; Keller, S. W. *Chem. Commun.* **2004**, 492–493.
230. Ouahab, L.; Golhen, S.; Triki, S.; Pope, M. T.; Müller, A. (Eds.) Conducting and Magnetic Organic/inorganic materials based on polyoxometalates, In: *"Polyoxometalate Chemistry: from Topology via Self-assembly to Application"*; Kluwer: Dordrecht, **2001**, 205–229.
231. Borrás-Almenar, J. J.; Clemente-Juan, J. M.; Clemente-León, M.; Coronado, E.; Galán-Mascarós, J. R.; Gómez-García, C. J.; Pope, M. T., Müller, A. (Eds.) Molecular materials from polyoxometalates, In: "*Polyoxometalate Chemistry: from Topology via Self-assembly to Application*"; Kluwer: Dordrecht, **2001**, 231–253.
232. Hagrman, P. J.; Hagrman, D.; J., Z.; Pope, M. T., Müller, A. (Eds.) Perspectives on the Solid State Coordination Chemistry of the Molybdenum Oxides, In: "*Polyoxometalate Chemistry: from Topology via Self-assembly to Application*"; Kluwer: Dordrecht, **2001**, 269–300.
233. Kurth, D. G.; Volkmer, D.; Pope, M. T., Müller, A. (Eds.) Polyoxometalate clusters in a supramolecular self-organized environment: steps towards functional nanodevices and thin film applications, In: "*Polyoxometalate Chemistry: from Topology via Self-assembly to Application*"; Kluwer: Dordrecht, **2001**, 301–318.
234. Inman, C.; Knaust, J. M.; Keller, S. W. *J. Chem. Soc., Chem. Commun.* **2002**, 156–157.
235. Lee, I. S.; Long, J. R.; Prusiner, S. B.; Safar, J. G. *J. Am. Chem. Soc.* **2005**, *127*, 13802–13803.
236. Nagano, O.; Y., S. *Acta Crystallogr.* **1979**, *B35*, 2387–2389.
237. You, W. S.; Wang, E. B.; Zhang, H.; Xu, L.; Wang, Y. B. *J. Mol. Struct.* **2000**, *554*, 141–147.
238. You, W. S.; Wang, E. B.; He, Q. L.; Xu, L.; Xing, Y.; Jia, H. Q. *J. Mol. Struct.* **2000**, *524*, 133–139.
239. You, W. S.; Wang, E. B.; Xu, L.; Zhu, Z. M.; Gu, Y. P. *J. Mol. Struct.* **2002**, *605*, 41–49.
240. Shivaiah, V.; Das, S. K. *Inorg. Chem.* **2005**, *44*, 7313–7315.
241. Li, Y.; Hao, N.; Wang, E.; Yuan, M.; Hu, C.; Hu, N.; Jia, H. *Inorg. Chem.* **2003**, *42*, 2729–2735.
242. You, W.; Wang, E.; Xu, Y.; Li, Y.; Xu, L.; Hu, C. *Inorg. Chem.* **2001**, *40*, 5468–5471.
243. Rajec, P.; Mikulaj, V.; Husarcik, P.; Svec, V. *J. Radioanal. Nucl. Chem.* **1997**, *219*, 123–125.
244. Rajec, P.; Svec, V.; Mikulaj, V.; Hanzel, R. *J. Radioanal. Nucl. Chem.* **1998**, *229*, 9–12.
245. Mikulaj, V.; Svec, V. *J. Radioanal. Nucl. Chem.* **1994**, *183*, 127–133.
246. Zhu, L.; Zhongqun, L.; Wenjun, C.; Shaojin, C. *J. Radioanal. Nucl. Chem.* **1996**, *205*, 49–56.
247. Srivastava, S. K.; Gupta, V. K.; Dwivedi, M. K.; Jain, S. *Indian J. Chem., Sect. A* **1994**, *33A*, 1042–1045.

248. Nazarenko, A. Y.; Zaitsev, S. A.; Sukhan, V. V. *Izvestiya Vysshikh Uchebnykh Zavedenii, Khimiya i Khimicheskaya Tekhnologiya* **1993**, *36*, 38–42.
249. Shih, J. S.; Tsay, L. M.; Wu, S. C. *Analyst* **1985**, *110*, 1387–1390.
250. Blasius, E.; Nilles, K. H. *Radiochim. Acta* **1984**, *36*, 207–214.
251. Blasius, E.; Nilles, K. H. *Radiochim. Acta* **1984**, *35*, 173–182.
252. Sheen, S. R.; Shih, J. S. *Analyst* **1992**, *117*, 1691–1695.
253. Shih, J. S.; Wang, D. *Jiemian Kexue Huizhi* **1991**, *14*, 13–21.
254. Diaz, C.; Vidal, J. C.; Galban, J.; Urate, M. L.; Lanaja, J. *Microchemical Journal* **1989**, *39*, 289–297.
255. Zhu, Y.; Cammers-Goodwin, A.; Zhao, B.; Dozier, A.; Dicky, E. C. *Chem. Eur. J.* **2004**, *10*, 2421–2427.
256. Kimura, E. In:"*Biomimetic and Bioorganic Chemistry*",vol.128; Springer: Berlin, West Germany, **1985**.
257. Bernhardt, P. V.; Lawrence, G. A. *Coord. Chem. Rev.* **1990**, *104*, 297–343.
258. Wainwright, K. P. *Coord. Chem. Rev.* **1997**, *166*, 35–90.
259. Kaden, T. A. *Top. Curr. Chem.* **1984**, *121*, 157–179.
260. Lu, X.; Zhong, R.; Liu, S.; Liu, Y. *Polyhedron* **1997**, *16*, 3865–3872.
261. Lu, X.-M.; Jin, X.-L.; Pu, X.-H.; Liu, S.-C. *Jiegou Huaxue* **1997**, *16*, 1–5.
262. Wang, D.; Zhang, W.; Grüning, K.; Rehder, D. *J. Mol. Struct.* **2003**, *656*, 79–91.
263. Korendovych, I. V.; Rybak-Akimova, E. V.; Roesner, R. A. 228th ACS National Meeting, Philadelphia, PA, United States, **2004**.
264. Korendovych, I. V.; Rybak-Akimova, E. V.; Roesner, R. A. Manuscript in preparation.

SUPRAMOLECULAR CHEMISTRY OF ENVIRONMENTALLY RELEVANT ANIONS

BRUCE A. MOYER[a], LÆTITIA H. DELMAU[a], CHRISTOPHER J. FOWLER[a], ALEXANDRE RUAS[a], DEBRA A. BOSTICK[a], JONATHAN L. SESSLER[b], EVGENY KATAYEV[b], G. DAN PANTOS[b], JOSÉ M. LLINARES[c], MD. ALAMGIR HOSSAIN[c], SUNG O. KANG[c] and KRISTIN BOWMAN-JAMES[c]

[a]Chemical Sciences Division, Oak Ridge National Laboratory, BLDG 4500S, MS-6119, P.O. Box 2008, Oak Ridge, TN 37831, USA
[b]Department of Chemistry and Biochemistry, University of Texas, 1 University Station – A5300, Austin, TX 78712-0165, USA
[c]Department of Chemistry, University of Kansas, 1251 Wescoe Hall Drive, Lawrence, KS 66045, USA

I. Introduction

A. The Problem

Certain anions, especially oxoanions, have been prominent as contaminants (e.g., pertechnetate), troublesome species (e.g., sulfate, chromate, and phosphate), or ubiquitous matrix components (e.g., nitrate) that not only pose a threat to the environment, but which can interfere with waste treatment processes in the US Department of Energy

ADVANCES IN INORGANIC CHEMISTRY
VOLUME 59 ISSN 0898-8838 / DOI: 10.1016/S0898-8838(06)59005-1

complex. In the first phase of this project, we approached the topic of anion recognition and separation broadly, targeting such oxoanions as nitrate, sulfate, and phosphate. In the past several years, however, the presence of sulfate in legacy radioactive tank waste has risen to be a critical concern in meeting the objectives of Mission Acceleration at the Hanford Site in Washington state (*1*), where some 54 million gallons of Cold War era reprocessing waste must be treated. All of the waste is scheduled to be vitrified in borosilicate glass, either as high-level waste (HLW) that will be sequestered in an underground repository or low-activity waste (LAW) that will be stored at Hanford. Treatment processes entail separations that will direct most of the radionuclides, which constitute less than 0.01% of the mass of the waste, to the HLW glass, leaving the bulk of the waste to be disposed of as LAW glass. Because the vitrification processes are expensive, it would be advantageous if the volume of LAW glass could be minimized. However, the problem arises in that sulfate is present in sufficient quantity in the waste that its low solubility in the glass has proven to be a key determinant of the volume of LAW glass that will be produced (*2*).

The sulfate problem has been spelled out in detail in various needs statements pertaining to the Hanford Site, recognizing sulfate management in LAW via pretreatment, vitrification, and off-gas approaches as having important beneficial consequences. It has been estimated that as much as 20% more glass would have to be produced without sulfate mitigation (*3*). Such a penalty represents a serious obstacle to the Mission Acceleration initiative (*2*), which seeks to reduce the time to clean up the Hanford tanks by 20 years and to reduce the cost of the cleanup by $20 billion. Sulfate is, in fact, present in the tank wastes at several USDOE sites, including the Savannah River Site and the Idaho National Environmental and Engineering Laboratory (INEEL), as well as Hanford. It is a particularly acute issue at Hanford, because of the unique requirement there that specifies vitrification of LAW. Owing to its low solubility (typically $<1\%$) in borosilicate glasses, sulfate at elevated levels will migrate to the top of the melt as a separate phase (*4*), as documented in studies of nuclear-waste vitrification (*5–10*). Specific processing problems include inhibition of melting rate, short-circuiting of the electrodes, corrosion of the melter, electrodes, and off-gas equipment. In addition, the final glass product containing high sulfate levels can exhibit increased leach rates, a feature that makes such products less desirable for use in long-term waste storage.

In view of the above problems associated with sulfate in vitrification of the Hanford LAW, recent studies have with limited success been directed toward identifying technologies for removal of the sulfate prior to vitrification. Suggested strategies have included evaporative crystallization of burkeite ($Na_6(SO_4)_2CO_3$) (*11*), which in tests to date has not proved sufficiently selective (*12,13*). Precipitating agents, such as barium or strontium nitrate, can effect sulfate removal, although not without selectivity and secondary-waste issues (*12,14*). Ion exchange

has also been tried but, again, has proved ineffective (*12,15*). In spite of this lack of success, planning in the Mission Acceleration initiative has included provision for sulfate removal (*2*) to reduce the volume of immobilized LAW and corresponding costs. Since options for removing the sulfate from the highly alkaline waste have so far proven unattractive, the suggested approach (*2*) involves acidification of the salt waste and precipitation of strontium sulfate. With options so clearly limited, the need for basic research to provide new alternatives seems obvious. Such alternatives might avoid waste acidification, for example, or they might prove more efficient.

B. Research Path toward a Solution

Jointly, the groups of Moyer, Sessler, and Bowman-James have been exploring an extractive approach. From a generic technology standpoint, solvent extraction is attractive since it is a venerable technique in the nuclear-separations industry and represents a known, potentially viable high-throughput technique (*16–24*). Although most applications have involved nitric acid aqueous phases, treatment of alkaline nuclear waste by solvent extraction has recently been demonstrated (*25–27*) in the case of the Caustic-Side Solvent Extraction (CSSX) process (*28–32*) for cesium removal from the Savannah River Site tank waste. The CSSX process uses a calixarene-crown ether as the cesium extractant and has been selected (*33*) for implementation in the Savannah River Site Salt Waste Processing Facility, which as of this writing is in privatized conceptual design (*34*). Crown ethers have also found application in the SREX process for strontium separation from acidic nuclear waste (*35*). Thus, precedent exists for applications for both acid and alkaline media using designed ion receptors. That anion receptors will work for specific anion extraction applications in nuclear or hydrometallurgical applications seems an obvious expectation, but to our knowledge, no such precedent currently exists.

The design of systems for *selective* recognition of anions is not straightforward. Much of the literature dealing with this problem has been within the framework of sensing and analysis. Fortunately, the principles of ion transport that make possible such applications are the same principles we are interested in for performing a separation. For example, electrode selectivities for simple anions tend to follow the Hofmeister series, $ClO_4^- > IO_4^- > SCN^- > NO_3^- > I^- > Br^- > Cl^- > HCO_3^- = H_2PO_4^- > SO_4^{2-}$, a pattern that is based on the lipophilicity of the anions in question (at a maximum for ClO_4^-) (*36,37*). This is the same order as the ease of dehydration of anions (*38*). Consequently, this order is observed in chemical reactions in which dehydration is the dominant thermochemical term. Because water is a very efficient hydrogen-bond donor (HBD), this condition is often met. In particular, processes in which anions are transported into another phase, to a pseudo phase (e.g., micelle), or to an interface, are typically associated with Hofmeister-type

selectivity (*39*). Accordingly it has proved extremely difficult to overcome this natural selectivity. Further, anions as a class are generally characterized by charge densities that are lower than cations and a range of shapes and sizes that are far more complex than seen in the case of simple metal salts. As a result, the field defined as the "supramolecular" chemistry of anions, involving the selective targeting and recognition of anions via non-covalent means, has been slow in developing and has only really blossomed within the last decade. Basic principles, such as the influence of hydrogen bonding, conformational changes, electrostatic, and dipole forces, as well as topological complementarity, have been clearly identified and are appreciated as playing a major role in terms of allowing or influencing selective anion coordination. However, at present, the understanding of these factors is at best qualitative, and there thus exists a need to understand such phenomena at the molecular level. From the outset, a critical goal of this project has been to provide such an understanding. We have done so through the synthesis and study of nitrogen-based anion receptors for which the targeted, ultimate application is the selective extraction of sulfate from nitrate-rich aqueous media including that present in radioactive waste tanks.

In this chapter, we describe the evolution of anion-binding ligands from simple ammonium-based systems through mixed amide/amine and thioamide/amine receptors. Thus, the emphasis will largely be on synthetic design strategy carried out in the Bowman-James group. However, a recent class of mixed pyrrole-imine amide systems from the Sessler group is also described, as are some results involving the calixpyrroles, a novel class of anion receptors that show promise for sulfate binding. Special attention is drawn to receptors with high affinities for sulfate and the progress of sulfate-selective extraction experiments. In this regard, this chapter provides an update on progress in this project, where published results are reviewed and some new results are presented.

II. Structure and Binding

A. Strategy for Ligand Design

The design of ligands in the Bowman-James group has now passed through various phases starting with simple polyammonium macrocycles, and progressing through mixed polyamide/amine, polyamide/quaternized amine, and polythioamide/amine receptors. This progression reflects strategies (1) to increase the hydrogen-bonding capability of the receptor, i.e., a progression from amide to thioamide functionalities; (2) to add an electrostatic attractive component, i.e., synthesis of the mixed polyamide/quaternized amine systems; and (3) to explore the influence of receptor dimensionality, i.e., monocycles vs. bicycles. Schemes 1 and 2 illustrate the general road map for monocyclic and bicyclic receptors,

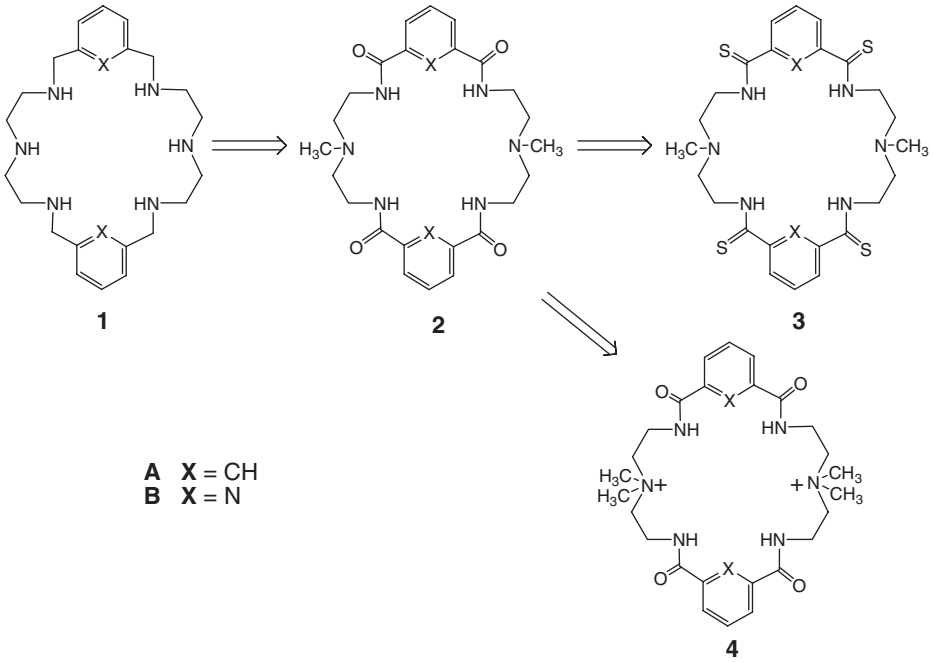

SCHEME 1. Two-dimensional monocycles.

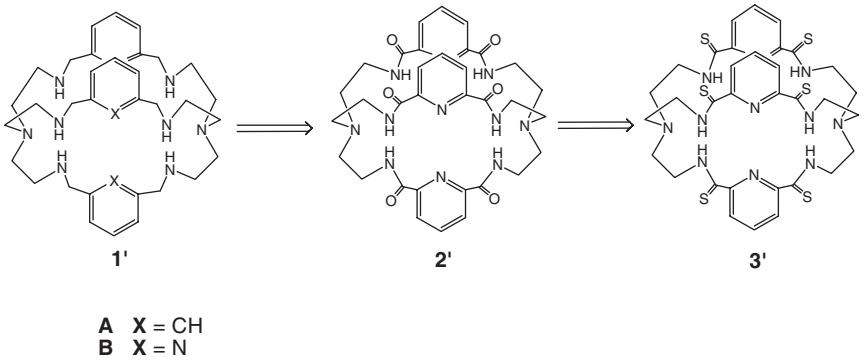

SCHEME 2. Three-dimensional bicyclic cryptands.

respectively. The strategy for ligand design in the Sessler group has focused on utilizing calixpyrrole frameworks containing multiple pyrrole functionalities for hydrogen bonding as shown later in Scheme 3. Ultimately, the merger of the two systems, the amides with the pyrroles, were envisioned as providing a more versatile receptor.

B. POLYAMMONIUM MACROCYCLES

Preliminary studies were performed on monocyclic and bicyclic polyammonium hosts derived from simple Schiff base condensations,

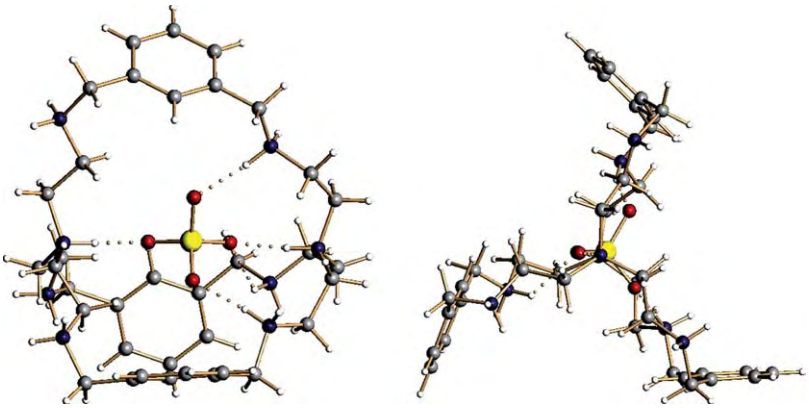

FIG. 1. Two perspective views of the sulfate inclusion complex of **1A**′ as determined by X-ray diffraction analysis.

followed by borohydride reduction to yield monocycles, **1** and bicycles, **1**′ (Schemes 1 and 2). These studies were done to lay the groundwork for understanding various structural aspects of selective recognition, as related to the design of topologically complementary systems. Binding studies for these receptors were performed in aqueous solutions, and binding was found to be maximimal at lower pHs, when the receptors are close to fully protonated (*40–48*). Dimensionality in the polyammonium receptors plays a major role on binding affinities in anion complexes (*40–49*). While monocyclic systems may bind multiply-valent anions with significant affinity, they do not have even measurable affinities in some cases for monoanions (*41,42,48*). Crystallographic results indicated that in general for the polyamine monocycles, alternating layers of anions and macrocyclic cations form throughout the crystal lattice, while encapsulation often occurred with the bicycles as seen for the sulfate complex of **1**′ derived from isophthalaldehyde (Fig. 1) (*41–49*). The nitrate complex of **1**′ was of special interest, since it showed the ditopic inclusion of two nitrates inside the cavity (Fig. 2) (*40,41*). In this bicycle, the trigonal arrangement of the receptor amines perfectly complements the D_{3h} symmetry of the nitrate, and allows for maximum utilization of hydrogen-bonding contacts.

C. Polyamide and Polythioamide Macromonocycles

For applications related to the remediation problem, polyamine systems have a number of drawbacks related to the fact that they are pH-sensitive, binding well usually at pHs lower than 7. They are also generally water soluble, a hindrance in liquid–liquid extraction applications when extractions are from water into another phase. Hence, structurally related polyamide monomacrocycles, **2**, were designed and synthesized. A key design feature of these receptors is that they

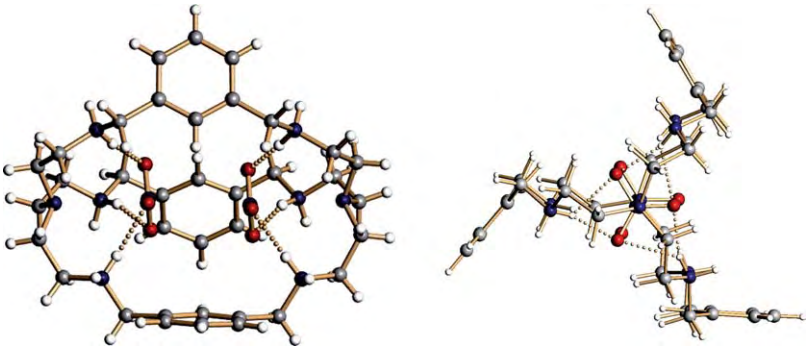

FIG. 2. Two perspective views of the single crystal X-ray diffraction structure of the nitrate complex of **1A**′ showing the ditopic inclusion of two nitrates inside the cavity.

incorporate two amine sites that were expected to play a major role defining their binding propensities. Proton NMR spectroscopic titrations, carried out in $CDCl_3$, indicated high affinities for oxo acid anions compared to simple halides, perchlorate, and nitrate (*50*). These receptors proved soluble in organic solvents, but generally not very soluble in water.

As expected, the inclusion of amines in these systems lends chemical versatility. As noted above, receptor **2A**, containing a *m*-xylyl spacer, shows a high affinity for protonated oxoanions, such as HSO_4^- and $H_2PO_4^-$, over other anions (Fig. 3). We attribute this finding to a complex interplay of the acid/base properties of both the anion and the macrocyclic amine. Crystals isolated from reacting HSO_4^- with **2A** indicated SO_4^{2-} (not HSO_4^-) sandwiched between two molecules of the receptor (Fig. 4). In the sulfate sandwich structure, each sulfate oxygen is held by two hydrogen bonds from the amides. This multiple hydrogen bond network is probably responsible for the high affinity seen for this complex with sulfate ($\log K = 4.50$ in $CDCl_3$) (*50*). The two macrocycles are rotated by 90° relative to one another, presumably to allow for the accommodation of the S_4 symmetry of the tetrahedral sulfate. Ligand **2B** with the pyridine spacer shows a lesser affinity for HSO_4^-, but still a very high affinity for $H_2PO_4^-$. With only minor exceptions, we have observed even greater affinity for anions by changing the *m*-xylyl spacer to pyridine (Fig. 3).

Since hydrogen bonding is one key to binding affinity in these complexes, an attempt to increase the HBD capability was explored, resulting in the design and synthesis of thioamide-based macrocycles **3** and bicycles **3**′ (*51,52*). By virtue of the soft polarizable sulfur atom, thioamide N–H bonds are weaker by about 10 kcal mol^{-1} (*53*), resulting in stronger hydrogen-bond interactions with a bound substrate. For the monocycles, as anticipated, results indicated increased affinity compared to the amide congeners (Fig. 3).

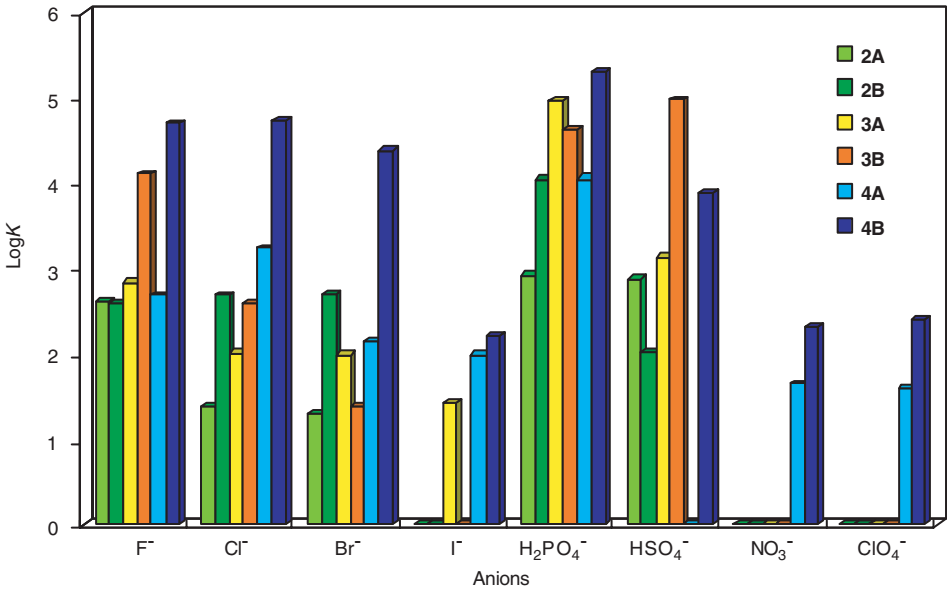

FIG. 3. Bar graph depicting binding of amides (greens), **2A** and **2B**; thiioamides (yellow and orange), **3A** and **3B**; and quaternized amides (blues) **4A** and **4B** with halides and oxoanions. Binding constants were determined in DMSO-d_6 using ^{1}H NMR spectroscopy.

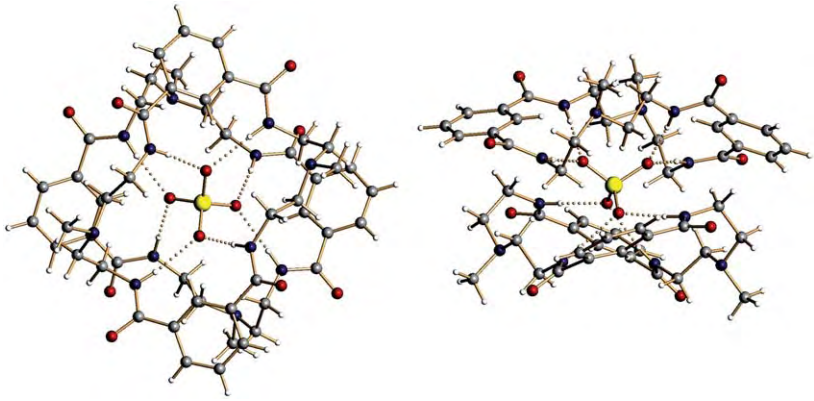

FIG. 4. Two perspective views of the sulfate sandwich complex formed with **2A** as determined by single crystal X-ray diffraction analysis.

D. POLYAMIDE/QUATERNIZED AMINE MACROMONOCYCLES

Another degree of complementarity, quaternization, is provided in the polyamide macrocycles of general structure **4**, namely increased charge matching (*54*). These new positively charged receptors showed

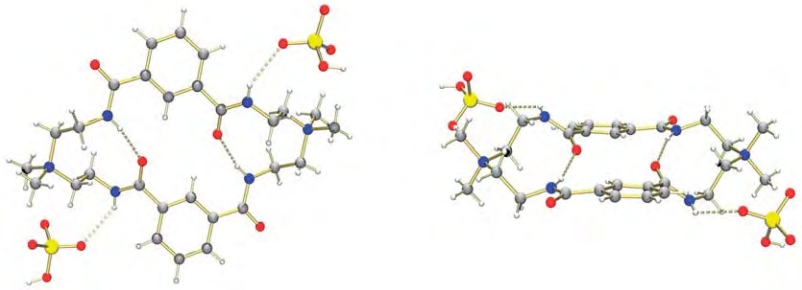

FIG. 5. Two perspective views of the single crystal X-ray diffraction structure of the 2:1 HSO_4^-; **4A**, complex as seen in the solid state.

significantly enhanced binding for anions (in most cases one or more orders of magnitude greater) (Fig. 3). However, they are less selective for HSO_4^-, and $H_2PO_4^-$ binding halides quite well. In this instance, the structure of **4A** (*m*-xylyl spacer) crystallized in the presence of HSO_4^- indicated a lack of inclusion of the anion in the cavity and only a single hydrogen bond holding the two bound HSO_4^- units to the outside of the macrocycle (Fig. 5). Again, we found that the pyridine analogs showed higher affinity than their *m*-xylyl corollaries in most cases, with HSO_4^- being the exception. This effect can probably be attributed to a preorganization influence provided by the pyridine nitrogens, which help orient the amide hydrogens in an inward-pointing fashion by hydrogen bonding. Alternatively, the increased affinity could reflect the presence of additional basic sites which serve to enhance oxoacid binding (although as noted earlier, the pyridine-based amide shows a reduced affinity for HSO_4^- compared with the corresponding *m*-xylyl analog).

E. POLY(THIO)AMIDE CRYPTANDS

In order to explore dimensionality in the amide- and thioamide-based series, receptors **2′** and **3′** were synthesized and characterized (*49,51,52,55*). While aza cryptands tend to bind anions more strongly than the corresponding monocycles, the affinities for oxoanions were found to decrease in the bicyclic amide- and thioamide-based series (Fig. 6). While the crystal structures to date indicate an inward orientation of the (thio)amide protons, it is possible that in solution a preferred geometry is with the sulfur or oxygen directed inward, promoted by a favorable hydrogen-bonding interaction with a (thio)amide on an adjacent arm. To the extent this is true, a greater reorganization energy would be required before anion binding is optimized. Nonetheless, the crystal structures of anion complexes isolated to date all show internal coordination of the anion. In fact, for fluoride, not only is a very symmetrical six-coordinate internal coordination observed (*52,55*), but in DMSO-d_6 deuterium exchange between the DMSO and cryptand amides is observed as a result of the highly basic nature

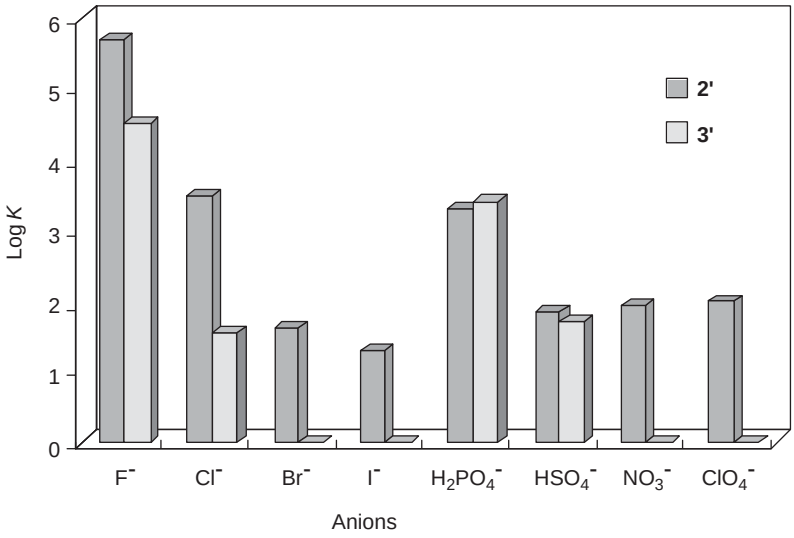

FIG. 6. Bar graph depicting binding of **2**′ and **3**′ with halides and oxoanions. Binding constants were determined in DMSO-d_6 using ^{1}H NMR spectroscopy.

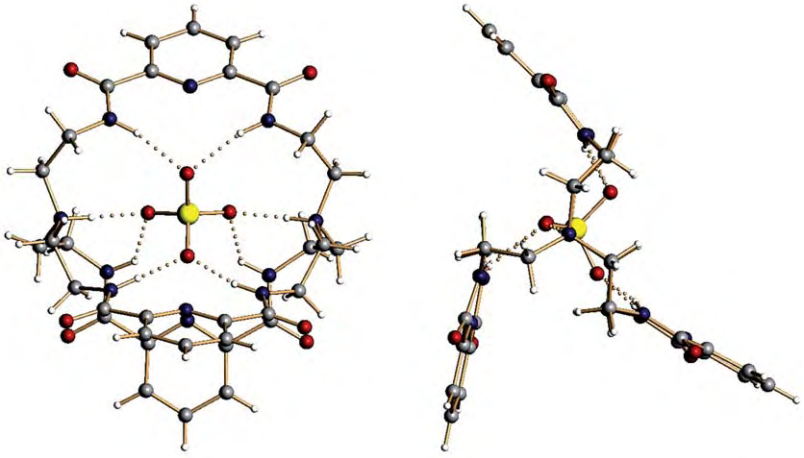

FIG. 7. Two perspective views of the single crystal X-ray diffraction structure of the HSO_4^- complex of **2**′ seen in the solid state.

of fluoride (*55*). A monohydrochloride salt was also isolated with one bridgehead amine protonated as well as a neutral ligand with encapsulated chloride (*52*).

For sulfate, a neutral complex was isolated with both bridgehead amines protonated and sulfate encapsulated (Fig. 7) (*49*), with an 8–fold hydrogen-bonding network reminiscent of the bis-macrocyclic

sandwich complex with sulfate stabilized by receptor **2A** (Fig. 4). In this instance, however, the orientation of the six amides and two bridgehead amines more closely approximates a bicapped trigonal prismatic geometry.

F. Calixpyrroles

In an approach that differs considerably from that pursued in the Bowman-James group, Sessler and collaborators have worked over the last decade to develop calixpyrroles (e.g., **5**) as neutral, NH donor-rich anion-binding agents (*56,57*). The calixpyrroles are extremely easy to make, being obtained generally in one step from the simple condensation of a monomeric pyrrole and a ketone (*56*). Although more constrained than acyclic systems, they are conformationally flexible. Nonetheless, they show high affinities for fluoride anion in organic media and, when fully substituted with fluorine atoms in the beta-pyrrolic positions (to give, e.g., **6**) (*58*), permit the selective extraction of sulfate anion from nitrate-rich media (*59*). Such findings, which are promising in their own right, led to the proposal that other pyrrole-containing receptors, including ones that incorporate amide and thioamide recognition elements and/or which possess a high degree of preorganization, would prove even better as sulfate anion extractants.

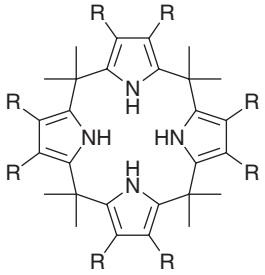

5 R = H
6 R = F

G. Hybrid Dipyrromethane Diamide Macrocycles

In an effort to pursue the above promise, it was decided to generate hybrid systems containing the key dipyrromethane fragment of calixpyrroles and the pyridine-2,6–dicarboxamide motif used so successfully by Bowman-James (*vide supra*) within a single macrocyclic receptor. This work was carried out in collaboration with Professor Yuri A. Ustynyuk of Moscow State University (*60,61*).

The synthesis of a first-generation hybrid macrocycle, **7**, is summarized in Scheme 3 (*60*). The key step involves the reaction of bis (2–aminophenyl)pyridine-2,6–dicarboxamide with diformyl dimethyldipyrromethane in the presence of a Brønsted acid catalyst. The best results (yields on the order of 90%) in the synthesis of macrocycle **7**,

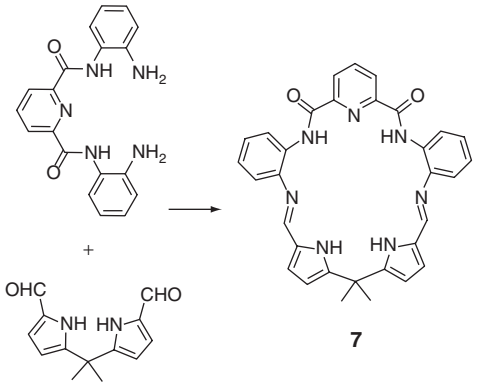

SCHEME 3. Synthesis of calixpyrrole hybrid receptor **7**.

were obtained using triflouroacetic acid in methanol, followed by treatment with triethylamine. Under these conditions, no precipitation was observed. By contrast, the use of other acid catalysts (HCl, CH_3COOH, HNO_3, H_2SO_4, and H_3PO_4) led to precipitation and yielded protonated salts of **7** contaminated with various oligomeric products. As a general rule, these precipitates displayed low solubility and could not be readily purified.

Receptor **7** was found to bind hydrogen sulfate in a strong 1:1 fashion in acetonitrile ($\log K = 4.81$). By contrast, no detectable affinity for nitrate anion was seen. Weak binding interactions were also seen in the case of cyanide, chloride, and bromide. This is rationalized in terms of the geometries of these anions (spherical: Cl^-, Br^-; linear: CN^-; and trigonal planar: NO_3^-), which do not match the deep cavity presumed to be present in **7**. Consistent with this supposition is the finding that acetate and phosphate, anions not particularly germane to the LAW remediation problem, are bound with appreciable affinity. In fact this latter anion interacts with receptor **7** in a strong, stepwise 2:1 (anion-receptor) fashion ($\log K_1 = 5.53$; $\log K_2 = 4.41$, acetonitrile). Such a sequential binding process is thought to reflect the presence of second binding site external to the macrocycle core that is not directly involved in sulfate recognition.

In an effort to obtain systems where the phosphate-binding affinity was reduced in comparison to that seen for sulfate and where the receptor-anion stoichiometries were in both cases 1:1, several new macrocycles were designed (*61*). Among these are receptors **8**, **9**, and **10**. The synthesis of the parent macrocycle **8** follows the same route as described for **7**, with the modification that a different, more rigid, dipyrromethane unit was used as starting material. The best results were obtained when the condensation reaction leading to Schiff base formation was carried out in methanolic solutions, under refluxing conditions, in the presence of 2.2 eqv. of H_2SO_4. Macrocycle **8** was obtained in 90% yield (for two steps) after quenching the reaction mixture with an excess of triethylamine. Macrocycles **9** and **10** were

obtained from **8** under reductive ($NaBH_4$) and oxidative ($KMnO_4$) conditions in quantitative and 75% yield, respectively.

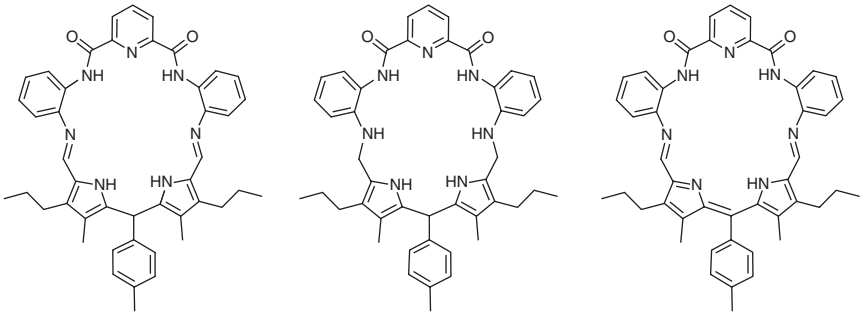

8 **9** **10**

Evidence in support of the suggestion that receptor **8** could function as a sulfate-binding receptor came from X-ray diffraction studies. As shown in Fig. 8, the diprotonated form of this system, crystallized as the 1:1 H_2SO_4 salt, was found to complex the sulfate counter anion within its central "cavity" as the result, presumably, of a combination of oriented hydrogen bonds and electrostatic interactions. In solution, receptor **8** was found to bind hydrogen sulfate in a strong 1:1 fashion

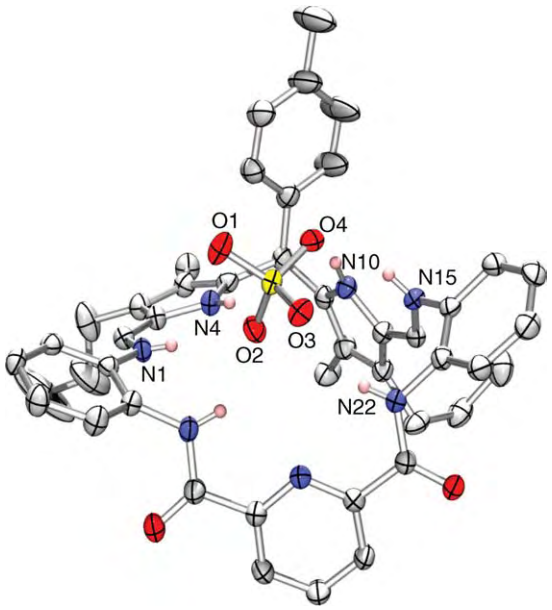

FIG. 8. ORTEP-POVray rendered view of $\mathbf{8} \cdot H_2SO_4$ as determined by single crystal X-ray diffraction analysis. Solvent molecules and most hydrogen atoms have been removed for clarity.

(log $K = 5.03$, acetonitrile), while the affinity for nitrate was found to be below the limits of detection. In contrast with the initial receptor, **7**, macrocycle **8** was found to interact with dihydrogen phosphate only moderately well and in a 1:1 fashion (log $K = 4.46$, acetonitrile). The change in selectivity, and more importantly the change in the binding stoichiometry (1:1 vs. 2:1 for dihydrogenphosphate with **8** and **7**, respectively), was rationalized as being the result of the tolyl group present in the *meso* position of the newer system **8**; presumably, this substituent acts as a *pseudo lid* for the macrocycle cavity. The tolyl group is also expected to reduce the conformational flexibility of the macrocycle as the result of steric interactions involving the methyl groups in the 4,4′ positions of the dipyrromethane subunit.

Receptor **9** was found to interact with chloride anion most strongly among of the anions studied (log $K = 5.06$, acetonitrile). It was inferred that the "hydrogen-rich" nature of this receptor, and its higher flexibility makes this receptor better suited for the binding of smaller, spherical anions (*61*).

Receptor **10** was found to interact only with bromide, albeit in a weak fashion (log $K = 3.44$, acetonitrile). Such a result is not surprising since this macrocycle possesses the fewest number of HBD atoms as compared to its congeners (*61*).

Taken in concert, these calixpyrrole-inspired systems serve to demonstrate further that the anion-binding properties of a given class of receptors may be readily modified via logical adjustments in terms of size, flexibility, and HBD number. As such, they set the stage for the generation of yet-improved systems that are appropriately fine-tuned for use in specified applications, including those associated with sulfate anion extraction.

III. Extraction Studies

A. Strategy

The transport of ions across interfaces has long been of interest to a broad array of scientists working across a full spectrum of disciplines. The importance of this phenomenon to mechanisms of solvent extraction, ion transport in biological membranes and, in general, the physical chemistry of the interfacial domain is obvious. Solvent extraction is of particular utility to researchers concerned with issues of radioactive waste remediation, since it provides a means for the selective removal of a targeted species by moving it from one phase into another. However, as noted in the introduction to this paper, a precedent has not yet been set using anion receptors for specific anion extraction in nuclear or hydrometallurgical applications.

Moyer and Bonnesen have recently introduced the concept of "bias" as opposed to "recognition" pertaining to anion extraction and separation (*39*). It is based on the fact that anion-transport processes have

historically tended to be solvation controlled and thus subject to the Hofmeister order (see above). Anion solvation is dominated by electrostatic interactions and hydrogen bonding, which are based primarily on ionic charge density and thus sensitive to the dielectric constant and HBD strength of the medium. In such cases, there is, in fact, no real recognition, and selectivity depends primarily on trends in size (or charge density more generally) plus solvation considerations. Although bias-type systems have proven extremely useful, their monotonic dependence on ionic charge density clearly limits their applicability. Recognition, on the other hand, should be capable of providing deviations from the trends observed in bias systems as a result of significant host–guest interactions through unique geometrical and hydrogen-bonding liaisons. Thus, the terms "bonding" and "coordination chemistry" become valid concepts in approaching the problem of anion recognition. Because of significant advances in recent years in anion recognition, in conjunction with the extensive base of understanding of recognition phenomena in general developed through studies of cation recognition, more highly efficient systems can now be designed for liquid–liquid extraction purposes, as discussed in more detail below.

Moyer and co-workers have been systematizing the use of host–guest chemistry in liquid–liquid ion transport (*62,63*), as presented in Table I. Three general strategies for ion extraction are apparent: Ion-pair (or salt) extraction, cation exchange, and anion exchange. Exchange is closely related to salt extraction if one envisions that a salt is so strongly extracted that negligible concentrations of the salt partition into the aqueous phase. In that case, the cation or the anion may be exchangeable with an aqueous ion that is relatively more attracted to the solvent phase. Cases #1–#5 in Table I entail transport of a salt into the organic solvent, which for our application would be sodium sulfate (or monohydrogen sulfate). There the cation may be bound by a host (Case #2); the anion may be bound by a host (Case #3); dual hosts may be used to bind cation and anion, but in separate complexes (Case #4); or a ditopic salt host can be used (Case #5). Among the salt-extraction options (Cases #1–#5), successful extraction of sodium sulfate would require receptors for both of these ions to compensate for the highly unfavorable partitioning of the ions to the solvent phase (*38,39*) and thus to wrest control of anion selectivity from Hofmeister bias. Accordingly, lack of cation binding disfavors Case #3, a very rarely observed case anyway, though anion binding proves effective for selectivity control (*59*). One thus can see that a dual-host system (Case #4) merits consideration (*64–68*). The ditopic case (#5) investigated recently by Bradley Smith and co-workers (*69–71*) represents a higher level of sophistication. This type of system confers one possible advantage in that if designed sufficiently well, the salt receptor may allow for an added electrostatic interaction between the bound cation(s) and anion(s).

TABLE I

ELEVEN APPROACHES TO RECOGNITION AND EXTRACTION OF SODIUM HYDROXIDE USING HOST–GUEST CHEMISTRY

Case	Name	Description
#1	No host	A polar solvent (e.g., 1-octanol) is used to solvate both cation and anion.
#2	Cation host	A cation host (e.g., crown ether) binds the cation. Anion remains primarily solvated.
#3	Anion host	An anion host binds the anion. Cation remains primarily solvated.
#4	Dual hosts	Cation host and anion host are used in synergistic combination.
#5	Ion-pair host	A single host binds both the cation and anion.
#6	Cation exchange	A lipophilic organic acid or its salt with hydrophilic cation is employed to effect cation exchange. No hosts are used.
#7	Synergistic cation exchange	A cation host is used in synergistic combination with a cation exchanger.
#8	Ditopic cation exchange	A cation-exchange functionality is incorporated into the cation host.
#9	Anion exchange	A salt of a lipophilic cation is employed to effect anion exchange. No hosts are used.
#10	Synergistic anion exchange	An anion host is used in synergistic combination with an anion exchanger.
#11	Ditopic anion exchange	An anion-exchange functionality is incorporated into the anion host.

Cases #6–#11 in Table I all represent ion exchange, either cation exchange (Cases #6–#8) or anion exchange (Cases #9–#11). For the present purposes, cation-exchange systems, proposed for hydroxide separation (*62,63*), are not of interest, but anion exchange is promising. For simple systems with no recognition component (Case #9), a highly lipophilic cation, such as a long-chain tetraalkylammonium cation is used as an anion exchanger, and well-known bias-type selectivity principles apply (*29*). To build-in anion recognition, Case #10 involves the case where an anion receptor is used as a separate entity in conjunction with an anion exchanger (e.g., a tetraalkylammonium cation); to the best of the authors' knowledge no examples of this strategy appear to have appeared in the literature. However, as recently reported, this strategy may be extended by employing a receptor that has a fixed positive charge, thus providing for built-in anion-exchange capacity (Case #11) (*72*).

Among the available options, salt extraction via Cases #4 and #5 and anion exchange via Cases #10 and #11 appear to have the most promise for sulfate separation. For those cases involving no anion binding (Cases #1, #2, and #9), bias-type Hofmeister selectivity dominated by solvation will disfavor sulfate relative to the abundant and less

charge-dense nitrate anion in the waste. In principle, it is possible to reverse the Hofmeister bias if the overall hydrogen-bonding environment of the solvent is stronger than that of water (*39*). Evidence for this phenomenon exists (*64*), but it would be difficult to achieve in the with our application, because compounds with strong enough HBD strength are likely to be deprotonated at the elevated alkalinity of the waste. Hence, anion receptors provide the best opportunity to achieve sulfate selectivity. For the two salt-extraction cases, part of the driving force of the extraction is the large sodium concentration in the waste, which provides for easy release of the salt when the loaded solvent is contacted with water. Stripping with water generates no secondary waste, generally has no adverse impact on downstream waste disposal, and is economically attractive. The two anion-exchange options offer a potential cost advantage in that no cation receptor is needed, but stripping, usually achieved by displacement, may be problematic.

B. Results

Below we survey the extraction behavior of illustrative liquid–liquid systems selected from Table I. For experimental design, it was recognized that the bulk of the tank waste may be characterized essentially as highly alkaline sodium nitrate containing numerous other ions at intermediate (e.g., potassium, nitrite, carbonate, and sulfate) and trace (e.g., noble metals and radionuclides) concentrations. However, at this stage of our progress, experiments were designed primarily to derive understanding of the principles of solvation, selectivity, and binding relevant to sulfate extraction. The need to approximate conditions of the waste or of processing, and expectations for results pertaining directly thereto, were considered secondary. Hence, aqueous-phase compositions were kept simple, and receptor concentrations were low. The latter limitation resulted both from the small quantities of receptor compounds available from custom synthesis and from their generally low solubilities in solvents of interest. Although distribution ratios were thus generally quite low, much higher values may be expected when more realistic extractant concentrations are used. Sulfate distribution measurements were made via β-scintillation counting using $^{35}SO_4^{2-}$ tracer. Distribution ratios are defined as the concentration of target species (e.g., sulfate) in the organic phase divided by that in the aqueous phase.

Case 1. Several experiments were conducted in which sodium sulfate extraction into 1–octanol was measured (Case #1). 1–Octanol is reasonably good at solvating both cations and anions, as it is both a good electron-pair donor and HBD (*73*). Even so, extraction was expected to be weak, as alcohols solvate ions more weakly than water, judging by tabulated values of the standard Gibbs energy of partitioning (ΔG_p°) (*38*). Using an aqueous phase consisting of 1 M NaOH, 0.1 mM Na_2SO_4, and tracer, a feeble D_{SO_4} of 2×10^{-6} was indeed obtained.

As it is known that anion partitioning, particularly that of small anions, is influenced mostly by the HBD ability of the solvent (*39*), it was postulated that addition of HBDs more acidic than 1–octanol to the 1–octanol solvent would enhance extraction. This modification may be thought of as a primitive Case #3 with a monofunctional anion receptor or perhaps just Case #1 with enhanced solvation. The simple monofunctional hydroxy compounds tested are given below:

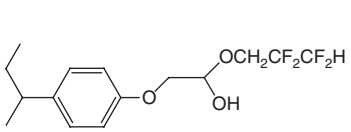

11

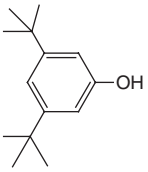

12

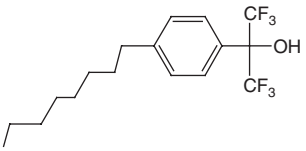

13

Compound **11** is the diluent modifier used in the CSSX process for $CsNO_3$ extraction by a calixcrown and is thought to function by solvation of the anion based on solvatochromic data (*74*). On adding **11**, **12**, or **13** at 0.2 M to 1–octanol, D_{SO_4} values were obtained as follows: 1.9×10^{-4}, 1.3×10^{-4}, and 3.4×10^{-4}, respectively. Although these are still very low distribution ratios, considerable extraction enhancement was observed, a factor of 170 for compound **13**. Sodium distribution was measured in parallel by gamma counting of ^{22}Na tracer. These measurements showed that the hydroxy proton of **11** is not significantly exchangeable with sodium under the experimental conditions used, and thus, the enhancement of extraction is interpreted as being due to enhanced solvation of sulfate by hydrogen bonding. Similar behavior has been observed in nitrobenzene (*63,75*), where the enhancement itself is anti-Hofmeister, though too weak to reverse the net Hofmeister effect. On the other hand, the hydroxy protons of **12** and **13** are sufficiently acidic that an appreciable fraction of each compound is converted to its sodium salt, 70% in the case of **12** and 98% in the case of **13**. The enhanced sulfate extraction observed for these two compounds must therefore involve some other mechanism involving ionic interactions.

Case 3. In accordance with expectations, Case #3 was confirmed to provide for only weak extraction. Addition of the anion receptor **2A** (Scheme 1) with a simple *m*-xylyl spacer to 1–octanol enhances sodium sulfate extraction from an aqueous solution containing 1 M NaOH, 0.1 mM Na_2SO_4, and $^{35}SO_4^{2-}$ tracer, but only slightly. In particular, it was seen that upon adding 10 mM **2A** to 1–octanol, D_{SO_4} increases from 2×10^{-6} to 3×10^{-5}. This is a feeble extraction, but the anion receptor does appear to have a noticeable effect. Because 1–octanol competes in the extraction, both by solvating the sulfate and the anion receptor, another type of experiment was sought that would better allow an examination of the selectivity of anion receptors in line with Cases #3 and #4 (Table I). As we recently demonstrated, certain cesium salts are

weakly extractable by nitrobenzene alone without any receptor at all, and it is therefore possible to quantify the enhancement of the cesium salt extraction when an anion receptor is added (*59*).

Nitrobenzene lacks HBD ability and thereby cannot compete with anion binding. Accordingly, it was possible to demonstrate that a derivative of **2A**, **14**, used alone (again Case #3, no cation receptor present) effects cesium salt extraction into nitrobenzene. Host **14** was synthesized by a variation of the methods for the synthesis of **2** using the *N*-dansyl derivative of diethylenetriamine (dien) as the precursor amine. The *N*-dansyl precursor was synthesized from dien with phthalimide-protected terminal amines. Receptor **14** at 3 mM in this diluent was used to extract cesium salts to which were added 1 mM NaOH and ^{137}Cs tracer. Distribution ratios of cesium salts of univalent anions were low but measurable. As an example, the distribution ratio for cesium nitrate (at 3 mM in the aqueous phase) was 0.0058 with 3 mM **14** vs. 0.0019 without **14**, a 3–fold enhancement. Not surprisingly, though, salts of divalent anions were extracted at levels that proved too low to allow for reliable determination. Evidence for Case #3 has been generally elusive in the literature, but limited data have been reported (*76–79*). Apparently, the anion receptor must be exceptionally strong to overcome the unfavorable cation partitioning. In other work we found that fluorinated calix[4]- and calix[5]pyrroles have the requisite strength and can effect the moderate extraction of cesium salts into nitrobenzene without a cation receptor and with a decidedly non-Hofmeister order (*59*).

Case 4. Dual-host extraction systems (Case #4) exhibited much stronger salt extraction with a synergistic effect being observed between cation and anion receptors. Extraction experiments were conducted with **14** in synergistic combination with the cesium-selective calixcrown, calix[4]arene-bis(*t*-octylbenzo)crown-6 (BOBCalixC6) **15** in nitrobenzene. Following previous dual-host experiments (*80*), cation receptor **15** was chosen for its strong binding of cesium (*81*) allowing the extraction of cesium salts of even divalent anions to be measured. This system thus facilitates evaluation of anion extraction selectivity, though ultimately a sodium receptor will be needed for a practical dual-host system relevant to sulfate extraction.

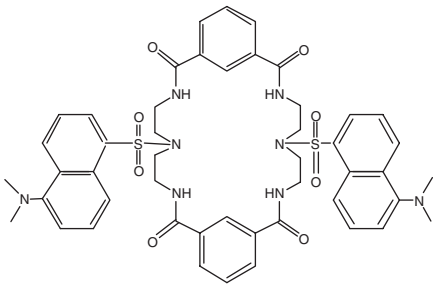

14

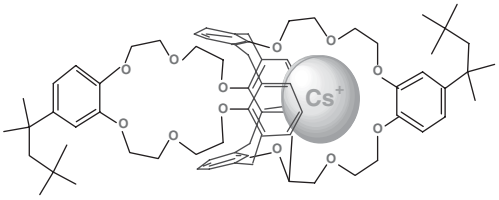

15

In dual-host systems, the expected synergism is ideally ascribable to a new reaction in which the cation receptor B binds the cation M^+ and the anion receptor R binds the anion X^{q-}, resulting in extraction of the M_qX salt in excess over that which would be extracted by B and R each acting independently (*82*). If the diluent is sufficiently polar that no ion-pairing occurs in the solvent phase, the new reaction may be expressed ideally in the following manner

$$qM^+(aq)+X^{q-}(aq) + qbB(org) + rR(org) \rightleftharpoons qMB_b^+(org) + R_rX^{q-}(org) \quad (1)$$

The polar diluent nitrobenzene minimizes (though may not altogether eliminate) the effect of ion-pairing interactions. The cation receptor **15** extracts simple salts of cesium according to (*81*)

$$Cs^+(aq) + X^-(aq) + B(org) \rightleftharpoons CsB^+(org) + X^-(org) \quad (2)$$

In many cases, including the present case, the anion receptor has negligible ability to extract CsX salts by itself (Case #3) relative to the dual-host system. When this is true, on addition of an anion receptor to the cation receptor **15**, an enhancement of extraction may be interpreted solely in terms of anion binding according to the new reaction given in Eq. (1). If the behavior is ideal, only 1:1 anion:receptor complexes form, and B and R do not form hydrogen-bonded aggregates B_bR_r, then one can in principle deduce the anion binding constant from the enhancement (*82*).

Extraction surveys were performed with various concentrations of **14** added to 10 mM **15** in nitrobenzene, revealing selective synergism for sulfate extraction. The aqueous phases consisted of single 1:1 or 2:1 Cs_qX ($q = 1$ or 2) salts to which were added 1 mM NaOH and ^{137}Cs tracer (for radiometric determination of the cesium distribution ratio D_{Cs}). Results are illustrated in Fig. 9. In general, it was found that **14** enhances Cs_qX extraction by **15**, and the enhancement increases with increasing anion hydration, decreasing anion radius for a given charge, increasing charge, and increasing anion-receptor concentration. Among the univalent anions, the enhancement is anti-Hofmeister. That is, anion binding tends to increase as the anions become smaller or more hydrated. This effect is typical, as the smaller the anion is, the stronger is the hydrogen bond with a given HBD. Among all of the anions, enhancement of sulfate extraction was one of the strongest (11–fold for **14**; it was 4–fold for **2A** which tended to be uniformly weaker than **14** for all anions). At 3 mM, **14** exhibited an even higher sulfate enhancement (16–fold), the highest seen for any of the anions at that receptor concentration; the decrease in enhancement at 10 mM vs. 3 mM is ascribed to formation of a third phase (i.e., the solubility limit of the complex was apparently exceeded). It is not definite whether the selectivity for

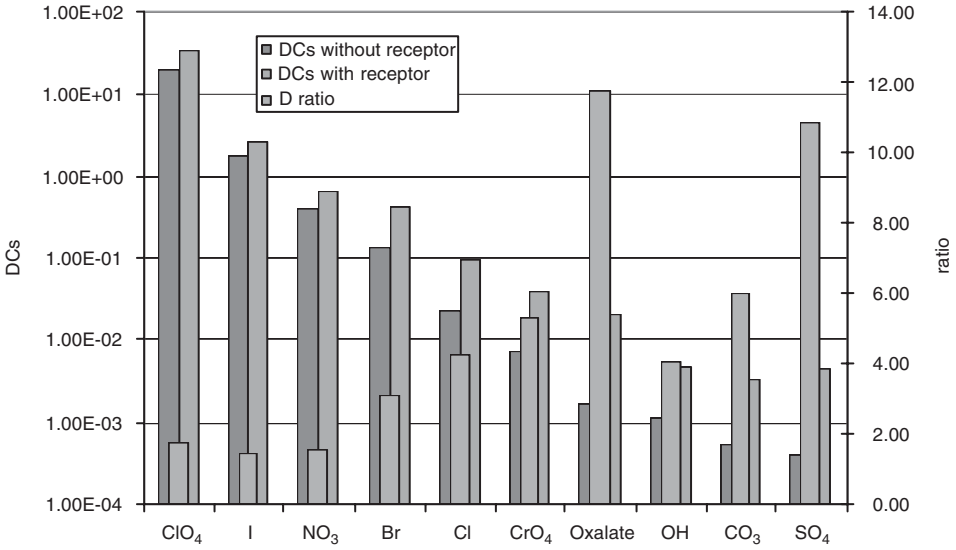

FIG. 9. Synergistic extraction of cesium salts into nitrobenzene by dual hosts **14** and BOBCalixC6, **15**. The cesium distribution ratio is shown on the left Y-axis, and the enhancement ratio D_{Cs}(**14**+BOBCalixC6)/D_{Cs}(BOBCalixC6 alone) is shown on the right Y-axis.

sulfate is due to special complementarity (e.g., sandwich formation (*50*)) or simply to the high charge density on sulfate. However, the pattern of enhancements with **14** vs. absolute D_{Cs} values without **14** in Fig. 9 provides evidence for recognition. We should keep in mind that we have been discussing *enhancement*, a measure of anion binding (*82*), whereas the small, charge-dense anions are difficult to extract in absolute terms, owing to their large hydration energies. The anions in Fig. 9 are arranged according to their order of decreasing D_{Cs} without anion receptor (Case #2, cation receptor only). It may indeed be seen that this order follows the Hofmeister order, at least insofar as the order originally noted by Hofmeister (sulfate > hydrogen phosphate > acetate > citrate > tartrate > hydrogen carbonate > chromate > chloride > nitrate > chlorate) (*36*). Among the univalent anions, the order of anions in Fig. 9 is identical to the order of decreasing thermochemical radius (*38*). As expected, divalent anions cluster at the right of the figure, though sulfate is out of order, where the order of decreasing thermochemical radii for the divalent anions is CrO_4^{2-} (0.240 nm) > SO_4^{2-} (0.230 nm) > $C_2O_4^{2-}$ (0.210 nm) > CO_3^{2-} (0.178 nm) (*38*). Clearly, the enhancement observed in the dual-host system is anti-Hofmeister, but one may note that the enhancement order is not the simple mirror image of the order of D_{Cs} values without anion receptor. Thus, a binding selectivity (i.e., a degree of recognition) would seem to be implicated, which agrees with the complementarity seen in the sandwich structure (*50*). Although the binding behavior thus proves very encouraging, one may observe that

the anti-Hofmeister *enhancement* still lacks sufficient magnitude to offset the dominant Hofmeister effect of Eq. (2). The net extraction observed thus follows Hofmeister behavior. Future work will thus be challenged by the need to obtain stronger binding as well as good selectivity.

Cases 9–11. On the basis of our systematized 11 approaches to extraction (Table I), it was considered advantageous to experiment with the anion-exchange systems represented by Cases #9–#11. In such systems, an aqueous cation is not co-transported with the anion, and thus all considerations of cation transport and binding are removed. Rather, anion exchange gives a direct measure of competitive extraction of one anion for the other. Having no anion receptor present, Case #9 is the baseline case, and for that we chose the classical extractant methyltri-*n*-octyl(decyl)ammonium nitrate. This extractant has major industrial uses and is marketed under the name Aliquat 336 in the chloride form; it is primarily a mixture of random substitution of normal octyl and decyl groups. Prior to use, it was converted to the nitrate form by contacting organic stock solutions of the chloride form with aqueous sodium nitrate. As discussed above, the choice of solvent is the main parameter controlling the selectivity, though the structure of the quaternary ammonium cation has an offsetting role via its influence on the strength of nonspecific ion-pairing (*39*). On addition of an anion host (Case #10), the resulting increase (synergism) or decrease (antagonism) in the distribution ratio of one of the anions reflects the direct competitive preference of the host for the two anions presented to it. It may be noted that this synergism of anion exchange using an anion receptor in bulk liquid–liquid extraction is fairly novel, though it has been in common use in membrane electrodes (*83*).

Liquid–liquid extraction experiments were conducted at 25°C by contacting equal volumes of the two phases for 1–2 hours, followed by centrifugation for several minutes at 25°C, and subsampling for scintillation counting. Contacting was carried out in small polypropylene vials by a gentle end-over-end tumbling on a rotating disk in a constant-temperature air box. Generally, kinetic experiments have shown that the contacting time using the described method is well in excess of that needed to reach equilibrium. Gamma scintillation techniques were employed for ^{22}Na and ^{137}Cs using an automatic counter (Cobra Quantum Model 5003, Packard Instruments, Downers Grove, IL) equipped with a through-hole-type NaI detector. Samples containing $^{35}SO_4^{2-}$ were analyzed by liquid scintillation counting of subsamples in Packard Ultima Gold cocktail using a Packard Tri-Carb 2500TR Liquid Scintillation Analyzer. Samples were run in duplicate or in higher replicate, and results are reported as the average value. Overall experimental precision is estimated to be $\pm$5–10%.

An experiment was devised to directly measure sulfate selectivity vs. nitrate, the key parameter for waste applications. One can envision the quaternary ammonium salt providing exchangeable nitrate anions

in the solvent phase. In a given solvent matrix, the exchange will give a characteristic value of D_{SO_4} measured by tracer techniques, reflecting whether a given receptor exhibits a greater affinity for sulfate vs. nitrate. Accordingly, values of D_{SO_4} were measured for 10 mM quaternary ammonium nitrate in a series of diluents. The aqueous phase contained 10 mM $NaNO_3$ plus 0.1 mM Na_2SO_4, and $^{35}SO_4^{2-}$ tracer. The sodium sulfate concentration was made small for convenience so that the extractants would not be significantly loaded with sulfate, making both the sulfate and nitrate distribution ratios effectively constant. In these systems, the figure of merit for assessing selectivity is the separation factor α_{SO_4/NO_3}, defined as the ratio D_{SO_4}/D_{NO_3}, which is presumed constant at small concentration of sulfate relative to nitrate in both phases. The value D_{NO_3} is approximately unity for these conditions, since $[NO_3^-]_{org} = \sim 10$ mM and $[NO_3^-]_{aq} = \sim 10$ mM. Thus, D_{SO_4} approximates α_{SO_4/NO_3}, and $D_{SO_4} > 1$ indicates sulfate selectivity. Results are shown in Table II. With no receptor added (Case #9), all values of D_{SO_4} may be seen to be less than 1, indicating nitrate selectivity, in accord with the higher hydration of sulfate and the normal

TABLE II

SURVEY OF ANION RECEPTORS AS SYNERGISTS FOR ANION EXCHANGE FOR VARIOUS DILUENTS[a]

Receptor	[Receptor] mM	Diluent	D_{SO_4}	Enhancement factor
None	0	1-octanol	4.4×10^{-3}	
11	200	”	9.7×10^{-3}	2.2
12	200	”	1.1×10^{-2}	2.3
13	200	”	1.1×10^{-2}	2.5
2A	10	”	7.3×10^{-3}	1.7
16	10	”	4.4×10^{-3}	1.0
16	10	”	6.4×10^{-3}	1.5
None	0	Toluene	3.9×10^{-4}	
11	200	”	3.6×10^{-3}	9.2
15	3	”	2.1×10^{-3}	5.4
16	3	”	2.4×10^{-2}	62
16	10	”	1.9×10^{-1}	490
		”		
None	0	1,2-dichloroethane	1.6×10^{-4}	
16	10	”	7.8×10^{-4}	4.9
None	0	2:1 Hexane/$CHCl_3$	1.7×10^{-4}	
16	10	”	2.0×10^{-1}	1200
None	0	0.5 M TBP, dodecane	2.3×10^{-3}	
16	10	”	5.5×10^{-3}	2.4

[a]All systems run at 10 mM Aliquat 336 in the indicated diluent. The aqueous phase contained 10 mM $NaNO_3$ plus 0.1 mM Na_2SO_4 and $^{35}SO_4^{2-}$ tracer. Contacting at 1:1 phase ratio at 25°C. Compounds were obtained or prepared as indicated: 2A(*50*), 6(*58*), 11(*84*), 12(ALDRICH), 13(*85*), AND 16(*86*).

expectation for solvation-based extraction selectivity. It was found that exchange with no anion receptor is most favorable (better stated as least unfavorable) for sulfate (highest D_{SO_4}) with 1–octanol as the diluent in comparison with toluene, dodecane, and 1,2–dichloroethane. This is not surprising, as the hydrogen bonding provided by 1–octanol will favor the more charge dense anion, sulfate.

Our investigations of anion receptors in synergistic anion exchange have produced exciting results. The tests have so far been limited to surveys of anion receptors and different solvents to quickly identify key parameters and most interesting behavior. Selected survey results for different receptors and different diluents are given in Table II. In addition to the simple monofunctional hydroxy compounds **11**–**13**, and the tetraamide macrocycle **2A**, a 1,3–benzene disulfonamide **16** and the octafluorinated calix[4]pyrrole **6** were examined. The two disparate diluents 1–octanol and toluene were explored most extensively, with more limited extension to other diluent systems. Solubility limitations were encountered for **2A** in toluene. Enhancement of anion exchange is taken quantitatively as the ratio of D_{SO_4} in the system with receptor vs. the system without the receptor. In no case was extraction by the anion receptor alone (Case #3) sufficiently strong to be taken into account.

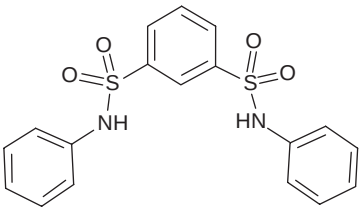

16

One may see at once from Table II a striking effect of both diluent and receptor type. In 1–octanol, enhancements tend to be weak overall, which is interpreted in terms of the ability of this diluent to compete with the receptor for anion binding and with the anion for receiving hydrogen bonds from the receptor. In this medium, **2A** somewhat outperforms the fluorinated calix[4]pyrrole **6**, and **16** exhibits no activity. Addition of hydroxy HBDs **11–13** at elevated concentration produces a positive effect. Selected tests were performed at 0.1 M quaternary ammonium salt in 1–octanol (not tabulated), where it was noted, for example, that addition of 10 mM of **2A** approximately halved the value of D_{SO_4} from 3.6×10^{-1} to 1.9×10^{-1}. This apparent dependence of the enhancement on the exchanger concentration strongly suggests an effect of aggregation. Quaternary ammonium salts are notorious for aggregating in organic solvents due to their high dipole moments. Hence, the exchanger is presumably at a higher state of aggregation when it is at 100 mM vs. 10 mM. Receptor **2A** was observed to interact more strongly with nitrate at the higher aggregation state.

Unfortunately, it was not possible to examine the effect of **2A** in toluene, as it was not soluble in the presence of the quaternary ammonium nitrate salt. For fluorinated calix[4]pyrrole **6**, the ordering of diluents with increasing enhancement of anion exchange was 1–octanol < 0.5 M tributylphosphate (TBP) in dodecane < 1,2–dichloroethane < toluene < 2:1 hexane:chloroform. It makes sense that in the TBP system, the good hydrogen bond accepting ability of the phosphoryl oxygen ties up the anion receptor, giving weak enhancement. Enhancements for **6** in toluene and 2:1 hexane:chloroform were quite striking, exceeding three orders of magnitude for the latter. In these two systems, the diluents are not polar nor are they capable of engaging in significant hydrogen bonding. Enhancement tended to correlate inversely with the sulfate distribution ratio without receptor, as anion binding and hence enhancement will be favored in the absence of competing strong solvation effects, which are otherwise favorable for sulfate relative to nitrate.

The results from Table II suggest that the needed selectivity and extraction strength for practical use will likely be attainable with continued research. One may note that no anion-receptor system in Table II meets the success criterion of $D_{SO_4} > 1$, and thus, we have not yet tipped the balance decisively in favor of sulfate. To a degree, this goal can be pursued with simple manipulation of concentrations of extractants, which will require generally more soluble anion receptors. That is, distribution ratios can be expected to increase when we are able to work at higher extractant concentrations commensurate with the concentration of sulfate in the waste (several tenths molar). Interestingly, the quaternary ammonium nitrate salt solubilizes **6** in toluene, undoubtedly owing to nitrate binding. This phenomenon allowed us to extend the exchange experiment to 100 mM **6** with 100 mM quaternary ammonium salt in toluene with the same aqueous conditions, when $D_{SO_4} = 1.6$ (*87*). Thus, the results show that we are within "striking distance" of systems that exhibit the requisite extraction selectivity and strength.

IV. Conclusions

These studies on the basic chemical aspects of anion receptor design of functional pH-independent systems have as an ultimate goal the targeting of selective binding of anions of environmental significance. In applications-oriented aspects of the research on the design of separations, strategies for selective and efficient removal of targeted anions have been a major long-term goal. Key findings from the extensive interdisciplinary program include (1) some of the first synthetic sulfate-selective anion-binding agents; (2) simple, structure-based methods for modifying the intrinsic anion selectivity of a given class of anion receptors; and (3) the first system capable of extracting sulfate

anion from acidic, nitrate-containing aqueous media. These initial findings point the way to more effective systems involving receptors with higher selectivity, binding strength, and solubility, as will be explored in future efforts.

Acknowledgments

Research sponsored by the Environmental Management Science Program, Office of Science, U.S. Department of Energy, under contract DE-AC05-00OR22725 with Oak Ridge National Laboratory, managed and operated by UT-Battelle, LLC; grant no. DE-FG02-04ER63741 to J.L.S.; and grant nos. DE-FG-96ER62307 and DE-FG02-04ER63745 to K. B.-J. The authors thank Peter V. Bonnesen for graciously providing the fluorinated alcohols **11** and **13** and a sample of phenol **12**. We also thank Victor Pastushok for synthesizing the disulfonamide **16**. Professor Sessler would like to acknowledge a fruitful collaboration with Professor Yuri A. Ustynyuk, which has allowed for the synthesis of macrocycles **7**–**10**. The participation of C.J.F. was made possible by an appointment to the Oak Ridge National Laboratory Postgraduate Program administered by the Oak Ridge Associated Universities.

References

1. "*Performance Management Plan for the Accelerated Cleanup of the Hanford Site*"; Report DOE/RL-2002-47, U.S. Department of Energy, Richland, WA, July 17, **2002**.
2. *"Research Needs for High-Level Waste Stored in Tanks and Bins at U.S. Department of Energy Sites"*; *National Research Council*, National Academy Press, **2001**; p. 55
3. Allen, R. W.; Josephson, G. B.; Westsik, J. H.; Nickola, C. L. "*Tanks Focus Area Site Needs Assessment*"; Report PNNL-13518, Pacific Northwest National Laboratory, Richland, WA, April **2001**.
4. Schreiber, H. D.; Fowler, R. W.; Ward, C. C. *Phys. Chem. Glasses* **1993**, *34*, 66–70.
5. Merrill, R. A.; Whittington, K. F.; Peters, R. D. "*Vitrification of High Sulfate Wastes*"; Report PNL-SA-24672, Pacific Northwest National Laboratory, Richland, WA, September **1994**.
6. Langowski, M. H. "*The Incorporation of P, S, Cr, F, Cl, I, Mn, Ti, U, and Bi into Simulated Nuclear Waste Glasses: Literature Study*"; Report PNNL-10980, Pacific Northwest National Laboratory, Richland, WA, February **1996**.
7. Li, H.; Langowski, M. H.; Hrma, P. R.; Schweiger, M. J.; Vienna, J. D.; Smith, D. E. "*Minor Component Study for Simulated High-Level Nuclear Waste Glasses*"; Report PNNL-10996, Pacific Northwest National Laboratories, Richland, WA, February **1996**.
8. Feng, X.; Schweiger, M. J.; Li, H.; Gong, M. "*Retention of Sulfur, Phosphorus, Chlorine, and Fluorine in Hanford Phase II Vendor LLW Glasses*"; Proceedings of the SPECTRUM '96; vol. 1; Seattle, WA, August 18–23, **1996**; pp. 555–562.
9. Feng, X.; Freeman, C. J.; Luey, J.; Li, H.; Schweiger, M. J.; Gong, M. "*Chemical Behavior of P, S, Cl, F, and Cr in Borosilicate Nuclear Waste Glasses*"; *Abstract of the ACS National Meeting*; vol. 36; Division of Environmental Chemistry, Orlando, FL, August **1996**; pp. 44–46.

10. Vienna, J. D.; Schweiger, M. J.; Smith, D. E.; Smith, H. D.; Crum, J. V.; Peeler, D. K.; Reamer, I. A.; Musick, C. A.; Tillotson, R. D. "*Glass Formulation Development for INEEL Sodium-Bearing Waste*"; Report PNNL-12234, Pacific Northwest National Laboratory, Richland, WA, July **1999**.
11. Merrill, R. A.; Whittington, K. F.; Peters, R. D. "*Vitrification of High Sulfate Wastes*"; Report PNL-SA-24672, Pacific Northwest National Laboratory, Richland, WA, September **1994**.
12. Hay, M.; Coleman, C.; Hassan, N.; McCabe, D.; King, B.; Nash, C.; Saito, H.; Calloway, B.; Crawford, C. "*Sulfate Removal Studies for River Protection Project Part B1*"; Report WSRC-TR-2000-00489, Westinghouse Savannah River Company, Aiken, SC, March **2001**.
13. Lumetta, G. J.; Klinger, G. S.; Kurath, D. E.; Sell, R. L.; Darnell, L. P.; Greenwood, L. R.; Soderquist, C. Z.; Steele, M. J.; Urie, M. W.; Wagner, J. J. "*Removal of Sulfate Ion from AN-107 by Evaporation*"; Report PNWD-3036, BNFL-RPT-018, Rev. 0, Pacific Northwest National Laboratory, Richland, WA, July **2000**.
14. Fiskum, S. K.; Kurath, D. E.; Rapko, B. M. "*Development and Demonstration of a Sulfate Precipitation Process for Hanford Waste Tank 241-AN-107*"; Report PNWD-3050, BNFL-RPT-029, Rev. 0, Pacific Northwest National Laboratory, Richland, WA, August **2000**.
15. Kurath, D. E.; Bontha, J. R.; Blanchard, D. L. Jr.; Fiskum, S. K.; Rapko, B. M. "*Ion Exchange Studies for Removal of Sulfate from Hanford Tank Waste Envelope C (241-AN-107) Using Superlig® Resin*"; Report PNWD-3053, BNFL-RPT-036, Rev. 0, Pacific Northwest National Laboratory, Richland, WA, August **2000**.
16. Horwitz, E. P.; Schulz, W. W. Solvent extraction in the treatment of acidic high-waste: Where do we stand? In: "*Recent Advances in Metal Ion Separation and Preconcentration*"; Eds. Rogers, R. D.; Dietz, M. L.; Bond, A. H.; ACS Symposium Series; American Chemical Society, Washington, DC, **1999**, pp. 20–50.
17. Schulz, W. W.; Horwitz, E. P. (Eds.) "*Chemical Pretreatment of Nuclear Waste for Disposal";* Plenum Press: New York, **1994**.
18. Wymer, R. G.; Vondra, B. L. (Eds.) "*Light Water Reactor Nuclear Fuel Cycle";* CRC: Boca Raton, **1981**.
19. Musikas, C.; Schulz, W. W.; Liljenzin, J. -O. Solvent extraction in nuclear science and technology. In: *Solvent Extraction*: *Principles and Practice*, 2nd Ed.; Eds. Rydberg, J.; Cox, M.; Musikas, C.; Choppin, G. R.; Marcel Dekker: New York, **2004**, pp. 507–557.
20. Danesi, P.R. Supported liquid Membranes In: "Developments in Solvent Extraction"; Ed. Alegret, S.; Ellis Horwood: Chichester, **1988**, pp. 188–214.
21. Cecille, L.; Casarci, M.; Pietrelli, L. (Eds.) "*New Separation Chemistry Techniques for Radioactive Waste and Other Specific Applications";* Elsevier Applied Science: Amsterdam, **1991**.
22. Schulz, W. W.; Lombardo, N. J. (Eds.) "*Science and Technology for Disposal of Radioactive Tank Wastes";* Plenum Press: New York, **1998**.
23. Logsdail, D. H.; Mills, A. L. (Eds.) "*Solvent Extraction and Ion Exchange in the Nuclear Fuel Cycle";* Ellis Horwood Ltd: Chichester, **1985**.
24. Choppin, G. R.; Khankhasayev, M. K. (Eds.) "*Chemical Separation Technologies and Related Methods of Nuclear Waste Management";* Kluwer: Dordrecht, **1999**.
25. Norato, M. A.; Campbell, S. G.; Crowder, M. L.; Geeting, M. W.; Kessinger, G. F.; Pierce, R. A.; Walker, D. D. "*High-Level Waste Demonstration of the Caustic-Side Solvent Extraction Process with Optimized Solvent in the 2-cm Centrifugal Contactor Apparatus Using Tank 37H/44F Supernate*"; WSRC-TR-2002-00243, Rev. 0, Westinghouse Savannah River Company, Aiken, SC, November 1, **2002**.
26. Norato, M. A.; Fink, S. D.; Fondeur, F. F.; Kessinger, G. F.; Pierce, R. A.; Walker, D. D. "*Demonstration of Caustic-Side Solvent Extraction with Optimized Solvent in the 2-cm Centrifugal Contactor Apparatus Using Dissolved Salt Cake from Tank 37H*"; WSRC-TR-2002-00307, Westinghouse Savannah River Company, Aiken, SC, September 3, **2002**.

27. Leonard, R. A.; Aase, S. B.; Arafat, H. A.; Conner, C.; Falkenberg, J. R.; Regalbuto, M. C.; Vandegrift, G. F. "*Simulant Flowsheet Test with Modified Solvent for Cesium Removal Using Caustic-Side Solvent Extraction*"; Argonne National Laboratory Technical Report ANL-02/22, Chemical Technology Division, Argonne National Laboratory, Argonne, IL, April 22, **2002**.

28. Moyer, B. A.; Sachleben, R. A.; Bonnesen, P. V.; Presley, D. J. "*Calixarene Crown Ether Solvent Composition and Use Thereof for Extraction of Cesium from Alkaline Waste Solutions*"; U. S. Patent 6,174,503, January 16, **2001**.

29. Bonnesen, P. V.; Moyer, B. A.; Sachleben, R. A. "*Fluoro-alcohol Phase Modifiers and Process for Cesium Solvent Extraction*"; Application Serial No. 09/703,899 to U.S. Patent Office, November 2, **2000**.

30. Bonnesen, P. V.; Delmau, L. H.; Moyer, B. A.; Leonard, R. A. *Solvent Extr. Ion Exch*. **2000**, *18*, 1079–1108.

31. Leonard, R. A.; Conner, C.; Liberatore, M. W.; Sedlet, J.; Aase, S. B.; Vandegrift, G. F.; Delmau, L. H.; Bonnesen, P. V.; Moyer, B. A. *Sep. Sci. Technol*. **2001**, *36*, 743–766.

32. Bonnesen, P. V.; Delmau, L. H.; Moyer, B. A.; Lumetta, G. J. *Solvent Extr. Ion Exch*. **2003**, *21*, 141–170.

33. "*Department of Energy Record of Decision: Savannah River Site Salt Processing Alternatives*"; vol. 66(201); Federal Register, October 17, **2001**; pp. 52752–52756.

34. "*Design, Construction, and Commissioning of a Salt Waste Processing Facility*"; Request for Proposal No. DE-RP09-02SR22210, Amendment 002, U. S. Department of Energy, Savannah River Operations Office, Aiken, SC, January 9, **2002**.

35. Dietz, M. L.; Horwitz, E. P.; Rogers, R. D. *Solvent Extr. Ion Exch*. **1995**, *13*, 1–17.

36. Hofmeister, F. *Arch. Ex. Pathol. Pharmakol*. **1988**, *24*, 247–260.

37. Wuthier, U.; Pham, H.; Pretsch, E.; Ammann, D.; Beck, A.; Seebach, D.; Simon, W. *Helv. Chim. Acta* **1965**, *68*, 1822–1827.

38. Marcus, Y. *"Ion Properties"*; Marcel Dekker: New York, **1997**.

39. Moyer, B.A.; Bonnesen, P.V. Historical view on the development of anion coordination chemistry In: "*Supramolecular Chemistry of Anions*"; Eds. Bianchi, A.; Bowman-James, K.; García-España, E.; Wiley-VCH: New York, **1997**, Ch. 1 pp. 1–44.

40. Mason, S.; Clifford, T.; Seib, L.; Kuczera, K.; Bowman-James, K. *J. Am. Chem. Soc.* **1998**, *120*, 8899–8900.

41. Clifford, T.; Danby, A.; Llinares, J. M.; Mason, S.; Alcock, N. W.; Powell, D.; Aguilar, J. A.; Garcia-Espana, E.; Bowman-James, K. *Inorg. Chem*. **2001**, *40*, 4710–4720.

42. Aguilar, J. A.; Clifford, T.; Danby, A.; Llinares, J. M.; Mason, S.; García-España, E.; Bowman-James, K. *Supramolec. Chem*. **2001**, *13*, 405–417.

43. Mason, S.; Llinares, J. M.; Morton, M.; Clifford, T.; Bowman-James, K. *J. Am. Chem. Soc.* **2000**, *122*, 1814–1815.

44. Hossain, M. A.; Llinares, J. M.; Mason, S.; Morehouse, P.; Powell, P.; Bowman-James, K. *Angew. Chem., Int. Ed. Engl.* **2002**, *41*, 2335–2338.

45. Hossain, M. A., Llinares, J. M., Miller, C., Seib, L., Bowman-James, K., *Chem. Commun*. **2000**, 2269–2270.

46. Hossain, M. A.; Llinares, J. M.; Alcock, N. W.; Powell, D.; Bowman-James, K. *J. Supramolec. Chem*. **2002**, *2*, 143–151.

47. Gerasimchuk, O. A.; Mason, S.; Llinares, J. M.; Song, M.; Alcock, N. W.; Bowman-James, K. *Inorg. Chem*. **2000**, *39*, 1371–1375.

48. Wiórkiewicz-Kuczera, J.; Kuczera, K.; Bazzicalupi, C.; Bencini, A.; Valtancoli, B.; Bianchi, A.; Bowman-James, K. *New J. Chem*. **1999**, *23*, 1007–1013.

49. Kang, S. O., Hossain, M. A., Powell, D., Bowman-James, K., *Chem. Commun*. **2005**, 320–321.

50. Hossain, M. A.; Llinares, J. M.; Powell, D.; Bowman-James, K. *Inorg. Chem*. **2001**, *40*, 2936–2937.

51. Hossain, M. A.; Kang, S. O.; Llinares, J. M.; Powell, D.; Bowman-James, K. *Inorg. Chem.* **2003**, *42*, 5043–5045.
52. Kang, S. O.; Llinares, J. M.; Powell, D.; VanderVelde, D.; Bowman-James, K. *J. Am. Chem. Soc.* **2003**, *125*, 10152–10153.
53. Lee, H.-J.; Choi, Y.-S.; Lee, K.-B.; Park, J.; Yoon, C.-J. *J. Phys. Chem. A.* **2002**, *106*, 7010–7017.
54. Hossain, M. A.; Kang, S. O.; Powell, D.; Bowman-James, K. *Inorg. Chem.* **2003**, *42*, 1397–1399.
55. Kang, S. O.; VanderVelde, D.; Powell, D.; Bowman-James, K. *J. Am. Chem. Soc.* **2004**, *126*, 12272–12273.
56. Gale, P. A.; Sessler, J. L.; Král, V.; Lynch, V. *J. Am. Chem. Soc.* **1996**, *118*, 5140–5141.
57. Custelcean, R.; Moyer, B. A.; Sessler, J. L.; Cho, W.-S.; Gross, D.; Bates, G. W.; Brooks, S. J.; Light, M. E.; Gale, P. A. *Angew. Chem. Int. Ed.* **2005**, *44*, 2537–2542. *Angew. Chem.* **2005**, *117*, 2513–2518.
58. Anzenbacher, P. Jr.; Try, A. C.; Miyaji, H.; Jurisíková, K.; Lynch, V. M.; Marquez, M.; Sessler, J. L. *J. Am. Chem. Soc.* **2000**, *122*, 10268–10272.
59. Levitskaia, T. G.; Marquez, M.; Sessler, J. L.; Shriver, J. A.; Vercouter, T.; Moyer, B. A. *Chem. Commun.* **2003**, 2248–2249.
60. Sessler, J. L.; Katayev, E.; Pantos, G. D.; Ustynyuk, Y. A. *Chem. Commun.* **2004**, 1276–1277.
61. Sessler, J. L.; Katayev, E.; Pantos, D. G.; Scherbakov, P.; Reshetova, M. D.; Khrustalev, V. N.; Lynch, V. M.; Ustynyuk, Y. A. *J. Am. Chem. Soc.* **2005**, *127*, 11442–11446.
62. Moyer, B. A., Bonnesen, P. V., Chambliss, C. K., Haverlock, T. J., Marchand, A. P., Chong, H.-S., McKim, A. S., Krishnudu, K., Ravikumar, K. S., Kumar, V. S., Takhi, M. In: "*Nuclear Site Remediation: First Accomplishments of the Environmental Science Program*"; Eds. Eller, P. G.; Heineman, W. R.; ACS Symposium Series 778; American Chemical Society, Washington, DC, **2001**; pp. 114–132.
63. Levitskaia, T. G.; Bonnesen, P. V.; Chambliss, C. K.; Moyer, B. A. *Anal. Chem.* **2003**, *75*, 405–412.
64. Cafeo, G.; Gattuso, G.; Kohnke, F. H.; Notti, A.; Occhipinti, S.; Pappalardo, S.; Parisi, M. F. *Angew. Chem. Int. Ed.* **2002**, *41*, 2122–2126.
65. Kavallieratos, K.; Danby, A.; Van Berkel, G. J.; Kelly, M. A.; Sachleben, R. A.; Moyer, B. A.; Bowman-James, K. *Anal. Chem.* **2000**, *72*, 5258–5264.
66. Chrisstoffels, L. A. J.; de Jong, F.; Reinhoudt, D. N.; Sivelli, S.; Gazzola, L.; Casnati, A.; Ungaro, R. J. *J. Am. Chem. Soc.* **1999**, *121*, 10142–10151.
67. Kavallieratos, K.; Moyer, B. A. *Chem. Commun.* **2001**, 1620–1621.
68. Murad, M. M.; Hayashita, T.; Shigemori, K.; Nishizawa, S.; Teramae, N. *Anal. Sci.* **1999**, *15*, 1185–1189.
69. Mahoney, J. M.; Beatty, A. M.; Smith, B. D. *J. Am. Chem. Soc.* **2001**, *123*, 5847–5848.
70. Deetz, M. J.; Shang, M.; Smith, B. D. *J. Am. Chem. Soc.* **2000**, *122*, 6201–6207.
71. Shukla, R.; Kida, T.; Smith, B. D. *Org. Lett.* **2000**, *2*, 3099–3102.
72. Sisson, A. L.; Clare, J. P.; Taylor, L. H.; Charmant, J. P. H.; Davis, A. P. *Chem. Commun.* **2003**, *17*, 2246–2247.
73. Reichardt, C. "*Solvents and Solvent Effects in Organic Chemistry*"; 2nd ed.VCH: Weinheim, **1990**.
74. Duchemin, C. R.; Engle, N. L.; Bonnesen, P. V.; Haverlock, T. J.; Delmau, L. H.; Moyer, B. A. *Solvent Extr. Ion Exch.* **2001**, *19*, 1037–1058.
75. Levitskaia, T. G.; Moyer, B. A.; Bonnesen, P. V.; Marchand, A. P.; Krishnudu, K.; Chen, Z.; Huang, Z.; Kruger, H. G.; McKim, A. S. *J. Am. Chem. Soc.* **2001**, *123*, 12099–12100.
76. Král, V.; Sessler, J. L.; Shishkanova, T. V.; Gale, P. A.; Volf, R. *J. Am. Chem. Soc.* **1999**, *121*, 8771–8775.

77. Fricke, T.; Hamann, J.; Bahadir, M.; König, B. *Anal. Bioanal. Chem.* **2002**, *374*, 148–154.
78. Berrocal, M. J.; Cruz, A.; Badr, I. H. A.; Bachas, L. G. *Anal. Chem.* **2000**, *72*, 5295–5299.
79. Kato, R.; Nishizawa, S.; Hayashita, T.; Teramae, N. *Tetrahedron Lett.* **2001**, *42*, 5053–5056.
80. Kavallieratos, K.; Moyer, B. A. *Chem. Commun.* **2001**, 1620–1621.
81. Haverlock, T. J.; Bonnesen, P. V.; Sachleben, R. A.; Moyer, B. A. *J. Inclusion Phenom. Macrocyclic Chem.* **2000**, *36*, 21–37.
82. Kavallieratos, K.; Bryan, J. C.; Sachleben, R. A; Van Berkel, G. J.; Espetia, O. D.; Kelly, M. A.; Danby, A.; Bowman-James, K.; Moyer, B. A. Dual host combinations: Using tripodal amides to enhance cesium nitrate extraction by crown ethers, In: "*Fundamentals and Applications of Anion Separations*"; Eds. Moyer, B. A.; Singh, R.; ACS Symposium Series; Kluwer: New York, **2004**, pp. 125–150.
83. Antonisse, M. M. G.; Reinhoudt, D. N. *Electroanalysis* **1999**, *11*, 1035–1048.
84. Bonnesen, P. V.; Delmau, L. H.; Moyer, B. A.; Lumetta, G. J. *Solvent Extr. Ion Exch.* **2003**, *21*, 141–170.
85. Haverlock, T. J.; Bonnesen, P. V.; Moyer, B. A. *Solvent Extr. Ion Exch.* **2003**, *21*, 483–504.
86. Kavallieratos, K.; Bertao, C. M.; Crabtree, R. H. *J. Org. Chem.* **1999**, *64*, 1675–1683.
87. Fowler, C. J.; Delmau, L. H.; Ruas, A.; Moyer, B. A.; Bowman-James, K.; Sessler, J. L.; Shriver, J. A.; Marquez, M., unpublished results.

ROLE OF CATION COMPLEXANTS IN THE SYNTHESIS OF ALKALIDES AND ELECTRIDES

JAMES L. DYE, MIKHAIL Y. REDKO, RUI H. HUANG and JAMES E. JACKSON

Department of Chemistry, Michigan State University, East Lansing, MI 48824, USA

I. Introduction

The common understanding of chemists about "permissible" oxidation states underwent a profound change with the synthesis by Neil Bartlett in 1962 of the solid noble gas compound $Xe[PtF_6]$ (*1*). To be sure, unusual oxidation states of the elements could be achieved in dilute gases or by matrix isolation. But, to prepare macroscopic samples that could be put into bottles was a major breakthrough. In a

ADVANCES IN INORGANIC CHEMISTRY
VOLUME 59 ISSN 0898-8838 / DOI: 10.1016/S0898-8838(06)59006-3

similar vein, for over a century all chemistry textbooks assigned the oxidation state of 1+ to the alkali metals (lithium through cesium) in nearly all of their compounds. Thus, the synthesis of crystalline salts of the alkali metal *anions*, Na^-, K^-, Rb^-, and Cs^- (alkalides) ranks as a second major assault on conventional wisdom (*2,3*). Perhaps even more remarkable was the synthesis of crystalline salts called *electrides,* in which all the anions are trapped electrons (*4*). Alkalides and electrides owe their existence to the powerful cation complexing ability and resistance to reduction of crown ethers, cryptands, and their aza analogs. This paper reviews the requirements, design and methodology involved in the synthesis of alkalides and electrides, culminating with the recent designed synthesis of a thermally stable electride (*5*). The very interesting optical, magnetic, electrical, and structural properties of these materials have been reviewed extensively (*6–16*) and the details are beyond the scope of this article.

A. Historical Perspective

The reaction of alkali metals with protonating solvents such as water is well-known. Remarkably, nearly 200 years ago, shortly after his preparation of the alkali metals, Sir Humphrey Davy noted that:

> When 8 grains of potassium were heated in ammoniacal gas – it assumed a beautiful metallic appearance and gradually became of a fine blue colour.

Unfortunately, that observation lay buried in his lab book until recently (*17*), and the first published account of alkali metals in ammonia was that of Weyl in 1864, who described the formation of "metal ammoniums," formed by the interaction of alkali metals with liquid ammonia (*18*). Confusion about the nature of these solutions was cleared up by the classic work of Charles Kraus from 1907 to 1953 (*19,20*). He correctly identified the nature of solvated electrons and the conversion to the metallic state at high concentrations. The properties of alkali and alkaline earth metals in liquid ammonia have been studied by many investigators in the years since Kraus coined the term "solvated electrons" (*21*).

A natural extension of metal-ammonia research was the use of other solvents. As early as 1918, Gibson and Argo (*22*) obtain the optical spectra of solutions of all the alkali metals plus calcium in liquid methylamine ($MeNH_2$). Although they were unable to investigate the IR region, they did see a common absorption peak at about 650 nm. Blades and Hodgins in 1955 (*23*) and Hohlstein and Wannagat in 1957 (*24*) used mixtures of $MeNH_2$ and ethylamine ($EtNH_2$) with ammonia. Fowles, McGregor, and Symons in 1957 (*25*) and Windwer and Sundheim in 1962 (*26*) studied alkali metal spectra in ethylenediamine (en). The most comprehensive study of absorption spectra in en was done by Dewald and Dye in 1964 (*27*).

All of these investigators found both metal – dependent and metal – independent bands. For example, a common peak at about 650 nm was

found for Na, K, and Li in en. Another common peak at about 1250 nm for Li, Rb, and Cs (with a shoulder for K) was similar to the single metal-independent peak attributed to solvated electrons in ammonia. Yet intermediate peaks were also seen for K, Rb, and Cs. Attempts to explain these confusing results included "amine and aliphatic traps," (*23*), "ionic-covalent dimers" (*28*), and "colloidal suspensions" (*29*).

Everything fell into place in 1968 when Hurley, Tuttle, and Golden (*30*) prepared solutions and examined the spectra in all-quartz vessels and cells. All previous workers had failed to realize that the glass they used to prepare the metal solutions contained sodium borosilicate! Exchange of Na^+ from the glass by Li^+ or K^+ yielded a sodium species with both metals. It was soon realized (*31,32*) that the diamagnetic species responsible for this "V-band" was Na^- and that K^-, Rb^-, and Cs^- were responsible for the metal-dependent "intermediate bands." The assignment of the "IR band" of Li, K, Rb, and Cs to solvated electrons remained unchanged.

Although species of stoichiometry M^- were invoked in 1969, the nature of these entities was still in question. Proposals ranged from ion-triples, $e^-M^+e^-$, to ion-pairs between M^+ and "dielectrons", $e_2^=$, to "genuine" alkali metal anions. The latter had been identified in the gas phase with ionization potentials of the anions ranging from 0.62 eV for Li to 0.47 eV for Cs (*33*). Although the existence of "genuine" alkali metal anions in solution seemed contrary to conventional wisdom, the completion of the outer *s* shell and the stability of M^- in the gas phase, made its existence in solution reasonable. Finally, in 1974, the ^{23}Na NMR spectra of solutions proved conclusively that "genuine" spherical Na^- anions were present (*34*). The stage was set for the formation of alkalide salts, but the low solubility of alkali metals in amine solvents made preparative chemistry difficult.

B. Alkali Metal Solubilization with Cation Complexants

When Pedersen and Lehn published their first papers on crown ethers and cryptands respectively (*35,36*), it became apparent that these complexants could compensate for the low solubility of alkali metals in amine and ether solvents. Indeed, the effects were remarkable. Simple equilibrium reactions and LeChatelier's Principle worked to greatly enhance metal solubility according to the equations:

$$2M(s) \rightleftharpoons M^+ + M^- \quad K_1 = K_{sp} = [M^+][M^-] \tag{1}$$

$$M^+ + nL \rightleftharpoons M^+L_n n = 1 \text{or} 2; \quad K_2 = [M^+L_n]/[M^+][L]^n \tag{2}$$

$$M^- + nL \rightleftharpoons M^+L_n + 2e^-_{solv} \quad K_3 = [M^+L_n][e^-_{solv}]^2/[M^-][L]^n \tag{3}$$

The enhancement in solubility was quickly confirmed (*32*). An added bonus was the ability to alter the ratio of e^-_{solv} to M^- in solution by

controlling the concentration and nature of the cation complexant, L. The solubility enhancement is remarkable! For example, no color is seen when K metal is added to dimethyl ether (Me_2O). This means that its concentration is 10^{-4} M or less. By adding 15-crown-5 (15C5, **1**, $n = 0$) to form the sandwich complex $K^+(15C5)_2$, the solubility increases to at least 0.4 M. In the absence of the complexant we have $[M^+] = [M^-] \leq 10^{-4}$ M so that $K_1 \leq 10^{-8}$ M^2. When 15C5 is added, such that $[K^+(15C5)_2] = [K^-] = 0.4$ M, we get $K_2 \geq 10^8$ M^{-2}. Whatever the exact values, the important feature is that the concentrations of complexed cations and alkali metal anions are high enough to permit bulk chemistry to be carried out with such solutions.

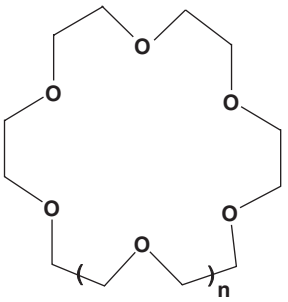

1

C. Solvent Properties

The properties of the solvents that can be used for metal solubility are important. That they are resistant to reduction by alkali metals is paramount. Primary amines are acceptable, but decomposition by proton abstraction from the R-NH_2 group makes it necessary to utilize pure solvents and low temperatures. The importance of high purity can be illustrated by our work with solutions of Cs in en (*37*). Normal purification of ethylenediamine by distillation from Na-K alloys permits formation of reasonably stable solutions with lifetimes of minutes to hours at room temperature. By first using a fractional freezing technique to purify the ethylenediamine, we were able to prepare 10^{-4} M solutions of Cs that were stable for many hours at room temperature. Solvents such as Me_2O and trimethylamine (Me_3N), with no acidic protons and no β hydrogens are very resistant to reduction. The former, with a dielectric constant of 6.3 at –30°C (about the same as that of THF at room temperature) is an excellent solvent when cation complexants are used. Trimethylamine, with a dielectric constant of only 2.4 makes an ideal precipitation and washing solvent. Even a good complexant cannot yield high metal solubility in such a low polarity solvent. However, if the solvent polarity is too high, as with NH_3, cation solvation competes with complexation and Eq. (2) above tends to be reversed. Of course, the solvation energy of the electron

also plays a role. In such solvents, metal anions are absent because the equilibrium

$$M^- \leftrightharpoons M^+_{solv} + 2e^-_{solv} \tag{4}$$

lies far to the right.

D. Prospects for Crystalline Alkalides and Electrides

The preparation of concentrated solutions that contained complexed alkali cations and alkali metal anions prompted us to consider the possibility that solid salts might be made by rapid solvent evaporation or crystallization. For example, a solution of sodium metal in $MeNH_2$ or $EtNH_2$ with cryptand[2.2.2] (C222, **2**, $n = 1$) consists primarily of Na^+(C222) and Na^- at concentrations as high as 0.5 M. By 1972 we had shown the generality of formation of solutions of all the alkali metals in the presence of crown ethers and cryptands in a number of solvents (*32,38,39*). We had also shown (*40*) that Na^- could be formed by pulse-radiolysis of solutions of NaBr in en via the reaction

$$Na^+ + 2e^-_{solv} \leftrightharpoons Na^- \tag{5}$$

This reaction was also observed by stopped-flow studies of the reaction of sodium salts with Cs and K in en (*37*).

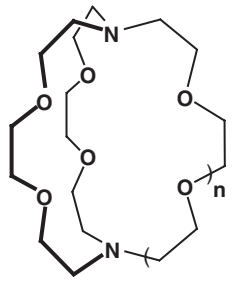

2

At the third Colloque Weyl (1972) on "Electrons in Fluids," Dye noted the following (*41*):

> If, indeed, identifiable alkali anions exist in metal solutions rather than just agglomerates of "old" species, then there is cause for excitement. The isolation of salts becomes a real possibility and the availability of new reducing agents varying from Na^- to Cs^- may be of utility in synthetic work.

A proposal to prepare a crystalline salt of Na^-, presented at an in-house seminar to faculty members at Michigan State University in March 1973, was met with considerable skepticism. After many years of hearing from colleagues and in the classroom that alkali metals are

characterized by the 1+oxidation state, chemists found it hard to believe that a compound with Na in the 1−oxidation state could be synthesized as a crystalline solid!

The possibility that a solid compound, $Na^+(C222)Na^-$, could be formed was enhanced by ^{23}Na NMR studies of exchange rates between free Na^+ and $Na^+(C222)$ in en, obtained by Ceraso and Dye in 1973 (*42*). This study yielded the first observation of separate signals from Na^+ in two environments. Extrapolation of the rate of dissociation of the complex $Na^+(C222)$ to –70°C indicated a half-life of about 20 h. This suggested that rapid evaporation of a solution of $Na^+(C222)Na^-$ in an amine solvent might permit the formation of a solid salt before reversion to the metal and free complexant could occur.

In October 1973, Joseph Ceraso attempted to measure the ^{23}Na NMR spectrum of a solution of $Na^+(C222)Na^-$ in $EtNH_2$ to see if he could obtain separate signals from $Na^+(C222)$ and Na^- (*34*). He needed a concentrated solution and wanted to work at low temperatures to minimize decomposition. When he cooled a concentrated solution from –30°C to –78°C, bright gold crystals precipitated from solution. The first crystalline salt of an alkali metal anion had been prepared! Furthermore, this first sodide was not only kinetically stable, but also thermodynamically stable to dissociation to the metal and complexant.

E. Crystal Structures

To convince the chemistry community that we had a "genuine" sodide salt would have been difficult without a crystal structure. Fortunately, Frederick Tehan in our lab persisted in growing and testing crystals of $Na^+(C222)Na^-$ until he found two (out of about 100) that were of high enough quality to obtain a structure and stable enough to determine the structure at room temperature (*3*). We naturally assumed in 1974 that many other alkalide structures would quickly follow, but it took a dozen years to develop the synthesis and handling techniques that permitted determination of the crystal structures of these reactive and unstable compounds. A review in 1996 (*14*) listed the crystal structures of 29 alkalides with complexed cations of all the alkali metals and with all of the alkali metal anions except Li^-. Structures of nine alkalides obtained since 1996 are listed in Table I.

The continuing search for crystalline alkalides and for corresponding materials with trapped electrons as anions (electrides) was given impetus by the ability to deposit thin, solvent-free films on the windows of optical cells. Flash evaporation of $MeNH_2$ from solutions that contained complexed cations and either alkali metal anions or solvated electrons left solvent-free solid films whose optical spectra could be measured. Such spectra were first obtained in Strasbourg with J. M. Lehn in 1976 (*43*). Although "blue powders" had been observed earlier (*3,44*) by evaporation of solutions that contained complexed M^+ and e^-_{solv}, the film spectra gave the first direct evidence for solid electrides

TABLE I

STRUCTURES OF ALKALIDES AND ELECTRIDES SINCE 1996 LISTING

Compound	Space group	Z	Cell parameters	R(%)	REF
$Ba^{+2}(H_5Aza222^{-})Na^{-} \cdot 2MeNH_2$	Mono. Cc	4	17.746,10.375,34.116, $\beta = 91.29$	7.23	(*74*)
$Na^{+}(TriPip222)Na^{-}$	Orth. Pccn	8	11.074,14.812,18.825	14.6	(*5*)
$Na^{+}(TriPip222)e^{-}$	Orth. Pccn	8	10.703,14.608,18.606	11.1	(*5*)
$Li^{+}(C211)Cs^{-}$	Mono C2/m	4	23.747,13.434,8.212 $\beta = 75.340$	9.8	(*78*)
$Rb^{+}(C222)e^{-}$	Tri P-1	2	8.730,11.565,13.947 $\alpha = 64.195$, $\beta = 71.931$, $\gamma = 84.744$	14.5	(*90*)
$K^{+}(Me_6Aza222)K^{-}$	[a]	2	15.44		(*53*)
$K^{+}(Me_5Aza222)Na^{-}$	[a]	2	15.24		(*53*)
$H^{+}(Adz)Na^{-}$	[b]	2	8.865,8.864,31.4578		(*66*)
$Cs_2^{+}(21C7)_2Na^{2-}$	Tri P1	2	10.469,10.032,12.708 $\alpha = 90.919$, $\beta = 73.385$, $\gamma = 107.453$	6.3	(*91*)
$K_2^{+}(21C7)_3Na_2^{-} \cdot MeNH_2$	Mono P21/n	2	9.140,36.574,19.475 $\beta = 94.63$	10.2	(*91*)
$K^{+}[24C8(C4H8)_2]Na^{-}$	Orth P212121	2	10.439, 10.954, 27.773	14.7	(*91*)

[a]Unable to refine structure; apparently cubic.
[b]Unable to refine structure; apparently orthorhombic.

and permitted introduction of the *electride* name for this new class of compounds. Electride powders and films were studied by various techniques for the next 10 years, culminating in the first electride crystal structure in 1986 (*4*). Since then, six additional electride structures have been determined, finally leading to the recent designed synthesis of a thermally stable electride that can be studied at room temperature (*5*). Structural information about the two electrides synthesized since the 1996 listing (*14*) are given in Table I.

II. Thermodynamics

A. SOLUTION EQUILIBRIA

Solid alkalides and electrides are formed by precipitation, crystallization or solvent evaporation from solutions that contain complexed cations and either alkali metal anions or solvated electrons. Cation complexation (Eq. (2)) provides the major driving force by converting the solvated cation into the complexed cation. Other solution equilibria are important in determining whether an alkalide or an electride will form and which alkalide is formed when two different metals are used in the synthesis.

No quantitative equilibrium data are available for complexant-free alkali metal solutions in the solvents used to synthesize alkalides and electrides ($MeNH_2$, $EtNH_2$, Me_2O). But the general trends can be predicted from solubility and optical absorbance data in ethylenediamine. Absorbance data, combined with approximate extinction coefficients of e^{-}_{solv} and M^{-}, yield the approximate concentration equilibrium

constants for Eq. (4)

$$K_4 = [M^+][e^-_{solv}]^2/[M^-].$$

Data from three sources (*27,45,46*) yield $10^6 K_4 = 3 \times 10^{-5}$, 2, 0.02–0.1, 40, for Na, K, Rb, and Cs, respectively. The most striking feature of these data is the extraordinary stability of Na^- to dissociation into solvated Na^+ and solvated electrons compared with the other alkali metals. Recall that Li^- has never been observed in solution, so lithium solutions always yield Li^+ and e^-_{solv} It appears that K^- has a greater tendency than Rb^- to form e^-_{solv} and that Cs^- readily produces solvated electrons.

Of course, just as the metal solubility is greatly enhanced by complexation of the cation, Eq. (4) is shifted to the right by cation complexation. This gives us some control over the solution composition. When the concentration of the complexant is one half that of the total dissolved metal, the solution contains primarily M^+L and M^- (except when M = Li). An increase in the complexant concentration generally increases the ratio e^-_{solv}/M^-, although, as noted above, when M = Na, the effect is small. The synthesis of alkalides and electrides generally reinforces these trends. Until the latest synthesis (*5*), we were unable to make any electride with Na^+L as the counter-ion because sodides always formed. Lithium forms only electrides while both alkalides and electrides can be made with K, Rb, and Cs. Mixed alkalides, in which the cation and anion are different alkali metals can also be made. Whenever sodium is present in equimolar amounts to another alkali metal, a sodide forms, as long as the complexant is capable of tying up the other alkali metal cation.

B. Thermodynamics of Formation of Crystalline Alkalides and Electrides

After we had synthesized the first alkalide, Na^+(Cryptand[2.2.2])Na^-, a number of questions came to mind: How general is this process? Can we estimate what alkalides are possible? What about electrides? Can metal anions be prepared with other elements than alkali metals? To provide plausible answers to these questions we developed a modified Born–Haber cycle (*47*) to permit rough estimates of ΔH° and ΔG° to be made for reactions of the type

$$nL(s) + M_a(s) + M_b(s) \rightarrow M_a^+ L_n M_b^-(s) \quad (6)$$

$$nL(s) + M(s) \rightarrow M^+ L_n e^-(s) \quad (7)$$

in which L is the complexant, $n = 1$ or 2, and M_a and M_b are the same or different metals.

At the time these estimates were made, we had determined the crystal structure of only one alkalide, $Na^+(C222)Na^-$. But the predictions made by this approximate method guided the synthesis of other alkalides and provided impetus for the synthesis of electrides. Although new measurements and calculations could improve the reliability of Born–Haber cycle estimates, the general trends developed in 1979 should still be valid. In addition to salts of the alkali metal anions, these calculations suggested that complexation of alkali cations by cryptands might lead to salts that contain Au^-, Ag^-, or even Cu^-. About the time that our manuscript was submitted to *Angewandte Chemie*, Lagowski, and coworkers prepared liquid ammonia solutions of alkali metal aurides, M^+Au^- (*48*). Later, solid salts of $M^+(C222)Au^-$ (with M = K, Rb, Cs) were prepared and studied (*49,50*) as well as tetramethylammonium auride (*51*). More recently, Tran and Lagowski reported evidence for Ag^- in liquid ammonia (*52*). Estimates from Born-Haber cycles (*47*) show that complexed alkaline earth cations such as $Ba^{2+}(C222)$ should form salts of Au^-, Ag^-, and Cu^- that are stable with respect to the elements and C222. The roadblock to formation of such salts has been decomposition of the complexant. Perhaps the aza-complexants described recently (*5,53*), which are very resistant to reductive decomposition, could lead to stable crystalline solids that contain these anions. It should be noted that salts that contain other monovalent metal anions from the alkaline earth and transition metal regions of the periodic table are predicted to be thermodynamically unstable. Platinum might be an exception because of the large electron affinity of Pt atoms. But the very large lattice energy of Pt(s) makes this unlikely.

As useful as the Born-Haber cycle calculations are, they are *quantitatively* incorrect since they predicted that $Na^+(C222)Na^-$ should be thermodynamically unstable to dissociation into C222(s) and 2Na(s) by some $+28\,kJ\,mol^{-1}$ [later (*54*) modified to $+22\,kJ\,mol^{-1}$]. Yet this compound does form, providing experimental proof that the estimate of ΔG_6^0 was in error! Collaboration with U. Schindewolf in 1982 yielded the first *experimental* determination of the thermodynamics of formation of $Na^+(C222)Na^-$ (*55*) that was later extended by using cryptand[2.2.1] (**2**, $n = 0$) to $Na^+(C221)Na^-$ (*54*). The key to these studies was the use of an electrode that is reversible to Na^+ by virtue of an Na^+-β-alumina membrane. The emf of the cell (for C222 as complexant)

$$Pt|Na(s)|Na^+ - \beta\text{-alumina}|Na^+(C222)Na^-(sat),\ C222(sat)|Pt$$

is independent of the solvent used as long as saturation of both the sodide and the complexant are maintained. The emf, E, then depends only on temperature and yields the thermodynamic values for the reaction.

$$2Na(s) + C222(s) \rightarrow Na^+(C222)Na^-(s) \qquad (8)$$

$\Delta G^0_8 = -2F\mathrm{E}$; $\Delta S\,^0_8 = 2F(\mathrm{d}E/\mathrm{d}T)$, in which F is the value of the Faraday. For $Na^+(C222)Na^-$, this yields $\Delta H^0_8 = -34 \pm 2\,\mathrm{kJ\,mol^{-1}}$ and $\Delta S^0_8 = -90 \pm 8\,\mathrm{J\,mol^{-1}\,K^{-1}}$ while the corresponding values for $Na^+(C221)Na^-$ are $\Delta H^0 = -37 \pm 3\,\mathrm{kJ\,mol^{-1}}$ and $\Delta S^0 = -83 \pm 8\,\mathrm{J\,mol^{-1}\,K^{-1}}$, respectively. The values of ΔH^0 are reasonably close to the estimates from the Born–Haber cycle (–35 and $-31\,\mathrm{kJ\,mol^{-1}}$ for C222 and C221, respectively) but the estimates of ΔS^0 are very different (–190 and $-140\,\mathrm{J\,mol^{-1}\,K^{-1}}$, respectively). Thus, the experimental entropy changes for formation of the crystalline salts are considerably less negative than the predictions of the cycle. The difference is probably caused by the neglect of changes in the configuration entropy of solvent and complexant in the steps

$$M^+L(sol) \rightarrow M^+L(g) \tag{9}$$

and

$$M^+_a L(g) + M^-_b(g) \rightarrow M^+_a L M^-_b(s) \tag{10}$$

The estimates were based on the entropy changes expected for hard spheres. Such calculations may be valid for alkali halides but not for species as complex as crown ethers or cryptands.

Since our original estimates were made, there have been a number of studies of the gas-phase complexation of alkali cations by various complexants (*56*). Thus, it is tempting to construct a Born–Haber type cycle based on these measurements. But the problem encountered is that the gas-phase conformations of metal ions bound to cryptands, for example, may not be the same as in solution or the solid state. For example, gas phase studies (*56*) show stronger binding of Na^+ by C211 than by either C222 or C221 – clearly not the case in solution. A stronger argument can be made for *theoretical* calculations of comparative gas phase binding energies of various complexants as was done for our recent ligand design considerations (*5*). However, such calculations do not provide information about the entropy change that occurs upon complexation.

III. Complexant Properties

A. Reducible Groups Ruled Out

There are a large number of macrocyclic and macrobicyclic complexants for alkali metal cations. In fact, even a molecular complexant as simple as ethylenediamine forms a crystalline sodide, $Li^+(en)_2Na^-$ (*57*). There is also evidence that solid sodides are formed in the Li-$EtNH_2$-Na (*58*) and Li-$MeNH_2$-Na (*59*) systems. But all of these sodides are subject to decomplexation and/or decomposition below 0°C, and we have not yet been able to obtain their crystal structures.

Clearly, macrocyclic complexation is important for stabilization of crystalline alkalides and electrides.

As with solvents for alkali metals, complexants must not contain easily reducible groups. Thus, the numerous cation complexants that contain acidic protons, carbonyl oxygens, reducible aromatic groups, amides, alcohols, etc. are clearly not candidates for alkalide or electride synthesis. Hydrogens on the nitrogens of primary and secondary amines are on the borderline, but complexants with these functionalities are subject to decomposition by reaction of M^- or e^- with the somewhat acidic amine hydrogens. Also, of course, the complexant must contain polar atoms or groups that can interact with the cation, so hydrocarbon chains alone cannot form the "arms" of a complexant. These restrictions leave ether oxygens and tertiary amine nitrogens as the best polar constituents of complexants for encapsulation of M^+ in the presence of M^- or e^-.

B. Complexation of Alkali Cations

Although alkalide and electride films can be prepared by direct codeposition of complexants and alkali metals (*60–65*), crystals must be grown from a solution that contains alkali metals and the complexant. This means that the complexant must be able to compete with cation solvation so that concentrated solutions of M_a^+L and either M_b^- or e_{solv}^- can be formed. The ether oxygens in crown ethers and cryptands are ideal for interaction with the "hard" alkali cations. The high dipole moment provided by ether oxygens results in strong ion-dipole interactions that can compete with ion-solvent forces. In addition, the presence of two lone pairs on oxygen makes the angular range for coordination of M^+ by ether oxygen large, so that a range of complexant conformations can be accommodated. These considerations show why crown ethers and cryptands were the complexants of choice for the early synthesis of alkalides and electrides. Yet the thermodynamic estimates and measurements described in Section II-B show that even $Na^+(C222)Na^-$ has only marginal stability with respect to the formation of Na(s) and C222(s). Thus, the ability of the complexant to strongly bind the alkali cation is paramount in preventing *decomplexation* of the cation by reversal of Eq. (6).

Aza complexants must rely on N-M^+ binding, which is intrinsically weaker than that of O–M^+. In addition, with only one lone pair on nitrogen, the angular requirement for optimal orientation of the lone pair with respect to the cation restricts the conformational freedom of the aza complexant. (See Fig. 1 of Ref. (*5*) for a comparison of O and N in this regard.) Unless the free complexant has a conformation similar to that of the complex, there is both an enthalpy and an entropy "cost" associated with the reorganization required for cation complexation.

Since ΔS for both reactions (6) and (7) is negative, $M_a^+LM_b^-$ and $M^+L \cdot e^-$ can be thermodynamically stable at low temperatures, but

they could *decomplex* to form the alkali metal or alloy and free complexant as the temperature is increased. This is a common occurrence with aza-complexants, but it is irreversible *decomposition* of oxa–complexants (to be considered later) rather than decomplexation that limits the temperature stability of alkalides and electrides that contain crown ethers and cryptands.

Until recently, stability toward decomplexation was dictated by thermodynamic considerations. It is also possible, however, to prevent decomplexation on the basis of kinetics. The most striking example is "inverse sodium hydride" (*66*) in which the proton is kinetically trapped in an adamanzane molecule, **3**. Another example is Na^+(TriPip)e^-, in which TriPip, **4**, is the recently designed and synthesized aza ligand with piperazine rings in each of the three "arms" (*5*). This electride is stable to about +45°C, at which temperature Na^+(TriPip) decomplexes and forms the sodide, Na^+(TriPip)Na^-, plus free TriPip. The sodide, in turn is stable to ~100°C, at which temperature the remaining Na^+(TriPip) decomplexes to form sodium metal and free (and partially decomposed) complexant. Because the kinetics of complex formation and dissociation are slow, it is necessary in these cases to form the cation complex at higher temperatures with a counter-ion that is subsequently displaced by e^- or M^-. The requirements for such *metathesis* reactions are considered later.

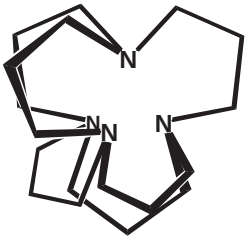

3

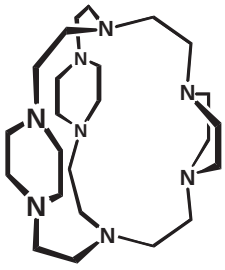

4

C. Complexant Stability

Research with alkalides and electrides would certainly have been simpler if crown ethers and cryptands were able to withstand the strong reducing power of alkali metal anions and trapped electrons. While reaction with air and moisture is intrinsic to these species, avoidance of such contaminants is easy. But when the reducing anion reacts with the complexant spontaneously, there is nothing one can do to prevent decomposition except to keep the temperature low enough to remain below the kinetic barrier. The oxa-complexants, such as crown ethers and cryptands are subject to C–O–C bond cleavage. Jedlinski, et al. showed (*67*) that $K^+(18C6)_2K^-$ in THF solution

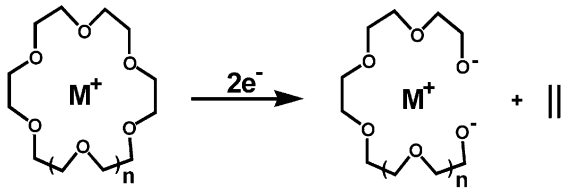

SCHEME 1.

decomposed in a manner expected for dimethylene fragments as leaving groups, resulting in the formation of ethylene and polyethylene glycol di-potassium salts. In our study of the decomposition products of some thirty solid alkalides and electrides that contained CH_2-O-CH_2-CH_2-O-CH_2 groups (*68*), we found that in all cases the initial products were ethylene and a glycolate. For example, crown ether-based alkalides and electrides decomposed as shown in Scheme 1.

Surprisingly, the ethylene that formed (or when C_2D_4 was added) was further reduced on standing to form ethane and butane products. The source of the extra hydrogens in the alkanes formed when ethylene is allowed to react with the solid alkalide or electride remains undetermined, but is likely to be other complexant molecules, the only H-containing species in the crystals.

We have known since 1989 that tertiary amine complexants are very resistant to reduction (*69*). Crystalline sodides were obtained with K^+, Rb^+, or Cs^+ complexed by hexamethyl hexacyclen (HMHCY), **5**, the permethylated peraza analogue of 18C6. The strong cation binding in these compounds results from the ability to form a "cage" around M^+ with coordination by all six nitrogens and four of the methyl groups completing the top of the cage. Additional stabilization results from the formation of a contact ion-pair between Na^- and the complexed cation (K^+, Rb^+, or Cs^+) via the open face of the cage. The structure of the K^+(HMHCY)Na^- unit is shown in Fig. 1.

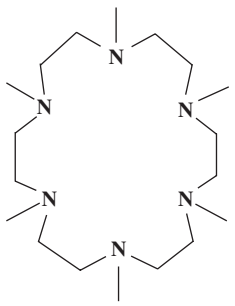

5

The remarkable resistance to irreversible reduction of HMHCY was shown by Differential Scanning Calorimetry (DSC) studies of

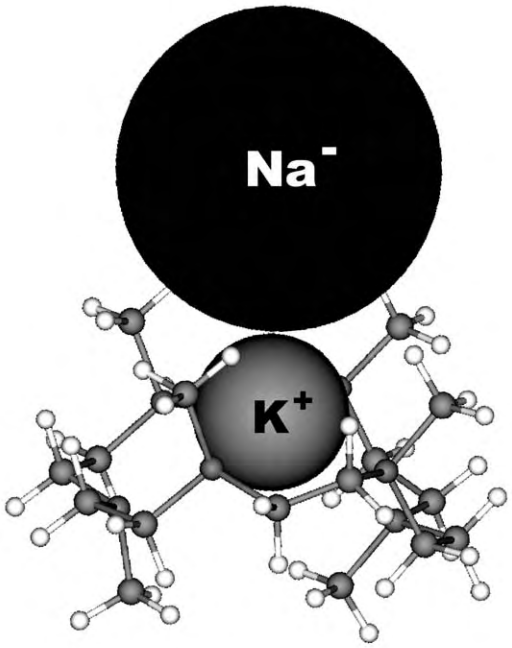

FIG. 1. Ion-pair formation in K^+(HMHCY)Na^-. Ion sizes are drawn to scale. The hexamethyl hexacyclen complexant (HMHCY) is depicted in the ball-and-stick mode.

K^+(HMHCY)Na^-. The compound melted at ~40°C and decomplexed completely at 60–70°C. Decomposition of the complexant did not occur until ~120°C. The DSC results were verified by visual observations and repeat formation of the sodide from a previous metal sample. The decomplexation is thermodynamically favored at room temperature but the process is slow. Samples left at room temperature for about four days underwent decomplexation. We concluded that K^+(HMHCY)Na^- is thermodynamically stable below about 0°C and very slow to decomplex at room temperature. Similar stability against reductive decomposition of peraza complexants TMPAND (**6**) and Me_6 Aza[2.2.2] (**7**) was observed for Li^+(TMPAND)Na^- (*70*) and K^+(Me_6 Aza[2.2.2])M^- (with M = Na & K) (*53*). However, in neither case were we able to prepare electrides. The strategy needed to prepare thermally stable alkalides and electrides was clear. We had to design tertiary amine aza-cryptands with complexing ability for M^+ comparable to oxa-cryptands. Since the latter were already on the borderline of thermodynamic stability, the new complexants needed to be pre-organized in a configuration similar to that of the complex, in order to minimize the enthalpy and entropy costs associated with cation complexation.

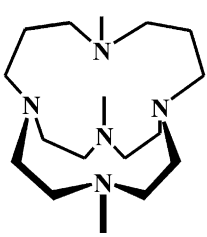

6

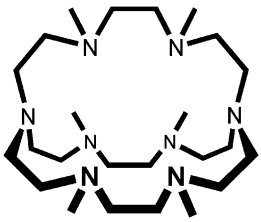

7

IV. Synthesis Methodology

A. Direct Combination

Direct combination of alkalides and electrides by reaction between a complexant and an alkali metal in solution is straightforward. It is only necessary to co-dissolve the alkali metal (or pair of alkali metals) in a solvent with the aid of a suitable cation complexant, decrease the solvent polarity by adding a less polar cosolvent, and grow crystals by slow cooling or slow evaporation of the more volatile polar solvent. There is, however, an important caveat; purity of solvents, complexants, and metals is of paramount importance. Reducible impurities not only remove alkali metal, but the reaction products often catalyze decomposition of the solutions. This is particularly troublesome when liquid ammonia and methylamine are the primary solvents, probably because of catalytic decomposition in the presence of the strongly basic amides. When one is fortunate enough to be able to use dimethylether as the primary solvent, these problems are greatly diminished. Yet, even in such cases, care must be taken to use pure complexants with the complete exclusion of air and moisture.

The synthesis methods that use "K-cells" have been described in detail elsewhere (*6*). These two-compartment cells are loaded with weighed amounts of alkali metals and complexants in a glove box and attached to a vacuum line for synthesis. We have found it very convenient to use a dual vacuum line, flexible stainless steel tubing, and Ultra-Torr fittings as described in detail by Wayda and Dye (*71*). This permits easy manipulation of the K-cells, cooling of one or both compartments in a Dry-Ice isopropanol bath and filtration. Purified solvents are distilled into and out of the cells as needed. A glass frit between the two compartments permits easy washing of the solid products with a solvent such as trimethylamine or pentane in which the alkalides or electrides are insoluble, but organic complexants and byproducts are soluble. Although some single crystal samples have been prepared by slow evaporation of Me_2O from a mixture with Me_3N or Et_2O, most crystals were grown by cooling saturated solutions from $\sim$–40°C to –70°C over a period of several days.

B. Metathesis

The direct combination methods described above work well when the rate of encapsulation of the metal is fast enough at the low temperatures required for syntheses. When, however, this rate is slow or when the free complexant cannot be made, the synthesis must use a salt, M^+LX^-, that has the cation pre-encapsulated. For example, H^+ cannot be removed from the 3^6 adamanzane (Adz) cage of **3**, so that the synthesis of "inverse sodium hydride", $AdzH^+Na^-$, required a metathesis reaction between a salt such as $AdzH^+HOCH_2COO^-$ and Na in liquid ammonia (*66*). Similarly, while the sodide, $Na^+(TriPip)Na^-$ could be made by direct combination, the electride $Na^+(TriPip)e^-$ required the use of a pre-formed salt (*5*).

Metathesis methods require prior formation of a salt of the complexed cation with an anion that can be removed from the metal solution in NH_3 or $MeNH_2$ by precipitation or reduction to an insoluble product. A major problem is the generally low solubility of such salts in liquid NH_3 and/or NH_3-$MeNH_2$ mixtures. The large size and hydrophobic exterior of the complexed cations leads to low cation solvation energies, so the anion needs to have a strong enough affinity for ammonia to yield sufficient solubility of M^+LX^-. At the same time, X^- must either form an insoluble salt with added alkali metals or be reduced to a product that is insoluble. Since salts of multiply charged anions are generally insoluble in NH_3 and $MeNH_2$, the most effective way to remove X^- during alkalide or electride synthesis is by reduction to form a dianion or trianion that can combine with the cations present to form an insoluble salt.

Salts that were used in the synthesis of $AdzH^+Na^-$ included the nitrate, glycolate, and isethionate anions (*66*). Excess sodium reduced the latter two to molecular hydrogen and insoluble sodium salts of the dianions, but low solubilities of the precursor salts resulted in poor yields of the desired product. The synthesis of $Na^+(TriPip)e^-$ first utilized the salt of the 2-anthraquinone anion, **8,** but low solubility was a major problem. After a lengthy search for a better "sacrificial anion," we found that the salt $Na^+(TriPip)$ $TAPS^-$ was highly soluble in ammonia and easily reducible to form an insoluble lithium salt (*5*). The formula for TAPS is given by **9**. It is likely that this will be the anion of choice for future syntheses by metathesis in liquid ammonia and/or methylamine.

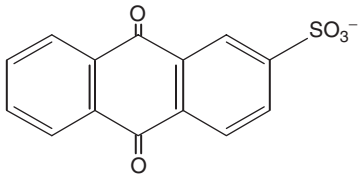

8

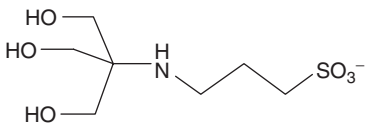

9

V. Structural Features of Alkalides

A. Isolated Anions

The structures of 12 alkalides are similar to corresponding salts that have "ordinary" spherical anions such as iodides. The complexants and anions form close-packed structures with anionic sites that are well separated from each other. For example, Fig. 2A shows clearly the separation of the Na^- ions in Na^+(TriPip)Na^-. Similar packing occurs for the other alkalides that have isolated anions.

Even when the alkalide contains the same alkali metal in two oxidation states, there is no perceptible charge-transfer from the anion to the cation. This is clearly shown for example, by the ^{23}Na MAS NMR spectrum of Na^+(C222)Na^- (72). The chemical shifts of Na^+ in the sodide and the corresponding iodide are –24 and –21 ppm respectively, while that of Na^- is at –61 ppm, which is within 1 ppm of the calculated value of Na^-(g). For isolated K^-, Rb^-, and Cs^- in solid alkalides the differences from the gas phase chemical shifts are 1, 20 and ~150 ppm, respectively. The heavier alkali metal anions are more strongly perturbed, presumably because of the introduction of orbital angular momentum into the ground state via interaction of complexant electron density with the filled outer *p* orbitals. The structures and NMR spectra verify the salt-like character of crystalline alkalides, thus justifying the representation $M_a^+LM_b^-$.

The addition of an electron to the alkali metal atom to form M^-, with two electrons in the outer *s* orbital, results in large, polarizable anions. Fig. 3 shows the relative diameters compared with that of I^-. The

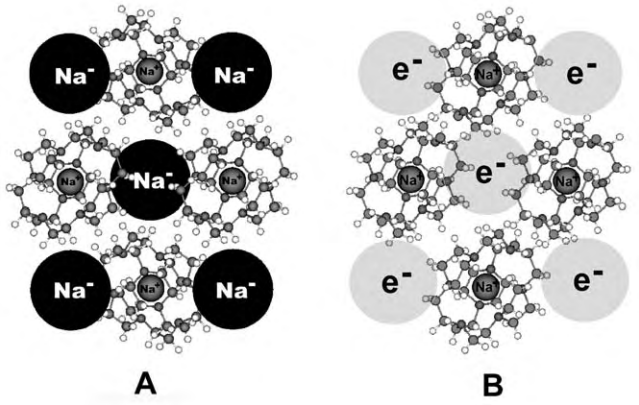

Fig. 2. The sodide (A) and electride (B) structures that have Na^+(TriPip222) as the counter-ion. Note that the Na^- ions in the sodide are isolated from each other. The two crystals are isostructural. The electron density in the electride is represented by the shaded area, but also extends through the channels that connect the cavities.

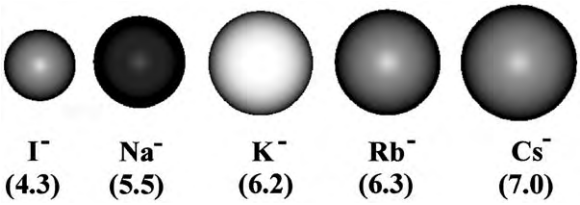

FIG. 3. Representation of the sizes of alkali metal anions compared to that of the iodide ion. The values in parentheses are the average diameters in Ångstroms.

volume occupied by Cs^- is more than four times that of I^-. Cs^- holds the current record as the largest monatomic species in the periodic table!

B. Dimers, Chains and Ion-Pairs

Alkali metals in the gas phase can form dimeric species such as neutral dimers, M_2, and ionic dimers, M_2^+. But an unexpected result with alkalides is the formation of dimers and chains *of alkali metal anions*. With a filled outer *s*-shell that contains two electrons and the expected repulsion between anions, one would expect these anions to remain well separated. Yet alkali metal anion dimers have been observed in three crystalline alkalides, $K^+(C222)K^-$, $Rb^+(C222)Rb^-$ (*73*), and $Ba^{2+}(H_5Aza222^-)\cdot(MeNH_2)_2Na^-$ (*74*). The inter-nuclear distances in these three dimers, K_2^{2-}, Rb_2^{2-}, and Na_2^{2-} are $>1{,}0$ Å shorter than predicted from the sizes of the isolated anions. That the result is not just caused by crystal packing forces is shown by theoretical calculations (*74,75*). The dimers are calculated to be stable in the presence of point positive charges (included to provide overall neutrality). The simplest orbital picture is mixing of *s* and *p* character to yield a "hybrid bond" with considerable charge delocalization. The structure of the Na_2^{2-} dimer and its surroundings in $Ba^{2+}(H_5Aza222^-)(MeNH_2)_2Na^-$ is shown in Fig. 4.

The mixing of *s* and *p* orbitals is also indicated by the MAS NMR results. Isolated Na^- species have a characteristic chemical shift of –61 ppm. The salt that contains dimers of Na^- has a chemical shift of only –32 ppm. The shift is even more dramatic for K_2^{2-} in its compounds with the complexant C222. The observed chemical shift of +19 ppm contrasts with the value of –102 ppm for isolated K^- (*76*). The admixture of *s* and *p* character introduces substantial spin-orbit coupling, which leads to a large Ramsey paramagnetic shift (*77*). The NMR spectrum of $Rb^+(C222)Rb^-$, which has Rb_2^{2-} dimers was too broad to permit determination of accurate chemical shifts, but the ^{87}Rb chemical shift of the dianion is positive and thus substantially more paramagnetic than the value of –190 ppm for isolated Rb^- anions (*76*).

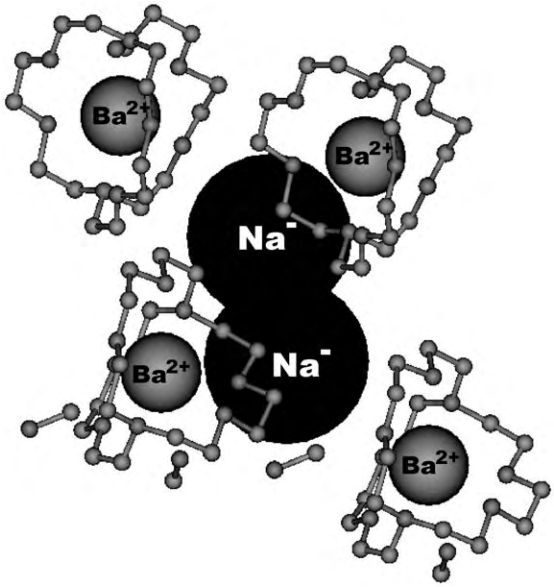

FIG. 4. Structure of the Na_2^{2-} species in Ba^{2+}(H6Aza222$^-$)$Na^-\cdot$2MeNH2. The sizes of Na^- and Ba^{2+} are drawn to scale, while the complexant is depicted in the ball-and-stick mode.

Two cesides, Cs^+(C222)Cs^- (*73*), and Li^+(C211)Cs^- (*78*) have infinite chains of Cs^-anions with internuclear distances shortened by 1.0 Å from the isolated Cs^- diameter. The ^{133}Cs NMR chemical shifts are shifted paramagnetically by about 300 and 350 ppm, respectively, from the shifts of isolated Cs^- anions. The chain structure of Cs^+(C222)Cs^- is shown in Fig. 5.

As described previously, M^+(HMHCY)Na^- structures contain M^+–Na^- contact ion-pairs. The only crown ether structure without encapsulation of the cation by two complexant molecules is Rb^+(18C6)Rb^-. This structure contains chains of Rb^- ions with shortened Rb^- to Rb^- distances as well as Rb^- to Rb^+ contact ion-pairs (*73*). It is remarkable that the complexation of Rb^+ by 18-crown-6 is so strong that a single compound contains two oxidation states of Rb *in contact*, with very little indication of charge transfer.

In conclusion, complexation of alkali cations by a number of complexants with oxa-and aza- cryptands and crown ethers has produced a great variety of alkalides. The simplest are those with isolated alkali metal anions, which are similar to normal salts, albeit with unusual anions. But the tendency of alkali metal anions to form dimers and chains has greatly expanded the range of alkalide properties. While this unusual class of ionic compounds has not been firmly established, it continues to amaze us with the variety of compounds that can be made.

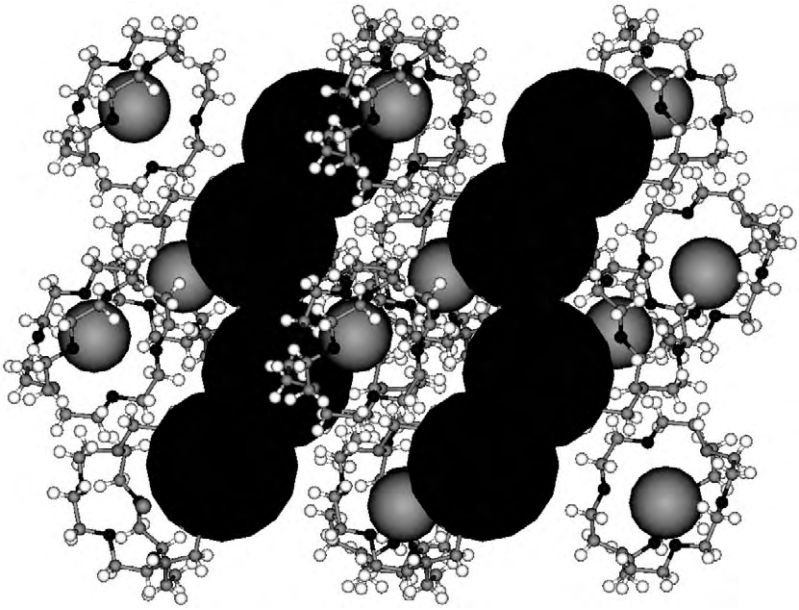

FIG. 5. The infinite Cs^- chain structure in $Cs^+(C222)Cs^-$. The Cs^- species (solid black) and the Cs^+ ions (gray) are drawn to scale. The complexant, C222, is depicted in the ball-and-stick mode.

VI. Electrides – Anionic or Electronic?

A. Electrides as Stoichiometric F-Centers

As unusual as alkalides are, they still provide us with well-defined anionic species. The situation is quite different with electrides. The idea that the "elusive electron" can serve as an anion in a crystalline ionic salt is quite revolutionary. The closest analogy is the case of F-centers in ionic solids, where electrons can be locally trapped at defect sites that are missing a conventional anion. Such "color centers" are readily produced in alkali halides by X-irradiation, electron bombardment, or even the discharge of a Tesla coil, and have been extensively studied since the 1930s (*79*).

F-center electrons are more-or-less localized in anionic sites and are far enough apart to prevent inter-electron interactions. It is true that adjacent trapped electrons can form coupled "dimers", the so-called "V-centers" as well as other combinations. But what would happen if we move to "stoichiometric F-centers" in which virtually *every* anionic site is occupied by electrons? This, indeed, is the simplest picture of electrides. When crystals are grown from solutions that contain complexed cations and solvated electrons, the overall neutral salts that are formed contain complexed alkali cations, with an equal number of electrons trapped in anionic cavities. But, unlike massive

alkali metal anions, electrons cannot be pinned down to specific sites and the electron density will tend to "leak out" into its surroundings. Thus, we can anticipate overlap with the complexant and its encapsulated alkali cation as well as with adjacent trapped electrons. Since the simple band picture of electrides is that of a half-filled conduction band, we might anticipate the formation of a metal. Electrides, therefore become ideal testing grounds for electron–electron interactions and for the non-metal to metal transition.

B. Synthesis of Electrides

The methods used to synthesize electrides are essentially the same as those used for alkalides. The major difference is that the concentration of alkali metal anions in solution must be suppressed. As described earlier, this can be done in favorable cases by increasing the concentration of complexant, so that the concentration of M^- is reduced by formation of $M^+(L)_n + e^-_{solv}$, caused by a shift of Eq. (3) to the right. This can be most easily accomplished in the more polar solvents, NH_3 (in which M^- does not form) and $MeNH_2$. However, in such solvents, decomplexation by reversal of Eq. (2) is also favored. The synthesis of pure electrides thus becomes a balance of solvent, metal, and complexant that requires much experimentation. As a result of improper balance, many alkalides are contaminated with trapped electrons, and even more electrides contain substantial concentrations of alkali metal anions. In spite of these difficulties, we have been able to synthesize and crystallize seven electrides in high enough purity to obtain crystal structures.

The synthesis of a thermally stable electride was a particular challenge. We knew that the vulnerability of oxa-complexants to reduction would require the use of tertiary amine aza-complexants. Permethylated aza-cryptand [2.2.2], **7**, yielded thermally stable sodides and potassides (*53*) but they were subject to decomplexation and, in addition, the complexing ability for K^+ was not strong enough for electride formation. Space-filling models suggested that an aza-cryptand with 6-membered piperazine rings in each of the three arms would have a conformation close to that of the complex with an internal alkali cation. This would minimize the energy and entropy costs associated with complexation. An extensive series of theoretical calculations was carried out that confirmed these predictions and led to the synthesis of Na^+(TriPip)e^- by the metathesis methods described in Section IV.B (*5*). The structure of this electride is shown in Fig. 2B.

C. Electride Structures and Properties

Electride structures are generally similar to those of alkalides. Where alkalides have M^- in the spaces between packed complexed cations, electride structures show X–ray empty cavities. The similarity

in structure between sodides and electrides is common; an example is shown in Fig. 2. Theory (*80*) and experiment (*10,16*) agree that most of the "excess" electron density in electrides resides in the cavities, with little charge transfer to the cation. A direct measure of such charge transfer is the NMR Knight shift (*81*), which can be easily identified by its temperature dependence. The *percent atomic character* of the encapsulated cation can be determined from the measured magnetic susceptibility and the slope of a plot of the chemical shift vs 1/T. Only ^{7}Li, ^{23}Na and ^{133}Cs have narrow enough solid-state NMR peaks to permit evaluation of the percent atomic character in electrides that contain these cations. The values are given in Table II.

Except for the mixed-crown ether electride (*82,83*), which has a complex structure, all electrides have major channels that connect the cavities along a particular direction. The electron density of the trapped electrons tends to avoid regions that are occupied by "filled-shell" molecules (Pauli Exclusion Principle). Therefore, the void spaces and the channels that connect them to form pseudo-1D chains become the regions of high "excess" electron density. The geometry of these "empty" regions has a profound effect on inter-electron coupling. *Isolated* trapped electrons would be paramagnetic and the magnetic susceptibility would follow the Curie Law,

$$\chi_{\mathrm{M}} = C/T + \mathrm{B} \tag{11}$$

or, for weak inter-electron coupling, the Curie-Weiss Law,

$$\chi_{\mathrm{M}} = C/(T-\theta) + \mathrm{B}, \tag{12}$$

in which the Weiss Constant, θ, is negative for the usual antiferromagnetic coupling. Inter-electron antiferromagnetic coupling along one-dimension results in a maximum in the susceptibility-temperature behavior. Expressions derived from Heisenberg theory (*84*) fit the data quantitatively in terms of a coupling parameter, *J*, which is negative for antiferromagnetic interactions of the electron spins. The magnitude of *J* depends on the extent of overlap of the wave functions, which for electrides is primarily determined by the size of the channels that connect the electron-trapping cavities (*12*). The values of J and the minimum cross-sectional areas of the connecting channels (along

TABLE II

Percent Atomic Character of the Cation in Some Electrides

Electride	Percent atomic character
$Cs^{+}(18C6)_2e^{-}$	0.036
$Cs^{+}(15C5)_2e^{-}$	0.063
$Na^{+}(TriPip222)e^{-}$	0.10
$Li^{+}(C211)e^{-}$	0.16

TABLE III

CORRELATION OF CHANNEL AREA WITH THE INTER-ELECTRON COUPLING CONSTANT IN ELECTRIDES

Electride	Channel area $(Å)^2$	$-J/k_B$ (K)
$Cs^+(15C5)_2e^-$	2.3	3.0
$K^+(15C5)_2e^-$	1.7	7.9
$Rb^+(C222)e^-$ (Phase α)	8.0	30
$Cs^+(18C6)_2e^-$	11.0	38
$Li^+(C211)e^-$	12.8	54
$K^+(C222)e^-$	21	430

the most open direction) are given in Table III. The importance of the "empty" regions to the magnitude of the inter-electron coupling provides strong confirmation that the "anionic" electrons in electrides tend to avoid "occupied" regions of space.

Another property of electrides that is strongly affected by geometry is the electrical conductivity. Pure electrides are *Mott insulators*, even though the "conduction band" is half-full, as in a metal. The energy cost of placing two electrons in the same cavity is too great to allow conductivity by double occupancy, and the average inter-electron distance is too large to meet the Mott criterion for a metal. Yet electrides *do* conduct electricity, with specific conductances that range from $10^{-10}\ \Omega^{-1}\,cm^{-1}$ for $Cs^+(18C6)_2e^-$ to $>20\ \Omega^{-1}\,cm^{-1}$ for $K^+(C222)e^-$ (*13*). All indications are that the conductivity is defect-dominated, but the cavity-channel geometry plays a dominant role in defect mobility. A simple defect is a cavity with a missing electron. Such a "hole" could migrate rapidly through open channels such as those in $K^+(C222)e^-$ and could "hop" through smaller channels that inter-connect the main ones. A detailed conductivity and EPR study of this electride has been published (*85*).

VII. Possible Future Developments

Now that we have demonstrated that it is possible to synthesize thermally stable electrides, the field is wide open for others with expertise in complexant synthesis to explore the many possibilities that exist. [See for example the excellent review "Coordination Chemistry of Azacryptands" by Nelson et al. (*86*)]. The complexant TriPip (compound **4**) is only one of a number of similar aza complexants that could be made. An obvious extension is to shorten or lengthen the arms to accommodate other cations from Li^+ to Cs^+. The deprotonation of one of the complexant nitrogens in $Ba^{2+}(H_5Aza\ 222^-)Na^-$ and the extraordinary stability of $Me_6Aza222$ in the potasside and sodide, suggests that it might be possible to methylate all but one nitrogen of $H_6Aza222$ to form the barium electride $Ba^{2+}(Me_5Aza222^-)e^-$. Complexation of

alkaline earths in an all-tertiary amine ligand such as TriPip to form $M^{2+}(L)(e^-)_2$ would produce an electride with roughly twice the density of anionic electride sites, which might enhance the electron coupling and conductivity. And as indicated by the consideration of Born–Haber cycles in Section II.B, a suitable non-reducible complexant for the alkaline earth cations opens the possibility of forming stable aurides, argentides and even cuprides. A salt of Cu^- would be a major breakthrough!

Another interesting possibility is the addition of appendages to the side arms of the polyamine complexants such as **4** and **7**. Such shape-changing modifications may alter the molecular and lattice structures of electrides in such a way as to open up large channels between the electron-trapping sites. This could lead to metallic electrides or to electrides with such weak electron binding that they could exhibit IR photoemission. Another intriguing possibility would be to incorporate aromatic or olefinic groups in the appendages that would compete with cavity trapping sites for the "extra" electron. The possibility that aromatic or alkenic radical anions and trapped electrons could co-exist in equilibrium is intriguing and worthy of exploration especially in light of our early observations of ethylene reduction and C–C bond formation (*68*).

Because even the thermally stable organic electrides are subject to decomplexation and decomposition at temperatures of ~100°C or so, the future of practical application of electrides in such areas as thermionic emission probably belongs to "inorganic electrides" in which electrons are trapped in cavities that are part of an inorganic framework. Progress in this area has been made with the addition of alkali metals to all-silica zeolites (*87,88*) and the formation of "electrides" in a calcium-aluminum oxide in which O^{2-} ions in anionic sites are replaced by trapped electrons (*89*). The truly ideal "inorganic electride" would be an all-silica zeolite that contains both sodalite cages and larger α-cages. The addition of an alkali metal might then place the cation in the sodalite cage and the electron in the large α-cage. This would be a "true inorganic electride."

References

1. Bartlett, N. *Proc. Chem. Soc. London* **1962**, *218* .
2. Dye, J. L.; Ceraso, J. M.; Lok, M. T.; Barnett, B. L.; Tehan, F. J. *J. Am. Chem. Soc.* **1974**, *96*, 608–609.
3. Tehan, F. J.; Barnett, B. L.; Dye, J. L. *J. Am. Chem. Soc.* **1974**, *96*, 7203–7208.
4. Dawes, S. B.; Ward, D. L.; Huang, R. H.; Dye, J. L. *J. Am. Chem. Soc.* **1986**, *108*, 3534–3535.
5. Redko, M. Y.; Jackson, J. E.; Huang, R. H.; Dye, J. L. *J. Am. Chem. Soc.* **2005**, *127*, 12416–12422.
6. Dye, J. L. *Prog. Inorg. Chem.* **1984**, *32*, 327–441.

7. Dye, J. L.; Huang, R. H.; Ward, D. L. *J. Coord. Chem.* **1988**, *B. 18*, 121–128.
8. Dye, J. L. In: *"Valency, The Robert A. Welch Foundation Conference on Chemical Research"*; vol. XXXII; Ed. Robert A.; Welch Foundation: Houston, TX, **1989**, pp. 65–91.
9. Dye, J. L. *Science* **1990**, *247*, 663–668.
10. Dye, J. L. *Nature* **1993**, *365*, 10–11.
11. Dye, J. L. *Chemtracts – Inorg. Chem.* **1993**, *5*, 243–270.
12. Dye, J. L.; Wagner, M. J.; Overney, G.; Huang, R. H.; Nagy, T. F.; Tomanek, D. *J. Am. Chem. Soc.* **1996**, *118*, 7329–7336.
13. Dye, J. L. *Inorg. Chem.* **1997**, *36*, 3816–3826.
14. Wagner, M.J.; Dye, J.L. In:*"Molecular Recognition: Receptors for Cationic Guests"*; 1st edn., vol. 1; Ed. Gokel, G. W.; Pergamon Press: Oxford, UK, **1996**, pp. 477–510.
15. Wagner, M. J.; Dye, J. L. *Annu. Rev. Mater. Sci.* **1993**, *23*, 223–253.
16. Dye, J. L. *Science* **2003**, *301*, 607–608.
17. Edwards, P. P. *Adv. Inorg.Chem. RadioChem.* **1982**, *25*, 135–185.
18. Weyl, W. *Ann. Physik u. Chemie* **1864**, *197*, 601–612.
19. Kraus, C. A. *J. Am. Chem. Soc.* **1907**, *29*, 1557–1571.
20. Kraus, C. A. *J. Chem. Educ.* **1953**, *30*, 83–87.
21. Kraus, C. A. *J. Am. Chem. Soc.* **1914**, *36*, 864–877.
22. Gibson, G. E.; Argo, W. L. *J. Am. Chem. Soc.* **1918**, *40*, 1327–1355.
23. Blades, H.; Hodgins, J. W. *Can. J. Chem.* **1955**, *33*, 411–425.
24. Hohlstein, G.; Wannagat, U. *Zeit. Anorgan Allege Chem.* **1957**, *288*, 193–200.
25. Fowles, G. W. A.; McGregor, W. R.; Symons, M. C. R. *J. Chem. Soc.* **1957**, 3329–3336.
26. Windwer, S.; Sundheim, B. R. *J. Phys. Chem.* **1962**, *66*, 1254–1258.
27. Dewald, R. R.; Dye, J. L. *J. Phys. Chem.* **1964**, *68*, 121–127.
28. Dye, J. L.; Dewald, R. R. *J. Phys. Chem.* **1964**, *68*, 135–142.
29. Dainton, F. S.; Wiles, D. M.; Wright, A. N. *J. Chem. Soc.* **1960**, 4283–4289.
30. Hurley, I.; Tuttle, T. R. J.; Golden, S. *J. Chem. Phys.* **1968**, *48*, 2818–2819.
31. Matalon, S.; Golden, S.; Ottolenghi, M. *J. Phys. Chem.* **1969**, *73*, 3098–3101.
32. Dye, J. L.; DeBacker, M. G.; Nicely, V. A. *J. Am. Chem. Soc.* **1970**, *92*, 5226–5228.
33. Kasdan, A.; Lineberger, W. C. *Phys. Rev. A* **1974**, *19*, 1658–1664.
34. Ceraso, J. M.; Dye, J. L. *J. Chem. Phys.* **1974**, *61*, 1585–1587.
35. Pedersen, C. J. *J. Am. Chem. Soc.* **1967**, *89*, 7017–7036.
36. Dietrich, B.; Lehn, J.-M.; Sauvage, J. P. *Tetrahedron Lett.* **1969**, 2889–2992.
37. DeBacker, M. G.; Dye, J. L. *J. Phys. Chem.* **1971**, *75*, 3092–3096.
38. Dye, J. L.; Lok, M. T.; Tehan, F. J.; Coolen, R. B.; Papadakis, N.; Ceraso, J. M.; DeBacker, M. G. *Ber. Bunsen-Ges. Phys. Chem.* **1971**, *75*, 659–662.
39. Lok, M. T.; Tehan, F. J.; Dye, J. L. *J. Phys. Chem.* **1972**, *76*, 2975–2981.
40. Dye, J. L.; DeBacker, M. G.; Eyre, J. A.; Dorfman, L. M. *J. Phys. Chem.* **1972**, *76*, 839–846.
41. Dye, J. L. In: "*Electrons in Fluids*"; Ed. Kestner, J. J. a. N. R.; Springer-Verlag: Berlin, **1973**, pp. 77–95.
42. Ceraso, J. M.; Dye, J. L. *J. Am. Chem. Soc.* **1973**, *95*, 4432–4434.
43. Dye, J. L.; Yemen, M. R.; DaGue, M. G.; Lehn, J.-M. *J. Chem. Phys.* **1978**, *68*, 1665–1670.
44. Harris, R. L.; Lagowski, J. J. *J. Phys. Chem.* **1978**, *82*, 729–734.
45. Dewald, R. R.; Dye, J. L. *J. Phys. Chem.* **1964**, *68*, 128–134.
46. Hurley, I.; Tuttle, T. R. J.; Golden, S. In: "*Metal-Ammonia Solutions*"; Eds. Lagowski, J. J.; Sienko, M. J.; Butterworths: London, **1969**, pp 449-480.
47. Dye, J. L. *Angew. Chem. Int. Ed. Engl.* **1979**, *18*, 587–598.
48. Peer, W. J.; Lagowski, J. J. *J. Am. Chem. Soc.* **1978**, *100*, 6260–6261.
49. Burns, R. C.; Corbett, J. D. *J. Am. Chem. Soc.* **1981**, *103*, 2627–2632.

50. Batchelor, R. J.; Birchall, T.; Burns, R. C. *Inorg. Chem.* **1986**, *25*, 2009–2015.
51. Dietzel, P. D. C.; Jansen, M. *Chem. Com.* **2001**, 2208–2209.
52. Tran, N. E.; Lagowski, J. *J. Inorg. Chem.* **2001**, *40*, 1067–1068.
53. Kim, J.; Ichimura, A. S.; Huang, R. H.; Redko, M.; Phillips, R. C.; Jackson, J. E.; Dye, J. L. *J. Am. Chem. Soc.* **1999**, *121*, 10666–10667.
54. Issa, D.; Dye, J. L. *Inorg. Chim. Acta.* **1989**, *160*, 111–113.
55. Schindewolf, U.; Le, L. D.; Dye, J. L. *J. Am. Chem. Soc.* **1982**, *86*, 2284–2286.
56. Chen, Q.; Cannell, K.; Nicoll, J.; Deardon, D. V. *J. Am. Chem. Soc.* **1996**, *118*, 6335–6344.
57. Concepcion, R.; Dye, J. L. *J. Am. Chem. Soc.* **1987**, *109*, 7203–7204.
58. DeBacker, M. G.; Mkadmi, E. B.; Sauvage, F. X.; Lelieur, J. P.; McMills, L. E. H.; Eglin, J. L.; Kim, J.; Guadagnini, R.; Wagner, M.; Concepcion, R.; Dye, J. L. *J. Am. Chem. Soc.* **1994**, *116*, 6570–6576.
59. DeBacker, M. G.; Mkadmi, E. B.; Sauvage, F. X.; Lelieur, J. P.; Wagner, M. J.; Concepcion, R.; Kim, J.; McMills, L. E. H.; Dye, J. L. *J. Am. Chem. Soc.* **1996**, *118*, 1997–2003.
60. Le, L. D.; Issa, D.; VanEck, B.; Dye, J. L. *J. Phys. Chem.* **1982**, *86*, 7–10.
61. Jaenicke, S.; Faber, M. K.; Dye, J. L.; Pratt, W. P. Jr. *J. Solid State Chem.* **1987**, *68*, 239–246.
62. Hendrickson, J. E.; Ph. D. Dissertation, Michigan State University, East Lansing, MI, 1994.
63. Hendrickson, J. E.; Kuo, C. T.; Xie, Q.; Pratt, W. P. Jr.; Dye, J. L. *J. Phys. Chem.* **1996**, *100*, 3395–3401.
64. Hendrickson, J. E.; Xu, G.; Pratt, W. P. Jr; Dye, J. L. *J. Phys. Chem. A* **1997**, *101*, 4149–4155.
65. Hendrickson, J. E.; Pratt, W. P. Jr.; Phillips, R. C.; Dye, J. L. *J. Phys. Chem. B* **1998**, *102*, 3917–3926.
66. Redko, M. Y.; Vlassa, M.; Jackson, J. E.; Misiolek, A. W.; Huang, R. H.; Dye, J. L. *J. Am. Chem. Soc.* **2002**, *124*, 5928–5929.
67. Jedlinski, Z.; Stolarzewicz, A.; Grobelny, Z. *Makromol. Chem.* **1986**, *187*, 795–799.
68. Cauliez, P. M.; Jackson, J. E.; Dye, J. L. *Tetrahedron Lett* **1991**, *32*, 5039–5042.
69. Kuchenmeister, M. E.; Dye, J. L. *J. Am. Chem. Soc.* **1989**, *111*, 935–938.
70. Eglin, J. L.; Jackson, E. P.; Moeggenborg, K. J.; Dye, J. L.; Bencini, A.; Micheloni, M. *J. Inclu. Phenom* **1992**, *12*, 263–274.
71. Wayda, A. L.; Dye, J. L. *J. Chem. Educ.* **1985**, *62*, 356–359.
72. Ellaboudy, A.; Tinkham, M. L.; VanEck, B.; Dye, J. L.; Smith, P. B. *J. Phys. Chem.* **1984**, *88*, 3852–3855.
73. Huang, R. H.; Ward, D. L.; Dye, J. L. *J. Am. Chem. Soc.* **1989**, *111*, 5707–5708.
74. Redko, M. Y.; Huang, R. H.; Jackson, J. E.; Harrison, J. F.; Dye, J. L. *J. Am. Chem. Soc.* **2003**, *125*, 2259–2263.
75. Tientega, F.; Dye, J. L.; Harrison, J. F. *J. Am. Chem. Soc.* **1991**, *113*, 3206–3208.
76. Kim, J.; Eglin, J. L.; Ellaboudy, A. S.; McMills, L. E. H.; Huang, S.; Dye, J. L. *J. Phys. Chem.* **1996**, *100*, 2885–2891.
77. Ramsey, N. F. *Phys. Rev.* **1950**, *78*, 699–703.
78. Ichimura, A. S., Huang, R. H.; Xie, Q.; Morganelli, P.; Burns, A.; Dye, J. L. *J. Phys. Chem. B* **2006**, 12293–12301.
79. Markham, J. J. *"F Centers in Alkali Halides"*; Academic Press: New York, **1966**.
80. Singh, D. J.; Krakauer, H.; Haas, C.; Pickett, W. E. *Nature* **1993**, *365*, 39–42.
81. Knight, W. D. *Phys. Rev.* **1944**, *76*, 1259–1260.
82. Wagner, M. J.; Huang, R. H.; Eglin, J. L.; Dye, J. L. *Nature* **1994**, *368*, 726–729.
83. Wagner, M. J.; Dye, J. L. *J. Solid State Chem.* **1995**, *117*, 309–317.
84. Bonner, J. C.; Fisher, M. E. *Phys. Rev. A* **1964**, *135*, 640–658.
85. Ichimura, A. S.; Wagner, M. J.; Dye, J. L. *J. Phys. Chem. B* **2002**, *106*, 11196–11202.

86. Nelson, J.; McKee, V.; Morgan, G. *Prog. Inorg. Chem.* **1998**, *47*, 167–316.
87. Ichimura, A. S.; Dye, J. L.; Camblor, M. A.; Villaescusa, L. A. *J. Am. Chem. Soc.* **2002**, *124*, 1170–1171.
88. Wernette, D. P.; Ichimura, A. S.; Urbin, S. A.; Dye, J. L. *Chem. Mater.* **2003**, *15*, 1441–1448.
89. Matsuishi, S.; Toda, Y.; Masashi, M.; Katsuro, H.; Toshio, K.; Hirano, M.; Tanaka, I.; Hosono, H. *Science* **2003**, *301*, 626–629.
90. Xie, Q.; Huang, R. H.; Ichimura, A. S.; Phillips, R. C.; Pratt, W. C., Jr.; Dye, J. L. *J. Am. Chem. Soc.* **2000**, 6971–6978.
91. Huang, S. Ph. D. Dissertation, Michigan State University, East Lansing, Michigan, 1994.

STRUCTURE–ACTIVITY STUDIES AND THE DESIGN OF SYNTHETIC SUPEROXIDE DISMUTASE (SOD) MIMETICS AS THERAPEUTICS

DENNIS P. RILEY[a] and OTTO F. SCHALL[b]

[a]Kereos, Inc., 4041 Forest Park Avenue, St. Louis, MO 63108, USA
[b]Metaphore Pharmaceuticals, Inc., 1910 Innerbelt Business Center drive, St. Louis, MO 63114, USA

I. Introduction

Low molecular weight catalysts which mimic a natural enzymatic function have potential utility for the treatment of diseases characterized by the overproduction of a deleterious metabolic by-product or foreign gene product. The discovery and development of pentaaza macrocyclic ligand complexes of manganese(II) as functional mimics of superoxide dismutase (SOD) enzymes serves as an example of rational design of catalytic drugs (enzyme mimetics). Two very important design factors are critical for design of a metal-based drug. Since the metal center in a complex is essential and will serve as the active site for SOD activity, it is necessary to not only be able to design a catalyst which affords the proper shape, ligand donor set, and donor number to afford fast catalytic rates, but it is also essential that the metal is tightly held/bound so that it does not dissociate from the complex *in vivo*.

We have been investigating for many years the development of synthetic enzymes (*synzymes*) as an approach to managing the types of

ADVANCES IN INORGANIC CHEMISTRY
VOLUME 59 ISSN 0898-8838 / DOI: 10.1016/S0898-8838(06)59007-5

diseases in which superoxide is known to play a significant role (*vide infra*). In this review we describe the discovery and subsequent development of highly *stable* Mn(II) complexes which possess high SOD activity – the two key attributes for an efficient SOD mimetic-based drug. Key to success in designing and synthesizing highly stable and highly active SOD mimetics was the development of a detailed understanding of the mechanism of action of this class of SOD mimetics, and the subsequent development of a computer-aided design (CAD) paradigm based on molecular mechanics (MM) that makes it possible to study and screen a large number of possible structures prior to embarking on complicated syntheses of highly substituted and constrained ligands.

II. Background

Superoxide dismutases (SODs) are a class of oxido-reductase enzymes which contain either Cu,

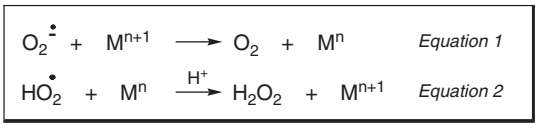

Fe, Mn, or Ni at the active site and catalyze the dismutation of superoxide (SO), the one-electron reduction product of molecular oxygen (Eqs. (1) and (2), where M^{n+} is the metalloenzyme in the reduced state and M^{n+} (*1*) is the enzyme in the oxidized state) to oxygen and hydrogen peroxide.(*1*) The SOD enzymes have been shown to have efficacy in animal models of disease states proposed to be, in part, mediated by superoxide, such as myocardial ischemia-reperfusion injury (*2–4*), inflammation (*4–7*), and cerebral ischemia-reperfusion injury (*8–10*). Evidence for superoxide (SO) as a mediator of disease states continues to accrue, such as in Parkinson's disease and neuronal apoptosis (*11–15*), cancer (*16–20*), and AIDS (*21,22*).

Owing to the limited therapeutic applications of the SOD enzymes arising from a number of negatives associated with their use (lack of oral activity, inability to gain access to the intracellular space of cells where superoxide is produced, immunogenicity when derived from non-human sources, bell-shaped dose– response curves, short half-lives, and cost) we have pursued the concept of designing synthetic, low molecular weight mimetics of the SOD enzymes which could overcome such limitations, and hence could serve as pharmaceutical candidates affording a new and promising approach to the treatment of disease.

III. Initial Structure Activity Studies – Catalyst/Drug Design

Initial efforts were focused on the synthesis of manganese-based complexes as low molecular weight SOD mimics – based largely on considerations of toxicity. Of the four metals known (Fe, Mn, Cu, Ni) to catalyze SO to hydrogen peroxide and oxygen, manganese is the least toxic to mammalian systems as the free aquated metal ion and is also the least likely of the four ions to react with hydrogen peroxide to generate hydroxyl radicals (Fenton chemistry). Early design efforts focused on the synthesis and screening of complexes of Mn(II) which could possess high chemical and thermodynamic stability. Much of the early synthetic efforts focused on complexes of Mn(II) with macrocyclic ligands which provide enhanced kinetic stability as compared to acyclic ligands.

From our initial structure/activity relationship (SAR) studies, we discovered that a class of manganese(II) complexes, **I** (Fig. 1), incorporating the macrocyclic ligand 1,4,7,10,13–pentaazacyclopentadecane (where $R_1 - R_{20}$ can be any number of defined substituents with known stereochemistry), effectively catalyze the dismutation of superoxide (*23,24*).

The discovery and efficacy of this class of Mn(II) complex as *functional* mimics of the SOD enzymes resulted from synthesis and screening studies utilizing a large number of different macrocyclic ligands complexes of Mn(II) (*23*). Even though over 40 complexes with different macrocylic ligands containing Mn(II) were synthesized, only the Mn(II) complex of the unsubstituted ligand derived from **I (Ia –** the 1,4,7,10,13-pentaazacyclopentadecane ligand, R_1-R_{20} = H), [Mn([15]a-neN_5)Cl_2], afforded measurable catalytic activity as monitored by stopped flow kinetic analysis of superoxide decay (*23*). This specificity of the pentaaza 15-membered ring ligands for affording SOD activity was somewhat surprising; e.g., the Mn(II) complex with the analogous

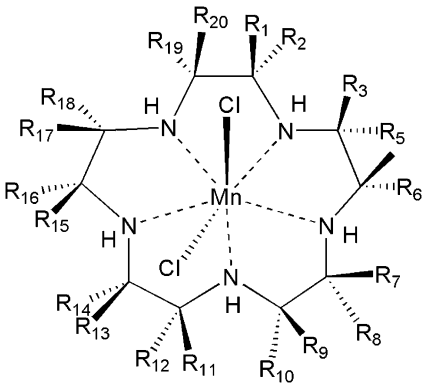

FIG. 1. Generic structure of the seven-coordinate Mn(II) complexes with 1,4,7,10,13-pentaazacyclopentadecane ligands.

16-membered ([16]aneN$_5$) ligand was at least two orders of magnitude less active and such simple changes to the ligand such as replacing one NH with an ether oxygen eliminated all activity. This complex, [Mn([15]aneN$_5$)Cl$_2$], is an excellent catalyst for the dismutation of superoxide to oxygen and hydrogen peroxide; possessing a k_{cat} of $4.1 \times 10^{+7}\,M^{-1}\,s^{-1}$ at pH = 7.4; i.e., about 20% of the activity of the native human Mn(SOD) enzyme (*23*) The complex crystallizes in either a seven-coordinate geometry, as exemplified by the *trans*-dichloro derivative with a planar macrocyclic ligand conformation or as a six-coordinate complex, as in the case of the nitrato-complex which possesses a folded ligand geometry and a six-coordinate pseudo octahedral geometry with a coordinated nitrate ligand and a nitrate counterion (*23,25*). In all cases the complexes are high-spin d^5 white materials possessing an average Mn(II) to N bond distance of ~2.28 Å. The Mn([15]aneN$_5$)Cl$_2$ complex possesses a reasonable thermodynamic stability at pH = 7.4 (log$K$ = 10.7) and excellent kinetic stability with the complex remaining intact at pH = 7.4 for many hours. This is still the case even in the presence of EDTA (*23*), which possesses a higher binding affinity for Mn(II) than does the [15]aneN$_5$ macrocycle. Additionally, this complex possesses excellent oxidative stability with the Mn(II) to Mn(III) oxidation occurring at +0.77 V (SHE) (*23*).

The observed stability of the Mn([15]aneN$_5$)Cl$_2$ complex was sufficient to assess this SOD mimetic's activity in a variety of *in vitro* and *in vivo* models of superoxide-mediated injury (*26*). Notably, this complex exhibits efficacy in *in vitro* (*27*) and *in vivo* models of inflammation (*28*), myocardial ischemia–reperfusion injury (*29–32*), vascular relaxation and restenosis (*33,34*). In addition, this and other complexes of this class of SOD mimetics derived from **I** have superior properties to that of the SOD enzymes in regard to their normal dose response curve (no deleterious effects observed at high doses in animal models), cellular permeability (dependent on the nature of the R groups), extended *in vivo* stability, non-immunogenicity, and projected lower cost of manufacture.

With positive biological concept data in hand, it was concluded that such synzymes may prove useful as therapeutic agents for the treatment of inflammation and myocardial ischemia–reperfusion injury, and other diseases mediated, in part, by overproduction of superoxide (*35,36*). As an added potential benefit, these SOD mimics have the unique property of increasing the circulating levels of nitric oxide, a vasorelaxant and anti-thrombotic (*33,34*) by reducing or eliminating the diffusion-controlled reaction between superoxide anion and nitric oxide that yields peroxynitrite, another toxic metabolite derived from oxygen (*37*). This nitric oxide reaction with superoxide proceeds with a nearly diffusion-controlled rate. We have also observed that SOD mimetics such as **Ia** limit the formation of peroxynitrite *in vivo* and hence can enhance the lifetime of nitric oxide *in vivo* (*33,37*). This provided a basis for testing the compound in an animal model of

platelet-mediated (NO blocks platelet aggregation) thrombosis in injured and stenotic arteries. The complex was shown to be protective in that restenosis of the damaged vessel was inhibited by the agent when administered over a two-week period (*34*).

IV. Development of Improved SOD Mimetics Derived from [Mn([15]aneN$_5$)Cl$_2$], Ia.

Having confirmed that the synthetic low molecular weight functional SOD mimetic, [Mn([15]aneN$_5$)Cl$_2$], **Ia**, possesses biological activity of pharmacological relevance to human disease states, provided the basis for pursuing this class of molecules for the development of a pharmaceutical agent. There are two key features necessary for improving the [Mn([15]aneN$_5$)Cl$_2$] complex for use as a therapeutic agent in humans: (1) increase the chemical stability via increasing the rigidity of the macrocyclic ligand (preorganization), and thereby increasing the inherent kinetic stability of the complex (*38*), and (2) increase the SOD activity, so that it would translate into a lower dose of agent and hence a diminished exposure to the metal-based drug.

Attempts to develop more active and more stable complexes probed the role that substituents (both on the N and C atoms of the parent macrocyclic ring) would exert on both the catalytic SOD activity and the overall chemical stability of the resultant complexes. How structural factors would affect these two key parameters was not immediately obvious, since it was not known at the outset how derivatized ligand systems would affect the catalytic activity. Thus, the number of substitutents, their placement, and their stereochemistry could all be critical design elements for maximizing catalytic activity and chemical stability.

Initial efforts showed that nitrogen-substituted complexes possess no catalytic activity. Thus, we focused on the synthesis of C-substituted derivatives, **I**. Unfortunately, standard procedures for the synthesis of aza crown macrocyclic ligands employing Atkins-Richman (*39*) chemistry were inadequate for the synthesis of C-substituted pentaaza crown ligands with stereo-defined centers. Cyclization yields were poor, because of both, higher oligomer formation and acid hydrolysis/detosylation giving stabilized carbonium ions that induce ring cleavage/elimination (*40*). While this chemistry is sufficient for the unsubstituted and even monosubstituted macrocycles, the yields for polysubstituted ligands were unworkably low. Consequently, we set out to devise better synthetic methods to such C-substituted ligands. New routes were successfully developed which utilized amide moieties as protecting groups for the amines during the cyclization (*41*). Such methods included acid chloride cyclization, bis-chloroacetamide protection schemes, and cyclic pentapeptide techniques (Fig. 2) which made it possible to run high concentration reactions and achieve high

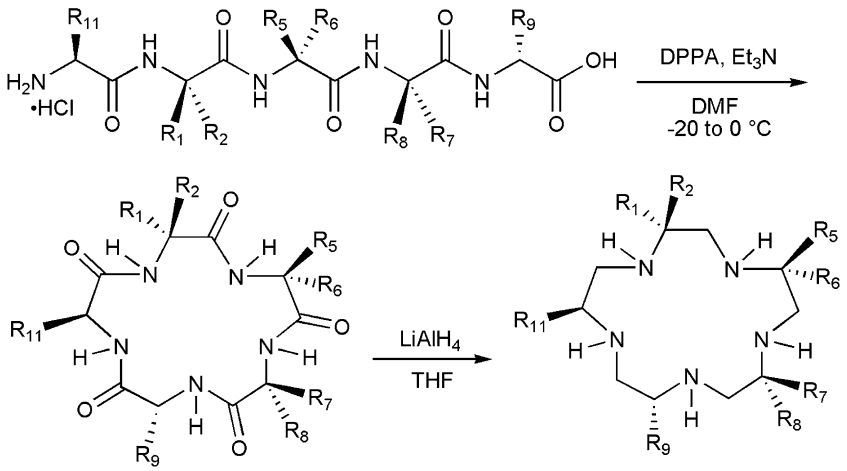

FIG. 2. Scheme for the synthesis of pentaaza 15-membered ring macrocyclic ligands with defined stereochemistry using the cyclic pentapeptide approach.

yields of pentaaza macrocycle (>50%, in most cases) (*39–42*). Additionally, combinations of these methods could be successfully incorporated into a single ligand preparation (*42*).

Employing such synthetic methodologies made it possible to synthesize highly substituted and stereochemically defined ligands and to probe the effect that stereochemically defined substituents exert on the stability and catalytic activity. For these studies we employed both methyl and fused-cycloalkyl substituents on the macrocyclic ring carbons to elicit the effect of stereochemistry on stability and rate. Examples of ligands employed are shown in Fig. 3. All of the resultant Mn(II) complexes were characterized and shown to be similar to the parent unsubstituted complex; e.g., high-spin d^5 Mn(II) *trans*-dichloro complexes with $E_{1/2}$(SHE) in the range of +0.74–0.78 V (*42*). Both the thermodynamic and kinetic stabilities of these complexes were assessed, (*42*) and several very significant features were discovered. First, increasing the number of C-substituents always increased the thermodynamic and kinetic stabilities of the complexes and in a nonlinear manner; i.e., stability increases geometrically with the number of substituents, so that, for example, the Mn(II) complex of the monomethyl ligand, **16**, is about twice as stable as the unsubstituted complex, **Ia**, the Mn(II) complex of the pentamethyl ligand, **10**, was over 160 times more stable than the unsubstituted complex. (*42*) We also observed that the *trans*-cyclohexano complex, [Mn(*trans*-cyclohexano[15]aneN_5)Cl_2], derived from ligand **11** (Fig. 3, see Table 1 for representative examples of complexes with k_{cat} and k_{diss} values) is more than twice as active as an SOD catalyst ($k_{cat} = 9.1 \times 10^{+7}\,M^{-1}\,s^{-1}$ at pH = 7.4) (*41*) and possessed both an improved thermodynamic

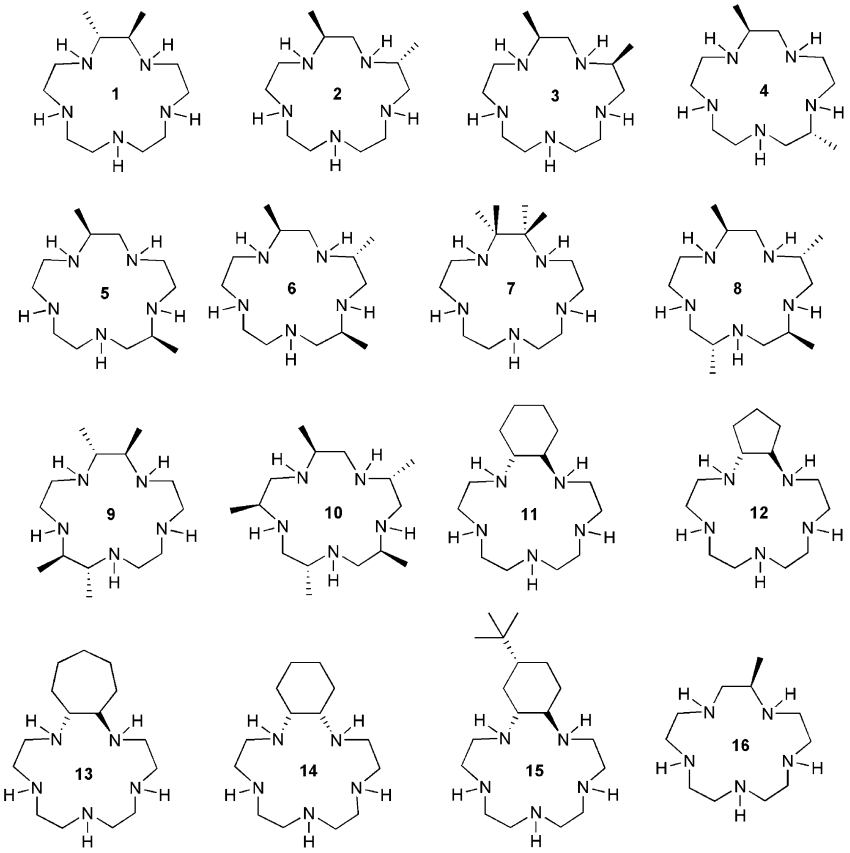

FIG. 3. Ligands utilized as their Mn(II) complexes to probe the effects of the number and stereochemistry and placement of substituents on the stability and catalytic rate of SO dismutation (*59*).

stability (log K of 11.6) and kinetic stability ($2\times$) over the unsubstituted complex.

Additionally, we observed that the stereochemistry of the methyl substituents exerts a large effect on the catalytic rate, but little effect on the stability of the complex as long as the number of substituents remains constant. A most remarkable aspect of the effect that substituents exert on the catalytic rate is revealed with the complexes of the macrocycles containing two *trans*-fused cyclohexano groups differing in the stereochemistry of their substitution.(*25*) Such a change can dramatically increase stability and have profound effects on activity. For example, the k_{cat} for the Mn(II) complex of the all *R*-ligand, **17** (Fig. 4, or its all *S*-enantiomer) [Mn(2*R*,3*R*,8*R*,9*R*-bis-cyclohexano[15]aneN$_5$)Cl$_2$], at pH 7.4 is $1.2\times10^8\,M^{-1}\,s^{-1}$ and possesses an increased thermodynamic stability (log $K = 13.3$) and an enhanced kinetic stability (at any pH over a 100-fold slower rate of dissociation

TABLE I

LIST OF Mn(II) complexes with various ligands and their catalytic rate constants for the dismutation of superoxide at pH = 7.4 and their second-order kinetic stabilities (first-order in [H+] and first-order in [Mn complex])

Complex	k_{cat} (pH = 7.4) $\times 10^{-7}\,M^{-1}\,s^{-1}$	k_{diss} $(M^{-1}\,s^{-1})$
Mn([15]aneN$_5$)Cl$_2$	4.1	2814
Mn(**10**)Cl$_2$	3.9	18
Mn(**11**)Cl$_2$	9.1	1375
Mn(**17**)Cl$_2$	12.1	28
Mn(**18**)Cl$_2$	<0.1	26
Mn(**19**)Cl$_2$	3.7	16
Mn(**20**)Cl$_2$	2.9	23
Mn(**28**)Cl$_2$	6.1	4.8
Mn(**29**)Cl$_2$	15.0	4.0
Mn(**30**)Cl$_2$	<0.1	5.9
Mn(**31**)Cl$_2$	4.56	1.42
Mn(**32**)Cl$_2$	2.0	<0.1
Mn(**33**)Cl$_2$	None	<0.03
Mn(**34**)Cl$_2$	1.6	<0.1
Mn(**35**)Cl$_2$	>200	<0.7

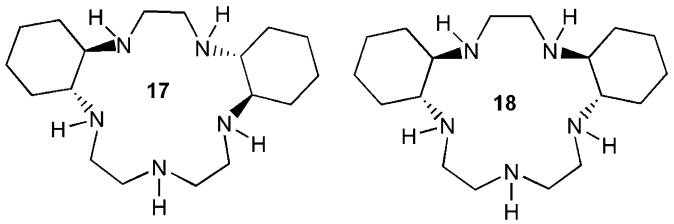

FIG. 4. Two diastereomeric bis(cyclohexano) substituted pentaazacyclopentadecane ligands **17** (2*R*,3*R*,8*R*,9*R*-bis-cyclohexano[15]aneN$_5$) and **18** (2*R*,3*R*,8*S*,9*S*-bis-cyclohexano[15]aneN$_5$).

results when compared to the unsubstituted complex, **Ia**). In contrast, the isomeric complex containing the 2*R*,3*R*,8*S*,9*S*-bis-cyclohexano[15]aneN$_5$ ligand, **18**, possesses a similar stability profile, but has no catalytic SOD activity (*25*).

Clearly, the stereochemical orientation of the carbon substituents exerts a major role in determining the ability of an Mn(II) complex of this class to function as an SOD catalyst. Thus, our synthesis and characterization efforts, initially focused on the role that C-substituents have on the complex's catalytic activity and chemical stability revealed that the interplay between position, number, and stereochemistry of substituents in dictating catalytic activity was subtle and unobvious.

It should be noted that the complex derived from ligand **18**, was characterized by X-ray crystallography and was shown to have the

Mn(II) arranged in a pentagonal bipyramidal geometry with *trans*-dichloro ligands and a planar macrocyclic orientation. (*25*) This complex, that of the parent unsubstituted complex, and the Mn(II) complex of ligand **7** (both also characterized by X-ray crystallography) all showed the same geometry and orientation of NHs. In each case the NH pattern is such that they alternate about the ring in an up: down: up: down: up orientation so that the two sides of the macrocyclic ring in the complex are chemically distinct. We also observed this same NH pattern in the Cd(II) complex of the unsubstituted complex (*43*).

Our initial design goal was to maximize the number of substituents on the macrocyclic ring, thereby increasing both preorganization and thus rigidity of the macrocyclic ligand, and hence the stability of the Mn(II) complex to dissociation (*38*). We initially had no way of knowing whether increasing the number of substituents on the parent macrocyclic ring would affect the catalytic activity in a beneficial or deleterious fashion. This evaluation required the development of a detailed mechanistic understanding of how these Mn(II) macrocyclic ligand complexes function as catalysts, and was predicated on the strong belief that once such information is in hand, the compounds could be subjected to computer-aided design (CAD) techniques in order to gain a quantitative and hence predictive understanding of how position, number, and stereochemistry of the substituents affect the catalytic rate.

Since the sole pathway for the loss of Mn(II) from these pentaaza crown ligands is a dissociative one, they possess a high inherent stability (*40,42*). In water, though, there exists a proton-dependent (1st-order in $[H^+]$) pathway for dissociation, and at or near physiological pH this is the major pathway for dissociation of the ligand from Mn(II) (*40,42*). Thus, in addition to the rigidity of the ligand, the basicity of the ligand itself, is also critical to determining the kinetic rate of dissociation. An excellent example of this effect is observed with the Mn(II) complex of the pyridino ligand **19** (*40*). This complex is nearly 175 times more kinetically stable at any pH than the parent unsubstituted ligand complex with Mn(II), **Ia**. This is undoubtedly due to some contribution from the rigidity conferred on the ligand by the pyridine substitution, but its complex with Mn(II) is even more stable than those complexes with the bis-cyclohexyl ligands (Figs. 3 and 4) of Mn(II). This enhanced stability is most likely attributable to the much lower basicity of the ligand itself; namely, a measure of the affinity of the ligand for a proton. For the aliphatic substituted ligands, three pK_a values are observed, with the values generally in the range: 10.5–11.0, 9.2–9.5, and 5.0–5.9 (*42*). With ligand **19** (Fig. 5), these values are lower, reflecting its weaker basicity: $pK_a = 9.4$, 8.8, and 5.3, and its lower affinity for a proton (*40*).

The structure of the Mn(II) complex of ligand **19**, [Mn(pyridine[15]aneN_5)Cl_2], is similar to other complexes of this class in that it crystallizes as a *trans*-dichloro pentagonal bipyramidal Mn(II) seven-coordinate complex with a planar array of the five nitrogens of

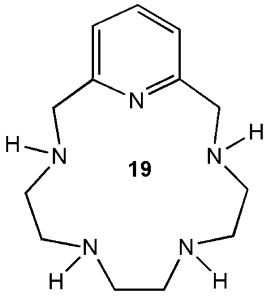

FIG. 5. The structure of the ligand **19** (pyridine[15]aneN$_5$).

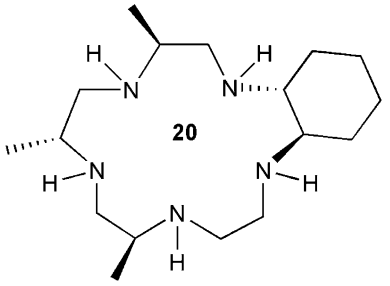

FIG. 6. Structure of the ligand **20** (cyclohexano-6*S*,9*R*, 12*S*-trimethyl[15]aneN$_5$) whose Mn(II) complex rivals in stability that of ligand **17**, but is very much less active as an SOD catalyst.

the macrocyclic ligand, while possessing an alternating up: down: up: down N–H orientation in relation to the plane defined by the metal and the five nitrogens (*40*). While it possesses an improved stability profile as compared to the parent unsubstituted complex **Ia**, it retains an SOD catalytic rate constant equivalent to it. Since there are an even number of NHs, the two sides of the macrocyclic plane, defined by the metal and the five nitrogens, are chemically equivalent.

The X-ray structure determination of the Mn(II) complex with ligand **20** has been carried out (*44*), revealing that this complex, as all the others that have been structurally characterized in this family of C-substituted [15]aneN$_5$ Mn(II) complexes (Fig. 6), possesses the alternating NH pattern described above. It is of interest to note that this complex crystallizes with a water in one coordination site *trans* to one of the chloride ligands, the second chloride ligand being present as an ionic component in the crystal lattice. Furthermore, the water is bound on the side of the macrocycle which possesses two *cis* non-adjacent NHs and the chloro ligand on the side with three *cis* NHs. At the time this complex was synthesized, its design was based on the empirical premise that more C-substitution is desirable for stability, but with no understanding of how to arrange the substituents to achieve a fast rate for the SOD reaction. In fact, the catalytic activity of this complex

is only about 70% of the parent unsubstituted complex at pH = 7.4 and almost 6 times less active than the Mn(II) complex of ligand **17**; thus, this complex represents an excellent example of the dilemma that was faced for the design of high activity catalysts; namely, while it is very stable, it has lower catalytic activity. Clearly, a sound mechanistic footing is necessary to solve the problem of how to design a maximally effective SOD mimic with its catalytic activity being at least as good as that of the Mn(II) complex with ligand **17**, but with an enhanced stability.

V. Mechanistic Studies

The need to understand the mechanistic details for the catalytic SOD reaction was a critical element for the design of highly substituted complexes possessing both high stability and high activity. From kinetic and mechanistic studies we have determined that the Mn(II) complexes of these pentaaza crown ligands function via a catalytic cycle in which the rate-determining step is oxidation of Mn(II) to Mn(III) (*23,25*). Two independent pathways operate for most of these complexes: (1) an outer-sphere proton-coupled electron transfer from a bound water to an incoming hydroperoxy radical (Eq. (3)):

$$Mn^{II}(L)(H_2O) + HO_2^{\bullet} \xrightarrow{k_1} Mn^{III}(L)(OH) + HOOH \qquad \textit{Equation 3}$$

and (2) an inner-sphere substitution involving coordination of superoxide anion to Mn(II) in a vacant axial site (Eq. (4)), followed by fast protonation of the bound superoxo creating a pseudo-octahedral Mn(III)-hydroperoxo complex (Eq. (5)):

$$Mn^{II}(L) + O_2^{\bullet-} \xrightarrow{k_2} Mn^{II}(L)(OO^{-}) \quad \text{inner-sphere substitution} \qquad \textit{Equation 4}$$

$$Mn^{II}(L)(OO^{-}) + H^{\oplus} \xrightarrow{fast} Mn^{III}(L)(OOH^{-}) \quad \text{oxidation} \qquad \textit{Equation 5}$$

Isotope studies using D_2O as the reaction solvent were particularly helpful in providing further insight into these pathways (*25*). Utilizing the fast catalyst derived from ligand **17** in both H_2O and D_2O, rate constants for both the proton independent and dependent pathways for oxidation of Mn(II) were measured (*25*). In H_2O, the pH independent water-exchange rate-limited path (Eqs. (4) and (5)) possesses a

rate constant of $1.58 \times 10^{+7}\,M^{-1}\,s^{-1}$ (*45*). In D_2O this rate is increased by ~10% consistent with water exchange rates on the Mn(II) ion having a role in dictating this rate (*45*). Other complexes showed similar small effects on the magnitude of this rate constant when measured in D_2O. This pathway is constrained to never be much faster than $\sim 1 \times 10^{+7}\,\ell M^{-1}\,s^{-1}$ (the water exchange rate for Mn(II)) owing to the limit imposed by the need to generate a vacant coordination site by loss of water from the metal.

The measured rates for the outer-sphere pH dependent pathway of Mn(II) oxidation with this complex and that of Mn(II) complex with ligand **11** were both dramatically lowered in D_2O showing an isotope effect of nearly 6 consistent with H-atom transfer for the proton-dependent pathway of oxidation of Mn(II) (*25*). This pathway is most significant and contributes all of the rate enhancement observed for those complexes with faster rates than about $1 \times 10^{+7}\,M^{-1}\,s^{-1}$.

For either pathway to be maximally efficient requires that the barrier to electron transfer must be minimal; i.e., the ligand reorganization barrier to electron transfer must be small (*46,47*). Thus, the precursor Mn(II) complex should adopt a six-coordinate pseudo-octahedral geometry similar to that required by the corresponding Mn(III) complex. Loss of an axial aquo ligand followed by folding of one of the secondary amine NHs of the macrocyclic ring so that it occupies an axial site would generate a pseudo-octahedral complex, $[Mn^{II}(L)X]^{n+}$, thereby accommodating the requirement for an octahedral six-coordinate Mn(III) complex. If the macrocyclic [15]aneN_5 ligand possesses C-substituents which, due to intramolecular steric repulsions and angle strains, could force the ligand to adopt this folded pseudo-octahedral geometry about the spherically symmetrical Mn(II) ion, then the Mn(II) complex would be poised to undergo facile electron transfer as the ligand reorganization barrier would be minimized; i.e., the shape of the reduced complex and its oxidized product will be similar. It is in this manner that the stereochemistry of the substituents would be expected to exert a major effect on the rate of electrontransfer via either pathway. This need to rearrange the ligand from a planar geometry into a folded conformation, stabilizing a pseudo-octahedral geometry on Mn(II), may be the reason why some complexes of this family show no measurable catalytic rate. It is intriguing to speculate whether the steric constraints imposed on the folding by the presence of a substituent positioned on a carbon of the ring would favor or inhibit a particular fold, and thereby promote or block the pathway for electron transfer.

Ligands **17** and **18** afford complexes which are either extremely active or inactive. Any attempt to rationalize the observed reaction rate constants for catalytic dismutation of superoxide must be able to predict a lack of SOD catalytic activity for the Mn(II) complex with ligand **18**.

VI. Computer-Aided Design (CAD)

Molecular modeling was utilized to test a theory of the details of this SOD catalysis with the goal of being able to correctly predict the effects that substitutents exert on the catalytic rate. The premise for the modeling paradigm is that the macrocyclic pentaaza ligand possesses C-substituents which, due to intramolecular steric repulsions and angle strains, force the ligand to adopt various degrees of folded pseudo-octahedral geometry about the spherically symmetrical Mn(II) ion. If the Mn(II) complex is constrained in a geometry which resembles a six-coordinate pseudo-octahedral geometry, then the Mn(II) complex would be poised to undergo facile electron-transfer as the ligand reorganizational barrier would be minimized. It is in this manner that the stereochemistry of the substituents could be expected to exert a major effect on the rate of electrontransfer via either pathway.

In order to better understand the effects that substituents exert, we utilized a combination of molecular mechanics calculations (*48*) and synthesis with the goal of rational design of highly substituted chemically stable synthetic enzymes. It needs to be stressed that while the prediction of properties and reactivity of small carbocyclic ring systems based on conformational control is widely practiced and relatively straightforward (*49*), the conformational analysis of large heterocyclic ring metal complexes undergoing redox chemistry offers a more difficult challenge.

The effective development of a rational modeling paradigm requires not only a detailed understanding of the mechanism of the rate-determining step in the catalytic process, but also a comprehensive database of chemical structures with their rate data so that the theoretical model could be subjected to stringent testing. Additional ligands, shown in Fig. 7, were also synthesized. The Mn(II) complexes of these ligands were then utilized as our source of rate and stability data for this **CAD** study (*50*). The Mn(II) complex of each ligand was completely characterized in terms of physical properties (e.g., the kinetic stability to dissociation in aqueous media) and the kinetics of their superoxide dismutase catalytic activity (*50*). In all cases, as we noted previously (*42*), increasing the number of the substituents on the macrocyclic ligand increases the kinetic stability of the complexes to dissociation in water.

The catalytic activities of the Mn(II) complexes of these ligands follow no apparent trend with regard to the number of substituents or their stereochemistry, other than that they both clearly have effects on the overall rate and on the two competing pathways for oxidation of Mn(II) during the catalytic cycle. Most striking is that for some of these complexes there is either no measurable inner-sphere or no outer-sphere rate. Complexes with the ligands **10, 18,** and **21** have no measurable k_{obs}. While these complexes were utilized in the original database to construct the modeling paradigm, complexes from ligands

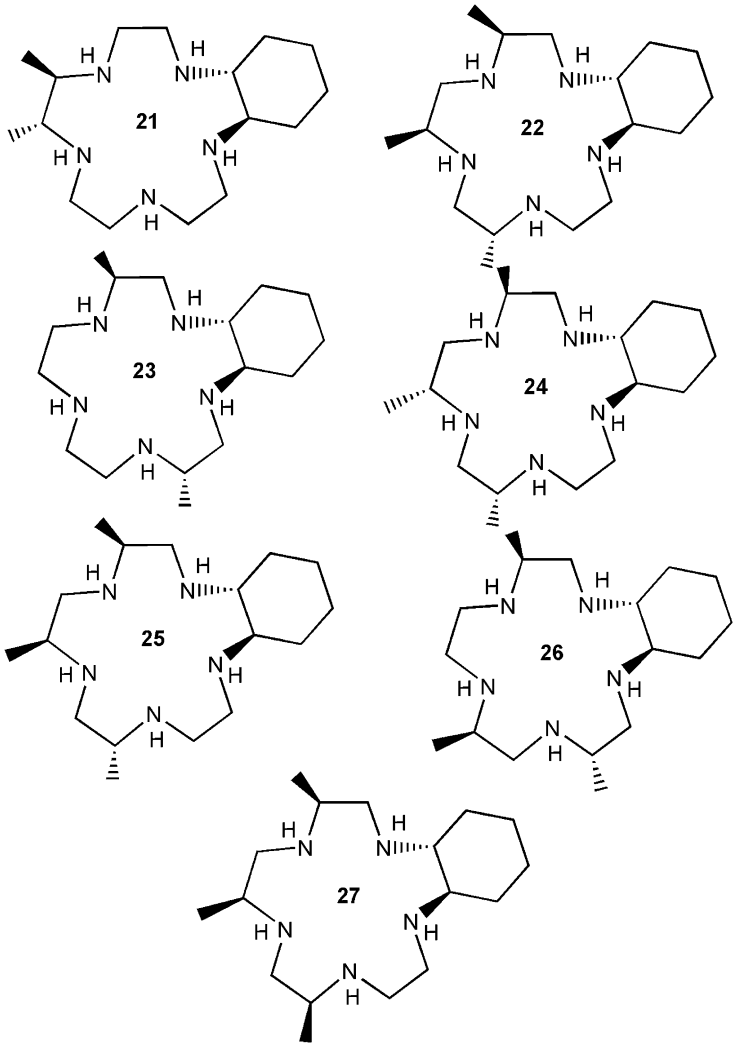

FIG. 7. Ligands **21**–**27** utilized as the database for substituted [Mn([15]aneN$_5$)X$_2$] complexes for probing the effects of substituents for molecular modeling (MM) studies.

28–31 (Fig. 8) were synthesized based on predictions of the model and provided tests of the predictive power of the MM calculations. For the complexes derived from ligands **28–31**, the kinetic stabilities and catalytic rate constants, k_{cat} (pH = 7.4), were also measured and are listed in Table 1.

While there are a number of computational methods available that could be used to predict structures and calculate the thermodynamic properties of a given structure for a coordination complex, the simplest level of calculation would be the use of molecular mechanics (MM)

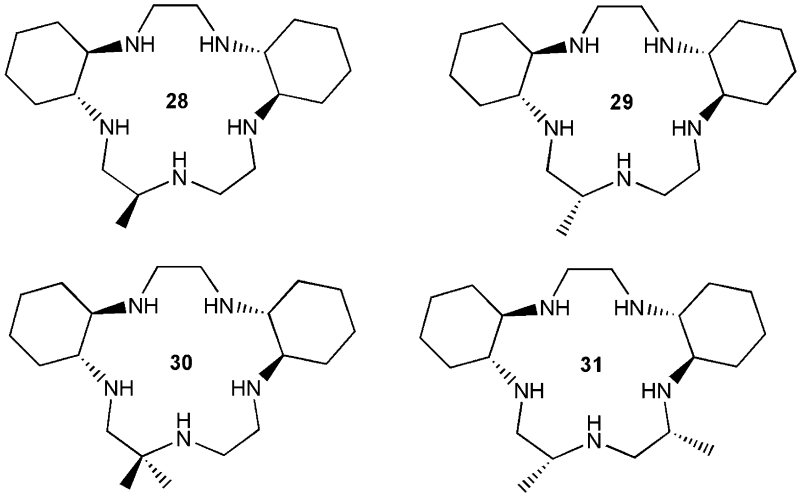

FIG. 8. Ligands **28–32** utilized for testing the predictive ability of the folding paradigm for MM calculations.

assuming appropriate parameters are available (*48,49*). We have completed the X-ray structure determinations and refinements of many complexes in this class and reported several crystal structures of this class of Mn(II) pentaaza crown complexes (*23,25,40,42,44*). This extensive X-ray structural database made it possible to refine the commercial parameters and utilize an improved R_{avg} for the Mn–Nitrogen distance, 2.283 Å, and also an R_{avg} for the Mn–Cl distance, 2.616 Å. In all cases, the NH stereochemical pattern is alternating; i.e., each side of the plane of the macrocyclic ring is chemically unique, since one side will have two non-adjacent NHs, while the other side possesses three (two in the case of pyridino ligands) NHs in a *cis* orientation. This motif provides a basis for probing the structural effects utilizing MM calculations.

The design premise requires that the ligand geometry about the Mn(II) ion dictates catalytic activity by promoting or preventing a particular folded structure. A good catalyst will be one in which the Mn(II) center is constrained in a geometry that promotes rapid electron transfer; i.e., the pseudo-octahedral geometry required by Mn(III). Consequently, the folding of an NH out of the plane defined by the metal and the five nitrogens of the ligand into an axial site governs the ability of the corresponding complex to function as a catalyst. The MM calculations can be utilized to determine the relative energies of all the possible folds for each complex (five possible, since each nitrogen can fold into an axial site, but only on the side of the macrocycle where the NH is located) and their relative energies compared. It should be emphasized that due to the symmetry of some ligands there may be fewer unique folding modes. For example, the

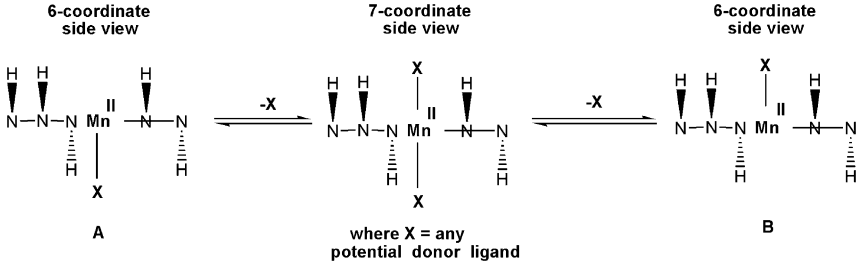

FIG. 9. Depiction of the equilibrium between two possible six-coordinate intermediate structures generated via ligand dissociation from a seven-coordinate intermediate Mn(II) complex.

pyridine[15]aneN_5 ligand, **19**, possesses a higher symmetry than other ligands of this class displayed here. It possesses four NHs and the two axial *trans* coordination sites are equivalent. As a consequence, only two unique folding motifs exist for this Mn(II) complex (folding of the pyridine nitrogen atom represents a very high-energy scenario and can be safely ruled out as a possible geometry in this system).

Our initial foray into the modeling using MM calculations involved probing the relative energies of two types of six-coordinate structures generated via loss of a ligand from a *trans*-seven-coordinate Mn(II) as depicted in Fig. 9. In solution and in the solid state, six- and seven-coordinate geometries exist for these complexes. In solution, a dynamic equilibrium involving such structures is expected (*25*). Two initial six-coordinate structures could be generated via the loss of an axial ligand from the seven-coordinate structure; i.e., the complex labeled **A** in Fig. 9, which has the vacant site on the side in which three NHs are *cis*, and the structure labeled **B,** which has the vacant site on the side with two non-adjacent NHs *cis*. Clearly, the two intermediates are chemically quite distinct and their relative energies can be calculated using **MM** approaches. Structure **A** (Fig. 9) was found to possess a much lower energy than that of structure **B** (their difference being in the range of 4–8 kcal for chloro as axial ligand and 8–12 kcal for aquo). The magnitude of this difference suggests that structure **A** should be considered a logical starting point as a common intermediate leading to catalysis for these complexes.

Using this approach, and assuming that the six-coordinate aquo complex is the Mn(II) complex that leads to productive chemistry, the simplest entry to the outer-sphere pathway presents itself as the aquo complex of structure **A** (where $\mathbf{X = H_2O}$). This suggests that for this path to be viable (fast rate) for a given complex, the substituents would force one of the three *cis* NHs on the side of the vacant coordination site out of the plane defined by the Mn(II) and the five nitrogen atoms (in effect, folded) into the axial pseudo-O_h site. When this is investigated for these complexes generated from the ligands specified above, we find, in general, that there is a most preferred NH (lowest energy

conformer) folding for one of the three *cis* NH nitrogens into an axial pseudo O_h site. This is the modeling paradigm which evolved for the outer-sphere correlation.

For those ligands in which there are five secondary NH donors, the inner-sphere, superoxide binding pathway, apparently, utilizes a folding motif generating a six-coordinate intermediate in which one of the NHs on the side with two *cis* NHs folds into the pseudo-axial site. This would arise from the common intermediate **A** by the coordination of superoxide anion to the vacant site trans to X followed by elimination of X to generate a six-coordinate intermediate of a structure as depicted for **B**. A unique lower energy folded conformer exists for all the complexes we have studied. This is consistent with the possibility that the inner-sphere pathway employs a folded structure which is unique and different from the outer-sphere pathway, and it is consistent with the inner-sphere path being accessed by an intermediate *common* to the outer-sphere path.

A scenario consistent with this follows. The outer-sphere path correlates with folding one of the three *cis* NHs fold into an axial site, and the inner-sphere path could utilize that same vacant site to bind superoxide. This negatively charged ligand will weaken the aquo ligand *trans*- to it and generate a vacant site on the side of the plane of the Mn(L) complex with the two non-adjacent *cis* NHs. Thus, loss of the bound *trans*-water and subsequent folding of either of the NHs on the side of the two *cis* NHs would generate a folded six-coordinate pseudo-octahedral complex. This correlation was validated by the modeling efforts, and it suggests that one common intermediate leads (geometry **A** in Fig. 9) to catalysis (*50*).

At the onset of this work, we relied on the consistency of our general mechanistic understanding and the chemical characterization of the various species involved in the superoxide dismutation (illustrated in Fig. 10) to guide us in the development of a modeling paradigm.

For all the above-described complexes utilized in the database, an evaluation of the energy difference (ΔE) of the folded six-coordinate structure for the Mn(II) and the corresponding Mn(III) complex were performed for each NH folded into an axial site. From this evaluation of different folded structures each complex will possess a lowest energy folded structure for the six-coordinate complex derived from an NH on the side of the three NHs occupying a pseudo-axial site, and also a lower energy structure for the six-coordinate complex derived from an NH on the side of two *cis* non-adjacent NHs occupying a pseudo-axial site. Thus, a correlation of the energy difference, ΔE ($\Sigma_{Mn(III)}$–$\Sigma_{Mn(II)}$), for a series of complexes for each of the two types of folds (potentially correlating with unique inner-sphere and outer-sphere folded structures) can be performed, where the ground state energy of both Mn(III) and Mn(II) are approximated by the summation of the various contributing energy terms: (*50*)

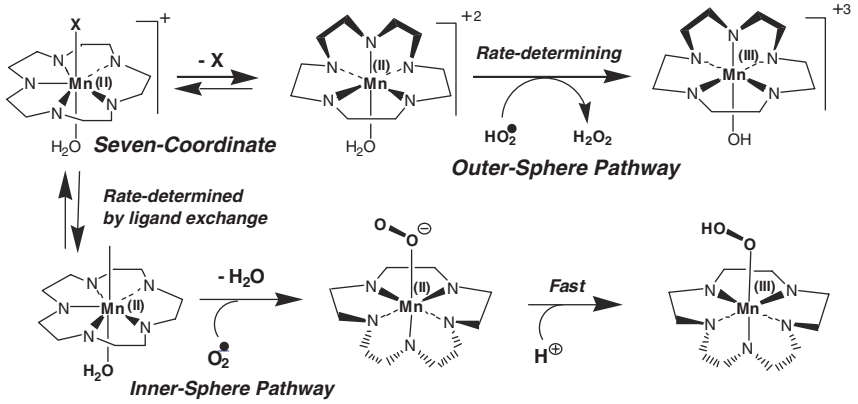

FIG. 10. Mn(II) and Mn(III) solution species involved in binding and dismutation of superoxide anion.

Equation 6 $$\text{Energy}_{\text{Mn(III)}} = U_{\text{electrostatics}} + U_{\text{H-bond}} + U_{\text{Bond Stretch}} + U_{\text{Ange Strain}} + U_{\text{torsional Strain}} + U_{\text{dihedral Strain}} + U_{\text{Van der Waals}} + U_{\text{Angle Deformation}};$$

Equation 7 $$\text{Energy}_{\text{Mn(II)}} = U'_{\text{electrostatics}} + U'_{\text{H-bond}} + U'_{\text{Bond Stretch}} + U'_{\text{Ange Strain}} + U'_{\text{torsional Strain}} + U'_{\text{dihedral Strain}} + U'_{\text{Van der Waals}} + U'_{\text{Angle Deformation}};$$

For a series of complexes a correlation of ΔE for the folded geometries (both the inner-sphere and the outer-sphere) is simplified by comparing a modified energy $\Delta E^{\#}$ in which the contribution of $(U_{\text{electrostatics}} - U'_{\text{electrostatics}}) + (U_{\text{H-bonding}} - U'_{\text{H-bonding}})$ are removed since they are maintained invariant among the series of complexes. Plots of $\Delta E^{\#}$ $(\Sigma_{\text{Mn(III)}} - \Sigma_{\text{Mn(II)}})_{\text{inner-sphere}}$ vs. k_{is} values (inner-sphere rate constant), and $\Delta E^{\#}$ $(\Sigma_{\text{Mn(III)}} - \Sigma_{\text{Mn(II)}})_{\text{outer-sphere}}$ vs. k_{os} values (outer-sphere rate constant) can be generated. Linear plots of $\Delta E^{\#}$ vs. k_{is} or k_{os} would indicate that the correlation is valid. In the cases described here with the ligands utilized for the database, excellent correlations were obtained relating the folding of one of the three *cis*-NHs as the outer-sphere H-atom transfer path and the folding of one of the two *cis* NHs as the inner-sphere SO binding pathway.

In general, we found a clear energy preference for a single, unique NH to fold on each side of the macrocycle and for each pathway (i.e., the energy differences between possible NH folding modes were large, sometimes as large as 70–100 kcal). Thus, ΔE $(E_{\text{Mn(III)}} - E_{\text{Mn(II)}})$ for the three outer-sphere folds and for the two inner-sphere folds for each

complex always affords a clear lowest energy choice for each type of fold with each complex. It is also clear from these modeling analyses that the orientation of the NHs is an important aspect of the strain energies required to fold the ligands. Implicit in this exercise is the assumption that the orientation of the NHs relative to the substituents is known. For those complexes in which crystallographic data exists, the orientations are known. Using this data, certain structural relationships (e.g., a *trans*-cyclohexano substituent dictates that the NHs α to the substituted carbons of the macrocyclic ring must also be *trans*), and MM calculations of the free ligands and for the Mn(II) planar 7-coordinate complexes, the NH pattern can be established with a high level of confidence for any complex of this family.

The goals of the correlations established above were to determine if (1) the folding paradigm is indeed consistent, (2) there are unique folding patterns for the innersphere and separate unique folding patterns for the outer-sphere pathways, and (3) if the MM calculation/modeling paradigm can be successfully used to predict structures in order to optimize the number of substituents for maximum stability while retaining high catalytic activity. This modeling paradigm based on MM calculations successfully addressed all three points. This meant that progress in developing highly substituted complexes with high catalytic activity could be made without the need to rely on trial and error synthesis, which can be exceedingly time-consuming for the synthesis of such highly substituted and stereo-defined ligands. Indeed, the excellent correlations allowed us to test the model in a predictive manner utilizing the four ligands of Fig. 8.

From the standpoint of ease of synthesis and the desire to maximize the stability with the minimum number of substituents, we chose to further elaborate the bis-cyclohexano structure of the high activity catalyst derived from ligand **17**. Note that the complex of this ligand with four of the macrocyclic ring carbons bearing a substituent achieves equivalent stability to those complexes bearing five methyl substituents. Thus, synthetically it was attractive to add an additional methyl to this ligand. Intuitively, to increase stability most efficiently, we chose to put the additional substituent on one of the chelate rings that did not possess a substituent. Thus, structures **28** and **29**, each bearing an additional methyl substituent, were modeled. The two complexes only differ in the stereochemistry of the added methyl substituent: **28** (*S*-Me) and **29** (*R*-Me). The predictions based on the use of these correlations are that the all *R* complex **29** should be a very good catalyst, especially via the outer-sphere pH dependent path, while complex **28** with the *S*-Me would be much less active via this mode, and they should possess comparable activities via the innersphere path. As predicted, the complex **29** is in fact very active with a large pH dependence; about $3\times$ that of complex **28**. In fact, complex **29** possesses a catalytic rate at pH = 7.4 in excess of $1.5 \times 10^{+8}\,M^{-1}\,s^{-1}$

and was the most active catalyst which we had synthesized up to that point.

Based on this level of success, it was intriguing to consider more highly substituted structures and whether they, in fact, would have catalytic activity. One type of substituent which we have observed to enhance stability is the *gem*-dimethyl; thus the *gem*-dimethyl complex **30** was subjected to the modeling paradigm. The results were quite clear and showed that no lower energy folded conformations exist (i.e., neither the inner- nor the outer-sphere pathway would be predicted to operate with this structure). The ligand and complex were synthesized and, indeed, only a trace of catalytic activity was observed.

The desire to increase stability by increasing the number of substituents on the macrocycle while retaining good catalytic activity led us to consider whether there were carbons of ligand **29** on which one could add a substituent and thereby increase the stability and retain good activity. Modeling led to the prediction that, of the five carbon atoms of the macrocyclic ring of **29** which were devoid of substituents, the 14-position could bear a methyl (or other substituent) and retain reasonable activity, but only if the stereochemistry of that additional substituent is *R* – generating the all *R* hexasubstituted ligand structure **31**. The modeling, in fact, predicts that the catalytic activity for such a complex **31** should be mid-range within this family via both pathways. The actual activity was actually better than the parent unsubstituted complex, [Mn([15]aneN$_5$)Cl$_2$], (**Ia)**; especially significant, considering that the complex bore six substituents. In fact, this complex not only has a better catalytic activity than **Ia**, but it possesses a kinetic stability of over 2000 times that of the original unsubstituted parent complex, [Mn([15]aneN$_5$)Cl$_2$], and a binding constant, log $K\sim$15.5 – more than 5 log units greater. An important structural insight into the driving force for the folding can be illustrated with this complex (Fig. 11). The 14*R*-Me substituent of the ligand **31** is in an axial position in the planar 7-coordinate Mn(II) complex structure. This high-energy strained conformation is dramatically relieved when the outer-sphere fold occurs generating the 6-coordinate aquo structure. This folding places the 14*R*-Me into an equatorial orientation; thus, relieving strain and providing an additional driving force for the fold.

Two complexes deserve additional comment since they exhibited a unique lack of activity: the Mn(II) complexes of ligand **10** and ligand **18**. For the complex with ligand **10**, no outer-sphere H-atom pathway was observed in its SOD catalysis. From the modeling experiments it was quite clear that such a path could not occur because the folding corresponding to the outer-sphere fold with this ligand was extremely unfavorable. Complex **18,** bearing the bis-cyclohexyl moiety, was also quite distinctive in that little or no catalytic activity was observed. Again the modeling was predictive of this; i.e., NH foldings were very high energy indicating that this ligand preferred a planar geometry and hence would be a poor catalyst, as observed.

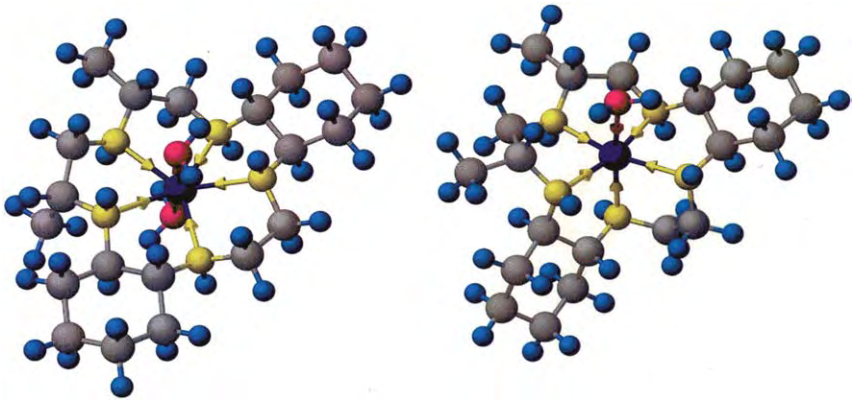

FIG. 11. Molecular structure of the complex [Mn(ligand **31**)] from MM calculations for the seven-coordinate bis(aquo) complex and the six-coordinate mono(aquo) complex showing the folded lowest energy structure for this complex.

In general, the linear correlations developed for this system of Mn(II) complexes lends support to the theory that folding is a critical aspect of catalytic activity for these synthetic enzymes and that the substituents, and their relative position and stereochemistry, influence folding in a predictable manner. Thus, we are able to model any given complex for the inner-sphere or the outer-sphere folding energetics and calculate the expected rate constant for each path for any ligand pattern! This paradigm has worked extremely well at correlating and predicting activity, and has made it possible to design highly substituted and stereodefined molecules and test their potential utility as a catalyst without the extraordinary effort required to synthesize such a structure in advance. We have been able to literally test hundreds of combinations of structures in this fashion and ascertain to a fair degree of certainty whether a ligand can provide an active catalyst prior to embarking on the complicated synthesis. In no case have we yet observed this modeling paradigm to fail to predict the approximate activity of a complex.

VII. Continuing Developments

Biological results generated with complexes designed using the MM2 technique and methods described here have provided additional confidence that these techniques hold great promise for the design of improved human therapeutics. Continuing efforts aimed at developing catalysts with activities approaching that of the Cu/Zn SOD enzymes ($k_{cat} > 1 \times 10^9\,M^{-1}\,s^{-1}$) and with enhanced stabilities are in progress. By building on these modeling successes with detailed knowledge of the factors affecting stability, we have designed and synthesized

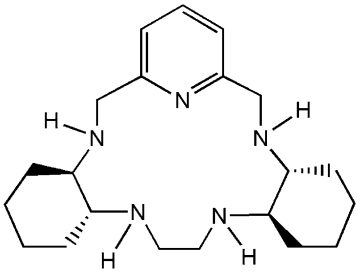

FIG. 12. The ligand **32** whose Mn(II) complex is the Metaphore Pharmaceutical's compound, **M40403**.

ligands and their Mn(II) complexes that not only possess dramatically enhanced stabilities and competent catalytic rates, but can be readily synthesized in few steps from commercially available building blocks. This last point is very important and it cannot be over-emphasized based on the ease and cost of synthesis and development, both very important elements in drug design. One notable success is the complex **M40403** [Mn(II) complex of ligand **32**, Fig. 12**]** which was successfully developed at Metaphore Pharmaceuticals and introduced into human clinical testing in 2001 (*51*,*52*).

The synthesis of **M40403** is achieved by a very atom efficient and chemically high yield template ring-closure in which the linear tetraamine, *N*,*N*′-bis-[(1*R*,2*R*)-2-aminocyclohexyl]-1,2-diaminoethane, is condensed in a mole ratio of 1 : 1 : 1 with $MnCl_2$ and 2,6-pyridinedicarboxaldehyde affording the precursor bisimine in a quantitative chemical yield and with complete stereochemical retention of the all *R* stereochemistry (*52*). The relative ease of synthesis of such a synthetic enzyme in high yield accomplishes one of the major design goals of any drug substance; namely, the cost/difficulty of manufacture. In addition to solving this design goal, this complex also addresses the need to have a ligand that can bind the Mn(II) very tightly and still afford a reasonable catalytic rate for superoxide dismutation at physiological pH. The marriage of the very high stability-imparting characteristics (i.e., lower basicity and rigidity) of the monopyridyl substituted ligand **19** combined with the propensity of the *R*,*R*,*R*,*R*-bis-cyclohexano moiety present in **17** to impart folding of one of the secondary NHdonors (into an axial binding site) was intellectually quite appealing. Molecular modeling experiments suggested that a complex such as **M40403** should be a competent catalyst as compared to that of the complex based on ligand **19**, but not as good as that derived from ligand **17** since it is more constrained to a planar geometry. In fact, at pH = 7.4, it was found that this was the case with most of the catalytic activity due to the inner-sphere superoxide binding pathway and only a small contribution to the overall rate being due to outer-sphere pH dependent (highly-folded six-coordinate intermediate) pathway (*53*).

Nevertheless, the incredibly high kinetic and thermodynamic stability of this complex, coupled with the ease of synthesis and its activity in a variety of pharmacologically relevant models of human disease (*51,54–57*), all contributed to the decision to pursue this compound as a human drug candidate. (Fig. 13)

Assuming that increasing the catalytic activity of the SOD mimetic will translate into a decreased human dose, it would be desirable to further increase the catalytic activity. Since the native SOD enzymes possess catalytic rate constants on the order of $10^9\,M^{-1}\,s^{-1}$, we attempted to design a low molecular weight mimic utilizing the **M40403** platform as a starting point for further structural modification/optimization studies using molecular modeling – with the provision and constraint that any structure selected for development following modeling must possess a reasonable synthetic route affording drug product with a pharmaceutically acceptable manufacturing cost.

One molecule that met the threefold design criteria of enhanced catalytic activity, ease of synthesis, and high stability is a dimethyl-substituted derivative of the ligand **32** (Fig. 14). This new ligand possesses the *S,S*-dimethyl stereochemistry and is readily synthesized in high yield via the template condensation utilizing 2,6-diacetypyridine in place of 2,6-pyridinedicarboxaldehyde (*53*). Two other isomers are possible when the *R,R*-diaminocyclohexane tetraamine is used and they have also been synthesized and characterized (*53*).

Modeling clearly predicts that the Mn(II) complex of the *S,S*-dimethyl-substituted ligand **35** (designated as Metaphore compound **M40401**) should be highly favored to fold into an octahedral geometry

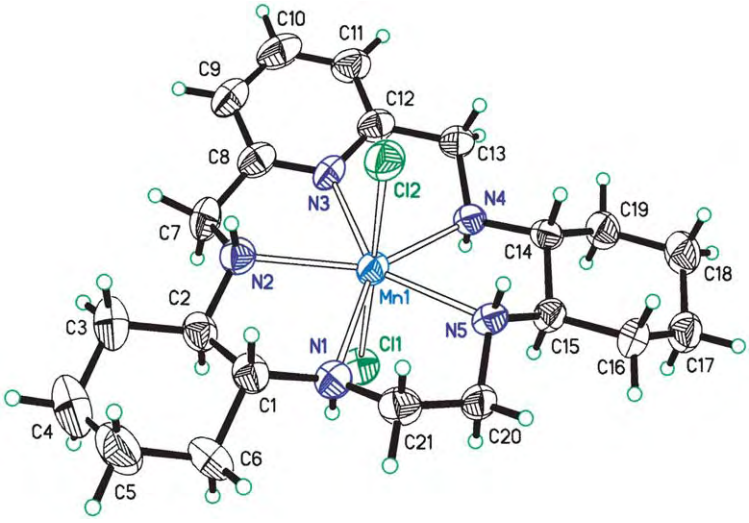

FIG. 13. Ortep drawing for the **M40403** complex ([Mn(ligand **32**)Cl_2] showing the 50% probability ellipsoids for the non-hydrogen atoms and the hydrogen atoms of the secondary amines (*53*).

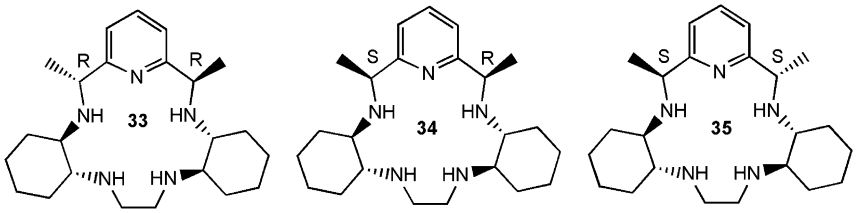

FIG. 14. Structure of the three isomeric dimethyl substituted derivatives of ligand **32**.

when complexed to Mn(II), while the complex with the ligand, **33**, of all *R*-stereochemistry, is constrained to be planar and is unable to fold, even as the Mn(III) ion. The *R,S*-ligand, **34**, when complexed to Mn(II) has an energetics for folding that is comparable to that with ligand **32**, the unsubstituted analogue. Measurement of the catalytic rates for these complexes validates these results and reveals that the complex with ligand **33** possesses no catalytic rate for the superoxide dismutation reaction and that the complex with ligand **34** possesses a catalytic rate profile virtually identical to that of **M40403** (complex with ligand **32**) (*53*). The most significant result is that the complex with ligand **35** possesses a catalytic rate constant for SOD activity greater than $10^9\,M^{-1}\,s^{-1}$ at pH = 7.4 – essentially as fast as the native Cu/Zn SOD enzyme!

The crystal structure of the dichloro complex, **M40401**, (crystallized from 1 : 1 : 1 THF:MTBE:MeOH) with this ligand **35** was determined and found to possess a very unique solid state structure (Fig. 15) (*53*). This complex crystallizes in a monoclinic space group ($P2_1$) with two distinctly different molecules in the unit cell. One form is the *trans*-dichloro seven-coordinate geometry observed with **M40403**, but the second molecule possesses a six-coordinate geometry in which one of the chlorides has moved away from the metal by nearly half an angstrom becoming a non-coordinated (ionic) chloride in which one of the secondary nitrogen atoms (on the unsubstituted chelate ring) has folded toward the vacated axial site generating a six-coordinate complex. The observed Cl-Mn-N angle for this folded nitrogen is 120.3 while the calculated angle is 124.6° (*53*).

To further probe the structure of this ligand when chelated to Mn(II) in a situation that can more closely parallel the solution structure of the complex, an attempt was made to crystallize the complex from water in the absence of any coordinating counter ions. This was accomplished by exchanging the chloride anion with hexafluorophosphate (a weakly coordinating anion). The resultant complex, [Mn(Ligand **35**)(H_2O)](PF_6)$_2 \cdot H_2O$, crystallizes as a six-coordinate mono aquo complex with two non-coordinating hexafluorophosphate counterions and an additional water molecule in its crystal lattice. The structure is shown in Figs. 16 and 17 (*58*).

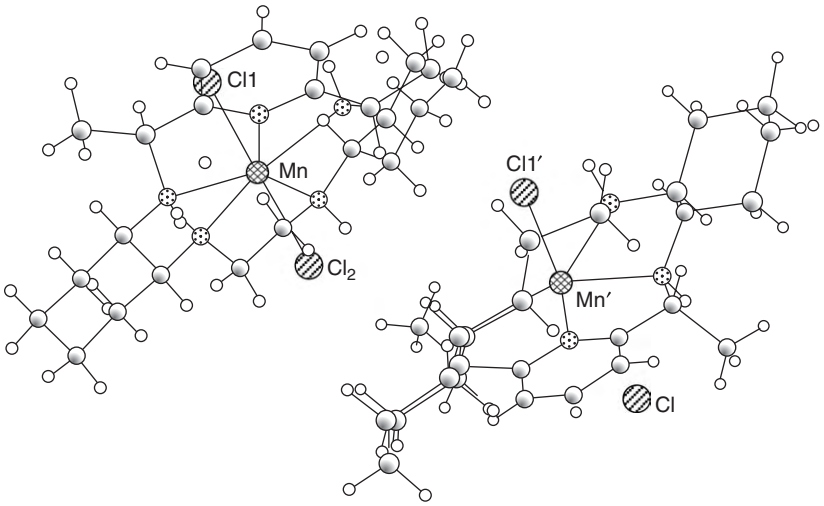

FIG. 15. Ortep drawing for the complex **M40401** ([Mn(ligand **35**)Cl_2]) showing the 50% probability ellipsoids for the non-hydrogen atoms and the hydrogen atoms of the secondary amines (*53*).

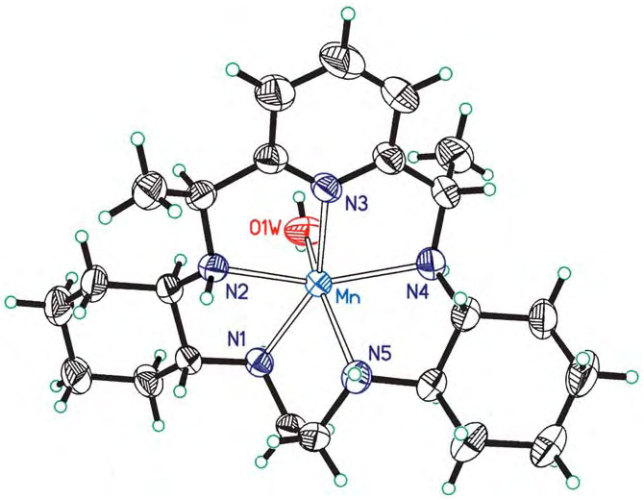

FIG. 16. ORTEP drawing for the complex [Mn(ligand **35**)(H_2O)](PF_6)$_2$ showing the labeling scheme and the 50% probability ellipsoids for the non-hydrogen atoms.

Table 2 lists some selected bond lengths and bond angles. A few very pertinent features stand out for this complex. First, this Mn(II) complex is very nearly a perfect octahedral structure with the macrocyclic ligand folded such that the secondary amine nitrogen atom N_5 (adjacent to one of the fused cyclohexano rings) is folded into a pseudo-octahedral axial coordination site with an aquo oxygen atom occupying

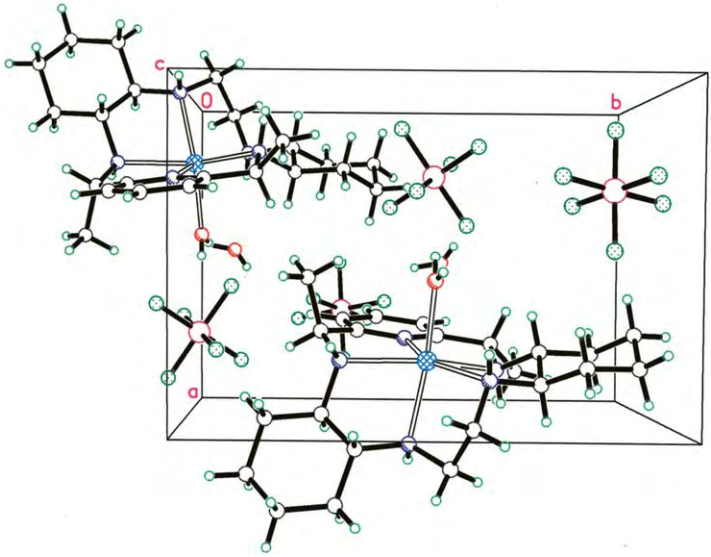

FIG. 17. Unit cell drawing for the complex [Mn(ligand **35**)(H_2O)](PF_6)$_2$ showing the disposition of the hexafluorophosphate anions in the lattice and oriented to show the very highly folded geometry of the macrocyclic ligand and the nearly octahedral shape of the complex.

TABLE II

REPRESENTATIVE BOND LENGTHS AND BOND ANGLES FOR THE COMPLEX [MN(LIGAND **35**)(H_2O)](PF_6)$_2$ AS DETERMINED BY X-RAY CRYSTALLOGRAPHIC DETERMINATION

Type	Length(Å)	Type	Angle (deg).
Mn–N_1	2.250(3)	OMnN_5	151.0(1)
Mn–N_2	2.293(3)	OMnN_1	86.5(1)
Mn–N_3	2.177(3)	OMnN_2	100.3(1)
Mn–N_4	2.296(3)	OMnN_3	91.6(1)
Mn-N_5	2.244(3)	OMnN_4	95.4(1)
Mn–O	2.164(3)	N_5MnN_1	79.2(1)
		N_5MnN_2	100.9(1)
		N_5MnN_3	113.0(1)
		N_5MnN_4	77.3(1)
		N_4MnN_1	133.7(1)
		N_4MnN_3	75.4(1)
		N_3MnN_2	74.4(1)
		N_2MnN_1	77.4(1)

the *trans-* position in this six-coordinate complex. The angle defined by the bound aquo and the folded nitrogen, O–Mn–N_5, is 151°. This is the most highly folded structure that we have observed for any of these pentaaza 15-membered macrocyclic ligands bound to Mn(II) and it is the most active catalyst that we have discovered in this class of Mn(II)

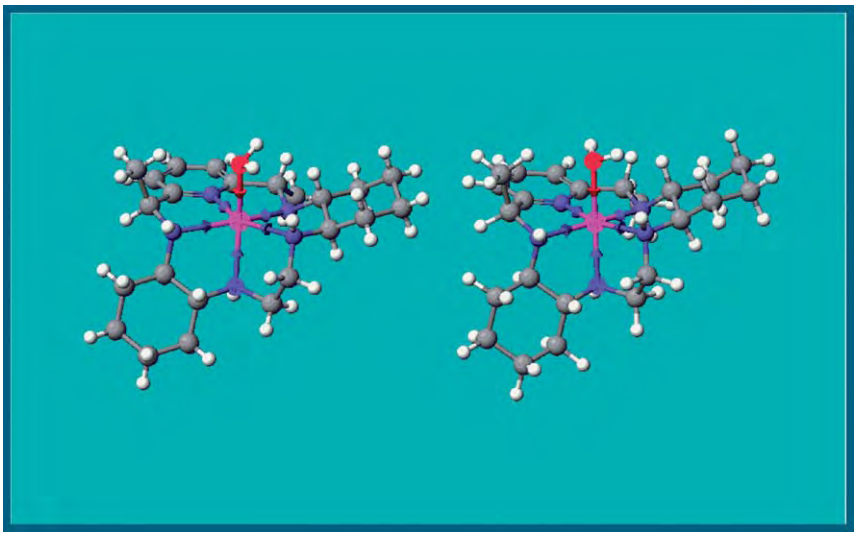

FIG. 18. Structure for [$Mn^{(II)}$(ligand **35**)(H_2O)](PF_6)$_2$, **M40401,** from X-ray diffraction and MM2 minimized structure of the octahedral [$Mn^{(III)}$(ligand **35**)(H_2O)]. *Right*: $<$O-Mn^{II}-N $= 151^\circ$ (left) versus $<$O-Mn^{III}-N $= 172^\circ$ (right).

complexes. Indeed, as is shown in Fig. 18 when the observed structure of this Mn(II) ion is compared to the calculated structure of its Mn(III) oxidation product, there is very little difference in the structure of the two complexes. The aquo six-coordinate solution structure of this complex is also the catalytically relevant structure for this complex. That this is the pseudo-octahedral structure predicted by modeling provides further support that Mn(II) complexes, such as **M40401**, when forced to adopt an octahedral geometry by the ligand will be more catalytically active.

VIII. Conclusion

An understanding of the details of the mechanism of action of these synthetic superoxide dismutase catalysts has made it possible to devise a computer modeling paradigm that allows one to design highly substituted (and hence highly stable) complexes that possess high catalytic activity. Molecular mechanics calculations have made it possible to correctly predict how substituents and their stereochemistry affect the energetics of ligand folding and thus catalytic activity. An excellent example of this is the comparison of predicted structures of the M40403 and **M40401** Mn(II) complexes (Fig. 19). The MM2 calculation for each structure reveals that the *S,S*-dimethyl substituted derivative (**M40401**) is more highly disposed to fold around the Mn(II) ion (as confirmed by X-ray diffraction) into a pseudo-octahedral

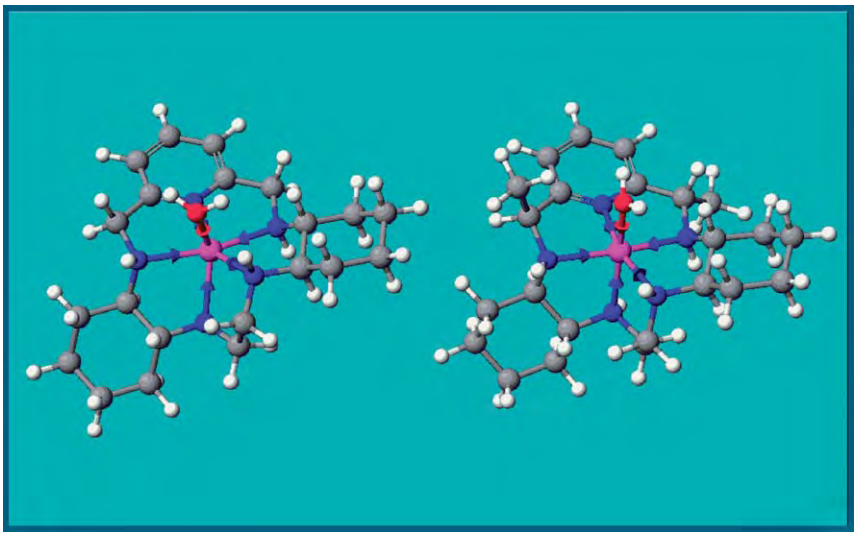

FIG. 19. MM2 minimized structures of **M40403** and **M40401** as monoaquo species showing the greater tendency of the macrocycle to fold into a pseudo-octahedral geometry with the **M40401** complex.

geometry required by the Mn(III) ion and is, as a result, predicted and is found to be the better catalyst for the dismutation of superoxide in which the rate-determining step is oxidation of the Mn(II) ion to Mn(III).

It should be noted that the complexes discussed here and the methodologies described here are aimed solely at the design of a core structure for an optimized catalyst. The compounds presented here only present a hydrocarbon surface; but, in fact, the optimum and final structure of a drug designed for any particular disease may well require a different log *P* or different type of functional substituent(s) to direct delivery of the compound, to optimize its efficacy, to minimize toxicity, and to facilitate its clearance as a drug. The chemistry presented here for designing and synthesizing core catalyst structures optimized for stability and catalytic activity, are amenable to the construction of complexes which have pendant functionality; e.g., alcohols, amines, amides, esters, acids, etc. Such chemistry is ready available from standard peptide chemistry and other methods using the available pool of natural and synthetic chiral amino acids. Thus, by adapting a promising core catalyst structure, such as that achieved with the Mn(II) complex of ligand **35** (**M40401**), it is possible to develop optimized structures with varying functionalities tailored to meet the need of the disease state. It is in such a manner that human pharmaceutical agents with minimal toxicity and maximal efficacy could be realized.

IX. Experimental

Crystals of **M40401 · $(PF_6)_2$** with the general formula $[Mn(N_5C_{23}H_{39})(H_2O)][PF_6]_2 \cdot H_2O$ were obtained from an aqueous ethanol solution as large faint yellow rectangular parallelepipeds.

Synthesis of $[Mn(N_5C_{23}H_{39})(H_2O)][PF_6]_2 \cdot H_2O$: $[Mn(N_5C_{23}H_{39})(Cl_2)]$ **M40401** (483 mg, 0.95 mmol) was dissolved in DI water (10 mL) and stirred while a solution of $AgPF_6$ (479 mg, 1.89 mmol) in 2 mL DI water was added dropwise. The resulting thick white gel was shaken, then stirred for 3–4 min and filtered through a pad of celite. The solid cake was air-dried and extracted with MeOH (2×10 mL, in the same filter funnel). The filtrate was then filtered through a 0.5 μm membrane, the solvent removed then the residue dried *in vacuo* (0.4 Torr, RT, 3 h) to afford the bis- hexafluorophosphato complex (610 mg, 90%) as a solid with a purity $\geq$99.5% by HPLC. A small amount (50 mg) of complex was added to 1–2 mL of boiling water. To this was then added ethanol dropwise until a clear solution resulted and the solution was then filtered through a plug of glass wool and allowed to sit undisturbed. Over the course of several days, the solution yielded crystals suitable for X-ray diffraction and were collected by filtration.

References

1. (a) McCord, J. M.; Fridovich, I. *J. Biol. Chem.* **1969**, *244*, 6049. (b) Fridovich, I. *J. Biol. Chem* **1989**, *264*, 7761. (c) Miller, A. F. Curr. Opin. Chem. Biol. 8**2004**, 162.
2. Werns, S. W.; Simpson, P. J.; Mickelson, J. K.; Shea, M. J.; Pitt, B.; Lucchesi, B. R. *J Cardiovasc. Pharmacol.* **1988**, *11*, 36.
3. Omar, B. A.; McCord, J. M. *Mol. Cell. Cardiol.* **1991**, *23*, 149.
4. McCord, J. K. *J. Free Radic. Biol. Med.* **1986**, *2*, 307.
5. Oyanagui, Y. *Biochem. Pharmacol.* **1976**, *25*, 1465.
6. Droy-Lefaix, M. T.; Drouet, Y.; Geraud, G.; Hosford, D.; Braquet, P. *Free Radic. Res. Commun.* **1991**, *12–13*, 725.
7. Shingu, M.; Takahashi, S.; Ito, M.; Hamamatu, N.; Suenaga, Y.; Ichibangase, Y.; Nobunaga, M. *Rheumatol. Int.* **1994**, *14*, 77.
8. Ando, Y.; Inoue, M.; Hirota, M.; Morino, Y.; Araki, S. *Brain Res.* **1989**, *477*, 286.
9. Chan, P. H.; Yang, G. Y.; Chen, S. F.; Carlson, E.; Epstein, C. J. *Ann. Neurol.* **1991**, *29*, 482.
10. Yang, G.; Chan, P. H.; Chen, J.; Carlson, E.; Chen, S. F.; Weinstein, P.; Epstein, C. J.; Kamii, H. *Stroke* **1994**, *25*, 165.
11. Deng, H. X.; Hentati, A.; Tainer, J. A.; Iqbal, Z.; Cayabyab, A.; Hung, W. Y.; Getzoff, E. D.; Hu, B.; Herzfeldt, R. P.; Roos, C.; Warner, G.; Deng, E.; Soriano, C.; Smyth, H. E.; Parge, A.; Ahmed, A. D.; Roses, R. A.; Hallewell, M. A.; Pericak-Vance; Siddique, T. *Science* **1993**, *261*, 12.
12. Rosen, D. R.; Siddique, T.; Patterson, D.; Figlewicz, D. A.; Sapp, P.; Hentati, A.; Donaldson, D.; Goto, J.; O'Regan, J. P.; Deng, H. X.; Rahmani, Z.; Krizus, A.; McKenna-Yasek, D.; Cayabyab, A.; Gaston, S. M.; Berger, R.; Tanzi, R. E.; Halperin, J. J.; Herzfeldt, B.; Van den Bergh, R.; Hung, W.-Y.; Bird, T.; Deng, G.; Mulder, D. W.; Smyth, C.; Laing, N. G.; Soriano, E.; Pericak-Vance, M. A.; Haines, J.; Rouleau, G. A.; Gusella, J. S.; Horvitz, H. R.; Brown, R. H. Jr. *Nature* **1993**, *362*, 59.

13. Brown, R. H. Jr. *Cell* **1995**, *80*, 687.
14. Troy, C. M.; Shelanski, M. L. *Proc. Natl. Acad. Sci. USA* **1994**, *91*, 6384.
15. Greenlund, L. J. S.; Deckwerth, T. L.; Johnson, E. M. Jr. *Neuron* **1995**, *14*, 303.
16. Bravard, A.; Sabatier, L.; Hoffschir, F.; Ricoul, M.; Luccioni, C.; Dutrillaux, B. *Int. J. Cancer* **1992**, *51*, 476.
17. Church, S. L.; Grant, J. W.; Ridnour, L. A.; Oberley, L. W.; Swanson, P. E.; Meltzer, P. S.; Trent, J. M. *Proc. Natl. Acad. Sci. USA* **1993**, *90*, 3113.
18. St. Clair, D. K.; Oberley, T. D.; Muse, K. E.; St. Clair, W. H. *Free Radic. Biol. Med.* **1994**, *16*, 275.
19. Safford, S. E.; Oberley, T. D.; Urano, M.; St. Clair, D. K. *Cancer Res.* **1994**, *54*, 4261.
20. Yoshizaki, N.; Mogi, Y.; Muramatsu, H.; Koike, K.; Kogawa, K.; Niitsu, Y. *Int. J. Cancer* **1994**, *57*, 287.
21. Flores, S. C.; Marecki, J. C.; Harper, K. P.; Bose, S. K.; Nelson, S. K.; McCord, J. M. *Proc. Natl. Acad. Sci. USA* **1993**, *90*, 7632.
22. Miesel, R.; Mahmood, N.; Weser, U. *Redox Report* **1995**, *1*, 99.
23. Riley, D. P.; Weiss, R. H. *J. Am. Chem. Soc.* **1994**, *116*, 387.
24. Riley, D. P.; Rivers, W. J.; Weiss, R. H. *Anal. Biochem.* **1991**, *196* (2), 344–349.
25. Riley, D. P.; Lennon, P. J.; Neumann, W. L.; Weiss, R. H. *J. Am. Chem. Soc.* **1997**, *119* (28), 6522–6528.
26. Weiss, R. H.; Flickinger, A. G.; Rivers, W. J.; Hardy, M. M.; Aston, K. W.; Ryan, U. S.; Riley, D. P. *J. Biol. Chem.* **1993**, *268* (31), 23049–23054.
27. Hardy, M. M.; Flickinger, A. G.; Riley, D. P.; Weiss, R. H.; Ryan, U. S. *J. Biol. Chem.* **1994**, *269*, 18535.
28. Weiss, R. H.; Fretland, D. J.; Baron, D. A.; Ryan, U. S.; Riley, D. P. *J. Biol. Chem.* **1996**, *271* (42), 26149–26156.
29. Zweier, J. L. *J. Biol. Chem.* **1988**, *263*, 1353.
30. Kilgore, K. S.; Friedrichs, G. S.; Johnson, C. R.; Schasteen, C. S.; Riley, D. P.; Weiss, R. H.; Ryan, U.; Lucchesi, B. R. *J. Mo. Cell Cardiol.* **1994**, *26*, 995.
31. Black, S. C.; Schasteen, C. S.; Weiss, R. H.; Riley, D. P.; Driscoll, E. M.; Lucchesi, B. R. *J. Pharmacol. Exp. Therapeut.* **1994**, *270*, 1208.
32. Venturini, C. M., Sawyer, W. B., Smith, M. E., Palomo, M. A., McMahon, E. G., Weiss, R. H., Riley, D. P.; Schasteen, C. S. A manganese-based superoxide dismutase mimic protects feline myocardium from necrosis after ischaemia and reperfusion. In: *"The Biology of Nitric Oxide 3: Physiological and Clinical Aspects"*; Eds. Moncada, S.; Feelisch, M.; Busse, R.; Higgs, E. A.; Portland Press: London, **1994**, pp. 65.
33. Kasten, T. P.; Settle, S. L.; Misko, T. P.; Riley, D. P.; Weiss, R. H.; Currie, M. G.; Nickols, G. A. *Proc. Soc. Exp. Biol. Med.* **1995**, *208*, 170.
34. Meng, Y. Y.; Trachtenburg, J.; Ryan, U. S.; Abendschein, D. R. *J. Am. Coll. Cardiol.* **1995**, *25*, 269.
35. Weiss, R. H.; Riley, D. P. Therapeutic aspects of manganese(II)-based superoxide dismutase mimics. In: "*Inorganic Chemistry in Medicine*"; Ed. Farrell, N., Royal Society of Chemistry.
36. Weiss, R. H., Riley, D. P., Rivers, W. J., Aston, K. W., Flickinger, A. G., Hardy, M. M.; Ryan, U. S. Manganese-based superoxide dismutase mimics: Design, discovery and pharmacologic efficacies. In: *"The Oxygen Paradox"*; Eds. Davies, K. J. A.; Ursini, F.; CLEUP University Press: Padova, Italy, **1995**, pp. 641.
37. Beckman, J. S.; Carson, M.; Smith, C. D.; Koppenol, W. H. *Nature* **1993**, *46*, 584.
38. Lindoy, L. F. *"The Chemistryof Macrocyclic Ligand Complexes"*; Cambridge University Press: Cambridge, Great Britain, **1989**.
39. Lennon, P. J.; Rahman, H.; Aston, K. W.; Henke, S. L.; Riley, D. P. *Tetrahed. Lett.* **1994**, *35*, 853.
40. Riley, D. P. *Ad. Supramol. Chem.* **2000**, *6*, 217–242.
41. Aston, K. W.; Henke, S. L.; Modak, A. S.; Riley, D. P.; Sample, K. R.; Weiss, R. H.; Neumann, W. L. *Tetrahed. Lett.* **1994**, *35*, 3687.

42. Riley, D. P.; Henke, S. L.; Lennon, P. L.; Weiss, R. H.; Neumann, W. L.; Rivers, W. J. Jr.; Aston, K. W.; Sample, K. R.; Rahman, H.; Ling, C.-S.; Shieh, J. J.-J.; Busch, D. H.; Szulbinski, W. *Inorg. Chem.* **1996**, *35* (18), 5213.

43. Franklin, G. W.; Riley, D. P.; Neumann, W. L. *Coord. Chem. Rev.* **1998**, *174*, 133.

44. Neumann, W. L.; Franklin, G. W.; Sample, K. R.; Aston, K. W.; Weiss, R. H.; Riley, D. P. *Tetrahed. Lett.* **1997**, *38*, 779.

45. Weiss, R.; Neumann, W.; Meeh, L.; Brown, T.; Lennon, P.; Sample, K.; Zweier, J. A. Samouilov, A.; Wang, P.; Riley, D. *Proceedings of the Society of Magnetic Resonance and the European Society for Magnetic Resonance in Medicine and Biology*, **Vol. 1**, abstract 43.

46. Eigen, M. *Pure Appl. Chem.* **1963**, *6*, 105.

47. Marcus, R. A. *Annu. Rev. Phys. Chem.* **1964**, *15*, 155.

48. Burkert, U.; Allinger, N. L. *Molecular Mechanics*, ACS Monograph 177, American Chemical Society: Washington, DC, **1982**.

49. (a) Hancock, R. D. *Acc. Chem. Res.* **1990**, *23*, 253. (b) Wade, P.W.; Hancock, R. D.; Boeyens, J. C. A.; Dobson, S. M. *J. Chem. Soc., Dalton Trans.* **1990**, 483. (c) Luckay, R.; Chantson, T. E.; Riebenspies, J. H.; Hancock, R. D. *J. Chem. Soc., Dalton Trans.* **1995**, 1363.

50. Riley, D. P.; Henke, S. L.; Lennon, P. J.; Aston, K. W. *Inorg. Chem.* **1999**, *38*, 1908.

51. Salvemini, D.; Zweier, J. L.; Misko, T. P.; Currie, M. G.; Cuzzocrea, S.; Sikorski, J. A.; Riley, D. P. *Science* **1999**, *286*, 304–306.

52. Salvemini, D.; Riley, D. P. *Drugs Future* **2000**, *25* (10), 1027–1033.

53. Aston, K. W.; Rath, N.; Naik, A.; Slomczynski, U.; Schall, O. F.; Riley, D. P. *Inorg. Chem.* **2001**, *40* (8), 1779–1789.

54. Salvemini, D.; Riley, D. P. *Cell Mol. Life Sci.* **2000**, *57*, 1489.

55. Macarthur, H.; Westfall, T.; Riley, D. P.; Misko, T.; Salvemini, D. *Proc. Natl. Acad. Sci. USA* **2000**, *97* (17), 9753.

56. Cuzzocrea, S.; Mazzon, E.; Dugo, L.; Caputi, A.; Riley, D. P.; Salvemini, D. *Eur. J. Pharm.* **2001**, *431* (1), 79–89.

57. Cuzzocrea, S.; Mazzon, E.; Dugo, L.; Caputi, A.; Riley, D. P.; Salvemini, D.; Serraino, I. *Br. J. Pharm.* **2001**, *132* (4), 815–827.

58. Crystal data for the complex [Mn(ligand **35**)(H_2O)](PF_6)$_2$: colorless, monoclinic, space group $P2_1$-C_2^2 (no. 4); $a = 8.978(1)$ Å, $b = 13.126(1)$ Å, $c = 14.175(1)$ Å; $\alpha = 90.000^\circ$, $\beta = 93.199(8)^\circ$, $\gamma = 90.000^\circ$; $V = 1667.8(3)$ Å^3; $Z = 2$; $\lambda = 0.71073$ Å; $\rho = 1.526$ gcm^{-3}; and final statistics from the fourth cycle of full matrix least-squares refinement for all reflection data (collected at -50°C) $R_1 = 0.049$ w$R_2 = 0.087$.

59. Reprinted with permission from reference 53. Copyright (2001) American Chemical Society.

ELECTRONIC TUNING OF THE LABILITY OF INERT Co(III) AND Pt(II) COMPLEXES

RUDI VAN ELDIK

Institute for Inorganic Chemistry, University of Erlangen-Nürnberg, Egerlandstr. 1, 91058 Erlangen, Germany

I. Electronic Tuning

In this contribution an account of possible ways to tune the lability of inert metal complexes through electronic effects is given. This is based on the selective variation of the electronic properties of the apparently innocent spectator ligands bound to inert metal centers and their effect on the lability (i.e. substitution reactivity) of the ligand participating in the substitution process. In general, ligand substitution reactions are the most fundamental chemical processes that can occur on a metal center and are of fundamental importance in all processes that deal with the activation of small molecules (such as dioxygen, carbon dioxide, nitrogen oxide and alkanes), oxidative addition/reductive elimination reactions, and electron transfer processes. A fundamental understanding of the labilization mechanisms can assist a systematic tuning of the reactivity of the metal complex and so affect the performance of the metal complex in the activation of small molecules and related catalytic functions. Inert metal complexes have the advantage

ADVANCES IN INORGANIC CHEMISTRY
VOLUME 59 ISSN 0898-8838 / DOI: 10.1016/S0898-8838(06)59008-7

of presenting stable centers for specific interactions that can promote chemical conversions in a selective manner. A full mechanistic understanding of such tuning abilities could result in a systematic control over reactivity of well-designed metal complexes.

The sequence followed in this presentation is the one adopted for the presentation at the ACS Symposium in Philadelphia. We start off with some general remarks about electronic tuning effects and the mechanistic approach adopted in this work. We then turn to a discussion of the electronic tuning of inert Co(III) and Pt(II) complexes, and finally draw some general conclusions based on this work. Most of the reported systems are taken from our own work in this area performed over the past few years. Where appropriate reference will also be made to relevant contributions from other groups, but this account is not intended to be a complete coverage of the theme since that would exceed the allotted space for this contribution.

Electronic tuning of the lability of metal centers can be accomplished through a systematic variation of σ-donor and π-acceptor effects of spectator ligands, or a combination thereof. The introduction of strong σ-donors such as metal–carbon or metal–phosphor bonds in general, labilize the *trans* position in octahedral and square-planar complexes and so induce an increase in the ligand displacement rate in that position. This can also be accompanied by a changeover in mechanism, i.e. from more associative (A or I_a) to more dissociative (D or I_d). The labilization can result from ground state effects in which case we generally refer to the *trans influence*, which results from structural modifications of the metal complex, or from transition state effects in which case we refer to the *trans effect*, which results from kinetic effects on the system. In many cases these *trans* effects go hand in hand since ground state bond labilization is bound to assist the displacement of the ligand during the substitution process and vice versa. In general, σ-donor effects can promote both associative and dissociative substitution processes in transition metal complexes.

The introduction of π-acceptor effects on spectator ligands, such as the introduction of in-plane pyridine or bipyridine ligands, causes an increase in the electrophilicity of the metal center, which in turn can promote the associative binding of an entering nucleophile and accelerate the ligand substitution process. Such π-acceptor effects can be offset by σ-donor effects, since the latter decreases the electrophilicity of the metal center. In this way it should in principle be possible through the systematic tuning of σ-donor and π-acceptor effects to reach almost any degree of lability of the metal complex, as will be shown in the forthcoming sections.

Our approach is a kinetic–mechanistic one since the lability of metal complexes can only be quantified through a kinetic analysis of the substitution behavior. The application of fundamental reaction kinetics has the advantage that not only information on the reactivity/lability of a metal complex can be obtained from the empirical rate law,

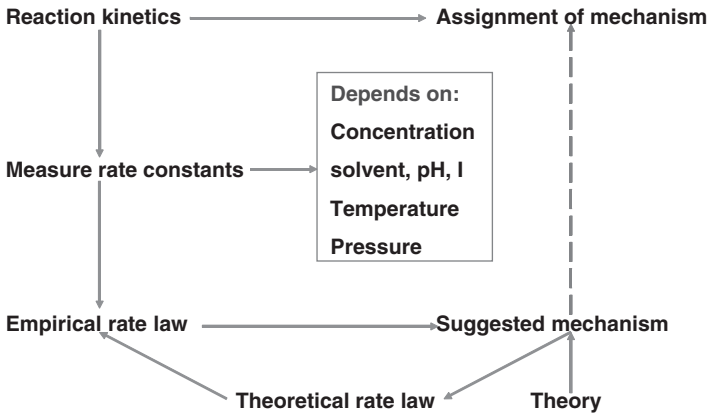

FIG. 1. Schematic presentation of the fundamental principles involved in the elucidation of inorganic reaction mechanisms through kinetic and theoretical considerations.

but in addition mechanistic information can be gained from a systematic variation of chemical and physical variables. In the latter case it is temperature and pressure effects that can through the application of the transition state theory reveal important mechanistic information in terms of the nature of the transition state from activation enthalpy, entropy and volume data. A schematic presentation of the fundamental ideas involved in inorganic reaction kinetics is given in Fig. 1. In order to come as close as possible to the 'real' mechanism, it is essential to gain as much as possible information from the empirical rate law, activation parameters, chemical knowledge on the studied system, evidence for possible intermediates and a theoretical analysis of the suggested mechanism or even the transition state. In this respect, based on our experience over many years, the application of high-pressure thermodynamic and kinetic techniques can reveal crucial mechanistic information through the construction of volume profiles for chemical processes. Such profiles not only complement free enthalpy profiles for the studied reaction but further enable a chemical picture to be visualized on the basis of partial molar volume changes that occur along the reaction coordinate. Numerous examples of such profiles are now available and have clearly demonstrated the ability of such profiles to contribute to the elucidation of inorganic, organometallic and bioinorganic reaction mechanisms (*1*).

II. Inert Co(III) Complexes

In general, classical Werner Co(III) complexes are inert and undergo ligand substitution reactions on a time scale of hours at 50–60°C. Many ligand substitution reactions of Co(III) ammine complexes have been studied in detail and most reactions occur according to a dissociative

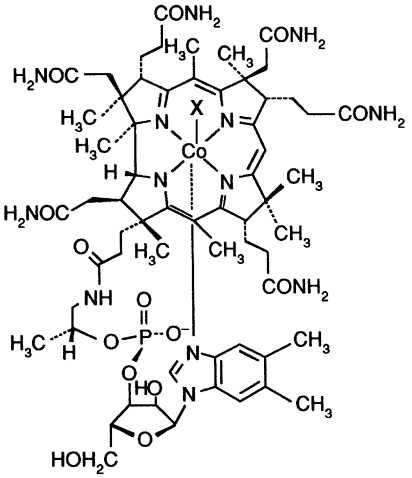

FIG. 2. Schematic structure of cobalamin, where $X = CN^-$ for cyanocobalamin (vitamin B_{12}), $X = H_2O$ for aquacobalamin (vitamin B_{12a}) and X = 5′-deoxyadenosyl for coenzyme B_{12}.

interchange (I_d) or limiting dissociative (D) mechanism. It could be nicely demonstrated that for the slow aquation reactions of a series of complexes of the type $[Co(NH_3)_5X]^{3+}$, where X is water or a neutral leaving group, all available kinetic evidence supports the operation of an I_d mechanism. By way of comparison, reversible ligand substitution reactions in the axial β-position of the Co(III) center in aquacobalamin, H_2OCbl (see structure of Vitamin B_{12}12 –> in Fig. 2), are orders of magnitude faster through the influence of the 15-member corrin ring and the chelated dimethylimidazole ligand in the axial α-position (*2–14*). The overall reaction can be formulated as in (1), where k_1 and k_{-1} represent the complex-formation and aquation rate constants, respectively. This scheme is valid for neutral pH since aquacobalamin has a pK_a value of 8.1. Some typical nucleophile concentration dependencies for the observed pseudo first-order rate constant for such reactions are shown in Fig. 3, from which it follows that reaction (1) is indeed a reversible process and the complex-formation reaction can involve precursor-formation as evidenced by the non-linear concentration dependence observed in some cases. Thus, reaction (1) typically proceeds via a dissociative interchange (I_d) mechanism as outlined in more detail in reactions (2) and (3), for which the rate law is given in (4).

$$B_{12}\text{-}H_2O + L \rightleftharpoons B_{12}\text{-}L + H_2O \quad k_1, k_{-1} \tag{1}$$

$$B_{12}\text{-}H_2O + L \rightleftharpoons \{B_{12}\text{-}H_2O.L\} \quad K_2 \tag{2}$$

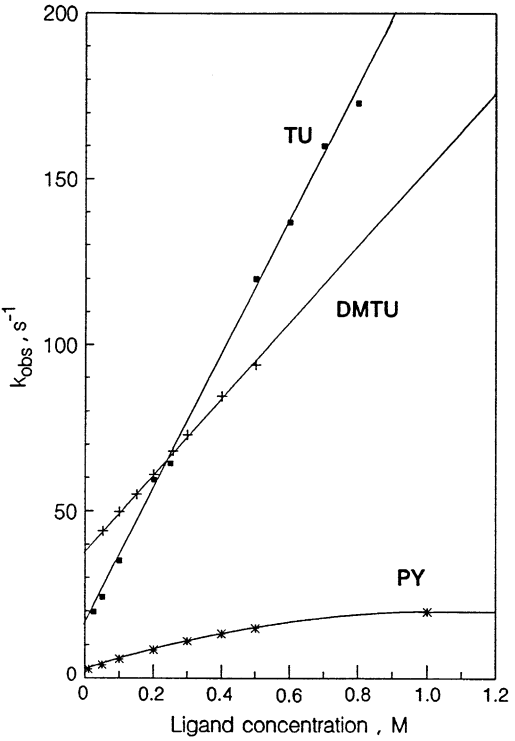

FIG. 3. Typical plots of k_{obs} versus entering ligand concentration at 25°C for reaction (1), TU = thiourea, DMTU = dimethylthiourea and PY = pyridine.

$$\{B_{12}\text{-}H_2O.L\} \rightleftharpoons B_{12}\text{-}L + H_2O \quad k_3, k_{-3} \tag{3}$$

$$k_{obs} = \{k_3K_2[L]/(1 + K_2[L])\} + k_{-3} \tag{4}$$

Under experimental conditions where no kinetic saturation is observed, i.e. in the absence of significant encounter complex formation, the rate expression (4) simplifies to (5), for which in comparison to the overall reaction (1), $k_3K_2 = k_1$ (the overall second-order complex-formation rate constant) and $k_{-3} = k_{-1}$ (the aquation rate constant). This is the case for thiourea and dimethylthiourea as entering ligands in Fig. 3.

$$k_{obs} = k_3K_2[L] + k_{-3} \tag{5}$$

Further evidence for the operation of an I_d substitution mechanism comes from the activation parameters determined from the temperature and pressure dependence of the reactions. Here it is especially the

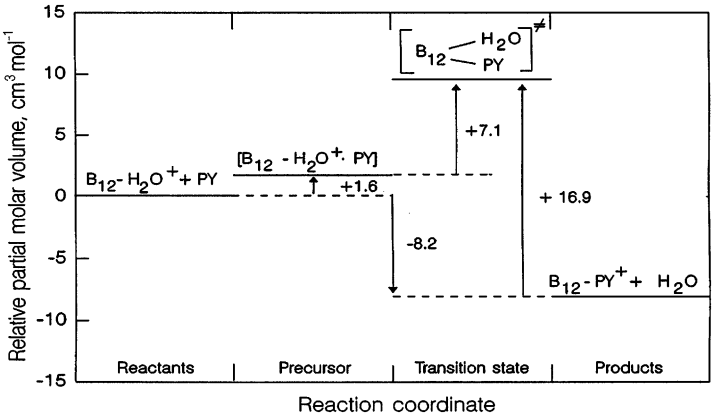

FIG. 4. Representative volume profile for reactions (2) and (3) for L = pyridine.

positive activation entropies and positive activation volumes that support the operation of an I_d mechanism. An example of a typical volume profile for reactions (2) and (3) is given in Fig. 4, which clearly demonstrates the dissociative interchange nature of the substitution process. In this particular case, plots of k_{obs} versus pyridine concentration are significantly curved (see Fig. 3) and enable the estimation of K_2, k_3 and k_{-3} as a function of temperature and pressure. Thus, all the observed kinetic trends are in agreement with the expectations for a labile d^6 metal center.

A. Substitution Reactions of Adenosylcobalamin (AdoCbl)

The introduction of a cobalt–carbon bond in coenzyme $B_{12}12 ->$ is expected to further increase the lability of the complex, especially in the position *trans* to this bond. The expected high lability will, in principle, require a very strong nucleophile to effectively bind to the Co(III) center. The reaction of 5′-deoxyadenosylcobalamin (AdoCbl) with CN^- has been known for several decades and involves heterolytic cleavage of the Co–C bond. The reaction products were isolated and characterized as $(CN)_2$Cbl, adenine and the cyanohydrin of D-erythro-2,3-dihydroxy-4-pentanol (*15*). The mechanism of this reaction, and the question whether CN^- first attacks the α- or the β-position of AdoCbl, were of considerable interest to inorganic chemists for quite some time.

The introduction of a metal–carbon bond in vitamin B_{12} is expected to labilize the *trans*-positioned dimethylbenzimidazole (DMBz) group. It is therefore reasonable to expect that ligand substitution will follow a dissociative mechanism. However, we found that AdoCbl reacts with CN^- in a single kinetically observable step, with no evidence for the displacement of DMBz in the α-position by CN^- in the first reaction step. The rate-determining step was suggested to involve the displacement of

the Ado group in the β-position (*16*). The study was carried out at pH 11.0, and the CN^- concentration was varied in the range 0.005–0.5 M. A linear plot of k_{obs} versus [CN^-] with a negligible intercept was obtained (Fig. 5), indicating that the reaction is irreversible and that no other parallel reaction occurred. This plot further showed no sign of curvature at the highest cyanide concentration employed. Surprising, however, is the fact that the observed reaction was much slower than expected for such a labile Co(III) center, and the slope of the plot gave a second-order rate constant of $7.4 \times 10^{-3}\,M^{-1}\,s^{-1}$ at 25°C (*16*). The reaction sequence given in Scheme 1 was suggested to account for the observed experimental data, in which the formation of (α-DMBz)(β-CN)Cbl is the rate-determining step and is followed by the rapid displacement of the DMBz group to produce $(CN)_2$Cbl.

The reaction between AdoCbl and CN^- was also studied as a function of temperature and pressure. $\Delta H^{\neq}$ and $\Delta S^{\neq}$ were found to be

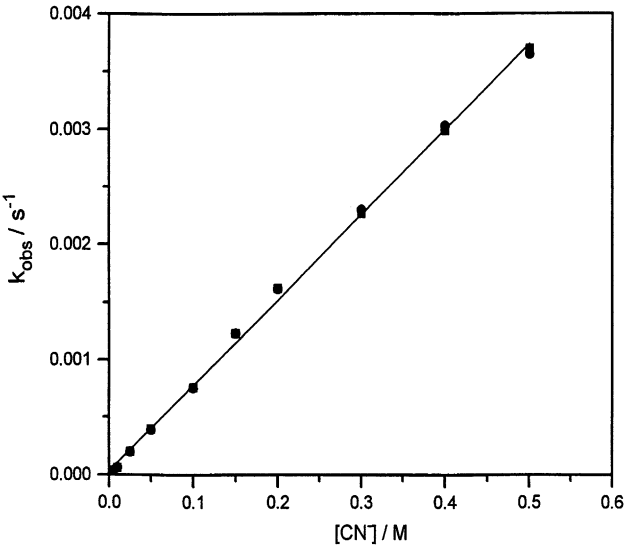

FIG. 5. Plot of k_{obs} versus [CN^-] for the reaction of AdoCbl with cyanide at pH 11.0 and 25.0°C.

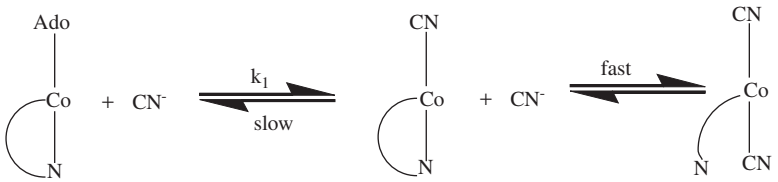

SCHEME 1.

$53 \pm 0.6\,\mathrm{kJ\,mol^{-1}}$ and $-127 \pm 3\,\mathrm{J\,K^{-1}\,mol^{-1}}$, respectively, whereas $\Delta V^{\neq}$ was calculated to be $-10.0 \pm 0.4\,\mathrm{cm^3\,mol^{-1}}$ (*16*). Thus, even more unexpected, both the values of $\Delta S^{\neq}$ and $\Delta V^{\neq}$ suggest that the reaction has a strongly associative character (*16*). But why? No reasonable explanation could be offered at that time. A logical solution to the problem would be to study model systems that would mimic the essential coordination sphere of the Co(III) center in the coenzyme.

B. Substitution Reactions of *trans*-[$Co(en)_2(Me)X$] as a Model for Coenzyme B_{12}

The rather confusing results obtained for the cyanation reaction cited above led us to investigate some model complexes for coenzyme B_{12}12 –>. There are many model complexes available for coenzyme B_{12}, of which Kofod *et al*. (*17,18*) prepared a series of complexes that contain ethylenediamine or NH_3 in the equatorial positions and a methyl group in one of the axial positions. They suggested that these complexes could be used as simple models for coenzyme B_{12}. We studied the substitution behavior of the methylpentaammine Co(III) complex and showed that the subsequent displacement of four ammine ligands by two ethylenediamine chelates, is followed by a slow *cis* to *trans* rearrangement of the bis(ethylenediamine) complex. The rate law for both steps showed saturation kinetics with respect to [en] and [NH_3], and the activation parameters suggested that the reactions follow a limiting D mechanism (*19*).

The axial ligand substitution of *trans*-$[Co(en)_2(Me)H_2O]^{2+}$ by CN^-, imidazole and NH_3, was investigated in detail to mimic the substitution behaviour of the coenzyme (*20,21*). For the reaction with CN^-, a good linear concentration dependence of the observed rate constant (notably faster than found for the coenzyme system) with a negligible intercept was obtained, suggesting that the reaction is irreversible and no parallel reaction occurs. The reaction was investigated as a function of temperature and pressure, and the activation parameters ($\Delta H^{\neq}$, $\Delta S^{\neq}$ and $\Delta V^{\neq}$) were found to be $50 \pm 4\,\mathrm{kJ\,mol^{-1}}$, $0 \pm 16\,\mathrm{J\,K^{-1}\,mol^{-1}}$ and $+7.0 \pm 0.6\,\mathrm{cm^3\,mol^{-1}}$, respectively. The volume of activation suggested that the reaction is dissociative in nature. For the reaction of *trans*-$[Co(en)_2(Me)H_2O]^{2+}$ with imidazole, the concentration dependence showed a significant intercept, which represented the back reaction. The rate law for this reaction is given in Eq. (6), where k_a and k_b represent the rate constants for the forward and the backward reactions, respectively (*20*).

$$k_{obs} = k_a[ImH] + k_b \tag{6}$$

$\Delta H^{\neq}$, $\Delta S^{\neq}$ and $\Delta V^{\neq}$ for the forward reaction were found to be $53 \pm 2\,\mathrm{kJ\,mol^{-1}}$, $-22 \pm 7\,\mathrm{J\,K^{-1}\,mol^{-1}}$ and $+4.7 \pm 0.1\,\mathrm{cm^3\,mol^{-1}}$, respectively, and those for the backward reaction were found to be

$94 \pm 8\,kJ\,mol^{-1}$, $+97 \pm 27\,J\,K^{-1}\,mol^{-1}$ and $+6.4 \pm 0.9\,cm^3\,mol^{-1}$, respectively. A volume profile for this reaction is shown in Fig. 6, which clearly illustrates the dissociative nature of the ligand substitution process (*20*). A similar concentration dependence and volume profile were obtained for the reaction with NH_3 (*21*). The aquation reaction of *trans*-$[Co(en)_2(Me)NH_3]^{2+}$ and the reaction of *trans*-$[Co(en)_2(Me)NH_3]^{2+}$ with SCN^-, N_3^- and CN^- were also studied in detail (*21*). Based on the kinetic data reported for these reactions and the corresponding activation parameters, it was suggested that these reactions all proceed via an intermediate aqua complex, such that aquation of the ammine complex becomes the rate-determining step at high concentrations of the entering ligand. Furthermore, *trans*-$[Co(en)_2(Me)NH_3]^{2+}$ could be used as a model for coenzyme B_{12}, since the NH_3 group in the axial position is very labile and mimics the DMBz group that occupies the axial position in cobalamin.

Unfortunately, the work on the model complexes described above did not clarify the abnormal behavior of the reaction of AdoCbl with CN^-, since the observed results were in exact agreement with our expectations. This then led us to investigate the substitution behavior of a series of alkylcobalamins, in which the σ-donor strength of the cobalt–carbon bond could be varied in a systematic manner. The selected series of alkylcobalamins cover a wide range of σ-electron donation ability, varying from Pr, Ado, Et and Me (strong σ-donors) to CF_2H, CF_3CH_2, and finally to $NCCH_2$, CF_3 and CN^- (weak σ-donors). Such a systematic variation of the σ-donor strength should in principle reveal the reasons for the unexpected behavior of AdoCbl.

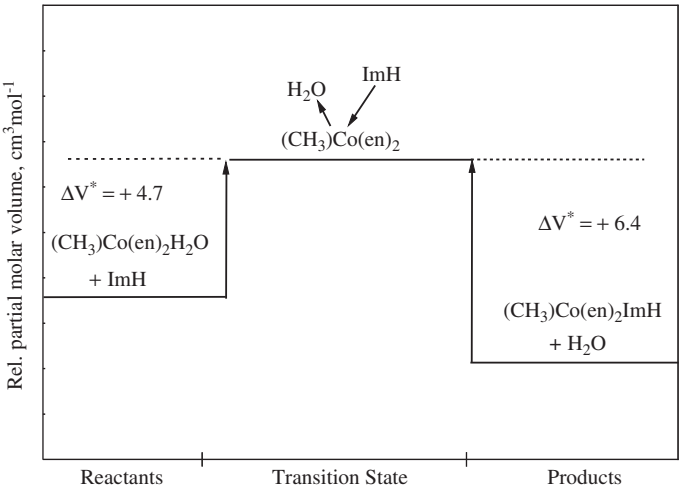

FIG. 6. Volume profile for the reaction of *trans*-$[Co(en)_2(Me)H_2O]^{2+}$ with imidazole.

C. Reactions of Alkylcobalamins with CN^-

It is known from the literature that the two active forms of vitamin B_{12} (AdoCbl and MeCbl), which are essential for some of the enzymatic reactions, undergo substitution of their axial benzimidazole ligand by the protein histidine residue during complexation to the MeCbl dependent methionine synthase (*22*), the class I AdoCbl dependent mutase (*23*), and the class III AdoCbl dependent D-lysine-5,6-aminomutase (*24*). The surprising results found for the cyanation of AdoCbl and the little information obtained from the studies on model complexes, led us to investigate the reaction of MeCbl and other alkylcobalamins with cyanide. It was previously found that MeCbl forms an adduct with CN^- when the $[CN^-]$ was varied in the range 0.01–1.1 M (*25*). The formation of this adduct was found to be very fast and difficult to monitor by stopped-flow techniques. However, it was reported later that a significant increase in the UV–Vis spectrum was observed in the range of 580–600 nm when a very high concentration of CN^- (1–6 M) was added to MeCbl (*26*). This observation suggested that the new band formed in this spectral range is due to substitution of the DMBz group in the α-position by CN^-. The value of the stability constant, K_{CN}, was found to be $0.38\,M^{-1}$ (*26*). In another study, this value was determined by ^1H NMR technique and found to be $0.35\,M^{-1}$, in good agreement with the spectrophotometric value (*27*). The low value of K_{CN} clearly indicates that the position *trans* to the methyl group is extremely labile and requires a high concentration of a strong nucleophile to stabilize the α-substituted complex.

We were not able to measure the kinetics of the first reaction step between 8×10^{-5} M MeCbl and 1.0 M CN^- at pH 11.0 and 5.0°C, since the reaction in aqueous solution was found to be too fast to be followed by stopped-flow technique (dead time 2–4 ms) (*26*). The reactions between CH_2BrCbl and *n*-PrCbl with CN^- were also too fast to be followed in this way. However, in the case of CF_2HCbl, the second-order rate constant at 10.0°C could be determined to be $10^3\,M^{-1}\,s^{-1}$ (*26*). Thus, the obvious alkylcobalamins to study were those with the less strong σ-donors, viz. R = CF_3CH_2, CF_3, $NCCH_2$ and CN.

We started our measurements on these systems by studying the reaction of β-CF_3CH_2Cbl with CN^- (0.005–0.4 M), which occurred in one kinetically observable step with no evidence for the displacement of DMBz from the α-site. The rate-determining step was found to be the displacement of the CF_3CH_2 group by CN^- (*26*). Under the selected conditions, a non-linear CN^- concentration dependence was observed with a second-order rate constant calculated from the initial slope of $0.24\,M^{-1}\,s^{-1}$ at 10°C. The corresponding activation parameters ($\Delta H^{\#}$, $\Delta S^{\#}$ and $\Delta V^{\#}$) were found to be $71 \pm 1\,kJ\,mol^{-1}$, $-25 \pm 4\,J\,K^{-1}\,mol^{-1}$ and $+8.9 \pm 1.0\,cm^3\,mol^{-1}$, which suggest the operation of an I_d mechanism.

Figure 7 shows a plot of k_{obs} versus $[CN^-]$ for the reaction of β-CF_3Cbl with excess CN^- at pH 11.0 ($[CN^-] = 0.0005$–0.25 M),

$I = 0.5\,M$ ($NaClO_4$) and 10.0°C. This plot shows saturation kinetics and a limiting value of k_{obs} ($= k_1$) is reached at high [CN^-]. The intercept can be assigned to a contribution of the reverse reaction, whereas the observed curvature can be considered as evidence in favor of a limiting D or I_d mechanism. The kinetic data are for the first reaction step that involves substitution of α-DMBz by CN^-, since the product spectrum clearly suggests the formation of an intermediate (β-CF_3)(α-CN)Cbl, which is accompanied by an increase in absorbance at 580–600 nm, and is also light sensitive as expected (*26*). The reaction was studied as a function of temperature and pressure. $\Delta H^{\neq}$ and $\Delta S^{\neq}$ for this reaction were found to be $77 \pm 3\,kJ\,mol^{-1}$ and $+44 \pm 11\,J\,K^{-1}\,mol^{-1}$, respectively. A good linear plot of ln$k$ versus pressure was obtained, from which $\Delta V^{\neq}$ was calculated to be $+14.8 \pm 0.8\,cm^3\,mol^{-1}$ (*26*).

On the basis of all the data, the suggested mechanism for the reaction between β-CF_3Cbl and CN^- can be represented by Eq. (7) (X = CF_3), which involves dissociative dechelation of DMBz to form a six-coordinate intermediate aqua complex. If k_{-2} has a significant value as seen in Fig. 7, then the observed rate law is expressed by Eq. (8), which can be simplified to $k_{obs} = k_1$ at high concentrations of CN^-. The data in Fig. 7 were fitted to Eq. (8) and resulted in $k_1 = 8.8 \pm 1.6\,s^{-1}$, $k_{-2} = 2.6 \pm 0.2\,s^{-1}$ and $k_2/k_{-1} = 42 \pm 4\,M^{-1}$ at 10°C, from which an overall equilibrium constant $k_1k_2/k_{-1}k_{-2} = 142 \pm 15\,M^{-1}$ could be calculated. The value of k_2[CN^-]/k_{-1} represents the efficiency of cyanide as compared to DMBz of the nucleotide loop to scavenge the six-coordinate intermediate, which will depend on the selected cyanide concentration.

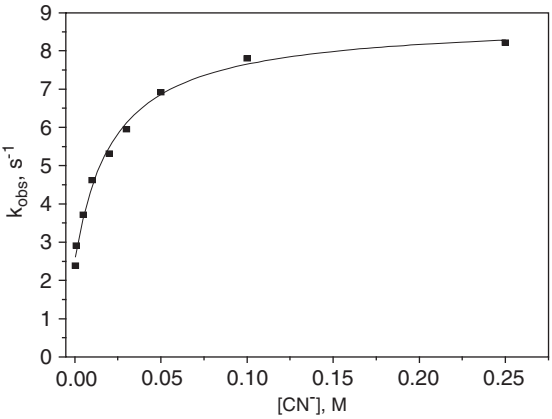

FIG. 7. Plot of k_{obs} versus CN^- concentration for the reaction of CF_3Cbl and CN^- at pH = 11.0, 10.0°C and $I = 0.5\,M$ ($NaClO_4$).

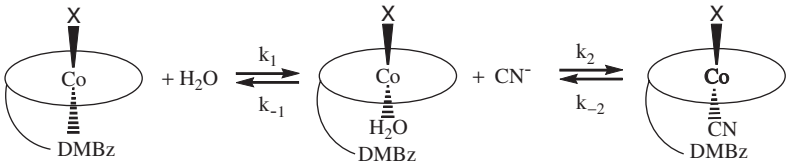

(7)

$$k_{obs} = (k_1 k_2[CN^-] + k_{-1}k_{-2})/(k_{-1} + k_2[CN^-]) \quad (8)$$

Similar plots to that shown in Fig. 7 were obtained for the reaction of the other two β-alkylcobalamins with CN^-, where $X = NCCH_2$ and CN^- (*28*). These plots also showed significant curvature at high cyanide concentration, and the intercepts were assigned to a contribution of the reverse reaction. The experimental data obtained in these cases were fitted to Eq. (8) and resulted in $k_1 = 64.7 \pm 0.7\,s^{-1}$, $k_{-2} = 27.4 \pm 0.8\,s^{-1}$ and $k_2/k_{-1} = 28 \pm 3\,M^{-1}$ at 5.0°C for $X = NCCH_2$, with an overall equilibrium constant $k_1k_2/k_{-1}k_{-2} = 66 \pm 3\,M^{-1}$. Those obtained in the case of $X = CN^-$ are: $k_1 = 0.042 \pm 0.001\,s^{-1}$, $k_{-2} = (7 \pm 3) \times 10^{-5}\,s^{-1}$ and $k_2/k_{-1} = 36.9 \pm 1.5\,M^{-1}$ at 25oC, with an overall equilibrium constant $k_1k_2/k_{-1}k_{-2} = (2.2 \pm 0.1) \times 10^4\,M^{-1}$ (*28*). The value of K is in agreement with that reported previously based on a spectrophotometric titration (*29*), and the values of K and k_1 are also in very good agreement with the data obtained by Reenstra and Jencks (*30*). They suggested that the mechanism is a limiting D one (*30*).

The reactions of β-alkylcobalamins with CN^- for $X = NCCH_2$ and CN^- were studied as a function of temperature and pressure at high cyanide concentration where $k_{obs} = k_1$. $\Delta H^{\neq}$, $\Delta S^{\neq}$ and $\Delta V^{\neq}$ in the case of $X = NCCH_2$ were found to be $85 \pm 2\,kJ\,mol^{-1}$, $+97 \pm 6\,J\,K^{-1}\,mol^{-1}$ and $+12.7 \pm 0.5\,cm^3\,mol^{-1}$, respectively, and in the case of $X = CN^-$ to be $105 \pm 2\,kJ\,mol^{-1}$, $+81 \pm 6\,J\,K^{-1}\,mol^{-1}$ and $+13.1 \pm 0.3\,cm^3\,mol^{-1}$, respectively (*28*). Table I summarizes the second-order rate constants for the cyanation reaction of XCbl measured at low cyanide concentration, the corresponding activation parameters and the overall binding constant for CN^-. It is clear from this table and the above discussion that the X group in XCbl has a significant influence on the rate of the axial substitution reaction of DMBz, located *trans* to X. Based on the reported kinetic data and the activation parameters obtained for the reactions of the series of XCbls with CN^-, it is reasonable to conclude that the reactions follow a dissociative mechanism. The operation of a limiting D mechanism requires the intermediacy of a five-coordinate transition state species. Such species are known for some alkylcobalt(III) complexes (*31–39*). Furthermore, the data for the X substituents that exhibit a much smaller σ-donor property than expected for AdoCbl, suggests that substitution of DMBz in AdoCbl should be very fast and even more dissociative in nature, in contrast with the experimentally observed results. Table I also shows that the value of (K_{CN}) decreases significantly from 10^3 for $X = CN^-$ to $0.7\,M^{-1}$ for $X = Et$.

TABLE I

RATE CONSTANTS AND ACTIVATION PARAMETERS FOR THE CYANATION REACTIONS OF A SERIES OF COBALAMINS (XCBLS)

R	$pK_{base\text{-}off}$	k_{CN} ($M^{-1}s^{-1}$)	K_{CN} (M^{-1})	$\Delta H^{\#}_{CN}$ ($kJ\,mol^{-1}$)	$\Delta S^{\#}_{CN}$ ($Jk^{-1}\,mol^{-1}$)	$\Delta V^{\#}_{CN}$ ($cm^3\,mol^{-1}$)
Et	4.2	Too fast	0.7			
n-Pr	4.1	Too fast	1.3			
Ado	3.7	7×10^{-3}	0.6	53.0 ± 0.6	-127 ± 3	-10.0 ± 0.4
CH_3	2.9	$\geq 10^4$	1.2			
CH_2CF_3	2.6	1,250 (3°C)	13			
CF_2H	2.1	1,000 (10°C)	3.3			
CH_2CN	1.8	483 (5°C)	64	85 ± 2	$+97 \pm 6$	$+12.7 \pm 0.5$
CF_3	1.4	217 (10°C)	123	77 ± 3	$+44 \pm 11$	$+14.8 \pm 0.8$
CN	0.1	1.1 (25°C)	3×10^3	105 ± 2	$+81 \pm 6$	$+13.1 \pm 0.3$

TABLE II

BOND LENGTHS AND THERMODYNAMIC DATA FOR A SERIES OF COBALAMINS (XCBLS)

R	Co-R (Å)	Co-N_{Bzm} (Å)	p$K_{base\text{-}off}$	Fraction base-off
CH_2CH_3			4.16	4.7×10^{-2}
$CH_2CH_2CH_3$			4.10	4.0×10^{-2}
Adenosyl	2.04	2.24	3.67	1.3×10^{-2}
CH_3	1.99	2.19	2.89	2.1×10^{-3}
CH_2CF_3	1.99	2.19	2.60	1.1×10^{-3}
CF_2H			2.15	3.8×10^{-4}
CH_2CN			1.81	1.8×10^{-4}
CF_3	1.88	2.05	1.44	7.7×10^{-5}
CN	1.86	2.01	0.10	3.4×10^{-6}

Table II summarizes the different alkylcobalamins (XCbl), the bond length between the cobalt center and the N-donor of DMBz in the *trans* position to the alkyl group (Co-N_{Bz}), the Co–C bond distance, p$K_{base-off}$ (for reaction (9)) and the fraction of the base-off form for these cobalamins (Eq. 10). It is clear from this table that the Co–N bond lengths and Co–C bond lengths in XCbls increase in the order $H_2O < CN < CF_3 < NCCH_2 < CF_2H < CF_3CH_2 < CH_3 < Ado$ (*40–42*). This suggests that AdoCbl can be expected to be the most labile complex in terms of ligand substitution reactions. The fraction of the base-off form of XCbl decreases significantly from 0.047 in the case of CH_3CH_2Cbl to 2×10^{-8} for H_2OCbl.

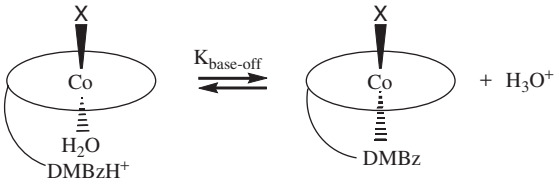

(9)

$$\text{Fraction base-off} = K_2/K_{base-off} \tag{10}$$

D. THE KINETIC *TRANS*-EFFECT ORDER

When the kinetic *trans*-effect order discussed earlier and shown in Table I, is taken into consideration, the displacement of DMBz in AdoCbl should be extremely fast, which is apparently not the case. An alternative interpretation of the data requires that the first cyanation reaction in Scheme 1 is indeed extremely fast and that the observed slow reaction is in fact the subsequent heterolysis of the Co–C bond

(*28*). If this is the case, there should be spectroscopic evidence for the rapid formation of the α-cyano complex followed by the slow subsequent heterolysis reaction. The original measurements included a cyanide concentration range of 0.05–0.5 M (Fig. 5), for which no evidence for such a rapid pre-equilibrium cyanation process was observed (*16*). Keeping in mind that the α-DMBz group maybe extremely labile in the case of the AdoCbl complex, evidence for the rapid cyanation pre-equilibrium may only be observed under extremely high cyanide concentration conditions, since the binding constant for CN^- to AdoCbl is expected to be very low (see Table I).

UV–Vis spectra recorded before and after mixing of AdoCbl with 2 M CN^- and higher, did show a significant increase in absorbance in the range 560–640 nm and a decrease in absorbance in the range 470–530 nm as shown in Fig. 8 (*28*). These spectral changes were not pronounced enough at low cyanide concentration, demonstrating that significantly higher concentrations of CN^- are required to displace the DMBz group from the α-position in a rapid step to form (β-Ado)(α-CN)Cbl, which then reacts to $(CN)_2$Cbl. Formation of $(CN)_2$Cbl is accompanied by good isosbestic points at 347, 380, 524 and 608 nm, a decrease in absorbance in the range 620–650 nm, and the appearance of new bands at 367, 540 and 580 nm as shown in Fig. 8. It is known that substitution of α-DMBz by CN^- is accompanied by an increase in absorbance in the range 580 620 nm due to a new d–d transition com-

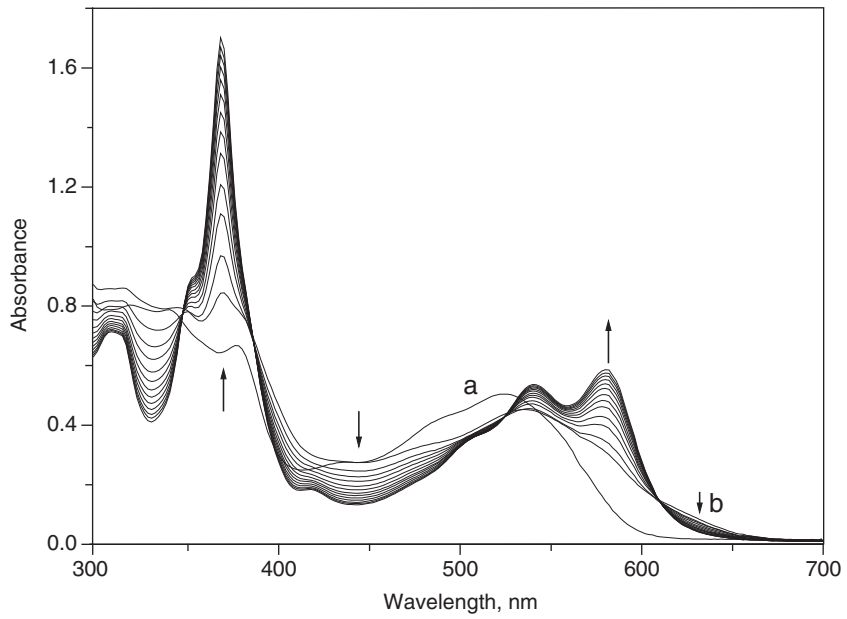

FIG. 8. (a) UV–Vis spectra of AdoCbl before and directly after mixing with 2 M CN^- at pH 11.0 and 25°C. (b) Selected visible spectra for the reaction of AdoCbl and 2 M CN^- at longer time scale (spectrum recorded every 20 s).

mon to all complexes of this type. Interestingly, the UV–Vis spectrum obtained directly after mixing AdoCbl with CN^-, matches that obtained for the reaction of AdoCbl and tetrabutyl ammonium cyanide in a less protic solvent (92 % DMF/8 % D_2O) (*43*). Also, the UV–Vis spectral changes that accompany the conversion of (β-Ado)(α-CN)Cbl to $(CN)_2$Cbl are almost identical in both cases (i.e. in aqueous and less protic solvents). The conversion of (β-Ado)(α-CN)Cbl to $(CN)_2$Cbl can be monitored by following the decrease in absorbance at 620–650 nm, or the increase in absorbance at 367 or 580 nm. In the case of less protic solvents, the rate-determining heterolytic Co–C cleavage was preceded by rapid addition of CN^- to AdoCbl to form (β-Ado)(α-CN)Cbl (*43*). This confirms that the first step in the reaction of AdoCbl and CN^- is indeed the substitution of α-DMBz by CN^- to form (β-Ado)(α-CN)Cbl.

A spectrophotometric titration was performed by following the rapid increase in absorbance at 600–620 nm as a function of cyanide concentration. It is important to note that the intermediate CN(X)Cbl, where X = Ado and CF_3CH_2, undergoes heterolytic Co–C cleavage and reacts with CN^- in the dark to give $(CN)_2$Cbl. Therefore, it is difficult to determine the value of K spectrophotometrically by the normal method (titrating XCbl with different concentration of CN^-). Consequently, the values of K in these two cases were determined spectrophotometrically by injecting a small volume of concentrated AdoCbl solution (to minimize dilution) into the buffer containing different concentrations of CN^-. Then the rapid absorbance increase at 600–620 could be followed. Typical changes in absorbance at 620 nm on addition of AdoCbl to CN^- are shown in Fig. 9, from which the value of K was calculated and found to be $0.6 \pm 0.1\ M^{-1}$. A similar spectrophotometric titration was carried out in the case of CF_3CH_2Cbl and the value of K

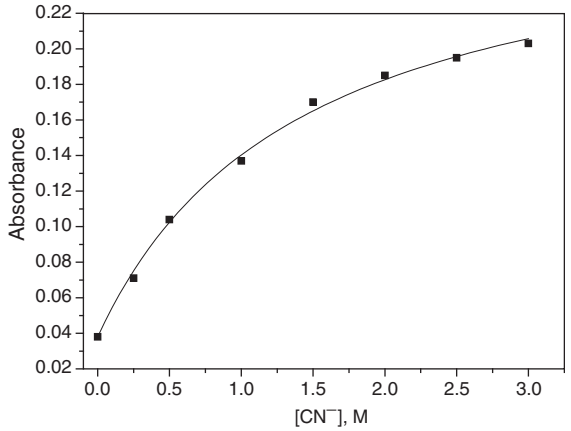

FIG. 9. Variation in absorbance at 620 nm on addition of CN^- to AdoCbl; the solid line is a fit of the data and gives a value of $K_{CN} = 0.6 \pm 0.1\ M^{-1}$.

was found to be $13 \pm 2\,M^{-1}$, which is in agreement with that determined previously from kinetic data (viz. $9.8 \pm 0.5\,M^{-1}$) (*28*).

We were not able to measure the kinetics of the first cyanation step between 8×10^{-5} M AdoCbl and 1 M CN^- at pH 11 and 5.0°C, since the reaction in aqueous solution was found to be too fast to be followed by stopped-flow technique (dead time 2–4 ms) (*28*). The kinetics of the reaction between 5×10^{-5} M β-CF_3CH_2Cbl and 0.4 M CN^- was followed at pH 11.0 and at 3.0°C, and the second-order rate constant was found to be $1.25 \times 10^3\,M^{-1}\,s^{-1}$. We have mentioned before that the reactions of CH_3Cbl, CH_2BrCbl and *n*-PrCbl with CN^- were also too fast to be followed in this way (*28*). This fits nicely with the kinetic *trans*-effect order expected for the data in Table I. The kinetic *trans*-effect order was found to decrease along the series Pr ≥ Ado ≥ Me ≥ $CF_3CH_2 > CF_2H > NCCH_2 > CF_3 > CN^-$. We can therefore conclude that the first step for the reaction of AdoCbl or CF_3CH_2Cbl with CN^- is a rapid pre-equilibration which cannot be monitored by stopped-flow techniques.

The second-order rate constant obtained previously for the reaction of AdoCbl with CN^- ($4.7 \times 10^{-3}\,M^{-1}\,s^{-1}$) does not agree with the kinetic *trans*-effect order of XCbl and must be assigned to the subsequent slow step. This led to a further study of the kinetics of the reaction of AdoCbl with CN^- in a higher concentration range. The reaction between AdoCbl and CN^- was studied at cyanide concentrations up to 4 M. Curvature is observed in the kinetic data as a function of cyanide concentration, as shown in Fig. 10, which is typical for saturation kinetics in which a rapid pre-equilibrium precedes the rate-determining Co–C bond cleavage as proposed in Scheme 2 (*28*). It is clear from this figure that for $[CN^-] \leq 0.50$ M, the plot is essentially linear, as found in

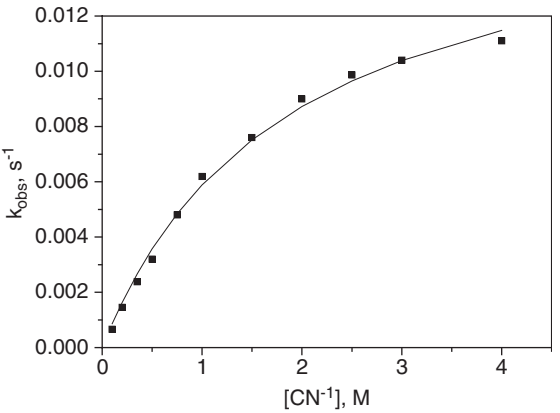

FIG. 10. Plot of observed rate constant (k_{obs}) versus CN^- concentration for the reaction between AdoCbl and CN^- at 25.0°C ([AdoCbl] ~5×10^{-5} M, [NaCN] = 0.10–3.0 M, H_2O, 0.10 M CAPS, pH 11.0, I = 5.0 M ($NaClO_4$)).

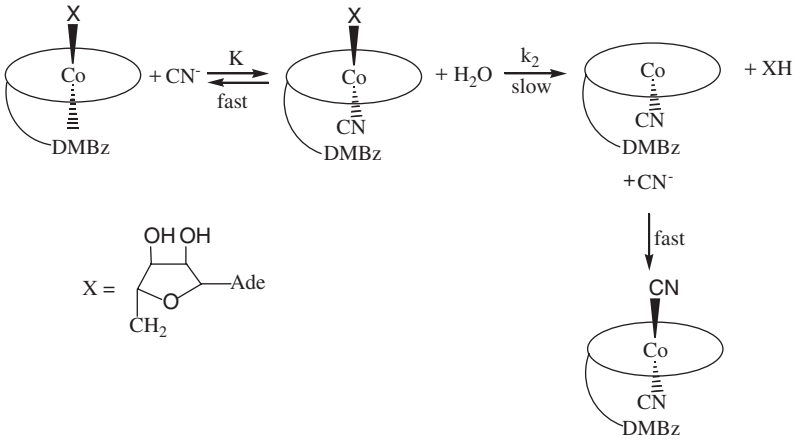

SCHEME 2.

our earlier study (*16*). The experimental data were fitted to the rate law given in Eq. (11) for the mechanism shown in Scheme 2.

$$k_{obs} = k_2K[CN^-]/(1 + K[CN^-]) \tag{11}$$

The reaction between AdoCbl and 4.0 M CN^- at pH 11.0 was studied as a function of temperature and pressure to probe the possible involvement of the solvent in formation of the transition state for Co–C heterolysis of the (β-Ado)(α-CN)Cbl intermediate (*44*). The activation parameters ($\Delta H^{\neq}$, $\Delta S^{\neq}$ and $\Delta V^{\neq}$) were found to be $55 \pm 1\,kJ\,mol^{-1}$, $-98 \pm 3\,J\,K^{-1}\,mol^{-1}$ and $-5.7 \pm 0.3\,cm^3\,mol^{-1}$, respectively.

In our earlier study, the activation parameters for the reaction between AdoCbl and cyanide in H_2O were studied at low cyanide concentration (7.50×10^{-2} M), and $\Delta H^{\neq}$, $\Delta S^{\neq}$ and $\Delta V^{\neq}$ were reported to be $53.0 \pm 0.6\,kJ\,mol^{-1}$, $-127 \pm 3\,J\,K^{-1}\,mol^{-1}$ and $-10.0 \pm 0.4\,cm^3\,mol^{-1}$, respectively (*16*). From Eq. (11) it follows that at low cyanide concentrations, $k_{obs} = k_2K[CN^-]$, or, in terms of the proposed mechanism in Scheme 2, $\Delta V^{\neq}(k_{obs}) = \Delta V^{\neq}(k_2)+\Delta V(1/K_{Co})+\Delta V(K_{CN})$, where $\Delta V(1/K_{Co})$ and $\Delta V(K_{CN})$ represent the reaction volumes for formation of the base-off AdoCbl and the subsequent formation of the intermediate (β-Ado)(α-CN)Cbl complex, respectively. If it is assumed that $\Delta V^{\neq}(k_2)$ for AdoCbl$\sim\Delta V^{\neq}(k_2)$ for $AdoCbi^+$, which seems quite reasonable, given the excellent agreement between rate constants for the two systems, then for the reaction between AdoCbl and cyanide, $\Delta V(1/K_{Co})+\Delta V(K_{CN})$ can be estimated to be $-4.3 \pm 0.8\,cm^3\,mol^{-1}$. These steps involve dechelation of the α-dimethylbenzimidazole accompanied by bond formation with the entering cyanide ligand, such that it is reasonable to

expect an overall small negative value for $\Delta V(1/K_{Co})+\Delta V(K_{CN})$, due to the larger volume decrease associated with the coordination of free cyanide as compared to the volume increase associated with the dechelation of the α-dimethylbenzimidazole group. Thus, on the basis of these arguments, and the mechanistic interpretation presented here, we conclude that the significantly negative volume of activation observed before (and incorrectly interpreted as evidence for associative binding of cyanide), results from approximately equal negative contributions for both the rapid formation of the (β-Ado)(α-CN)Cbl intermediate and the subsequent solvent-assisted heterolysis reaction. We conclude that the negative entropies and volumes of activation give further support to a mechanism involving solvent-assisted Co–C bond heterolysis (*44*).

It was suggested earlier on the basis of the effect of the solvent (i.e., D_2O versus 92 % DMF/8 % D_2O) on the magnitude of the rate constant for Co–C heterolytic bond cleavage that a solvent molecule is involved in the transition state for this process (*45*). If this is indeed the case, it is reasonable to expect $\Delta V^{\neq}(k_2)$ to have a small negative value, resulting from partial binding of a solvent molecule and heterolysis of the Co–C bond, as experimentally observed. Note that if the solvent was not involved in the bond cleavage process, dissociative activation parameters (i.e., a significantly positive value of $\Delta V^{\neq}$) would be expected for the heterolysis process. Similar arguments can be adopted to account for the negative activation entropy found for this reaction in aqueous solution. Hence, both the volume and entropy of activation provide further evidence that Co–C heterolytic cleavage of the intermediate is indeed a solvent-assisted process.

It is reasonable to expect a similar behavior to that obtained in the case of AdoCbl for CF_3CH_2Cbl, and we conclude that based on the agreement between the value of K_{CN} determined thermodynamically ($13 \pm 2\,M^{-1}$) and that obtained from kinetic data ($9.8 \pm 0.5\,M^{-1}$) (*28*), and the kinetic *trans*-effect order for the reaction of XCbls with CN^-, that the reaction between β-CF_3CH_2Cbl and CN^- proceeds in a similar way as the reaction of AdoCbl with CN^- shown in Scheme 2. This scheme shows that the rate-determining step is the cleavage of the Co–C bond and is preceded by a rapid step for the formation of (β-CF_3CH_2)(α-CN)Cbl ($K_{CN} = 13\,M^{-1}$ and $k_{CN} = 1.25 \times 10^3\,M^{-1}\,s^{-1}$ at 5°C) which then decomposes in the dark in the presence of CN^- to give $(CN)_2Cbl$. We conclude that these arguments based on our kinetic observations and supported by spectroscopic measurements now present a consistent mechanistic picture to account for the surprising associative mechanism initially proposed for the reaction of coenzyme B_{12} with cyanide. By studying a variety of related reactions and systems, and through a tedious investigation of all possible explanations, finally led to a satisfactory self-consistent overall mechanistic picture in which the basic concept of the kinetic *trans*-effect order was not violated anymore.

III. Inert Pt(II) Complexes

Following Rosenberg's discovery of the anti-tumor properties of *cis*-platin in 1969 (*46*), studies on the substitution behavior of Pt(II) complexes have attracted much attention. Since *cis*-platin was only active against some specific cancers, new drugs had to be developed for possible application in the treatment of other types of cancer. Two approaches were adopted: a wide variety of different Pt(II) complexes were synthesized and tested for their possible biological activity; systematic investigations were launched in efforts to resolve the factors that control the reactivity (lability) of Pt(II) complexes (*47*). Once such factors are well understood, it should in principle be possible to design Pt(II) complexes with specific kinetic and thermodynamic properties to reach a desired activity in a specific biological environment.

Studies have shown that steric hindrance above and below the square-planar plane of the Pt(II) complex can significantly slow down the rate of the substitution reaction (*48–50*), whereas steric crowding in the plane of the complex can result in an increase in reactivity (*51,52*). In addition, many studies have focused on the electronic tuning of the reactivity of Pt(II) complexes by changing the nature of the ligand *trans* to the reactive site. The observed trend, depending on the selected system, is an increase (even as high as 10^{11} fold) in the lability of the investigated complexes for stronger *trans*-labilizing ligands (*53–59*). This has, in general, been ascribed to σ-donor properties of coordinated ligands.

A. σ-Donor Effects

Much attention has in recent years been given to the substitution behavior of Pt(II) complexes that contain one or more Pt–C bonds. A reason for this is that two *cis* Pt–C bonds can induce a mechanistic changeover from the usual associative substitution mode to a dissociative mechanism (*60–65*). It could be shown that in the case of complexes of the type *cis*-$[Pt(L)_2(R)_2]$ (L = Me, Ph; R = thioethers or dmso), the 14 valence electron intermediate participating in a dissociative substitution mechanism is stabilized by the two strong σ-donor carbon atoms. If one of the thioethers is displaced by CO, the mechanism changes again from a dissociative to an associative one. This can be accounted for by the strong π-acceptor ability of CO which removes the high electron density from the metal center, and favors a five-coordinate 18 valence electron intermediate encountered in an associative substitution mechanism (*66*). Astonishingly, a comparison of the substitution reactions of the complexes *cis*-$[Pt(Ph)_2(SMe_2)_2]$ and $[Pt(2,2'\text{-biphenyl})(SMe_2)_2]$, showed that the latter reacts 10^2 times faster and still dissociative despite its presumed π-acceptor ability. It was concluded from these findings that in-plane disposition of single

aryl ligands does not increase the electrophilicity of the platinum center through π-back bonding (*67*).

This leads to another reason for the significant interest in this area. Over the past decade, the role of cyclometalation in controlling the reactivity of platinum complexes has been studied extensively (*56,57,67–71*). For example, it was discussed whether the remarkable enhancement in rate observed for the substitution of water in the complexes [Pt(N-C)(N)(H_2O)] (N–CH = *N*,*N*-dimethylbenzylamine, N = pyridine-3-sulfonic acid) (*56,68*) and [Pt(N–C–N)(H_2O)]$^+$ (N–CH –N = 2,6-bis((dimethylamino)methyl)phenyl)) (*57*), is due to π-back donation into the empty anti- or non-bonding π-orbitals of the in-plane aryl ligand (*56,57*), or due to the strong *trans*-labilizing effect of the Pt–C bond (*69,70*), as also suggested by the investigations mentioned above (*66*). Further kinetic studies on the role of cyclometalation have shown that the importance of cyclometalation for aliphatic carbon donors is minute, but in the case of phenyl as carbon donor, the in-plane configuration of the phenyl ring as induced by cyclometalation, enables effective π-back bonding comparable to that of an in-plane pyridine ring and therefore enhances the reaction rate ([Pt(N–N–C)Cl], N–N–CH = 6-phenyl-2,2′-bipyridine, reacts 10^2 times faster than [Pt(2-2′bipyridine)(phenyl)Cl]) due to an enhanced electrophilicity of the metal center (*71*). In this case, only Pt–C bonds *cis* to the leaving ligand were investigated, whereas the above-mentioned studies focused on substitution reactions *trans* to the Pt–C bond. At least for the *cis* position it could be shown that the electrophilicity of the metal center benefits from the π-back bonding to the in-plane phenyl ring, whereas the importance of π-back bonding of an in-plane phenyl ring in the *trans* position still remains uncertain.

B. π-Acceptor Effects

Although many studies on the *trans* effect have been performed, considering both σ and π contributions, the influence of π-acceptors only has not been studied in as much detail, except for the case of Zeise's anion, [$PtCl_3(C_2H_4)$]$^-$, where the ligand exchange kinetics *trans* to the very strong π-acceptor ethylene have been studied in detail (*54*). Furthermore, it is known that the complex [Pt(terpy)(L)]$^{(2-n)+}$ (terpy = 2,2′:6′,2″-terpyridine) shows a very high lability relative to the corresponding [Pt(dien)(L)]$^{(2-n)+}$ (dien = diethylenetriamine, the terpy complex being 10^4–10^5 times more labile), which is assigned to π-back bonding from the metal to the empty π* orbitals of the pyridine subunits of the terpy ligand (*71–73*). Another possible reason offered for this high reactivity is the steric strain on the [Pt(terpy)(L)]$^{(2-n)+}$ complexes (*74*).

In spite of all the evidence for the influence of π-accepting pyridine ligands on the electronic properties of the Pt(II) center, no investigation has been performed in which a systematic variation of the

π-acceptor effect by replacing amines with π-accepting pyridines in tridentate N-donor systems was undertaken. Since this effect seems to play a major role in going from $[Pt(dien)(L)]^{(2-n)+}$ to $[Pt(terpy)(L)]^{(2-n)+}$ complexes, and both complexes are of biological interest in terms of their cytotoxicity (*75*,*76*), it seemed appropriate to study the behavior of these types of complexes in more detail. We therefore investigated the effect of a systematic displacement of amine donors by π-accepting pyridines in tri-dentate N-donor chelates (of the dien and terpy type) on the thermodynamic and kinetic behavior of Pt(II) complexes. We studied the substitution behavior of the corresponding aqua complexes, since these are considered to be the reactive species in the key step of the binding of *cis*-platin to DNA. Furthermore, with a neutral leaving group it is possible to prevent charge separation/neutralization effects that could complicate the mechanistic interpretation of the kinetic activation parameters.

From a systematic variation of the π-accepting ability of the chelate on the substitution lability, it was possible to observe some important trends that are often hidden in other studies by stronger σ-donor or steric effects. We clearly observed a decrease in electron density on the Pt(II) center, an increase in the ability of the complex to stabilize further incoming electron density on the Pt(II) center, and a decrease in the energy separation of the frontier molecular orbitals in these Pt(II) complexes, with increasing number of π-acceptors in the coordination sphere, which in turn affected the kinetic and thermodynamic parameters that control the ligand substitution process. In addition, our observations enabled a systematic comparison of *cis* and *trans* π-acceptor effects of pyridine rings in ligand substitution reactions, and the introduction of an acceleration concept based on 'electronic communication' between the π-accepting pyridine rings.

In order to investigate the effect of adding π-acceptor units to tris(N-donor) chelates on the water substitution rates in divalent platinum complexes, a total of six mono(aqua) Pt(II) derivatives were synthesized and characterized. Their DFT-calculated structures are shown in Fig. 11. The similarities and differences between the aqua complexes **aaa**, **aap**, **apa**, **pap**, **app** and **ppp** were first studied by determining the pK_a values of the coordinated water molecules, followed by a study of the ligand substitution reactions as a function of nucleophile concentration for different nucleophiles, pH, temperature and pressure. The deprotonation reaction can therefore be presented by reaction (12), for which the pK_a values are summarized in Table III.

$$'L3'Pt^{II} - OH_2^{2+} + H_2O \overset{K_a}{\rightleftharpoons} 'L3'Pt^{II} - OH^+ + H_3O^+ \qquad (12)$$

The kinetics of the substitution of coordinated water (reaction (13)) was studied for five, neutral and anionic nucleophiles, viz. thiourea (TU), *N*,*N*-dimethylthiourea (DMTU), *N*,*N*,*N*′,*N*′-tetramethylthiourea

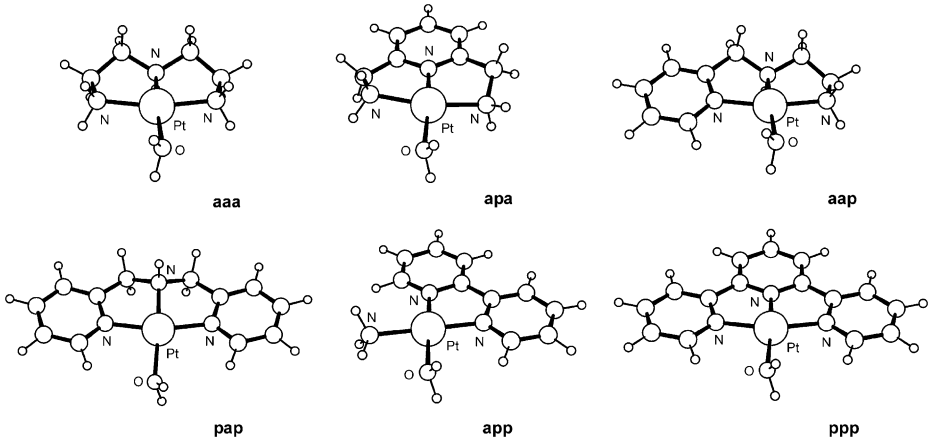

FIG. 11. DFT-calculated minimum energy structures for Pt(II) aqua complexes of the type $[Pt^{II}(L)(OH_2)]^{2+}$, where L represents a tridentate N-donor chelate or bipy/NH_3.

(TMTU), iodide and thiocyanate, which have different nucleophilicities and steric hindrance.

$$'L3'Pt^{II}\text{-}OH_2^{2+} + Nu^{n-} \underset{k_{-1}}{\overset{k_1}{\rightleftharpoons}} 'L3'Pt^{II}\text{-}Nu^{(2-n)+} + H_2O \qquad (13)$$

All kinetic experiments were performed under pseudo-first-order conditions, and at a pH between 2.0 and 2.5, where the complexes exist in the aqua form based on the data in Table III. The pseudo-first-order rate constants, k_{obs}, were plotted against the concentration of the entering nucleophile. A linear dependence on the nucleophile concentration with no meaningful intercept was observed for all reactions. Plots showing representative results for one complex are shown in Fig. 12. The results imply that k_{obs} can be expressed by Eq. (14).

$$k_{obs} = k_1[Nu] + k_{-1} \approx k_1[Nu] \qquad (14)$$

In the case of strong nucleophiles, the reaction is irreversible and $k_{-1} \approx 0$. The substitution reactions of the complexes with thiourea (TU) were studied over the entire pH range in order to determine the pK_a values kinetically (see typical results in Fig. 13). The coordinated water molecule on Pd(II) and Pt(II) centers has been shown to be very labile and can easily be substituted compared to stronger nucleophilic leaving groups. However, following deprotonation the resulting hydroxo ligand was found to be practically inert to substitution, presumably due to a back-bonding effect of the lone pair electrons on the hydroxo ligand with the p_z orbital of the metal, by which the Pt–OH bond obtains a quasi double bond character (*77*,*78*). This phenomenon was also observed in

TABLE III

SUMMARY OF THE SECOND-ORDER RATE CONSTANTS FOR THE REPLACEMENT OF WATER BY A RANGE OF NUCLEOPHILES IN COMPLEXES OF THE TYPE $[Pt^{II}(L)(OH_2)]^{2+}$. KINETIC AND THERMODYNAMIC pK_a VALUES FOR PLATINUM-BOUND WATER IN THESE COMPLEXES ARE ALSO GIVEN[a]

	k_1 ($M^{-1} s^{-1}$)					
Nucleophile	**aaa**	**apa**	**aap**	**pap**	**app**	**ppp**/10^4
TU[b]	29.1±0.4	101±1	110±1	393±2	1,429±6	16.3±0.2
DMTU[c]	11.9±0.2	41.2±0.3	80.4±0.5	393±5	1,690±21	21.7±0.3
TMTU[d]	3.20±0.02	12.3±0.1	29.3±0.2	182±2	1,196±29	15.3±0.3
I^-	67.3±0.5	180±1	246±2	854±6	1,690±21	22.4±0.4
SCN^-	40.4±0.5	88.3±0.5	115±1	367±6	953±17	11.9±0.1
Cl^-		1.91±0.01	2.29±0.01			
Br^-		10.4±0.1	13.9±0.1			
			pK_a			
pK_a[e]	6.35±0.03	5.96±0.05	5.60±0.06	5.30±0.03	4.37±0.02	4.42±0.05
pK_a[f]	6.26±0.10	6.04±0.08	5.71±0.03	5.53±0.07	4.68±0.03	4.62±0.04

[a]Experimental conditions: ionic strength = 0.1 M ($NaClO_4$), 25°C, pH = 2.0–2.5.
[b]Thiourea.
[c]Dimethylthiourea.
[d]Tetramethylthiourea.
[e]Kinetic value.
[f]Thermodynamic value.

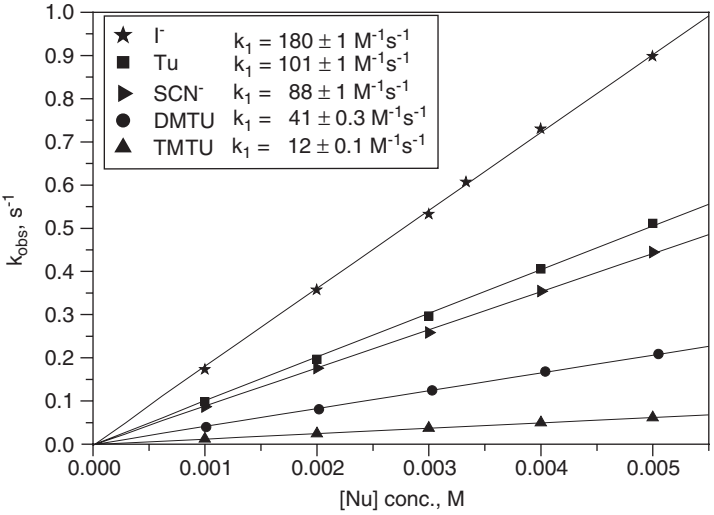

FIG. 12. Plots of k_{obs} versus nucleophile concentration for the **apa** complex. $I = 0.1$ M ($NaClO_4$), Temperature = 25°C, pH = 2 ($HClO_4$).

the systems studied here. The substitution process can therefore be represented by the mechanism outlined in Scheme 3.

The rate law for this mechanism is given by Eq. (15). The resulting pH profile for the **apa** complex fitted using Eq. (15) is shown in Fig. 13,

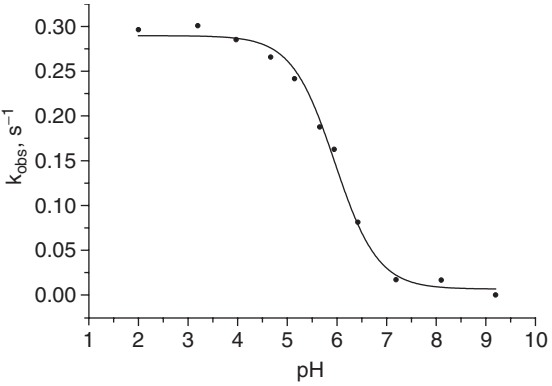

FIG. 13. pH dependence of k_{obs} for the reaction between the **apa** complex and thiourea at 25°C, $I = 0.1$ M ($NaClO_4$), [**apa**] = 0.1 mM, $\lambda = 300$ nm.

and the calculated pK_a values are summarized in Table III. These values can be related to the second-order rate constant, k_1, by a Hammett-plot as shown in Fig. 14.

$$k_{obs} = \left\{ \frac{k_1[H^+] + k_2 K_a}{K_a + [H^+]} \right\} [Nu] \qquad (15)$$

Figure 15 shows plots of log k_1 for the displacement of water in the complexes **aaa**, **aap**, **apa**, **pap**, **app** and **ppp** versus the calculated van der Waals volumes (a measure of steric bulk) of the incoming nucleophiles I^-, SCN^-, TU, DMTU and TMTU. The plots for **app** and **ppp** have zero slopes, indicative of a substitution process that is essentially independent of steric effects. The steepest slope is observed for the dien derivative **aaa**. The log k_1 values for **aaa**, **apa**, **aap** and **pap** therefore show a clear dependence on the steric bulk of the entering nucleophile, with the fastest and slowest substitution rates being observed for the smallest (I^-) and largest (TMTU) nucleophiles, respectively.

The thermodynamic data in Table III demonstrate that there is a remarkable correlation between the pK_a values for the coordinated water molecule and the structure, especially the π-acceptor character of the individual spectator ligands; the more π-acceptors in the system, the lower the pK_a value. This can be explained in terms of the electron-withdrawing ability of each added pyridine ring, which controls the electrophilicity of the metal center and stabilizes the negatively charged hydroxo ligand.

Although it is not a novel finding that the pK_a value of coordinated water is an experimental indicator of the electron density around the metal center (79), it is interesting that in all of the complexes except **ppp**, the pK_a value is an experimental gauge of the lability of the aqua

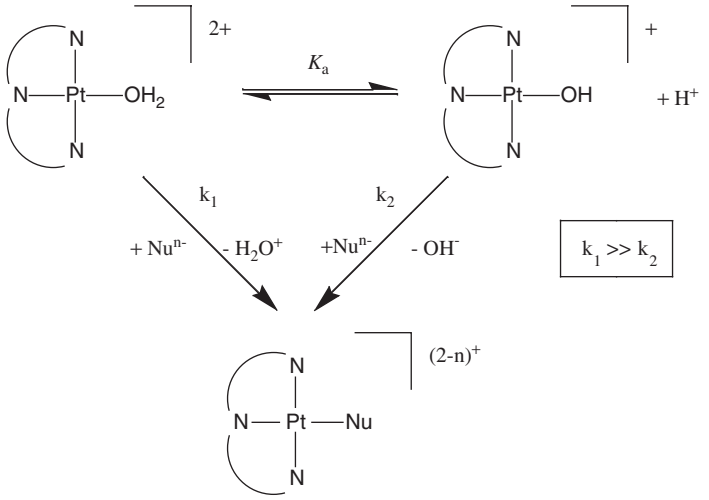

SCHEME 3.

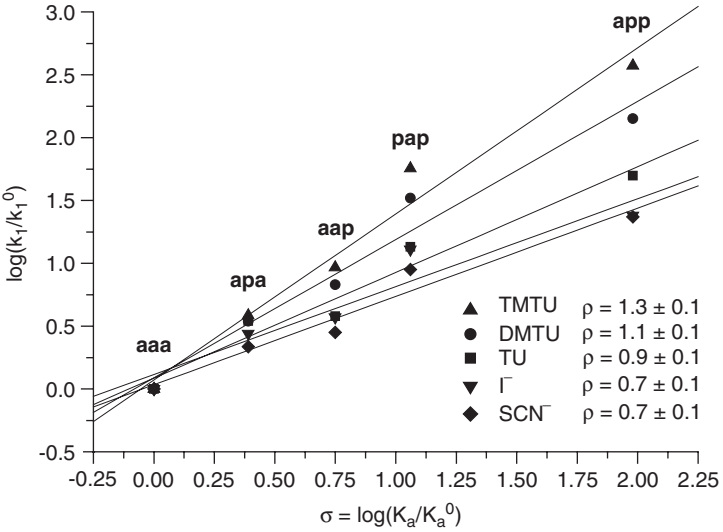

FIG. 14. Hammett-plot of $\log(k_1/k_1^0)$ versus $\log(K_a/K_a^0)$ according to Eq. (16) for the aqua complexes at 25°C for the entering nucleophiles I^-, SCN^-, TU, DMTU and TMTU. The values for **aaa** were used as reference (k_1^0, K_a^0).

complex (as shown by the Hammett-plot in Fig. 14, *vide infra*). This experimental finding is paralleled by a similar, though not perfect, trend in the DFT-calculated charges on the Pt(II) ion.

Interestingly, our observed reactivity order for the Pt(II) aqua complexes, viz. **aaa** < **apa** < **aap** < **pap** < < **app** < < **ppp**, is in good agreement with that expected for this series of complexes, but only partly

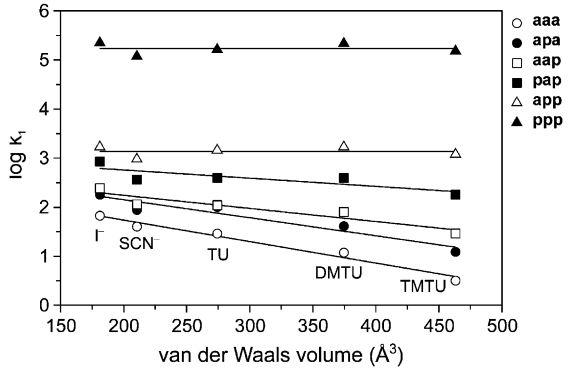

FIG. 15. Plot of log k_1 for the replacement of water in six $[Pt(L)(OH_2)]^{2+}$ derivatives against the calculated van der Waals volumes of the incoming nucleophiles I^-, SCN^-, TU, DMTU and TMTU.

matches that reported for substitution reactions of the analogous chloro complexes in methanol by Pitteri *et al.* (*80*). These workers found that [Pt(bis(2-pyridylmethyl)amine)Cl]$^+$ reacts slower than [Pt(2,6-bis-aminomethylpyridine)Cl]$^+$, which contradicts our findings for the reactions of the corresponding aqua complexes. This maybe related to the fact that they investigated the reactions of the chloro complexes in methanol as solvent, such that the two studies are not that compatible.

From the observed reactivity order, the questions remain of how the number and position of the π-acceptor ligands can affect the observed reactivity, and in which way two or three π-acceptor pyridine rings can interact with each other. It seems logical that if the introduction of one π-acceptor in the *cis* position (**aap** as compared to **aaa**) results in an enhancement of about a factor of 3.8 (for TU), the introduction of a second π-acceptor group (**pap**) results in a further acceleration factor of 3.8, i.e. an overall factor of 14.4. From the values in Table III it follows that the reaction of **pap** with TU is 13.6 times faster than the reaction of the **aaa** complex with TU. The other nucleophiles behave in a similar way; only the factors that are squared as done above vary due to the reduced importance of steric hindrance on increasing the electrophilicity of the metal center (see below). It can, therefore, be concluded that the effects of the π-acceptor groups can to some extent be combined in a multiplicative manner.

It is widely accepted in inorganic textbooks that the electronic *trans* effect is much stronger than the electronic *cis* effect in Pt(II) complexes (as soon as steric hindrance plays a role, the importance is reversed) (*81*). However, this statement is based mainly on investigations with σ-donor ligands or ligands which have both σ-donating and π-accepting properties. It is therefore interesting to compare the influence of only the π-effect (in the absence of a variation of the σ-donor properties) in

the *trans* (**apa**) to that in the *cis* position (**aap**). Since the pK_a value for the latter complex is slightly smaller, we would expect a higher reactivity for **aap**. The data in Table III show that this expectation is perfectly correct. The k_1 values for the substitution reactions with TU, I^- and SCN^- are 10–30 % higher, and in the case of the sterically hindered nucleophiles DMTU and TMTU, the values are two to three times higher, respectively. To our knowledge, this is the first time that it is shown that the *cis* effect for a specific ligand can be larger than its *trans* effect, as long as steric hindrance is excluded. The effect can rather easily be accounted for in terms of the orbitals involved. The π-effect results mainly from an interaction between the perpendicular $6p_z$ Pt orbital (accepting additional electron density) and the perpendicular non-/anti-bonding π-orbitals of the ligands. Since all the involved orbitals are perpendicular to the square-planar plane, the same interaction of the orbitals should occur in the *cis* and *trans* position. This would account for the similar influence of a *cis* or a *trans* aromatic ring on the thermodynamic and kinetic findings, but offers no explanation for the enhanced reactivity/decrease in pK_a of the **aap** system (in comparison to **apa**). The accumulation of electron density on the Pt(II) center in the case of the **apa** complex leads to a less electrophilic metal center, which results in a higher pK_a and a slower substitution reaction. This then explains why the *cis* effect is slightly larger than the *trans* effect on considering only the π-acceptor interactions. This demonstrates once more (*51,82*), that it is necessary to distinguish between σ-donor and π-acceptor effects of the ligands when referring to *cis* and *trans* effects.

If we ignore the fact that the *trans* π-acceptor has a slightly smaller influence on the rate than the *cis* π-acceptor, the **pap** and **app** complexes should be comparable in their kinetic and thermodynamic behavior since they both have two π-acceptor rings. However, the opposite was found. The pK_a value for the **app** complex is about 0.9 units lower than that of the **pap** complex, and the rate of substitution is about 2 (I^-) to 6 times (TMTU) faster than for **pap**. These data imply that the platinum center is more electrophilic when two pyridine rings are adjacent to each other. We accounted for this effect in terms of 'electronic communication' between the ligands that resulted in very efficient π-back bonding (*83*). In the case of the **ppp** complex, the same effect is at hand. Since we now know that the acceleration effect on the addition of π-acceptors is multiplicative (see above), it would be reasonable to expect the **ppp** complex to be about 20–226 (**apa** combined with **pap**) times faster than the **aaa** complex, depending on the nature of the entering nucleophile. However, a much larger increase in the rate constant of 3×10^3 to 5×10^4 is observed. This must be due to the effect of efficient electronic communication between the chelate partners. The large increase in the rate constant as compared to the **app** complex can be accounted for by the fact that in the **ppp** complex, three rings are adjacent to each other instead of only two in the case of the **app** complex.

Using the Swain–Scott relationship (*84*) for the nucleophiles Cl^-, Br^- and I^-, the nucleophilic discrimination factor s can be calculated for the **aap** and **apa** systems. In both cases, the value of s is 0.8 ± 0.1 and therefore much higher than for **aaa** ($s = 0.4 \pm 0.1$), which can be accounted for by the better π-accepting abilities of **aap** and **apa** that affect the nucleophilic discrimination (*85*). However, there is no difference in s for **apa** and **aap**, showing that the difference in the HOMOs has no effect on the nucleophilic discrimination factor.

As already mentioned, substitution of coordinated water by the sterically hindered nucleophiles *N*,*N*′-dimethlythiourea (DMTU) and *N*,*N*,*N*′,*N*′-tetramethylthiourea (TMTU) shows a clear dependence on the steric bulk of the nucleophiles. The most sterically hindered nucleophile TMTU reacts significantly slower than the less hindered TU in the case of the **aaa** complex (Table III). Upon the introduction of one pyridine π-acceptor ring in the *cis* position (**aap**), DMTU becomes nearly as fast as TU and the rate for TMTU is now only a third of the rate for TU. In the case of the **pap** complex, the rates for both TU and DMTU are within the experimental error limits almost identical, and TMTU is now only about half as fast as TU. Astonishingly, DMTU becomes even faster than TU on going to the **app** or **ppp** complex, and the most sterically hindered TMTU reacts with these complexes as fast as the non-hindered TU. It can be concluded that the effect of steric hindrance on the rate of substitution along the series of complexes from **aaa** to **ppp** decreases and is offset completely by the electronic effects in the case of the **ppp** complex. This conclusion is fully consistent with the plots of the second-order rate constants for the replacement of water against the calculated van der Waals volumes of the incoming nucleophiles (Fig. 15). More specifically, both **app** and **ppp** have zero slopes, i.e., zero dependence on the steric bulk of the nucleophile. This trend can be accounted for in terms of the increase in electrophilicity of the Pt(II) center which reaches a maximum for the **ppp** complex, such that the bulkiness of the attacking nucleophiles is compensated for by the higher nucleophilicity of DMTU and TMTU as a result of the inductive effects of the methyl substituents. It should be kept in mind that the displacement of amines by pyridines also reduces the steric hindrance caused by the solvated hydrogen atoms on NH_2R. This is confirmed by the DFT-calculated geometries of the complexes in Fig. 11, showing both **app** and **ppp** to be effectively planar, particularly in the region closest to the Pt-bound aqua ligand. However, this effect is not expected to be very significant. Alternatively, the observed changes in reactivity could also be due to different σ-donor abilities of the N-donors on the displacement of amines by pyridines. The σ-donor abilities of amine-N and pyridine-N donors are almost the same, so that the observed kinetic effects must mainly be due to π-acceptor and not to σ-donor effects.

Since both the pK_a value of the coordinated water molecule and the rate of substitution depend on the π-acceptor properties of the ligands,

it seems reasonable to expect a correlation between these two quantities. Such a free-energy relationship is known from organic chemistry, where the K_a values of ring-substituted benzoic acids are correlated with their reactivity in substitution reactions (*86*). Since this Hammett relationship deals with the same kind of data (K_a and k_1 values), it is reasonable to use this well-known relationship for the interpretation of our inorganic systems. We took the standard Hammett Eq. (16) (*86*) and used the data for the **aaa** complex as a reference system for K_a^0 and k_1^0.

$$\log(k_1/k_1^0) = \rho * \log(K_a/K_a^0) = \rho * \sigma \qquad (16)$$

The Hammett-plot is shown in Fig. 14 for all entering nucleophiles and all studied complexes, except for **ppp** which does not fit the linear correlation at all. The linear dependence observed for five of the six complexes, has slopes (ρ) of 0.7 ± 0.1, 0.7 ± 0.1, 0.9 ± 0.1, 1.1 ± 0.1 and 1.3 ± 0.1, for I^-, SCN^-, TU, DMTU and TMTU as entering nucleophiles, respectively. The positive values of ρ indicate that the reaction is accelerated by the introduction of electron-withdrawing groups (π-acceptors) on the chelate. This means that during the reaction an increase in electron density is developed at the reaction center, as would be expected for an associative substitution mechanism. Higher values for ρ indicate that the amount of electron density developed in the transition state is higher. This means that for the present system the inductive effect of the methyl groups on the substituted thioureas, increase the electron density that is stabilized in the transition state. Although the Hammett relationship has been used in the past to account for the reactivity trend in substituted Pt(II) terpy complexes by using σ values of the substituents on the terpy ring system (*87*), this is, to our knowledge, the first time that the Hammett relationship has been applied to Pt(II) complexes with σ values based on the K_a values of the aqua complexes.

The only exception in the linear correlation is the **ppp** complex, which according to the correlation should have a significantly smaller pK_a value in order to fit in with its much higher reactivity. A possible explanation for this exceptional behavior is that it maybe impossible to drain more electron density from the already very electrophilic center in the ground state to further decrease the pK_a value. However, during an associative substitution reaction with an entering nucleophile, the additional electron density can be spread over the total ligand system to stabilize the transition state and result in an enhanced substitution process. The correlation in Fig. 6 therefore suggests that it is possible to predict the kinetic behavior of such systems from thermodynamic data and vice versa, as long as one stays within reasonable limits.

The trend in the reactivity of the complexes of **aaa** to **ppp** can also be seen in the activation enthalpies for the investigated reactions

(Table IV). With increasing electrophilicity of the metal center, there is a decrease in the activation enthalpy due to the stabilization of the transition state. This decrease in $\Delta H^{\#}$ is more pronounced for the **ppp** complex, where a two-fold decrease in $\Delta H^{\#}$ is observed for all studied nucleophiles. Based on the activation enthalpies, it appears that charged nucleophiles (I^- and SCN^-) do not benefit as much as the neutral nucleophiles from the strong π-acceptor effect of bipy and terpy in case of **app** and **ppp**, respectively. As mentioned in the discussion of the kinetic data, the difference in $\Delta H^{\#}$ for the nucleophiles TU, DMTU and TMTU reduces in going from **aaa** to **ppp**.

The activation parameters were determined through a systematic variation of temperature and pressure, for which the data are

TABLE IV

ACTIVATION PARAMETERS FOR THE REACTION OF DIFFERENT NUCLEOPHILES WITH $[Pt^{II}(L)(OH_2)]^{2+}$ AT 25°C

Chelate L	Nucleophile	$\Delta H^{\#}$ (kJ mol^{-1})	$\Delta S^{\#}$ (J K^{-1} mol^{-1})	$\Delta V^{\#}$ (cm^3 mol^{-1})
aaa	TU	44.2±1.1	–69±4	–6.0±0.1
	DMTU	52.0±1.5	–50±5	–8.9±0.4
	TMTU	62.9±1.4	–11±5	–8.8±0.7
	I^-	53.7±0.7	–30±2	
	SCN^-	55.6±1.1	–29±4	
apa	TU	42.3±0.7	–65±2	–5.3±0.6
	DMTU	45.0±0.5	–63±2	–6.9±0.4
	TMTU	48.4±0.8	–62±3	–10.3±1.4
	I^-	51.6±0.3	–29±1	
	SCN^-	48.7±0.9	–45±3	
aap	TU	42.2±1.0	–65±3	–5.3±0.5
	DMTU	44.7±0.9	–59±3	–8.5±0.9
	TMTU	44.4±0.9	–68±3	–9.1±0.8
	I^-	49.7±1.1	–33±4	
	SCN^-	49.3±0.2	–40±1	
pap	TU	40.1±0.4	–61±1	–6.8±0.3
	DMTU	46.2±1.7	–41±6	–6.3±0.4
	TMTU	43.2±1.7	–57±6	–8.2±0.4
	I^-	46.2±0.7	–41±1	
	SCN^-	46.9±1.2	–46±5	
app	TU	36.4±0.5	–63±2	–6.0±1.3
	DMTU	38.2±0.5	–56±2	–6.1±1.1
	TMTU	41.1±0.6	–48±2	–8.0±0.8
	I^-	49.8±0.6	–14±2	
	SCN^-	48.9±1.4	–24±4	
ppp	TU	21.5±0.3	–73±1	–6.0±0.4
	DMTU	17.6±0.4	–84±1	–6.5±0.4
	TMTU	18.9±0.4	–82±1	–8.1±0.1
	I^-	30.3±1.1	–47±4	
	SCN^-	31.3±0.9	–52±3	

summarized in Table IV. It is worth noting that the values of the activation entropy, $\Delta S^{\#}$, and the activation volume, $\Delta V^{\#}$, are significantly negative for all studied reactions (Table IV). This is consistent with an associative substitution mechanism and a net increase in bond order in the transition state. Minor trends can be observed for these parameters along the series of complexes. The value of the activation entropy for the negatively charged nucleophiles is much smaller than for the neutral nucleophiles. This is ascribed to charge neutralization effects on bond formation in the transition state. The activation volumes were only determined for the neutral entering nucleophiles, since it is well known that this parameter is also affected by changes in electrostriction as a result of charge neutralization. The reported activation volumes are very typical for associative substitution reactions on square-planar complexes (*88–90*), where the volume collapse resulting from bond formation with the entering nucleophile is partially offset by a volume increase resulting from a geometric change from square planar to trigonal bipyramidal in forming the five-coordinate transition state. The activation volumes are independent of the nature of the selected chelate, but do become more negative for the larger entering nucleophile TMTU. This can be ascribed to a more effective overlap of the van der Waals radii on forming the five-coordinate transition state with the larger nucleophile.

The reactivity of the studied complexes results mainly from the electrophilicity of the metal center, as a result of the electron back donation of incoming electron density to the ligand orbitals. The electronic communication between the π-acceptor ligands as found in the case of the **app** and **ppp** complexes is responsible for the drastic increase in lability observed in these cases. This is because of their ability to withdraw π-electron density more strongly from the metal center. The effect of breaking this electronic communication between π-acceptor groups has, in fact, been recently shown to lower the substitution rate by a factor of 60 (*71*). The π-acceptor effects on their own (in the *cis* or *trans* position) are of minor significance in influencing the lability of d^8 square-planar complexes because of the absence of a direct electronic communication.

Revealed here for the first time is the observation that the rate of substitution is inversely proportional to the basicity of the complex as a whole, and not just that of the leaving or entering groups. This can be correlated with the Hammett relationship, which is usually applied to the reactions in organic compounds. The present investigation also demonstrates that it is possible, through π-acceptor effects, to tune the pK_a and the reactivity of $[Pt(L)(OH_2)]^{2+}$ complexes. Since we have found that the hydroxo species of the tridentate $[Pt(L)OH]^+$ derivatives are much less reactive than the corresponding aqua complexes, the pH of the environment can control the reactivity of the complex in terms of the fraction of the aqua complex available in solution. This may prove to be important in terms of the anti-tumor activity of such

complexes, since it is known that cancer cells are distinguishable from normal cells by a difference in the pH of their cytoplasm. We could show by modifying the π-acceptor properties of the spectator ligands that it is possible to tune the pK_a values of the aqua complexes in such a manner that the maximum reactivity is attained under specific pH conditions, for instance in cancer cells. Since one of the reasons for the specific activity of *cis*-platin against certain cancer cells is the pK_a value of its hydrolysis product in combination with the cell pH, this finding may prove to be important in drug design.

C. Combined σ-Donor and π-Acceptor Effects

In the study on the π-acceptor effects of in-plane pyridine donors, we could show that π-back bonding in the *cis* position seems to enhance the electrophilicity of the metal center slightly more than in the *trans* position. Nevertheless, there is still a thermodynamically and kinetically measurable increase in the electrophilicity if a *trans* amine is substituted by a *trans* in-plane pyridine ligand (*91*). We have therefore investigated the effect of a strong σ-donor Pt–C bond in the *cis* or *trans* position to the leaving group on the reactivity of the complex in the presence of a strong π-acceptor ligand backbone. We systematically studied the ligand substitution reactions of the complexes [Pt(N–C–N)Cl] (N-CH-N = 1,3-di(2-pyridyl)benzene) and [Pt(N–N–C) Cl] (N–N-CH = 6-phenyl-2,2′-bipyridine) in comparison to [Pt(N–N–N)Cl] Cl (N–N–N = 2,2′:6′,2″-terpyridine) (see Fig. 16). In the remaining text these complexes are referred to as **NCN**, **NNC** and **NNN**, respectively. In these complexes, the in-plane phenyl/pyridine rings act as π-acceptors, delocalize negative charge away from the reaction center and thereby increase the electrophilicity of the Pt(II) center (*71,73,80, 83,91,92*).

It was also our objective to gain more insight into the relationship between σ-donor and π-acceptor effects in Pt(II) chemistry. Are these effects cumulative, do they counteract each other, or are they independent effects in which their importance is defined by the underlying reaction mechanism? Dissociative substitution reactions are expected to benefit mostly from σ-donor properties, whereas associative reactions are expected to be mainly enhanced by π-acceptor effects. Another

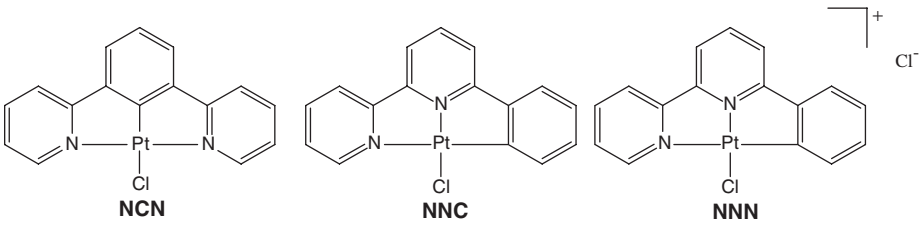

Fig. 16. Schematic structures of the investigated complexes.

question concerns the position of the σ-donor (*cis* or *trans*) to the leaving group. Furthermore, the investigated complexes allow us to analyze the *trans* and *cis* σ-donor effects and influence of the phenyl group, without affecting the steric or π-acceptor properties (*71*) of the *trans* or *cis* position, which often camouflage the relatively small *cis* σ-donor effect.

In order to investigate the *cis* and *trans* σ-donor effect of a Pt(II)-carbon bond in the presence of the strong π-accepting terpyridine type of ligand backbone, three Pt(II) derivates were synthesized, characterized and their ligand substitution reactions studied kinetically. For the reactions of TU, DMTU and TMTU with **NNC** and **NCN**, the corresponding activation parameters ($\Delta H^{\#}$, $\Delta S^{\#}$ and $\Delta V^{\#}$) were also determined. The obtained pseudo-first-order rate constants, k_{obsd}, were plotted against the concentration of the entering nucleophile. A linear dependence on the nucleophile concentration was observed for all reactions. An intercept was observed for all reactions with **NCN**. Since the error in the intercept (k_S) was considerably higher for the reactions with TU ($k_S = 12 \pm 6\,s^{-1}$, at 25.0°C), these values were not used in further calculations (i.e. temperature dependence). In the case of the weakest investigated nucleophile Br^-, an intercept could also be observed in the concentration dependence of **NNN** and **NNC**. The intercept observed for reactions with **NNC** and **NCN** can be ascribed to a parallel solvolysis reaction pathway, well known in Pt(II) chemistry. In the case of **NNN**, however, the solvolysis reaction of the bromo complex also contributes to the observed back reaction as shown in Scheme 4. Since it is impossible to separate k_S and k_{-S} experimentally in this particular case, the relative values of k_S and k_{-S} had to be predicted. It is known from the literature that the solvolysis rate constants for the complexes $[Pt(dien)(Br)]^+$ and $[Pt(dien)(Cl)]^+$ are within $\pm 30\,\%$ almost

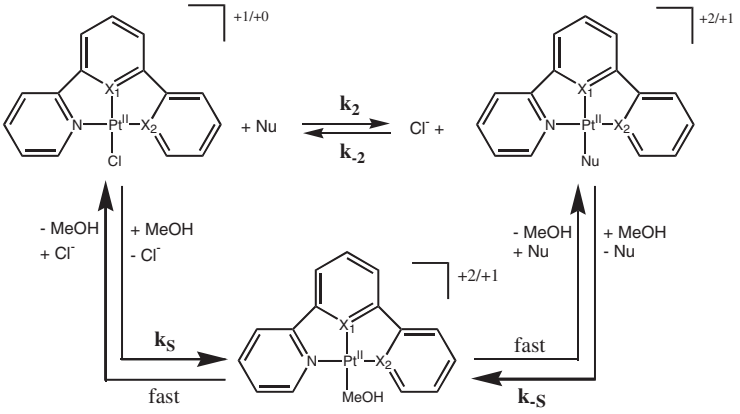

SCHEME 4.

the same (*93–95*). Therefore, it is reasonable to assume that k_S and k_{-S} contribute equally to the observed intercept. In fact, it is more the order of magnitude of k_S and k_{-S} that is important for the subsequent treatment of the data. The overall substitution process can therefore be represented by the mechanism outlined in Scheme 4, and the corresponding expression for k_{obsd} is given by Eq. (17).

$$k_{obsd} = k_S + k_2[Nu](+k_{-2}[Cl^-] + k_{-S} \text{ in the case of } \mathbf{NNN}) \qquad (17)$$

Note that the solvolysis pathway occurs for all investigated reactions, but since its contribution to k_{obsd} in the reaction with the stronger nucleophiles is rather small, the observed intercept is smaller than the experimental error. The resulting rate constants are summarized in Table V. The activation parameters for the reactions of **NCN** and **NNC** with TU, DMTU and TMTU were determined from a systematic variation of temperature and pressure. Since k_{obsd} consists of two independent rate constants k_S and k_2 in the case of the reactions with **NCN** (see Eq. (17)), a concentration dependence at different temperatures was performed, whereas the temperature dependence for **NNC** was studied at only one nucleophile concentration. The thermal activation parameters for k_S and k_2 ($\Delta H^{\#}$ and $\Delta S^{\#}$) were calculated from the Eyring equation. For the effect of pressure on the reaction rates of **NCN**, a pressure dependence study at different TMTU concentrations was performed. The obtained pressure-dependent values of k_S were subtracted from the corresponding k_{obsd} values observed for the reactions of **NCN** with TU and DMTU, which were performed at one nucleophile concentration only. This enabled us to calculate the

TABLE V

SUMMARY OF RATE CONSTANTS FOR THE DISPLACEMENT OF CHLORIDE BY A RANGE OF NUCLEOPHILES IN METHANOL AT 25.0°C AND 0.1 M ($LiSO_3CF_3$) IONIC STRENGTH

	Complexes		
Nucleophile	**NCN**	**NNC**	**NNN**
TU,[a] k_2 ($M^{-1}s^{-1}$)	44,500 ± 2,000	98 ± 2	1,500 ± 10[d]
DMTU,[b] k_2 ($M^{-1}s^{-1}$)	18,400 ± 500	42.5 ± 0.4	450 ± 10[d]
TMTU,[c] k_2 ($M^{1}s^{-1}$)	7,400 ± 300	32.3 ± 0.3	95 ± 4[d]
Br^-, k_2 ($M^{-1}s^{-1}$)	157 ± 9	0.0145 ± 0.0006	6.5 ± 0.1
I^-, k_2 ($M^{-1}s^{-1}$)	1,464 ± 14	0.64 ± 0.02	267 ± 1
MeOH, k_S (s^{-1})	16.4 ± 0.9[e]	$(2.2 \pm 0.1) \times 10^{-4}$ [f]	$(2.1 \pm 0.4) \times 10^{-4}$ [f,g]

[a] Thiourea.
[b] *N,N*-dimethylthiourea.
[c] *N,N,N′,N′*-tetramethylthiourea.
[d] Data taken from literature.
[e] Average value for the reactions with DMTU, TMTU, Br^- and I^-.
[f] Obtained from the reaction with Br^-.
[g] k_S was assumed to be equal to k_{-S}.

activation volume for k_2 independently of k_S. In the case of **NNC**, the pressure dependence was studied at a single nucleophile concentration. The values of k_{obsd} and k_S increase with increasing pressure, and the dependences of $\ln(k_{obsd/S})$ on the applied pressure were in all cases linear. The acceleration of the reaction by pressure is indicative of an associative substitution mechanism. This is also supported by the negative $\Delta S^{\#}$ values calculated from the temperature dependence of the reactions. All activation parameters are summarized in Table VI.

In order to gain further information on the influence of a single Pt–C bond in the *cis* or *trans* position on the nucleophilic discrimination ability of the complex, the rate constants for substitution of Cl^- by MeOH, Br^- and I^- were measured and the corresponding $\log(k_2)$ values plotted against their n_{Pt} values ($n_{Pt}(MeOH) = 0$, $n_{Pt}(Br^-) = 4.18$, $n_{Pt}(I^-) = 5.42$), as shown in Fig. 17. To obtain the k_2 value for substitution by MeOH, the rate constant for the solvolysis pathway (k_S) was divided by the concentration of methanol as solvent (24.7 M). Although the values for TU as entering nucleophile are also included in the plot, they were omitted from the fit since it is known that their behavior in determining the nucleophilic discrimination factor (s) is misleading due to their biphilic character. The resulting values for s are 0.61 ± 0.04 (**NCN**), 0.9 ± 0.1 (**NNC**) and 1.39 ± 0.02 (**NNN**), respectively.

A major part of the following discussion is based on the assumption that the π-acceptor effect of a phenyl ligand is comparable to that of a pyridine ligand, at least as far as the kinetic effects are concerned. Romeo *et al*. could demonstrate that the reactivity of the complex [Pt(2,2′bipyridine)(phenyl)Cl] is enhanced by a factor of 191, as soon as the phenyl ring becomes part of the π-acceptor system due to its in-plane arrangement in **NNC** (*71*). Nearly the same rate enhancement (factors 114–133) is achieved, when ammonia in the complex [Pt(2,2′bipyridine)(NH_3)OH_2] is displaced with an in-plane pyridine

TABLE VI

ACTIVATION PARAMETERS FOR THE REACTIONS OF TU, DMTU AND TMTU WITH **NCN** AND **NNC**

Nucleophile	Complex	$\Delta H^{\#}$ (kJ mol^{-1})	$\Delta S^{\#}$ (J K^{-1} mol^{-1})	$\Delta V^{\#}$ (cm^3 mol^{-1})
TU	**NNC**	40.8 ± 1.5	-70 ± 5	-8.9 ± 0.4
	NCN	21.1 ± 1.4	-85 ± 5	-7.1 ± 0.4
DMTU	**NNC**	39.2 ± 0.8	-82 ± 3	-10.5 ± 0.6
	NCN	16.1 ± 1.3	-109 ± 4	-7.9 ± 0.3
TMTU	**NNC**	29.1 ± 1.6	-119 ± 5	-13.1 ± 0.7
	NCN	10.5 ± 0.9	-135 ± 3	-10.7 ± 1.7
MeOH	**NCN**	55.0 ± 1.0^a	-37 ± 3^a	-8.7 ± 2.2^b

[a] Average value of the temperature dependence of the intercept (k_S) from the reactions with DMTU and TMTU.

[b] From the intercept of the reaction with TMTU.

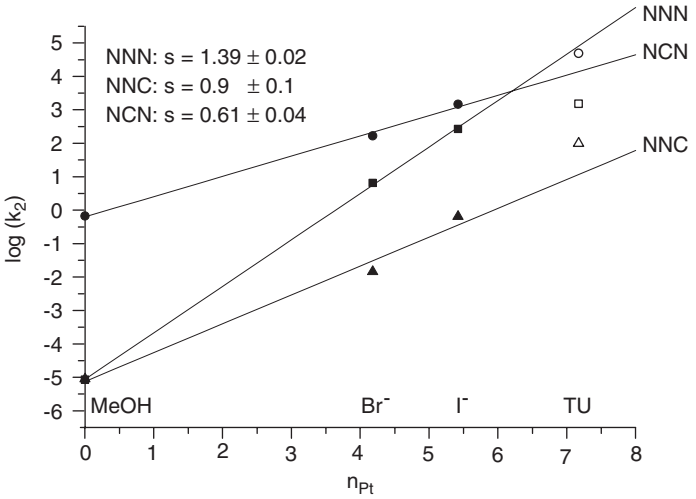

FIG. 17. Plots of $\log(k_2)$ versus n_{Pt} for the determination of the nucleophilic discrimination factor s. Note that the empty points (TU) are not considered in the linear fit, due to the biphilic behavior of TU.

to give [Pt(2,2′:6′,2″-terpyridine)OH_2], due to the π-acceptor properties of the in-plane pyridine ring (*91*). In both cases, the increased reactivity has its origin in the π-acceptor properties of the in-plane pyridine/phenyl ring (*71,91*), showing clearly that these are indeed approximately the same. Therefore, the π-acceptor environment of **NNC** can be considered to be similar to that of **NNN**, as already suggested by Romeo *et al* (*71*).

The X-ray structure of **NNC** enabled us to compare the *trans* influence of the phenyl group in the complex **NCN** with its *cis* influence, by a comparison of the lengthening of the Pt–Cl bond on displacing a *trans* or *cis* pyridine in **NNN** by a phenyl ligand. In the case of **NCN**, a Pt–Cl distance of 2.417(2) Å is reported (*96*), which is in perfect agreement with other Pt–Cl bond lengths *trans* to the phenyl carbon donor. The average Pt–Cl bond length for [Pt(terpy)Cl]ClO_4 (*97*) and [Pt(terpy)Cl]SO_3CF_3 (*98*) is 2.304 Å. This bond length is therefore increased by ~0.113 Å through the *trans* labilizing influence of the phenyl group. This rather large increase in bond length is not surprising, since it is known that the phenyl group is a very strong *trans*-labilizing ligand (an approximate *trans* influence sequence is: Cl < S < Sn,P < C,H < Si) due to its high σ-donor strength. Perhaps more interesting is how this strong σ-donor affects the Pt–Cl bond in case of the **NNC** complex. It is known that the *cis* influence for a specific ligand is usually much smaller than its *trans* influence. It is therefore not surprising that the average Pt–Cl bond length of **NNC** is 2.312 Å and only 0.008 Å longer than in the $[Pt(terpy)Cl]^+$ complex. Considering three standard deviations, this difference in bond length is too small to allow a convincing

interpretation. Nevertheless, two independent structures of **NNN** type complexes and two independent structures of **NNC** do show the same trend, viz. the Pt–Cl bond is always longer in the latter ligand arrangement. This may indicate a slight *cis* labilization via the σ-bond framework due to the higher σ-donor strength of the phenyl group as compared to the pyridine group. However, if there is such an effect, it is too small to be observed clearly in the available X-ray structures.

Despite the fact that the *trans* influence of the carbon σ-donor in the **NCN** complex is in perfect agreement with literature values (see discussion above), the observed reactivity of this complex is orders of magnitude higher than in comparable complexes. To our knowledge, the observed rate constants are the highest ever found for the substitution of chloride *trans* to a Pt(II)-carbon bond by the selected nucleophiles. Since there is no evidence for a larger *trans* influence that would indicate a higher σ-donor strength of the *trans* phenyl group and therefore a higher ground state labilization, other reasons must account for this unusual high reactivity. There are two possible explanations: Firstly, the planar coordination sphere of the metal center as induced by the in-plane pyridine/phenyl ligand system, offers only minute steric hindrance to the entering nucleophile, which leads to faster substitution reactions compared to complexes which are sterically more crowded in the *cis* positions (*99*). Secondly, the in-plane arrangement of pyridine/phenyl rings at Pt(II) centers is known to accelerate associative substitution reactions by stabilizing the additional electron density in the transition state via their π-acceptor ability, thereby increasing the electrophilicity (and therefore the nucleophilic discrimination factor *s*) of the complex (*56,57,71,83,91*). We believe that both effects contribute to the observed high reactivity. On the one hand, the influence of steric crowding in the *cis* position on the substitution rate has been very well investigated for square planar Pt^{II}/Pd^{II} complexes, and it is therefore known that reducing the steric crowding in the *cis* position accelerates the reaction. On the other hand, the nucleophilic discrimination factor *s* of **NCN** is about 0.61, whereas for the complexes $[Pt\{C_6H_3(CH_2NMe_2)_2\text{-}2,6\}(OH_2)]^+$ and $[Pt\{C_6H_4(CH_2NMe_2)\text{-}2\}(NC_5H_4SO_3\text{-}3)(OH_2)]$ this factor is significantly smaller (0.40 and 0.43, respectively) (*57*). This indicates that transition state stabilization due to π-back bonding to the in-plane pyridine/phenyl groups also contributes to the observed high reactivity, at least for strong nucleophiles which benefit more from the nucleophilic discrimination ability of the metal center.

On comparing the reactivity of **NCN** with **NNN**, it is seen that the substitution reaction is accelerated by five orders of magnitude in the case of the solvolysis reaction in methanol, but only by a factor of five in the case of the reaction with iodide, on displacing one nitrogen donor by a much stronger carbon donor. There is a simple explanation for this strange behavior. The high reactivity of **NCN** is mainly due to the *trans*-labilizing effect of the Pt–C bond which induces a high

intrinsic reactivity, whereas the high reactivity of **NNN** is due to the increased electrophilicity of the metal center that causes a high nucleophilic discrimination. On displacing the *trans* pyridine of **NNN** by the strong phenyl σ-donor, the intrinsic reactivity goes up five orders of magnitude but the nucleophilic discrimination factor drops from 1.39 (**NNN**) to 0.61 (**NCN**) because the electron-withdrawing effect of the π-acceptor rings is partially cancelled by the electron-donating effect of the carbon atom. Therefore, on comparing the reaction rates of **NNN** and **NCN**, the nucleophilicity of the incoming ligands is very important. Weak nucleophiles such as methanol will benefit most from the increased intrinsic reactivity of **NCN**, whereas strong nucleophiles will benefit more from the higher nucleophilic discrimination ability of **NNN**. For the reaction of a medium strong nucleophile like iodide with **NCN**, the gain in reactivity by the first factor is almost cancelled by the reduced nucleophilic discrimination as compared to **NNN**.

Following these arguments, it is expected that the stronger nucleophiles TU, DMTU and TMTU should react faster with **NNN** than with **NCN**. However, the opposite is true and must be due to the biphilic character of these nucleophiles. Their high nucleophilicity is partly due to their π-acceptor ability that assists the stabilization of the electron-rich five-coordinate transition state. This means that electron-rich metal centers as in **NCN** (and **NNC**) will benefit much from this specific ability of the nucleophile, whereas the already very electrophilic metal center of **NNN** cannot take advantage of this effect. Therefore, the reactivity of biphilic nucleophiles depends on the electrophilicity of the reactant complexes. If the electrophilicity of the investigated complex is higher than that of the reference complex for the calculation of the n_{Pt} value for a specific nucleophile (viz. *trans*-[Pt(pyridine)$_2$Cl$_2$]), the reaction rate for a biphilic nucleophile will be smaller than predicted by its n_{Pt} value and vise versa. This assumption only considers electronic effects, whereas steric effects which also affect nucleophilic discrimination are not considered. From the n_{Pt} versus log k_2 plots in Fig. 17, it can clearly be seen that TU reacts faster with **NNC** and **NCN**, and slower with **NNN** than predicted from the linear fit based on the other nucleophiles (MeOH, Br^- and I^-) as expected from the above outlined arguments.

The *cis* effect has not been studied in much detail before and the experimental findings are to some extent contradictory. The obvious reason for these different results lies in the fact that changes in the σ-donor, π-acceptor and steric properties of the *cis* ligand have opposite effects on the reactivity of the complex. In the present study, the steric and π-acceptor properties of the *cis* and *trans* ligands were not changed (*71*), only the σ-donor ability was changed by displacing the weak σ-donor nitrogen by the strong σ-donor carbon.

From a comparison of the reactivity of **NNN** and **NNC**, it follows that the substitution reactions of the latter complex are up to 450 times slower (Nu = Br^-) for all nucleophiles, except for the solvolysis

rate constants which are similar within the experimental error limits. This behavior emphasizes the general assumption that the *cis* effect is smaller and has the opposite trend than the *trans* effect (*100–102*). Since only the σ-donor property of the chelating ligand was altered, we conclude that this finding only applies in cases where only the σ-donor properties of the *cis* and *trans* ligands are altered, meaning that stronger σ-donors in the *cis* position result in slower substitution reactions. Taking into account that π-acceptors behave in exactly the opposite way, viz. the reactivity is enhanced more if stronger π-acceptors are in the *cis* position than if they are in the *trans* position (*83,91*), it seems clear why such different results are reported in the literature. If a ligand possesses both σ-donor and π-acceptor properties, its observed *cis* effect depends on whatever effect is stronger since the former decelerates and the latter accelerates the reaction.

Romeo *et al*. showed that the reactivity of a complex which benefits from a strong π-acceptor environment is decreased, if a strong σ-donor is placed in the *cis* position, because the electron-donating effect of the σ-donor counteracts the electron-withdrawing effect of the π-acceptors (*71*). Based on our data, we believe that this deceleration of the substitution rate of **NNC** as compared to **NNN** is caused by the reduced nucleophilic discrimination of the **NNC** complex ($s = 0.9$ as compared to $s = 1.39$ for **NNN**). This means that *cis* σ-donor lowers the nucleophilic discrimination as its *trans* counterpart by reducing the electrophilicity of the platinum metal center due to their electron-donating effect. However, the decrease in nucleophilic discrimination for **NNC** is smaller than for **NCN** ($s = 0.61$). Important to note, is that the intrinsic reactivity of **NNC** is comparable with that of **NNN**, which indicates that the observed decrease in reactivity is mainly caused by the reduced nucleophilic discrimination and therefore depends on the nucleophilicity of the entering nucleophile.

The substitution of chloride by the nucleophiles TU, DMTU and TMTU shows a clear dependence on the steric hindrance of the nucleophile. With increasing steric hindrance the substitution rate decreases for all the studied complexes. The observed rate constant for the substitution of chloride by TU is about 6 (**NCN**) to 16 (**NNN**) times larger than for the reaction with TMTU, which is in good agreement with literature values for the corresponding reactions in methanol. However, in the case of the **NNC** complex the difference in rate is much smaller; TU reacts only three times faster than the steric demanding TMTU ligand. This cannot be due to the reduced nucleophilic discrimination of **NNC**, since **NCN** is even less able to discriminate between different nucleophiles. Therefore the reduced influence of steric crowding on the nucleophile must be due to the reduced steric demand of the complex. The steric bulk of the investigated chelates themselves is comparable, but in the case of **NNC** the overall N–Pt–C distance of the *cis* ligands is 4.145 Å due to the strong *trans* influence of the phenyl carbon donor, and therefore significantly longer than the

corresponding N–Pt–N distance in the case of **NNN** or **NCN** (viz. 4.048 and 4.074 Å, respectively) (*96,97*). Since it is known that associative substitution reactions on Pd(II)/Pt(II) centers are very sensitive to steric hindrance in the *cis* position, we believe that *cis* bond lengthening reduces the steric hindrance of the complex and therefore also reduces its ability to discriminate between nucleophiles with differing steric bulk. This can also account for the slightly reduced steric discrimination of **NCN** (TU:DMTU:TMTU = 6.0:2.4:1) as compared to **NNN** (TU:DMTU:TMTU = 15.8:3.3:1) since the N–Pt–N distance is 0.026 Å longer for **NCN** due to the *cis* influence of the *trans* carbon donor. This suggests that the ratio of the rate constants (TU/TMTU) is an indication of the steric discrimination ability of the complexes.

The much higher reactivity of **NCN** as compared to **NNC** is also reflected by a large decrease in activation enthalpy $\Delta H^{\#}$ (a difference of $\sim$20 kJ mol^{-1}) for the substitution reactions of the **NCN** complex with the investigated thioureas (see Table VI). This can be ascribed to the *trans* influence of the phenyl group, which destabilizes the ground state, makes it easier to cleave the bond to the leaving group and has a large influence on the observed reactivity. It is interesting to compare the activation enthalpies for the reactions of TU, DMTU and TMTU with a specific complex. In the case of **NNC**, the observed sequence for increasing $\Delta H^{\#}$ is TMTU < DMTU $\approx$ TU, whereas for **NCN** it is TMTU < DMTU < TU, respectively. This is not in accordance with the observed reactivity sequence, where DMTU reacts faster than TMTU, and TU has the highest reaction rate of all investigated thioureas. Therefore, it can be concluded that the difference in the activation entropies must be responsible for the observed steric retardation.

Since it is known from the literature that not a single *trans* Pt–C bond or a single *cis* Pt–C bond, but only the combination of a *trans* and a *cis* Pt–C bond can induce a mechanistic changeover in the substitution behavior from associative to dissociative, negative values for both the activation entropy $\Delta S^{\#}$ and activation volume $\Delta V^{\#}$ are expected for the investigated reactions. This is exactly what is observed for both **NNC** and **NCN**, and the reported values are in good agreement with literature values for related complexes (*57*). The observed volume collapse in the transition state results from bond formation with the entering nucleophile, which is partially offset by a volume increase that results from a square planar to a trigonal bipyramidal change in geometry on forming the five-coordinate transition state. The latter volume increase is larger in the case where platinum-ligand bonds of the entering and leaving ligands are longer, as in the case of **NCN** due to the large *trans* influence. This explains why the observed activation volumes for the investigated nucleophiles are less negative for **NCN** than for **NNC**, where the bonds to the leaving and entering groups are significantly shorter.

The activation entropies behave in the opposite direction; they are more negative for the reactions of **NCN** than for **NNC**. This can be

ascribed to an increase in solvent electrostriction in the transition state as a result of partial charge separation that accompanies the lengthening of the platinum chloride bond in the transition state and induces an increase in the dipole moment of the complex. Therefore, the dipole character of **NCN** in the transition state is larger than that of **NNC**, and there is a stronger influence on the reorganization of the polar solvent that leads to more negative $\Delta S^{\#}$ values for the **NCN** complex. Both $\Delta S^{\#}$ and $\Delta V^{\#}$ become more negative on increasing the size of the entering thiourea nucleophile for a specific complex. This can be ascribed to a more effective overlap of the van der Waals radii on forming the five-coordinate transition state with larger entering nucleophiles.

From a comparison with literature data, it could be shown that the electron-withdrawing effect of in-plane aryl/phenyl rings (the in-plane arrangement being achieved through cyclometalation) increases the reactivity, although the strong σ-donor carbon weakens the π-acceptor effect dramatically since the electron-donating properties of the σ-donor counteract the electron-withdrawing effect of the π-acceptors. Taking the nucleophilic discrimination factor as an indicator for the electrophilicity of the metal center, it can be seen that the decrease in the π-acceptor effect is smaller for *cis* than for *trans* carbon-donors, indicating that in the case of a Pt–C bond *trans* to the leaving group, the additional benefit from π-acceptor pyridyl/phenyl rings is small, but still significant. The reactivity of the **NCN** complex is therefore the highest observed among comparable complexes of the type *trans*-[Pt(C)(L_1)(L_2)Cl] due to the highly destabilized ground state (labilization of the Pt–Cl bond by the *trans* influence of phenyl) and the additional small π-acceptor contributions.

In the case of the **NNC** complex, the nucleophilic discrimination is lower than for **NNN**, which results in slower substitution reactions with all investigated nucleophiles except for methanol. The intrinsic reactivity of **NNC** is not affected by the introduction of the *cis* σ-donor phenyl and remains equal to that of **NNN**. On the basis of the present work and earlier investigations, the *cis* effect in Pt(II) substitution chemistry can be summarized in the following way. The direction (acceleration or deceleration) and magnitude of the *cis* effect (as compared to the *trans* effect of the same ligand) depends on three factors, viz. the σ-donor strength, π-acceptor ability and steric property of the *cis* ligand. (i) With increasing σ-donor strength, the reactivity decreases because nucleophilic discrimination is reduced. Whether this deceleration is larger or smaller than the accelerating *trans* effect of the same σ-donor depends on the nucleophilicity of the investigated nucleophile. (ii) With increasing π-acceptor ability of the *cis* ligand the reactivity is increased by an enhanced nucleophilic discrimination of the complex. This π-*cis* effect is larger than the corresponding π-*trans* effect (*83,91*). (iii) With increasing steric bulk of the *cis* ligand, the

reaction is slowed down due to an increase in steric hindrance in the five-coordinate transition state. This steric *cis* effect reduces the reactivity more than the corresponding steric *trans* effect.

The results of this and earlier studies clearly demonstrate the ability to systematically tune the reactivity of Pt(II) complexes via σ-donor and π-acceptor effects, to the point where a fine tuning as a result of a combination of these effects is indeed possible. This may be of significance in the systematic tuning of the reactivity of Pt(II) complexes in applications such as anti-tumor drug design, C–H activation and homogeneous catalysis.

IV. Conclusions

The emphasis in this contribution was to demonstrate how the lability of inert Co(III) and Pt(II) complexes can be tuned electronically to the point that the metal centers become remarkably labile even to the extent that the reactions become too fast to be followed by rapid reaction trechniques. In the case of octahedral Co(III) complexes electronic effects in general induce a more dissociative activation mode that is caused by the labilization of the leaving ligand. In the case of square-planar Pt(II) complexes the electronic effects can be used to labilize the leaving group and to accelerate the ligand displacement reaction even to the extent that a changeover in mechanism, i.e. from the usual associative to the unusual dissociative reaction mode, can occur. The application of rather fundamental chemical principles can cause this impressive lability tuning by which the reactivity of the metal center changes over many orders of magnitude. In the case of Pt(II) complexes a reactivity typical for Pd(II) complexes can be reached. It is this electronic tuning ability in coordination chemistry that makes the underlying chemistry fascinating and can serve as model for many other inert metal complex systems. Along these lines the reactivity of homogeneous catalytic systems can systematically be adjusted to the degree required under specific experimental conditions. Thus, a fundamental understanding of the mechanistic implications of electronic tuning effects can indeed advance our ability to apply the gained knowledge to processes of industrial importance.

Acknowledgments

The author gratefully acknowledges the continuous financial support from the Deutsche Forschungsgemeinschaft, Fonds der Chemischen Industrie, the Alexander von Humboldt foundation and the Max-Buchner Research Foundation. He furthermore appreciates the fine colloboration he has enjoyed over many years with graduate and post-doctoral collaborators whose names are given on the papers cited from his group.

References

1. (a) van Eldik, R.; Dücker-Benfer, C.; Thaler, F. *Adv. Inorg. Chem.* **2000**, *49*, 1. (b) van Eldik, R.; Hubbard, C. D. van Eldik, R.; Klärner, F.-G. (Eds.) *"High Pressure Chemistry: Synthetic, Mechanistic and Supercritical Applications";* Weinheim, Germany: VCH-Wiley, **2002** pp. 340 (c) van Eldik, R.; Hubbard, C. D. Riad Manaa, M. (Ed) Chemistry at Extreme Conditions **2005**. Amsterdam: Elsevier, pp. 109–164.
2. Marques, H. M.; Munro, O. Q.; Cumming B. M.; de Nysschen, C. *J. Chem. Soc., Dalton Trans*. **1994**, 297.
3. Marques, H. M.; Breet, E. L. J.; Prinsloo, J. J. *J. Chem. Soc., Dalton Trans.* **1991**, 2941.
4. Marques, H. M. *J. Chem. Soc., Dalton Trans*. **1991**, 339.
5. Stochel, G.; van Eldik, R.; Kunkely, H.; Vogler, A. *Inorg. Chem*. **1989**, *28*, 4314.
6. Prinsloo, F. F.; Meier, M.; van Eldik, R. *Inorg Chem*. **1994**, *33*, 900.
7. Meier, M.; van Eldik, R. *Inorg. Chem*. **1993**, *32*, 2635.
8. Prinsloo, F. F.; Breet, E. L. J.; van Eldik, R. *J. Chem. Soc., Dalton Trans.* **1995**, 685.
9. Marques, H.; Knapton, L. *J. Chem. Soc., Dalton Trans.* **1997**, 3827Marques, H. M.; Bradley, J. C.; Brown, K. L.; Brooks, H. *J. Chem. Soc., Dalton Trans*. **1993**, 3475Marques, H. M. *S. Afr. J. Chem*. **2003**, *44*, 114
10. Perry, C. B.; Fernandes, M. A.; Brown, K. L.; Zou, X.; Valente, E. J.; Marques, H. M. *Eur. J. Inorg. Chem*. **2003**, *11*, 2095.
11. Moreno-Esparza, R.; Lopez, M.; Pannell, K. H. *J. Chem. Soc., Dalton Trans.* **1992**, 1791.
12. Thusius, D. *J. Am. Chem. Soc.* **1971**, *93*, 2629. Randall, W. C.; Alberty, R. A. *Biochemistry* **1973**, *6*, 1520. Nome, F.; Fendler, J. H. *J. Am. Chem. Soc.* **1973**, *99*, 1557Nome, F.; Fendler, J. H. *J. Chem. Soc., Dalton Trans*. **1976**, 1212;Poon, C. K. *Coord. Chem. Rev.* **1973**, *10*, 1.
13. Marques, H. M. *J. Chem. Soc., Dalton Trans*. **1991**, 1437;Marques, H. M.; Egan, T. J.; Marsh, J. H.; Mellor, J. R.; Munro, O. Q. *Inorg. Chim. Acta* **1997**, *166*, 249Marques, H. M.; Bradley, J. C.; Campbell, L. A. *J. Chem. Soc., Dalton Trans.* **1992**, 2019.
14. Hamza, M. S. A. *J. Chem. Soc., Dalton Trans*. **2002**, 2831.
15. Johnson, A. W.; Shaw, N. *J. Chem. Soc. A*. **1962**, 4608.
16. Brasch, N. E.; Hamza, M. S. A.; van Eldik, R. *Inorg. Chem*. **1997**, *36*, 3216.
17. Kofod, P.; Harris, P.; Larsen, S. *Inorg. Chem*. **1997**, *36*, 2258.
18. Kofod, P. *Inorg. Chem*. **1995**, *34*, 2768.
19. Dücker-Benfer, C.; Hamza, M. S. A.; Eckhardt, C.; van Eldik, R. *Eur. J. Inorg. Chem*. **2000**, 1563.
20. Hamza, M. S. A.; Dücker-Benfer, C.; van Eldik, R. *Inorg. Chem*. **2000**, *39*, 3777.
21. Alzoubi, B. M.; Hamza, M. S. A.; Dücker-Benfer, C.; van Eldik, R. *Eur. J. Inorg. Chem*. **2002**, 968.
22. Drennan, C. L.; Matthews, R. G.; Ludwig, M. L. *Curr. Opin. Struct. Biol*. **1994**, *4*, 919.
23. Golding, B. T.; Buckel, W. In: "*Comprehensive Biological Catalysis*"; vol. III, vol. III; Ed. Sinnott, M. L.; Academic Press: London, **1997**, pp. 239–259.
24. Chang, C. H.; Frey, P. A. *J. Biol. Chem*. **2000**, *275*, 106.
25. Brasch, N. E.; Müller, F.; Zahl, A.; van Eldik, R *Inorg. Chem*. **1997**, *36*, 4891.
26. Hamza, M. S. A.; Zou, X.; Brown, K. L.; van Eldik, R. *Inorg. Chem*. **2001**, *40*, 5440.
27. Brodie, S. J.; Cregan, A. G.; van Eldik, R.; Brasch, N. E. *Inorg. Chim. Acta* **2003**, *348*, 221.
28. Hamza, M. S. A.; Zou, X.; Brown, K. L.; van Eldik, R. *J. Chem. Soc., Dalton Trans.* **2002**, 3832.
29. George, P.; Irvine, D. H.; Glauser, S. C. *Ann. NY Acad. Sci.* **1960**, *88*, 393.
30. Reenstra, W. W.; Jencks, W. P. *J. Am. Chem. Soc.* **1979**, *101*, 5780.

31. Costa, G.; Mestroni, G.; Tauzher, G.; Stefani, L. *J. Organomet. Chem.* **1966**, *6*, 181.
32. Costa, G.; Mestroni, G.; Stefani, L. *J. Organomet. Chem.* **1967**, *7*, 493.
33. Bigotto, A.; Costa, G.; Mestroni, G.; Pellizer, G.; Puxeddu, A.; Reisenhofer, E.; Stefani, L.; Tauzher, G. *Inorg. Chim. Acta. Rev.* **1970**, 41.
34. Summers, M. F.; Marzilli, L. G.; Bresciani-Pahor, N.; Randaccio, L. J **1984**,*Am. Chem. Soc.* **1984**, *106*, 4478.
35. Brucker, S.; Calligaris, M.; Nardin, G.; Randaccio, L. *Inorg. Chim. Acta,* **1969**, *3*, 308.
36. Marzilli, L. G.; Summers, M. F.; Bresciani-Pahor, N.; Zangrando, E.; Charland, J. P.; Randaccio, L. *J. Am. Chem. Soc.* **1985**, *107*, 6880.
37. Brown, K. L.; Lyles, D.; Pencovici, M.; Kallen, R. G. *J. Am. Chem. Soc.* **1975**, *97*, 7338.
38. Brown, K. L.; Awtrey, A. W. *Inorg. Chem.* **1978**, *17*, 111.
39. Ogoshi, H.; Watanabe, E.; Koketsu, N.; Yoshida, Z. *Bull. Chem. Soc. Jpn.* **1976**, *49*, 2529.
40. Randaccio, L.; Furlan, M.; Geremia, S.; Slouf, M.; Srnova, I.; Toffoli, D. *Inorg. Chem.* **2000**, *39*, 3403.
41. Wagner, T.; Afshar, C. E.; Carrell, H. L.; Glusker, J. P.; Englert, U.; Hogenkamp, H. P. C. *Inorg. Chem.* **1999**, *38*, 1785.
42. Zou, X.; Brown, K. L. *Inorg. Chim. Acta* **1997**, *267*, 305.
43. Brasch, N. E.; Haupt, R. J. *Inorg. Chem.* **2000**, *39*, 5469.
44. Hamza, M. S. A.; Cregan, A. G.; Brasch, N. E.; van Eldik, R. *J. Chem. Soc., Dalton Trans.* **2003**, 596.
45. Brasch, N. E.; Cregan, A. G.; Vanselow, M. E. *J. Chem. Soc., Dalton Trans.* **2002**, 1287.
46. Rosenberg, B.; Van Champ, L.; Trosko, J. E.; Mansour, V. H. *Nature* **1969**, *22*, 385.
47. Lippert, B. (Ed.) *"Cisplatin: Chemistry and Biochemistry of a Leading Anticancer Drug";* Weinheim: Wiley-VCH, **1999**.
48. Romeo, R.; Minniti, D.; Trozzi, M. *Inorg. Chim. Acta* **1975**, *14*, L15.
49. Romeo, R.; Minniti, D.; Trozzi, M. *Inorg. Chem.* **1976**, *15*, 1134.
50. Krüger, H.; van Eldik, R. *J. Chem. Soc., Chem. Commun.* **1990**, 330.
51. Romeo, R.; Scolaro, L. M.; Nastasi, N.; Arena, G. *Inorg. Chem.* **1996**, *35*, 5087.
52. Clark, R. J. H.; Fanizzi, F. P.; Natile, G.; Pacifico, C.; van Rooyen, C. G.; Tocher, D. A. *Inorg. Chim. Acta* **1995**, *235*, 205.
53. Gosling, R.; Tobe, M. L. *Inorg. Chem.* **1983**, *22*, 1235.
54. Otto, S.; Elding, L.I. *J. Chem. Soc., Dalton Trans.* **2002**, 2354.
55. Cusumano, M.; Marricchi, P.; Romeo, R.; Ricevuto, V.; Belluco, U. *Inorg. Chim. Acta* **1979**, *34*, 169.
56. Schmülling, M.; Ryabov, A. D.; van Eldik, R. *J. Chem. Soc., Dalton Trans.* **1994**, 1257.
57. Schmülling, M.; Grove, D. M.; van Koten, G.; van Eldik, R.; Veldman, N.; Spek, A. L. *Organometallics* **1996**, *15*, 1384.
58. Wendt, O. F.; Elding, L. I. *Inorg. Chem.* **1997**, *36*, 6028.
59. Wendt, O. F.; Elding, L. I. *J. Chem. Soc., Dalton Trans.* **1997**, 4725.
60. Lanza, S.; Minniti, D.; Moore, P.; Sachinidis, J.; Romeo, R.; Tobe, M. L. *Inorg. Chem.* **1984**, *23*, 4428.
61. Lanza, S.; Minniti, D.; Romeo, R.; Moore, P.; Sachinidis, J.; Tobe, M. L. *J. Chem. Soc., Chem. Commun.* **1984**, 542.
62. Alibrandi, G.; Bruno, G.; Lanza, S.; Minniti, D.; Romeo, R.; Tobe, M. L. *Inorg. Chem.* **1987**, *26*, 185.
63. Minniti, D.; Alibrandi, G.; Tobe, M. L.; Romeo, R. *Inorg. Chem.* **1987**, *26*, 3956.
64. Frey, U.; Helm, L.; Merbach, A. E.; Romeo, R. *J. Am. Chem. Soc.* **1989**, *111*, 8161.
65. Alibrandi, G.; Minniti, D.; Monsù Scolaro, L.; Romeo, R. *Inorg. Chem.* **1989**, *28*, 1939.
66. Romeo, R.; Grassi, A.; Monsù Scolaro, L. *Inorg. Chem.* **1992**, *31*, 4383.

67. Plutino, M. R.; Monsù Scolaro, L.; Romeo, R.; Grassi, A. *Inorg. Chem.* **2000**, *39*, 2712.
68. Schmülling, M.; Ryabov, A. D.; van Eldik, R. *J. Chem. Soc., Chem. Commun.* **1992**, 1609.
69. Elding, L.I.; Romeo, R. *J. Chem. Soc., Dalton Trans.* **1996**, 1471.
70. Wendt, O. F.; Oskarsson, A.; Leipold, J. G.; Elding, L. I. *Inorg. Chem.* **1997**, *36*, 4514.
71. Romeo, R.; Plutino, M. R.; Monsù Scolaro, L.; Stoccoro, S.; Minghetti, G. *Inorg. Chem.* **2000**, *39*, 4749.
72. Mureinik, R. J.; Bidani, M. *Inorg. Chim. Acta* **1978**, *29*, 37.
73. Pitteri, B.; Marangoni, G.; Cattalini, L.; Bobbo, T. *J. Chem. Soc., Dalton Trans.* **1995**, 3853.
74. Basolo, F.; Gray, H. B.; Pearson, R. G. *J. Am. Chem. Soc.* **1960**, *82*, 4200.
75. Palmer, B. D.; Wickham, G.; Craik, D. J.; McFadyen, W. D.; Wakelin, L. P. G.; Baguley, B. C.; Denny, W. A. *Anti-Cancer Drug Des.* **1992**, *7*, 385.
76. Lowe, G.; Droz, A. S.; Vilaivan, T.; Weaver, G. W.; Tweedale, L.; Pratt, J. M.; Rock, P.; Yardley, V.; Croft, S. L. *J. Med. Chem.* **1999**, *42*, 999.
77. Mahal, G.; van Eldik, R. *Inorg. Chem.* **1985**, *24*, 4165.
78. Mahal, G.; van Eldik, R. *Inorg. Chim. Acta* **1987**, *127*, 203.
79. Dadci, L.; Elias, H.; Frey, U.; Hörnig, A.; Koelle, U.; Merbach, A. E.; Paulus, H.; Schneider, J. S. *Inorg. Chem.* **1995**, *34*, 306.
80. Pitteri, B.; Marangoni, G.; Cattalini, L.; Visentin, F.; Bertolasi, V.; Gilli, P. *Polyhedron* **2001**, *20*, 869.
81. Tobe, M. L.; Burgess, J. *"Inorganic Reaction Mechanisms"*; 1st edn.Addison-Wesley Longman Limited: Essex, England, **1999**.
82. Wendt, O. F.; Deeth, R. J.; Elding, L. I. *Inorg. Chem.* **2000**, *39*, 5271.
83. Jaganyi, D.; Hofmann, A.; van Eldik, R. *Angew. Chem. Int. Ed.* **2001**, *40*, 1680.
84. Swain, C. G.; Scott, C. B. *J. Am. Chem. Soc.* **1953**, *75*, 141.
85. Belluco, U.; Cattalini, L.; Basolo, F.; Pearson, R. G.; Turco, A. *J. Am. Chem. Soc.* **1965**, *87*, 241.
86. Hansch, C.; Leo, A.; Taft, R. W. *Chem. Rev.* **1991**, *91*, 165.
87. Carr, C. A.; Richards, J. M.; Ross, S. A.; Lowe, G. *J. Chem. Research (S)* **2000**, *12*, 566.
88. Stochel, G.; van Eldik, R. *Coord. Chem. Rev.* **1999**, *187*, 329.
89. Helm, L.; Elding, L. I.; Merbach, A. E. *Helv. Chim. Acta* **1984**, *67*, 1453.
90. Helm, L.; Elding, L. I.; Merbach, A. E. *Inorg. Chem.* **1985**, *24*, 1719.
91. Hofmann, A.; Jaganyi, D.; Munro, O. Q.; Liehr, G.; van Eldik, R. *Inorg. Chem.* **2003**, *42*, 1688.
92. Annibale, G.; Brandolsio, M.; Bugarcic, Z.; Cattalini, L. *Trans. Met. Chem.* **1998**, *23*, 715.
93. Belluco, U.; Ettorre, R.; Basolo, F.; Pearson, R. G.; Turco, A. *Inorg. Chem.* **1966**, *5*, 591.
94. Rindermann, W.; Palmer, D. A.; Kelm, H. *Inorg. Chim. Acta* **1980**, *40*, 179.
95. Palmer, D. A.; Kelm, H. *Inorg. Chim. Acta* **1976**, *19*, 117.
96. Cárdenas, D. J.; Echavarren, A. M.; Ramírez de Arellano, M. C. *Organometallics* **1999**, *18*, 3337.
97. Bailey, J. A.; Hill, M. G.; Marsh, R. E.; Miskowski, V. M.; Schaefer, W. P.; Gray, H. B. *Inorg. Chem.* **1995**, *34*, 4591.
98. Yip, H. -K.; Cheng, L. -K.; Cheung, K. -K.; Che, C. -M. *J. Chem. Soc., Dalton Trans.* **1993**, 2933.
99. Kapoor, P.; Kukushkin, Y. V.; Lövquist, K.; Oskarsson, A. *J. Organomet. Chem.* **1996**, *517*, 71.
100. Burdett, J. K. *Inorg. Chem.* **1977**, *16*, 3013.
101. Okeya, S.; Wakamatsu, K.; Shibahara, T.; Yamakado, H.; Nishimoto, K. J **2002**,*Comput. Chem. Jpn.* **2002**, *1*, 97.
102. Braddock, P. D.; Romeo, R.; Tobe, M. L. *J. Chem. Soc., Dalton Trans.* **1993**, 233.

INDEX